SLIDING DISPLACEMENTS IN REINFORCED MASONRY WALLS SUBJECTED TO IN-PLANE LATERAL LOADS

by

Jose Centeno

M.A.Sc. The University of British Columbia, 2009

B.E.Sc. Escuela Superior Politécnica del Litoral, 2004

A THESIS SUBMITTED IN PARTIAL FULFILLMENT OF

THE REQUIREMENTS FOR THE DEGREE OF

DOCTOR OF PHILOSOPHY

in

The Faculty of Graduate and Postdoctoral Studies

(Civil Engineering)

THE UNIVERSITY OF BRITISH COLUMBIA

(Vancouver)

March 2015

Abstract

Seismic design provisions in the Canadian Masonry Code often lead to indications that the governing yield mechanism for a reinforced masonry wall with a height/length (H/L) ratio below 1.0 and under low axial loads will not achieve the design objective of a flexural yield mechanism and instead, will develop a sliding shear mechanism. In addition to this, results of previous experimental research studies indicate that even for squat walls that yield in flexure, the displacements at the top are the result of both flexure and sliding shear mechanisms. Currently, there is a limited understanding on how sliding shear displacements develop and how they affect the response of a building. The following work sets out to study the sliding shear mechanism and to develop tools for determining the corresponding displacements for seismic design. This study proposes to modify the current definition for a sliding shear mechanism, re-classifying yield mechanisms of Reinforced Masonry (RM) walls with sliding displacements into three separate mechanisms: sliding shear (SS) mechanism, dowel-constrained failure (DCF) mechanism and combined flexural-sliding shear (CFSS) mechanism. In addition, a 2D analytical model is developed and calibrated in this study using the experimental test results of wall specimens with recorded sliding shear displacements. This calibrated model simulates sliding in RM walls based on the effects of frictional resistance, dowel action and flexural hinging, which will be the basis for a procedure that can estimate sliding displacements in an RM wall design.

Preface

This dissertation is original, unpublished and based on independent work undertaken by the author.

Table of Contents

List of Tables

List of Figures

List of Symbols

A_{db}:	cross-sectional area of an individual reinforcing bar
A_s:	total area of reinforcing steel
c:	depth of compression zone
C_{DA}	dowel action yield strength coefficient
C_{Fl}:	flexural yield coefficient
C_k:	dowel action secant stiffness coefficient
C_o:	overturning moment coefficient
C_p:	coefficient of plastic moment
C_{SS_U}	upper bound sliding shear yield coefficient
C_y:	yield resistance coefficient
d':	masonry cover
DA:	dowel action force
DA_y:	dowel action yield resistance
d_b:	rebar diameter
E_m:	modulus of elasticity for masonry
E_s:	modulus of elasticity for steel
E_{sh}:	modulus for strain-hardening in steel
f'_g:	masonry grout compression strength
f'_m:	masonry compression strength
Fr:	frictional resistance
Fr_A:	frictional resistance due to axial compression
Fr_{Fl}:	frictional resistance due to flexural-compression
Fr_{Fl_U}:	Upper bound frictional resistance due to flexural-compression
f_s:	steel stress
F_{si}:	axial force in reinforcing bar
f_{su}:	steel ultimate strength
f_y:	steel yield strength
G:	shear modulus

H:	wall height
h:	plastic hinge height
H/L:	wall height to length aspect ratio
I_g:	wall gross moment of inertia
I_s:	rebar moment of inertia
k_b:	wall bending stiffness in elastic beam-column element
k_{DA}:	dowel action shear stiffness
k_e:	wall elastic shear stiffness
k_g:	grout bearing stiffness
k_s:	wall shear stiffness in elastic beam-column element
k_{sec}:	dowel action secant stiffness
k_{shear}:	wall post-cracking shear stiffness
L:	wall length
M:	overturning moment
M_o:	overturning moment to close flexural crack
M_p:	plastic moment at design ductility
n_{db}:	number of vertical reinforcing bars
n_{db_y}:	number of vertical reinforcing bars that yield in tension
Nmf:	number of masonry fibers
P:	axial compression force
s:	spacing of reinforcing bars
t:	wall thickness
u_{DA}:	dowel action deformation
u_y:	dowel action yield displacement
V:	lateral force
V_{Fl}:	flexural resistance
V_m:	diagonal tension shear resistance
V_o:	lateral force to close flexural crack
V_{SF}:	shear friction resistance,
V_{SS}:	sliding shear resistance

V_{SS_U}	upper bound sliding shear resistance
V_y:	yield resistance
α:	modification coefficient for masonry strength
α_1:	parameter in equation 5.6
β:	modification coefficient for the steel yield strength
β_1:	parameter in equation 5.6
γ:	parameter in equation 5.6
Δ_{Base}:	base sliding displacement
$\Delta_{Base}/\Delta_{Top}$	base sliding displacement
Δ_{Top}:	total displacement at top of wall
Δ_p:	plastic displacement of wall
Δ_y:	yield displacement of wall
δ_y	friction yield displacement
ε_m:	masonry strain
ε_s:	steel strain
ε_{sy}:	steel strain
ϕ_m:	resistance factor for masonry
ϕ_s:	resistance factor for steel reinforcement
$\frac{M}{Vd}$:	shear span ratio
μ:	displacement ductility ratio
μ_{Fr}:	coefficient of friction
ρ_v:	vertical steel reinforcement ratio
σ_{mx}:	vertical stress in masonry at distance x from the extreme compression fiber
υ:	Poisson ratio

Acknowledgements

I would like to thank my supervisor, Professor Carlos E. Ventura, for giving me the opportunity to participate in several of his research projects conducted at the Earthquake Engineering Research Facility at UBC. These experiences have shaped my understanding of structural dynamics and the seismic response of structures. I'm grateful to him for the guidance, support and attentions that I received from him throughout our years learning together.

I'm thankful to Dr. Svetlana Brzev for sharing her knowledge of masonry structures. She guided me to present my research findings in a practical way that could be applied directly in engineering practice. She also provided many editorial comments which have helped me improve my technical writing. Her belief in this research topic was instrumental in its development.

I am also indebted to Dr. Donald Anderson for his committed collaboration in this research study. He was influential in the methodology presented in this thesis. His constant pursuit of knowledge inspired me to strive for a thorough understanding of my research data and its implications. It has been a privilege to work with such an insightful scholar.

The experimental results that I present in this thesis were kindly shared with me by Professor Richard Klingner and Dr. Farhad Ahmadi from the University of Texas at Austin. This data proved essential in my research study.

Also, I thank my sister, Maria Gracia Centeno, for taking the time to edit the first draft of this thesis. With her editorial suggestions, I succeeded in presenting a more refined first draft to my research committee.

I wish to extend my gratitude to Dr. Otton Lara who first taught me many valuable lessons about research in earthquake engineering. The academic training I received from him had an important influence in this PhD thesis. I'm grateful to him for his financial assistance throughout my PhD. I'm also honoured to have enjoyed his friendship and constant encouragement.

Throughout my years at UBC I was very fortunate to have the company of friends Manuel Archila, Alejandro Bohl, Alfredo Bohl, Seku Catacoli, Jason Dowling, Miguel Fraino, Yavuz Kaya, Sheri Molnar, Devin Sauer and Martin Turek. I will remember fondly our time together.

Special thanks go to my friends who commenced their PhDs before me and led by example: Juan Carlos Carvajal, Bishnu Pandey, Freddy Piña and Hugon Juarez Garcia. I am grateful for our conversations wherein we discussed everything from engineering, higher education and other great mysteries of the universe.

To my parents, Cuty and Pepe, for their unconditional love and financial support shown to me and to my sisters, Cristina and Maria Gracia. My parents taught us, the Centeno-Grunauer children, the value of education, integrity and perseverance; and they allowed us the freedom to discover our own paths in the world.

This thesis is dedicated to

my mother and father.

Chapter 1: Introduction

1.1 Sliding Shear Mechanism In Seismic Masonry Design

Reinforced Masonry (RM) squat shear walls are common in low-rise masonry buildings such as school buildings and fire halls. The latter ones must be designed as post-disaster facilities following the NBCC 2010 design provisions. This requirement forces the design of RM squat shear walls to follow provisions for moderately ductile squat shear walls.

RM squat shear walls subjected to in-plane seismic loads develop different levels of ductility capacity depending on the yield mechanism. In seismic design of RM shear walls, an acceptable yield mechanism has the property of having sufficient ductility capacity to prevent a loss of lateral strength at the design displacement.

RM squat shear walls can be designed to develop a ductile yield mechanism by applying the capacity design approach (Park and Paulay, 1975). The objective of the capacity design approach is to force the structure to yield in a ductile manner, by avoiding brittle yield mechanisms.

For RM shear walls, the design yield mechanism is a ductile flexural mechanism. However, RM shear wall with a Height to Length (H/L) ratio below 1.0 and with low axial loads cannot develop a flexural yield mechanism. This occurs since the wall's sliding shear resistance is less than the flexural resistance, resulting instead in a sliding shear yield mechanism. Moreover, if a

new design iteration is made and more dowels are added to increase sliding shear resistance, the governing mechanism continues to be sliding shear (Anderson & Brzev, 2009). Current code provisions do not address this problem and there is no guidance on the estimation of seismic performance of a sliding shear mechanism. As a result, the wall is designed either by assuming the ductility capacity in the sliding shear mechanism; or by ignoring the possibility of wall sliding.

Current seismic design of RM squat shear walls require a better understanding and better tools to estimate what conditions influence wall sliding displacements. In addition, there exists the need to evaluate if wall sliding is an acceptable seismic performance.

1.2 Research Motivation, Goals and Objectives

Current engineering practice requires design tools to estimate the onset of the sliding shear response in RM squat shear walls. There is a need to understand when wall sliding shear can be used as a ductile mechanism for seismic design of RM shear walls.

The goal of this research is to provide a methodology to accurately estimate the magnitude of sliding displacements that can develop RM squat walls subjected to seismic loading and provide a better understanding of their seismic performance. Following, are the main objectives to achieve this goal:

- Study the mechanics of the sliding shear mechanism based on previous experimental studies on reinforced masonry wall specimens.

- Propose and calibrate an analytical model that can accurately simulate the interaction between flexural and sliding shear behaviours.
- Use the calibrated model to conduct numerical simulations over a large range of design parameters to the determine the effects of design conditions on wall response, and
- Develop a design methodology for estimating sliding shear displacements.

1.3 Scope

The scope of this thesis is limited to RM shear walls, fully grouted, with uniformly distributed vertical reinforcement and designed with sufficient diagonal shear resistance to prevent a brittle diagonal shear failure in the wall.

1.4 Thesis Organization

Chapter 2 presents a review of relevant studies on the development of the sliding shear mechanism in RM shear walls. The chapter begins an overview of the sliding shear design provisions of the Canadian masonry design code (CSA S304.4, 2004). Next, a theoretical model proposed by Priestley (1977) is presented to explain how sliding displacement develops in RM walls during pseudo-static cyclic loading. In addition, this chapter provides a review of reported cases of sliding shear mechanism formed in walls.

Chapter 3 looks at the mechanics of the sliding shear mechanism based on observations from previous research studies. The sliding shear behaviour may be associated with one of the following yield mechanisms: i) sliding shear mechanism, ii) dowel-constrained failure

mechanism and iii) combined flexural sliding shear mechanism. Furthermore, this chapter presents a methodology for modeling friction and dowel action to account for the development of any of the three aforementioned mechanisms.

Chapter 4 presents the development and calibration of a 2D analytical macro model for simulating sliding shear displacements in RM cantilever walls. Modeling parameters are calibrated using 10 different wall configurations from previous experimental studies with a variety of design conditions, such as: shear span ratio, level of axial compression and vertical reinforcement ratio.

Chapters 5 and 6 present the results of an extensive parametric study on the behaviour of RM squat shear walls using the calibrated model. The parameters used in the analyses are wall dimensions, properties of vertical reinforcement, material strengths and level of axial compression. The first part of the parametric study (presented in Chapter 5) is focused on studying sliding displacements in RM shear walls when subjected to monotonic loading. This chapter also proposes equations for sliding shear resistance, V_{SS}, and flexural resistance, and V_{Fl} in RM cantilever walls. The second part of the parametric study (presented in Chapter 6) is focused on the sliding behaviour of RM walls subjected to cyclic loading.

Chapter 7 outlines a new procedure proposed for assessing the sliding shear displacements for seismic design of RM squat walls, based on the results presented in Chapters 5 and 6. A design example is presented to illustrate its application in design.

Finally, Chapter 8 presents conclusions and major contributions of this research study and outlines recommendations for future research studies.

Chapter 2: Literature Review

This chapter presents a review of relevant studies on the sliding shear mechanism, as observed in RM shear walls. First, background information on the current sliding shear resistance model is presented, based on the provisions in the Canadian Masonry Code (CSA S304.1, 2004), also known as the shear friction design model in the reinforced concrete design code ACI-318 (2011). The second section in this chapter shows a review of studies that have reported cases of sliding shear mechanisms formed in RM shear walls. This chapter ends with a summary and discussion of key findings.

2.1 The Shear Friction Model

The shear friction model is used for estimating shear transfer across cracked interfaces in reinforced concrete structures. In design, this model is implemented to determine the amount of reinforcement required to enable this shear transfer and thereby, limit the degree of slip across the interface.

The shear friction mechanism in reinforced concrete structures is used to estimate the shear transfer capacity between adjacent surfaces. A hypothesis first proposed by Birkeland and Birkeland (1966) and Mast (1968), is based on the assumption that the shear plane is located along a cracked concrete interface having a certain extent of roughness. When a shear force is applied along the shear crack, it initiates a slip along this roughened interface, as illustrated in Figure 2.1. The aggregates exposed along the crack develop a wedging action resisting the slip - this resistance is referred to as aggregate interlock. In order to slide along the cracked surface,

the movement must occur in the direction parallel to the plane and there must also be dilation, i.e., movement in a direction perpendicular to the plane (Walraven et al., 1987). Because of dilation, tensile strains develop in the reinforcement crossing the shear plane; this results in a tension force and a balancing compression force on the masonry. This compression force produces a frictional resistance along the cracked interface. Sliding across the cracked interface applies a shearing action to each individual reinforcing bar. The resistance of the bars to this shearing action is often referred to as dowel action (Mattock & Hawkins, 1972).

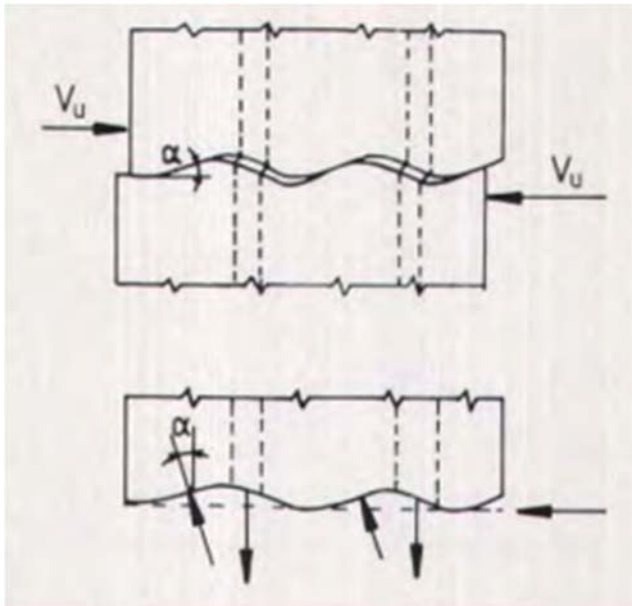

Figure 2.1 Illustration of shear friction mechanism showing aggregate interlock and crack dilation (Walraven et al., 1987)

Based on the shear friction model, the shear capacity of a structure across the shear plane subjected to a relative slip can be estimated as the sum of friction due to compression forces, dowel action, aggregate interlock, and friction forces due to rebar yielding caused by dilation. Research studies using shear tests on precracked push-off specimens (Mattock & Hawkins, 1972; Dulácska, 1972; Walraven, et al, 1987) have quantified what is the contribution for each of these

parameters towards the total shear transfer capacity. Further information on various shear transfer capacity equations based on the shear friction model is available in a state-of-the-art review by Santos and Julio (2012).

The shear friction model cannot be applied directly for cases where the sliding plane is a cold joint between two adjoining elements. Unlike for a cracked interface, a cold joint will not have aggregates along the surface and therefore, will not have the contribution by aggregate interlock or friction from rebar yielding due to dilation. This is why a cold joint, also referred to as a smooth surface, has a shear transfer capacity considerably lower than that of a cracked joint.

For bonded surfaces, also referred to as uncracked surfaces, the shear transfer capacity has been found to be greater than that of a cracked shear plane (Mattock & Hawkins, 1972). An uncracked shear plane consists of two surfaces that are bonded together through a cohesion force. In estimating the shear transfer capacity of an uncracked surface, this cohesion force must be considered in addition to the shear friction model.

2.2 The Design Shear Friction Equation

The sliding shear resistance equation used in current design standards is presented in equation 2.1. It is included in the Canadian masonry design standard (CSA S304.1, 2004) and the American Reinforced Concrete Code ACI 318 (2011). The design approach is based on the shear friction model. In the case of RM shear walls, the critical sliding plane is commonly identified as the construction joint between the base of the wall and the foundation interface. Its

sliding resistance is determined using the sliding shear resistance equation (equation 2.1) with a value of coefficient of friction, μ_{Fr}, following design conditions in Table 2.1.

$$V_{SF} = \mu_{Fr}(A_s f_y + P) \tag{2.1}$$

Where:

V_{SF} is the shear friction resistance,

μ_{Fr} is the coefficient of friction,

P is the compression force acting perpendicular to the shear plane, and

$A_s f_y$ is the clamping force due to tension in the reinforcement crossing the shear plane.

Table 2.1 Coefficients of friction for sliding shear resistance (CSA S304-14)

Masonry to masonry	1.0
Masonry to roughened concrete sliding plane	1.0
Masonry to smooth concrete sliding plane	0.7
Masonry to bare steel sliding plane	0.7

Table 2.1 shows the values of coefficient of friction, μ_{Fr}, to be used in design, which varies depending on the surface conditions of the shear plane. Elwood and Moehle (2005) point out that these values, used in design, are not equal to coefficients of friction but include the effects of aggregate interlock, dilation and dowel action. Therefore, the values in Table 2.1 allow using a single sliding shear resistance equation to model the sliding shear problem.

2.3 Experimental Studies

Several experimental studies have shown that sliding displacements occurred during the testing of RM specimens subjected to in-plane lateral loading. An overview of the studies that have made significant contributions to the current understanding of how the sliding shear mechanism develops in reinforced masonry structures is presented below.

2.3.1 Priestley (1977)

Priestley performed tests on six RM squat shear wall specimens with a Height to Length aspect ratio, H/L, of 0.75. The walls were heavily reinforced with horizontal reinforcement to prevent diagonal tension failure. The experimental program was set out to prove that RM shear walls could be designed for higher shear stress demands than allowed at the time. These tests showed that all wall specimens tested yielded in flexure and did not develop diagonal tension failure during cyclic loading. However, all tested walls developed sliding displacements along the base-foundation interface, which contributed to the total displacements and a reduction in stiffness. Priestley concluded that, although flexural failure modes could be achieved, the sliding mechanism limited the energy dissipation by the structure.

Based on the results of these tests and previous experimental studies on reinforced clay brick masonry walls (Priestley & Bridgeman, 1974), Priestley explained that the sliding shear mechanism occurs due to significant plastic tensile strains developed in the wall's vertical reinforcement during reverse cyclic loading.

"After the wall has suffered significant inelastic displacement in one direction, inelastic steel strains result in a wide open crack at the base course on removal of the load. As the load direction is reversed, the crack becomes open over the full length of the wall. Since the base mortar course is very smooth, aggregate interlock is totally ineffective, and all shear has to be resisted by dowel action of the vertical steel." (Priestley, 1977).

In order to continue with the shear transfer adequately, dowel action must develop significant sliding displacements in the RM wall. "As the load is increased, the compression steel yields, the base crack closes at the compression end, and shear can once more be transmitted across the compression zone of the blockwork. Consequently, sliding ceases, and the load level rises rapidly" (Priestley, 1977).

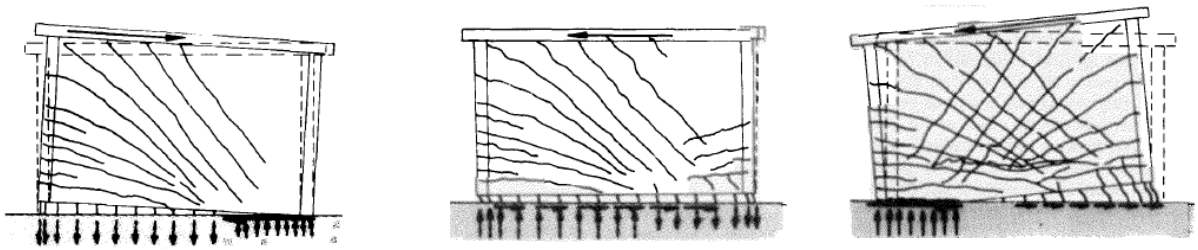

a) Flexural yielding occurs with tensile strains developing in reinforcement on one wall end.

b) Loading direction is changed, open crack has formed along the base, the shear is resisted through dowel action and the sliding is initiated

c) Flexural crack has closed and the sliding has ceased.

Figure 2.2 Sliding shear mechanism combined with flexural yielding (Paulay, Priestley, Synge, 1982).

Priestley demonstrated that sliding displacements at the wall base were more significant as the specimen was subjected to top displacement on the order of 4 times the yield displacement. These researchers pointed out that sliding displacements did not occur when applied loads reached the maximum wall strength but rather during the lowest levels of lateral loading. These

observations led Priestley to conclude that using a force-based criterion for sliding shear design did not appear to be valid.

Force-displacement hysteresis curves characterizing sliding behaviour in RM shear walls are shown in Figure 2.3. These plots show shear force versus the measured sliding displacement at the base of the specimen. These curves illustrate the pinched hysteresis behaviour and the strength degradation that develop due to an increase in sliding displacements. It was observed that sliding displacements increased during the second and third cycle of every displacement level, as shown in Figure 2.3a.

Priestley also highlighted the beneficial influence of vertical loads in limiting sliding by comparing sliding shear hysteresis plots for wall specimens A3 and A6, shown in Figure 2.3. It is believed that this effect occurs due to an early closing of the base crack due to the additional vertical load.

2.3.2 Abrams (1988)

Abrams observed significant sliding displacements in RM walls while performing shake table testing on a scaled model (¼ scale) of a two-storey RM building model with openings. Sliding shear displacements developed after the flexural cracks were formed at the top of the piers, as shown in Figure 2.4. During sliding, the storey shear was redistributed to one pier forcing it to fail in shear; which resulted in near collapse of the model.

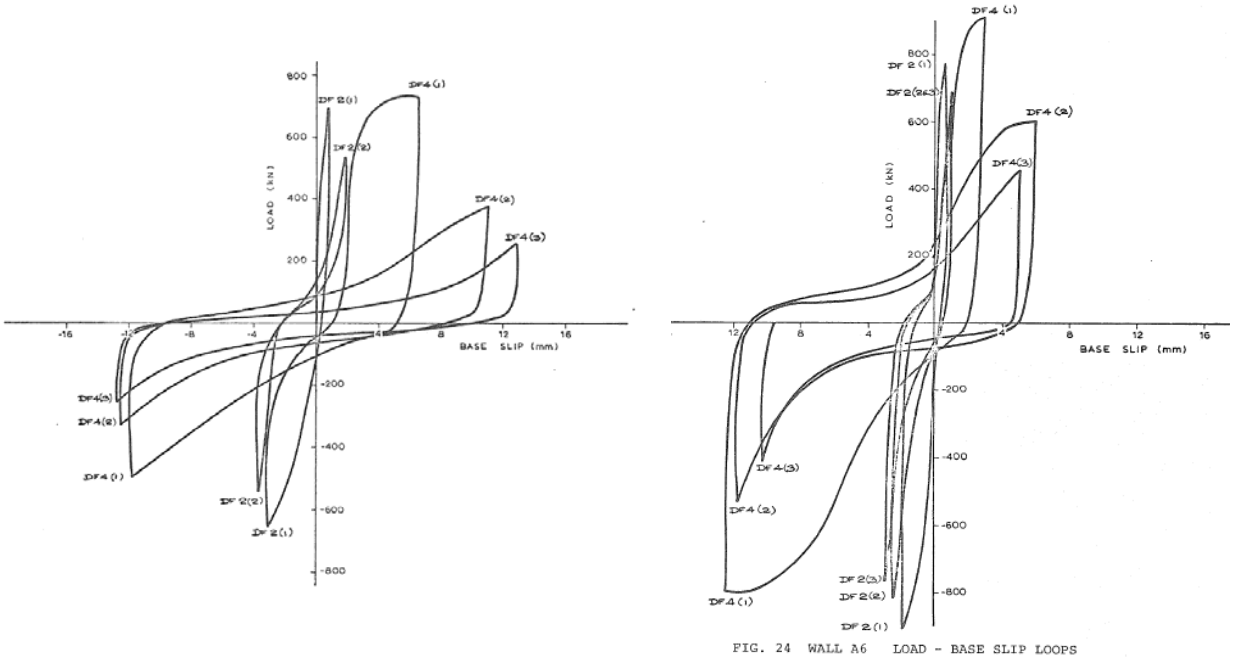

a) b)

Figure 2.3 Lateral force vs sliding displacement plots: a) Wall specimen A3 no additional axial loads; b) Wall specimen A6 – 240 kN axial load; (Priestley, 1977).

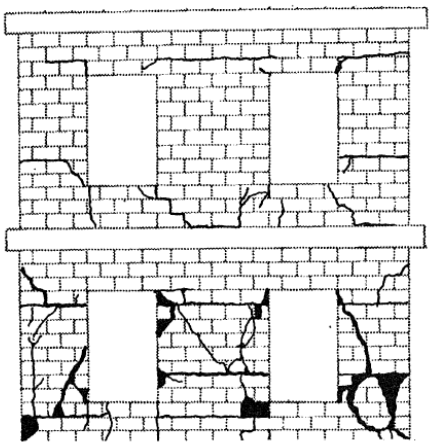

Figure 2.4 Final crack pattern for the test building model (Abrams, 1988)

2.3.3 Shing et al., (1989)

The researchers studied the effect of the applied axial stress and vertical and horizontal reinforcement on the lateral resistance, failure mechanism, ductility and energy dissipation capability of RM walls. Out of sixteen specimens, three specimens with an H/L ratio of 1.0 experienced sliding at the base in combination with either a flexural or a shear mechanism. All three wall specimens (#6, #8, and #11) were tested under zero axial stress conditions. When the walls were loaded to the ultimate lateral load capacity, the contribution of base wall sliding to the total deformation was approximately 10%. As the walls were loaded at higher ductility levels, base sliding contributed to 25% of the total deformation for specimens 6 and 11, and more than 50% for specimen 8. In addition, it was reported that base sliding influenced the degradation in lateral load capacity and, to a lesser extent, the ultimate lateral strength.

2.3.4 Anderson and Priestley (1992)

Anderson and Priestley proposed a modification to the parameters in equation (2.1) for estimating sliding shear resistance. The authors proposed that, for a cantilever wall approaching yielding in flexure, the sliding shear resistance equation should not include the area of vertical reinforcing steel at its ends. It was assumed that the tension steel force at one end of the wall would be balanced out by the compression steel force at the opposite end, thus reducing the flexural-compression force in the masonry. Based on limited available test data (Matsumura, 1987), the authors found that equation (2.1) with the modified area of steel, provided good results when the coefficient of friction, μ_{Fr}, was equal to 1.3.

2.3.5 Kikuchi et al. (2004)

The researchers performed pseudo-static testing on fourteen RM wall specimens, varying the H/L ratio, axial compressive stress, quantity of wall reinforcement, and strengthening techniques for preventing wall sliding failure. All wall specimens that had been designed to yield in flexure developed sliding shear displacements at the wall-to-foundation interface. Initially, these walls yielded in flexure and gradually developed sliding shear displacements as testing continued. The authors noted that no remarkable degradation in lateral strength was observed until flexural rebars buckled and pushed out the concrete cover. At the final loading cycle, sliding shear displacements were in the order of 70 to 90% of the total wall displacement.

The authors developed an equation (2.2) for predicting the ultimate sliding capacity for the wall specimens. The coefficient of friction μ_{Fr} had to be increased as the wall aspect ratio decreased. The value μ_{Fr}=0.93 was used for specimens with H/L ratio of 0.90 and μ_{Fr}=1.18 for specimens with H/L ratio of 0.75. These authors recognized that in some cases, the estimated sliding capacity values obtained were conservative after using the proposed equation.

$$V_{SF} = \mu_{Fr} P_n + 0.7 A_s f_y \tag{2.2}$$

The strengthening techniques for preventing wall sliding consisted of adding dowels in the middle third of the wall length. This study found that, with one exception, specimens strengthened by dowels did not develop a sliding shear mechanism. However, these authors found that specimens with dowels had less ductility than those without dowels. It was also found that in the occasion where dowels were added, sliding failure was formed at the top of lowest masonry course coinciding with the location of the end of the dowel bars. Overall, the authors

concluded that adding dowels was an effective way of strengthening the sliding shear resistance at the foundation-to-wall interface.

2.3.6 Voon and Ingham (2006)

Voon and Ingham performed a research study on the shear strength of reinforced concrete masonry walls and tested ten full scale RM walls with different H/L ratios. In the case of Wall 3, which was designed to yield in flexure, sliding contributed to about 20% of the wall lateral displacement at the end of testing. Figure 2.5 shows the cracking pattern and lateral force versus top displacement hysteresis loops for this specimen. The specimen reached only 93% of the expected flexural yielding force, F_n, as shown in Figure 2.5b. The authors attributed this effect in flexural yielding force to the sliding behaviour and the shear force transfer through dowel action.

2.3.7 Shedid, Drysdale, and El-Dakhakhni (2008)

Shedid, Drysdale and El-Dakhakhni performed cyclic lateral loading tests on six fully grouted RM shear walls with H/L ratio of 2.0, different amounts and distribution of vertical reinforcement, and varying level of axial compressive stress. One of the four wall units tested under zero axial load conditions, Wall #3, experienced significant sliding displacements. The recorded sliding displacements were associated with a continuous wide crack between the wall and the wall foundation. The authors observed that the sliding may have led to the rapid strength degradation by about 20% developed at lower drifts and reduced overall ductility capacity compared to other tested walls.

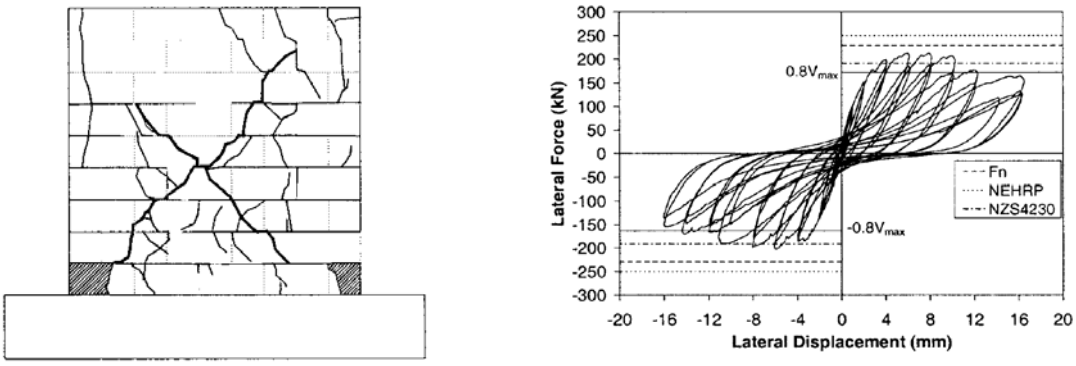

a) b)

Figure 2.5 Results of lateral loading of Wall 3 designed to fail in flexure: a) Final cracking pattern; b) Load-deflection hysteresis loops (Voon and Ingham, 2006).

2.3.8 San Bartolomé et al. (2007 & 2009)

The authors performed an experimental testing program on cyclic loading of five RM wall specimens with H/L ratio of 1.0 to establish design solutions for preventing the formation of the sliding shear mechanism. Various design solutions were tested, such as roughening the foundation surface and including additional vertical reinforcement dowels to splice the vertical reinforcement. The study found that the roughening of the foundation surface improved the mortar's bond to the foundation; however it did not prevent the formation of the sliding shear mechanism. The study also found that the wall specimen with all lap splices provided at the same height, formed two sliding shear planes during testing: one at the foundation-to-wall interface and the other at the end of lap splices. All other wall specimens with lap splices developed sliding shear planes at the base of the wall only. This can be explained because the design specified staggered location of individual lap splices.

The authors concluded that sliding displacements could be significantly reduced by adding extra dowels close to the centre of the wall base and by concentrating the vertical reinforcement at the ends to meet the required design vertical reinforcement ratio.

2.3.9 Hernandez (2012)

Hernandez performed pseudo-static loading tests on six RM shear wall specimens with H/L ratio of 1.0 which were designed to develop a flexural yield mechanism. The study aimed to establish the effect of vertical reinforcement and the level of applied axial compressive stress upon the flexural behaviour of an RM wall. One of the key findings was that the flexural ductility capacity and the contribution of base wall sliding to the total wall displacement decreased with an increase in the applied axial load level. Wall specimens without applied axial loads developed sliding displacements that contributed to more than 23% of the total wall displacement.

2.3.10 Ahmadi (2012)

Ahmadi proposed a displacement-based approach for seismic design of reinforced masonry structures. In developing the design procedure, Ahmadi performed pseudo-static and dynamic tests on RM walls with low H/L aspect ratios and found that several specimens developed significant sliding shear displacements. As a part of his research, he attempted to develop an equation to account for sliding shear behaviour in the analysis and design of RM wall structures.

2.3.10.1 Pseudo-Static Experimental Program

Ahmadi tested six RM wall specimens with an H/L ratio of 1.0 and fixed-fixed support conditions. The specimens were built using different reinforcement ratios and different levels of

applied axial compressive stress. Results of testing showed that four out of six wall specimens experienced significant sliding shear displacements which contributed to more than 45% of the top lateral displacement.

The total sliding displacement is due to the combination of sliding along the base and the top of the wall. Similar to the study by Priestley (1977), Ahmadi developed force versus displacement hysteresis plots for each sliding interface and a combined plot showing the total sliding displacement. Figure 2.6 shows the force versus sliding displacement plots obtained for a wall specimen subjected to lateral loads only (no axial loads).

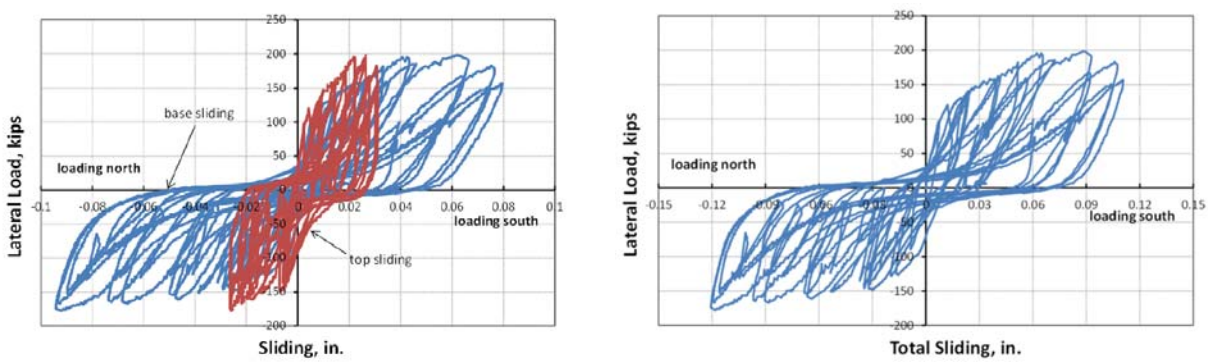

a) b)

Figure 2.6 Force-deformation hysteresis loops along sliding interfaces specimen PBS-01: a) At individual supports, b) Total sliding behaviour (Ahmadi, 2012).

Ahmadi studied various equations for sliding shear capacity equations that are available in the literature, and evaluated their accuracy using results from pseudo-static reverse cyclic tests on masonry shear walls which had developed significant sliding shear displacements. The author put together a data set that included the results from his pseudo-static testing and previous research studies by others (Shing et al.1989; Tanner et al., 2005; Voon and Ingham, 2006; and Hernandez, 2012). He found that equation 2.1, with an average value of coefficient of friction of

μ_{Fr} = 0.68, had the best line fit for all the experimental sliding shear capacities. Ahmadi also concluded that the coefficient of friction μ_{Fr} was independent of the degree of roughening of the specimen's foundation.

2.3.10.2 Shake Table Experimental Program

The study also included in-plane shake table testing of two full scale RM wall structures. The testing was performed on a three-storey RM wall structure, and a two-storey RM wall structure with openings. The test results showed that lintel beams above openings acted as coupling beams. The coupling effect effectively reduced the H/L ratio of the walls, and exposed them to higher shear demands than anticipated in the design. Due to the coupling effect, RM wall W-2 showed significant sliding shear displacements in both test structures during shake table testing (Note that these walls were located in the middle of the respective floor plans and were subjected to low axial compressive stresses). The final failure mechanisms for both walls were significantly different, as shown in Figure 2.7. In the case of the three-storey structure (Figure 2.7a), wall W-2 showed lateral stiffness degradation but developed only minor cracks along the wall height. In the case of the two-storey structure (Figure 2.7b), wall W-2 experienced extensive diagonal cracking, crushing of diagonal struts, face shell spalling and shear failure.

The results of this study indicated that for both cantilever and fixed-fixed support conditions, W-2 type RM walls developed sliding shear displacements, which affected their expected energy dissipation properties. Ahmadi observed that no provisions were available in the 2008 MSJC Code to limit the observed base sliding. This study suggested that the Masonry Standards Joint

Committee (MSJC) should develop criteria to limit interstorey drifts caused by base wall sliding that may lead to the collapse of other elements in the structure.

a) b)

Figure 2.7 Damage observed in shake table tests: a) Three-storey structure, Wall W-2; b) Two-storey structure, Wall W-2; (Ahmadi, 2012).

2.3.11 Robazza (2013)

Robazza performed pseudo-static loading tests on two RM shear wall specimens to study the out-of-plane stability of RM shear walls for different levels of axial compression. Specimen dimensions were 3.8 m height by 2.6 m length, with 140 mm thickness. Specimen reinforcement consisted of one 15M rebar concentrated at each wall end, plus 10M rebar spaced at 400 mm on centre along the length of the wall. Specimen W1 was loaded with a compression force of P = 660 kN and specimen W2 was tested with no axial compression force.

Robazza reported that during the initial loading cycles, test specimen W2 developed a flexural crack at the base of the bottom course, along the wall length. This flexural crack resulted in the RM wall sliding at the base with sliding displacements of 25 mm, which corresponded to 30% of the total wall displacement. On the other hand, specimen W1 with an axial compression load, P, of 660 kN, did not develop any significant base wall sliding.

2.4 Analytical Studies

There have been few attempts to model sliding shear in RM shear walls. The following presents the results and observations presented by researchers on their approaches to modeling this mechanism.

2.4.1 Ahmadi (2012)

Ahmadi developed an analytical model to predict the behaviour of a full-scale two-storey RM wall structure subjected to a shake table testing described in Section 2.2.10. He developed a 3D model using the software package PERFORM 3D (CSI, 2007), which was able to accurately simulate the overall results of the 2-storey model up to a shaking level corresponding to an amplitude of 145% of the "El Centro" acceleration record.

For the shake table test using the "El Centro" record at 160% amplitude, significant sliding was observed at the top of wall W-2, which was not captured by the analytical model. Ahmadi modified the model in an attempt to improve the accuracy of analytical predictions, which consisted of replacing the shear strength in wall W-2 with its sliding shear capacity using equation 2.1. He reported that this modification did not improve the simulation of the total wall

displacements for wall W-2, or the accuracy of the overall results for the two-storey model, as shown in Figure 2.8b.

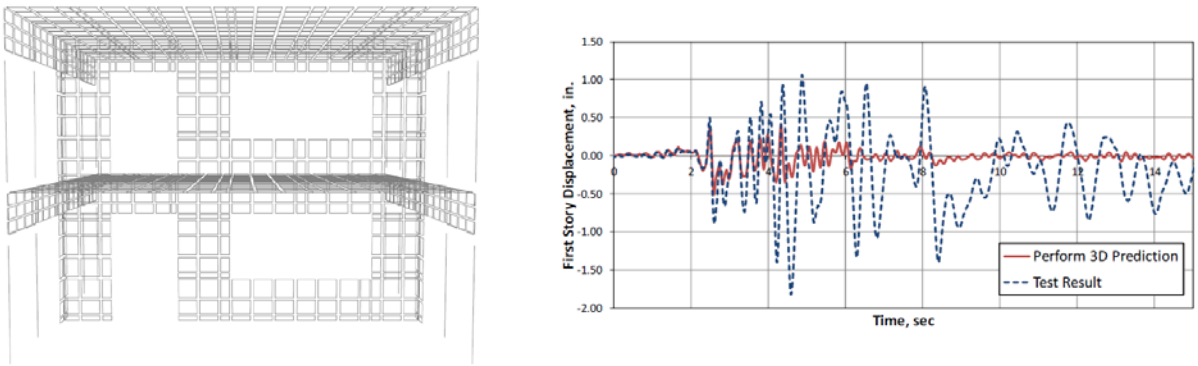

a) b)

Figure 2.8 Modeling sliding shear for a two-story structure subjected to shake table testing: a) Illustration of 3D model; b) Comparison of analytical and experimental time history results for 160% El Centro earthquake (Ahmadi, 2012).

2.4.2 Williams (2013)

Williams proposed a new approach to modeling RM shear walls by modifying an existing nonlinear truss model method shown in Figure 2.9a. This modification consisted of adding a sliding interface to the model in order to allow the development of a sliding shear mechanism.

This sliding interface, as shown in Figure 2.9b, consists of one shear spring, one axial spring, and one flat slider bearing element that connects the bottom of the truss model to a fixed foundation. The shear spring element represents the combination of dowel action and shear friction contributed by the vertical steel reinforcement crossing the sliding plane. The axial spring is a tension-only spring and is used to resist the overturning of the wall, while the flat bearing slider element is used to model friction due to compressive loads. These springs connect from the

centre node at the bottom of the wall to an additional node with the same coordinates with a fixed boundary condition.

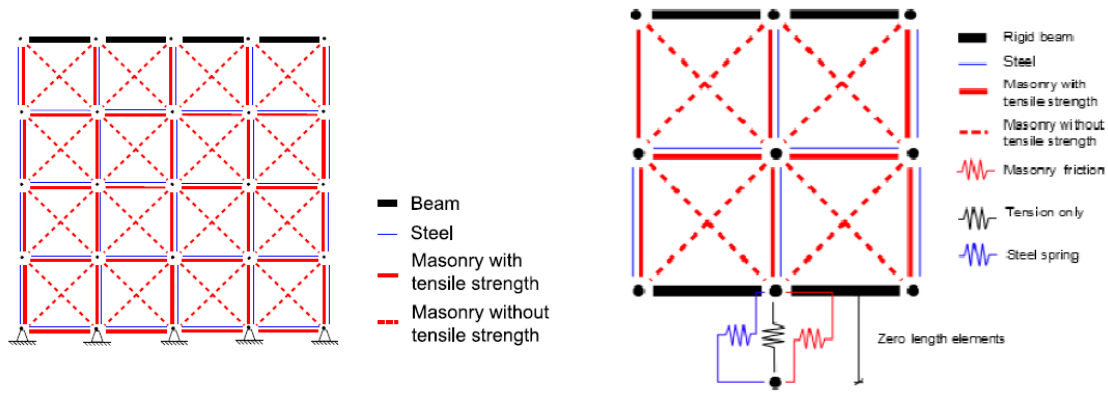

a) b)

Figure 2.9 Modified nonlinear truss model for RM shear walls: a) 16 cell truss model, b) Addition of a sliding interface at the base of a truss model (Williams, 2013).

Williams compared the model results with those obtained from an experimental study (Shing et al., 1989). The comparison showed that the proposed model required further examination in order to capture the sliding shear mechanism. Williams suggests that a way to improve the prediction of the sliding shear resistance would be to incorporate the effects of the interaction between flexure and shear into the sliding shear interface.

2.5 Discussion

The following observations can be made based on the studies discussed in this chapter:

1. The Canadian Masonry Code CSA S304.1 recommends estimating sliding shear resistance using equation 2.1 based on the shear friction model. However, the experimental studies shown in this literature review present evidence that, when a flexural crack is formed along the wall length, the sliding shear resistance in RM shear

walls is not developed through friction but through dowel action. Therefore, recommendations on the contribution of dowel action to sliding shear resistance and its variation during loading cycles are necessary.

2. The approach proposed by Priestley (1977) has been widely accepted and used in many studies on cyclic loading of RM walls. However, this theory has not yet been implemented into a method for determining whether or not an RM wall would develop a sliding shear mechanism.
3. Despite the current progress related to understanding the sliding shear mechanism, there is still no method to estimate the sliding displacement demands in RM shear walls.

2.6 Summary

Key findings of previous research studies relevant for this thesis are summarized below:

1. The current Canadian Masonry Code equation for sliding shear resistance is based on the shear friction concept. This concept establishes that the sliding shear resistance along a roughened surface is the result of a combined friction due to compression forces, dowel action, aggregate interlock and additional friction resistance caused by rebar yielding due to dilation. In the case of smooth surfaces, the sliding resistance is the sum of friction from compression forces and dowel action.
2. Evidence from experimental studies has shown that RM walls that yield in flexure can develop sliding displacements after flexural cracks formed along the wall length.
3. Priestley (1977) proposed the current conceptual model for the sliding shear mechanism in RM shear walls. This model indicates that sliding displacements occur after a flexural crack opens along the full length of an RM wall, due to residual strains in the steel

reinforcement. During this behaviour, shear is transferred along the crack through dowel action alone.

4. Provision of additional rebar dowels has shown to improve the response of RM squat walls subjected to low axial stresses (Kikuchi et. al, 2004, San Bartolomé et.al, 2009). Tests showed that adding dowel bars in the middle third of the wall's cross section resulted in significant increase of its sliding shear resistance.

Chapter 3: Mechanics of the Sliding Shear Behaviour

This chapter establishes the mechanics of the sliding shear mechanism based on the state-of-the-art analytical and experimental studies reviewed in Chapter 2. This chapter proposes ways to incorporate current knowledge related to sliding shear behaviour, as well as frictional and dowel action resistance to model the development of sliding displacements in RM walls.

3.1 Sliding Shear Resistance

The onset of sliding displacements can be modeled using a resistance model which is consistent with the observed behaviour reported in experimental studies. The resistance model used in this study is the shear friction resistance model for smooth surfaces described in Chapter 2. According to this model, the sliding shear resistance is provided by frictional, Fr, and dowel action, DA, resisting forces, as summarized in equation 3.1, as follows:

$$V_{SS} = Fr + DA_y \tag{3.1}$$

Where

V_{SS} = Sliding shear resistance

Fr = Friction resistance

DA_y = Dowel Action yield strength

Contributions of aggregate interlock and dilation are assumed to be negligible due to the small aggregate sizes (less than 12 mm) used in most masonry grouts (MIBC, 2009).

3.2 Frictional Resistance

The friction force that acts along the sliding plane and contributes to sliding shear resistance is developed through both axial and flexural compression. These compression forces vary throughout flexural response and should not be considered constant during in-plane loading.

Axial and flexural compression forces can be determined by modeling the normal stresses and strains in the masonry, following the assumption that plane sections remain plane, as shown in Figure 3.1. Coulomb's friction model can be used to determine the frictional forces that result from compression forces, using a constant coefficient of friction, μ_{Fr}. In this way, the frictional resistance function could be expressed using Equation 3.2. Frictional resistance is a function of normal stresses acting in the masonry; thus it is possible to model the variations in friction resistance during the loading history.

$$Fr = \mu_{Fr} \int_0^L f(\sigma_{mx})\, t\, dx \tag{3.2}$$

$$f(\sigma_{mx}) = \begin{cases} \sigma_{mx}, & \sigma_{mx} > 0 \\ 0, & \sigma_{mx} \leq 0 \end{cases}$$

Where:

Fr is the resulting friction force.

σ_{mx} is the stress in masonry at distance x from the extreme compression fiber

t is the wall thickness

L is the wall length

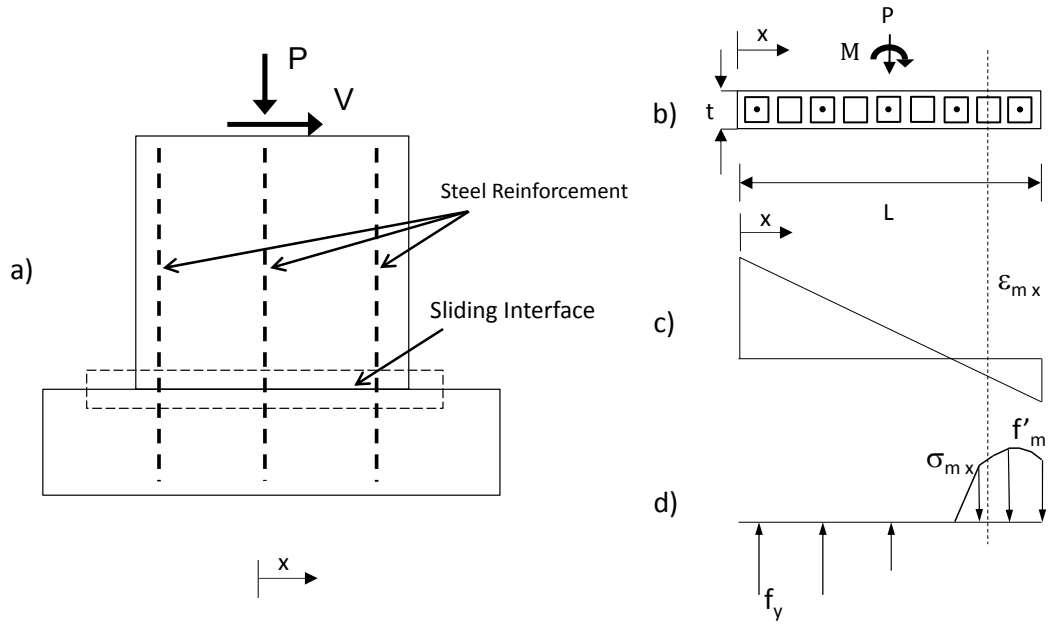

Figure 3.1 RM shear walls subjected to external loads: a) Elevation view of an RM cantilever wall; b)External forces acting on the sliding interface; c) Strain distribution, and d) Normal stress distribution.

3.3 Dowel Action of Reinforcing Bars

In the study of shear transfer mechanism in reinforced concrete and masonry structures, dowel action is recognized as an important component that must be considered. However, experimental evidence regarding the shear transfer by dowel action is limited, and some aspects of dowel action have not been investigated (He and Kwan, 2001). This is because the shear force transferred through dowel action is often embedded with other shear transfer components, such as friction and aggregate interlock, thereby making it difficult to measure the individual contribution of these components. Uncertainties related to the behaviour of dowel action have resulted in few attempts to model it. It is often not directly included in nonlinear models, but it is commonly accounted for by lumping it together with frictional resistance using the shear friction model described in Chapter 2.

This section reviews the properties of dowel action based on findings from previous research studies. These properties are used as modelling parameters for a dowel action model independent from frictional resistance.

3.3.1 The Mechanics of Dowel Action

Determining the lateral force deformation behaviour along a reinforcing bar due to dowel action requires an accounting for the compatibility between transverse deformations of the reinforcing bar and the surrounding masonry. Previous research studies (Priestley and Bridgeman, 1974; He and Kwan 2001; El-Ariss, 2007) have analysed this interaction by using "beam on elastic foundation" theory (Hetenyi, 1958), which treats the reinforcing bar as a beam supported by Winkler springs. By taking the reinforcing bar subjected to dowel action at the inflexion point, the bar is treated as a semi-infinite beam resting on a foundation subjected to a concentrated load at one end, as shown in Figure 3.2.

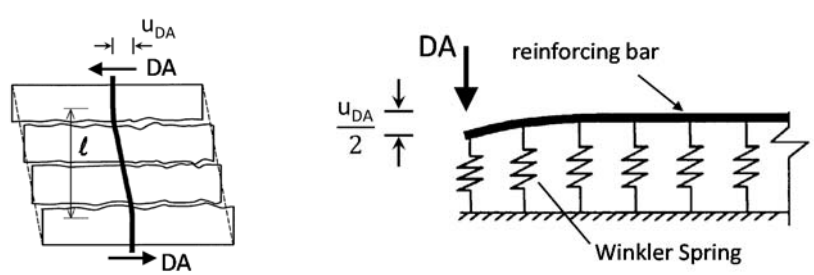

a) b)

Figure 3.2 Modeling of dowel action: a) Reinforcing bar loaded in transverse direction, b) Modeling of reinforcing bar as "beam on elastic foundation" (El-Ariss, 2007).

3.3.2 Dowel Action Shear Stiffness

Using the analytical solutions from the "beam on elastic foundation" problem, He and Kwan (2001) proposed a value of linear elastic shear stiffness k_{DA} for dowel action (see equation 3.3) to

establish the relationship between dowel action force, DA, and transverse deformation, u_{DA}. The dowel stiffness k_{DA} is expressed as a function of flexural properties of the rebar and the bearing stiffness provided by the surrounding grout. The bearing stiffness, k_g, of the surrounding grout is estimated using the data-fitting expression in equation 3.4 proposed by Soroushian et al, (1987). Equations 3.3 and 3.4 were originally developed for dowel action in reinforced concrete structures and have been implemented in this study for estimating dowel action shear stiffness in reinforced masonry structures.

$$k_{DA} = E_s I_s \left(\frac{k_g d_b}{4 E_s I_s}\right)^{3/4} \tag{3.3}$$

$$k_g = \frac{127\sqrt{f'_g}}{{d_b}^{2/3}} \quad \left(\frac{N}{mm^3}\right) \tag{3.4}$$

Where

E_s: modulus of elasticity of steel

I_s: moment of inertia of the bar

d_b: diameter of the bar

k_g: bearing stiffness of the surrounding grout

f'_g: masonry grout compressive strength

3.3.3 Dowel Action Yield Resistance

Several research studies have proposed dowel action yield resistance expressions for reinforced concrete assuming the reinforcing bars deform in flexure. Although most of these studies correspond to reinforced concrete structures, it is believed that observations are applicable to

reinforced masonry. Therefore, grout strength, f'_g, was used instead of concrete strength, f'_c. These resistance equations are presented in Table 3.1.

Table 3.1 Dowel action resistance equations developed in various research studies.

$DA_y = 1.66\ A_{db}\sqrt{f'_g f_y}$ A_{db}: rebar cross-section area f'_g: grout compression strength f_y: steel yield strength	(Rasmussen, 1962)
$DA_y = 1.47 A_{db}\sqrt{f'_g f_y}\sqrt{1-\left(\frac{N}{N_f}\right)^2}$ N: Tension force of rebar N_f: Tensile force inducing yield in pure tension	(Dulascka, 1972)
$DA_y = 0.79\ A_{db}\sqrt{f'_g f_y}$	(Priestley and Bridgeman, 1974)
$DA_y = 1.72\ A_{db}\sqrt{f'_g f_y}\left(\sqrt{1+9\zeta^2}-3\zeta\right)$ $\zeta = \frac{e}{d_b}\sqrt{f'_g / f_y}$ e: eccentricity of artificial compression force used to simulate bonding between reinforcing bar and grout.	(Pruijssers, 1988)

These studies consider localized yielding of the rebar and local crushing of the surrounding material. Figure 3.3 shows that, as the bar deforms in flexure, it generates high local stresses on the surrounding masonry grout with eventual crushing of the material near the dowel. This crushing forms a gap between the masonry and the reinforcing bar, which for subsequent loading cycles results in a decrease in the dowel action shear stiffness.

Shear transfer through dowel action could potentially develop shear or kinking failure in the reinforcing bars, as illustrated in Figure 3.4. However, in this study it is considered that a sufficient eccentricity is provided by the crack width, and that the length over which grout crushes near the crack is sufficient and allows for flexural behaviour. It is also assumed that shear behaviour is not significant. Kinking behaviour, characteristic for dowel action, could take place only if large inelastic deformations develop through the dowel's plastic hinge mechanism.

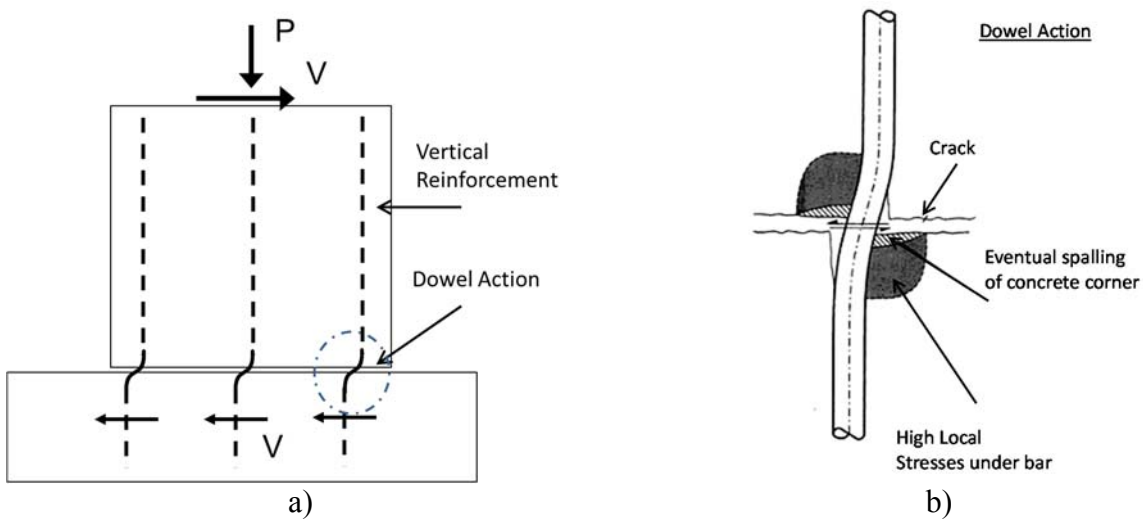

Figure 3.3 Dowel action behaviour in RM shear walls: a) Sliding resistance through dowel action; b) Common representation of dowel action (Walraven, 1999)

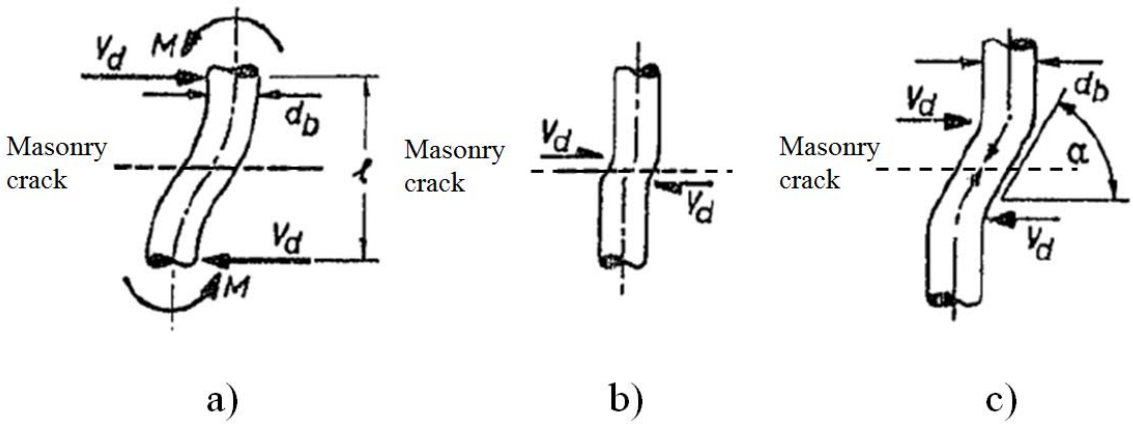

Figure 3.4 Behaviour modes in dowel action: a) Flexure, b) Shear, c) Kinking (Park and Paulay, 1975).

The key design parameters that appear in all dowel action yield resistance equations are: 1) grout compression strength, f'_g; 2) steel yield strength, f_y; and 3) rebar cross-section area, A_{db}. Therefore, the proposed expression for estimating dowel action yield resistance, DA_y, to be used in this study is shown in equation 3.5. The value of coefficient, C_{DA}, is considered at this stage as unknown and needs to be determined through calibration.

$$DA_y = C_{DA} n_{db} A_{db} \sqrt{f'_g f_{sy}} \tag{3.5}$$

Where

C_{DA}: coefficient of dowel action yield strength

n_{db}: number of vertical reinforcing bars

f'_g: grout compression strength

f_y: steel reinforcement yield strength

A_{db}: area of one vertical reinforcing bar

3.3.4 Dowel Action Hysteresis Rule

The hysteresis rule for dowel action proposed for this study is based on the base shear versus sliding shear displacement curves from cyclic testing of RM squat wall specimens under zero axial loads (Priestley, 1977; Ahmadi, 2012). These walls showed combined flexure and sliding shear mechanisms. While the flexural crack was open, sliding shear resistance was provided only by the dowel action. This behaviour is characterized by stiffness degradation and pinched hysteresis loops, but without cyclic strength degradation. Figure 3.5 highlights the force versus displacement hysteresis curves for a wall specimen that experienced dowel action and was tested by Priestley (1977).

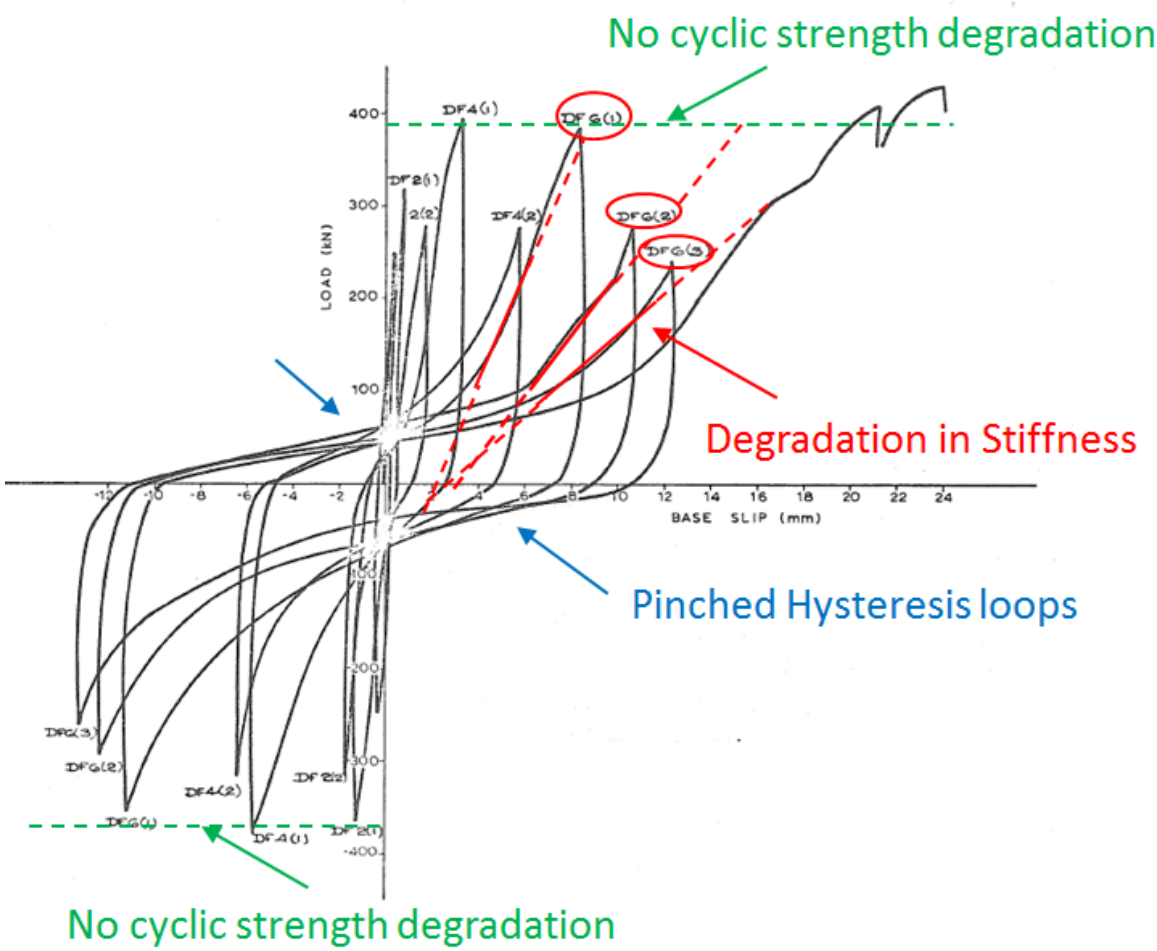

Figure 3.5 Dowel action hysteretic behaviour based on base shear versus sliding displacement curves per Priestley (1977)

This pinched hysteretic behaviour reflects a loss in dowel action shear stiffness during dowel action flexural response. This occurs when the reinforcing bar deforms onto crushed grout from an earlier loading cycle, as previously shown in Figure 3.3b. Dowel action shear stiffness is restored when the reinforcing bar bears onto undamaged grout.

In addition to the pinching effect, hysteresis curves show that cyclic strength degradation does not occur during the hysteretic response. The hysteresis curves show that the maximum sliding

shear resistance is maintained until the final displacement cycle, however there is an apparent loss of strength when a loading cycle is repeated at the same displacement amplitude. Nevertheless, during the following cycle, the strength is recovered with a larger displacement amplitude. This behaviour was observed in experimental studies using reinforced concrete specimens (Soroushian et al., 1988) and also RM cantilever shear walls (Kikuchi et al., 2004; Voon and Ingham, 2006).

Figure 3.5 also indicates hysteresis curves showing stiffness degradation during cyclic loading, as highlighted for loading cycles corresponding to a displacement factor, DF, equal to 6. However, the highest reduction in stiffness is observed as a result of the first loading cycle.

3.4 RM Shear Wall Yield Mechanisms

By studying the available literature on sliding shear behaviour in RM shear walls, this study proposes that a distinction is required between RM wall yield mechanisms that develop sliding displacements:

a) Sliding shear mechanism: The RM shear wall develops sliding displacements when the lateral force, V, is equal or greater than the sliding shear resistance of the RM wall.

b) Combined Flexural-Sliding Shear Mechanism: The RM wall yields in flexure and forms an open flexural crack along the wall length. Wall inelastic displacements are equal to the sum of flexural and sliding displacements.

c) Dowel-Constrained Failure Mechanism: The RM wall yields in flexure and has insufficient dowel action yield resistance to transfer shear across an open flexural crack

along the wall length. RM wall sliding displacements are developed due to dowel action yielding.

3.4.1 Sliding Shear Mechanism

The sliding shear mechanism will develop when the sliding shear resistance, V_{SS}, is less than the lateral force, V_{Fl}, required to induce flexural yielding in an RM shear wall (Figure 3.6a). As a result, the RM wall does not experience flexural yielding and its inelastic displacements are only due to inelastic sliding shear displacements.

3.4.2 Combined Flexural and Sliding Shear (CFSS) Mechanism

When the sliding shear resistance, V_{SS}, is equal to or greater than V_{Fl}, then the RM wall will yield in flexural yield mechanism during monotonic loading, as illustrated in Figure 3.6b. For cyclic loading, this flexural yield mechanism changes into a CFSS mechanism, developing sliding displacements when a flexural crack opens along the full wall length, as Priestley (1977) explained. The wall will switch back to a flexural mechanism when the flexural crack is closed. Sliding displacements will increase at higher ductility demands in the flexural hinge region (Priestley, 1977).

Hysteretic behaviour characteristics for the CFSS mechanism are illustrated in Figure 3.7. As explained by Priestley (1977), when the wall is subjected to lateral loading in one direction, yielding takes place in the tension reinforcement (point A). As the wall yields in flexure, a wide open crack develops at the tension end of the wall. Upon the load reversal (point B), the end of the wall, which used to be in compression, is now under tension. At this stage a new flexural

crack opens at the tension end of the wall, while the previously formed flexural crack at the opposite end has not closed yet. As a result, a large flexural crack forms along the wall length and causes a loss of masonry contact and frictional resistance along the wall's interface. When the crack closes due to flexural-compression, frictional resistance becomes re-established and sliding ceases. When the wall is subjected to increasing lateral displacements, vertical reinforcement yields again in tension, and the top lateral displacement is due to flexure-induced inelastic rotation and residual sliding displacement (point C). Similar behaviour is observed when the wall is loaded in the opposite direction (points D and E).

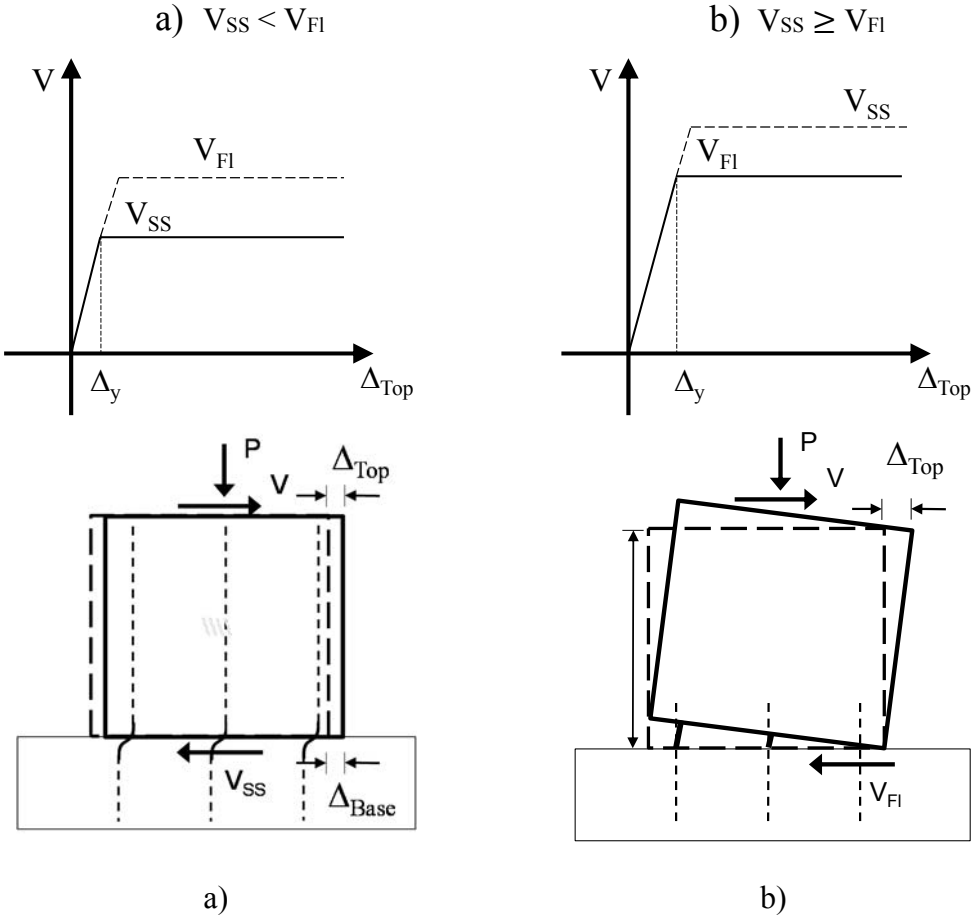

Figure 3.6 Development of yield mechanism in RM shear walls subjected to monotonic loading: a) Sliding shear mechanism, and b) Flexural yield mechanism

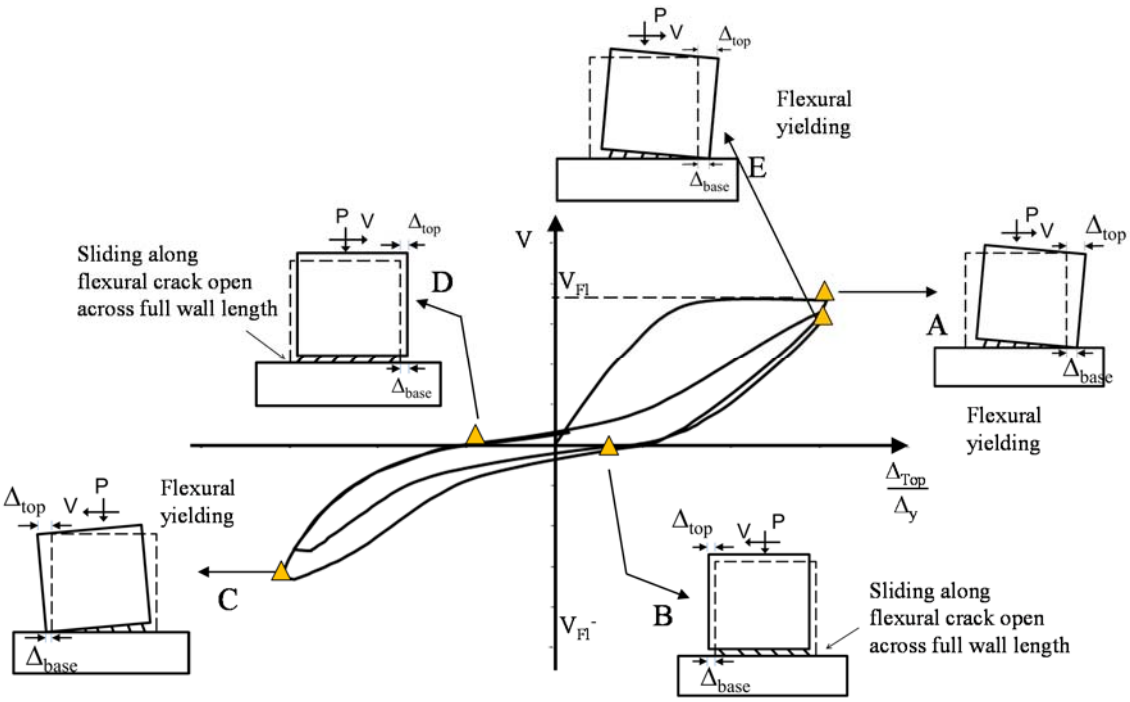

Figure 3.7 Lateral force versus displacement hysteretic behaviour of an RM shear wall experiencing a CFSS mechanism

3.4.2.1 Overturning Moment, M_o, and Shear Force, V_o

Figure 3.8 shows an internal force distribution in an RM wall with open flexural crack at the base. While the flexural crack is open, the in-plane shear force and overturning moment are resisted by the vertical reinforcing bars through dowel action and axial forces, respectively. This flexural crack can close if sufficient shear can be resisted through dowel action to develop an overturning moment, M_o, that causes vertical reinforcement on one end of the wall to yield in compression (Priestley, 1977). An expression for this overturning moment, M_o, is presented in equation 3.6. This equation is determined from equilibrium of internal moments, and expresses M_o as a function of the area of the vertical reinforcement, A_{db}, the axial stress in the reinforcement f_s, and the vertical bar's lever arm, d, as shown in Figure 3.8b.

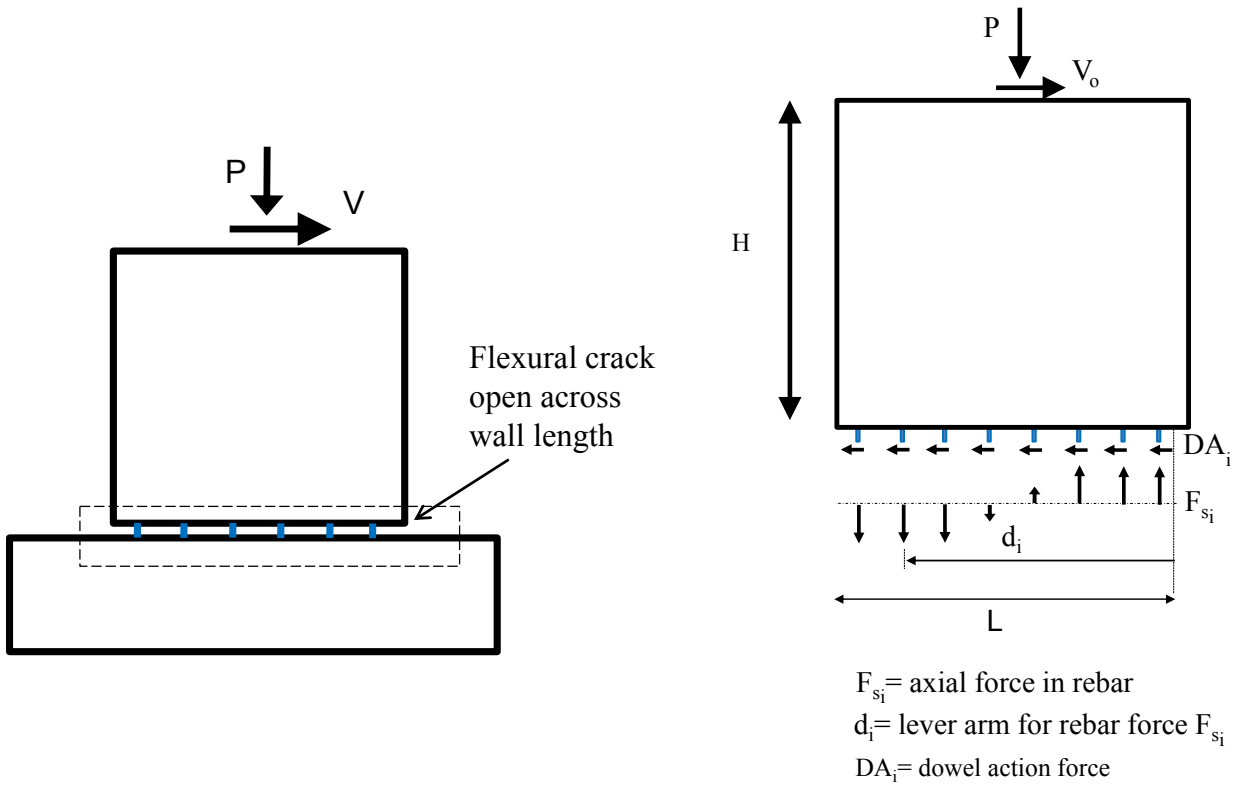

a) b)

Figure 3.8 Lateral resistance of an RM shear wall with open flexural crack:

a) Wall loading and cracked at wall-foundation interface;

b) Vertical reinforcement resisting external loading through dowel action, DA, and axial forces, F_s.

$$M_o = V_o H = \sum_{i=1}^{n} A_{db_i} f_{s_i} d_i + P\frac{L}{2} \tag{3.6}$$

The overturning moment M_o can also be expressed as shown in equation 3.7 for RM walls with distributed reinforcement. In this expression, M_o is a function of the total area of the vertical steel reinforcement, A_s, the yield stress of the reinforcement, f_y, and the length of the RM wall, L; where the coefficient, C_o, is calculated using equation 3.8. A generalized expression for C_o as a

function of the RM wall's design parameters will be derived through various parametric studies shown in Chapter 6.

$$M_o = C_o A_s f_y L \tag{3.7}$$

$$C_o = \frac{\left(\sum_{i=1}^{n} A_{db_i} f_{s_i} d_i\right) + P\frac{L}{2}}{A_s f_y L} \tag{3.8}$$

The lateral force V_o required to develop M_o in an RM cantilever wall can be determined through equation 3.9. An RM wall can close the flexural crack that causes sliding, when the dowel action yield resistance, DA_y, is sufficient to resist the lateral force V_o , as expressed in equation 3.10.

$$V_o = \frac{M_o}{H} \tag{3.9}$$

$$V_o < DA_y \tag{3.10}$$

3.4.3 Dowel-Constrained Failure (DCF) Mechanism

AN RM wall experiences a DCF mechanism when dowel action yield resistance is insufficient to resist the lateral force V_o, as expressed in equation 3.11. This behaviour is defined as failure as it stops the closing of the flexural crack and thus, prevents development of a flexural mechanism. Instead, the DCF mechanism develops significant inelastic transverse displacement demands; with a low lateral resistance equal to the dowel action yield resistance, DA_y. The hysteretic behaviour characteristic of a DCF mechanism is illustrated in Figure 3.9.

$$V_o \geq DA_y \tag{3.11}$$

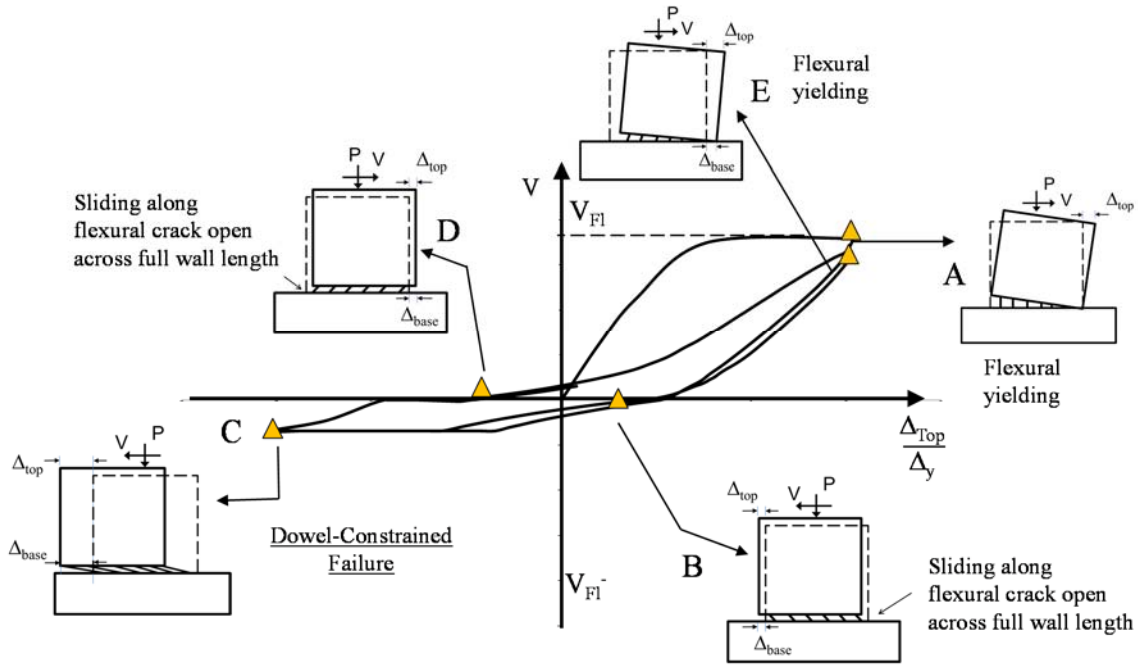

Figure 3.9 Lateral force versus displacement hysteretic behaviour of an RM shear wall experiencing a DCF mechanism.

3.5 Summary

A few relevant remarks are summarized below:

1. Sliding shear resistance is proposed as the sum of frictional and dowel action resistances.
2. A key aspect of the proposed approach is that frictional resistance is modeled as a function of the flexural compression force acting along the sliding plane. This will allow for the of capture the loss of frictional resistance as described by Priestley (1977).
3. This approach proposes simple expressions to model dowel action resistance and hysteretic behaviour.
4. This study identifies three yield mechanisms in which RM walls develop sliding displacements, namely, sliding shear (SS) mechanism, combined flexural-sliding shear (CFSS) mechanism and dowel-constrained failure (DCF) mechanism.

Chapter 4: Proposed Analytical Model for Simulating Sliding Shear Behaviour

4.1 Introduction

A novel 2D analytical macro model is presented in this chapter for simulating base sliding displacements in RM cantilever shear walls. This model is developed to simulate the interaction between the sliding shear and flexural behaviours in the development of an RM wall's yield mechanism. The input parameters for the model need to be calibrated using test results from previous experimental studies involving pseudo-static testing of RM shear wall specimens.

4.2 Model Properties

The model is based on the Multiple Vertical Line Element Model (MVLEM) approach originally proposed by Vulcano, Bertero and Colotti (1988) to simulate flexural behaviour. The MVLEM approach has been used to successfully balance the simplicity of a macroscopic model and the refinements of a microscopic model in order to simulate the combined effects of axial compression and flexural behaviour in RC shear walls (Orakcal, Massone and Wallace, 2006). The MVLEM approach discretizes the wall cross-section into a number of vertical uniaxial springs representing the axial strains and stresses acting on the masonry and reinforcing steel. As a result, the model is able to simulate shifting of the compression block length, the effect of axial compression on flexural strength and the development of an open flexural crack along the wall length.

The MVLEM approach was modified in this study to take into account effects of combined flexural compression and friction and it will be referred to as Modified MVLEM approach. This modification consisted of using friction bearing elements for modeling masonry in compression instead of axial springs. As a result, the plastic hinge zone of the RM wall is modeled using a combination of three components: friction bearing elements, nonlinear axial springs and nonlinear shear springs. The portion of the wall above the plastic hinge zone is modelled using an elastic beam-column element. These components are linked through two rigid beams (AA and BB). The proposed RM wall model is illustrated in Figure 4.1.

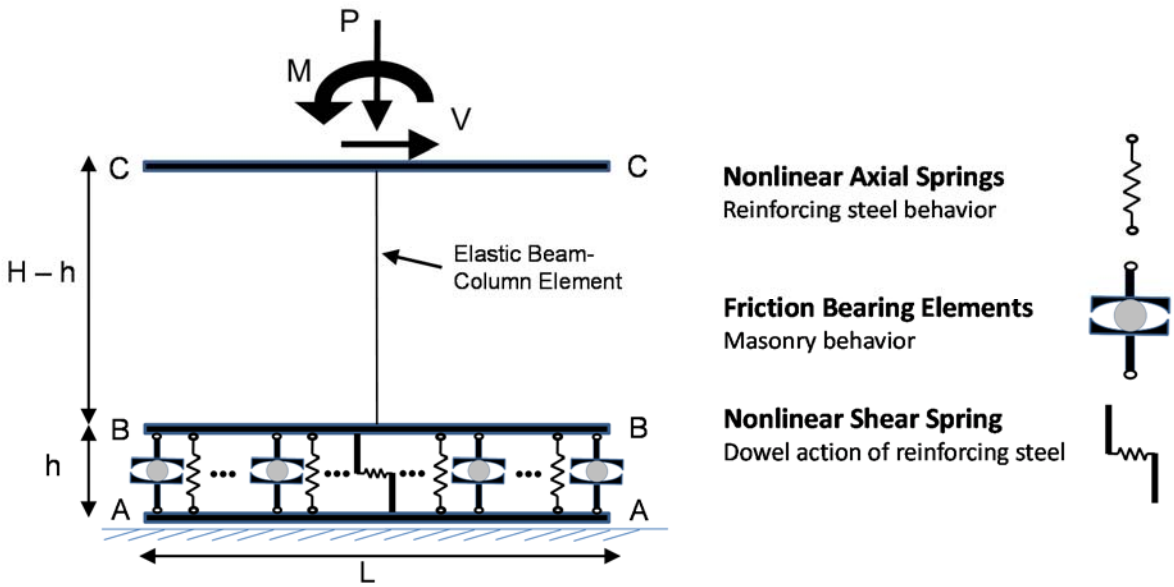

Figure 4.1 RM cantilever wall model.

4.2.1 Friction Bearing Elements

The use of the Friction Bearing (FB) element allows for modeling of the frictional force developed by the masonry in compression. The FB is an element commonly found in structural analysis software platforms, such as OpenSees (OpenSeesWiki, 2012).

The FB element is the combination of three internal springs (see Figure 4.2):

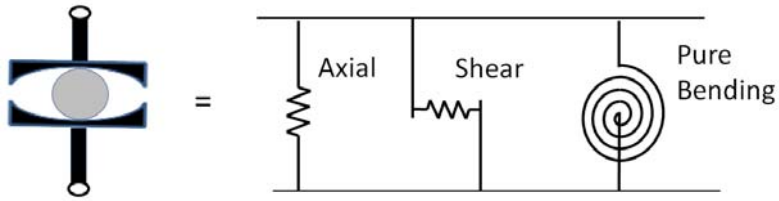

Figure 4.2 Springs that make up the friction bearing (FB) element.

1. The shear spring models the frictional resistance in the element using the Coulomb Friction model with a constant friction coefficient, μ_{Fr}.
2. The axial spring is a compression-only nonlinear spring suitable for modeling the masonry's compression behaviour.
3. The rotational spring models the bending behaviour along the component length as infinitely rigid. Its rotational spring is assigned a high rotational stiffness, k_θ.

The constitutive model for the FB shear spring is defined using yield displacement as the input parameter. This allows the FB element to model shear stiffness as proportional to the frictional resistance. The yield displacement, δ_y, for the shear spring was set at 1 mm as the lowest displacement value that did not cause numerical instability during analysis.

The axial spring for modeling masonry behaviour, uses the modified Kent and Park concrete model, presented as an envelope model in Scott, Park and Priestley, (1982). The hysteresis rule follows the properties developed by Yassin (1994). An illustration of the stress-strain backbone curve with hysteretic rule is shown in Figure 4.3. This material model is available as Concrete02 stress-strain material model in Opensees (OpenSeesWiki., 2010).

The axial spring's cross-sectional area is equal to its tributary area. Therefore, its cross sectional area will depend on the number of axial springs (Nmf) used to discretize the wall cross-section. The area can be calculated as the product of the RM wall's thickness, t, and the length equal to the sum of the two half distances to adjacent masonry axial springs.

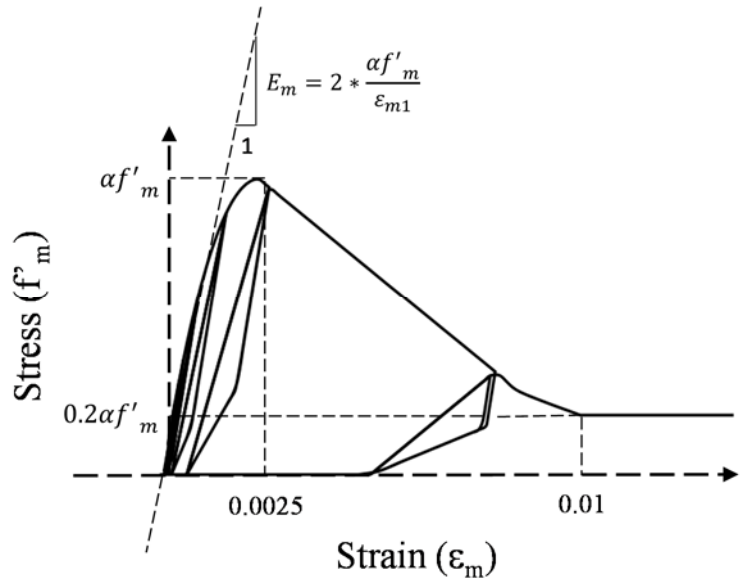

Figure 4.3 Masonry material stress-strain curve (Kent and Park concrete model).

4.2.2 Nonlinear Axial Springs

Nonlinear axial springs are also used to model the stress and strain response in vertical steel bars. The nonlinear axial spring uses a Giuffre-Menegotto-Pinto steel material model (Menegotto and Pinto, 1983) with isotropic strain hardening (Filippou, Popov, and Bertero, 1983). An illustration of steel stress-strain backbone curve with hysteretic rule is shown in Figure 4.4. The cross-sectional area assigned to each spring is equal to the area of the reinforcing bar, A_{db}. The spring locations correspond to the vertical reinforcing bars in the RM wall.

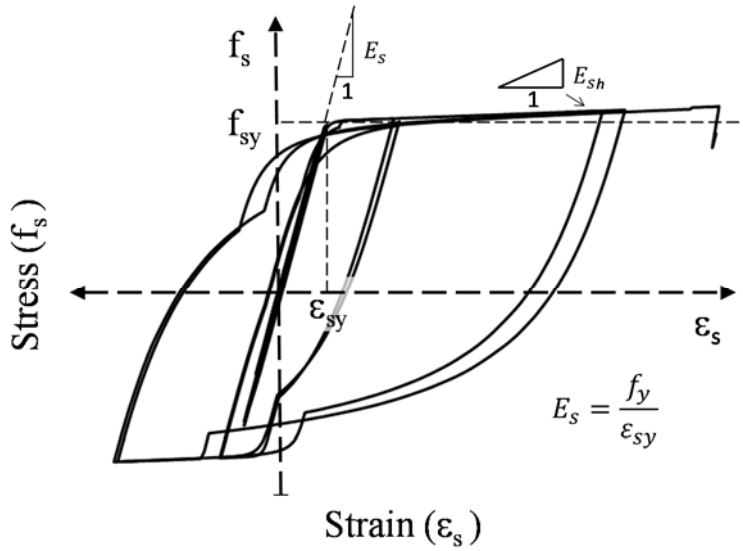

Figure 4.4 Steel material stress-strain curve (Giuffre-Menegotto-Pinto steel material model).

4.2.3 Nonlinear Shear Spring

The nonlinear shear spring in the model is used to model the total dowel action across the sliding plane. A backbone curve and a hysteresis rule are proposed for this study, as shown in Figure 4.5. These properties are based on the observations presented in Chapter 3 on dowel action behaviour. The values for lateral stiffness, k_{DA}, and yield strength, DA_y, are determined using equations 3.4 and 3.5, respectively.

4.2.4 Elastic Beam-Column Element

The beam-column element is assigned elastic bending and shear stiffness properties. Following Canadian Masonry Code provisions (CSA S304.1-14), the value of elastic modulus, E_m, is determined using equation 4.1.

$$E_m = 850f'm \text{ (MPa)} \tag{4.1}$$

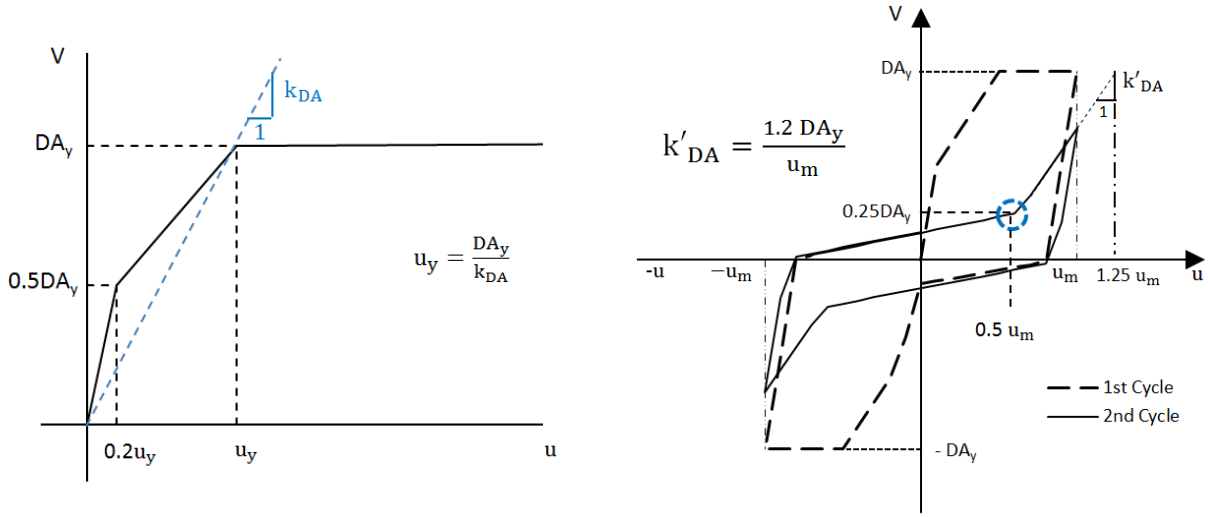

a) Monotonic Envelope b) Hysteresis rule

Figure 4.5 Plot of dowel action force deformation behaviour

The bending stiffness, k_b, is modeled as uncracked bending stiffness as shown in equation 4.2, where I_g is the value of the gross moment of inertia. For shear stiffness, k_s, shear stiffness is calculated following equation 4.3 with shear modulus G set equal to 0.4 E_m.

$$k_b = \frac{E_m I_g}{H} \tag{4.2}$$

$$k_s = \frac{GA_y}{H} \tag{4.3}$$

4.2.5 Connection of Spring Components

Each spring component has its own set of nodes, independent from those nodes in the two rigid beams (AA and BB). These nodes are connected together by constraining their Degrees of Freedom (DOF). The connection of each spring component to the rigid beams is shown in Figure 4.6.

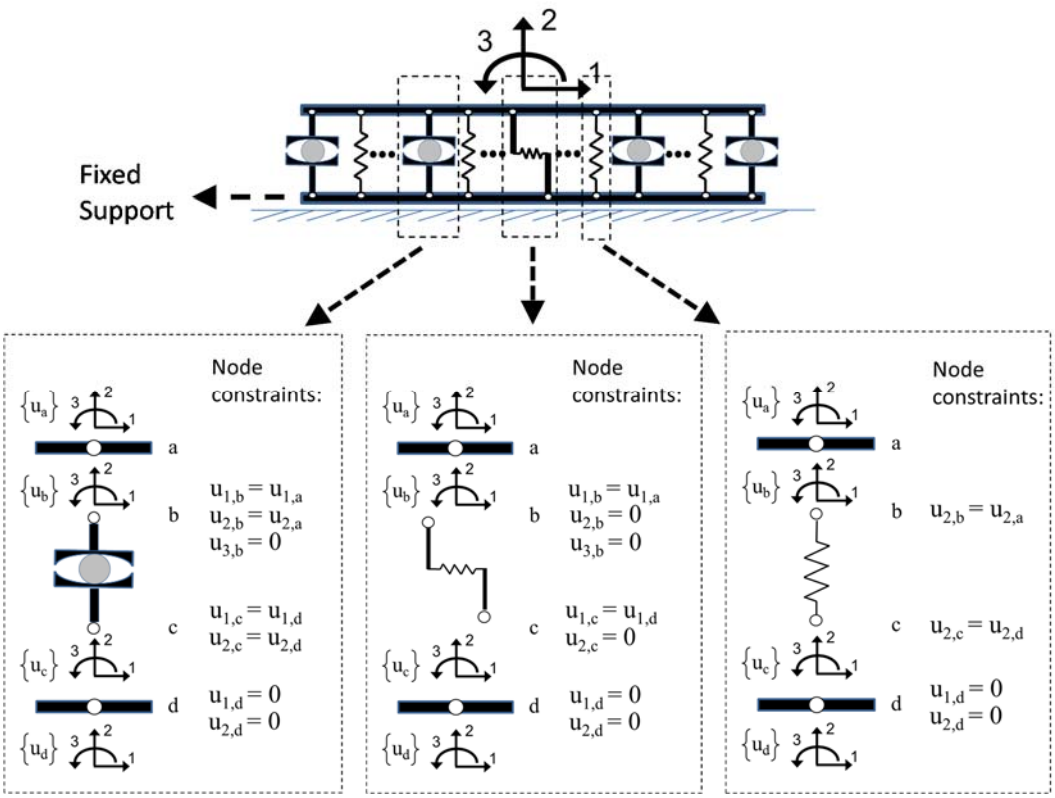

Figure 4.6 Connection of spring components forming a plastic hinge zone of the wall.

The DOFs constrained to have equal displacements with rigid beams are the following:

- FB element: u_1, u_2 (horizontal and vertical DOFs).
- Nonlinear axial spring: u_2 (vertical DOF).
- Nonlinear shear spring: u_1 (horizontal DOF).

The rotational DOFs in the spring components are not constrained to the rigid beams to ensure that no external moments act at the supports. In this way, the moment resistance can be developed through a force couple created by the axial forces in the vertical elements. In addition, in order to model the fixed support conditions of a cantilever RM wall, the DOFs for

each node in the lower rigid beam are set equal to pinned support conditions ($u_{1,d}=0$, $u_{2,d}=0$, $u_{3,d}\neq 0$).

4.2.6 Plastic Hinge Height (h)

The proposed model assumes that a plastic hinge is formed at the base of the wall. The hinge allows the RM cantilever wall to yield in flexure or shear, as shown in Figure 4.7. This hinge is defined by the height, h, of the spring components.

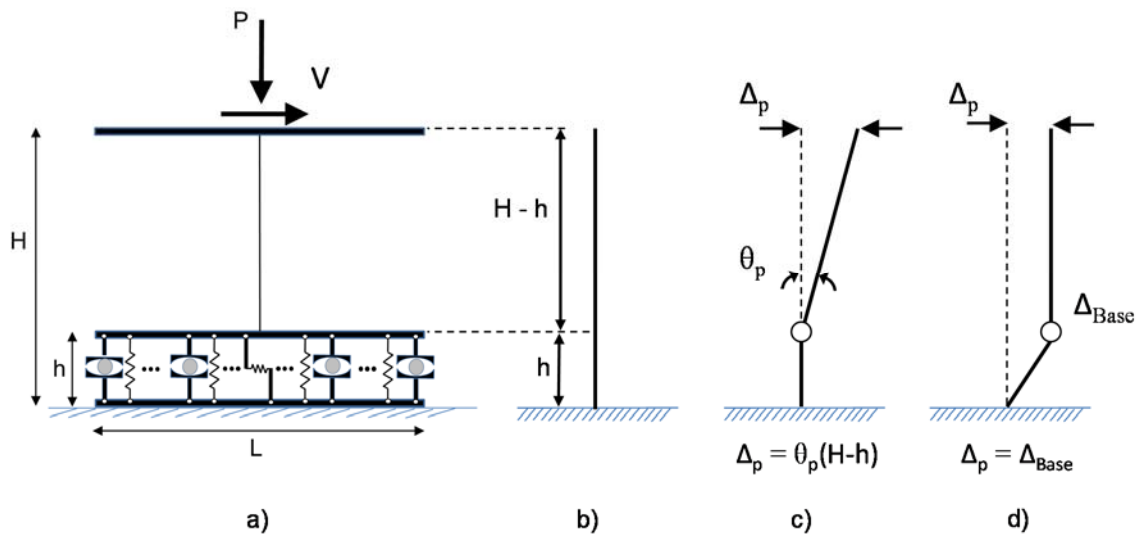

Figure 4.7 Plastic hinge model and wall displacements: a) RM wall cantilever model; b) Undeformed shape; c)Flexural mechanism; d) Sliding shear mechanism.

When the model develops a flexural mechanism, the plastic hinge's behaviour is equivalent to a flexural hinge; as shown in Figure 4.7c. For this behaviour, the inelastic wall displacement, Δ_p, is influenced by the plastic hinge's location. Therefore, the plastic hinge height will influence the accuracy of the inelastic flexural displacements.

When the model yields in a sliding shear mechanism, the plastic hinge's behaviour is equivalent

to a shear hinge; as shown in Figure 4.7d. In this case the wall displacement, Δ_p, does not depend on the plastic hinge height, h. In addition, the Δ_p value is equal to Δ_{Base} and therefore it is used to represent the base sliding displacement of the wall.

4.3 Calibration of the Model for Different Wall Support Conditions

The model has been calibrated to match test results from previous experimental studies on RM shear walls subjected to static reverse cyclic loading. The results used for calibration consist of five RM walls with cantilever support conditions (Hernandez, 2012) and five RM walls with fixed-fixed support conditions (Ahmadi, 2012). The available data set is used to calibrate the proposed model for different cases of effective shear-span/depth ratio, $\frac{M}{Vd}$, reinforcement ratio, ρ, and axial load, P.

The goal of the calibration process is to establish standard model parameters for the components such as: coefficient of friction, μ_{Fr}; dowel action resistance coefficient, C_{DA}; and plastic hinge height, h. A calibration is considered to be complete when the analysis adequately matches the experimental time history results from the onset of sliding up to a strength degradation of 20% or higher.

4.3.1 RM Walls with Cantilever Support Conditions

The experimental program (Hernandez, 2012) consisted of three wall specimens, PBS-03, PBS-04 and PBS-04G, tested without axial compression, and three wall specimens, PBS-11, PBS-12

and PBS-12G, subjected to axial loads equal to 10% of their estimated axial load capacity. Wall specimen properties are tabulated in Table 4.1.

Due to a malfunction in the instrumentation during the testing, data from specimen PBS-11 was not available for calibration. Specimens PBS-04G and PBS-12G shared the same seismic design parameters as walls PBS-04 and PBS-12, respectively, but were constructed using concrete block units made of recycled material and were referred to as "Green" masonry units.

Table 4.1 Properties of RM cantilever wall test specimens (Hernandez, 2012)

Wall Dimensions:	PBS-03	PBS-04	PBS-04G	PBS-12	PBS-12G
Height (m)	2.4	2.4	2.4	2.4	2.4
Length (m)	2.4	2.4	2.4	2.4	2.4
Aspect ratio (H/L)	1.0	1.0	1.0	1.0	1.0
Plastic hinge height (m)	1.0	1.0	1.0	1.2	1.0
Reinforcement					
ρ reinf. ratio	0.30%	0.17%	0.17%	0.17%	0.17%
Bar diameter (mm)	12	12	12	12	12
Bar Area (mm^2)	126	126	126	126	126
Number of bars	11	6	6	6	6
Vertical Loads					
Axial Comp. Ratio (Masonry): $P/(A_g f'_m)$	0%	0%	0%	10%	10%
Axial Comp. Ratio, (Steel): $P/(A_s f_y)$	0%	0%	0%	250%	250%
Axial Load, P (kN)	0	0	0	814	814
Material Strength					
f'_m (MPa)	17.5	17.5	17.5	17.5	17.5
f_y (MPa)	420	420	420	420	420
f_{su} (MPa)	680	680	680	680	680

Each wall specimen is modeled as a cantilever RM wall model. To represent cantilever end support conditions, the model has fixed support conditions at the base and free support conditions at the top. The analytical model used for calibration is illustrated in Figure 4.8. The

estimated sliding displacement, Δ_{Base}, represents the relative displacement at point A (see Figure 4.8a).

Displacement-controlled nonlinear analysis is performed by applying increasing lateral displacement, Δ_{Top}, at the top of the specimen. The vertical loads include: the external axial force, P, applied at the top node of the beam-column element; and the self-weight of the specimen, W, applied at the lower node of the linear elastic beam-column element, and estimated to be equal to 23 kN assuming a weight density of 21 kN/m^3.

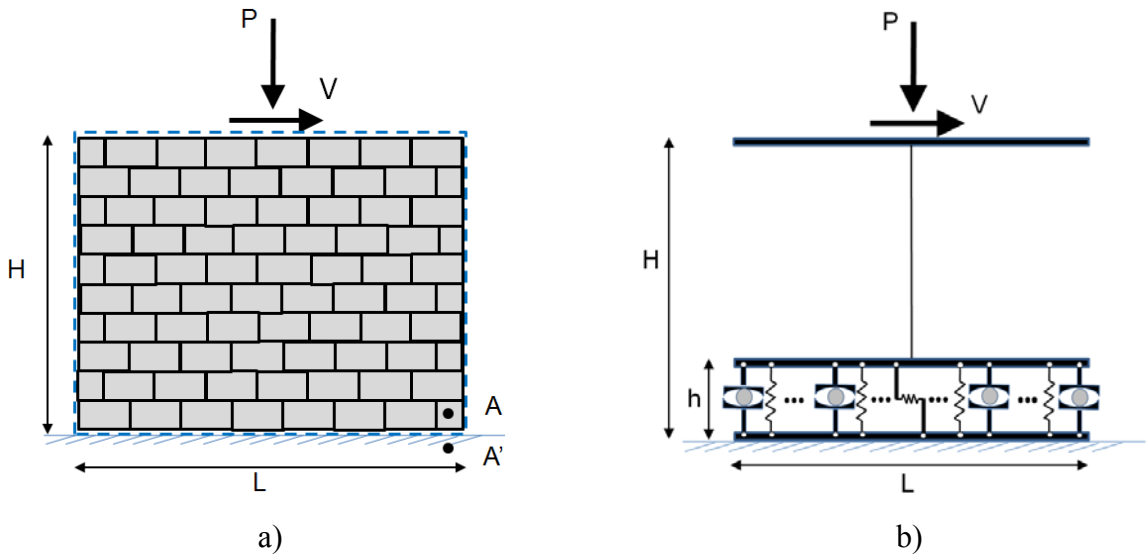

Figure 4.8 Modeling of cantilever RM wall using modified MVLEM:
a) RM wall test specimen; b) Analytical Model using modified MVLEM.

The calibration is done following an iterative process, with the first iteration performed using the wall dimensions and material properties (see Table 4.1). Sliding shear behaviour parameters to be calibrated are given preliminary values and later adjusted; with the values of frictional coefficient, μ_{Fr}, equal to 0.6, and dowel action yield strength coefficient, C_{DA}, equal to 1.00, and plastic hinge height, h, taken as 25% of the overall wall height, H.

The analysis results obtained from the model are then compared to the experimental results. The initial comparison is made for the flexural displacements and strength. For these tests, flexural contribution to the total wall displacement was significant. Adjusting the plastic hinge height, h, improved the results for wall displacements. For strength, improving the match with flexural resistance required adjusting the masonry strength, f'_m, and the steel yield strength, f_y. The masonry strength is multiplied by coefficient α and the steel yield strength by coefficient β. The adjusted strengths, shown in equations 4.4 and 4.5, are replaced as input parameters in the corresponding stress-strain material models. The values of masonry elastic modulus, E_m, and dowel action yield resistance, DA_y, are also recalculated using the adjusted material strengths. However, steel material properties of elastic modulus, E_s, and strain hardening slope, E_{sh}, are not changed.

$$f'_{m_i} = \alpha_i f'_{m_0} \tag{4.4}$$

$$f_{y_i} = \beta_i f_{y_0} \tag{4.5}$$

Where:

f'_m = masonry compression strength (MPa)

f_y = steel yield strength (MPa)

α: modification coefficient for masonry strength

β: modification coefficient for the steel yield strength

i: number in the iteration of the calibration process

The calibration of the sliding shear behaviour consists of matching the sliding shear displacements and hysteretic curves from the experimental results. In the case of the wall specimens without axial precompression (PBS-03, PBS-04, and PBS-04G), this required adjusting the dowel action model parameters. On the other hand, for the wall specimens under high axial stresses (PBS-12 and PBS-12G), the adjustments were needed for friction properties.

Several iterations are made, and the model parameters are adjusted, until the results of the analysis matched the experimental data to satisfactory level. The calibrated values of each cantilever RM wall model are presented in Table 4.2. A comparison of experimental and analytical results after calibration is presented in Figure 4.9. These models correctly estimated the governing yield mechanism for the corresponding wall specimens: Combined Flexural-Sliding Shear Mechanism (CFSS) mechanism for specimens PBS-03, PBS-04, PBS-04G, and flexural yield mechanism for specimens PBS-12 and PBS-12G.

Table 4.2 RM wall cantilever model component properties after calibration

Wall Specimen:	PBS-03	PBS-04	PBS-04G	PBS-12	PBS-12G	**Average**	**Standard Deviation / Average**
h / H	0.20	0.21	0.15	0.20	0.22	0.20	12%
Nmf *	24	20	20	30	30	25	18%
Axial Springs							
α	0.5	0.5	0.5	0.5	0.5	0.5	0%
β	1.1	1.05	1.05	1.1	1.1	1.08	2%
(E_{sh}/E_s)	0.5%	0.5%	0.5%	1.0%	0.5%	0.6%	33%
Friction Properties							
μ_{Fr}	0.60	0.60	0.60	0.55	0.55	0.58	4%
δ_y (mm)	1.0	1.0	1.0	1.0	1.0	1.0	0%
Dowel Action Properties							
C_{DA}	1.27	1.17	1.17	1.20	1.26	1.21	4%

Nmf = Number of masonry fibers

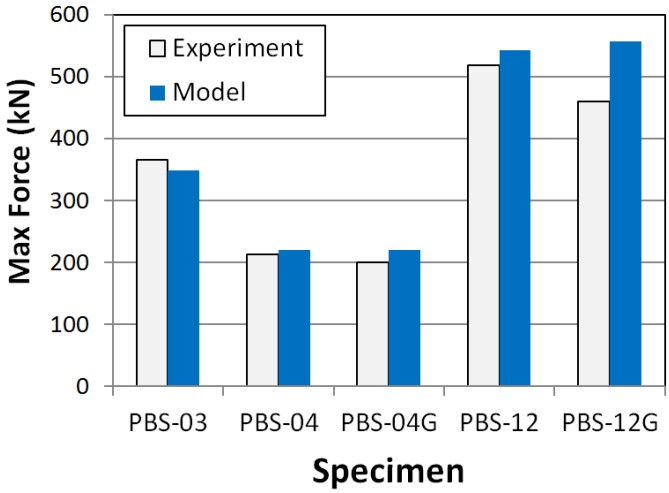

a)

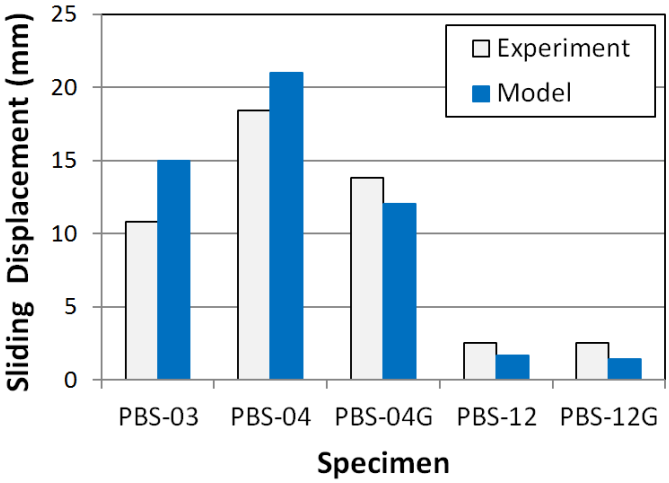

b)

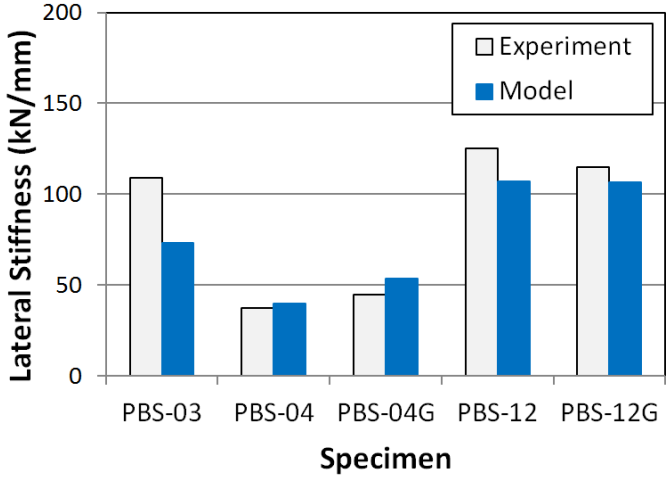

c)

Figure 4.9 Comparison of experiment results vs. analytical results for RM cantilever wall specimens: a) Maximum lateral force; b) Maximum sliding displacements; and c) Lateral stiffness.

The cyclic loading protocol used for specimen PBS-03 is shown in Figure 4.10a. This displacement history is applied as input for the analytical model. After the calibration process, the sliding displacements for each cycle matched the peak sliding displacements in the range from 97% to 127% of those developed in the experiment. The sliding displacement histories for the experiment and the model are compared in Figure 4.10b.

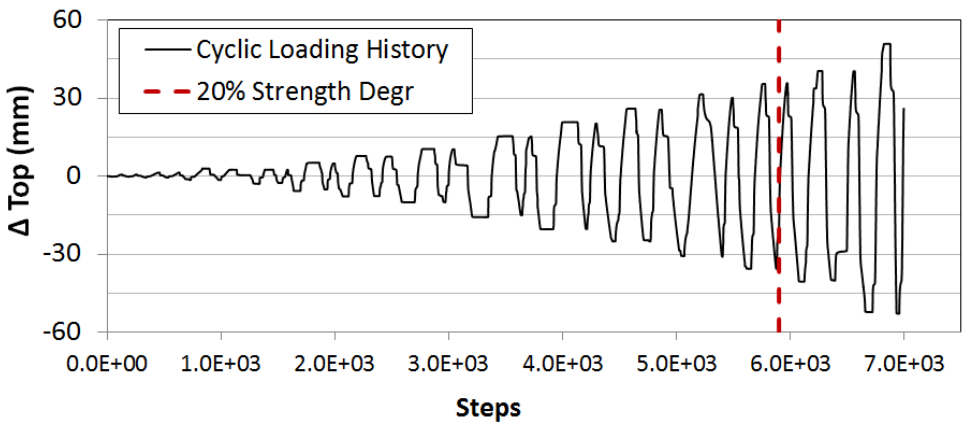

a)

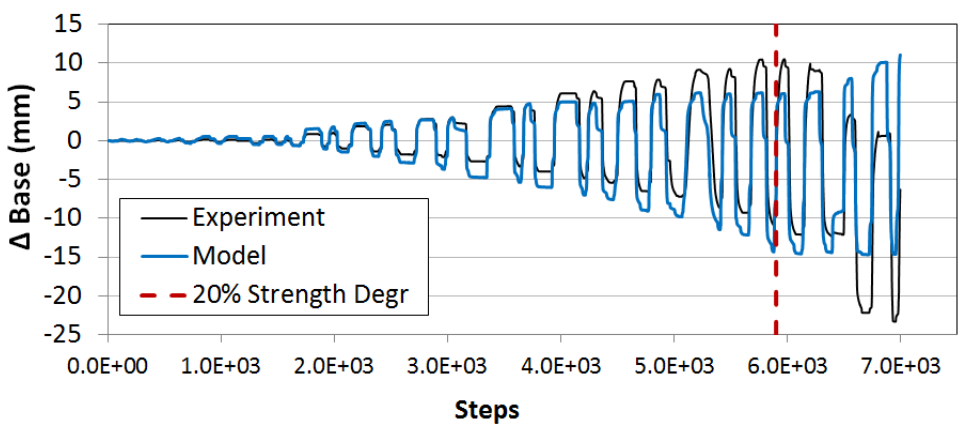

b)

Figure 4.10 Displacement histories for Specimen PBS-03:
a) At top of the wall; b) At base of the wall (sliding displacement).

The RM wall model with calibrated parameters is able to simulate the sliding hysteresis behaviour for the specimen PBS-03 prior to strength degradation, as shown in Figure 4.11. It

can be seen from the figure that the test specimen and the model have similar levels of stiffness degradation and pinching in their hysteresis loops.

The sliding shear resistance estimated by the model is equal to the sum of frictional and dowel action resistances. The friction hysteresis in Figure 4.12a shows a severely pinched hysteresis without dissipation of energy. This occurs due to loss of frictional resistance when the flexural crack is open along the wall length. On the other hand, the dowel action hysteresis in Figure 4.12b shows that dissipation of energy in the specimen occurred through dowel action alone.

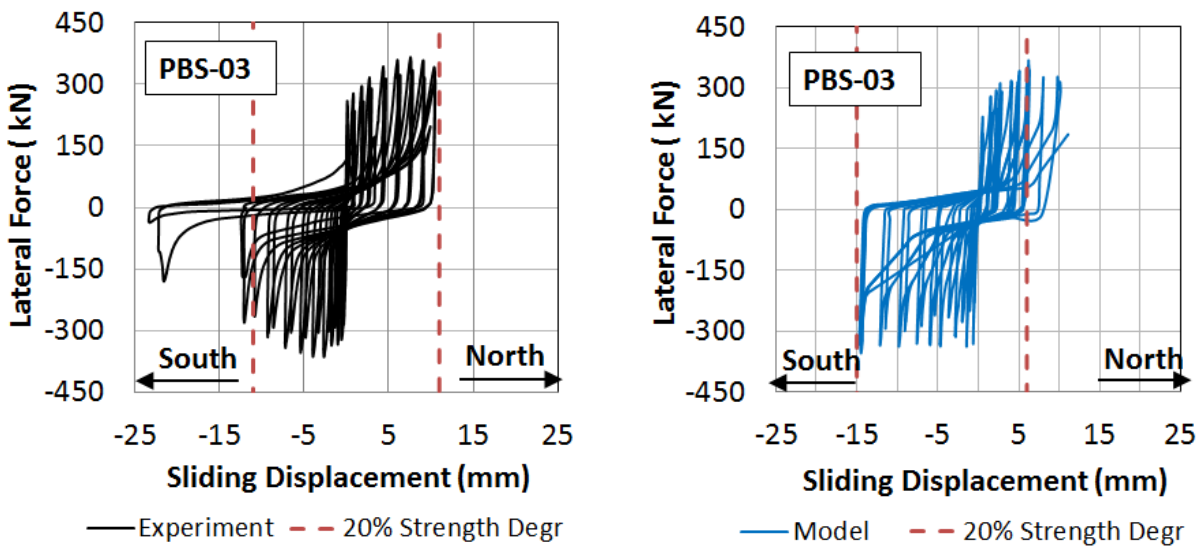

a) b)

Figure 4.11 Sliding hysteresis curves at the base of the wall for specimen PBS-03: a) Experiment; and b) Analytical model.

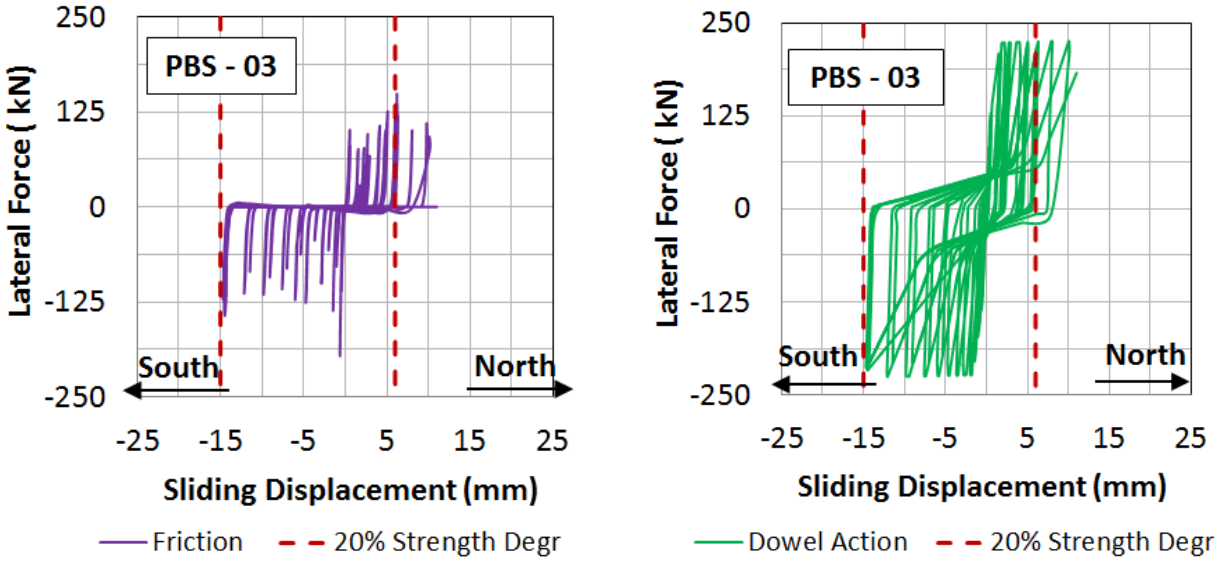

a) b)

Figure 4.12: Contributions to sliding shear resistance - Specimen PBS-03: a)Friction hysteresis and b) Dowel action hysteresis.

The model assumes the flexural crack is open when the outermost fibers at opposite ends of the wall both develop tensile strains. Figure 4.13 shows that, during loading cycles (steps 1900 to 5800) most of the model's sliding displacements developed when the flexural crack was open.

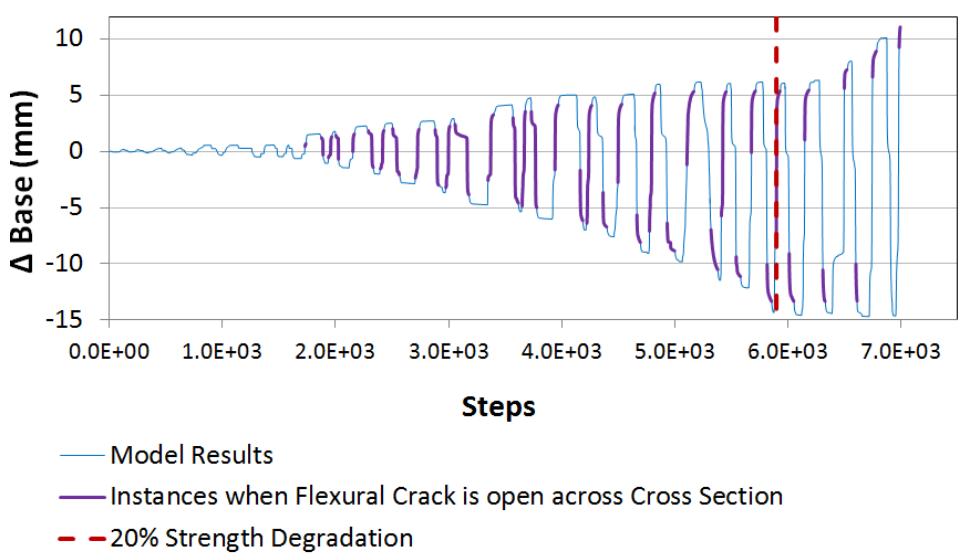

Figure 4.13 Tracking of instances when flexural crack opened along wall length for Specimen PBS-03.

For the lateral force vs. top displacement curves shown in Figure 4.14, the RM wall model is able to predict the lateral force when the peak top displacement, Δ_{Top}, exceeded the yield displacement, Δ_y, equal to 5 mm. These values range from 94 to 104% of that developed in the experiment. However, the model overpredicts the energy dissipated at each cycle, as observed in the difference in areas under the hysteretic curves shown in Figure 4.14. This can be explained by the shear stiffness degradation that occurred during the experiment at lateral displacement level Δ_{Top} of more than 15 mm, which was caused by a large concentration of shear cracks developed at the wall mid-height (Hernandez, 2012). The analytical model assumes shear stress-strain behaviour to be linear-elastic and therefore cannot capture this behaviour.

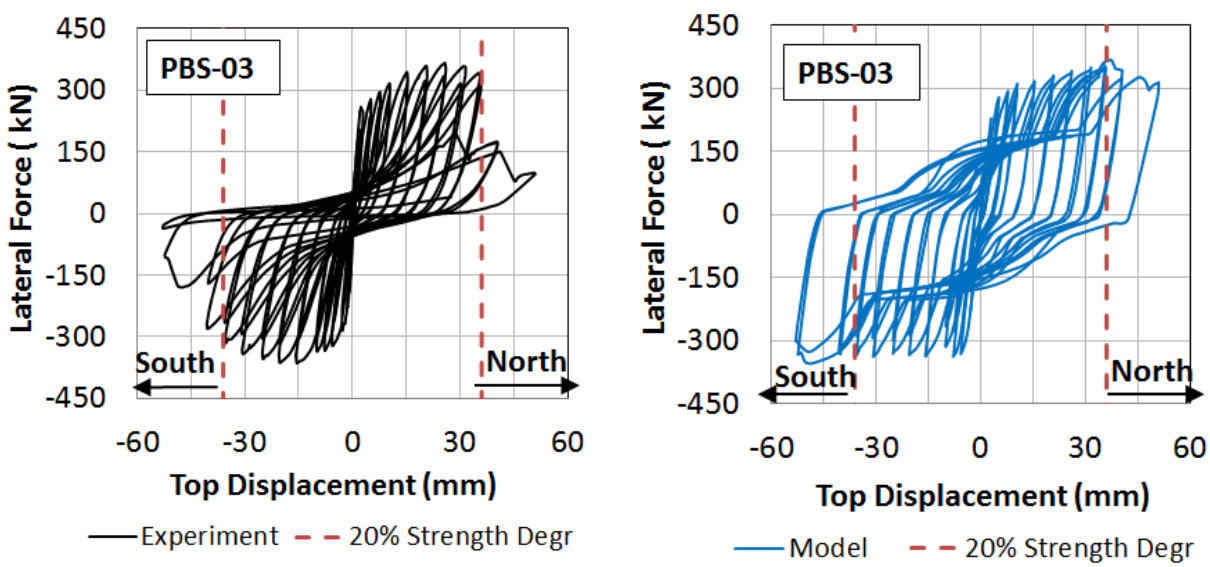

a) b)

Figure 4.14 Lateral force vs top displacement hysteresis – Specimen PBS-03: a)Experiment, b) Analytical Model.

The specimen developed a 25% loss of lateral strength in the south direction during the 2nd cycle of lateral displacement, Δ_{Top}, of 36 mm. This resulted in the crushing of the compression toe of

the specimen and subsequent buckling of the vertical reinforcement. The model is not able to capture this loss of strength since rebar elements are modeled as non-buckling axial springs.

4.3.2 RM Walls with Fixed-Fixed Support Conditions

The pseudo-static test program conducted by Ahmadi (2012) consisted of cyclic loading tests on wall specimens with aspect ratio H/L=1.0 with fixed-fixed support conditions. From this testing program five wall specimens are used in the model's calibration process: PBS-01, PBS-05, PBS-06, PBS-09 and PBS-10. Wall specimen properties are tabulated in Table 4.3.

Table 4.3 Properties of RM cantilever wall test specimens (Ahmadi, 2012)

Wall Dimensions:	PBS-01	PBS-05	PBS-06	PBS-09	PBS-10
Height (m)	1.8	1.8	1.8	1.8	1.8
Length (m)	1.8	1.8	1.8	1.8	1.8
Aspect ratio, H/L	0.5	0.5	0.5	0.5	0.5
Reinforcement					
Reinf. Ratio (ρ)	0.75%	0.33%	0.18%	0.33%	0.18%
Bar diameter (mm)	19	12	12	12	12
Bar Area (mm^2)	284	126	126	126	126
Number of bars	9	9	5	9	5
Vertical Loads					
Axial Comp. Ratio (Masonry): $P/(A_g f'_m)$	2%	6%	5%	10%	10%
Axial Comp. Ratio, (Steel): $P/(A_s f_y)$	20%	73%	114%	122%	222%
Axial Load (kN)	89	361	304	608	608
Material Strength					
f'_m (MPa)	17.5	17.5	17.5	17.5	17.5
f_y (MPa)	430	430	430	430	430
f_{su} (MPa)	693	693	693	693	693

All specimens, with the exception of specimen PBS-01, developed a sliding shear mechanism. Although wall specimen PBS-01 experienced a diagonal shear failure, it was used to provide a

lower limit for the sliding shear resistance of fixed-fixed RM walls since it had a low axial compression level, $P/A_g f'_m$, equal to 2%.

For a specimen with fixed-fixed end support conditions, flexural cracks can develop both at the top and bottom of the wall, creating possible sliding planes. These sliding planes can be modeled using the modified MVLEM approach, as shown in Figure 4.15. The estimate of sliding displacement, Δ_{Base}, is calculated as the sum of the relative displacements at the supports, which correspond to the relative displacements at points A and B, shown in Figure 4.15a.

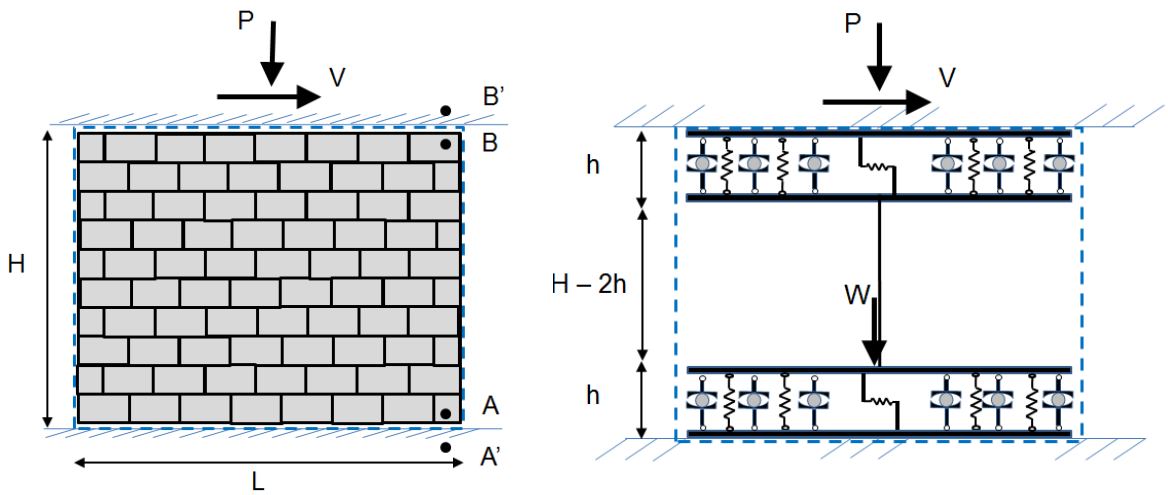

Figure 4.15 Model of fixed-fixed RM wall using modified MVLEM:
a) RM wall test specimen; b) Analytical Model using modified MVLEM.

Displacement-controlled nonlinear analysis is performed by applying lateral displacements, Δ_{Top}, at the top of the specimen. The vertical load, P, and self-weight of the specimen, W, are applied as illustrated in Figure 4.15b. The W value used is equal to 13 kN, assuming a weight density of 21 kN/m^3.

The first iteration of the calibration used material properties presented in Table 4.3 and values of coefficient, μ_{Fr}, equal to 0.6, coefficient of dowel action yield resistance, C_{DA}, equal to 1.21; and plastic hinge height, h, taken as 20% of the overall wall height, H. These values correspond to the average results of the calibration process for RM cantilever walls shown in Table 4.2.

The first step in the calibration process involved improving the match with the specimen's lateral resistance. For the first iteration, the RM wall model's predictions of sliding shear resistance were 60% of that obtained through experimental testing. The C_{DA} coefficient was then changed from the original value of 1.21 and made equal to 2.18; this improved the matching of sliding shear resistance to an average of 90%. This C_{DA} value reflects the upper limit for dowel action yield strength, DA_y, as shown in equation 4.6, because it corresponds to the maximum shear resistance for steel reinforcing bars.

$$DA_y \leq \frac{1}{\sqrt{3}} A_s f_y \tag{4.6}$$

The strain hardening parameter, E_{sh}, (see Figure 4.4) cannot be calibrated based on the available test results for fixed-fixed conditions. Flexural demands for all five specimens were below their flexural yield strength, V_y. Therefore, no recommendation on the E_{sh} value is made based on the calibration results from the fixed-fixed wall tests.

It took a few iterations before a satisfactory match between experimental data and analysis results was achieved. The calibrated values for the fixed-fixed RM wall models are presented in Table 4.4. The comparison between experimental and model results is shown in Figure 4.16.

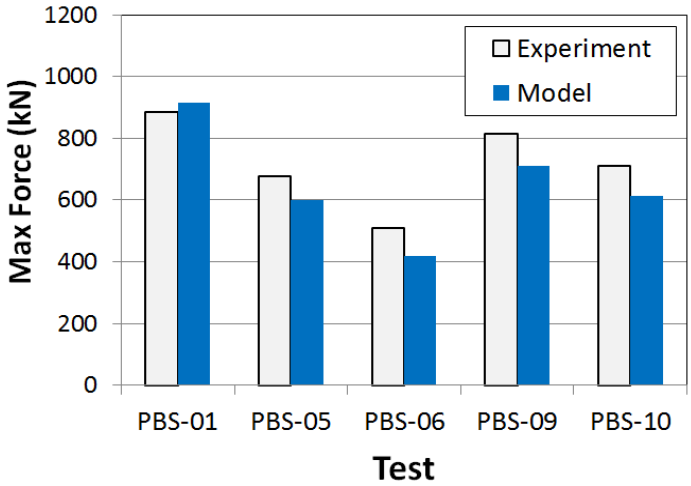

a)

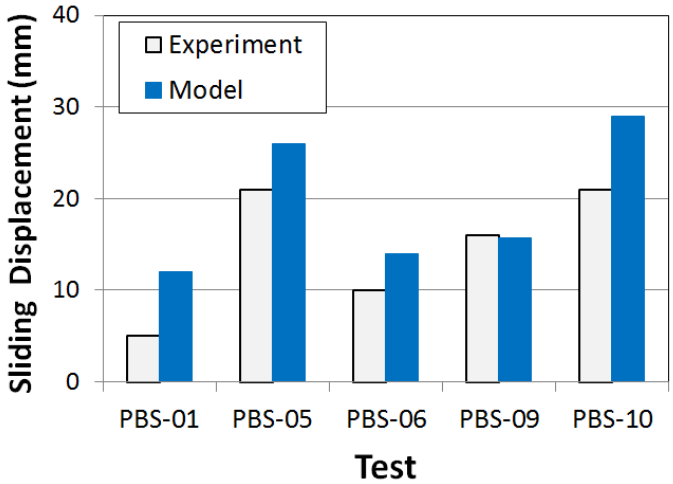

b)

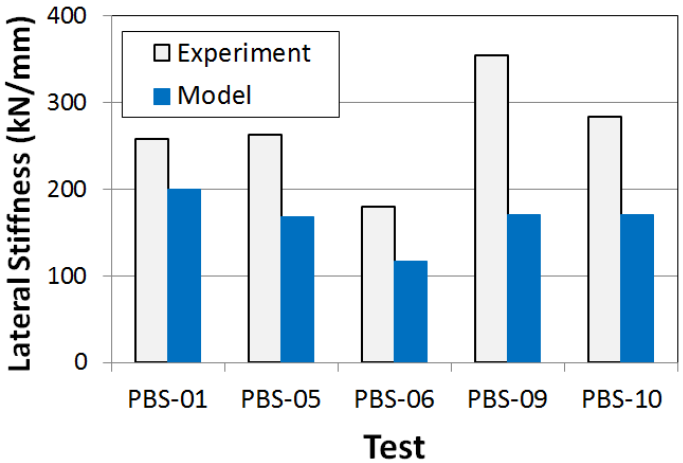

c)

Figure 4.16 Comparison of experiment results vs. analytical results for RM wall with fixed-fixed end support conditions: a) Maximum lateral force; b) Maximum sliding displacements; and c) Lateral stiffness.

Table 4.4 RM wall fixed-fixed model component properties after calibration

Wall Specimen:	PBS-01	PBS-05	PBS-06	PBS-09	PBS-10	Average	Standard Deviation / Average
h/ H	0.15	0.15	0.15	0.15	0.15	0.15	0%
Nmf *	27	27	18	27	18	23	20%
Axial Springs							
α	0.5	0.5	0.5	0.5	0.5	0.5	0%
β	1.1	1.1	1.1	1.1	1.1	1.1	0%
E_{sh}/E_s	N/A	N/A	N/A	N/A	N/A	N/A	N/A
Friction Properties							
μ_{Fr}	0.6	0.6	0.6	0.6	0.6	0.6	0%
Dowel Action Properties							
C_{DA}	2.18	2.18	2.18	2.18	2.18	2.18	0%

Nmf= number of masonry fibers

It has been shown that the modified MVLEM approach correctly predicts the yield mechanism for wall specimens that developed a sliding shear mechanism. The maximum sliding displacements obtained from the model range from 100 to 140% of experimental values.

The cyclic loading protocol used for testing the specimen PBS-06 is shown in Figure 4.17a. This same displacement history is applied as input for the analytical model. After the calibration, the predictions for sliding displacement for each cycle are in the range of 130 to 190% of that developed in the experiment. The sliding displacement histories for both the experiment and the model are compared in Figure 4.17b.

The calibrated RM wall model acceptably recreates the sliding hysteresis behaviour developed in specimen PBS-06 (prior to developing strength degradation). Hysteresis curves obtained experimentally and through MVELM simulation in Figure 4.18 shows similar energy dissipation.

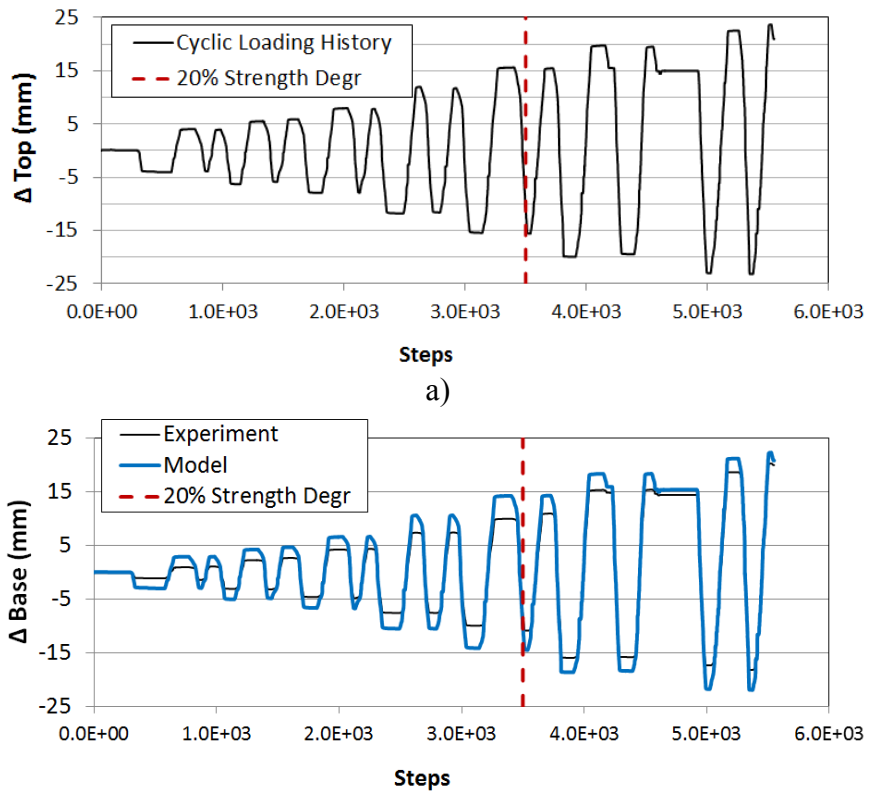

Figure 4.17 Displacement histories for Specimen PBS-06:

a) Wall total displacement; b) Sliding displacement.

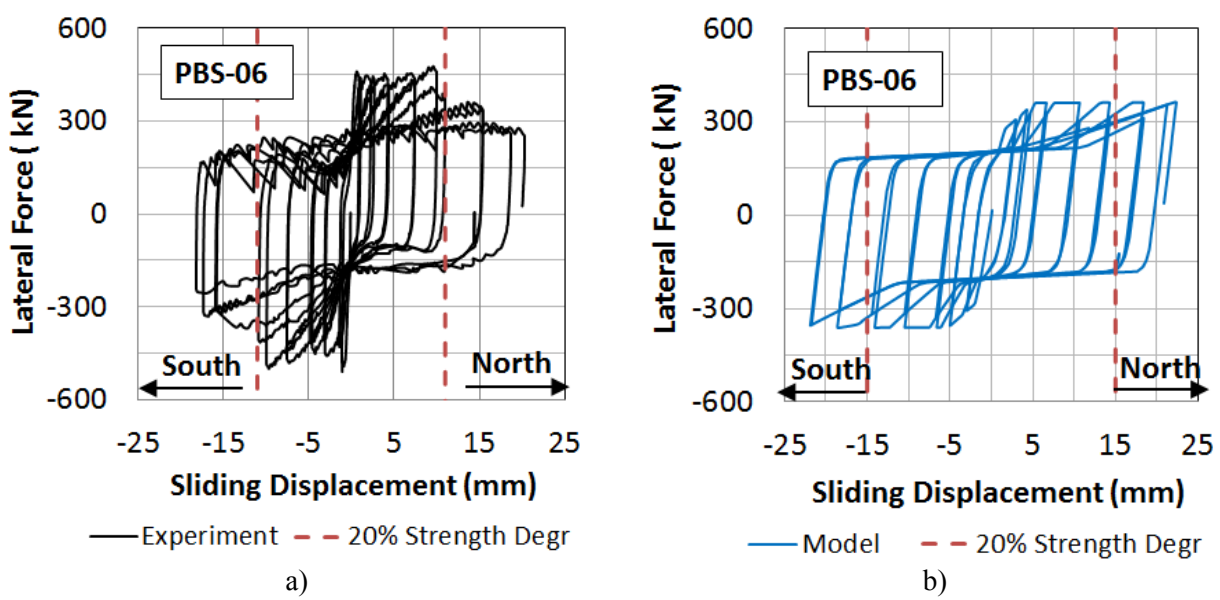

Figure 4.18 Sliding hysteresis curves of specimen PBS-06: a) Experiment; and b) Analytical model.

Figure 4.19 illustrates the friction and dowel action hysteresis curves corresponding to sliding displacements at the top support of the wall (point B in Figure 4.15). The friction hysteresis shows elastic-plastic hysteresis behaviour and the dowel action hysteresis shows stiffness degradation and pinching. These results show that both friction and dowel action contribute to energy dissipated through sliding at the wall supports.

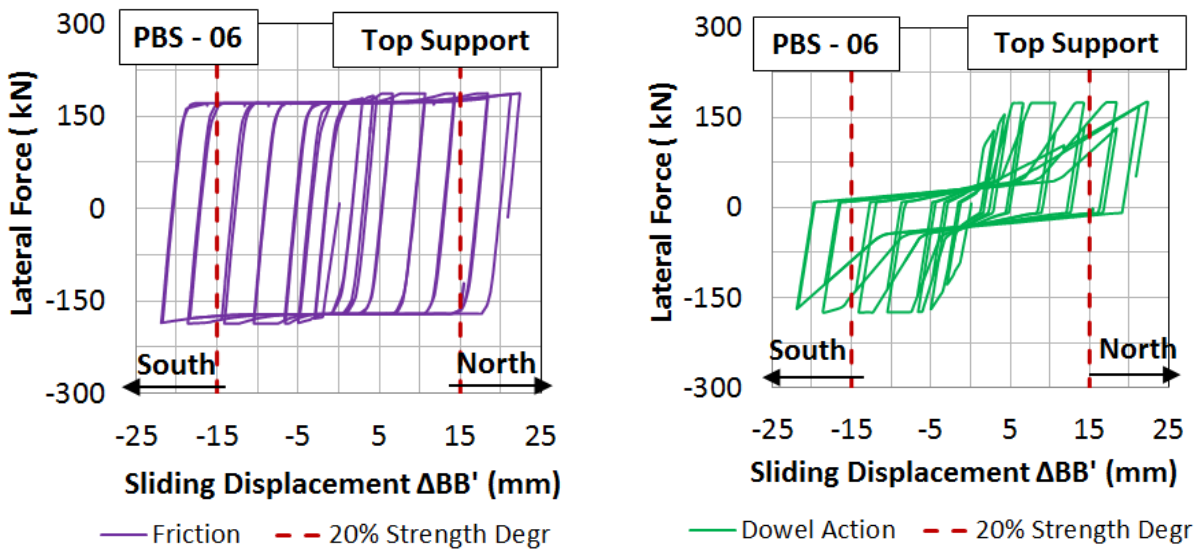

a) b)

Figure 4.19 Contributions to sliding shear resistance in top support (B) - Specimen PBS-06: a) Friction hysteresis and b) Dowel action hysteresis.

Figure 4.20 indicates that analysis results for specimen PBS-06 do not show instances of an open flexural crack across the wall's length. This behaviour is consistent with RM walls that experience a sliding shear mechanism, in which sliding displacements develop as inelastic displacements, Δ_p, (see Section 3.4.1). Therefore, the model adequately simulates the sliding shear mechanism.

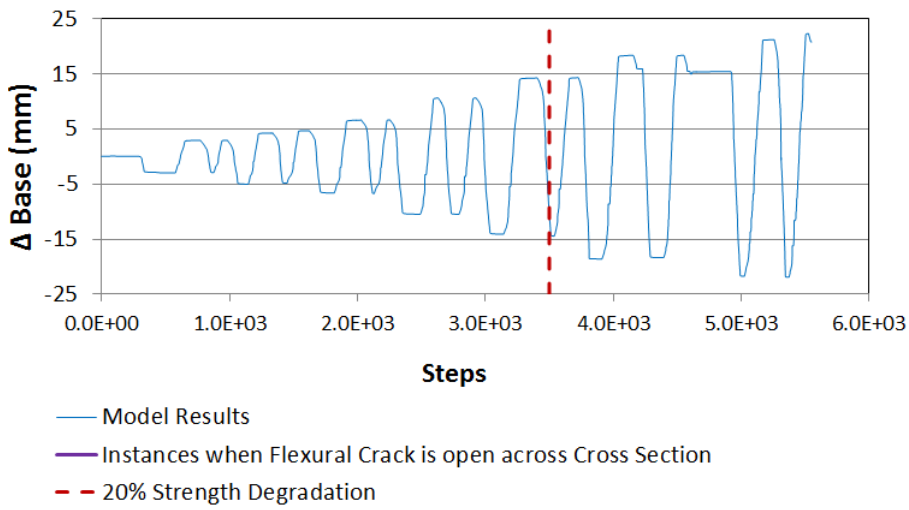

Figure 4.20 Tracking of instances when flexural crack opened along wall length for Specimen PBS-06.

Hysteresis curves for lateral force vs. top displacement are shown in Figure 4.21. The RM wall model showed a satisfactory simulation of hysteretic behaviour developed by the wall specimen at each cycle.

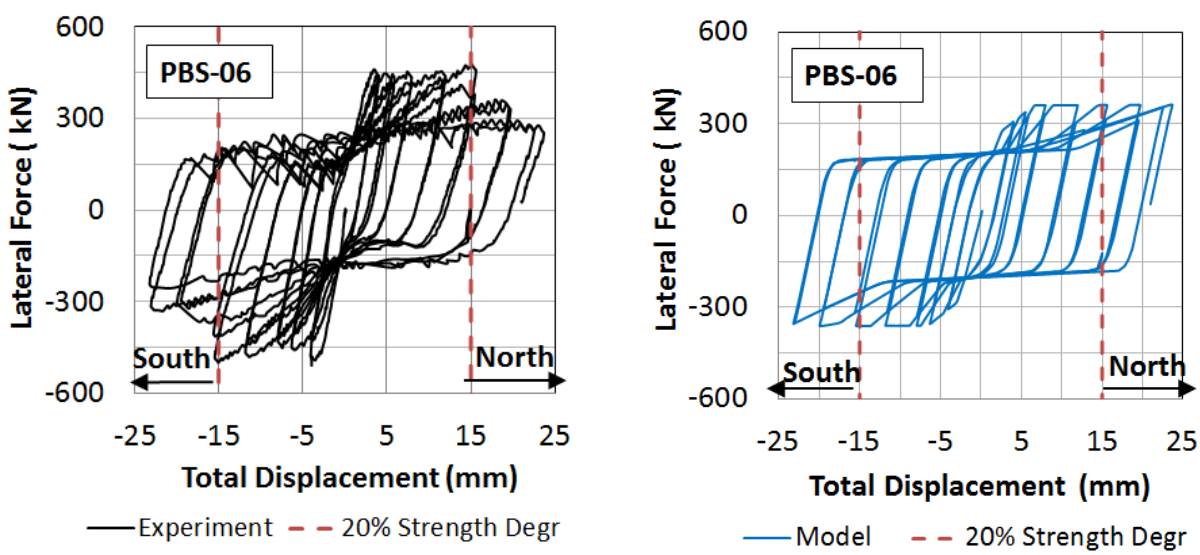

a) b)

Figure 4.21 Lateral force vs top displacement hysteresis – Specimen PBS-06: a)Experiment, b) Analytical Model.

4.3.3 Calibrated Values for the Proposed RM Cantilever Wall Model

In this study, analytical models have been calibrated to match results of experimental studies on RM shear walls with cantilever and fixed-fixed support conditions. Based on the average calibrated parameters obtained from these analyses, two sets of calibration factors are proposed for modeling RM walls, as shown in Table 4.5.

These parameters are recommended based on the assumption that the averaged calibrated parameters obtained for RM fixed-fixed walls can be used to model RM walls with shear span ratios less than 0.5, while the averaged calibrated parameters for RM cantilever walls can be used for modeling those with shear span ratios equal or greater than 1.0. In the case of RM walls with shear span ratios between 0.5 and 1.0, the recommended values are to be determined through linear interpolation. Note that shear span ratio is equal to H/L ratio.

Table 4.5 Recommended calibration parameters for RM Wall Models

Aspect Ratio (H/L)	Axial Springs			Friction		Plastic Hinge		Dowel Action
	α	β	E_{sh}/E_s	μ_{Fr}	δ_y (mm)	E_{sh}/E_s	h/H_{Wall}	C_{DA}
$H/L \leq 0.5$	0.5	1.08	0.5%	0.6	1.0	25	0.15	2.2
$H/L \geq 1.0$	0.5	1.08	0.5%	0.6	1.0	25	0.20	1.2

Nmf*= number of masonry fibers

The difference in dowel action yield resistance coefficient, C_{DA}, as a function of an RM wall's H/L ratio is assumed to reflect a difference in local dowel action yield mechanism:

- In RM walls with H/L ratios less than 0.5, dowel action is developed through shear deformations in the vertical reinforcement, illustrated in Figure 3.4b. This local yield

mechanism occurred in the reinforcing bars since specimens experienced a sliding shear mechanism.

- In RM walls with H/L ratios greater than 1.0, dowel action is developed through flexural deformations in the vertical reinforcement, as illustrated in Figure 3.4a. This local yield mechanism occurred in the reinforcing bars since the specimens experienced a combined flexural-sliding shear mechanism.

4.4 Resistance Properties Based on Calibration Results

After calibrating the 2D model to match experimental results, there are several observations regarding the in-plane behaviour of RM shear walls that can be applied in seismic design. Based on these observations and the results in Table 4.5, this section presents recommendations on design equations for friction coefficient, dowel action resistance and RM wall shear stiffness.

4.4.1 Friction

The recommended frictional resistance developed due to axial compression can be determined using in equation 4.7, based on the Coulomb friction model. The recommended coefficient of friction, μ_{Fr}, corresponds to a masonry-to-concrete sliding plane, based on the roughness reported for test specimens in Hernandez (2012) and Ahmadi (2012).

$$\mathrm{Fr_A} = \mu_{\mathrm{Fr}}\mathrm{P} \tag{4.7}$$

Where

$\mu_{\mathrm{Fr}} = 0.6$, (for masonry-to-concrete sliding plane, not intentionally roughened)

This recommended friction coefficient is lower than that recommended in the Canadian Masonry Code (CSA S304-14). This difference in μ_{FR} values occurs because the friction coefficient in the Canadian Masonry Code, following the design shear friction equation discussed in Section 2.2, accounts for the combined effects of friction and dowel action. In contrast, this study proposes independent expressions for frictional and dowel action resistance, and therefore a lower value of friction coefficient μ_{FR} is proposed.

4.4.2 Dowel Action

An expression for estimating dowel action yield resistance is presented below. The coefficient of dowel action resistance, C_{DA}, is presented in equation 4.5 and developed based on recommended resistance parameters shown in Table 4.5.

$$DA_y = C_{DA} n_{db} A_{db} \sqrt{f'_g f_y} \tag{3.5}$$

$$C_{DA} = \begin{cases} 2.2, & H/L \leq 0.5 \\ \left[2.2 - 2\left(\frac{H}{L} - 0.5\right)\right], & 0.5 < H/L < 1.0 \\ 1.2, & H/L \geq 1.0 \end{cases} \tag{4.8}$$

The coefficient of C_{DA} is presented as a function of wall aspect ratio to reflect the variation in resistance observed in experimental data. For RM walls with aspect ratios of $H/L \leq 0.5$, the C_{DA} value is based on results of RM walls with fixed-fixed conditions; for aspect ratios of $H/L \geq 1.0$, the C_{DA} value is based on results of RM walls with cantilever conditions. For RM walls with aspect ratios between H/L = 0.5 and H/L = 1.0, dowel action resistance is determined as a linear interpolation between the corresponding C_{DA} values.

4.4.3 RM Wall Lateral Stiffness

This study proposes for calculating an RM wall's lateral stiffness, k_{shear}, to use the expression shown in equation 4.9. This was developed empirically by Shing et al. (1990), based on experimental tests on RM wall specimens and shows a good prediction of the experimental data used in this study.

$$k_{shear} = \left(0.2 + 0.1073\frac{P}{Lt}\right)k_e \tag{4.9}$$

$$k_e = \frac{E_m Lt}{2.4H(1+\upsilon)} \tag{4.10}$$

where:

k_e: elastic shear stiffness

k_{shear}: post-cracking shear stiffness

E_m: Elastic Modulus of Masonry

υ: Poisson ratio, (for Masonry, $\upsilon = 0.2$)

Figure 4.22 shows lateral stiffness values k_{shear} obtained through equation 4.9 versus results of experimental tests (Hernandez, 2012; Ahmadi, 2012). The reference line represents an ideal one-to-one match between prediction from equation 4.9 and the experimental results. As shown in Figure 4.22, the set of data points of k_{shear} follow the reference line with a linear correlation factor of 0.92.

4.5 Summary

A few key observations from this chapter are summarized below.

1. A modified MVLEM was proposed to simulate sliding shear displacements in RM walls. This model was based on the effects of frictional resistance, dowel action and flexural hinging.

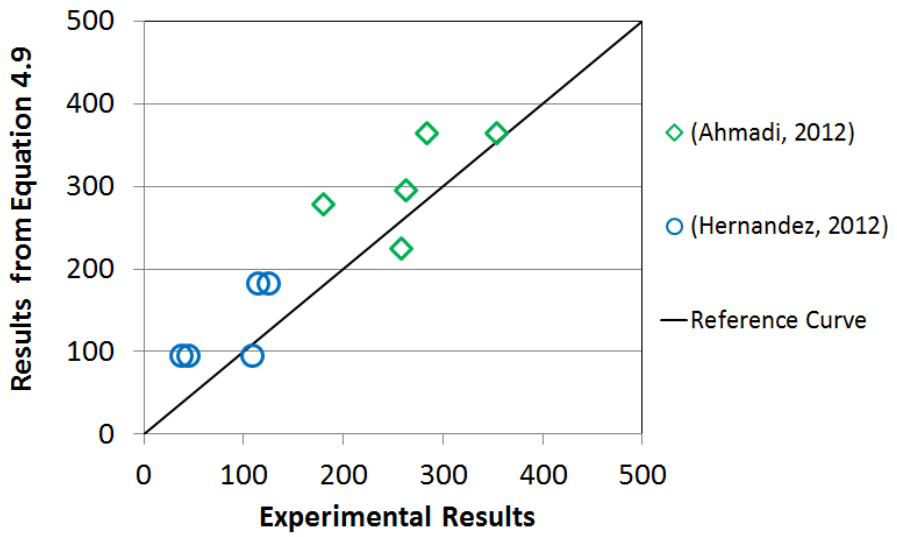

Figure 4.22 Estimation of RM wall lateral stiffness, k_{shear}, from equation 4.9 vs results from experimental data.

2. A calibration of the model parameters was performed using 10 different RM wall specimens, with variations in the following design parameters: shear span ratio, level of axial compression and vertical reinforcement ratio.

3. A set of calibration parameters for the model was determined based on the average adjusted values obtained from 10 individual calibrations.

4. The proposed model was found to be successful in simulating the sliding behaviour of an RM shear wall that experiences a sliding shear mechanism or a combined flexural-sliding shear mechanism.

Chapter 5: Nonlinear Static Analysis of RM Cantilever Walls – Monotonic Loading

5.1 Introduction

In this chapter, the calibrated model is used for studying the response of RM cantilever walls with flexural and sliding shear mechanisms subjected to increasing monotonic loading. The parameters used in the analyses include wall dimensions, properties of vertical steel reinforcement, masonry strength and axial compression level. The findings of these parametric studies will be used to develop an equation for sliding shear resistance, V_{SS}, of an RM cantilever wall as a function of its design parameters.

In these parametric studies, the friction force is separated into two forces: friction due to axial compression, Fr_A, and friction due to flexural compression, Fr_{Fl}. Therefore, the sliding shear resistance in equation 3.1 is modified to consider these two components as follows:

$$V_{SS} = Fr_A + Fr_{Fl} + DA_y \tag{5.1}$$

Where:

V_{SS}: Sliding shear resistance

Fr_A: Friction resistance due to axial compression

DA_y: Dowel Action yield strength

Fr_{Fl}: Friction resistance due to flexural compression

5.2 Pushover Analysis

In this study, the lateral force and displacement behaviour of RM walls subjected to monotonic loading is determined through pushover analyses. Each of these pushover tests determine the RM wall´s yield point and yield mechanism. For these pushover tests, monotonic loading is stopped upon reaching a maximum displacement of 45 mm.

The yield point in each pushover analysis is determined through the lateral force vs top displacement curve. This yield point corresponds to the point in which the curve's slope, k_i, becomes less than 10% of the initial slope, k_0. The yield point indicates the yield displacement, Δ_y, and lateral yield force, V_y, at which the RM wall develops its yield mechanism.

5.3 Characteristics of Yield Mechanisms

Two possible yield mechanisms for RM walls are considered in the following pushover analyses: a flexural mechanism and a sliding shear mechanism. These mechanisms will be illustrated in the following examples in Sections 5.3.1 and 5.3.2. The key parameters to be considered for these mechanisms are: flexural resistance, V_{Fl}, sliding shear resistance, V_{SS}, yield displacement, Δ_y, wall top displacement, Δ_{Top}, and base sliding displacement, Δ_{Base}.

5.3.1 Flexural Mechanism

As an example of a flexural yield mechanism during monotonic loading, the pushover test results of an RM wall model are presented in Figure 5.1. The RM wall's height to length aspect ratio, H/L, is 1.0 with a reinforcement ratio, ρ_v, of 0.2% and with an axial compression force, P, of 0 kN. The key design properties are presented in Table 5.1.

Table 5.1 Design properties of wall specimen with aspect ratio, H/L = 1.0

Wall dimensions	Reinforcement	Masonry Material Properties
Length = 3000 mm	Vertical: 12-10M bars	Masonry compression strength: f'_m =10 MPa
Height = 3000 mm	Grade 400 steel f_y = 400 MPa	Grout compression strength: f'_g = 35 MPa
Thickness = 190 mm	Reinforcement ratio ρ = 0.2%	

For the RM wall's sliding plane, the resistance parameters for friction and dowel action are determined using equations 4.7 and 4.8, respectively. For a wall with aspect ratio H/L = 1.0, these values result in a friction coefficient, μ_{Fr}, of 0.6 and dowel action yield coefficient, C_{DA}, of 1.2.

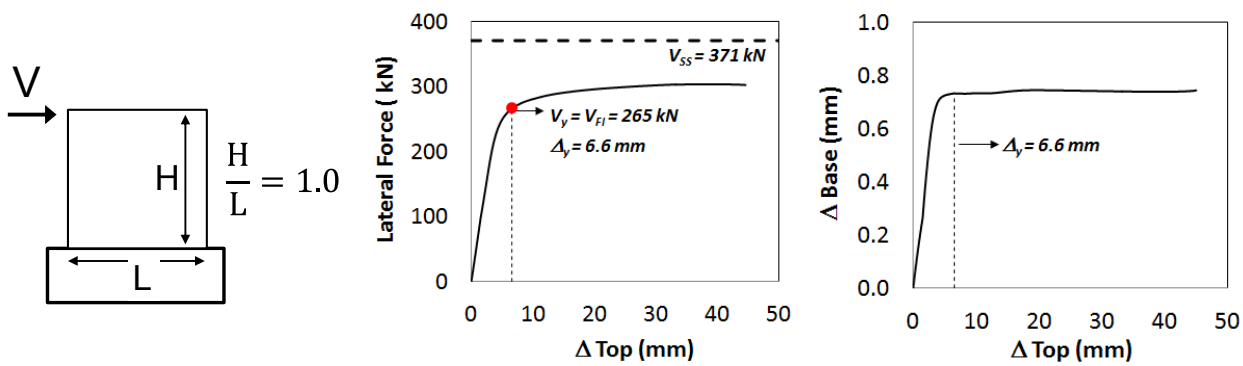

a) b) c)

Figure 5.1 Pushover analysis for an RM wall with H/L=1.0: a) Wall dimensions, b) Lateral force vs displacement, c) Top vs base displacement history.

The pushover analysis results indicated in Figure 5.1b show that the yield displacement, Δ_y, is equal to 6.6 mm and the lateral yield force, V_y, is equal to 265 kN. The yield mechanism corresponds to a flexural mechanism, where V_y is equal to the flexural resistance, V_{Fl}, and is less than the wall's sliding resistance, V_{SS}, of 371 kN. As monotonic loading continues, the wall's lateral resistance increases due to strain; and a lateral force, V, of 303 kN is reached.

Figure 5.1c indicates that the base sliding displacement, Δ_{Base}, is linearly proportional to the Δ_{Top} value when the RM wall's force vs displacement behaviour is elastic. When the RM wall yields in flexure, base sliding stops and reaches a maximum Δ_{Base} value of 0.7 mm. Therefore, as the displacement ductility demand, μ, increases from 1 to 2, the ratio $\Delta_{Base}/\Delta_{Top}$ referred to herein as "sliding ratio", decreases from 11 to 6%.

5.3.2 Sliding Shear Mechanism

As an example of a sliding shear mechanism during monotonic loading, the pushover test results of an RM wall model with H/L ratio of 0.5 are shown in Figure 5.2. The RM wall has a reinforcement ratio, ρ_v, of 0.2% and an axial compression force, P, of 0 kN. The key design properties are presented in Table 5.2.

Table 5.2 Design properties of wall specimen with aspect ratio, H/L = 0.5

Wall Dimensions	Reinforcement	Masonry Material Properties
Length = 6000 mm	Vertical: 24-10M bars	Masonry compression strength: f'_m =10 MPa
Height = 3000 mm	Grade 400 steel f_y = 400 MPa	Grout compression strength: f'_g = 35 MPa
Thickness = 190 mm	Reinforcement ratio ρ = 0.2%	

For the RM wall's sliding plane, the resistance parameters for friction and dowel action are determined following equation 4.7 and 4.8, respectively. For a wall with an H/L ratio of 0.5, these values result in a friction coefficient, μ_{Fr}, of 0.6 and dowel action yield coefficient, C_{DA}, of 2.2.

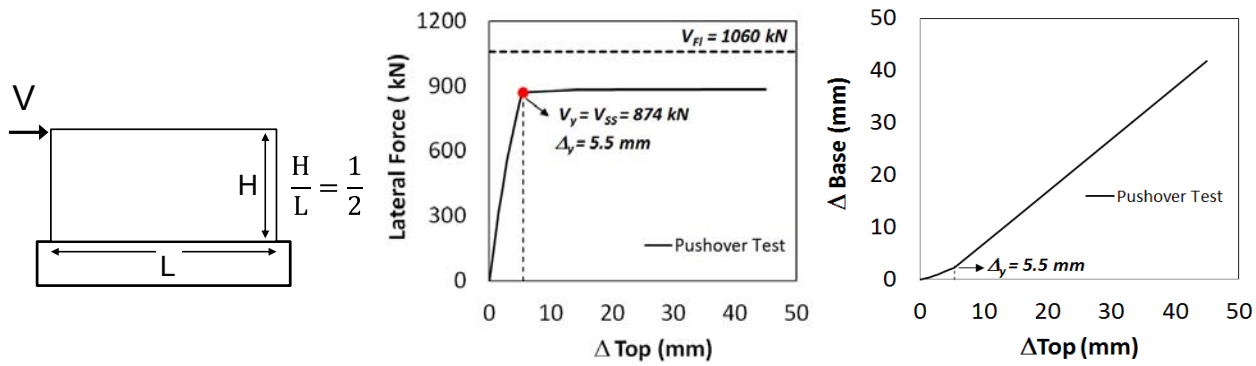

a) b) c)

Figure 5.2 Pushover analysis RM wall with H/L=0.5: a) Wall dimensions, b) Lateral force vs displacement, c) Top vs base displacement history.

In Figure 5.2b, the RM wall model's pushover curve shows that the yield displacement, Δ_y, is equal to 5.5 mm and the lateral yield force, V_y, is equal to 874 kN. The yield mechanism corresponds to a sliding shear mechanism; where V_y is equal to the sliding shear resistance, V_{SS}, and is less than the wall's flexural resistance, V_{Fl}, of 1060 kN.

After yielding takes place, the wall model displaces as a rigid body through base sliding. As shown in Figure 5.2c, the Δ_{Base} value increases proportionally with top lateral displacement, Δ_{Top}, during monotonic loading. Therefore, as the displacement ductility demand, μ, increases from 1 to 2, the sliding ratio, $\Delta_{Base}/\Delta_{Top}$, increases from 27 to 63%.

5.4 Parametric Study – Monotonic Loading

Results of pushover analyses on RM wall models are used to determine the critical design parameters that influence the development of an RM wall's yield mechanism. For each parametric study, one design property is varied, while others are kept constant. The key results

include the flexural resistance, V_{Fl}, sliding shear resistance, V_{SS}, and sliding displacement ratio, $\Delta_{Base}/\Delta_{Top}$.

The analytical models intend to simulate behaviour of RM shear walls with a given set of design parameters. In this study the wall height, H, is set equal to 3 m, and wall thickness, t, is 0.19 m, while the wall length, L, is varied to produce different values of aspect ratio, H/L. Material properties include masonry compression strength, f'_m, set to 10 MPa, and steel yield strength, f_y, set to 400MPa. The grout compression strength, f'_g, is set to 35 MPa, following grout strength properties shown in experiments (Hernandez, 2012; Ahmadi, 2012). The resistance parameters for friction and dowel action are determined following equations 4.7 and 4.8, respectively. The axial compression level, P/Asfy, is set equal to 0%. These properties are kept constant for all parametric studies, unless noted otherwise.

5.4.1 Wall Aspect Ratio (H/L)

This section presents a study on the influence of wall aspect ratio on an RM wall's sliding behaviour. This section is separated into two parts: a parametric study for various H/L ratios and a study on the relation between the RM wall's H/L ratio and the frictional resistance developed from flexural compression, Fr_{Fl}.

5.4.1.1 Parametric Study

The effect of the aspect ratio, H/L, on the RM wall's yield mechanism is studied through pushover analyses on RM wall models with H/L ratios less than 2.0. Each RM wall is modelled assuming 10M vertical reinforcing bars with the reinforcement ratio, ρ_v, of 0.2%.

The results show that RM walls with H/L ratios of less than 0.6 develop a sliding shear mechanism, while those with higher H/L ratios develop a flexural mechanism. This can also be proven by considering the relationship between the RM wall's yield mechanism and its sliding ratio for displacement ductility, μ, of 2. A sliding ratio, $\Delta_{\mathrm{Base}}/\Delta_{\mathrm{Top}}$, greater than 0.50 indicates that the RM wall's yield mechanism is a sliding shear mechanism (see Section 5.3.2); while a $\Delta_{\mathrm{Base}}/\Delta_{\mathrm{Top}}$ value less than 10% corresponds to a flexural mechanism (see Section 5.3.1).

Figure 5.3 shows the relationship between the RM wall's H/L ratio and the analysis results for sliding ratio, $\Delta_{\mathrm{Base}}/\Delta_{\mathrm{Top}}$, for a displacement ductility of μ of 2. This curve shows that for H/L ratios less than 0.5, the wall behaviour is governed by a sliding shear mechanism because sliding ratios are greater than 71%, while for H/L ratios greater than 0.6, wall behaviour is governed by a flexural mechanism since the sliding ratios are lower than 10%. The sliding ratio curve also shows a decrease in sliding ratios, from 71 to 12%, for H/L ratios increasing from 0.5 to 0.6. This range of H/L ratios develops a sliding shear mechanism in which the wall initially yields in flexure and develops a sliding shear mechanism after strain hardening (see Section 5.4.3).

In this study, the upper limit for an H/L ratio at which an RM wall develops a sliding shear mechanism is defined as Triggering Aspect Ratio #1 (TAR1). For these analyses, the TAR1 value is taken as 0.6. Sliding ratio vs H/L ratio curves are used herein to determine the influence of design parameters on the TAR1 value and the criterion for development of an SS mechanism.

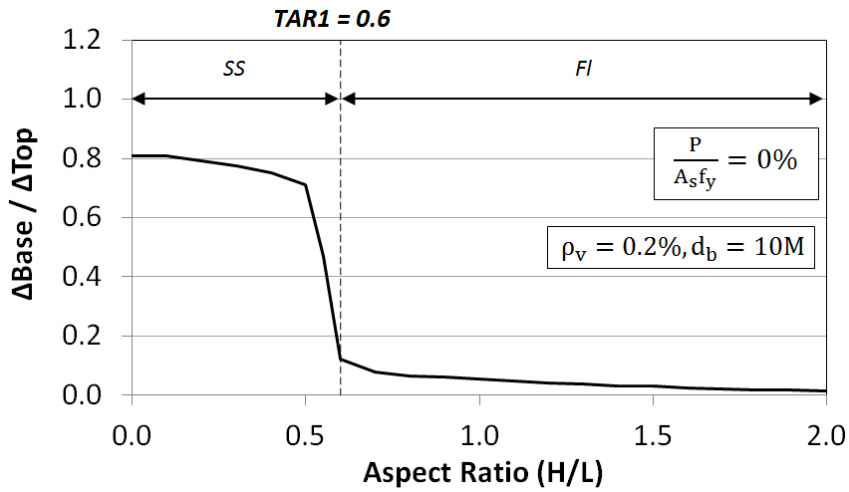

Figure 5.3 Sliding ratio vs H/L ratio at displacement ductility of μ=2.

Figure 5.4a shows the relation between RM walls' overturning moment at yield, and the H/L ratio. For RM walls with H/L ratios greater than 0.55, the normalized overturning moment, $M/A_s f_y L$, is constant at 0.53; while for RM walls with an H/L ratio less than 0.55, the normalized overturning moment is proportional to the wall's H/L ratio.

In Figure 5.4b, the curve of yield force, V_y, determined through pushover analyses indicates that the yield force of an RM wall is equal to the lesser of the wall's flexural resistance, V_{Fl}, and the wall's sliding shear resistance, V_{SS}. This statement is expressed through equation 5.2. For RM walls with H/L ratios less than 0.55, the sliding shear resistance, V_{SS}, is less than flexural resistance, V_{Fl}, whereas for walls with higher H/L ratios, the flexural resistance, V_{Fl}, is less than the sliding shear resistance, V_{SS}, thus:

$$V_y = \min(V_{Fl}, V_{SS}) \tag{5.2}$$

The values of yield force V_y, flexural resistance, V_{Fl}, and sliding shear resistances, V_{SS}, for each RM wall are divided by the reinforcement's tension resistance, $A_s f_y$, to obtain the yield

coefficient C_y and resistance coefficients, C_{Fl} and C_{SS}, as shown in equation 5.3. Curves of these resistance coefficients are plotted against the H/L ratio in Figure 5.5.

$$C_y = \frac{V_y}{A_s f_y} \qquad C_{SS} = \frac{V_{SS}}{A_s f_y} \qquad C_{Fl} = \frac{V_{Fl}}{A_s f_y} \tag{5.3}$$

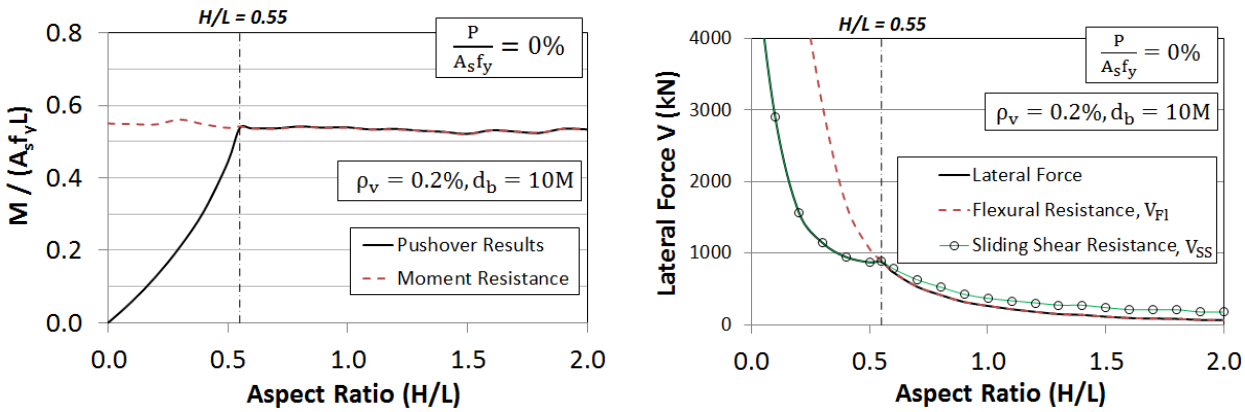

a) b)

Figure 5.4 Comparison of pushover results: a) Normalized overturning moment at yield vs H/L ratio, b) Lateral force at yield vs H/L ratio.

The flexural resistance coefficient, C_{Fl}, is inversely proportional to H/L, as shown in the C_{Fl} vs H/L curve in Figure 5.5. The C_{Fl} curve intersects the curve of sliding shear resistance coefficient, C_{SS}, at H/L = 0.55, which corresponds to the highest value in the C_y curve. For other wall aspect ratios, the value of C_y corresponds to the lower of the two resistance coefficients, (C_{SS} and C_{Fl}).

The coefficient of sliding shear resistance, C_{SS}, is shown to depend on the wall's H/L ratio because the sliding shear resistance, V_{SS}, is equal to the sum of the friction force due to flexural compression, Fr_{Fl}, and the dowel action strength, DA_y. These two forces develop different yield strengths depending on the wall's aspect ratio H/L, as illustrated in Figure 5.6. Therefore, the variation of C_{SS} for walls with H/L ratios less than 0.55 is due to effects of frictional resistance,

Fr_{Fl}; while variations for H/L ratios from 0.50 to 1.0 are due to effects of dowel action resistance, DA_y.

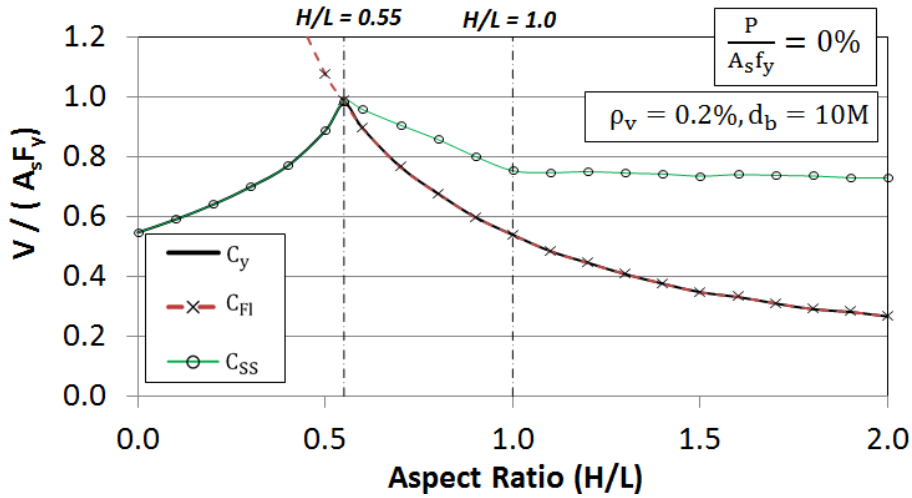

Figure 5.5 Resistance coefficient vs aspect ratio (H/L).

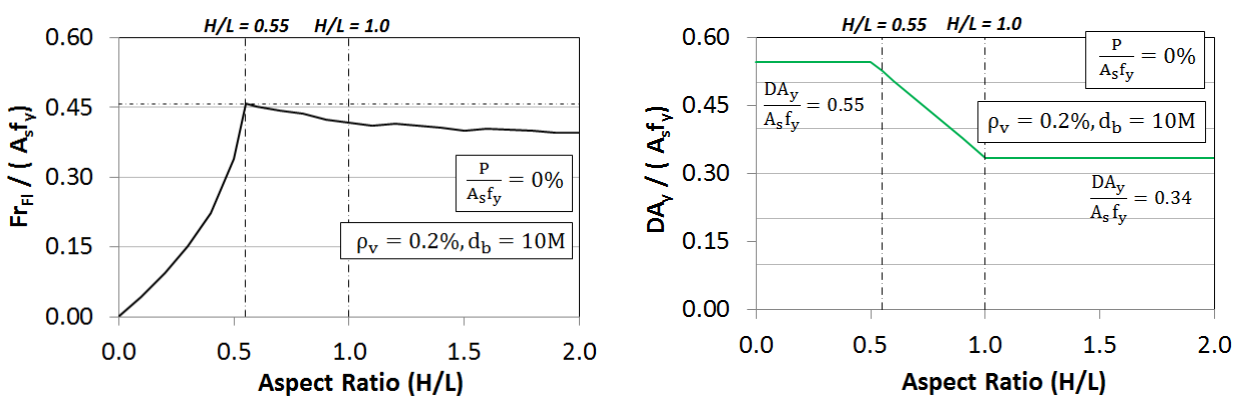

a) b)

Figure 5.6 Components of sliding shear resistance: a) Frictional resistance, b) Dowel action resistance.

5.4.1.2 Frictional Resistance Due to Flexural Compression as a Function of H/L Ratio

Lower values of frictional resistance, Fr_{Fl}, for walls with H/L ratios less than 0.55 can be explained by considering the internal strains, stresses and frictional resistances of two RM wall models analysed in the study with H/L ratios equal to 0.4 and 0.6. When the RM wall model with an H/L ratio of 0.4 develops its sliding shear mechanism, flexural behaviour is in the elastic

range and reinforcing bars do not yield in tension (see Figure 5.7a). As a result, the friction force Fr_{Fl} developed at the compression toe of the wall is equal to $0.22A_sf_y$. For the case of the RM wall model with an H/L ratio of 0.6, the yield mechanism is a flexural mechanism and therefore 73% of all reinforcing bars yield in tension, (see Figure 5.7b), and consequently the friction force Fr_{Fl} is equal to $0.45A_sf_y$. Therefore, as observed in these cases, the friction force developed through flexural compression depends on the ratio of rebars that yield in tension over the total number of rebars, (see equation 5.4).

$$Fr_{Fl} \propto \left(\frac{n_{db_y}}{n_{db}}\right) \tag{5.4}$$

Where:

Fr_{Fl}: frictional resistance due to flexural compression

n_{db}: total number of reinforcing bars

n_{db_y}: number of reinforcing bars that yield in tension

Based on the above observations, the upper bound value for frictional resistance corresponds to a case when an RM wall develops a flexural yield mechanism. Equation 5.5 enables estimation of the upper bound value, Fr_{Fl_U}, as a function of the length of the compression zone, c, and the bar spacing, s. The accuracy of this expression is later verified in the parametric studies for reinforcement ratio, ρ_v and level of axial compression, P/A_sf_y.

$$Fr_{Fl_U} = \mu_{Fr}\left[0.9\left(\frac{1-\frac{c}{L}-\frac{d'}{L}}{1+\frac{s}{L}-2\frac{d'}{L}}\right)\right]A_sf_y \tag{5.5}$$

Where:

Fr_{Fl_U}: upper bound of frictional resistance due to flexural compression

μ_{Fr}: Coefficient of friction

d': masonry cover

L: Wall length

s: vertical rebar spacing

c: depth of compression zone

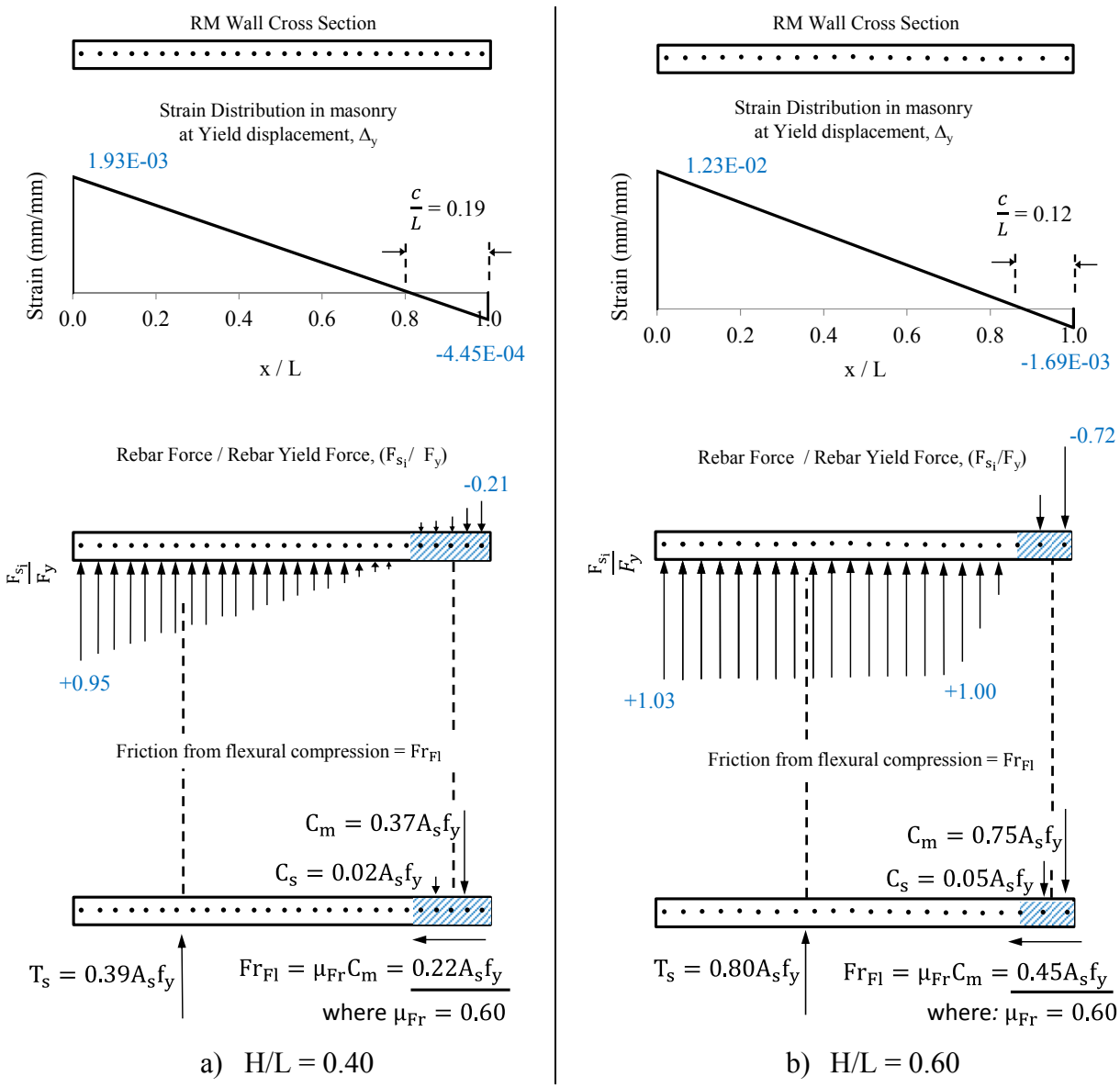

a) H/L = 0.40 b) H/L = 0.60

Figure 5.7 Internal strains and forces in RM walls with aspect ratios: a) H/L = 0.40 & b) H/L = 0.60.

The depth of the compression zone, c, can be determined from equation 5.6, which was developed by Cardenas and Magura (1973). This equation was recommended as part of the procedure for determining moment capacity of rectangular wall sections by Anderson and Brzev (2009). The c/L ratio can be determined as follows:

$$\frac{c}{L} = \frac{\omega + \gamma}{2\omega + \alpha_1\beta_1} \tag{5.6}$$

Where:

$$\omega = \frac{A_s f_y}{f'_m L t} \qquad \gamma = \frac{P}{f'_m L t}$$

$$\alpha_1 = 0.85 \qquad \beta_1 = 0.80$$

For RM walls that develop a sliding shear mechanism, the frictional resistance due to flexural compression, Fr_{Fl}, is only a fraction of the frictional resistance, Fr_{Fl_U}, expected for RM walls that develop a flexural mechanism. An expression is presented in equation 5.7 to model the friction force, Fr_{Fl}, based on the results shown in Figure 5.6a.

$$Fr_{Fl} = \left(\frac{H/L}{TAR1}\right)^2 Fr_{Fl_U} \quad \leq Fr_{Fl_U} \tag{5.7}$$

The frictional resistances, Fr_{Fl_U} and Fr_{Fl}, obtained using equations 5.5 and 5.7, respectively, are compared in Figure 5.8 against the frictional resistance determined through pushover analysis. This comparison shows that the proposed equations are able to capture the variation of frictional resistance due to wall aspect ratio, H/L.

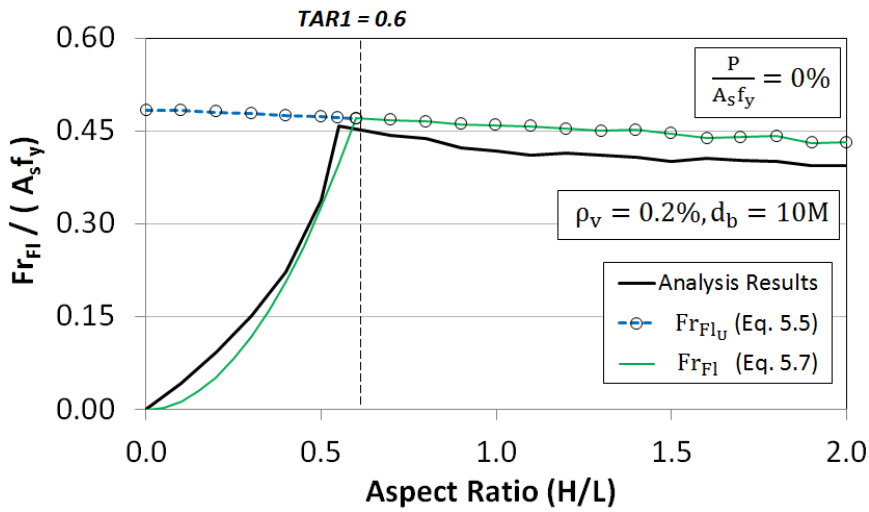

Figure 5.8 Frictional resistance vs aspect ratio, H/L – proposed equations vs analysis results.

5.4.2 Wall Height (H)

A parametric study of wall height, H, is performed to determine the variation of sliding behaviour for RM walls with larger dimensions. The analysis results for H values of 2, 3, 4.5, and 6 m are presented in Figure 5.9.

The value of sliding ratio, $\Delta_{Base}/\Delta_{Top}$, shows that sliding ratio decreases with an increase in wall height, H. Although Δ_{Top} and Δ_{Base} share a direct relation to height, H, Δ_{Top} increases at a steeper rate with respect to H than Δ_{Base}, as shown in Figure 5.10. As a result, the expected sliding ratio, $\Delta_{Base}/\Delta_{Top}$, of an RM wall decreases for higher height values.

The curve of yield coefficient, C_y, is shown not to be sensitive to the H value, as shown in Figure 5.9b. Similarly, the triggering aspect ratio, TAR1, is also not influenced by wall height, H.

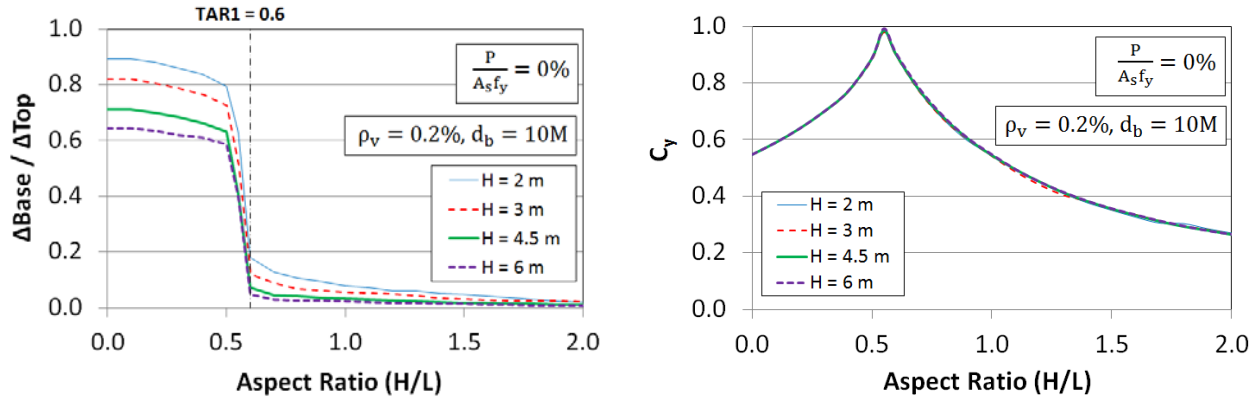

a) b)

Figure 5.9 Effect of wall height: a) Sliding ratio vs aspect ratio (H/L), at μ=2, b) Yield coefficient vs aspect ratio (H/L).

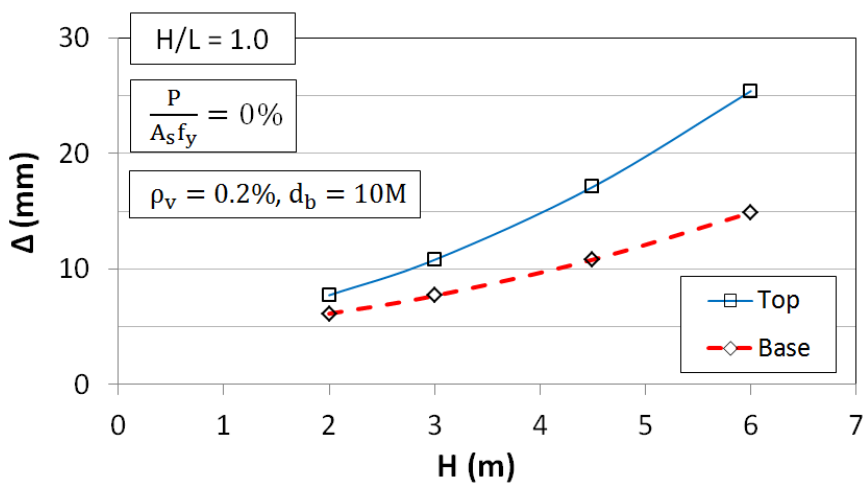

Figure 5.10 Maximum wall displacements in RM walls with H/L=1.0 at μ=2, for different wall heights, H.

5.4.3 Displacement Ductility (μ)

Parametric studies varying the displacement ductility, μ, show that the wall's sliding ratio depends on its yield mechanism, as illustrated in Figure 5.11. In RM walls with H/L ratios less than TAR1, (RM walls which experience a sliding shear mechanism), the sliding ratio increases as the displacement ductility, μ, increases from 1 to 4. However, an opposite effect is observed in walls with H/L ratios greater than TAR1, (RM walls which experience a flexural mechanism),

where the sliding ratios decrease as the μ value increases. This behaviour is illustrated in Figure 5.11 by highlighting the sliding ratio values for H/L ratios of 0.55 and 0.60 for different ductility demands, μ.

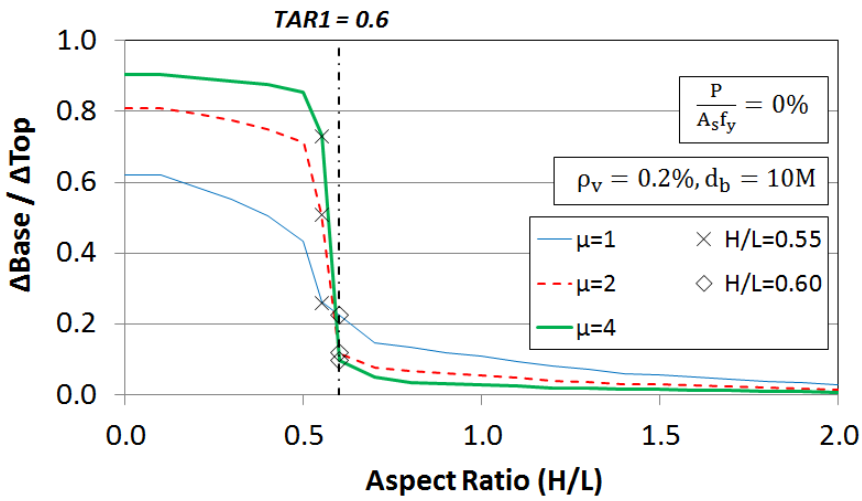

Figure 5.11 Sliding ratio vs aspect ratio (H/L), at μ=2, for different displacement ductility values, μ.

Normalized lateral resistance values, V/A_sf_y, are shown in Figure 5.12 corresponding to μ values of 1, 2 and 4. For RM walls with H/L ratios less than 0.53, the V/A_sf_y values are constant with respect to the ductility demand, μ. However, for RM walls with H/L ratios greater than 0.53, the lateral force resistance increases with the displacement ductility, μ, as a result of strain hardening effects in flexural yielding. This increase in V/A_sf_y value due to strain hardening is observed to lead into the development of a sliding shear mechanism in RM walls with H/L ratios between 0.53 and 0.60, as shown in Figure 5.13.

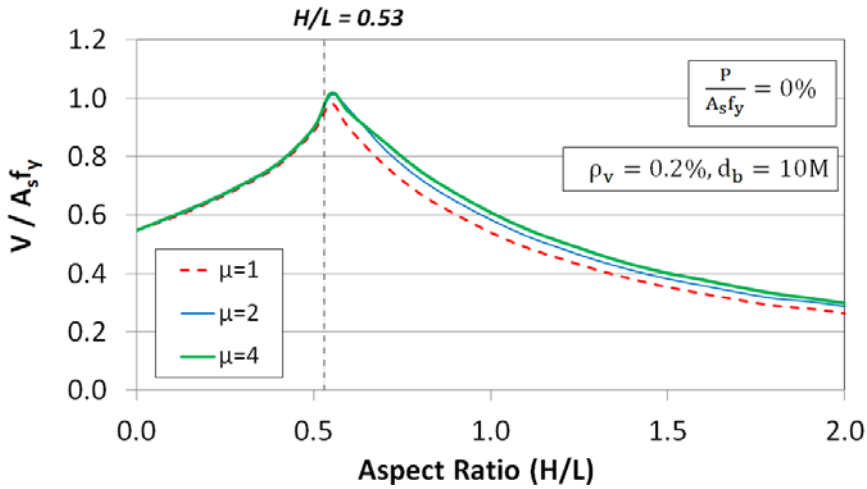

Figure 5.12 Normalized resistance vs aspect ratio (H/L) for different displacement ductility values, μ.

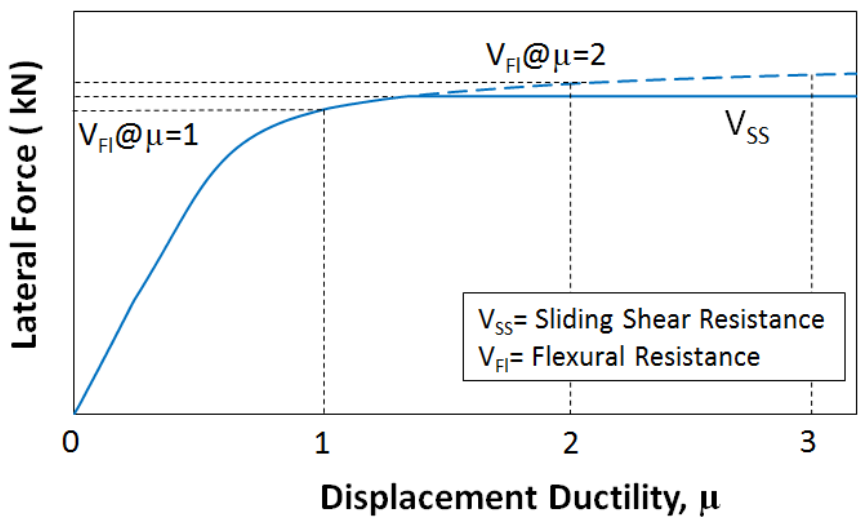

Figure 5.13 Development of a sliding shear mechanism due to strain hardening.

As illustrated in Figure 5.13, at a displacement ductility of μ = 1, the flexural resistance, V_{Fl}, is lower than the sliding shear resistance, V_{SS}, therefore the RM wall develops a flexural mechanism. However, as the wall's ductility demand increases, strain hardening causes the V_{Fl} value to become greater than the V_{SS} value and as a result, the yield mechanism changes to a sliding shear mechanism. This indicates that to predict the yield mechanism for an RM wall with a ductile behaviour (μ values greater than 1), the sliding shear resistance, V_{SS}, should be

compared to a flexural resistance, V_{Fl}, value which includes the effects of strain hardening at a displacement ductility, μ, value equal to or higher than 2.

5.4.4 Vertical Reinforcement Ratio (ρ_v)

Pushover analyses are performed on RM walls with vertical reinforcement ratios, ρ_v, of 0.1, 0.2 and 0.3%. The results of yield coefficient, C_y, and sliding ratio, $\Delta_{Base}/\Delta_{Top}$, for different H/L ratios are shown in Figure 5.14.

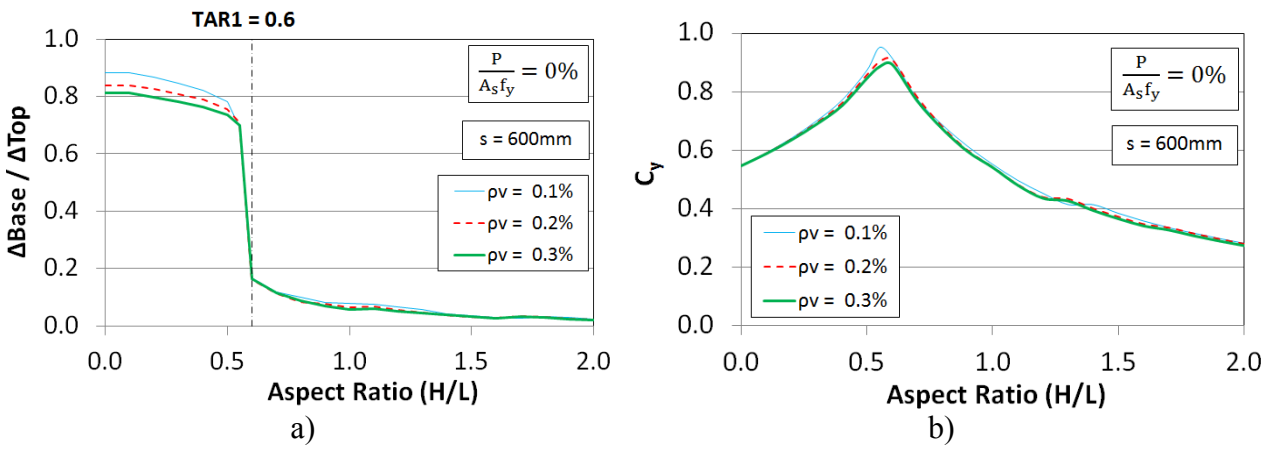

Figure 5.14 Effect of vertical reinforcement ratio (ρ_v): a) Sliding ratio vs aspect ratio (H/L), at μ=2, b) Yield coefficient vs aspect ratio (H/L).

The sliding ratio, $\Delta_{Base}/\Delta_{Top}$, for H/L ratios less than TAR1 is shown to decrease as the reinforcement ratio, ρ_v, increases from 0.1 to 0.3%. In contrast, for walls with H/L ratios greater than TAR1, the sliding ratio is not affected by the ρ_v value.

The results of analysis shown in Figure 5.14a also show that the TAR1 value is not influenced by the reinforcement ratio, ρ_v. For all three ρ_v values, the TAR1 value is equal to 0.60.

Figure 5.14b shows that the yield coefficient, C_y, value is influenced by the reinforcement ratio, ρ_v, when the H/L ratio is close to TAR1. However, for other H/L values, C_y does not depend on the ρ_v value.

The upper bound frictional resistance, Fr_{Fl_U}, values are determined for ρ_v values ranging from 0.05 to 0.35%, at their corresponding TAR1 value. These Fr_{Fl_U} values are compared with the values obtained from equation 5.5, as shown in Figure 5.15. These results show that equation 5.5 provides a satisfactory match for the pushover analysis results and it can be used to estimate the upper bound frictional resistance due to flexural compression, Fr_{Fl_U}.

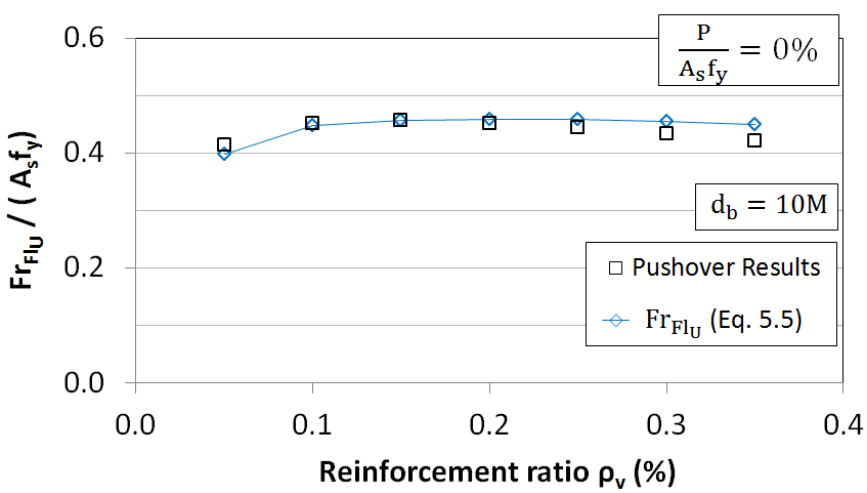

Figure 5.15 Upper bound frictional resistance due to flexural compression vs vertical reinforcement ratio (ρ_v).

5.4.5 Vertical Reinforcement Spacing (s)

Pushover analyses are performed on RM shear walls with reinforcement spacing, s, values of 400, 600 and 800 mm. A constant reinforcing bar size of 10M is used for all analyses.

Figure 5.16a shows variation in sliding ratios depending on the H/L ratio. The variation in the TAR1 value indicates that the reinforcement spacing influences the development of a sliding shear mechanism in RM walls. The TAR1 value is equal to 0.6 for values of 400 and 600 mm; and 0.7 for s values of 800 mm.

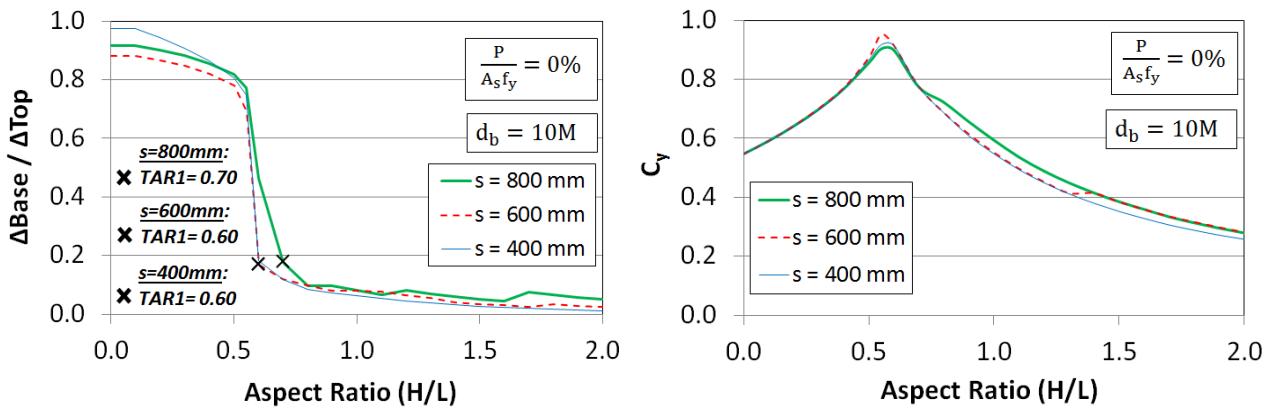

a) b)

Figure 5.16 Effect of vertical reinforcement spacing (s): a) Sliding ratio vs aspect ratio (H/L), at μ=2, b) Yield coefficient vs aspect ratio (H/L).

Figure 5.16b shows the relation between yield coefficient, C_y, and H/L ratio. The results suggest that rebar spacing has a moderate effect on the yield coefficient of RM walls that develop a flexural yielding mechanism. A maximum increase in C_y value of 9% occurs when the rebar spacing increases from 600 to 800 mm.

5.4.6 Diameter of Reinforcing Bar (d_b)

The results for RM wall models showing the effect of reinforcing bar diameters, d_b, equal to 10M (11 mm), 15M (16 mm) and 20M (19 mm), are presented in Figure 5.17. For this study, the reinforcing spacing parameter is kept constant at 400 mm, in order to establish the effect of rebar diameter on sliding behaviour, independent from rebar spacing.

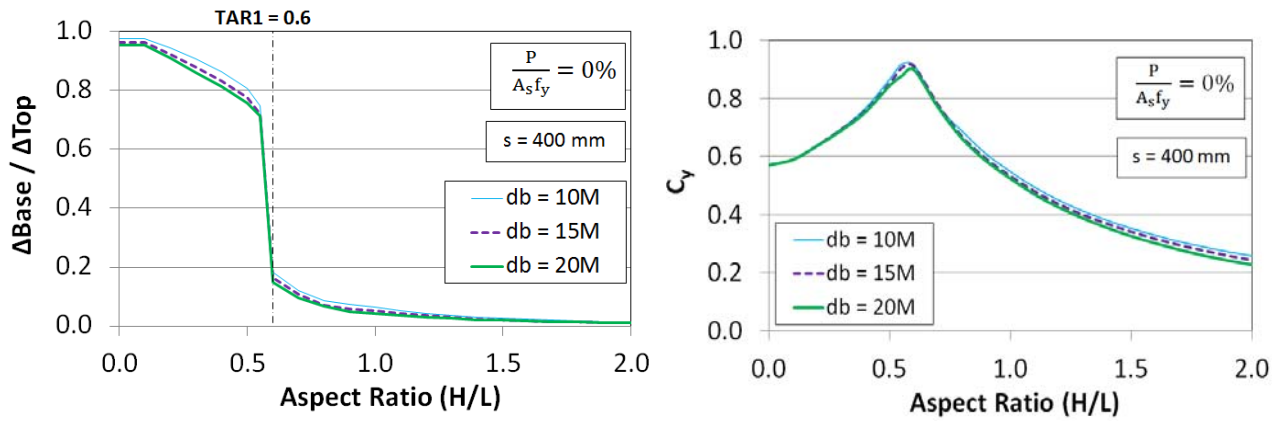

a) b)

Figure 5.17 Effect of vertical reinforcement diameter (d_b): a) Sliding ratio vs aspect ratio (H/L), at μ=2, b)Yield coefficient vs aspect ratio (H/L).

The results in Figure 5.17 show that sliding ratio and yield coefficient, C_y, values are not dependent on the d_b values. Differences in results are determined to be within a 5% range.

These results also show that the TAR1 value is equal to 0.60 irrespective of reinforcing bar diameter. This finding indicates that the reinforcing bar diameter does not influence the sliding shear behaviour.

5.4.7 Masonry Compression Strength (f'_m)

Masonry compression strengths, f'_m, of 5, 10 and 15 MPa are used in this parametric study. The results of the analysis are presented in Figure 5.18.

The sliding ratio curve shown in Figure 5.18a indicates that the f'_m value has a moderate influence on the sliding ratio in RM walls, with differences in the range of 10% between f'_m

values of 10 MPa and 5 MPa. These results also show that the TAR1 value is independent of the f'$_m$ value.

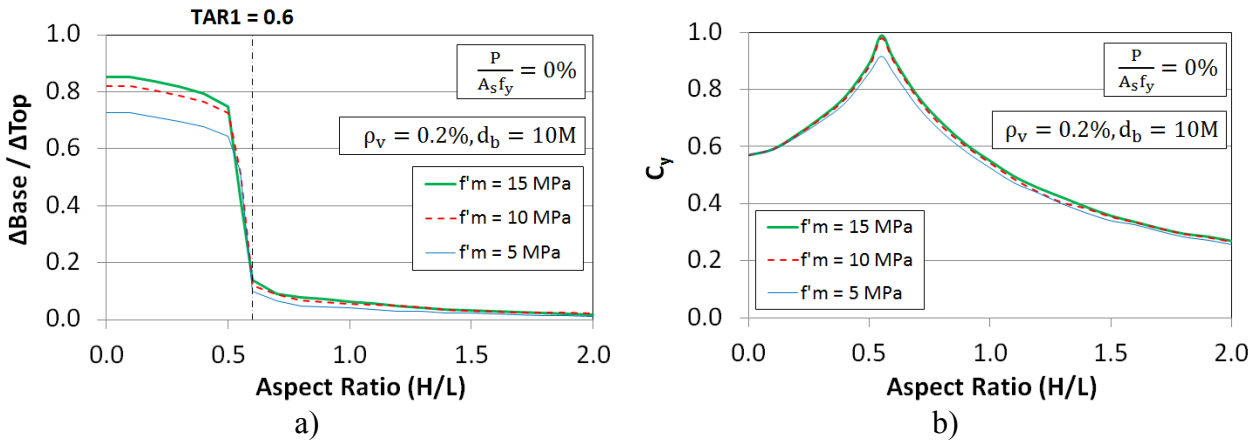

Figure 5.18 Effect of masonry compression strength, f'$_m$: a) Sliding ratio vs aspect ratio (H/L), at μ=2, b)Yield coefficient vs aspect ratio (H/L).

The curves of yield coefficient, C_y, in Figure 5.18b show that f'$_m$ has a minor influence on the yield coefficient, C_y. The highest variation in C_y value is of 6%, corresponding to variation in f'$_m$ values from 5 to 10 MPa.

5.4.8 Grout Compression Strength (f'$_g$)

This study examines the effects of grout compression strength, f'$_g$, on sliding behaviour. Three grout strengths values are considered: 5, 15 and 35 MPa, representing low, medium and high strength values, respectively. In this study, the grout compression strength, f'$_g$, is assumed to be independent of masonry compression strength, f'$_m$, which is set at 10 MPa.

The relationship between sliding ratio and H/L ratio presented in Figure 5.19a, shows the influence of grout compression strength, f'$_g$, on the TAR1 value and the development of a sliding shear mechanism. These results show that f'$_g$ has an inverse relation with regards to the TAR1

value. As the grout compressive strength, f'$_g$, increases from 5 to 35 MPa, the TAR1 values decrease from 1.1 to 0.6. It is also observed that in RM walls with H/L ratios less than TAR1, the sliding ratios, $\Delta_{Base}/\Delta_{Top}$, decrease as the f'$_g$ values increase.

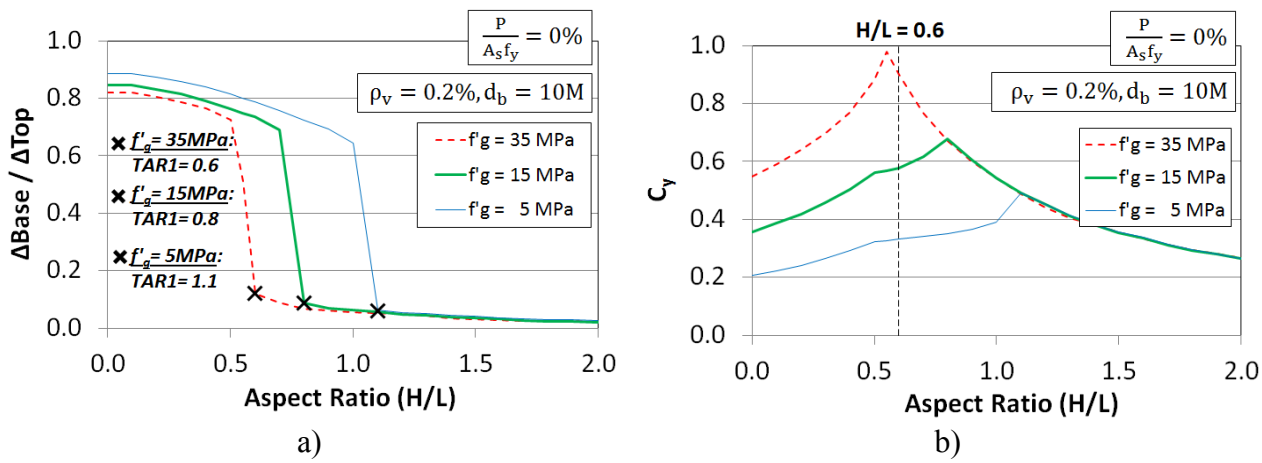

Figure 5.19 Effect of grout compression strength f'$_g$: a) Sliding ratio vs aspect ratio (H/L), at μ=2, b)Yield coefficient vs aspect ratio (H/L).

Figure 5.19b indicates that the f'$_g$ value has a significant influence on the yield coefficient, C_y, for RM walls. The curve of yield coefficient, C_y, shows that for H/L ratios less than TAR1, higher f'$_g$ values result in higher yield coefficient values (see Figure 5.19b). In the case of an RM wall with H/L ratio equal to 0.6, an increase in f'$_g$ value from 15 to 35 MPa results in an increase in C_y value of 56%. However, for H/L ratios greater than TAR1, values of C_y remain constant irrespective of the f'$_g$ value.

The influence of grout compression strength on the sliding ratio and yield coefficient of an RM wall is due to its relation with regards to dowel action resistance, DA_y, as shown in equation 3.5. Figure 5.20a indicates that, for all H/L ratios, an increase in the f'$_g$ value from 5 to 35 MPa results in an increase in DA_y value by a factor of 2.6.

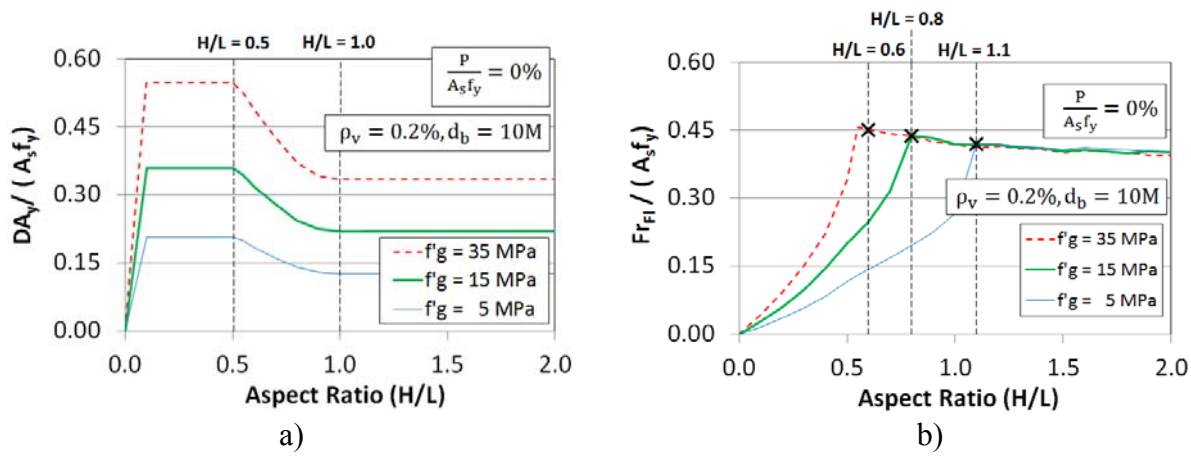

Figure 5.20 Effect of grout compression strength, f'$_g$: a) Dowel action resistance vs aspect ratio (H/L), b) Frictional resistance vs aspect ratio (H/L).

Grout compression strength, f'$_g$, also has an indirect influence on the frictional resistance, Fr_{Fl}, in RM walls that develop a sliding shear mechanism (H/L ratios less than TAR1). This occurs because the TAR1 value is influenced by f'$_g$ and this affects the Fr_{Fl} value, as shown in equation 5.7. However, the frictional resistance is shown to be independent of the grout compression strength, f'$_g$, when an RM wall develops a flexural mechanism (H/L ratios greater than TAR1).

5.4.9 Steel Yield Strength (f_y)

Analyses are performed on RM wall models using steel yield strength values, f_y, of 350, 400 and 500 MPa. It can be seen from the curve of sliding ratio vs H/L ratio shown in Figure 5.21a that the f_y value has a minor influence on the value of sliding ratio, $\Delta_{Base}/\Delta_{Top}$. These curves also show that f_y has a minimal influence on the TAR1 value, where TAR1 is equal to 0.55 for f_y values of 350 MPa; and equal to 0.60 for f_y values of 400 MPa and 500 MPa, respectively.

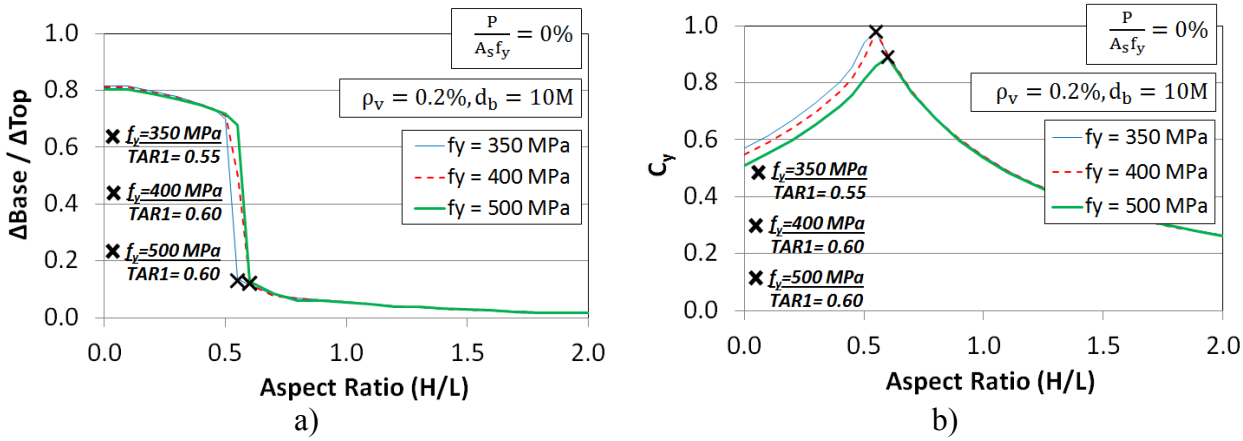

Figure 5.21 Effect of steel yield strength: a) Sliding ratio vs aspect ratio (H/L), at μ=2, b)Yield coefficient vs aspect ratio (H/L).

The C_y curve in Figure 5.21b shows that for H/L ratios less than TAR1, an increase in steel reinforcement strength, f_y results in a lowers C_y value. As the f_y value is increased from f_y of 350 MPa to 500 MPa, the C_y coefficient decreases from 0.98 to 0.86, which corresponds to a reduction of 13%. However, for H/L ratios greater than H/L, the C_y coefficient is not influenced by the f_y value.

5.4.10 Axial Compression Level (P/A_sf_y)

This parametric study models the effects of axial compression on the sliding behaviour of RM walls. The axial compression levels, P/A_sf_y, considered are 0%, 25%, 50% and 100%.

For this study, the axial compression forces are modeled as a fraction of the vertical reinforcement's resistance, A_sf_y, instead of the masonry material's compression resistance, f'_mA_g. The P/A_sf_y ratio is chosen for this study because it influences the plastic moment, M_p, of RM walls (see Section 5.5.1), as well as the development of a CFSS mechanism (see Section 3.4.2).

It can be seen from the curves of yield coefficient, C_y, vs H/L ratio in Figure 5.22 that higher axial compression levels, P/A_sf_y, result in higher C_y values for all values of H/L ratio. This result occurs because axial compression has a significant effect on the sliding shear resistance as well as the flexural resistance.

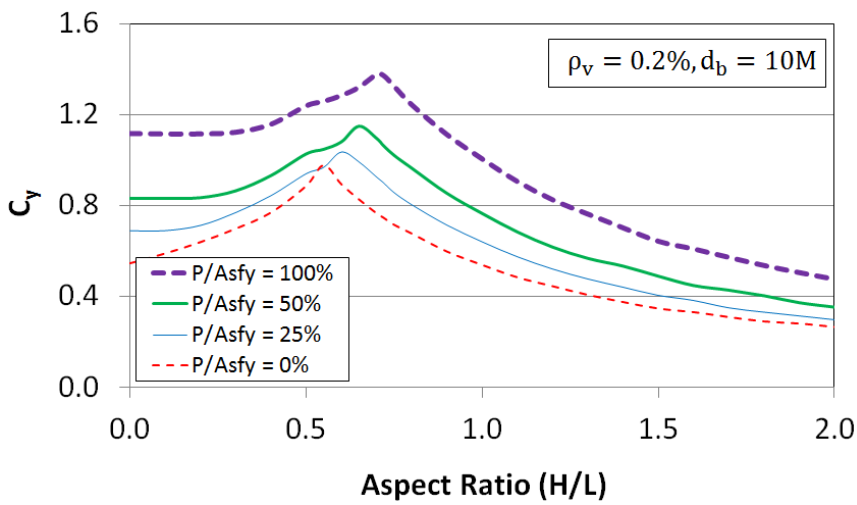

Figure 5.22 Yield coefficient vs aspect ratio (H/L). for different axial compression levels, P/A_sf_y.

Figure 5.23 shows the normalized values of flexural resistance, V_{Fl}/A_sf_y, and sliding shear resistance, V_{SS}/A_sf_y, for an RM wall subjected to different axial compression levels, P/A_sf_y. For instance, when the axial compression level is close to 0%, V_{SS}/A_sf_y is higher than V_{Fl}/A_sf_y, which results in a flexural yield mechanism. However, for axial compression levels of more than 12%, this trend is reversed and V_{SS}/A_sf_y becomes lower than V_{Fl}/A_sf_y; this results in the RM wall experiencing a sliding shear yielding mechanism. These results show that a change in axial compression level, P/A_sf_y, can affect the RM wall's expected yield mechanism from a flexural mechanism to a sliding shear mechanism.

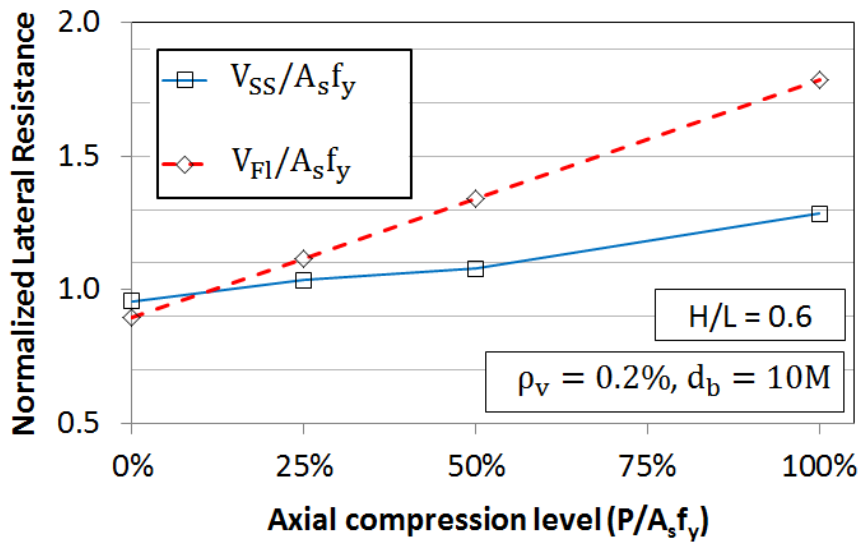

Figure 5.23 RM wall resistance vs axial compression level, for RM wall with an H/L ratio of 0.6.

Figure 5.24 shows the relation between the sliding ratios and axial compression levels in RM walls. When a variation in P/A_sf_y changes an RM wall's yield mechanism from flexural mechanism to sliding shear mechanism, the wall's sliding ratio increases by approximately 430%. However, when variations in P/A_sf_y do not affect the yield mechanism, differences in the sliding ratio are within a 3% range.

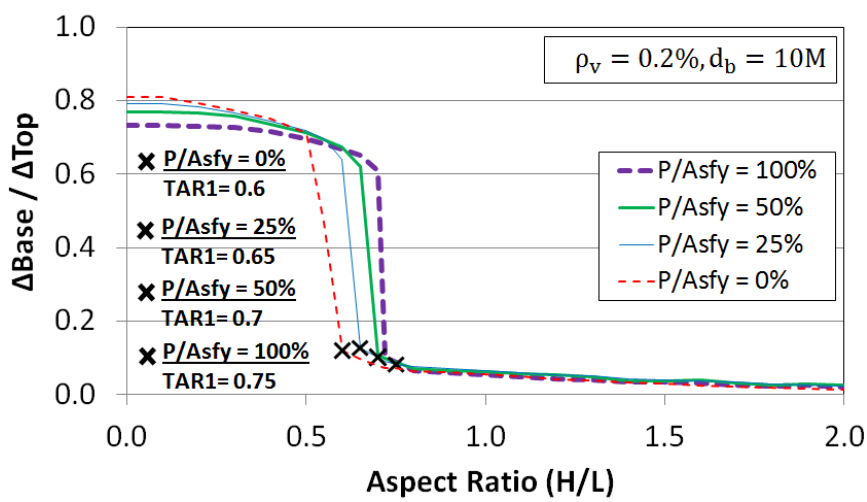

Figure 5.24 Sliding ratio vs H/L ratio at displacement ductility of μ=2, for different axial compression level, P/A_sf_y.

This study also shows that the axial compression level, P/A_sf_y, influences the upper bound frictional resistance developed due to flexural compression, Fr_{Fl_U}. Figure 5.25 illustrates the normalized results of the frictional resistance, $\frac{Fr_{Fl_U}}{A_sf_y}$, vs axial compression level, P/A_sf_y, for a constant reinforcement ratio, ρ_v, of 0.2%. This curve shows that the $\frac{Fr_{Fl_U}}{A_sf_y}$ value decreases as the axial compression level increases. Figure 5.25 also shows that the proposed equation predicts similar results as those determined through pushover analysis.

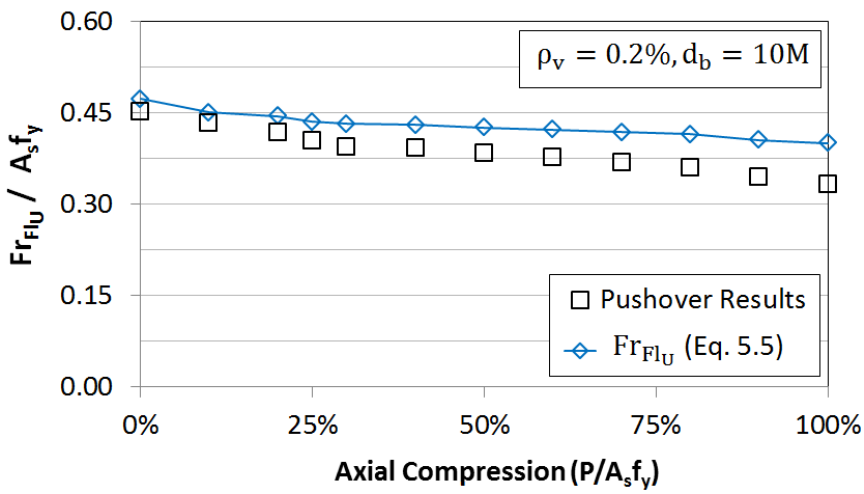

Figure 5.25 Normalized upper bound frictional resistance due to flexural compression for various axial compression levels, (P/A_sf_y).

5.4.11 Summary of Results of Parametric Studies

From the results of the parametric studies, the design parameters have a different extent of influence upon the sliding shear response parameters: i) TAR1, ii) sliding shear resistance coefficient, C_{SS}, and iii) flexural resistance coefficient, C_{FL}. A summary of the results of the parametric studies is presented in Table 5.3. This table indicates the design parameters that showed low, moderate and high influence on the sliding shear response parameters. A low influence refers to a variation of less than 5% between consecutive design parameters; moderate

influence to a variation of between 5% and 20%; and high influence for a variation greater than 20%.

Table 5.3 Design parameters that influence SS parameters in RM walls

Design Parameters	TAR1	C_{SS}	C_{Fl}	Development of SS Mechanism
H/L	N/A	●	●	●
H	○	○	○	○
μ	◑	○	◑	◑
ρ_v	○	○	○	○
s	◑	○	◑	◑
d_b	○	○	○	○
f'_m	○	◑	◑	○
f'_g	●	●	○	●
f_y	◑	◑	○	◑
P/A_sf_y	◑	●	●	◑

● High influence: Variations greater than 20%.
◑ Moderate influence: Variations ranging from 5% to 20%.
○ Low influence: Variations lower than 5%.

Table 5.3 indicates that an RM wall's H/L ratio has a high influence on all sliding shear response parameters, irrespective of wall height, H. The displacement ductility, μ, reflects the effects of strain hardening and as a result shows a medium influence on the flexural resistance coefficient, C_{FL}, and a low influence on sliding shear resistance coefficient, C_{SS}. Vertical reinforcement spacing, s, is shown to have a medium influence on TAR1 value due to its relation with frictional resistance, Fr_{Fl}. Grout compression strength, f'_g, has a high influence on the C_{SS} and TAR1 values as a result of its influence on dowel action yield resistance, DA_y. Steel yield strength, f_y, also influences DA_y, however, for the range of f_y values to be expected in construction practice, it has only a medium influence on C_{SS} and TAR1 values. Masonry compression strength, f'_m,

showed a low influence on TAR1 and C_{Fl} values and a medium influence on C_{SS} value. Axial compression level, $P/A_s f_y$, has a high influence on lateral resistance coefficients C_{SS} and C_{Fl} and a medium influence on the TAR1 value.

From the design parameters considered, only the vertical reinforcement ratio, ρ_v, and the reinforcing bar diameter, d_b, showed low influences on all sliding shear response parameters. These results indicate that in the design of an RM wall, the development of a sliding shear mechanism cannot be altered by varying the vertical reinforcement ratio, ρ_v, nor the diameter of reinforcing bars, d_b; this is consistent with observations made by Anderson and Brzev (2009) on design solutions for a sliding shear mechanism.

5.5 Flexural and Sliding Shear Resistance: Proposed Equations

The yield mechanism of an RM wall can be estimated by determining the lower resistance value between the wall's flexural resistance, V_{Fl}, and the wall's sliding shear resistance, V_{SS}. This section proposes design expressions for these two resistances and for the triggering aspect ratio value, TAR1.

5.5.1 Flexural Resistance, V_{Fl}

In an RM wall, its flexural resistance, V_{Fl}, is proportional to the plastic moment, M_p, developed at the base of the wall, as illustrated in Figure 5.26. The relation between V_{Fl} and M_p is shown in equation 5.8.

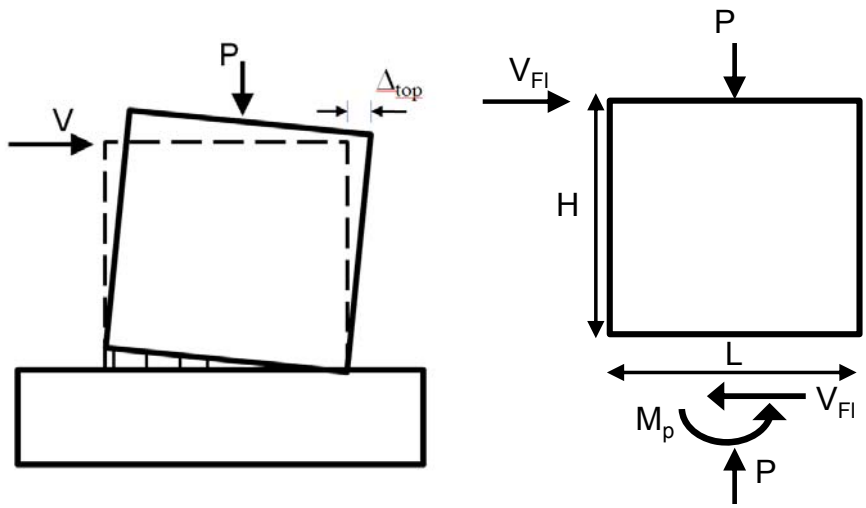

a) b)

Figure 5.26 Flexural resistance a) RM wall develops flexural yield mechanism, b) Development of plastic moment, M_p.

$$V_{Fl} = \frac{M_p}{H} \tag{5.8}$$

The expression for an RM wall's plastic moment, M_p, has been determined through curve fitting using results from various parametric studies, as shown in equation 5.9:

$$M_p = [C_p] A_s f_y L \tag{5.9}$$

where

$$C_p = \left[0.6\left(1 + \frac{5}{6}\frac{P}{A_s f_y}\right)\left(1 - \frac{c}{L}\right)\left(\mu^{1/15}\right)\right] \tag{5.10}$$

Figure 5.27 shows plastic moment coefficient, C_p, obtained from equation 5.10 paired with results of analysis using the 2D model. The analysis results include data of RM walls that yield in flexure from the parametric studies for reinforcement ratio, ρ_v, vertical reinforcement spacing, s, axial compression level, $P/A_s f_y$ and displacement ductility, μ. The reference line represents an

ideal one-to-one match between prediction from equation 5.10 and the result of the 2D model. Data points for C_p follow the reference line closely. The correlation factor between these values is determined to be 0.97.

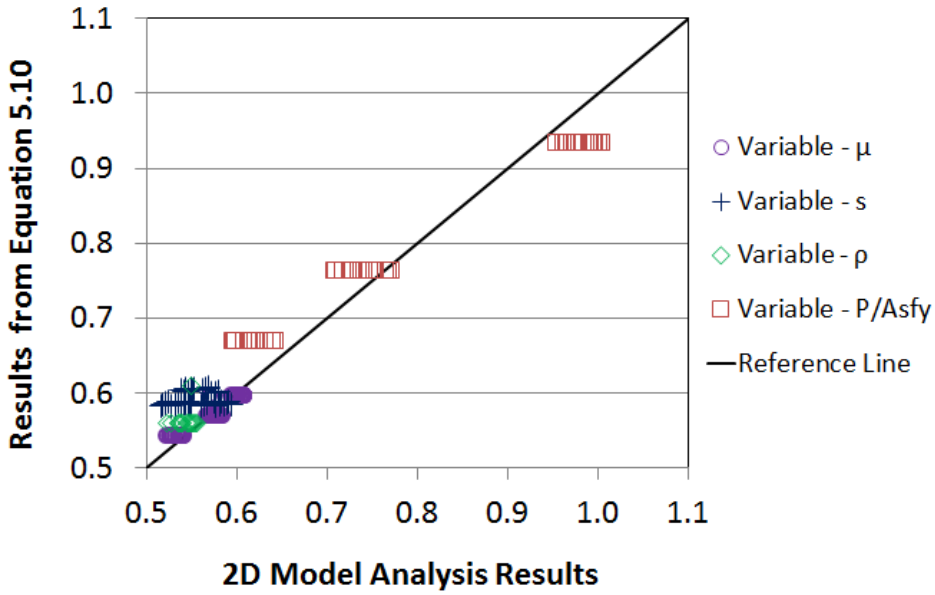

Figure 5.27 Plastic moment coefficient, C_p, results from equation 5.10 vs results from pushover analysis.

Figure 5.28 shows a comparison of two curves of plastic moment, M_p, vs. displacement ductility, μ, in which one curve increases due to strain hardening and the other has a constant plastic moment resistance after a displacement ductility μ greater than 1. This comparison shows that the M_p value at a μ of 2 can be used to represent the average effect of strain hardening for μ values ranging from 1 to 4. This approach allows for a simplification of equation 5.9 to equation 5.11 as follows:

$$C_p = \left[0.63\left(1 + \frac{5}{6}\frac{P}{A_s f_y}\right)\left(1 - \frac{c}{L}\right)\right] \tag{5.11}$$

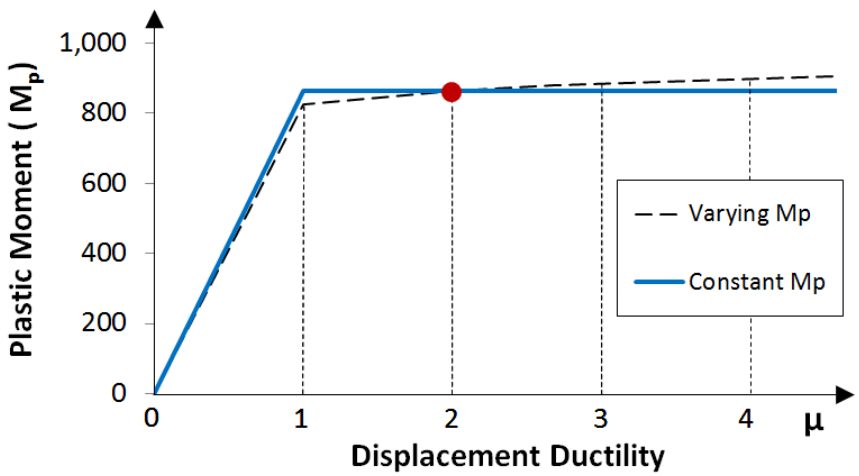

Figure 5.28 Curve of plastic moment, M_p, vs displacement ductility, μ.

5.5.2 Upper Bound Sliding Shear Resistance, V_{SS_U}

RM walls that experience a flexural mechanism develop an upper bound sliding resistance, V_{SS_U}, in which the frictional resistance developed from flexural compression is equal to the upper bound frictional resistance, Fr_{Fl_U}. The upper bound sliding shear resistance can be determined through equation 5.12.

$$V_{SS_U} = Fr_A + Fr_{Fl_U} + DA_y \tag{5.12}$$

where:

V_{SS}: Sliding shear resistance

Fr_A: Friction resistance due to axial compression

DA_y: Dowel Action yield strength

Fr_{Fl}: Friction resistance due to flexural compression

Figure 5.29 shows V_{SS_U} values from equation 5.12 plotted against the values obtained through analysis using the 2D model. Data points of V_{SS_U} obtained through equation 5.12 follow the

reference line and show a correlation factor of 0.99 with analysis results. It can be concluded that equation 5.12 yields satisfactory predictions of V_{SS_U} values compared to the results obtained from the 2D model.

5.5.3 Sliding Shear Resistance, V_{SS}

For RM walls that experience a sliding shear mechanism, the lateral force at yield corresponds to the sliding shear resistance determined following equation 5.1, where the frictional resistance developed from flexural compression, Fr_{Fl}, is less than the upper bound frictional resistance, Fr_{Fl_U}, and can be determined through equation 5.7. In Figure 5.30 the results of V_{SS} using equation 5.1 are plotted against those obtained through analysis using the 2D model. The equation for V_{SS} yields a correlation factor of 0.99 with the results obtained from the 2D model.

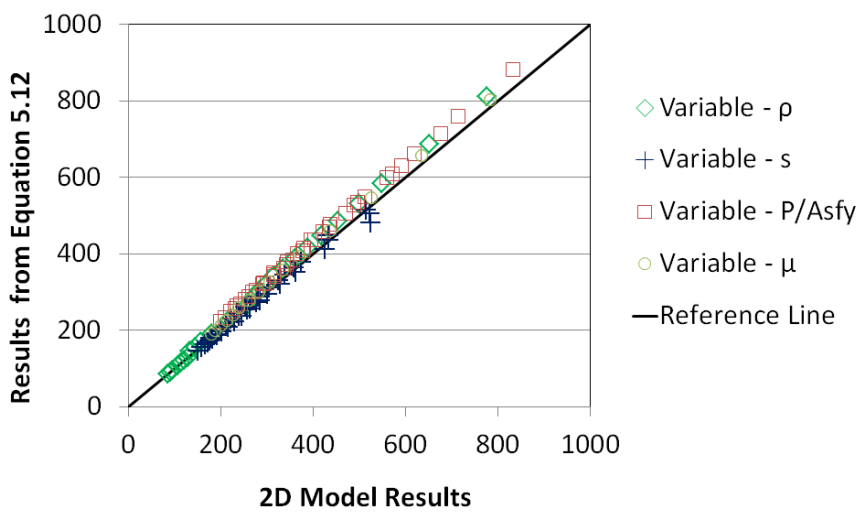

Figure 5.29 Upper bound sliding shear resistance, V_{SS_U}, from equation 5.12 vs results from 2D model.

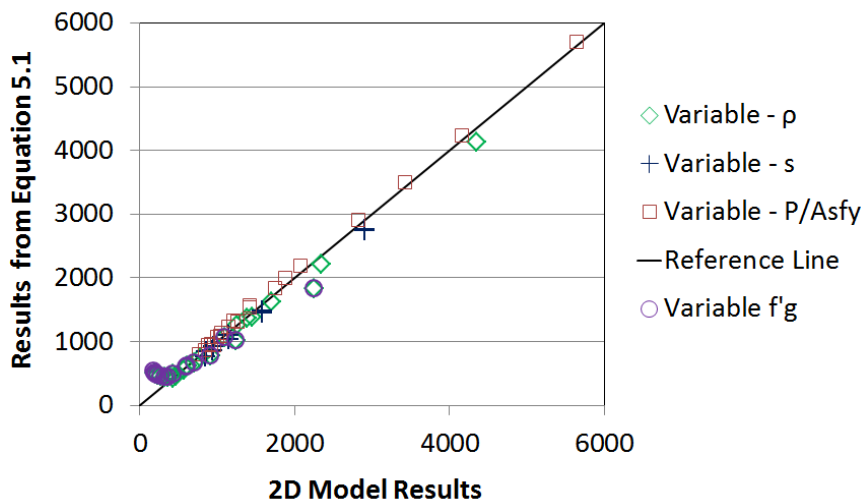

Figure 5.30 Sliding shear resistance, V_{SS}, from equation 5.1 vs results from 2D model.

5.5.4 Triggering Aspect Ratio #1, TAR1

The TAR1 value indicates the upper limit aspect ratio in which an RM wall will develop a sliding shear mechanism, as illustrated in Figure 5.31. This TAR1 value can be determined through equation 5.13.

$$\mathrm{TAR1} = \frac{\mathrm{H}}{\mathrm{L}}, \text{when } \mathrm{V_{SS}} = \mathrm{V_{Fl}} \tag{5.13}$$

5.5.5 Estimating Sliding Displacements in a SS Mechanism

The RM wall's base sliding displacement, Δ_{Base}, corresponds to the inelastic displacement, Δ_p, developed during the wall's sliding shear mechanism, as expressed in equation 5.14. Base sliding occurs when the RM wall yields at a lateral resistance equal to the sliding shear resistance, V_{SS}, as illustrated in Figure 5.32, where the Δ_p value can be expressed as a function of displacement ductility, μ, as shown in equation 5.15.

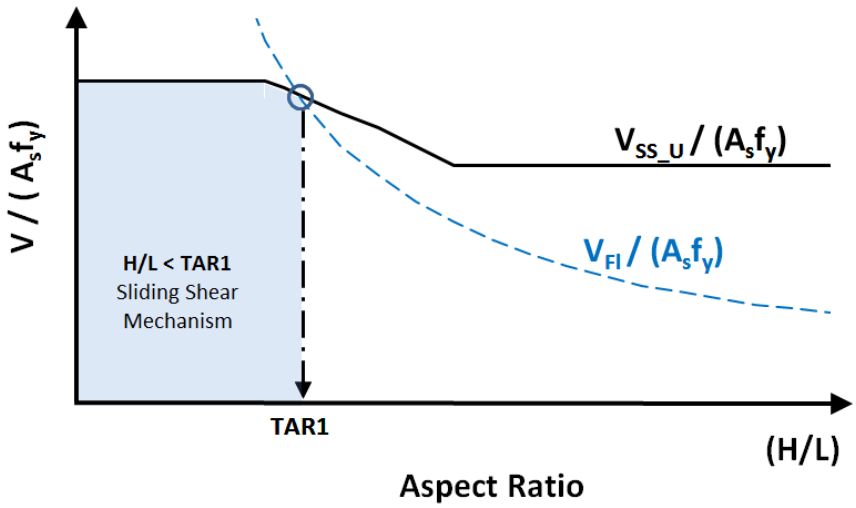

Figure 5.31 Determining the triggering aspect ratio #1, TAR1.

$$\Delta_{Base} = \Delta_p \ , \quad \mu \geq 1 \tag{5.14}$$

$$\Delta_p = (\mu - 1)\Delta_y \ , \quad \mu \geq 1 \tag{5.15}$$

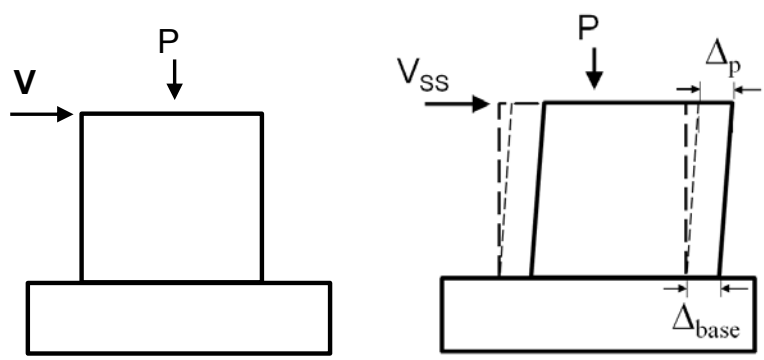

a) b)

Figure 5.32 Base sliding displacements in an RM wall that experiences a SS mechanism, a) Lateral force, V, applied on RM wall, b) RM wall yields in sliding shear mechanism.

Where the yield displacement, Δ_y, can be expressed using equation 5.16, with lateral shear stiffness, k_{shear}, determined using equation 4.9.

$$\Delta_y = \frac{V_{SS}}{k_{shear}} \tag{5.16}$$

Base sliding displacement, Δ_{Base}, can be obtained by substituting (5.14) and (5.16) into (5.15). The resulting expression for the Δ_{base} value is as follows:

$$\Delta_{Base} = (\mu - 1)\frac{V_{SS}}{k_{shear}}, \quad \mu \geq 1 \tag{5.16}$$

5.6 Summary

In this chapter, the sliding shear behaviour in RM shear walls subjected to increasing monotonic loading (known as pushover analysis) has been studied through parametric studies considering various design parameters. The key findings are summarized below:

1. Sliding shear resistance of RM shear walls can be estimated as the sum of three forces: friction due to axial compression, Fr_A, friction due to flexural compression, Fr_{Fl}, and dowel action resistance, DA_y.
2. The development of a sliding shear mechanism in an RM shear wall occurs when its sliding shear resistance, V_{SS}, is lower than its flexural resistance, V_{Fl}.
3. The sliding ratio, $\Delta_{Top}/\Delta_{Base}$, at a displacement ductility $\mu = 2$, is proposed as a measure of the behaviour of an RM wall during a pushover test. Sliding ratio values greater than 50% indicate that the RM wall's yield mechanism is a sliding shear mechanism, while the values less than 10% indicate a flexural mechanism.
4. The TAR1 value is defined as the upper limit H/L ratio for which an RM wall experiences a sliding shear mechanism.
5. Frictional resistance developed due to flexural compression, Fr_{Fl}, is proportional to the fraction of vertical reinforcement yielding in axial tension.

6. Parametric studies showed that the following design parameters have a high influence on the sliding shear response parameters: H/L ratio, grout compressive strength, f'_g, and axial compression level, $P/A_s f_y$.
7. The vertical reinforcement ratio, ρ_v, and the reinforcing bar diameter, d_b, have minimal influence on all sliding shear response parameters; this suggests that changes in these design parameters may not be effective in preventing the development of a sliding shear mechanism.

Chapter 6: Nonlinear Static Analysis of RM Cantilever Walls – Cyclic Loading

6.1 Introduction

This chapter studies the sliding behaviour of RM cantilever walls subjected to cyclic loading and the effect of design parameters on this behaviour. The design parameters considered in this study are: wall dimensions, vertical reinforcement ratio, ρ_v; bar spacing, s; bar diameter, d_b; masonry and steel strengths; and axial compression level, $P/A_s f_y$.

6.2 Nonlinear Static Analysis – Cyclic Loading

Several nonlinear static analyses are performed applying a reverse cyclic loading at the top of an RM wall model. The cyclic loading history is presented in Figure 6.1. For each loading cycle, the peak top displacement is expressed as the product of the yield displacement, Δ_y, and the displacement ductility demand μ; where the yield displacement, Δ_y, is obtained from the monotonic loading analysis in Chapter 5.

6.2.1 Characteristic Response of Yield Mechanisms

Four possible yield mechanisms can develop in an RM wall subjected to cyclic loading: a Sliding Shear (SS) mechanism, a Combined Flexural-Sliding Shear (CFSS) mechanism, a Dowel-Constrained Failure (DCF) mechanism and a Flexural (Fl) mechanism. An example for each yield mechanism is presented. In each example, it is assumed that diagonal shear failure has been prevented by design.

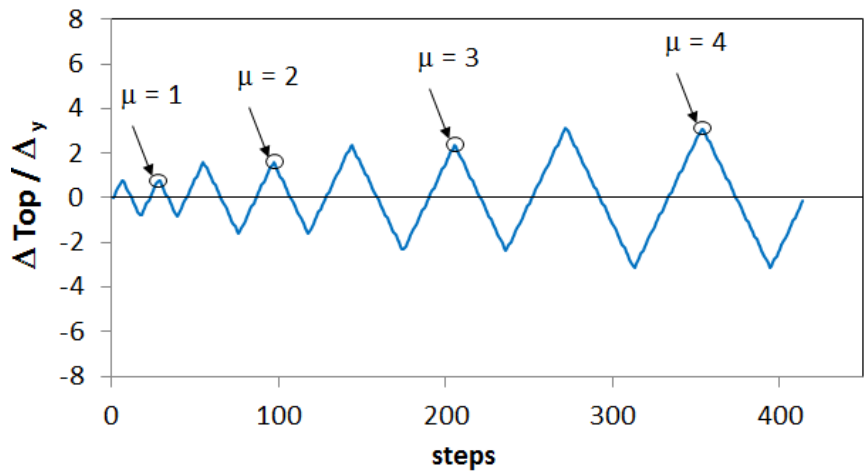

Figure 6.1 Cyclic loading history.

The following analysis cases will help identify the sliding behaviour parameters that influence the development of different yield mechanisms and their respective base sliding displacements. These parameters include: sliding ratio, $\Delta_{\text{Base}}/\Delta_{\text{Top}}$; overturning moment required to close a flexural crack along the wall length, M_o; and dowel action secant stiffness coefficient, C_k.

With the exception of the "Dowel-Constrained Failure" case, the material properties used for these analyses cases include: masonry compression strength, f'_m, of 10 MPa, grout compression strength, f'_g, 35 MPa and steel yield strength, f_y, of 400 MPa. Also, wall dimensions are set at a height, H, of 3 m and a thickness, t, of 190 mm.

6.2.1.1 Sliding Shear (SS) Mechanism.

The results of cyclic loading analysis for an RM wall model with a H/L ratio of 0.5 are used to illustrate the behaviour of an RM wall experiencing a SS mechanism. The RM wall's reinforcement ratio, ρ_v, is set equal to 0.2% and the axial compression level, P/A_sf_y, set at 0%.

In a SS mechanism, an RM wall develops inelastic displacements through base wall sliding. Figure 6.2 shows the displacement results for an RM wall model with an SS yield mechanism. This mechanism develops sliding ratios, $\Delta_{Base}/\Delta_{Top}$, that are above 0.5 for displacement ductility demands, μ, greater than 1. At a displacement ductility, μ, of 2, sliding displacement contributes to approximately 80% of the total wall displacement; this corresponds to a base displacement, Δ_{Base}, of 8.9 mm.

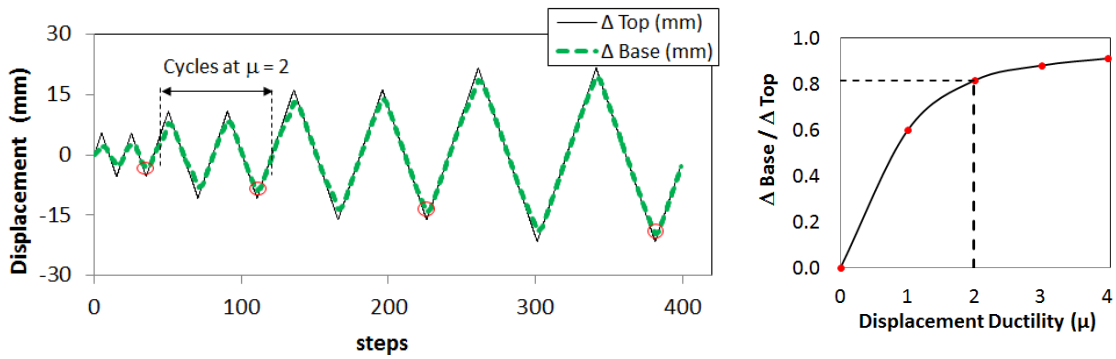

a) b)

Figure 6.2 Sliding displacements for an RM wall with H/L=0.5 and SS mechanism: a) Displacement history, b) Sliding ratio vs displacement ductility, μ.

Hysteresis curves shown in Figure 6.3 indicate low energy dissipation due to pinching and stiffness degradation. The yield resistance is unsymmetrical with a higher yield strength, V_y, in the positive direction (V_y^+=874 kN) than for the negative direction (V_y^-=762 kN).

The force vs displacement hysteresis curves for friction and dowel action resistances, shown in Figure 6.4, indicate low energy dissipation capacity for this specimen. In comparison, the energy dissipated through dowel action is higher than the energy dissipated through frictional resistance. Frictional resistance has low dissipation of energy because it is developed only due to flexural

compression. Frictional resistance due to axial compression is not developed because the $P/A_s f_y$ value is equal to 0%.

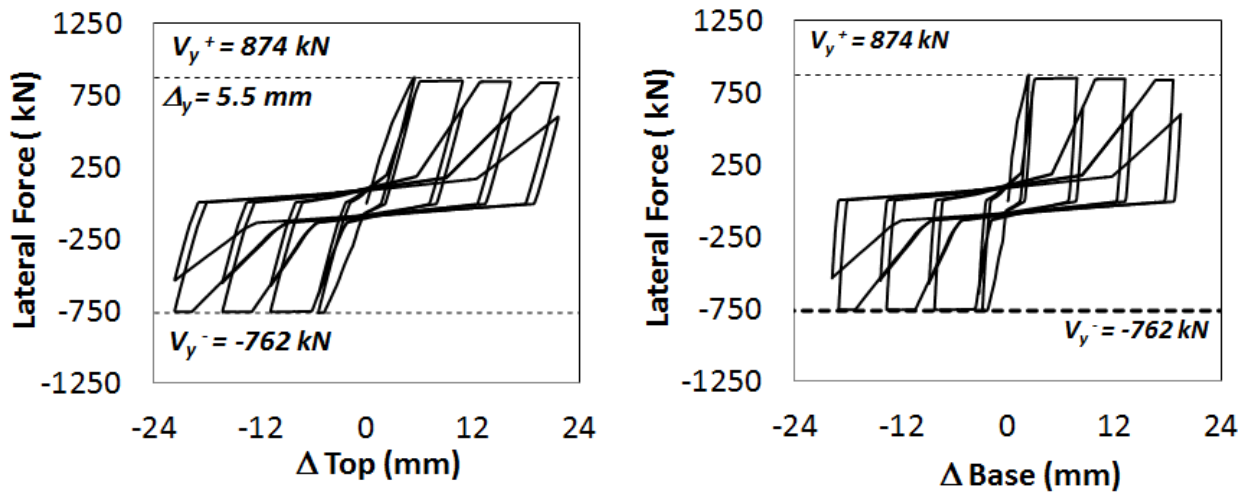

a) b)

Figure 6.3 Hysteresis curves for RM wall with H/L=0.5 and SS mechanism:

a) Lateral force vs top displacement, b) Lateral force vs base displacement.

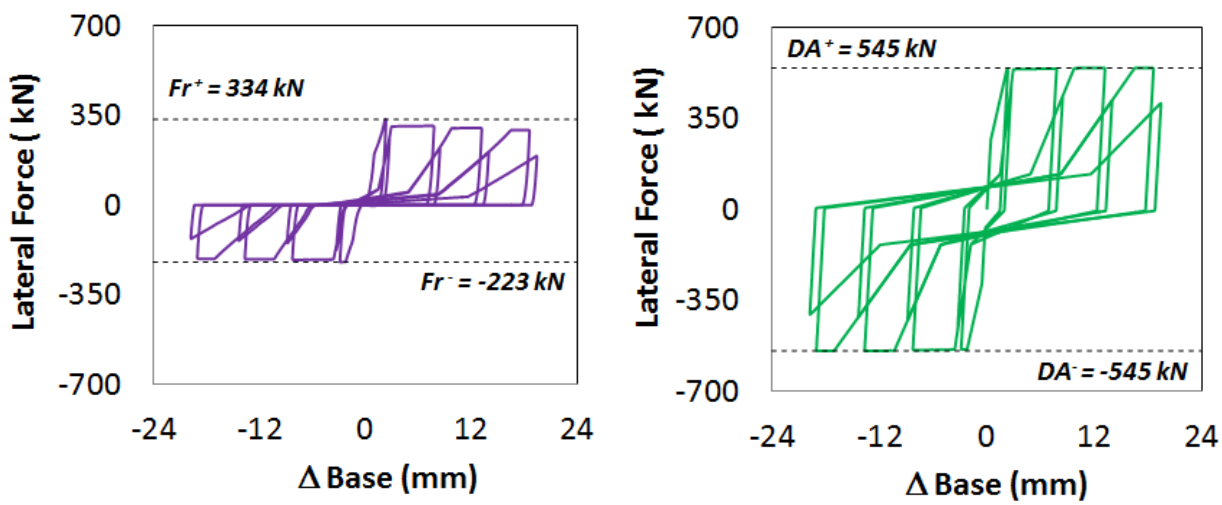

a) b)

Figure 6.4 Cyclic response of an RM wall with H/L=0.5 and SS mechanism:

a) Friction hysteresis, b) Dowel action hysteresis.

The hysteresis curve for friction resistance in Figure 6.4a shows an unsymmetrical resistance. This effect in frictional resistance due to flexural compression is due to different bars yielding in

tension for the positive direction and for the negative direction, as observed in Section 5.4.1.2. When the wall is loaded in the negative direction, the number of bars that yield in tension is less than for the wall loaded in the positive direction.

6.2.1.2 Combined Flexural-Sliding Shear (CFSS) Mechanism

The results of cyclic loading analysis for an RM wall model with an H/L ratio of 1.0, reinforcement ratio, ρ_v, of 0.2% and axial compression level, $P/A_s f_y$, of 0%, are used to study the behaviour of an RM wall experiencing a CFSS mechanism.

Cyclic displacements of an RM wall that experiences a CFSS mechanism are equal to the sum of the displacements due to flexural rotations and base sliding. These displacements account for 5 to 90% of the RM wall's total displacement. For the wall example under consideration, the level of sliding shown in Figure 6.5 indicates that at a displacement ductility, μ, of 2, wall sliding is equal approximately to 25% of the total wall displacement; this corresponds to a base displacement, Δ_{Base}, of 3.3 mm.

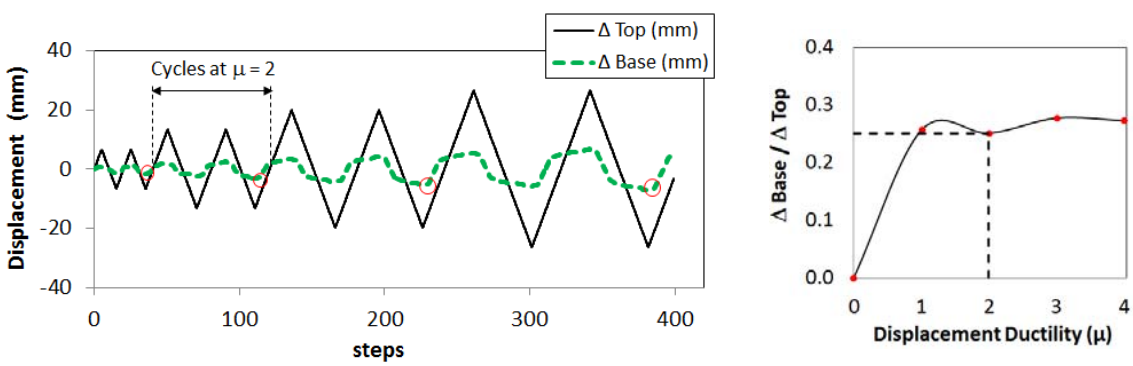

a) b)

Figure 6.5 Sliding displacements for an RM wall with H/L=1.0 and CFSS mechanism: a) Displacement history, b) Sliding ratio vs displacement ductility, μ.

The displacement history in Figure 6.5a shows that base wall sliding displacements increase with an increase in the ductility demand, μ. However, it is found that the sliding ratio, $\Delta_{Base}/\Delta_{Top}$, stays approximately constant for μ values greater than 1, as observed in Figure 6.5b. This indicates that sliding displacements in the CFSS mechanism develop in proportion to the wall's inelastic rotation.

Figure 6.6 shows hysteresis curves for an RM wall which experienced a CFSS mechanism. It can be seen that the RM wall's force vs displacement behaviour is not symmetric. Figure 6.6a shows that for the positive displacement direction, the yield force, V_y^+, is 265 kN, while for the negative direction, the yield force, V_y^-, is -235 kN. In the first case, V_y^+ is equal to the flexural resistance, V_{Fl}, while in the latter case V_y^- is equal to 89% of V_{Fl}.

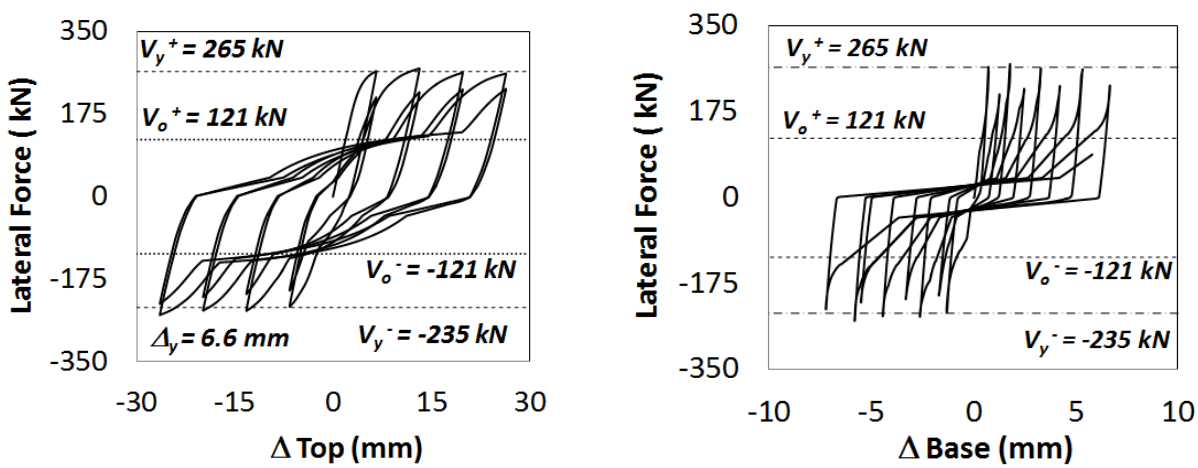

a) b)

Figure 6.6 Hysteresis curves for RM wall with H/L=1.0 and CFSS mechanism: a) Lateral force vs top displacement, b) Lateral force vs base displacement.

The hysteresis curves in a CFSS mechanism are characterized by pinching and stiffness degradation, which are the effects of an open flexural crack along the wall length, as discussed in Section 3.4.2. In this example, the lateral force required to close the flexural crack, V_o, is equal

to 121 kN. After the flexural crack is closed, the masonry at opposite sides of the crack comes into contact and the wall restores its lateral strength and stiffness.

Figure 6.7 presents the changes in the CFSS mechanism for the example RM wall example at a displacement ductility demand, μ, equal to 2. At point A, the RM wall is at zero lateral force and its reinforcement on the compression end has residual tensile strains that prevent a flexural crack from closing (see Figure 6.7a). When the load increases from points A to B, as shown in Figure 6.7b, rebar yields at the tension end of the RM wall, causing the base of the RM wall to form an open flexural crack along the wall length. Transfer of shear and overturning moments along this open crack is achieved by vertical reinforcement, through dowel action and axial forces, respectively. At this stage, a low shear stiffness is provided by dowel action causing wall displacements to be governed by base sliding displacements. However, for points B to C, dowel action restores stiffness as it bears onto new undamaged grout, causing the wall to resist higher overturning moments and develop flexural rotations. For points C to D, the flexural crack begins to close, as shown in Figure 6.7c and Figure 6.7d. As a result, compression strains begin to develop in the masonry due to flexural compression. At point D, frictional resistance is restored and wall displacements are governed by flexural rotation.

In a CFSS mechanism, frictional resistance is zero during wall sliding, as shown in Figure 6.8a. This effect occurs while the flexural crack is open which causes a loss of contact between masonry and the loss of frictional resistance. Frictional resistance is regained when the flexural crack is closed and masonry is once more in contact.

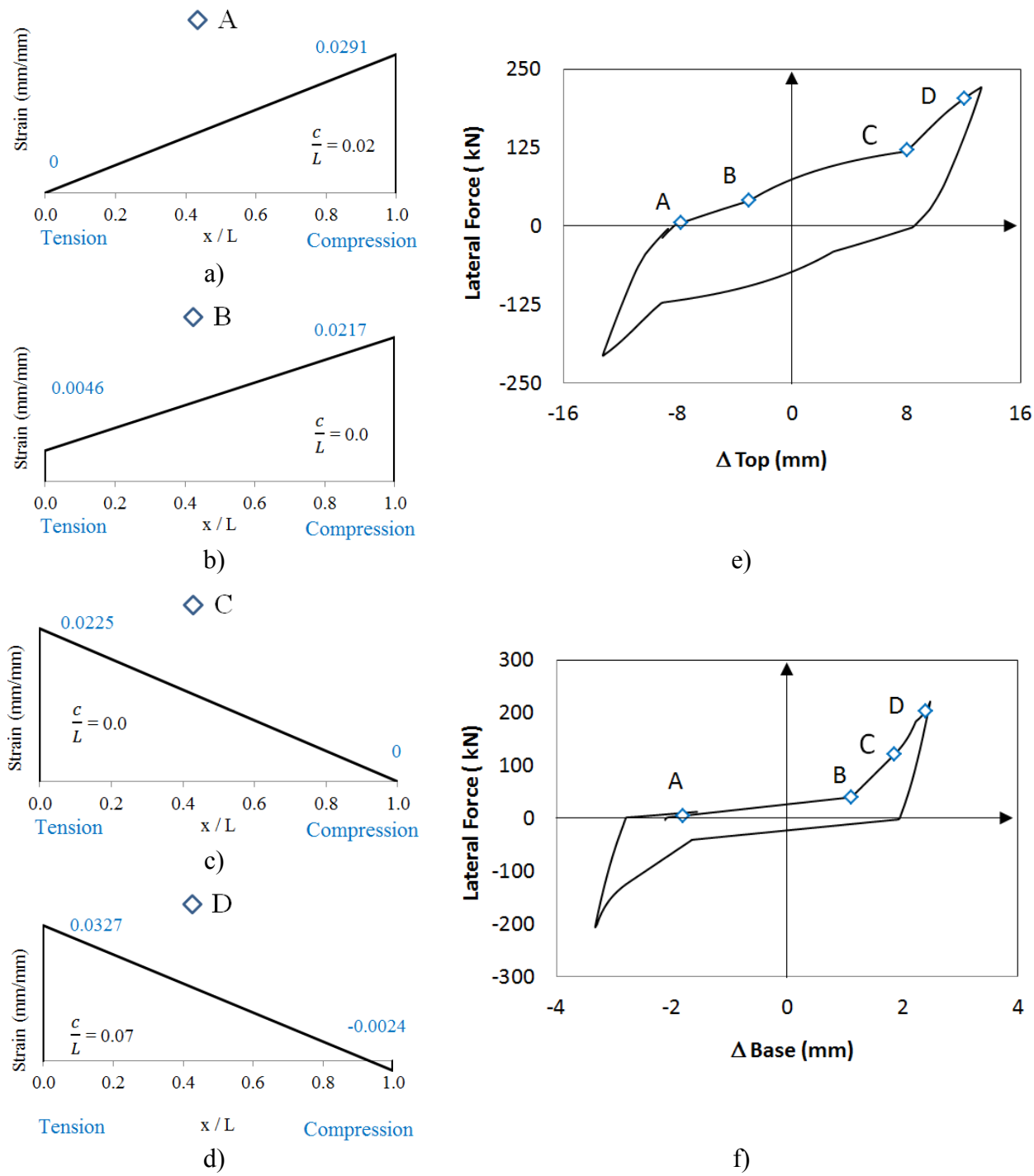

Figure 6.7 Sliding behaviour for various loading points of an RM wall experiencing a CFSS mechanism at a displacement ductility demand of μ=2: a) Strain distribution at point A; b) Strain distribution at point B; c) Strain distribution at point C; d) Strain distribution at point D; e)Lateral force vs top displacement; f) Lateral force vs base displacement.

In a CFSS mechanism, sliding displacements develop due to dowel action deformations which are required to enable shear transfer across the open flexural crack along the wall length. In each loading cycle, 80% of these deformations correspond to elastic dowel action deformations and 20% correspond to inelastic dowel action deformations. In addition, dowel action shear stiffness degrades after each increase in displacement ductility, μ, causing higher elastic dowel action deformations for each subsequent loading cycle, as shown in Figure 6.8b. For instance, at a displacement ductility, μ, equal to 2, the dowel action deformation is equal to 2.5 times the dowel action deformation developed at a μ value of 1.

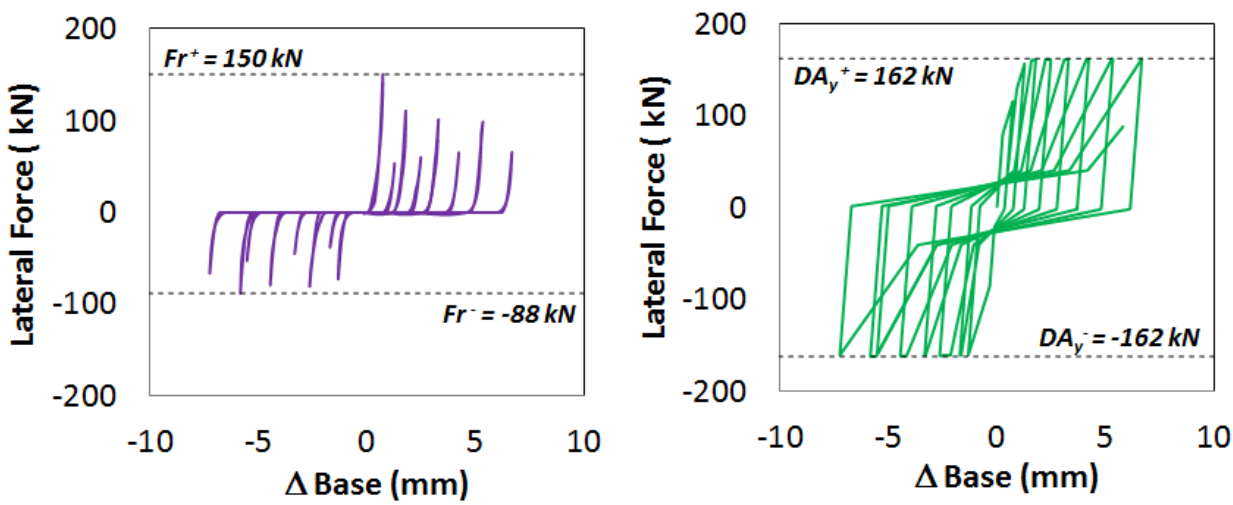

a) b)

Figure 6.8 Cyclic response of an RM wall with aspect ratio H/L=1.0 and CFSS mechanism: a) Friction hysteresis, b) Dowel action hysteresis.

After an increase in displacement ductility demand, μ, dowel action hysteresis shows pinching behaviour and stiffness degradation. To measure this stiffness degradation, the dowel action secant stiffness, k_{sec}, is determined for each μ value during cyclic loading, as shown in equation 6.1. Figure 6.9 shows that at a μ value of 2, the k_{sec} value is equal to 49 kN/mm. This stiffness value amounts to 39% of the total dowel action elastic stiffness, k_{DA}.

$$k_{sec} = \frac{DA}{u_{DA}}, \qquad DA \leq DA_y \tag{6.1}$$

Where:

DA: shear force transferred through dowel action.

u_{DA}: dowel action deformation.

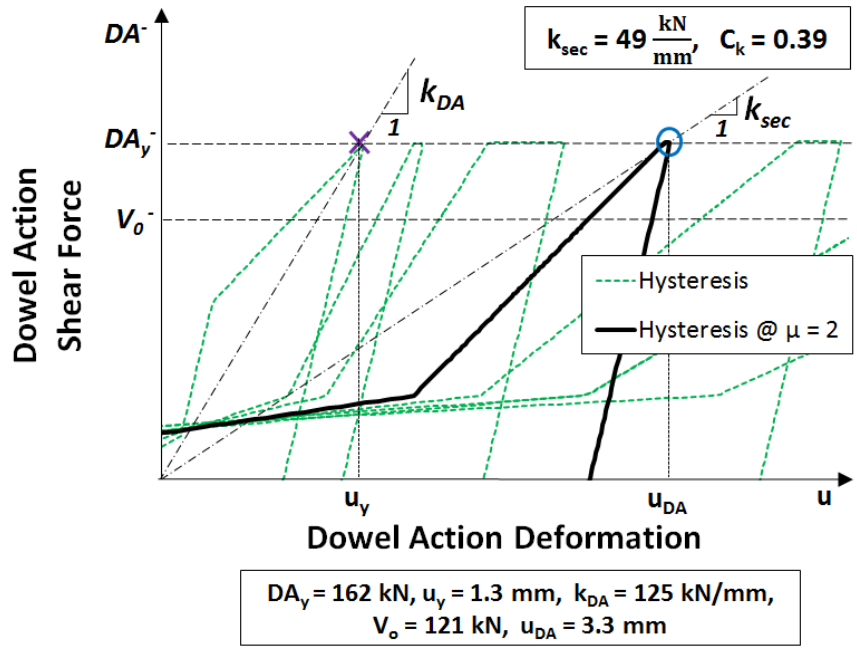

Figure 6.9 Dowel action secant stiffness, k_{sec}, in a CFSS mechanism.

The dowel action stiffness ratio, C_k, is used to evaluate the variation in dowel action secant stiffness, k_{sec}, during cyclic loading and is determined using equation 6.2. For RM walls that experience a CFSS mechanism, the dowel action stiffness ratio, C_k, is less than 1.0. The RM wall example develops a C_k value of 0.39 at a displacement ductility, μ, equal to 2.

$$C_k = \frac{k_{sec}}{k_{DA}} \tag{6.2}$$

Where:

k_{sec}: dowel action secant stiffness at displacement ductility, μ.

k_{DA}: dowel action elastic stiffness.

6.2.1.3 Dowel-Constrained Failure (DCF) Mechanism

The sliding behaviour of an RM wall that experiences a DCF mechanism during cyclic loading analysis is illustrated using the results of an RM wall model with an H/L ratio of 1.0. The wall model's design parameters used are: vertical reinforcement ratio, ρ_v, equal to 0.2%; grout compression strength, f'_g, of 15 MPa; and an axial compression level, $P/A_s f_y$, of 0%.

For a DCF mechanism, wall displacements are due to flexure in the positive direction and base sliding in the negative direction (see Figure 6.10a). As a result, the sliding displacement history is non-symmetrical and base sliding increases with an increase in ductility demand, as shown in Figure 6.10b. For inelastic demands, base sliding can be significant, resulting in sliding ratios, $\Delta_{Base}/\Delta_{Top}$, between of 0.50 to 3.0.

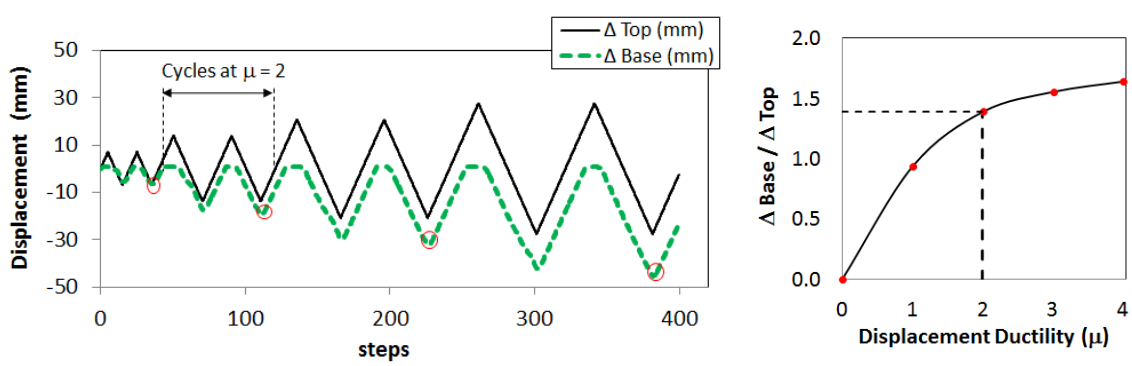

a) b)

Figure 6.10 Sliding displacements of an RM wall with H/L=1.0 experiencing a DCF mechanism: a) Displacement history, b) Sliding ratio vs displacement ductility, μ.

The lateral force vs top displacement curve shown in Figure 6.11a indicates that, for the positive direction, the wall's yield force, V_y^+, is 267 kN, which amounts to 100% of the flexural

resistance, V_{Fl}. For the negative direction, V_y^-, is 107 kN, which amounts to 40% of $V_{Fl.}$ and 100% of the dowel action yield resistance, DA_y. It should be noted that the yield resistance, V_y^-, is lower than the force necessary to close the open flexural crack that causes sliding, V_o, of 121 kN. As a result, the flexural crack remains open and the RM wall slides at the base in the negative direction.

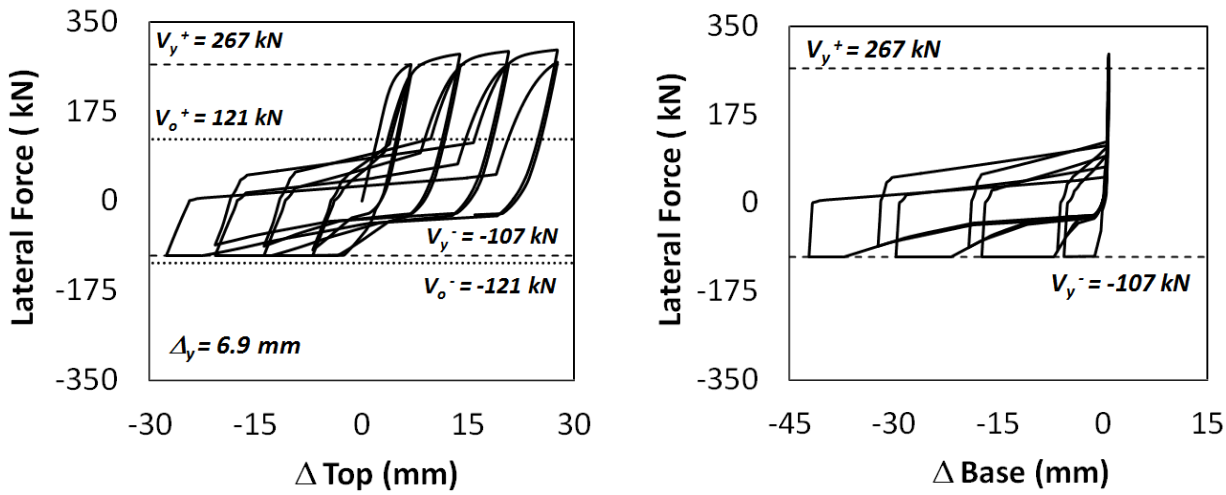

Figure 6.11 Hysteresis curves for RM wall with H/L=1.0 and DCF mechanism: a) Lateral force vs top displacement, b) Lateral force vs base displacement.

The friction hysteresis in Figure 6.12a shows loss of frictional resistance and moderate dissipation of energy for the negative direction, and high elastic shear stiffness in the positive loading direction. For the negative direction, when sliding develops during the first loading cycle at displacement ductility, μ, frictional resistance is zero. However, for the following cycle with the same μ value, sliding displacements develop while the flexural crack is closed, thus frictional resistance, Fr^-, reaches a maximum value of 26 kN.

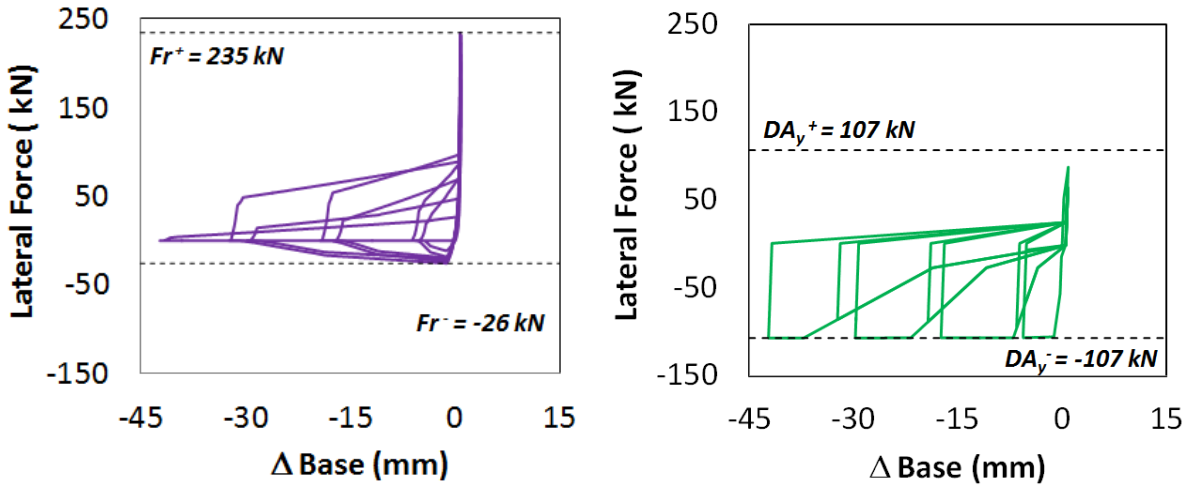

a) b)

Figure 6.12 Cyclic response of an RM wall with H/L=1.0 and DCF mechanism: a) Friction hysteresis, b) Dowel action hysteresis.

The dowel action force displacement curve in Figure 6.12b shows elastic response for loading in the positive direction and significant plastic yielding in the negative direction. For a displacement ductility demand, μ, sliding develops during the first loading cycle due to dowel action yielding while the flexural crack remains open along the wall length. Subsequently, in the second loading cycle for the same μ value, sliding occurs due to pinching in the dowel action hysteretic behaviour without the formation of an open flexural crack.

RM walls that experience a DCF mechanism are characterized by low values of dowel action secant stiffness coefficient, C_k. As illustrated in Figure 6.13, the RM wall example develops a C_k value of 0.06 at a displacement ductility, μ, of 2. These C_k values indicate that significant dowel action deformations are associated with this mechanism.

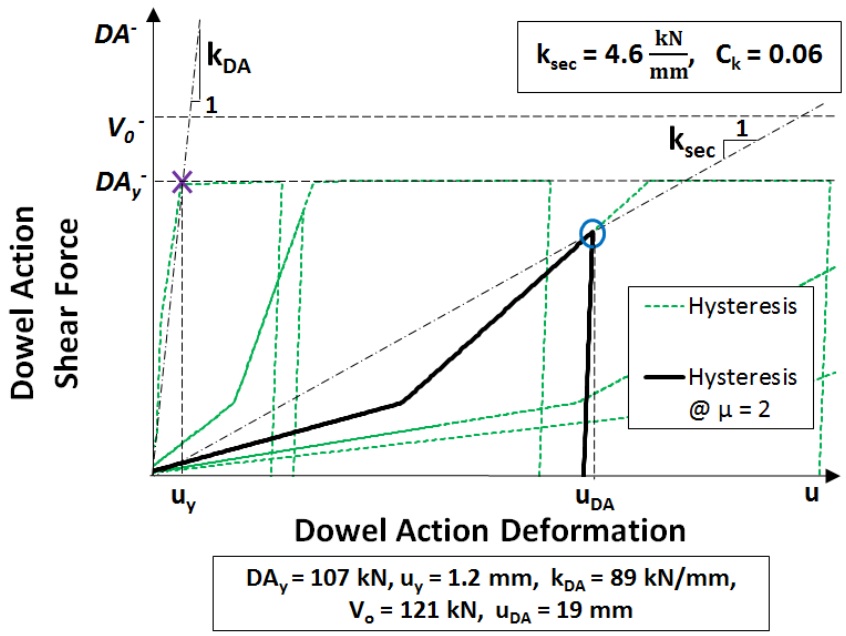

Figure 6.13 Dowel action secant stiffness, k_{sec}, in a DCF mechanism.

6.2.1.4 Flexural (Fl) Mechanism

The results of cyclic loading for an RM wall model with H/L ratio of 1.6, reinforcement ratio, ρ_v of 0.2%, and axial compression level, $P/A_s f_y$, of 0%, are used to represent the behaviour of an RM wall experiencing a CFSS mechanism.

It can be seen from Figure 6.14 that in a flexural mechanism, base sliding has an insignificant contribution to total wall displacement. The results of displacement history in Figure 6.14a indicate that the maximum sliding displacement, Δ_{Base}, is less than 1 mm. The curve of sliding ratio vs displacement ductility in Figure 6.14b, shows that for a ductility μ=2, the sliding ratio is 6%, however as the ductility demand increases to μ=4, the ratio drops to 3%.

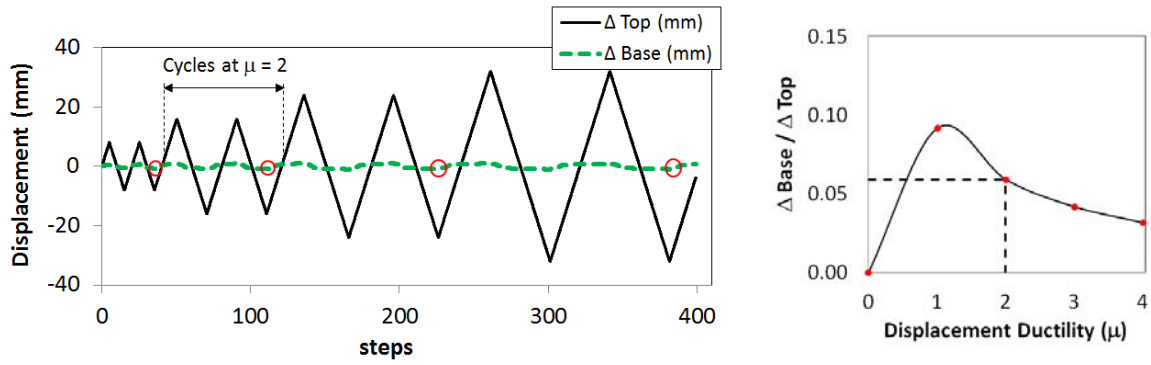

a) b)

Figure 6.14 Sliding displacements for an RM wall with H/L=1.6 and Fl mechanism:

a) Displacement history, b) Curve of sliding ratio vs displacement ductility, μ.

The force vs top displacement curve shown in Figure 6.15a, is symmetrical, with a yield force, V_y, of 95 kN. It can be seen from the figure that the wall develops 100% of its flexural resistance, V_{Fl}, for both loading directions. The hysteresis behaviour shows pinching when lateral force is less than V_o= 44 kN; this occurs due to the opening and closing of a flexural crack along the wall length. However, unlike the CFSS mechanism, the sliding shear hysteresis shows that the wall develops only small sliding displacements, Δ_{Base}, of less than 1mm.

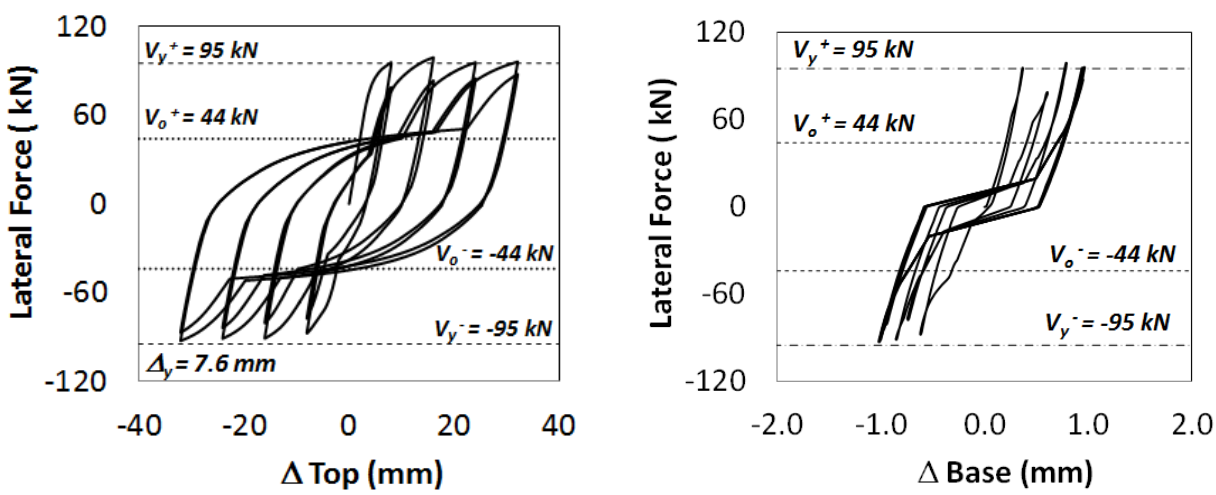

a) b)

Figure 6.15 Hysteresis curves for RM wall with H/L=1.6 and Fl mechanism:

a) Lateral force vs top displacement, b) Lateral force vs base displacement.

The friction and dowel action hysteresis curves are shown in Figure 6.16. The friction hysteresis shows slip without energy dissipation when the flexural crack is open, and high shear stiffness when the crack is closed. The dowel action hysteresis shows that shear forces transferred through dowel action are less than the dowel action yield resistance, DA_y, of 96 kN.

For RM walls that experience a flexural mechanism, the dowel action stiffness ratio, C_k, is equal to or higher than 1.0; this indicates that dowel action shear stiffness is not significantly affected by pinching and stiffness degradation. As illustrated in Figure 6.17, the RM wall example has a C_k value of 1.0 at a displacement ductility, μ, of 2.

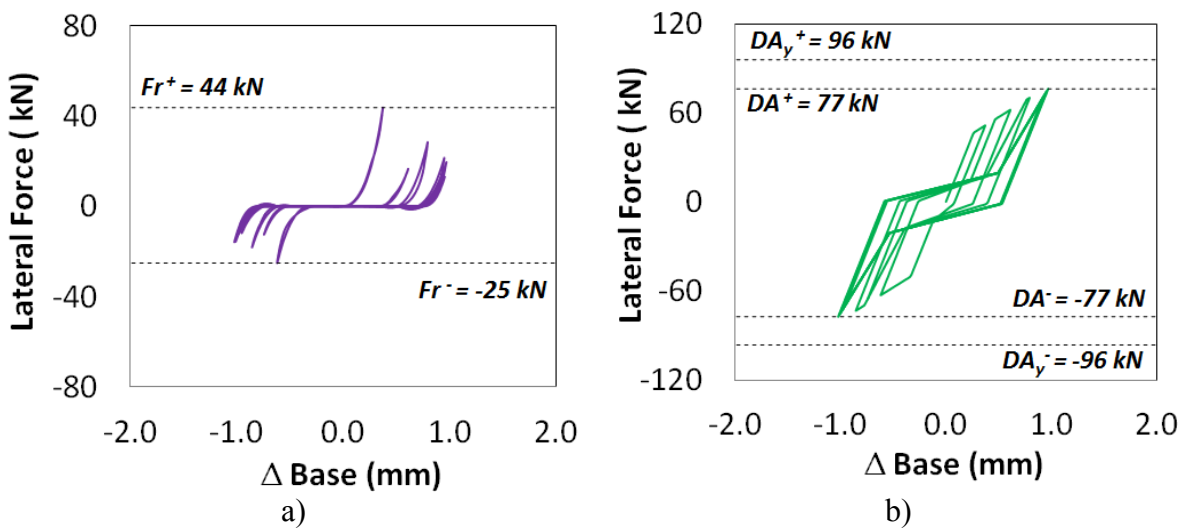

Figure 6.16 Cyclic response of an RM wall with aspect ratio H/L=1.6 and Fl mechanism: a) Friction hysteresis, b) Dowel action hysteresis.

6.3 Parametric Study – Cyclic Loading

These parametric studies focus on determining the influence of specific design parameters on the level of sliding that occurs in RM shear walls subjected to cyclic loading. In each analysis, the following response parameters were evaluated: sliding ratio, $\Delta_{\mathrm{Base}}/\Delta_{\mathrm{Top}}$, the overturning

moment required to close the flexural crack along the wall length, M_o, and the dowel action secant stiffness coefficient, C_k.

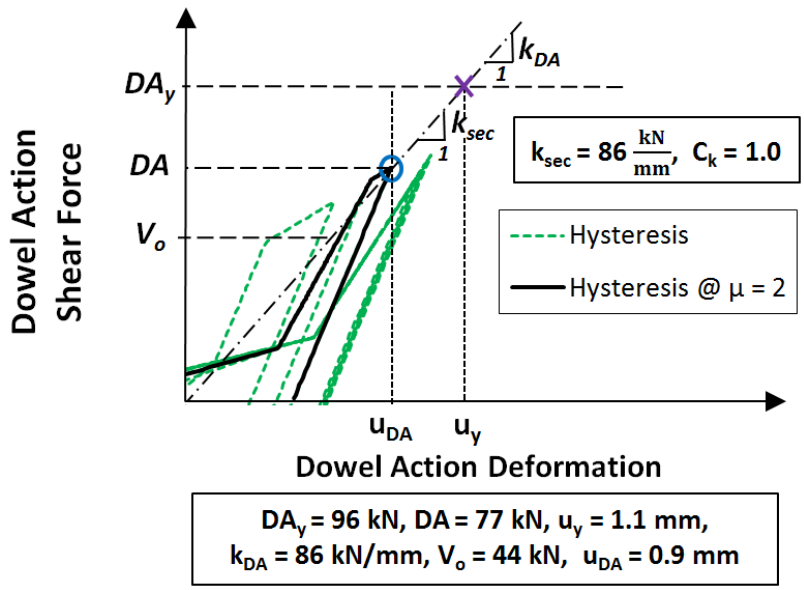

Figure 6.17 Dowel action secant stiffness, k_{sec}, in a Fl mechanism.

Unless specified in the study, each model has the same dimensions: wall height, H = 3 m, wall thickness, t= 0.19 m, however the length, L, is variable. Material properties used are masonry compression strength, f'_m, of 10 MPa, grout compression strength, f'_g, of 35 MPa, and steel yield strength, f_y, of 400 MPa. The f'_g value is set to 35 MPa following grout strength properties shown in experiments (Hernandez, 2012; Ahmadi, 2012). The axial compression level, P/A_sf_y, is 0%.

6.3.1 Aspect Ratio (H/L)

For this parametric study, cyclic loading analyses are performed on RM wall models with H/L ratios less than 2.0. The values of H/L ratio considered in this study are varied in increments of 0.1. The vertical reinforcement ratio at ρ_v, is 0.2%, and 10M diameter bars are used.

The results of this parametric study show an RM wall develops a SS mechanism when its sliding shear resistance, V_{SS}, is less than its flexural resistance, V_{Fl}. For RM walls, with V_{SS} value higher than V_{Fl}, and a C_k coefficient of less than 1.0, the yield mechanism corresponds to a CFSS mechanism. Otherwise, an Fl mechanism develops when the C_k coefficient is equal or greater than 1.0. Possible yield mechanisms for RM walls depending on H/L ratio are shown in Table 6.1.

Figure 6.18 illustrates the sliding ratio at a displacement ductility, μ, equal to 2; for each of the RM walls analysed. The sliding ratios, $\Delta_{\mathrm{Base}}/\Delta_{\mathrm{Top}}$, values range from 0.6 to 0.8 for RM walls that experience a SS mechanism; from 0.05 to 0.60 for a CFSS mechanism, and below 0.05 for an Fl mechanism.

Table 6.1 Yield mechanism depending on wall H/L ratio

H/L Ratio	**Yielding Mechanism**
H/L < 0.6	Sliding Shear (SS) Mechanism
0.6 ≤ H/L < 1.6	Combined Flexural-Sliding Shear (CFSS) Mechanism
H/L ≥ 1.6	Flexural (Fl) Mechanism

Figure 6.18 also shows a comparison of the sliding ratio values for RM walls subjected to monotonic and cyclic loading. This comparison indicates that sliding ratios developed through

cyclic loading are higher than those developed through monotonic loading. The largest differences in sliding ratio are found for RM walls that develop a CFSS mechanism.

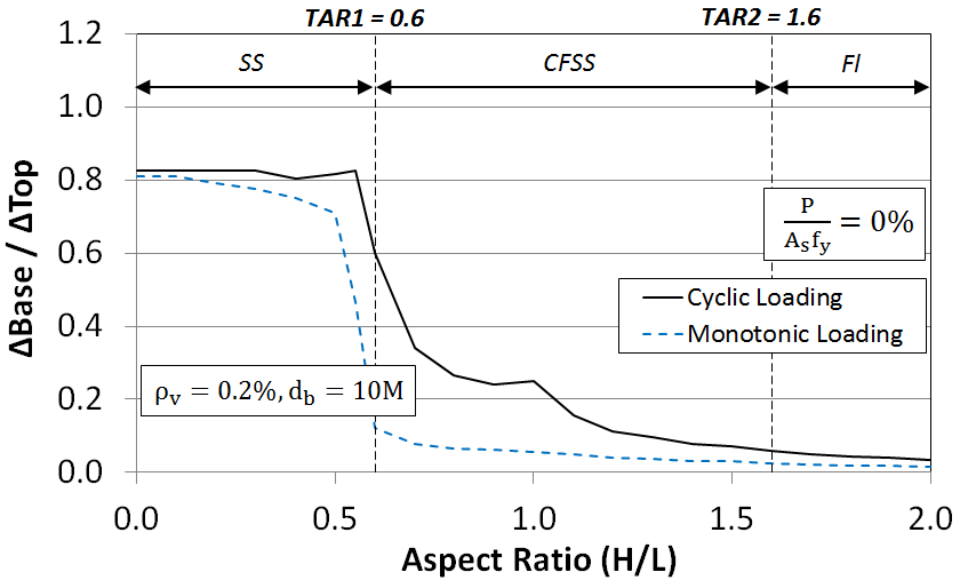

Figure 6.18 Sliding ratio vs H/L ratio at μ=2 for ρ_v=0.2%.

The upper H/L limits for the SS and CFSS mechanisms are 0.6 and 1.6, respectively. The upper H/L limit for the SS mechanism is determined from equation 5.13. On the other hand, the upper limit for a CFSS mechanism is defined as the value equal to the H/L ratio that corresponds to an RM wall that has a C_k ratio equal to 1.0 for a displacement ductility, μ, equal to 2, as highlighted in Figure 6.19. The upper limit aspect ratio for a CFSS mechanism is referred to herein as Triggering Aspect Ratio #2, (TAR2).

The dowel action secant stiffness ratio, C_k, in each RM wall varies depending on the H/L ratio and the wall's yield mechanism, as shown in Figure 6.19. In RM walls experiencing a SS mechanism, the C_k ratio ranges between 0.19 and 0.23. For RM walls with a CFSS mechanism, the C_k ratio follows a trend of increasing values that start at approximately C_k of 0.20 at a

H/L ratio equal to TAR1, and reaches a C_k value of 1.0 at an H/L ratio equal to TAR2. For RM walls that experience a Fl mechanism, the C_k ratio is greater than 1.0, this indicates that dowel action deformations are less than the dowel action yield deformation, u_y, as illustrated in the dowel action hysteresis curve in Figure 6.17.

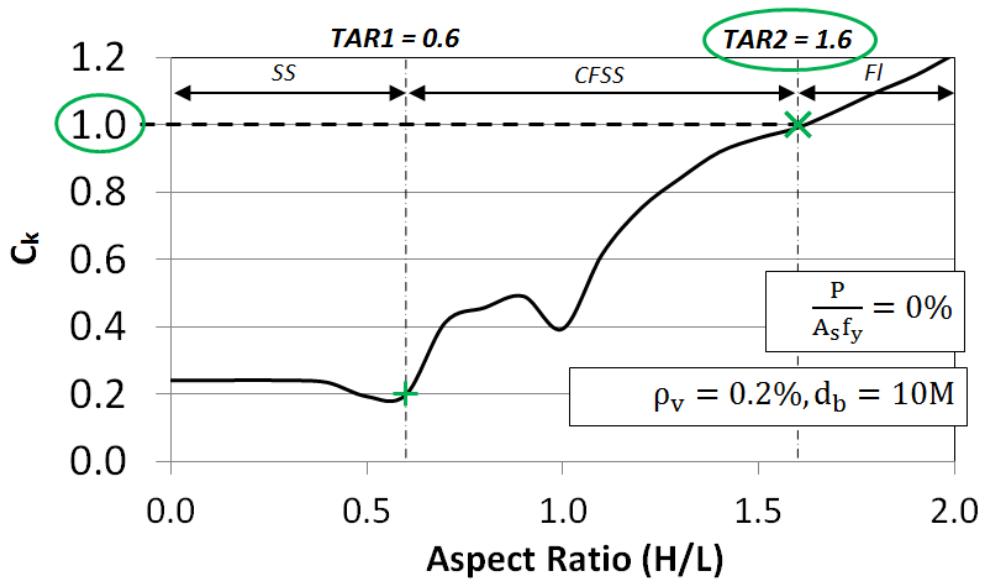

Figure 6.19 C_k vs H/L ratio at μ = 2.

For each RM wall considered, the overturning moment coefficient, C_o, is calculated from equation 3.8. As shown in Figure 6.20, for RM walls with a CFSS mechanism and an Fl mechanism, C_o is equal to 0.25, irrespective of a wall's H/L ratio. Therefore, it is determined that the RM wall's aspect ratio, H/L, does not influence the coefficient C_o which is used in the M_o expression (see equation 3.7).

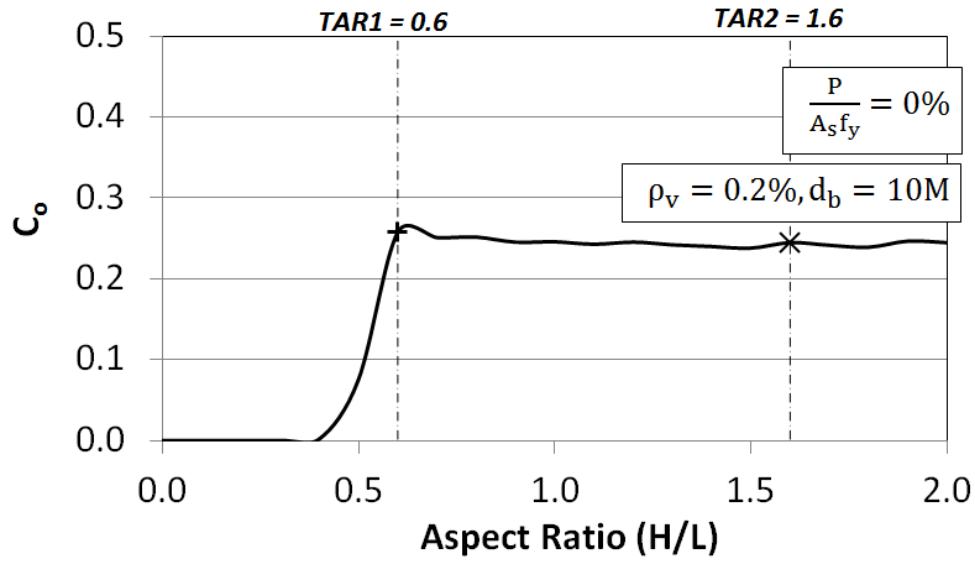

Figure 6.20 C_o vs H/L ratio at μ=2.

6.3.2 Wall Height (H)

The effect of wall height is studied by performing cyclic loading analyses on RM walls with wall height, H, value of 2, 3, 4.5 and 6 m. The range of H/L ratios for each wall height is set at H/L greater than 2.0. The reinforcement ratio, ρ_v, is set 0.2% and 10M diameter bars are used.

The results show that variations in H value do not affect the H/L ratio at which an RM wall develops a yield mechanism. Therefore, TAR1 and TAR2 values remained constant for all wall heights, H.

It can be seen from the sliding ratio curves for different H values in Figure 6.21 that as wall height increases, sliding ratio decreases. This behaviour occurs due to Δ_{Top} increasing at a higher rate than Δ_{Base} as the H value increases. This was also observed in Section 5.4.2 related to monotonic loading.

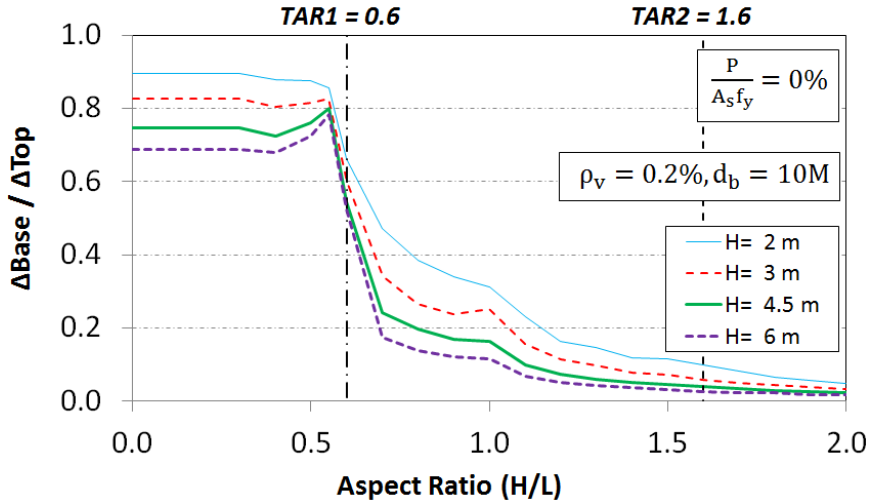

Figure 6.21 Sliding ratio vs H/L ratio at μ=2 for different wall heights, H.

Figure 6.22a, shows the relationship between C_o and H/L ratio for different wall heights. For RM walls that experience a CFSS mechanism, the coefficient C_o value is constant (on average equal to 0.25) and independent from wall height, H.

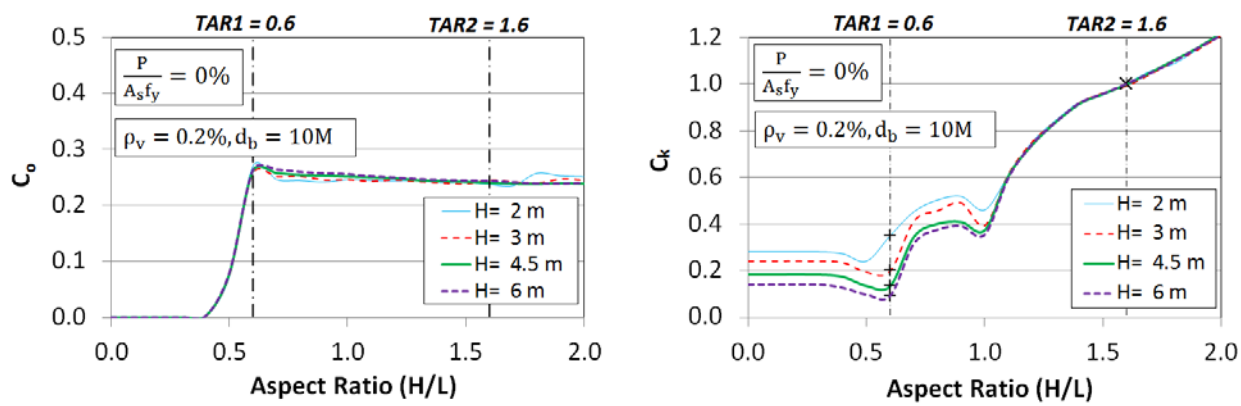

a) b)

Figure 6.22 Effect of wall height (H): a) C_o vs H/L ratio, b) C_k vs H/L ratio.

The curves of C_k ratio vs H/L ratio shown in Figure 6.22b indicate that wall height H has an inverse influence on C_k value for H/L ratios less than 1.1, that is, C_k value decreases as wall

height H increases. The results show that for H/L ratios greater than 1.1, the C_k value is not influenced by the wall height.

6.3.3 Displacement Ductility (μ)

This section studies the sliding behaviour of RM walls for various displacement ductility, μ, values ranging from 1 to 4. These μ values can be seen on the cyclic loading protocol shown in Figure 6.1.

Figure 6.23 shows that the ductility demand, μ, influences the sliding behaviour in an RM wall depending on its H/L ratio. For H/L ratios less than or equal to 1.0, sliding ratios increase with ductility demand, while an opposite trend is observed for H/L ratios greater than 1.0.

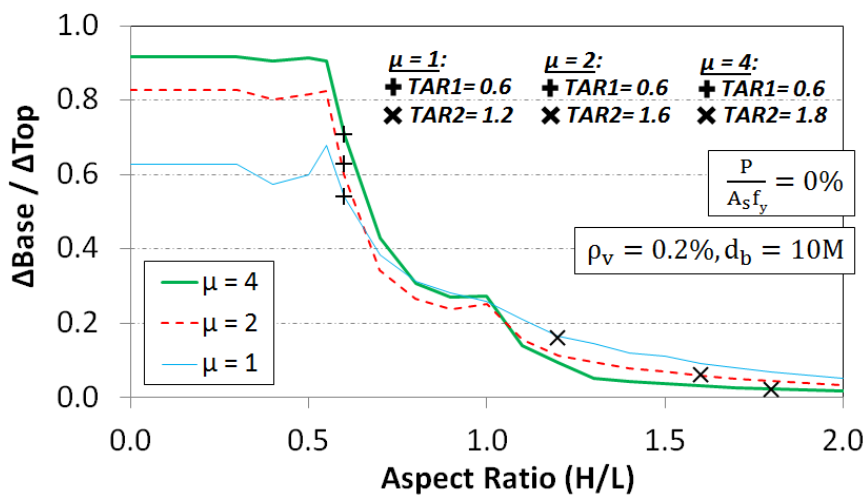

Figure 6.23 Sliding ratio vs H/L ratio at μ=2, for different displacement ductility values.

Figure 6.24a indicates that the C_o coefficient is higher at higher values of displacement ductility, μ. This trend is also observed for an average C_o value determined for RM walls with H/L ratios greater than TAR1 and less than 2.0 (see Table 6.2).

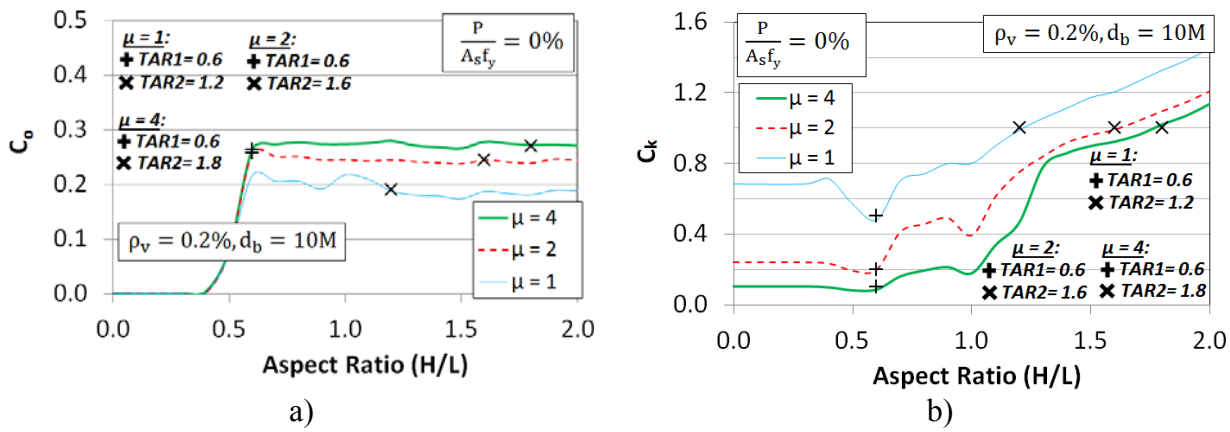

a) b)

Figure 6.24 Effect of displacement ductility (μ): a) C_o vs H/L ratio, b) C_k vs H/L ratio.

Table 6.2 Average C_o coefficients for various displacement ductility, μ, values.

Displacement Ductility, μ	Average Coefficient, C_o
1	0.21
2	0.25
4	0.27

It can be seen from Figure 6.25a that the relation between C_o and μ value is approximately linear with a gradual slope. This chart indicates that the C_o value begins to plateau at μ values greater than 3. The highest increase in C_o value is equal to 13% when the μ value is increased from 1 to 2.

Figure 6.24b indicates that the C_k value decreases as the ductility demand increases. For example, for an RM wall with an H/L ratio of 1.0, an increase in μ value from 1 to 4 results in a decrease in C_k value from to 0.80 to 0.18. Therefore, C_k, coefficient value is inversely proportional to the μ value.

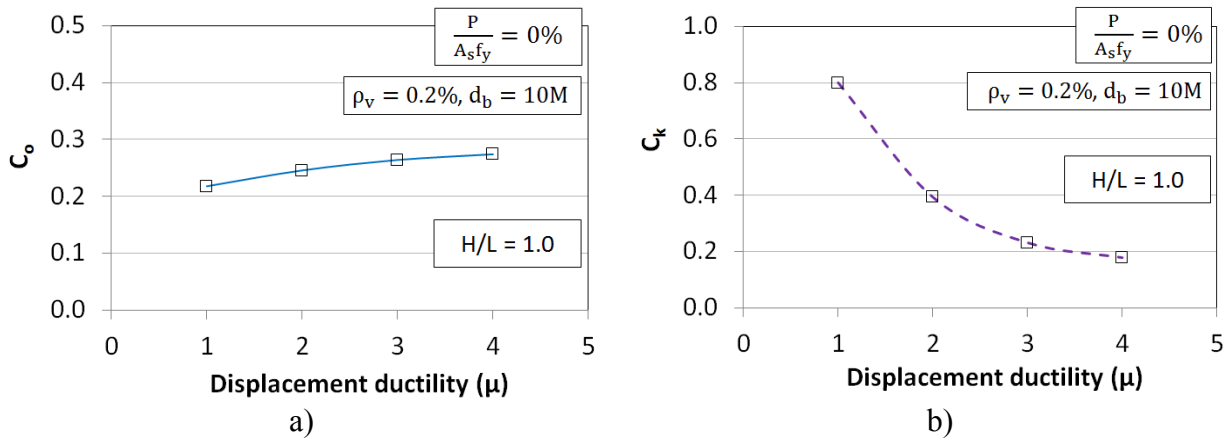

Figure 6.25 Effect of displacement ductility for RM wall with H/L = 1.0: a) C_o value vs displacement ductility, μ; b) C_k vs displacement ductility, μ.

Figure 6.24 also shows that increase in ductility demand, μ, causes an increase in the upper limit TAR2. For μ values of 1, 2 and 4; TAR2 is equal to 1.2, 1.6 and 1.8, respectively.

6.3.4 Vertical Reinforcement Ratio (ρ_v)

A parametric study is performed on RM walls with vertical reinforcement ratios, ρ_v, of 0.1%, 0.2% and 0.3%. The reinforcement spacing, s, is set constant at 600 mm with rebar diameters of 10M, 15M and 20M for reinforcement ratios, ρ_v, of 0.1%, 0.2% and 0.3%, respectively.

Figure 6.26 shows that the sliding ratio in RM walls with H/L ratios greater than TAR1, are not significantly affected by changes in reinforcement ratio, ρ_v. For a wall with an H/L ratio of 1.0, the sliding ratio is equal to 0.36, 0.35, and 0.33, for ρ_v values of 0.1%, 0.2% and 0.3%, respectively. These results indicate that changes in ρ_v value cause minor differences in sliding ratio (in the range of 5%).

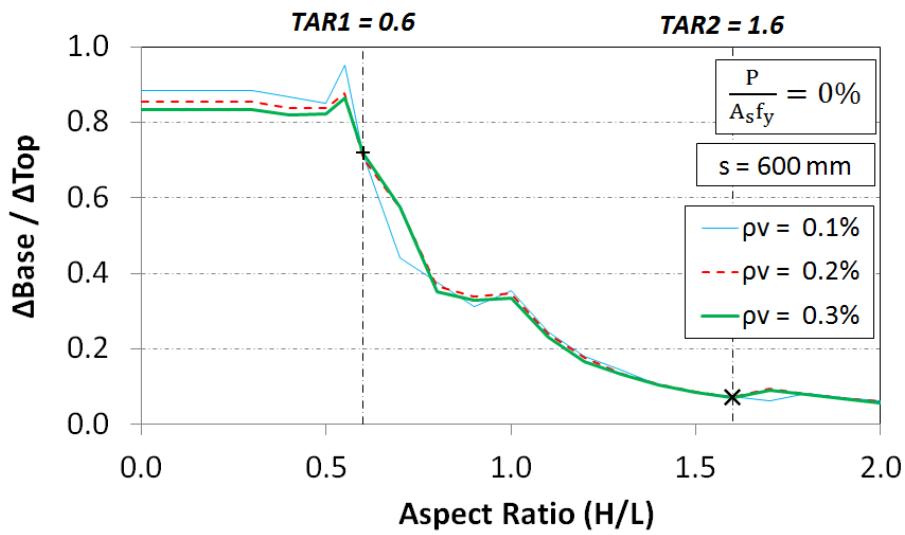

Figure 6.26 Sliding ratio vs H/L ratio at μ=2,
for different vertical reinforcement ratios (ρ_v).

Figure 6.27a indicates that the ρ_v value has a moderate influence on the C_o coefficient. As the ρ_v value increases from 0.1 to 0.3%, the average C_o coefficient, increases from 0.27 to 0.29 (see Table 6.3). These variations in ρ_v value correspond to an increase of up to 8% in the C_o coefficient.

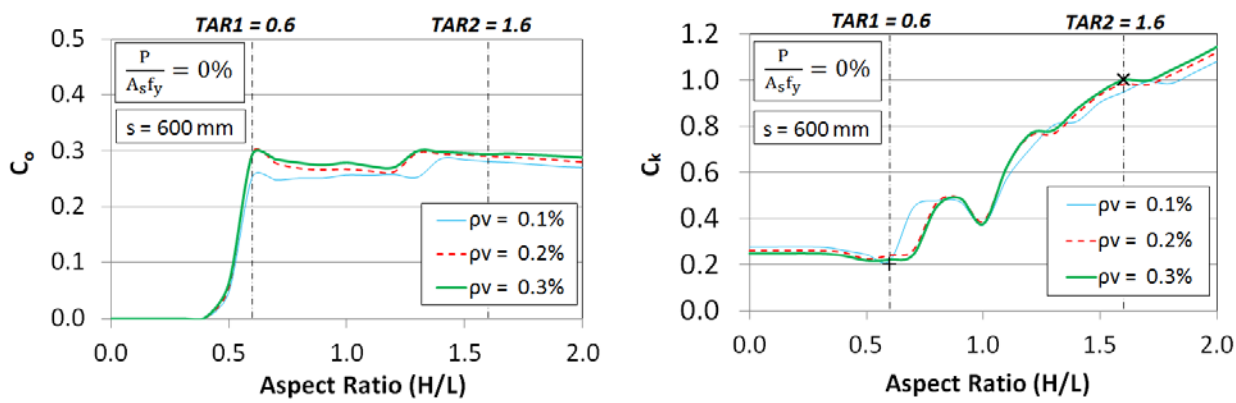

a) b)

Figure 6.27 Effect of vertical reinforcement ratio (ρ_v):
a) C_o vs H/L ratio at μ=2, b) C_k vs H/L ratio at μ=2

Table 6.3 Average C_o coefficients for different reinforcement ratios, ρ_v.

Vertical reinforcement ratios, ρ_v,	Average coefficient, C_o
0.1%	0.27
0.2%	0.28
0.3%	0.29

Figure 6.27b indicates that the ρ_v value has a moderate influence on the C_k coefficient. Differences in C_k values are in the range of 11% for ρ_v values ranging from 0.1 to 0.3%. The figure also shows that the TAR2 value is equal to 1.6 irrespective of the ρ_v value; this indicates that changes the ρ_v value do not influence the TAR2 value.

6.3.5 Vertical Reinforcement Spacing (s)

The effect of the spacing between reinforcing bars, s, is studied in this section by performing an analysis on RM wall models using s values of 400, 600 and 800 mm. All RM walls are modeled using 10M diameter bars.

It can be seen in Figure 6.28 that vertical reinforcement spacing, s, has a significant influence on the sliding ratio values. Increasing reinforcement spacing, s, from 400 to 800 mm results in higher sliding ratios for walls with H/L ratios greater than TAR1. Also observed in Figure 6.28, is that varying the reinforcement spacing from 600 to 800 mm results in a change in yield mechanism from CFSS mechanism to DCF mechanism in RM walls with H/L ratios from 0.7 to 1.0.

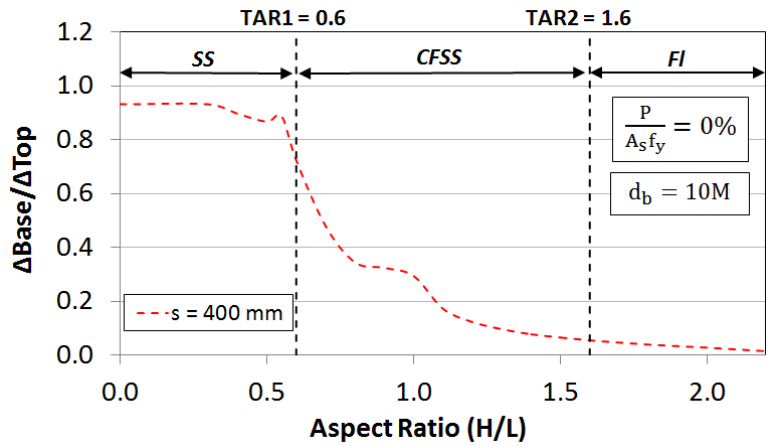

a)

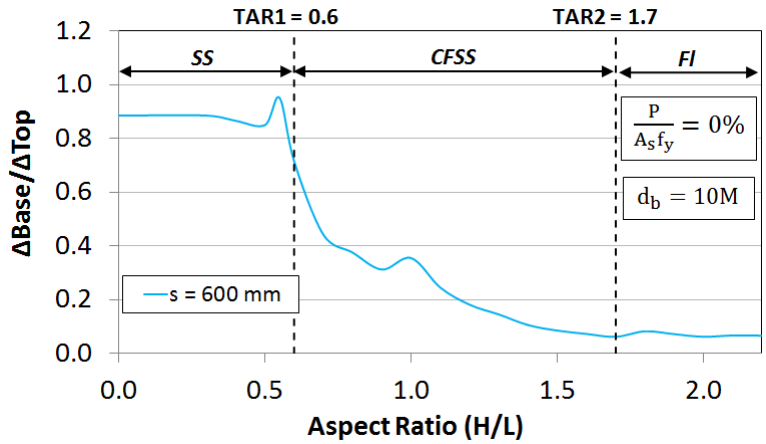

b)

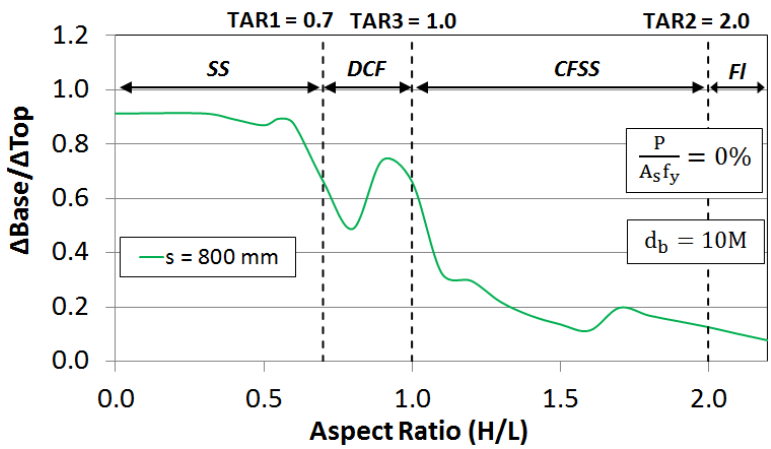

c)

Figure 6.28 Sliding ratio vs H/L ratio at μ=2, for different values of vertical reinforcement spacing, s: a) s = 400mm, b) s = 600mm, c) s = 800mm.

The upper H/L limit for an RM wall required to develop a DCF mechanism is referred to herein as the Triggering Aspect Ratio #3 (TAR3). The TAR3 value corresponds to the highest H/L ratio of an RM wall for which its dowel action resistance, DA_y, is insufficient to resist the shear force, V_o, required to close the flexural crack that causes sliding, as shown in equation 6.3. It should be noted that for RM walls with s = 800 mm, the TAR3 value is equal to 1.0.

$$H/L = TAR3, \text{ when } V_o = DA_y \tag{6.3}$$

The curves of C_o vs H/L ratio shown in Figure 6.29 indicate that the C_o coefficient increases in proportion to the reinforcement spacing, s. This effect is also observed for the average C_o values in Table 6.4, determined for RM walls with H/L ratios between H/L = TAR1 and H/L = 2.2. The average C_o value increases from 0.24 to 0.33 as the reinforcement spacing, s, increases from 400 to 800 mm. Therefore, a change in reinforcement spacing by 100% can cause a 38% variation in the C_o coefficient.

Figure 6.29 also shows shifts in the C_o value for reinforcement spacing values of 600 and 800 mm at H/L ratios of 1.4 and 1.5, respectively. These shifts in the C_o value occur because the number of vertical bars, n_{db}, for each RM wall model used in the analysis is reduced as the H/L ratio increases. The lower n_{db} value requires a different arrangement of vertical bars which results in a significant difference in C_o value for consecutive H/L ratios. The relation between n_{db} and the C_o coefficient was determined in Chapter 3 in the derivation of equation 3.8.

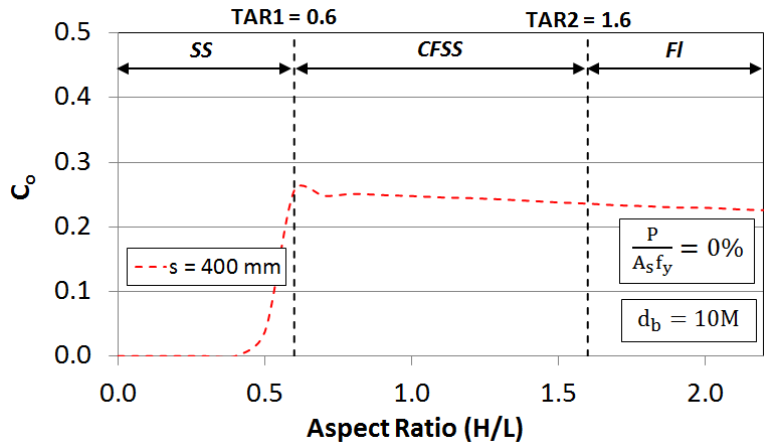

a)

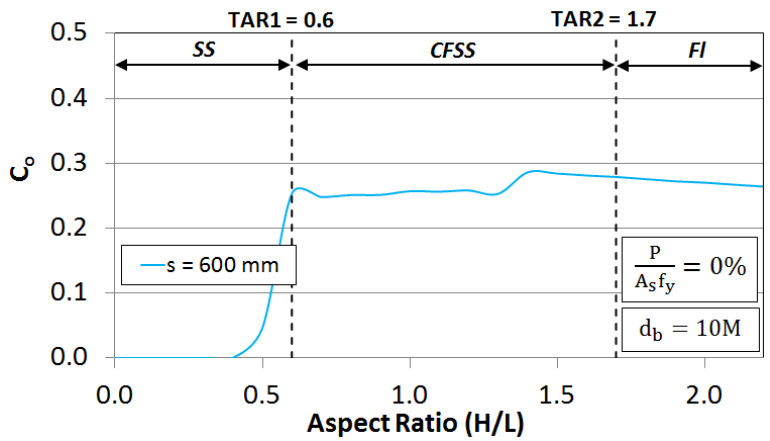

b)

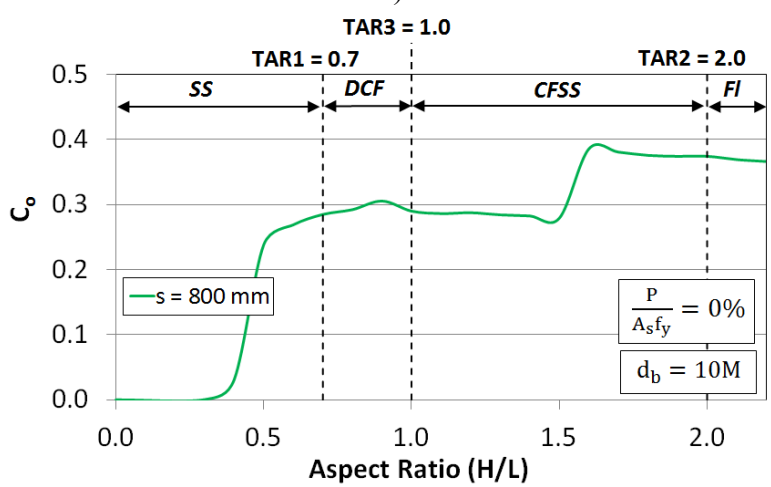

c)

Figure 6.29 Effect of vertical reinforcement spacing, s, on C_o vs H/L ratio, at μ=2: a) s = 400mm, b) s = 600mm, c) s = 800mm.

Table 6.4 Average C_o coefficients for various reinforcement spacing, s.

Reinforcement Spacing, s	Average Coefficient, C_o
400 mm	0.24
600 mm	0.27
800 mm	0.33

Figure 6.30 shows that the TAR3 value can be determined as the intersection of the curves of shear force V_o and dowel action resistance, DAy. The shear force V_o is determined using equation 3.9 and using the average C_o values shown in Table 6.4; while the dowel action resistance, DAy, is determined through equations 3.5 and 4.8.

Figure 6.30 also shows that RM walls with H/L ratios ranging from TAR1 to TAR3 develop a DCF mechanism only when the TAR1 value is less than the TAR3 value. This condition reflects the two physical conditions that are required for an RM wall to develop a DCF mechanism:

1) Developing an open flexural crack along the RM wall's full length, or
2) Dowel action resistance, DA_y, is insufficient to resist the shear force V_o required to close the open flexural crack.

Condition 1 corresponds to RM walls with H/L ratios greater than TAR1, while condition 2 corresponds to RM walls with H/L ratios less than TAR3. Therefore, an RM wall with an H/L ratio between TAR1 and TAR3 will develop a DCF mechanism only if TAR3 is greater than TAR1.

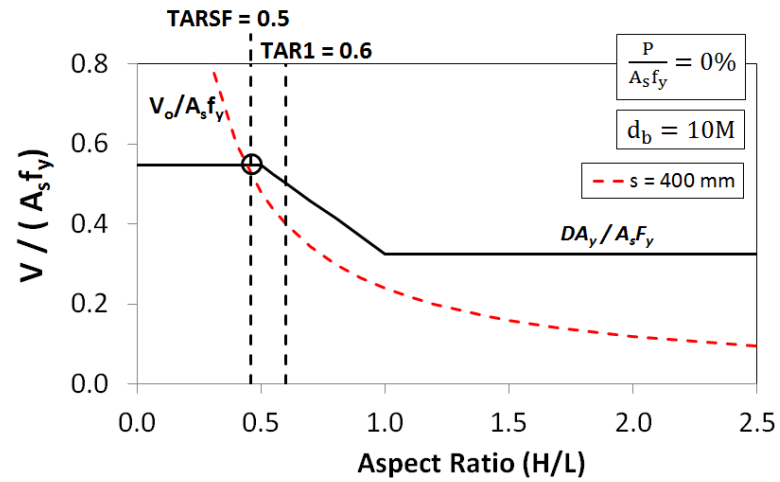

a)

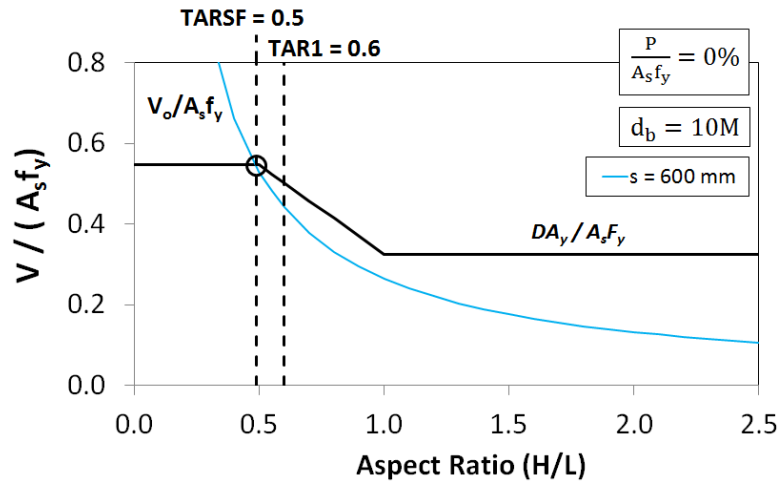

b)

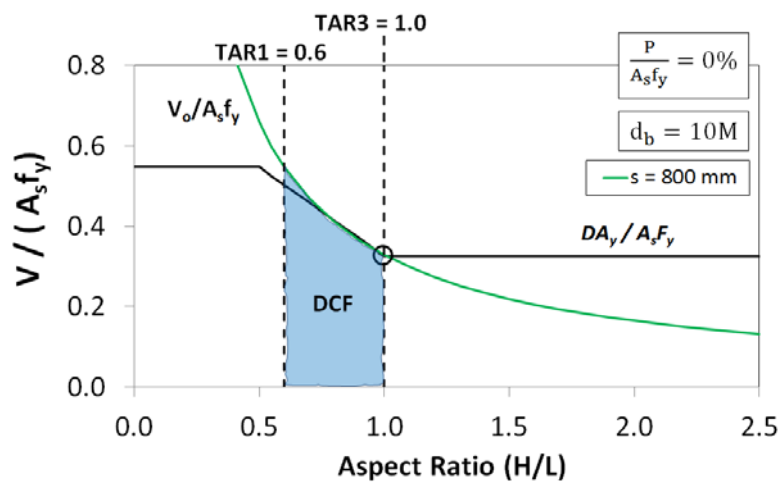

c)

Figure 6.30 Effect of vertical reinforcement spacing, s, on relation between shear force, V_o, and dowel action resistance, DA_y, a) s = 400mm, b) s = 600mm, c) s = 800mm.

Figure 6.31 shows C_k values at a displacement ductility of $\mu = 2$ for various values of reinforcement spacing, s. These curves show that the influence of the s value on yield mechanism also results in changes in C_k values. For all three values of reinforcement spacing, s, the C_k value for RM walls that experience a CFSS mechanism follows a linear ascending pattern starting at C_k of 0.2 for the lower limit H/L ratio, and reaches a C_k value of of 1.0 at the upper limit H/L ratio. In the case of RM walls that experience a DCF mechanism, the C_k coefficient shows significant variation with respect to H/L ratio, with its average value equal to 0.24 and its standard deviation equal to 0.06.

6.3.6 Diameter of Reinforcing Bar (d_b)

The effect of reinforcing bar diameter is studied performing analyses for different bar diameter values (10M, 15M and 20M), while rebar spacing, s, is set constant at 400 mm.

Figure 6.32 shows that the sliding ratio in an RM wall does not depend significantly on the reinforcement diameter. For instance, for an RM wall with an H/L ratio of 1.0, increasing the bar diameter from 10M to 15M results in a change in sliding ratio from 0.29 to 0.26. This corresponds to a reduction in the sliding ratio of 10%.

Figure 6.33a illustrates that the C_o values are not significantly affected by changes in d_b values. This effect is also observed for the average C_o values shown in Table 6.5, determined for RM walls with H/L ratios greater than TAR1 and less than 2.0. For instance, the average C_o value increases from 0.24 to 0.25 as the reinforcing bar diameter, d_b, increases from 10M to 15M. These results indicate that the d_b value can cause variations in the C_o value in the range of 4%.

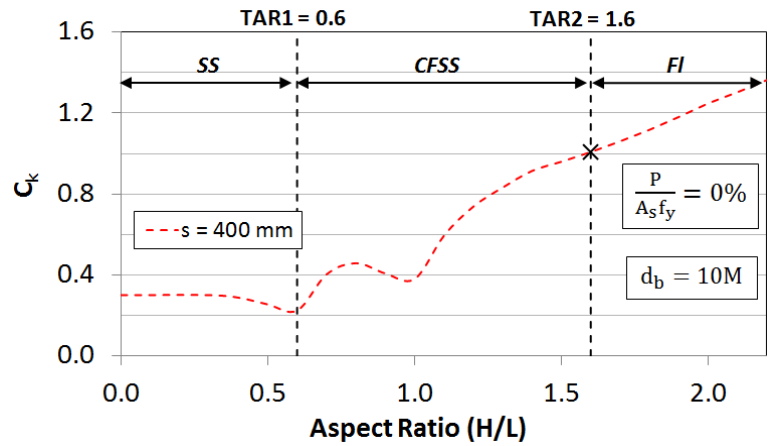

a)

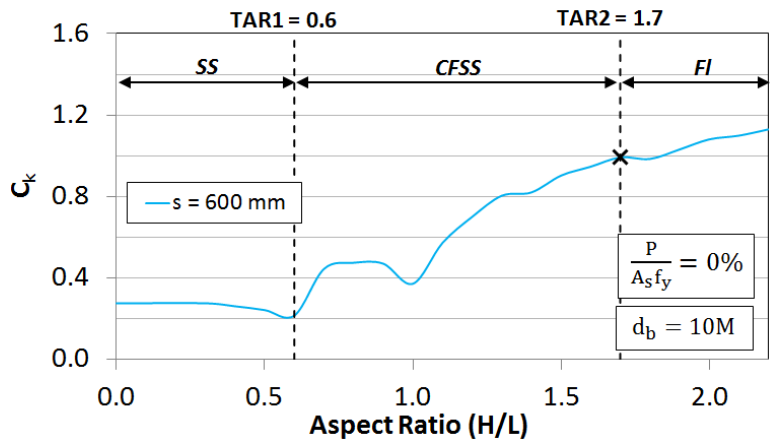

b)

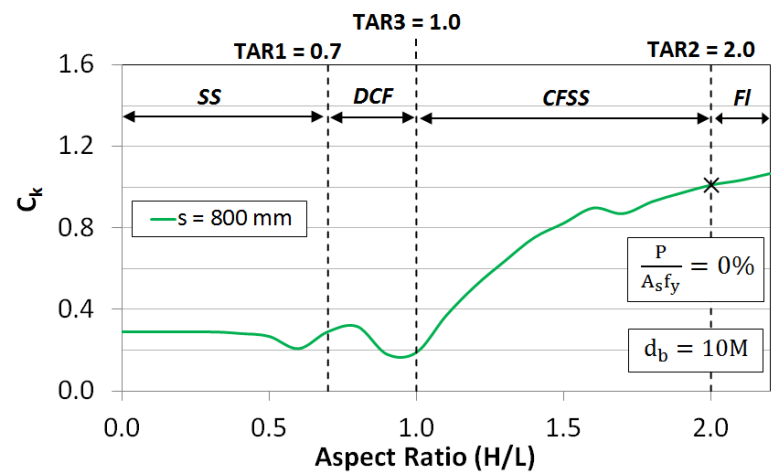

c)

Figure 6.31 Effect of vertical reinforcement spacing, s, on C_k vs H/L ratio, at μ=2: a) s = 400mm, b) s = 600mm, c) s = 800mm.

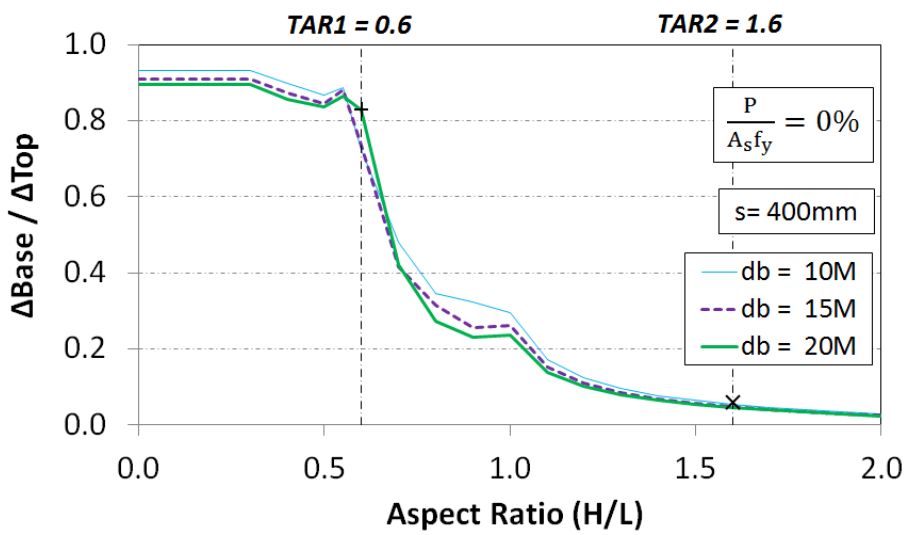

Figure 6.32 Sliding ratio vs H/L ratio at μ=2,
for different values of rebar diameter, d_b.

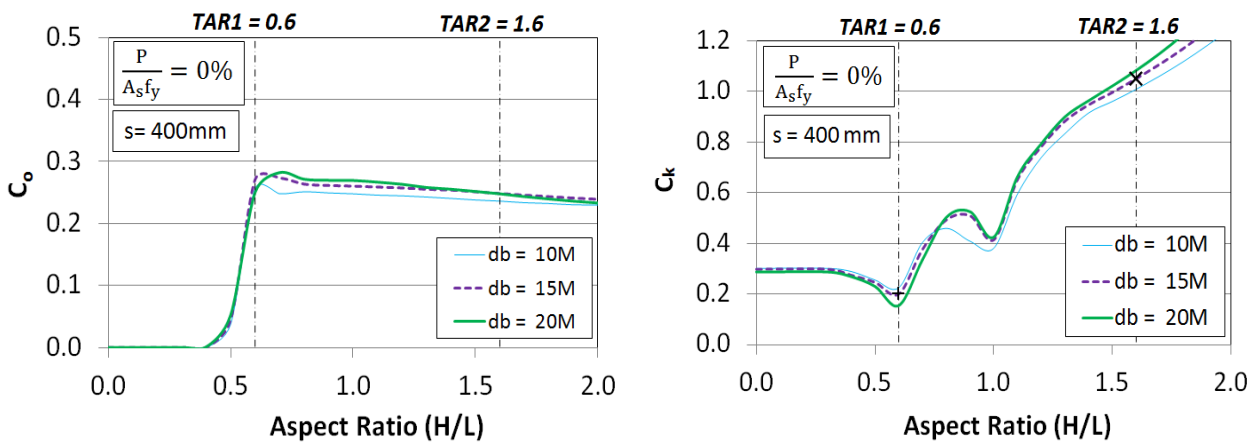

a) b)

Figure 6.33 Effect of rebar diameter, d_b:
a) C_o vs H/L ratio, at μ=2, b) C_k vs H/L ratio, at μ=2.

Figure 6.33b shows reinforcing bar diameter, d_b, has a moderate influence on C_k values. The variations in C_k value range from 4% to 9% for consecutive d_b values. In addition, the TAR2 remains constant at 1.6, irrespective of changes in d_b value.

Table 6.5 Average C_o coefficients for various reinforcement bar diameters, d_b.

Diameter of reinforcing bar, d_b	Average Coefficient, C_o
10M	0.24
15M	0.25
20M	0.26

6.3.7 Masonry Compression Strength (f'_m)

The effect of masonry compression strength, f'_m, is studied using the values of 5 MPa, 10 MPa, and 15 MPa. The reinforcement ratio, ρ_v, is set constant at 0.2% and using 10M diameter bars.

In Figure 6.34, for each H/L ratio it can be observed that higher f'_m values result in higher sliding ratios. For instance, for an RM wall with an H/L ratio of 1.0, an increase in f'_m value from 5 to 10 MPa results in an increase in the sliding ratio from 0.20 to 0.25. Therefore, changes in f'_m value can result in differences in the sliding ratio in the range of 30%.

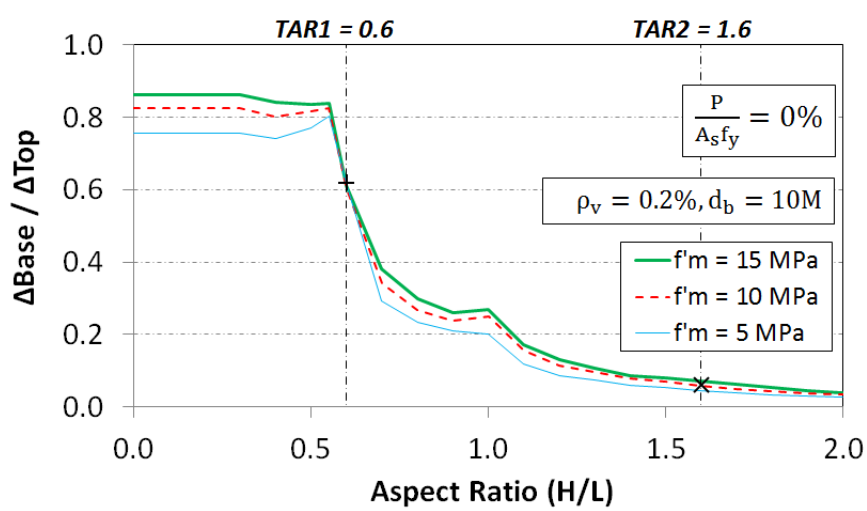

Figure 6.34 Sliding ratio vs H/L ratio at μ=2,
for different values of masonry compression strength (f'_m).

Curves in Figure 6.35a show that higher f'_m values result in lower C_o coefficients. For example, when an H/L ratio is equal to 1.0, the C_o coefficient is equal to 0.26, 0.25 and 0.24 for the f'_m values of 5, 10 and 15 MPa, respectively. This effect is also observed for the average C_o coefficient determined for H/L ratios from 0.6 to 2.0, shown in Table 6.6. The variation in average C_o coefficient is equal to 4% when the f'_m value is increased from 5 MPa and 10 MPa.

Figure 6.35b shows that masonry compression strength, f'_m, has some influence on C_k values. For H/L ratios less than 1.0, C_k increases with an increase in the f'_m value. On the other hand, for H/L ratios greater than 1.0, C_k is not affected by the f'_m value. The C_k results also show that f'_m values have no significant effect on the TAR2 value. In all three cases considered, the upper limit TAR2 value is equal to 1.6.

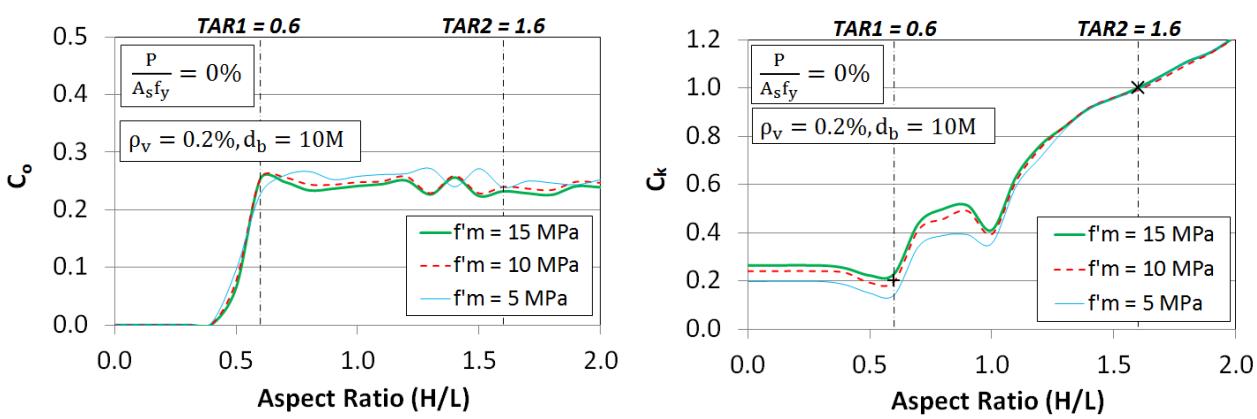

a) b)

Figure 6.35 Effect of masonry compression strength (f'_m) on:

a) C_o vs H/L ratio at μ=2, b) C_k vs H/L ratio at μ=2.

6.3.8 Grout Compression Strength (f'_g)

The masonry grout compression strength, f'_g, values are 5, 15 and 35 MPa, which represent low, medium and high strength values, respectively. For the sake of simplicity in modeling, the

masonry grout strength, f'_g, is assumed to be independent of the masonry compression strength f'_m, which is set at 10 MPa. The reinforcement ratio, ρ_v, is set constant at 0.2% using 10M diameter bars.

Table 6.6 Average C_o coefficients for masonry compression strength, f'_m.

Masonry Compression Strength, f'_m	Average coefficient, C_o
5 MPa	0.24
10 MPa	0.25
15 MPa	0.25

Figure 6.36 shows that the sliding behaviour in RM walls is significantly influenced by the masonry grout strength, f'_g. For example, an RM wall with an H/L ratio equal to 1.0 experiences a reduction in the sliding ratio from 1.40 to 0.25 when the f'_g value increases from 15 MPa to 35 MPa. Therefore, changes in grout compressive strength can result in a variation in sliding ratio in the range of 88%.

The curves of C_o vs H/L ratio shown in Figure 6.37 indicate that the average C_o coefficient remains equal to 0.25 for RM walls that experience a CFSS mechanism and Fl mechanism, irrespective of the f'_g value. For RM walls that experience a DCF mechanism, the C_o value is less than 0.25. This difference in behaviour occurs when dowel action has reached its yield resistance, DA_y, and therefore the overturning moment developed is less than the moment required to close the flexural crack, M_o.

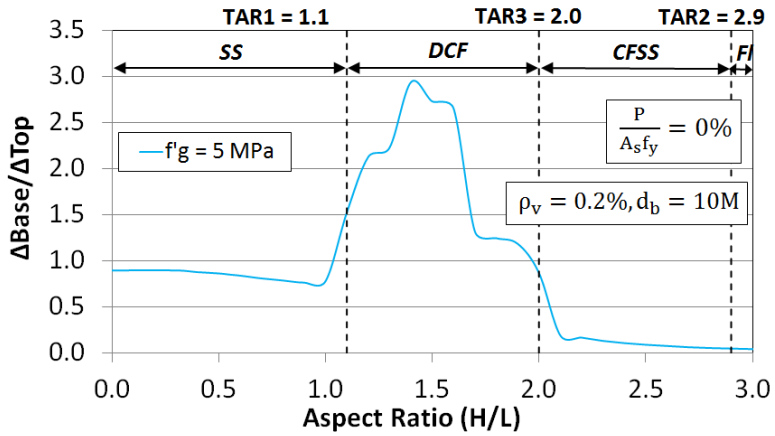

a)

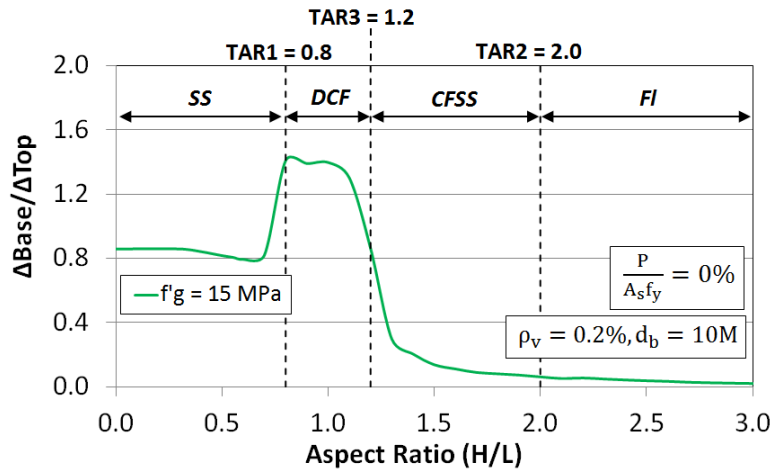

b)

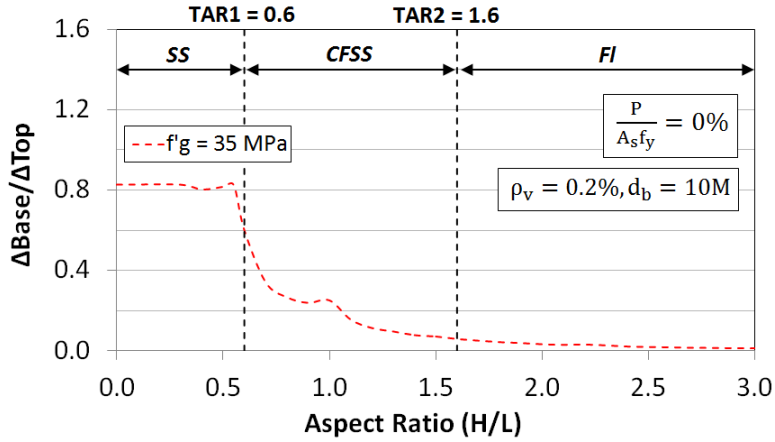

c)

Figure 6.36 Sliding ratio vs aspect ratio (H/L), at μ=2, for different f'$_g$ values: a) f'g = 5 MPa, b) f'g = 15 MPa, c) f'g = 35 MPa.

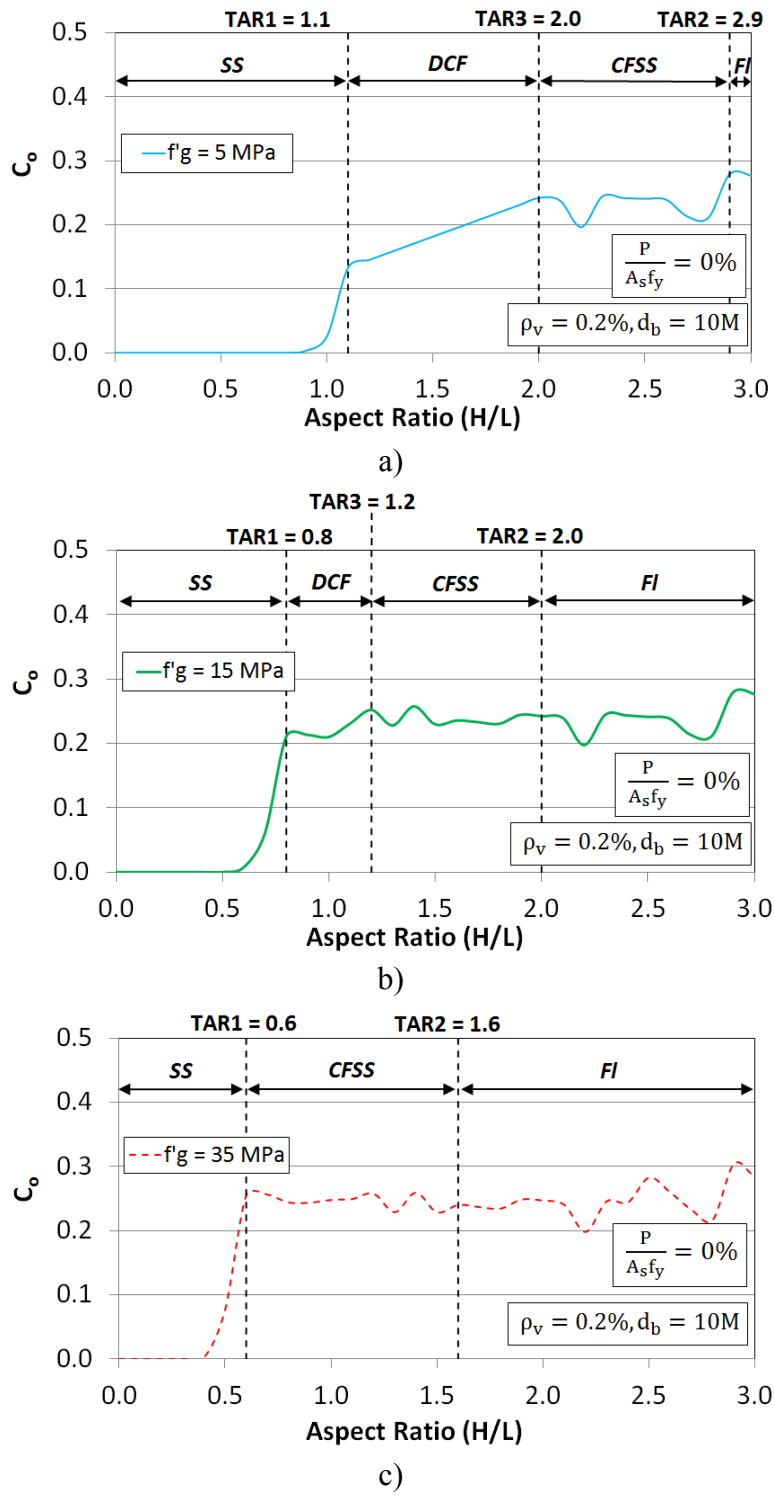

Figure 6.37 Effect of grout compressive strength, f'_g, on C_o vs H/L ratio, at μ=2: a) f'g = 5 MPa, b) f'g = 15 MPa, c) f'g = 35 MPa.

Figure 6.38 shows that the TAR3 value can be determined as the intersection of the curves of shear force V_o and dowel action resistance, DA_y. The shear force, V_o, is determined using equation 3.9, with the C_o value equal to 0.25; while the dowel action resistance, DAy, is determined through equations 3.5 and 4.8. An RM wall will experience a DCF mechanism if its H/L ratio is greater than TAR1 and less than TAR3.

Figure 6.39 shows, that when a displacement ductility demand, μ, is equal to 2, the C_k coefficient varies depending on the f'_g value and the wall's yield mechanism. For RM walls that experience a DCF mechanism, the C_k value is approximately constant and equal to 0.03 and 0.06 for f'_g values of 5 MPa and 15 MPa, respectively. For RM walls that experience a CFSS the mechanism, the C_k value follows a linear ascending pattern beginning at a minimum value and reaching a maximum value of 1.0 at an H/L ratio equal to TAR2. The minimum C_k value in a CFSS mechanism, as shown in Figure 6.39, varies depending on the f'_g value. For f'_g values of 5, 15 and 35 MPa, the minimum C_k values are equal to 0.07, 0.11 and 0.20, respectively.

Figure 6.39b also shows that the TAR2 value decreases with an increase in f'_g value. The TAR2 value decreases from 2.90 to 1.60 as the f'_g value increases from 5 to 35 MPa.

6.3.9 Steel Yield Strength (f_y)

In this study the effect of the sliding behaviour of RM walls is examined for common values of steel yield strength, f_y, of 350, 400 and 500 MPa. The reinforcement ratio, ρ_v, is set at 0.2%, using 10M diameter bars.

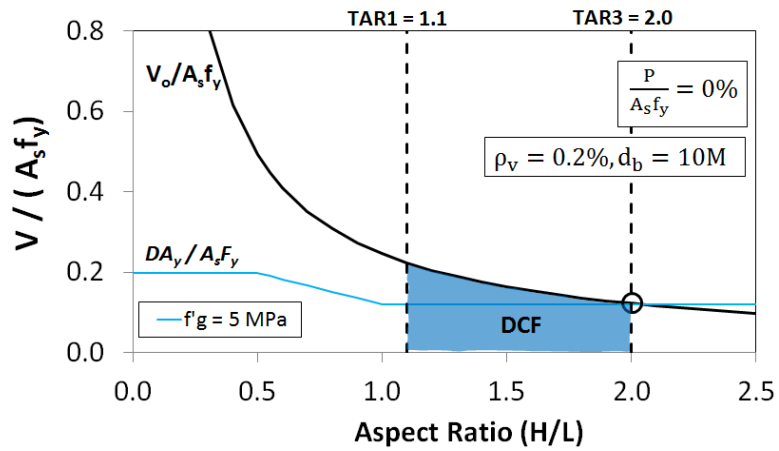

a)

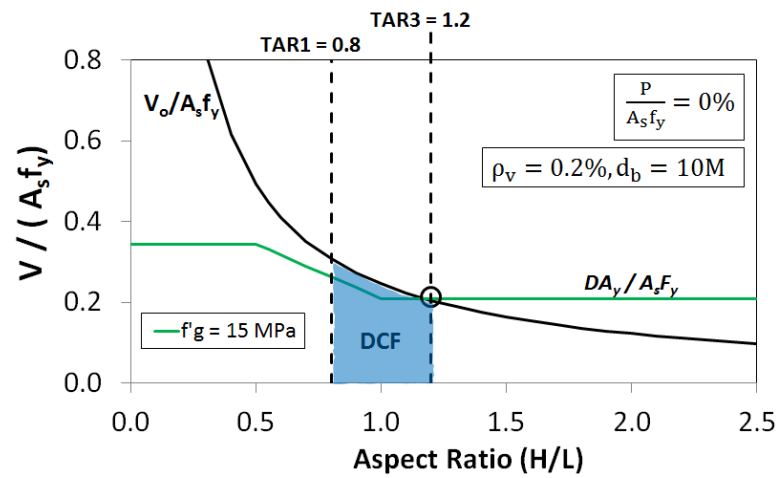

b)

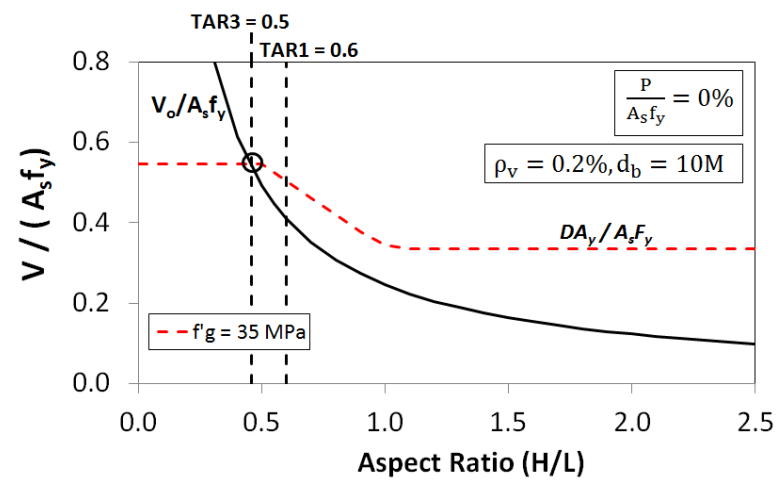

c)

Figure 6.38 Effect of grout compressive strength, f'_g, on relation between shear force, V_o, and dowel action resistance, DA_y: a) f'g = 5 MPa, b) f'g = 15 MPa, c) f'g = 35 MPa.

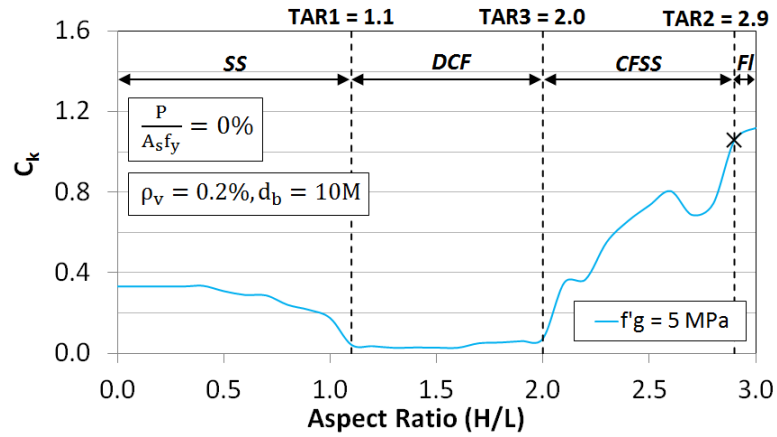

a)

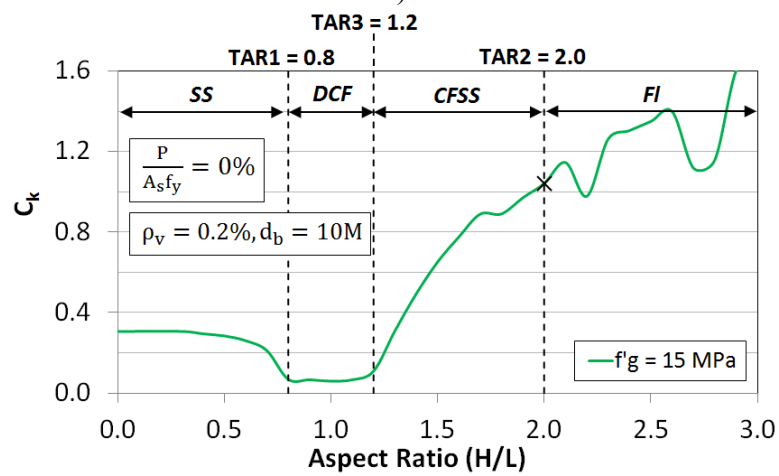

b)

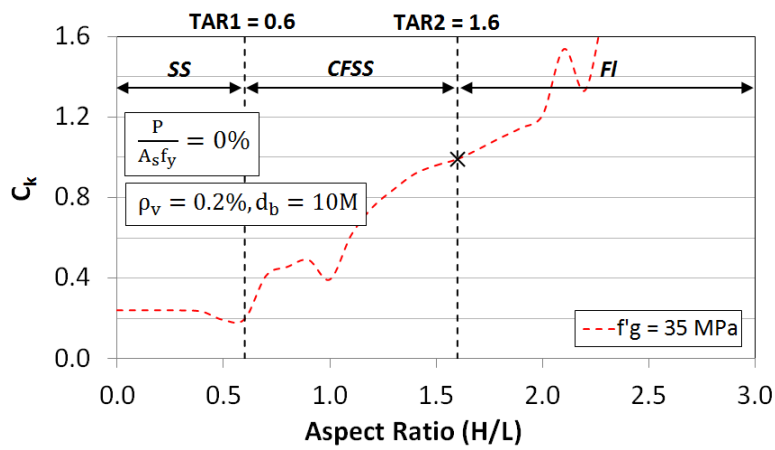

c)

Figure 6.39 Effect of grout compression strength, f'$_g$, on C_k vs H/L ratio, at μ=2: a) f'g = 5 MPa, b) f'g = 15 MPa, c) f'g = 35 MPa.

The sliding ratio curves in Figure 6.40 show that steel reinforcement with higher f_y values cause an increase in the sliding ratio for walls experiencing a CFSS mechanism. For instance, for an RM wall with an H/L ratio equal to 1.0, an increase in f_y value from 350 to 400 MPa results in an increase in the sliding ratio from 0.18 to 0.25. Therefore, changes in the steel yield strength can result in differences in $\Delta_{Base}/\Delta_{Top}$ values in the range of 40%.

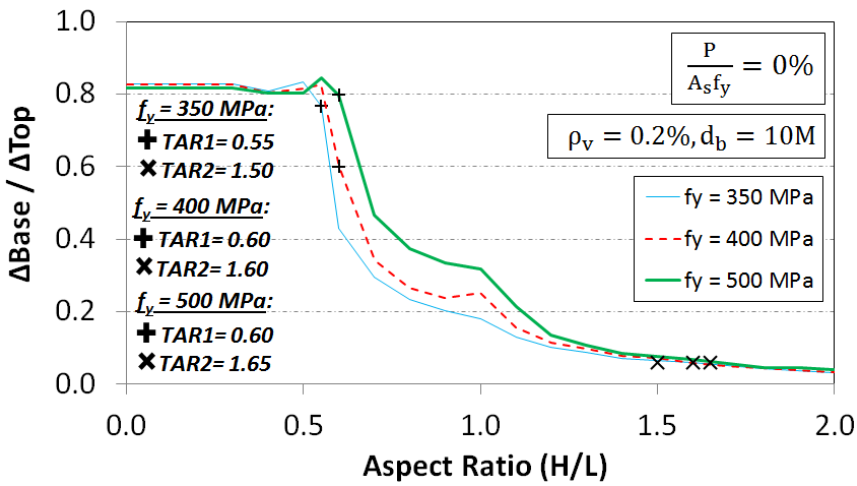

Figure 6.40 Sliding ratio vs H/L ratio at μ=2, for various steel reinforcement strength values.

Figure 6.41a shows the C_o coefficient is not influenced by the steel yield strength, f_y. Its value is shown to remain at 0.25 irrespective of the f_y value.

Figure 6.41b, shows that for RM walls that experience a SS mechanism (H/L ratios less than TAR1), the C_k coefficient is in dependent of the f_y value. In the case of RM walls that experience a CFSS mechanism (H/L ratios between TAR1 and TAR2), the C_k coefficient is inversely proportional to the f_y value.

Figure 6.41b also shows that the TAR2 value increases with an increase in f_y value. The TAR2 value increases from 1.50 to 1.65 as the f_y value increases from 350 to 500 MPa.

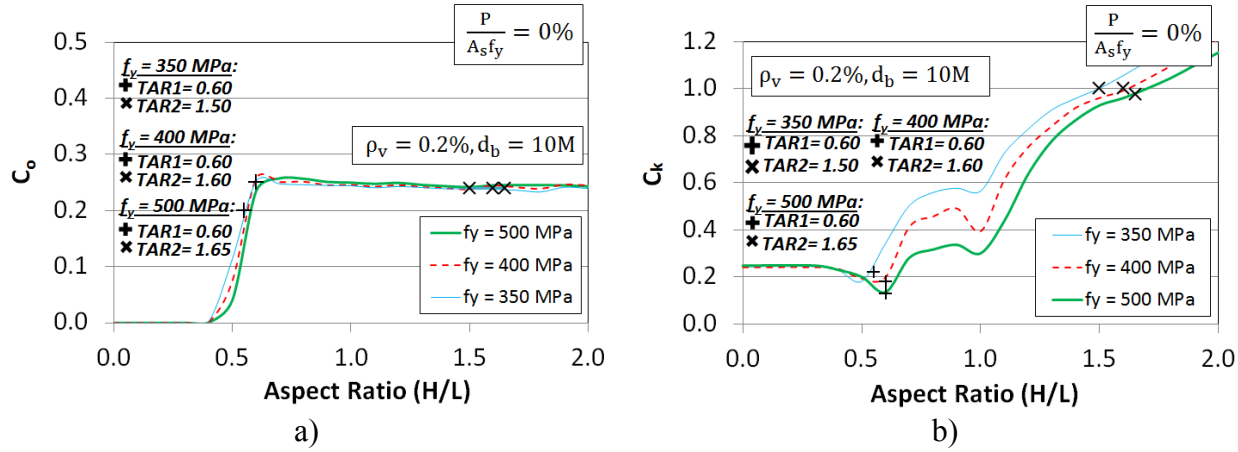

Figure 6.41 Effect of steel reinforcement strength (f_y): a) C_o vs H/L ratio, at μ=2, b) C_k vs H/L ratio, at μ=2.

6.3.10 Axial Compression Level (P/A_sf_y)

In this section the axial compression level, P/A_sf_y, is studied, considering values of 0%, 25%, 50% and 100%. For all RM wall models, the reinforcement ratio is set at ρ_v=0.2% using 10M diameter bars.

Figure 6.42 shows that higher axial compression levels can cause a decrease in the sliding ratios developed in RM walls with a CFSS mechanism. For instance, for an RM wall with an H/L ratio equal to 1.0, an increase in the P/A_sf_y value from 0% to 50% results in the decrease in sliding ratio, $\Delta_{Base}/\Delta_{Top}$, from 0.25 to 0.15. This variation corresponds to a 40% reduction in the RM wall's sliding ratio.

Figure 6.43 shows that the C_o coefficient varies in proportion to the axial compression level, P/A_sf_y. Results show that the C_o coefficient decreases at higher P/A_sf_y values. This effect is also

observed for the average C_o values shown in Table 6.7, determined for RM walls with H/L ratios between TAR1 and 2.0. For instance, the average C_o value decreases from 0.25 to 0.11 as the axial compression level, P/A_sf_y, increases from 0% to 50%.

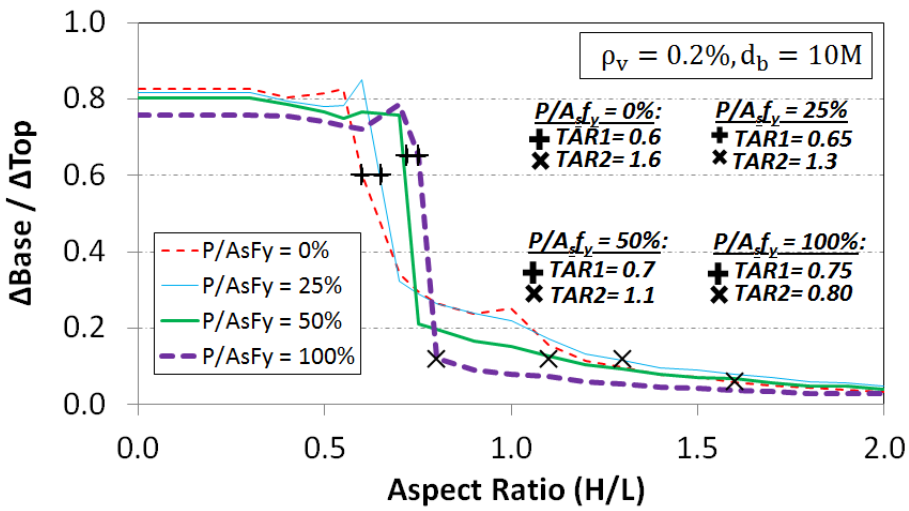

Figure 6.42 Sliding ratio vs H/L ratio at μ=2, for various axial compression levels, P/A_sf_y.

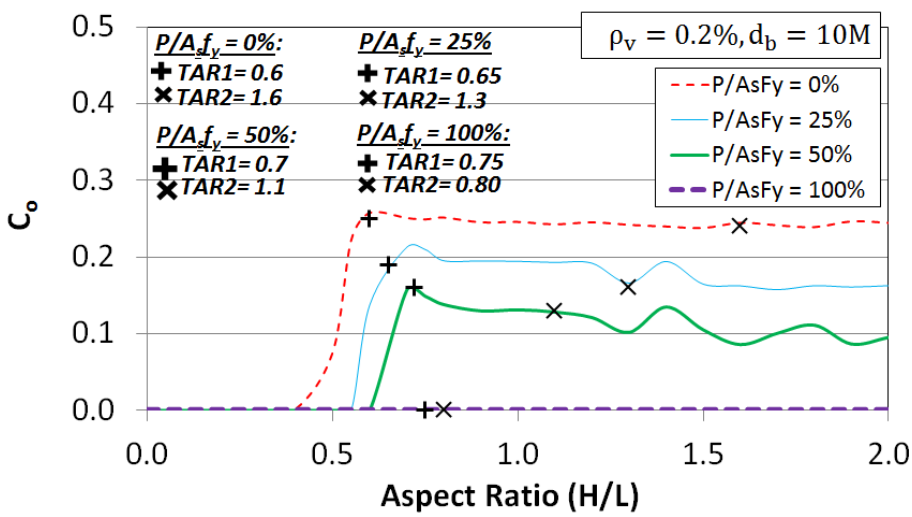

Figure 6.43 Effect of axial compression level (P/A_sf_y) on C_o vs H/L ratio, at μ=2

Table 6.7 Average C_o coefficients for masonry compression strength, f'_m.

Axial Compression Level, P/A_sf_y	Average Coefficient, C_o
0%	0.25
25%	0.18
50%	0.11
100%	0.0

Figure 6.44 shows that in RM walls with a sliding shear mechanism (H/L ratios less than TAR1) the C_k coefficient is, on average, equal to 0.25 and it is not influenced by P/A_sf_y. For RM walls with a CFSS mechanism (H/L ratios between TAR1 and TAR2), higher axial compression levels result in higher C_k values.

The results also show that higher axial compression levels result in a reduction in the upper limit TAR2. It can be seen from Figure 6.44 that as P/A_sf_y values increase from 0 to 100%, the TAR2 values decrease from 1.6 to 0.8, respectively.

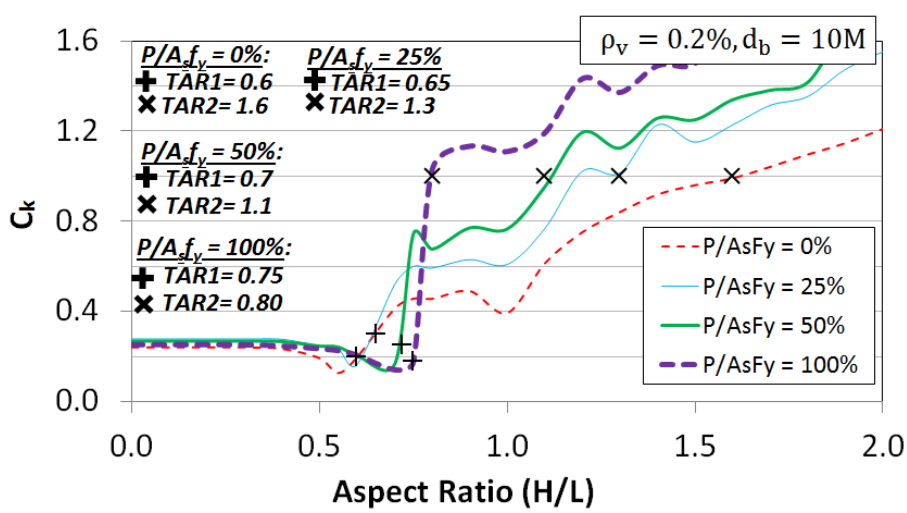

Figure 6.44 Effect of axial compression level, P/A_sf_y, on C_k vs H/L ratio, at μ=2

6.3.11 Summary of Results of Parametric Studies

From the results of the parametric studies it has been observed that various design parameters have different levels of influence on the sliding behaviour of an RM wall. A summary of these results is presented in Table 6.8, where variations in sliding behaviour parameters were evaluated for RM walls with H/L ratios between TAR1 and TAR2 values. This table identifies the design parameters that showed low, moderate and high influence on the sliding behaviour parameters. A low influence refers to a variation of less than 5% between consecutive design parameters; medium influence to a variation between 5% and 20%; and high influence to a variation greater than 20%.

Table 6.8 Design parameters that influence sliding behaviour parameters in RM walls.

Design Parameters	$\frac{\Delta Base}{\Delta Top}$	C_o	C_k	**TAR2**
H/L	●	○	●	N/A
H	●	○	●	○
μ	●	◑	●	◑
ρ_v	○	◑	◑	○
s	●	●	●	●
d_b	◑	○	◑	○
f'_m	●	○	●	○
f'_g	●	○	●	●
f_y	●	○	●	◑
$P/A_s f_y$	●	●	●	●

○ Low influence: Variations lower than 5%.
◑ Moderate influence: Variations ranging from 5% to 20%.
● High influence: Variations greater than 20%.

It can be seen that the sliding ratio, $\Delta_{Base}/\Delta_{Top}$, and C_k coefficient show the highest sensitivity to changes in values. On the other hand, the C_o coefficient is shown to be influenced mostly by the spacing of reinforcing bars, s, and the axial compression level, P/A_sf_y. The TAR2 values are mostly influenced by the spacing of the reinforcing bars, s; the axial compression level, P/A_sf_y, and the grout compression strength, f'_g.

It has been observed that the reinforcement ratio, ρ_v, and the reinforcing bar diameter, d_b, show the lowest influence on the sliding behaviour of RM walls subjected to cyclic loading. These results indicate that, changing the vertical reinforcement density ratio, ρ_v, or the diameter of reinforcing bars, d_b, will not prevent the formation of a CFSS mechanism or a DCF mechanism in the RM wall.

6.4 Design Equations for RM walls that Experience a DCF Mechanism and a CFSS Mechanism

The sliding response parameters of RM walls subjected to cyclic loading studied in this chapter were the C_o coefficient, the C_k coefficient and the TAR2 value. These parameters need to be estimated to predict the yield mechanism, overturning moment, M_o, and the base sliding displacements in an RM wall subjected to cyclic loading. Equations for determining these parameters are proposed in this section based on the results from the parametric studies performed in this chapter.

6.4.1 Overturning Moment to Close Flexural Crack, M_o

The overturning moment required to close the flexural crack along the wall length, M_o, is influenced by: i) the axial compression level, $P/(A_s f_y)$ and ii) the spacing of the reinforcing bars, s. Based on this observation and through curve fitting of analytical data, empirical expressions for estimating M_o and C_o values are proposed below.

$$M_o = [C_o] A_s f_y L \tag{6.4}$$

$$\text{where } C_o = \left[0.21\left(1 + \frac{s}{L}\right)\left(1 - \frac{P}{A_s f_y}\right)\right] \tag{6.5}$$

Figure 6.45 shows the M_o values from equation 6.5 plotted against the values obtained from the parametric studies performed in this chapter. The M_o values are determined for the H/L ratios greater than TAR1 and varying: reinforcement ratios, ρ_v; rebar spacing, s; axial compression level, $P/A_s f_y$; and displacement ductility demand, μ. The reference line represents an ideal match between prediction from equation 6.5 and the analysis results. Most data points are shown to be close to the reference line. The highest deviation from the reference line is obtained in cases where μ value is equal to 1 and the $P/A_s f_y$ value is equal to 50%. In that case, Equation 6.5 presents a standard deviation of 22% with respect to the value in the reference line. The correlation factor between these values is determined to be 0.97.

6.4.2 Upper Limit for a CFSS Mechanism, TAR2

Based on the parametric studies presented in this chapter, an empirical expression for estimating the TAR2 value is presented in equation 6.6. This is developed through the curve fitting of the analysis results. TAR2 is expressed as a function of the C_o coefficient, the grout compression

strength, f'_g, and the steel yield strength, f_y, as shown in Figure 6.46. The values obtained through this equation have a correlation factor of 0.97 with analysis results.

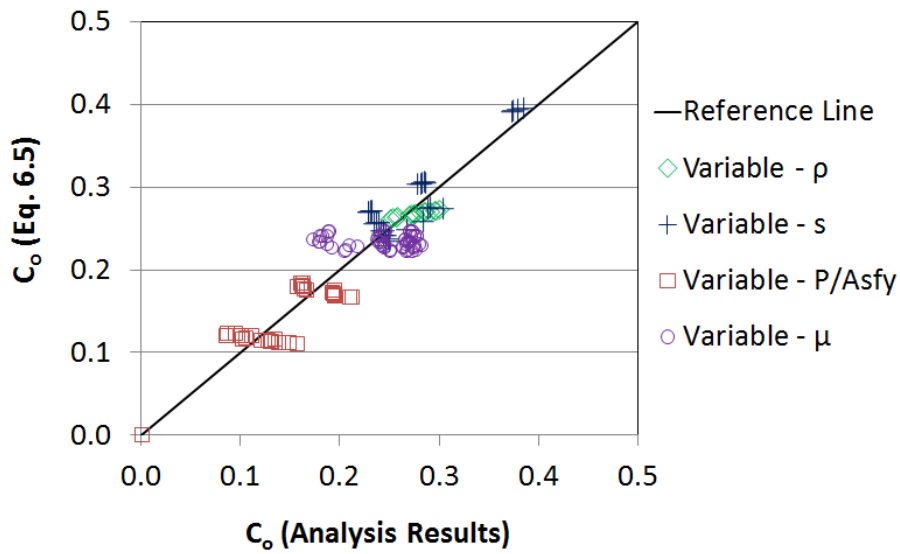

Figure 6.45 Comparison of C_o values obtained from parametric studies and equation 6.5.

$$\mathrm{TAR2} = 0.8\left[1 + C_o\sqrt{\frac{f_y}{f'_g}}\right] \tag{6.6}$$

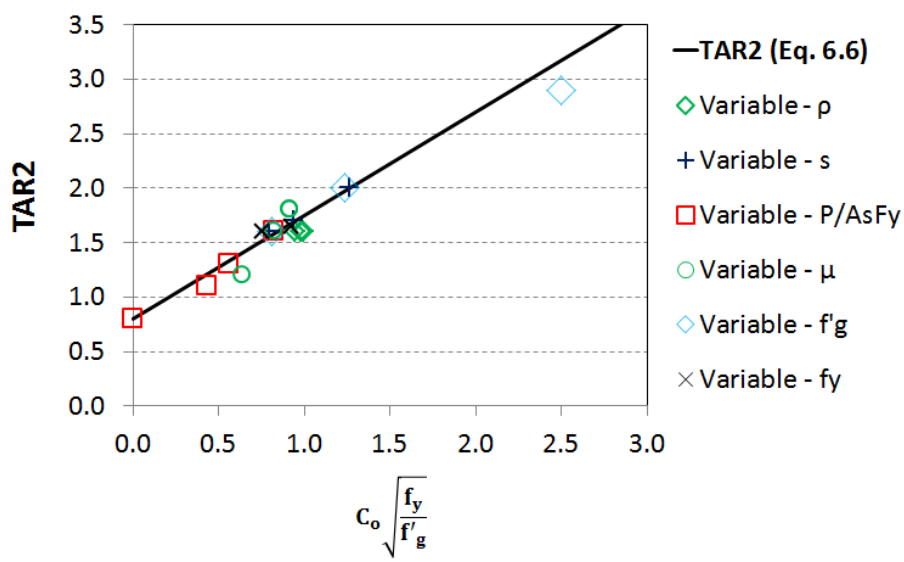

Figure 6.46 Relation between TAR2 and parameters C_o, f_y, f'_g.

6.4.3 Dowel Action Secant Stiffness Coefficient, C_k

This section proposes an approach to estimate the dowel action secant stiffness coefficient, C_k, for the design of an RM wall that experiences either a DCF mechanism or a CFSS mechanism. The C_k coefficient has been shown, through parametric studies, to vary as a function of the yield mechanism, the wall H/L ratio and the displacement ductility, μ.

For RM walls that experience a DCF mechanism an expression is proposed for the C_k coefficient as a function of displacement ductility, μ, as shown in equation 6.7:

$$C_k = \frac{0.12}{\mu} \tag{6.7}$$

For a CFSS mechanism, the C_k coefficient varies as a function of wall H/L ratio and displacement ductility, μ. The C_k value also depends on whether the TAR3 value is greater or less than the TAR1 value. The C_k coefficient for a CFSS mechanism can be obtained from equations 6.8a and 6.8b.

$$C_k = \left[\frac{0.40}{\mu} + \left(1 - \frac{0.40}{\mu}\right)\left(\frac{H/L - TAR1}{TAR2 - TAR1}\right)\right], \qquad \text{if } TAR3 < TAR1 \tag{6.8a}$$

$$C_k = \left[\frac{0.12}{\mu} + \left(1 - \frac{0.12}{\mu}\right)\left(\frac{H/L - TAR3}{TAR2 - TAR3}\right)\right], \qquad \text{if } TAR3 \geq TAR1 \tag{6.8b}$$

Figure 6.47 shows a comparison of C_k values obtained from equation 6.8 and analysis results from the 2D model for RM walls with a CFSS mechanism. For both cases, the C_k values estimated using equation 6.8 are shown to be a satisfactory estimation of analysis results.

Estimations of C_k values for RM walls with a DCF mechanism are also compared in Figure 6.47b. The comparison indicates that equation 6.7 provides a suitable estimation of analysis results obtained from the 2D model.

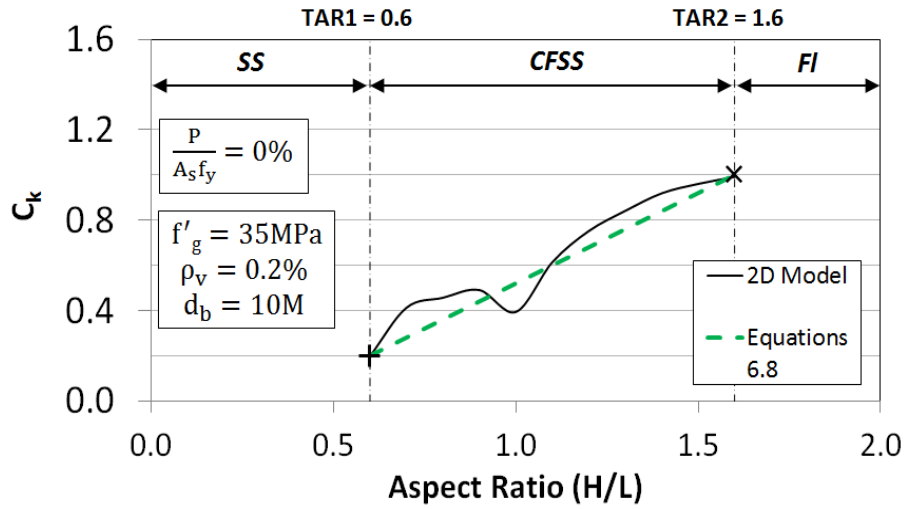

a)

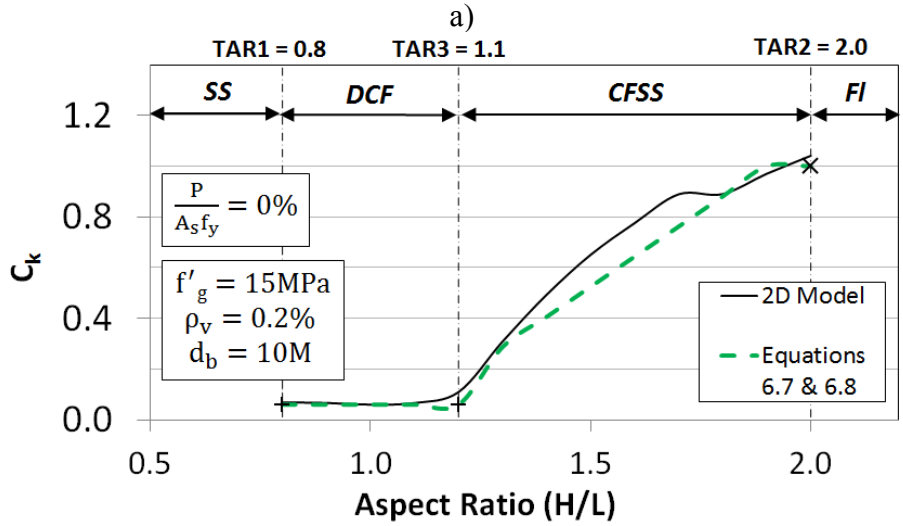

b)

Figure 6.47 C_k, values obtained from equations 6.7 and 6.8 vs results from 2D model: a) TAR3 < TAR1, b) TAR3 ≥ TAR1.

6.4.4 Estimating Sliding Displacements in a CFSS Mechanism

An empirical expression for estimating the base sliding displacement in RM walls that experience a CFSS mechanism is presented in equation 6.9 and has been developed through the

curve fitting of analysis results. The expression is based on the observation that sliding displacements develop due to elastic dowel action deformations while transferring the shear force V_o across the open flexural crack, and that dowel action secant stiffness, k_{sec}, degrades in proportion to the ductility demand, μ.

$$\Delta_{Base} = 1.25 \frac{V_o}{C_k k_{DA}} \tag{6.9}$$

Figure 6.48 shows a comparison of base sliding displacements obtained from equation 6.9 and those from analysis results of the 2D model. The results obtained using equation 6.9 show a satisfactory match, and the corresponding correlation factor is 0.98.

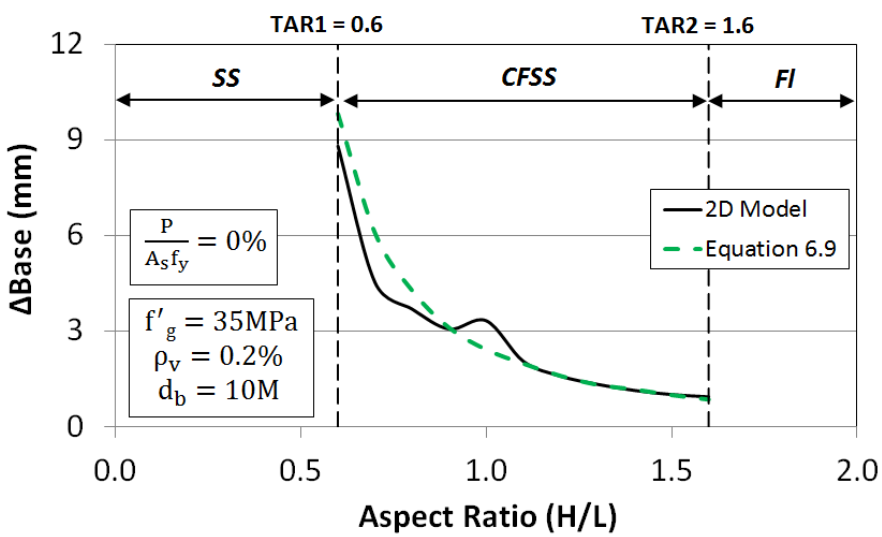

Figure 6.48 Base sliding displacement values obtained from equations 6.9 vs results from 2D model.

Figure 6.49 shows the Δ_{Base} values obtained from equation 6.9 plotted against the results from the parametric studies performed in this chapter. Most data points are shown to be close to the reference line. The highest eccentricity from the reference line is equal to 46% which

corresponds to cases where the μ value is equal to 4.0. The correlation factor between the 2D model results and results from equation 6.9 is equal to 0.87.

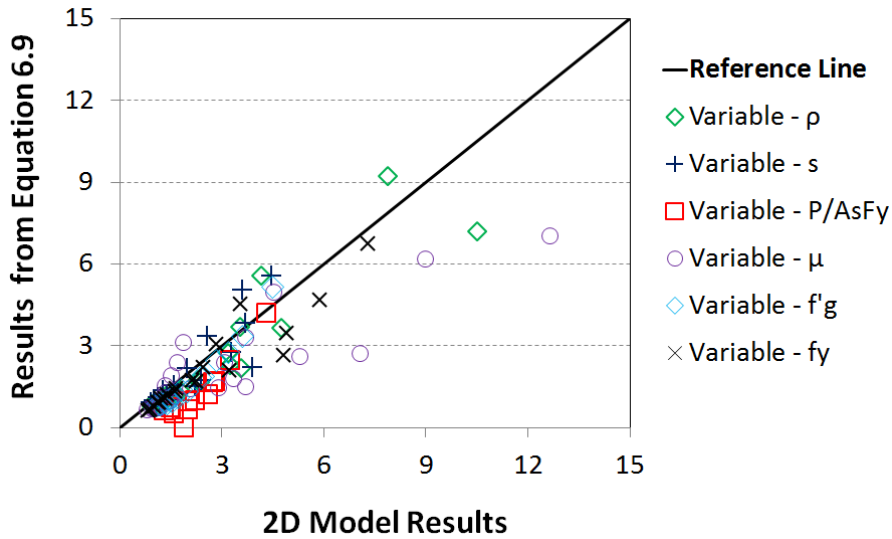

Figure 6.49 Comparison of Δ_{Base} values obtained from parametric studies and equation 6.9.

6.4.5 Estimating Sliding Displacements in a DCF Mechanism

An expression for estimating the base sliding displacement in RM walls that experience a DCF mechanism is presented in equation 6.10. The expression is derived based on the observation that base sliding displacements for this mechanism are caused by dowel action yielding. By substituting equation 6.7 into 6.10 the base sliding displacement can be obtained as a function of displacement ductility, μ, as shown in equation 6.11.

$$\Delta_{Base} = \frac{DA_y}{C_k k_{DA}} \tag{6.10}$$

$$\Delta_{Base} = \left(\frac{DA_y}{0.12 k_{DA}}\right)\mu \tag{6.11}$$

Figure 6.50 shows the calculated base sliding displacement obtained using equations 6.9 and 6.10 with those from analysis results of the 2D model. The comparison shows a satisfactory match between results obtained through the proposed equations and analysis results. The results from equation 6.10 show a satisfactory match, and the corresponding correlation factor is 0.98.

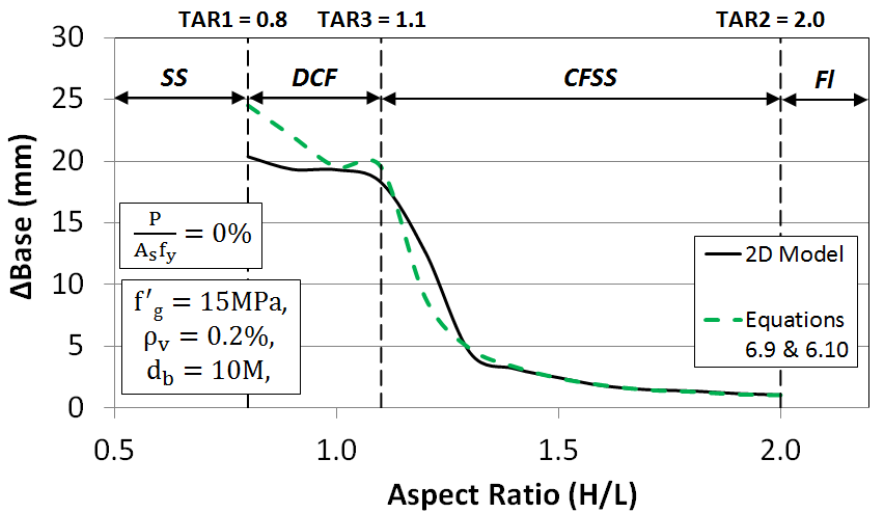

Figure 6.50 Base sliding displacement values obtained from equations 6.10 vs results from 2D model.

6.5 Summary

The results of nonlinear static analyses on RM shear walls subjected to reversed cyclic loading are presented in this chapter. The objective of these parametric studies was to examine the sensitivity of several design parameters: wall height to length ratio, H/L; vertical reinforcement ratio, ρ_v; wall height, H; spacing of reinforcing bars, s; masonry compression strength, f'_m; and wall axial compression level, $P/A_s f_y$. A summary of key findings is presented below:

1. The dowel action secant stiffness coefficient, C_k, can be used as a measure of the degradation in dowel action shear stiffness of RM walls subjected to cyclic loading.
2. The TAR2 and TAR3 values were defined as the upper limit H/L ratios in which an RM wall experiences a CFSS and a DCF mechanism, respectively.

3. The sliding response parameters studied in this chapter were the C_o coefficient, the C_k coefficient, and the TAR2 value. These parameters are required to predict the yield mechanism and the base sliding displacements in an RM wall subjected to cyclic loading. Empirical equations were developed for each sliding behaviour parameter obtained through the curve fitting of the analysis results.
4. In RM walls that experience a DCF mechanism, a base sliding displacement is caused by dowel action yielding.
5. In RM walls that experience a CFSS mechanism, base sliding displacements develop due to dowel action deformations that occur in order for dowel action to enable shear transfer across an open flexural crack. In addition, dowel action shear stiffness degrades with each increase in displacement ductility, μ, and higher elastic dowel action deformations develop in each subsequent loading cycle.
6. For RM walls that experience an Fl mechanism, dowel action shear stiffness is not significantly affected by pinching and stiffness degradation. As a result, dowel action deformations and base sliding displacements were found to be less than the dowel action yield deformation, u_y; and are therefore not significant.
7. The vertical reinforcement ratio, ρ_v, and the reinforcing bar diameter, d_b, have insignificant influence on sliding behaviour; which suggest that changes in these design parameters are not effective as solutions to prevent the development of either a CFSS mechanism or a DCF mechanism.

Chapter 7: Sliding Shear Behaviour Method for Estimating Sliding Displacements in RM Shear Walls

7.1 Introduction

In this chapter a novel method is proposed for estimating sliding displacements to aid in the seismic design of RM walls. The method will be referred as Sliding Shear Behaviour (SSB) Method. First, the theoretical basis of the method is presented, based on the findings from this study. Next, the proposed design method and corresponding equations are introduced. Finally, a design example case of an RM shear wall is presented where the proposed method is applied.

7.2 Yield Mechanisms and Key Criteria

This section summarizes the key criteria used in the SSB method for identifying the governing yield mechanism and the sliding displacements in RM shear walls. Each yield mechanism is introduced, indicating the key criteria that cause its development. Next, the sliding displacement expression for the mechanism is presented. The following yield mechanisms that need to be considered are as follows:

- Sliding Shear (SS) mechanism,
- Dowel-Constrained Failure (DCF) mechanism,
- Combined Flexural-Sliding Shear (CFSS) mechanism, and
- Flexural (Fl) mechanism.

7.2.1 Sliding Shear (SS) Mechanism

7.2.1.1 Key Criteria for the Development of the Mechanism:

An RM wall will develop an SS mechanism when the following condition is met:

1. The upper bound sliding shear resistance, V_{SS_U}, is less than or equal to the flexural resistance, V_{Fl}. ($V_{SS_U} \leq V_{Fl}$).

7.2.1.2 Sliding Displacements in a SS Mechanism

For an RM wall experiencing a SS mechanism, the wall's inelastic displacement, Δ_p, is equal to the base sliding displacement, Δ_{Base}, as illustrated in Figure 7.1. Based on this observation an expression for base sliding displacement, Δ_{Base}, was derived in Section 5.5.5, as a function of the displacement ductility, μ, as shown below:

$$\Delta_{Base} = (\mu - 1)\frac{V_{SS}}{k_{shear}} \qquad \text{when } \mu \geq 1 \tag{5.16}$$

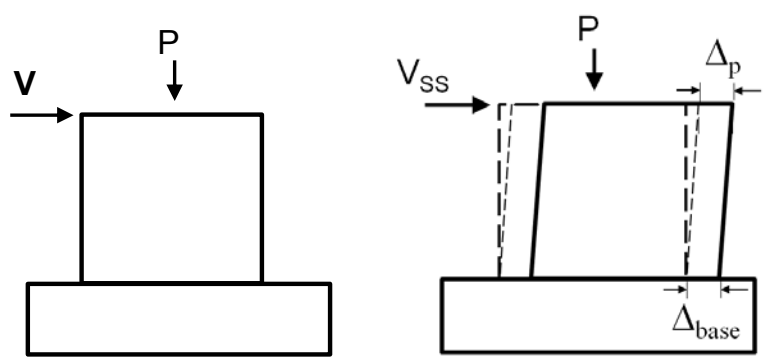

a) b)

Figure 7.1 Base sliding displacements in an RM wall that experiences a SS mechanism: a) Lateral force, V, applied at the top of the RM wall, b) RM wall yields in a SS mechanism.

7.2.2 Dowel-Constrained Failure (DCF) Mechanism

7.2.2.1 Key Criteria for the Development of the Mechanism:

An RM wall will develop a DCF mechanism when the following conditions are met:

1. The upper bound sliding shear resistance, V_{SS_U}, is greater than the flexural resistance, V_{Fl}, ($V_{SS_U} > V_{Fl}$), and
2. Dowel action resistance, DA_y, is insufficient to resist the lateral force required to close the flexural crack, V_o, ($DA_y \leq V_o$).

7.2.2.2 Sliding Displacements in a DCF Mechanism

For an RM wall experiencing a DCF mechanism, base sliding displacements develop due to dowel action inelastic deformations while transferring the shear force V_o across the open flexural crack, as illustrated in Figure 7.2. This base sliding displacement, Δ_{Base}, was derived in Section 6.4.5 as a function of the displacement ductility, μ, as follows:

$$\Delta_{Base} = \left(\frac{DA_y}{0.12k_{DA}}\right)\mu \qquad \text{when } \mu \geq 1 \tag{6.11}$$

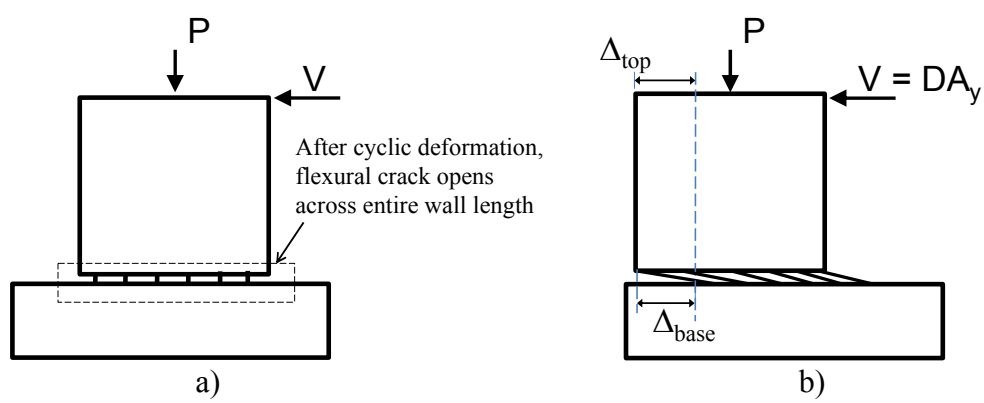

Figure 7.2: Base sliding displacements in an RM wall that experiences a DCF mechanism: a) Flexural crack forms along the wall length, b) Dowel action yielding prevents closure of flexural crack.

7.2.3 Combined Flexural-Sliding Shear (CFSS) Mechanism

7.2.3.1 Key Criteria for the Development of the Mechanism:

1. The upper bound sliding shear resistance, V_{SS_U}, exceeds the flexural resistance, V_{Fl}, ($V_{SS_U} > V_{Fl}$),
2. Dowel action resistance, DA_y, exceeds the lateral force required to close the flexural crack, V_o, ($DA_y > V_o$), and
3. The RM wall's H/L ratio is less than TAR2, (H/L < TAR2).

7.2.3.2 Sliding Displacements in a CFSS Mechanism

For an RM wall experiencing a CFSS mechanism, base sliding displacements develop due to elastic dowel action deformations while transferring the shear force V_o across the open flexural crack, as illustrated in Figure 7.3. As displacement ductility demands are increased, larger dowel action deformations develop due to degradation in dowel action shear stiffness. To estimate the resulting base sliding displacement, an expression is presented below which was first derived in Section 6.4.4:

$$\Delta_{Base} = 1.25 \frac{V_o}{C_k k_{DA}} \qquad \text{when } \mu \geq 1 \tag{6.9}$$

7.2.4 Flexural (Fl) Mechanism

7.2.4.1 Key Criteria for the Development of the Mechanism:

1. The upper bound sliding shear resistance, V_{SS_U}, exceeds the flexural resistance, V_{Fl}, ($V_{SS_U} > V_{Fl}$).

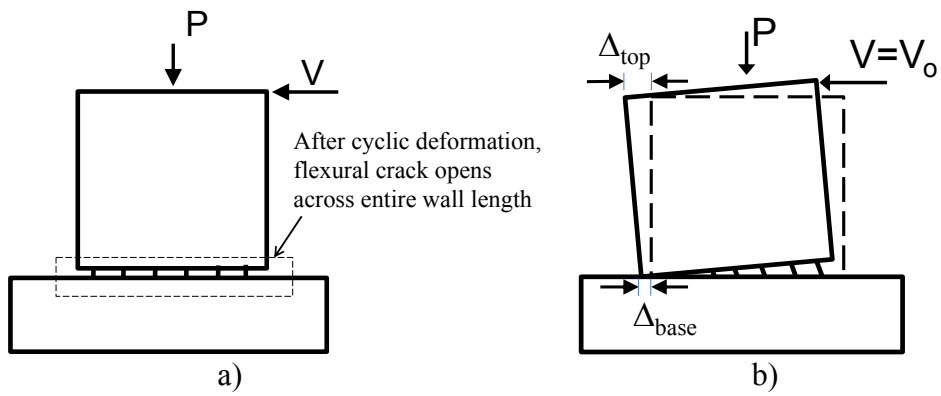

Figure 7.3: Base sliding displacements in an RM wall that experiences a CFSS mechanism: a) Flexural crack forms along wall length, b) Elastic dowel action deformations develop while transferring the shear force required to close the flexural crack, V_o.

2. Dowel action resistance, DA_y, exceeds the lateral force necessary to close flexural crack, V_o, ($DA_y > V_o$), and
3. The RM wall's H/L ratio is greater than or equal to TAR2, ($H/L \geq TAR2$).

7.2.4.2 Sliding Displacements in an Fl Mechanism

For an RM wall experiencing an Fl mechanism, base sliding displacements occur due to elastic dowel action deformations when transferring the shear force V_o across the open flexural crack, as illustrated in Figure 7.3. However, dowel action shear demands are low and do not cause degradation in dowel action shear stiffness. Therefore, base sliding displacements are expected to be less than 1 mm and are considered to be insignificant.

7.3 SSB Method

This section outlines the procedure for predicting the in-plane yield mechanism for an RM wall and estimating for corresponding base sliding displacements. The SSB method consists of

several equations developed throughout this study. The flowchart shown in Figure 7.4 summarizes the procedure.

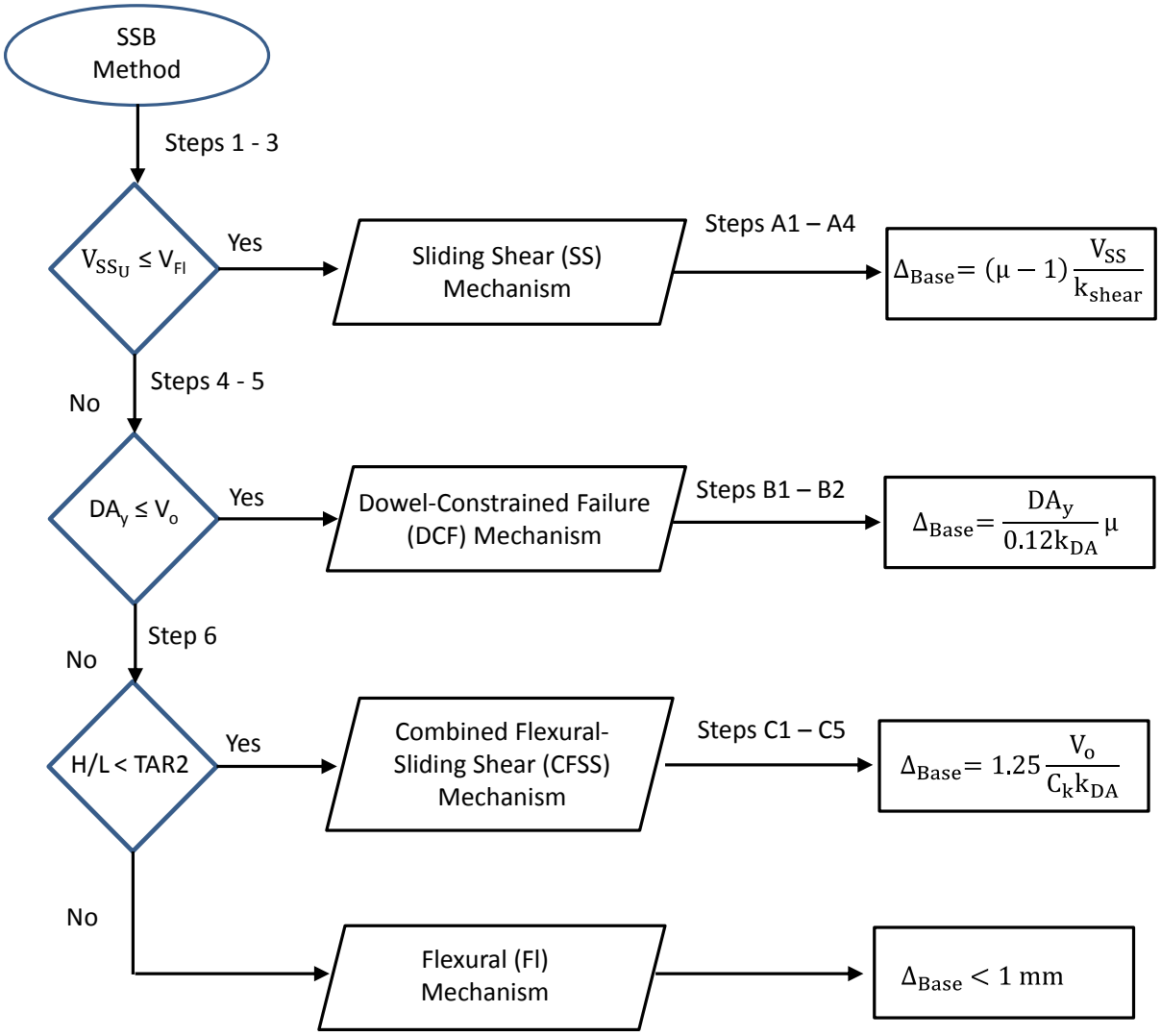

Figure 7.4 Flowchart of steps in the SSB method.

7.3.1 Determining the Yield Mechanism

Step 1: Calculate RM wall flexural behaviour parameters.

Assume the governing yield mechanism in the RM wall is a flexural yield mechanism, with internal stress and strain distributions as illustrated in Figure 7.5.

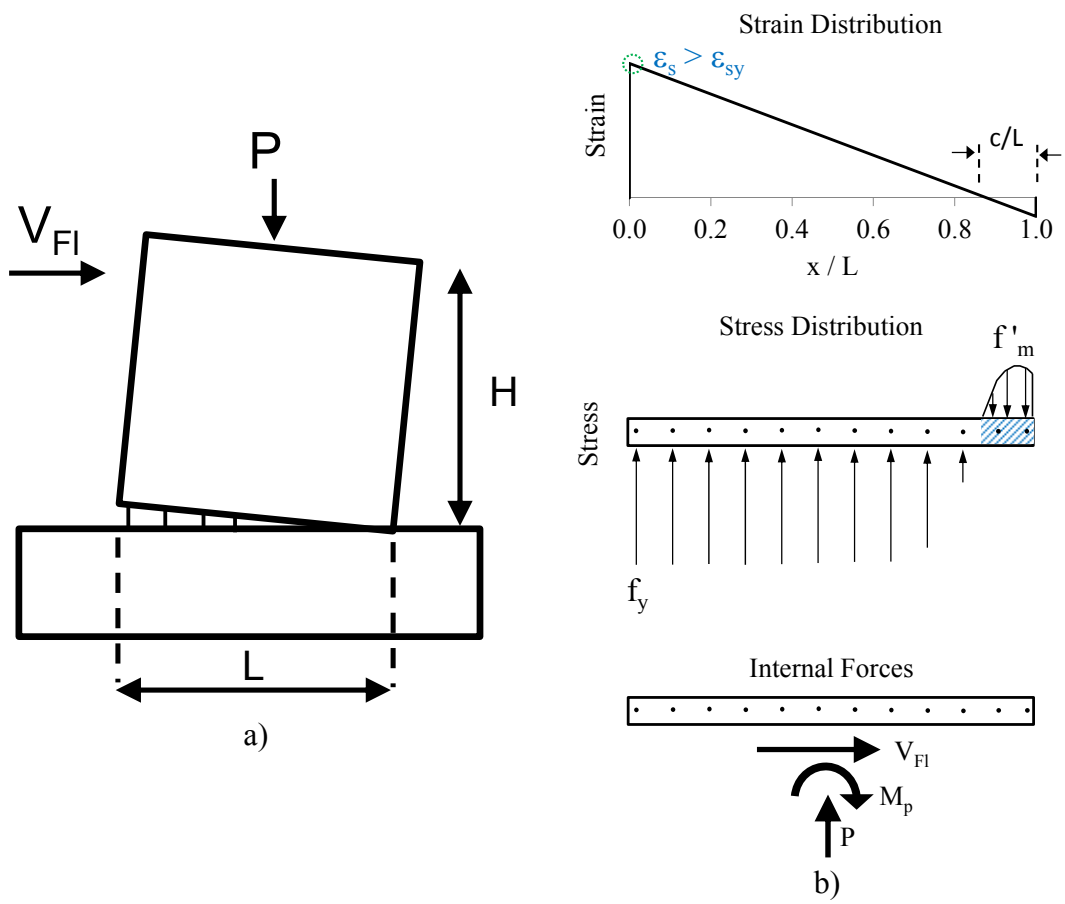

Figure 7.5 RM wall developing a flexural yield mechanism: a) RM wall loading and behaviour, b) Strain and stress distributions and internal forces along wall length.

1.1: Determine depth of compression zone, c.

$$\frac{c}{L} = \frac{\omega + \gamma}{2\omega + \alpha_1 \beta_1} \tag{5.6}$$

Where:

$$\omega = \frac{A_s f_y}{f'_m L t} \qquad \gamma = \frac{P}{f'_m L t}$$

$$\alpha_1 = 0.85 \qquad \beta_1 = 0.80$$

1.2: Determine the plastic moment resistance, M_p.

$$M_p = C_p A_s f_y L \tag{5.9}$$

Where:

$$C_p = 0.63\left(1 + \frac{5}{6}\frac{P}{A_s f_y}\right)\left(1 - \frac{c}{L}\right) \tag{5.11}$$

1.3: Determine the flexural resistance, V_{Fl}.

$$V_{Fl} = \frac{M_p}{H} \tag{5.8}$$

Step 2: Determine the upper bound sliding shear resistance, V_{SS_U}.

2.1: Calculate frictional resistance due to axial compression, Fr_A.

$$Fr_A = \mu_{Fr}(P_n) \tag{4.7}$$

where:

$$\mu_{Fr} = 0.6$$

Note: Frictional coefficient, μ_{Fr}, corresponds to a masonry-to-concrete sliding surface.

2.2: Calculate the upper bound frictional resistance due to flexural compression, Fr_{Fl_U}.

$$Fr_{Fl_U} = \mu_{Fr}\left[0.9\left(\frac{1 - \frac{c}{L} - \frac{d'}{L}}{1 + \frac{s}{L} - 2\frac{d'}{L}}\right)\right]A_s f_y \tag{5.5}$$

2.3: Calculate the dowel action yield resistance, DA_y.

$$DA_y = \left(C_{DA}\sqrt{f'_g f_y}\right)A_s \tag{3.5}$$

Where:

$$C_{DA} = \begin{cases} 2.2, & H/L \leq 0.5 \\ \left[2.2 - 2\left(\frac{H}{L} - 0.5\right)\right], & 0.5 < H/L < 1.0 \\ 1.2, & H/L \geq 1.0 \end{cases} \tag{4.8}$$

2.4: Calculate the upper bound sliding shear resistance, V_{SS_U}.

$$V_{SS_U} = Fr_A + Fr_{Fl_U} + DA_y \tag{5.12}$$

Step 3: Determine whether yield mechanism is a SS Mechanism.

3.1: Compare the upper bound sliding shear resistance, V_{SS_U}, and the flexural resistance, V_{Fl}, as follows:

- If $V_{SS_U} \leq V_{Fl}$, then the yield mechanism is an SS Mechanism.

  Continue to Step A1 (Section 7.3.2).

- If $V_{SS_U} > V_{Fl}$, continue to Step 4.

Step 4: Determine the conditions required for closing a flexural crack along the wall length.

During cyclic loading, residual tensile strains in the vertical reinforcement can cause a flexural crack along the wall length. This flexural crack can be closed when an overturning moment, M_o, is developed that induces the reinforcing bars to yield in compression, as shown in Figure 7.6. The overturning moment, M_o, and the corresponding lateral force, V_o, are determined as follows:

4.1: Determine M_o.

$$M_o = [C_o]A_s f_y L \tag{6.4}$$

Where

$$C_o = \left[0.21\left(1+\frac{s}{L}\right)\left(1-\frac{P}{A_s f_y}\right)\right] \tag{6.5}$$

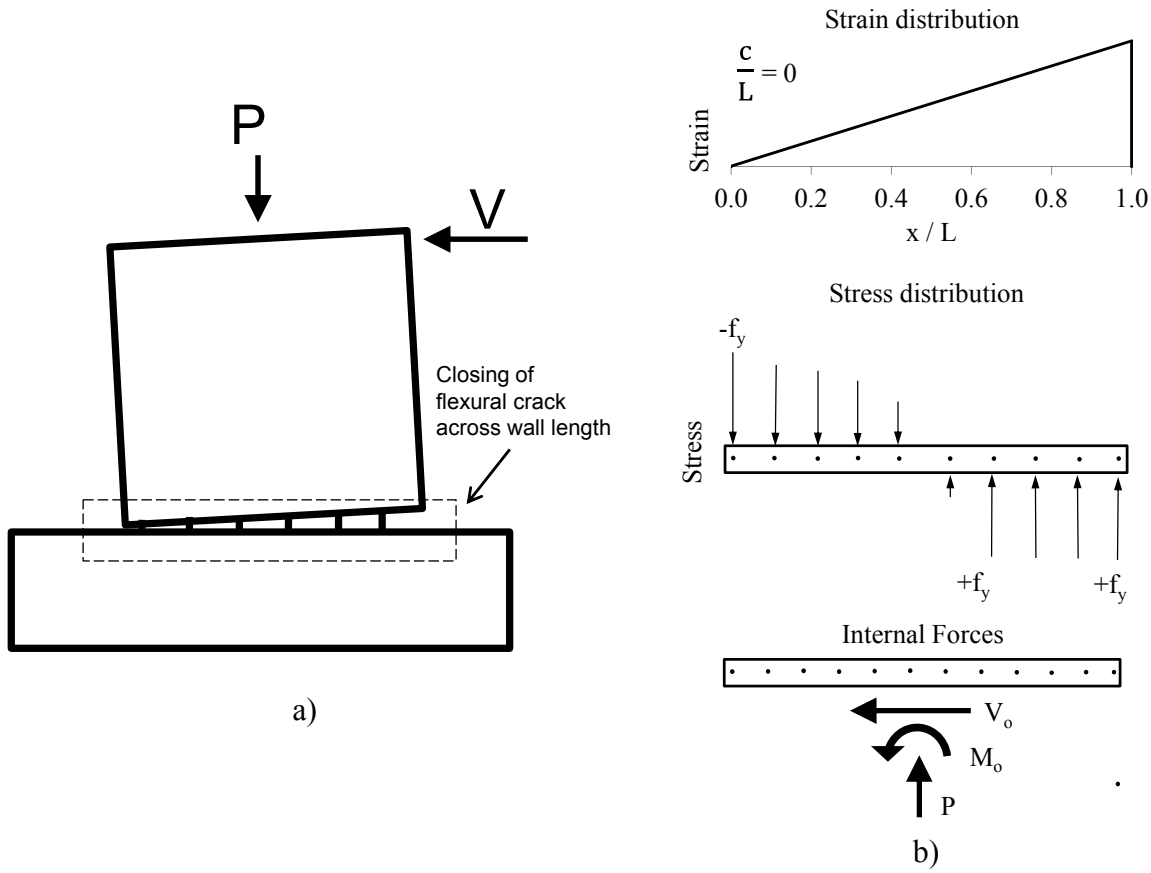

Figure 7.6 RM wall at the stage when the flexural crack closes: a) RM wall loading behaviour, b) Strain and stress distributions and internal forces along wall length.

4.2: Determine the lateral force required to close flexural crack, V_o.

$$V_o = \frac{M_o}{H} \tag{3.9}$$

Step 5: Determine whether yield mechanism is a DCF mechanism.

5.1: Compare the lateral force required to close flexural crack, V_o, and the dowel action yield resistance, DA_y, as follows:

- If $DA_y \leq V_o$, then the yield mechanism is a DCF Mechanism. Continue to Step B1, (Section 7.3.2).
- If $DA_y > V_o$, continue to Step 6.

Step 6: Determine whether the yield mechanism is a CFSS Mechanism.

6.1: Calculate the TAR2 value.

$$TAR2 = 0.8\left[1 + C_o\sqrt{\frac{f_y}{f'_g}}\right] \tag{6.6}$$

6.2: Determine whether the wall's H/L ratio is less than TAR2.

- If H/L < TAR2, then the yield mechanism is a CFSS Mechanism. Continue to Step C1, (Section 7.3.2).
- If H/L ≥ TAR2, then the yield mechanism is an Fl Mechanism.

  In this case, base sliding displacements are expected to be small (less than 1 mm) and are considered to be insignificant.

7.3.2 Estimating Base Sliding Displacements

Step A: Estimate base sliding displacements for an SS mechanism.

A1: Calculate the TAR1 value.

$$H/L = TAR1, \text{ when } V_{Fl} = V_{SS_U} \tag{5.13}$$

A2: Adjust values of frictional resistance and sliding shear resistance.

In an RM wall that experiences a SS mechanism, the frictional resistance due to flexural compression, Fr_{Fl}, and the sliding shear resistance, V_{SS}, are lower than the upper bound values calculated in Step 2 of Section 7.3.1. The adjusted resistance values are determined as follows:

$$Fr_{Fl} = \left(\frac{H/L}{TAR1}\right)^2 Fr_{Fl_U} \quad \leq Fr_{Fl_U} \tag{5.7}$$

$$V_{SS} = Fr_A + Fr_{Fl} + DA_y \tag{5.1}$$

A3: Determine wall lateral stiffness, k_{shear}.

$$k_{shear} = \left(0.2 + 0.1073\frac{P}{Lt}\right)k_e \tag{4.9}$$

$$k_e = \frac{E_m Lt}{2.4H(1+\upsilon)} \tag{4.10}$$

A4: Calculate base sliding displacement, Δ_{Base}.

$$\Delta_{Base} = (\mu - 1)\frac{V_{SS}}{k_{shear}} \quad \text{when } \mu \geq 1 \tag{5.16}$$

Step B: Estimate base sliding displacements for a DCF mechanism.

B1: Determine dowel action yield stiffness, k_{DA},

$$k_{DA} = n_{db}E_sI_s\left(\frac{k_g d_b}{4E_sI_s}\right)^{3/4} \tag{3.3}$$

$$k_g = \frac{127\sqrt{f'_g}}{d_b^{\,2/3}}, \qquad \text{Note: } f'_g \text{ (MPa), } d_b \text{ (mm)} \tag{3.4}$$

B2: Calculate base sliding displacement, Δ_{Base}.

$$\Delta_{Base} = \left(\frac{DA_y}{0.12k_{DA}}\right)\mu \qquad \text{when } \mu \geq 1 \tag{6.11}$$

Step C: Estimate base sliding displacements for a CFSS mechanism.

C1: Calculate the TAR1 value.

$$H/L = TAR1, \text{ when } V_{Fl} = V_{SS_U} \tag{5.13}$$

C2: Calculate the TAR3 value.

$$H/L = TAR3, \text{ when } V_o = DA_y \tag{6.3}$$

C3: Calculate dowel action secant stiffness coefficient, C_k.

$$C_k = \left[\frac{0.40}{\mu} + \left(1 - \frac{0.40}{\mu}\right)\left(\frac{H/L - TAR1}{TAR2 - TAR1}\right)\right], \qquad \text{if } TAR3 < TAR1 \tag{6.8a}$$

$$C_k = \left[\frac{0.12}{\mu} + \left(1 - \frac{0.12}{\mu}\right)\left(\frac{H/L - TAR3}{TAR2 - TAR3}\right)\right], \qquad \text{if } TAR3 \geq TAR1 \tag{6.8b}$$

C4: Determine dowel action yield stiffness, k_{DA}.

$$k_{DA} = n_{db}E_sI_s\left(\frac{k_g d_b}{4E_sI_s}\right)^{3/4} \tag{3.3}$$

$$k_g = \frac{127\sqrt{f'_g}}{{d_b}^{2/3}}, \qquad \text{Note: } f'_g \text{ (MPa)}, d_b \text{ (mm)} \tag{3.4}$$

C5: Calculate base sliding displacement, Δ_{Base}.

$$\Delta_{Base} = 1.25 \frac{V_o}{C_k k_{DA}} \tag{6.9}$$

7.4 Validation of the SSB Method

To illustrate the accuracy of the SSB method, the method is used to estimate the sliding displacements in RM wall specimens A3 and A6 from Priestley (1977). Both these wall specimens experienced sliding displacements during static cyclic loading, as illustrated in lateral force vs sliding displacements plots shown previously in Figure 2.3.

The two wall specimens had identical design properties, which are shown in table 7.1. Material strength values, f'_m and f_y, are nominal design values; while the masonry grout strength value, f'_g, corresponds to grout cylinder tests (Priestley, 1977). Wall specimen A3 was tested without external vertical loads and specimen A6 had an external vertical load of 240 kN (0.71 MPa).

Table 7.1 Design summary of example RM shear wall.

Wall dimensions	Reinforcement	Masonry Material Properties
L = Length = 2400 mm	Vertical: 8 - 19 mm	Masonry compression strength: f'_m = 8.3 MPa
H = Height = 1800 mm	Horizontal: 1 – 19 mm @ 200 bond beam	Grout compression strength: f'_g = 25 MPa
t = thickness = 140 mm	Grade 400 steel (f_y = 414 MPa)	All masonry cells are fully grouted

Through the use of the SSB method it is determined that both wall specimens would experience a CFSS mechanism. As shown in Figure 7.7, for both specimens when the displacement ductility value, μ, is less than 3.0, the SSB method estimates sliding displacements, Δ_{Base}, greater than

those observed in experiments, while an opposite trend is observed for μ values greater than 3.0. In the most extreme case, specimen A6 at a μ value of 4, the estimated Δ_{Base} value is 42% less than the 12 mm sliding displacement reported in the experiment. Therefore, it can be concluded that the SSB method gives conservative estimates of sliding displacement for ductility values less than 3.0.

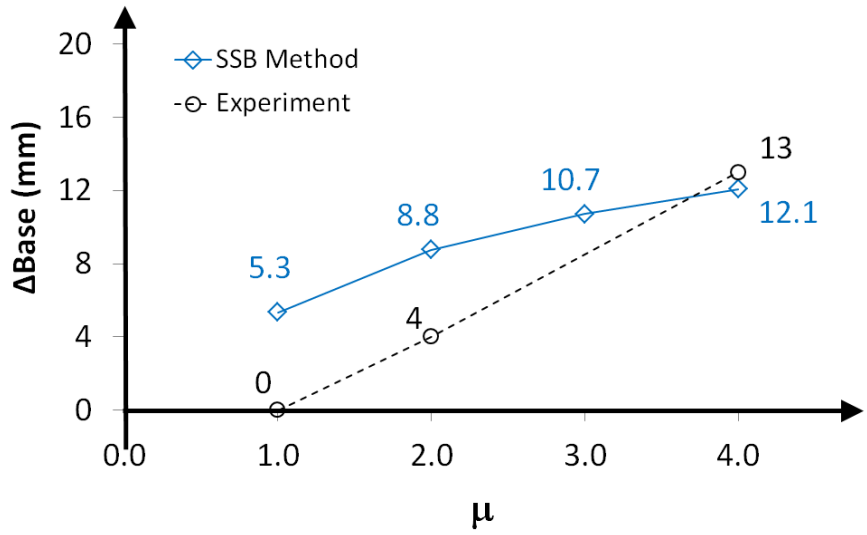

a)

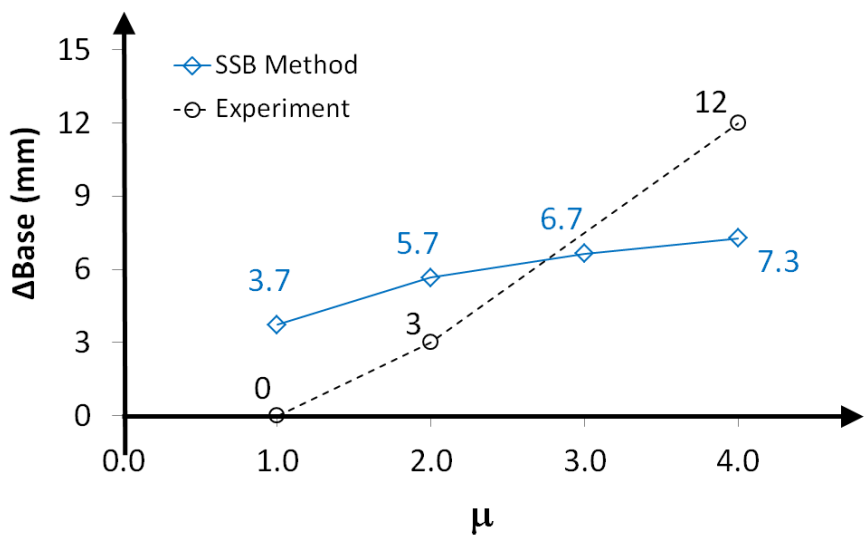

b)

Figure 7.7 Comparison of sliding displacement estimates using SSB method and experimental results from Priestley, 1977: a) Wall specimen without external vertical loads; b) Wall specimen with external vertical load of 240 kN.

7.5 Design Example

Determine the yield mechanism and base sliding displacement for a single storey RM squat wall designed according to NBCC 2010 and CSA S304.1, following seismic requirements for moderate ductility shear wall. The building site is located in Ottawa, ON, on site class C soil and the seismic hazard index $I_E F_a S_a(0.2)$ is 0.66. The wall is designed for the in-plane loads shown in Figure 7.8, and a force reduction factor, R_d, equal to 2.0. The reinforcement design properties are presented in Table 7.2. Neglect height-to-thickness limits and out-of-plane effects in this design, (Source: Example 4.c from Anderson & Brzev, 2009).

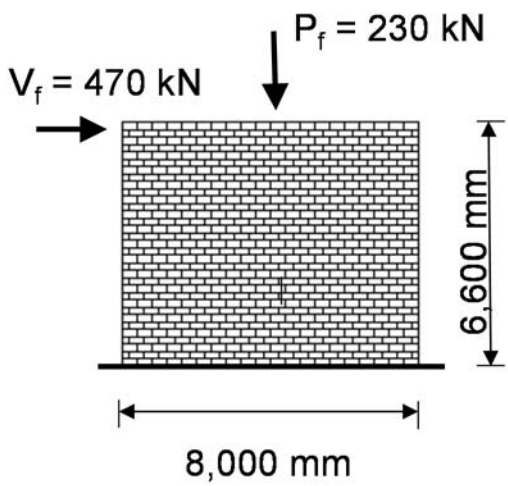

Figure 7.8 Loading conditions of single story squat RM wall (Anderson and Brzev, 2009).

7.5.1 Capacity Based Design Check (CBDC) According to CSA S304.1-14

The CBDC in CSA S304.1 Cl.10.16.3.3 is used to determine if a flexural mechanism takes place in the RM shear wall before a diagonal tension shear mechanism or a sliding shear mechanism has been initiated. This design requirement determines whether the flexural resistance, V_{FL}, is less than the diagonal tension shear resistance, V_m, as well as the sliding shear resistance, V_{SS}.

Table 7.2 Design summary of example RM shear wall.

Wall Dimensions	Reinforcement	Masonry Material Properties
L = Length = 8000 mm	Vertical: 11-15M	Masonry compression strength: f'_m =7.5 MPa
H = Height = 6600 mm	Horizontal: 2 – 15 M @ 1200 bond beam	Grout compression strength: f'_g = 15 MPa
t = thickness = 190 mm	Grade 400 steel (f_y = 400 MPa)	All masonry cells are fully grouted

1. Calculate flexural resistance.

V_{Fl} = 652 kN, following resistance equations in Section C1.1.2 (Anderson & Brzev, 2009).

2. Calculate diagonal tension shear resistance.

V_m = 778 kN, following resistance equations in Cl.10.10.1 (CSA S304.1-14).

3. Calculation of sliding shear resistance.

μ_{Fr} = 1, frictional coefficient for a masonry-to-roughened concrete sliding plane (see Table 2.1).

ϕ_m = 0.60, resistance factor for masonry.

ϕ_s = 0.85, resistance factor for steel reinforcement.

Total area of longitudinal reinforcement:

$A_s = 11*200mm^2 = 2200\ mm^2$

Steel tensile resistance:

$T_y = \phi_s A_s f_y = 0.85*2200*400 = 748$ kN

Total gravity load:

$P_d = 0.9 * P_f = 0.9 * 230 = 207$ kN

$P_2 = P_d + T_y = 207 + 748 = 955$ kN

Sliding shear resistance

$V_{SS} = \phi_m \mu_{Fr} P_2 = 0.6*1.0*955 = 573$ kN

$V_{SS} = 573$ kN

4. Determine the Yield Mechanism.

It is important to consider all possible yield mechanisms and identify the one that governs in this design. There are three lateral resistances:

$V_{Fl} = 652$ kN, flexural resistance,

$V_m = 778$ kN, diagonal tension shear resistance, and

$V_{SS} = 573$ kN, sliding shear resistance.

Since the sliding shear resistance, V_{SS}, value is the smallest, it can be concluded that the sliding shear mechanism is critical in this case.

5. Summary of Results.

The CBDC in CSA S304.1-14 finds that the RM shear wall will develop a sliding shear mechanism. The RM wall's yield resistance, V_y, is equal to 573 kN. The design check does not provide estimates for base sliding displacements.

7.5.2 Estimate Sliding Displacements According to SSB Method

7.5.2.1 Determine Yield Mechanism.

The procedure determines the governing yield mechanism by following Steps 1 through 6 presented in Section 7.3.1 of this study.

Step 1: Calculate RM Wall flexural behaviour parameters.

1.1: Determine depth of compression, c.

$\alpha_1 = 0.85$

$\beta_1 = 0.80$

$$\omega = \frac{A_s f_y}{f'_m L t}$$

$$\omega = \frac{(2200\text{mm}^2)(400\text{MPa})}{7.5\text{MPa}(8000\text{mm})(190\text{mm})} = 0.077$$

$$\gamma = \frac{P}{f'_m L t}$$

$$\gamma = \frac{230\text{ kN}}{7.5\text{MPa}(8000\text{mm})(190\text{mm})} = 0.02$$

$$\frac{c}{L} = \frac{\omega + \gamma}{2\omega + \alpha_1 \beta_1}$$

$$\frac{c}{L} = \frac{0.077 + 0.02}{2(0.077) + (0.85 * 0.8)} = 0.12$$

$$c = \left(\frac{c}{L}\right) L = 0.12 * 8000\text{mm} = 960\text{ mm}$$

1.2: Determine the plastic moment resistance, M_p.

$$C_p = 0.63\left(1 + \frac{5}{6}\frac{P}{A_s f_y}\right)\left(1 - \frac{c}{L}\right)$$

$$C_p = 0.63\left(1 + \frac{5}{6}\frac{230\text{kN}}{(2200\text{mm}^2)(400\text{MPa})}\right)(1 - 0.12)$$

$$C_p = 0.68$$

$$M_p = C_p A_s f_y L$$

$$M_p = (0.68)(2200\text{mm}^2)(400\text{MPa})(8000\text{mm})$$

$$M_p = 4787\ \text{kNm}$$

1.3: Determine the flexural resistance, V_{Fl}.

$$V_{Fl} = \frac{M_p}{H}$$

$$V_{Fl} = \frac{4787\ \text{kNm}}{6600\text{mm}}$$

$$V_{Fl} = 725\ \text{kN}$$

Step 2: Determine the upper bound sliding shear resistance, V_{SS_U}.

2.1: Calculate friction force due to axial compression, Fr_A.

$\mu_{Fr} = 0.6$, (Frictional coefficient for a masonry-to-concrete sliding plane).

$$Fr_A = \mu_{Fr}(P_f)$$

$$Fr_A = 0.6(230\ \text{kN})$$

$$Fr_A = 138\ \text{kN}$$

2.2: Calculate the upper bound friction force due to flexural compression, Fr_{Fl_U}.

$$Fr_{Fl_U} = \mu_{Fr}\left[0.9\left(\frac{1-\frac{c}{L}-\frac{d'}{L}}{1+\frac{s}{L}-2\frac{d'}{L}}\right)\right]A_s f_y$$

$$Fr_{Fl_U} = 0.6\left[0.9\left(\frac{1-\frac{960\text{mm}}{8000\text{mm}}-\frac{100\text{mm}}{8000\text{mm}}}{1+\frac{800\text{mm}}{8000\text{mm}}-2\frac{100}{8000}}\right)\right](2200\text{mm}^2)(400\text{MPa})$$

$$Fr_{Fl_U} = 383\ \text{kN}$$

2.3: Calculate the dowel action yield strength, DA_y.

$$\frac{H}{L} = \frac{6600\text{mm}}{8000\text{mm}} = 0.825$$

$$\frac{H}{L} = 0.83$$

$$C_{DA} = \begin{cases} 2.2, & H/L \leq 0.5 \\ \left[2.2 - 2\left(\frac{H}{L} - 0.5\right)\right], & 0.5 < H/L < 1.0 \\ 1.2, & H/L \geq 1.0 \end{cases}$$

Since $0.5 < H/L < 1.0$:

$$C_{DA} = [2.2 - 2(0.82 - 0.5)] = 1.56$$

$$DA_y = \left(C_{DA}\sqrt{f'_g f_y}\right)A_s$$

$$DA_y = \left(1.56\sqrt{(15\text{MPa})(400\text{MPa})}\right)(2200\text{mm}^2)$$

$DA_y = 266\ kN$

2.4: Calculate the upper bound sliding shear resistance, V_{SS_U}.

$V_{SS_U} = Fr_A + Fr_{Fl_U} + DA_y$

$V_{SS_U} = 138\ kN + 383\ kN + 266\ kN$

$V_{SS_U} = 787\ kN$

Step 3: Determine whether the yield mechanism is a SS Mechanism.

3.1: Compare upper bound sliding shear resistance, V_{SS_U}, and flexural resistance, V_{Fl}.

V_{SS_U} value is greater than V_{Fl} value (787 kN > 725 kN), then continue to Step 4.

Step 4: Determine conditions required to close a flexural crack along the wall length.

4.1: Determine M_o.

$$C_o = \left[0.21\left(1 + \frac{s}{L}\right)\left(1 - \frac{P}{A_s f_y}\right)\right]$$

$$C_o = \left[0.21\left(1 + \frac{800mm}{8000mm}\right)\left(1 - \frac{230kN}{(2200mm^2)(400MPa)}\right)\right]$$

$C_o = 0.17$

$M_o = [C_o]A_s f_y L$

$M_o = 0.17(2200mm^2)(400MPa)(8000mm)$

$M_o = 1197\ kNm$

4.2: Determine the lateral force required to close flexural crack, V_o.

$$V_o = \frac{M_o}{H}$$

$$V_o = \frac{1197\ \text{kNm}}{6600\ \text{mm}}$$

$$V_o = 181\ \text{kN}$$

Step 5: Determine whether the yield mechanism is a DCF mechanism.

5.1: Compare the lateral force required to close flexural crack, V_o, and the dowel action yield strength, DA_y.

Since DA_y value is greater than V_o value (266 kN > 181 kN), then continue to Step 6.

Step 6: Determine whether the yield mechanism is a CFSS Mechanism.

6.1: Calculate the TAR2 value.

$$TAR2 = 0.8\left[1 + C_o\sqrt{\frac{f_y}{f'_g}}\right]$$

$$TAR2 = 0.8\left[1 + 0.17\sqrt{\frac{400\text{MPa}}{15\text{MPa}}}\right]$$

$$TAR2 = 1.50$$

6.2: Determine whether the wall's H/L ratio is less than TAR2.

- If the H/L ratio is less than TAR2, (0.82 < 1.50), then the governing yield mechanism in this RM shear wall is a <u>CFSS mechanism</u>.

7.5.2.2 Estimate Base Sliding Displacements for a CFSS Mechanism.

The procedure determines the base sliding displacement corresponding to a CFSS mechanism by following Steps C1 to C5 in Section 7.3.2 of this study.

Step C1: Calculate the TAR1 value.

H/L = TAR1, when $V_{Fl} = V_{SS_U}$

First iteration, assume H/L = 0.5.

H = 0.5*8000 mm = 4000 mm

$$V_{Fl} = \frac{M_p}{H} = \frac{4787\ \text{kNm}}{4000\ \text{mm}}$$

$$V_{Fl} = 1197\ \text{kN}$$

$$Fr_A = 138\ \text{kN}$$

$$Fr_{Fl_U} = 383\ \text{kN}$$

For H/L = 0.5, C_{DA} = 2.2.

$$DA_y = \left(2.2\sqrt{(15\text{MPa})(400\text{MPa})}\right)(2200\text{mm}^2) = 375\ \text{kN}$$

$$V_{SS_U} = 138\ \text{kN} + 383\ \text{kN} + 375\ \text{kN}$$

$$V_{SS_U} = 896\ \text{kN}$$

Since $V_{Fl} \neq V_{SS_U}$, then TAR1 ≠ 0.5

For the next iteration, use

$H = \frac{M_p}{V_{SS_U}} = \frac{4787\ \text{kNm}}{896\ \text{kN}}$ = 5343 mm and hence H/L = 0.67

After three additional iterations, with $V_{SS_U} = 821$ kN and $V_{Fl} = 823$ kN, it follows that

<u>TAR1 = 0.72</u>.

C2: Calculate the TAR3 value.

H/L = TAR3, when $V_o = DA_y$

First iteration: assume H/L = 0.5.

$DA_y = 375$ kN

$$V_o = \frac{M_o}{H} = \frac{1197\ \text{kNm}}{4000\ \text{mm}}$$

$V_o = 300$ kN

Since $V_o \neq DA_y$, then TAR3 ≠ 0.5,

Second iteration, $V_o = 375$ kN and $DA_y = 375$ kN,

<u>TAR3 = 0.40</u>.

C3: Calculate dowel action secant stiffness coefficient, C_k.

$TAR3 < TAR1$

$$C_k = \left[\frac{0.40}{\mu} + \left(1 - \frac{0.40}{\mu}\right)\left(\frac{H/L - TAR1}{TAR2 - TAR1}\right)\right]$$

Assume $\mu = R_d$.

$\mu = 2$

$$C_k = \left[\frac{0.40}{2} + \left(1 - \frac{0.40}{2}\right)\left(\frac{0.82 - 0.72}{1.50 - 0.72}\right)\right]$$

$$C_k = 0.30$$

C4: Calculate dowel action yield stiffness, k_{DA}.

$$k_g = \frac{127\sqrt{f'_g}}{{d_b}^{2/3}}$$

$$k_g = \frac{127\sqrt{15\text{MPa}}}{(16\text{mm})^{2/3}} = 77.46\ \frac{\text{N}}{\text{mm}^3}$$

$$I_s = \frac{\pi(d_b)^4}{64}$$

$$I_s = \frac{\pi(16\text{mm})^4}{64} = 3217\text{mm}^4$$

$$k_{DA} = n_{db}E_sI_s\sqrt[4]{\left(\frac{k_gd_b}{4E_sI_s}\right)^3}$$

$$k_{DA} = 11(200\text{GPa})(3217\text{mm}^4)\left(\frac{77.46\ \frac{\text{N}}{\text{mm}^3}\,16\text{mm}}{4(200\text{GPa})(3217\text{mm}^4)}\right)^{3/4}$$

$$k_{DA} = 129\ \frac{\text{kN}}{\text{mm}}$$

C5: Calculate base sliding displacement, Δ_{Base}.

$$\Delta_{Base} = 1.25\frac{V_o}{C_kk_{DA}}$$

$$\Delta_{\text{Base}} = 1.25 \frac{181 \text{ kN}}{(0.30)\left(129 \frac{\text{kN}}{\text{mm}}\right)}$$

$$\Delta_{\text{Base}} = 5.8 \text{ mm}$$

7.5.2.3 Summary of Results

The SSB method finds that the RM shear wall will develop a CFSS mechanism. The RM wall's shear force corresponding to yield resistance, V_y, is equal to 725 kN. The SSB method determines, Δ_{Base}, that the wall's base sliding displacement is equal to 5.8 mm for a ductility $\mu = 2$.

7.5.3 Discussion

The CBDC method is used to check whether an RM squat wall will develop a sliding behaviour and if it governs in the design. The SSB method enables the designer to predict the sliding behaviour and estimate sliding displacements. The two methods determined that the RM squat wall will develop sliding behaviour, but differ in the expected yield mechanism (the CBDC method determines a sliding shear mechanism; the SSB method determines a CFSS mechanism). Only the SSB method is able to estimate the expected base sliding displacement, Δ_{Base}, with a value equal to 5.8 mm for a displacement ductility demand, μ, equal to 2. The SSB method enables the designer to evaluate whether the expected Δ_{Base} value can be considered acceptable for the wall structure.

7.5.3.1 Relation Between Δ_{Base} and R_d Factor

The SSB method can be applied to the design example case for different R_d values to determine the relation between the expected Δ_{Base} value and the corresponding R_d value. For each calculation, it is assumed that the displacement ductility demand, μ, is equal to the R_d value. Figure 7.8 shows that an increase in the R_d value in the design results in higher Δ_{Base} value. It can be seen that expected Δ_{Base} increases from 5.8 to 7.2 mm when the R_d increases from 2 to 3. This is not a considered to be a significant increase.

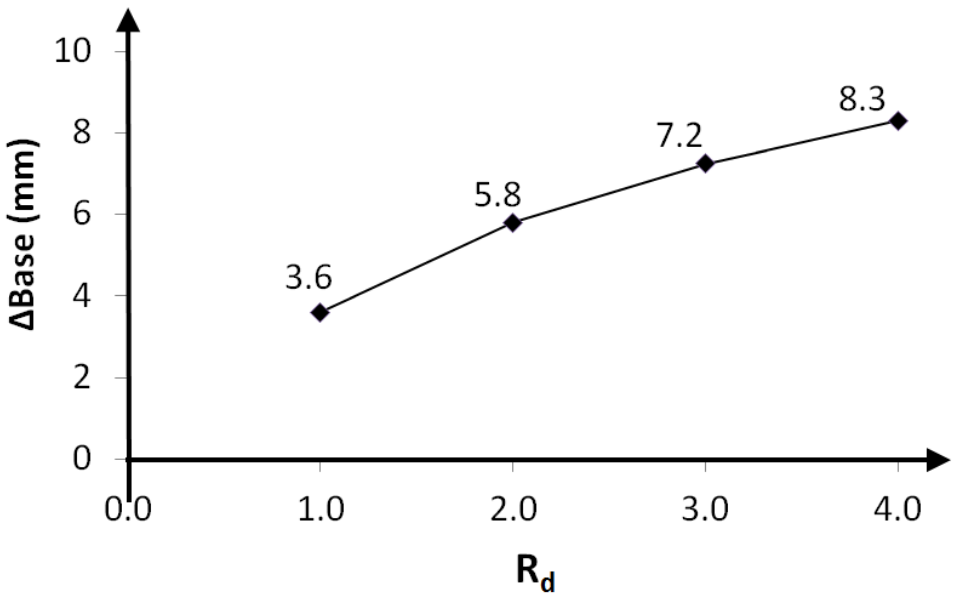

Figure 7.9 Curve of base sliding displacement, Δ_{Base}, vs strength reduction factor, R_d.

7.6 Summary

Key findings from Chapter 7 are summarized below:

1. The SSB method is proposed for predicting the yield mechanism and estimating sliding displacements in RM shear walls subjected to in-plane loads.

2. The proposed method is developed based on the findings from various parametric studies on RM shear walls subjected to monotonic and cyclic loading.

3. Comparison of estimations using the SSB method and experimental results shows that the SSB method gives conservative estimates of sliding displacement for ductility values less than 3.0.

4. The SSB method represents an improvement over the current capacity-based design procedure specified in CSA S304.1-14, because it enables the designer to estimate the base sliding displacement and evaluate whether the wall's seismic performance is acceptable.

5. The SSB method can be used in a performance-based seismic design of RM shear walls.

Chapter 8: Conclusions and Future Work

This study has proposed a modeling approach for accurately estimating sliding displacements in RM shear walls subjected to in-plane lateral loads. This approach determines the onset of sliding displacements by modeling the wall's sliding shear resistance as the sum of frictional and dowel action resistances, and accounting for their nonlinear behaviour during cyclic loading.

This approach has been used to develop an analytical model for simulating the sliding behaviour of cantilever RM shear walls subjected to monotonic and cyclic loading. Calibration of the model parameters was performed using 10 different RM wall specimens, and it accounted for a few parameters, including: shear span ratio, level of axial compression and vertical reinforcement ratio. The model was able to correctly estimate the yield mechanism and sliding behaviour of all 10 wall specimens subjected to cyclic loading.

A significant contribution of this research study has been identifying three RM shear wall yield mechanisms that develop base wall sliding displacements, which are: i) Sliding Shear (SS) mechanism, ii) Combined Flexural-Sliding Shear (CFSS) mechanism, and iii) Dowel-Constrained Failure (DCF) mechanism. This study proves that these three mechanisms have different sliding behaviours. In RM walls that experience a SS mechanism, sliding displacements occur when lateral loading exceeds the RM wall's sliding shear resistance. In RM walls that experience a CFSS or a DCF mechanism, sliding displacements are equal to dowel action deformations that occur in order for dowel action to transfer shear across an open flexural crack. In a CFSS mechanism, dowel action deformations are elastic and influenced by

degradation in dowel action shear stiffness, while in a DCF mechanism, these deformations are inelastic and occur when the applied shear force exceeds the dowel action yield resistance.

Parametric analyses studying the influence of several design parameters on sliding behaviour found that the masonry grout compressive strength and reinforcing bar spacing have a high influence on an RM wall's sliding behaviour. This occurs since grout compressive strength affects the dowel action's yield resistance and because spacing of reinforcing bars influence the resulting overturning moment required to close the flexural crack along the wall length. These results suggest these design parameters have to be considered in order to have acceptable values of sliding displacement in RM shear walls.

In addition, parametric studies determined that the vertical reinforcement ratio, ρ_v, and the reinforcing bar diameter, d_b, have insignificant influence on sliding behaviour which suggests that changes in these design parameters are not effective as solutions to prevent the sliding displacements in RM shear walls.

The Sliding Shear Behaviour (SSB) method is developed for estimating sliding displacements in RM walls based on results from comprehensive parametric studies using the calibrated model. The SSB method represents an improvement over the current capacity-based design procedure specified in CSA S304.1-14, because it enables the designer to estimate the base sliding displacement and evaluate whether the wall's seismic performance is acceptable.

8.1 Future Work

This research study's had the goal to provide a methodology to accurately estimate the sliding displacements that can develop in the seismic response of an RM squat wall. In that sense, the SSB method has achieved the proposed objective of the study.

However, it has been observed that there are other aspects that require further research regarding sliding behaviour in RM walls. The following suggestions can be conducted on future analysis in order to expand the understanding of the proposed method for estimating sliding displacements:

- Study how concentrating steel reinforcement at the ends of RM walls affect the sliding behaviour of RM walls.
- Perform experimental tests to determine the effect of various masonry grout strengths, f'_g, on sliding shear behaviour of RM shear walls. The experiments should measure resulting masonry compression strength, f'_m, dowel action yield resistance, DA_y, and sliding displacement values in wall specimens. This information could be used to improve predictions in the SSB method.
- Perform experimental studies to determine the sliding displacement response of RM shear walls with wall H/L ratios greater than 1.0. The experiments should also measure the maximum shear force developed while a flexural crack is open across the wall length.
- Perform experimental studies on the sliding shear behavior of RM shear walls designed for low vertical reinforcement ratios ($\rho_v < 0.1\%$). Wall specimens would consider the

maximum vertical reinforcement spacing of 2.4 m allowed in the Canadian Masonry Code for low seismic demand conditions.

- Study how wall openings in the RM shear wall would affect the estimates of sliding displacements using the SSB method.
- Study how sliding shear behaviour on an RM wall is affected by the interaction with an adjacent perpendicular RM wall.
- Develop simplified models of force vs deformation behaviour of the SS mechanism and CFSS mechanisms to be used for nonlinear dynamic analysis of RM walls.
- Perform nonlinear dynamic studies using different ground motions in order to identify the ductility demands of RM wall structures with sliding mechanisms.

References

Abrams, D. P., 1988 "Dynamic and Static testing of Reinforced Concrete Masonry Structures", Proceedings of 9th WCEE, August 1988, Tokyo-Kyoto Japan Vol. VI., pp. 169-174.

ACI 318-11, 2011. Building Code Requirements for Structural Concrete (ACI 318–11) and Commentary. American Concrete Institute: Farmington Hills, MI.

Ahmadi, F., 2012. "Displacement-based Seismic Design and Tools for Reinforced Masonry Shear-Wall Structures", PhD Dissertation, University of Texas, Austin, Texas.

Anderson, D.L., and Brzev, S. (2009). Seismic Design Guide for Masonry Buildings, Canadian Concrete Masonry Producers Association, Toronto, Canada, 317 (free download available at www.ccmpa.ca)

Anderson, D. L., and Priestley, M. J. N., 1992. "In plane shear strength of masonry walls" Proceedings of the 6th Canadian Masonry Symposium, Saskatoon, Saskatchewan.

ASCE 7-05, 2005. "Minimum Design Loads for Buildings and Other Structures" (with Supplement), American Society of Civil Engineers, Reston, Virginia.

Birkeland, P.W. and Birkeland, H.W., 1966. "Connections in Precast Concrete Construction". Journal ACI 1966; Vol. 63, No. 3, pp 345–68.

Cardenas, A.E., and Magura, D.D., 1973. "Strength of High-Rise Shear Walls - Rectangular Cross Section", *Response of Multistory Concrete Structures to Lateral Forces*, ACI Publication SP-36, American Concrete Institute, Detroit, pp. 119–150.

CSA (2014). “Design of Masonry Structures", CAN/CSA S304.1-04, Canadian Standards Association, Mississauga, Ontario, Canada

CSA (2004). “Mortar and Grout for Unit Masonry”, CAN/CSA A179-04, Canadian Standards Association, Mississauga, Ontario, Canada

CSI (2007). “PERFORM 3D V5, Nonlinear Analysis and Performance Assessment for 3D Structures”, Computer and Structures, Inc., Berkeley, California.

Dulascka, H., 1972. “Dowel Action of Reinforcement Crossing Cracks in Concrete”, ACI Structural Journal, Vol.69, No. 12, pp. 754-757.

El-Ariss, B. 2007. “Behaviour of beams with dowel action” Engineering Structures Vol. 29 No.6, pp. 899–903.

Elwood, K.J. and Moehle, J.P., 2005. “Axial Capacity Model for Shear-Damaged Columns”, ACI Structural Journal, Vol. 102, No. 4, pp 578-587.

Filippou, F. C., Popov, E. P., and Bertero, V. V. 1983. “Effects of Bond Deterioration on Hysteretic Behaviour of Reinforced Concrete Joints”. Report EERC 83-19, Earthquake Engineering Research Center, University of California, Berkeley.

He X.G. and Kwan A.K.H., 2001. “Modeling of dowel action of reinforcement bars for finite element analysis of concrete structures”, Computers and Structures Vol. 79, No. 6, pp 595-604

Hernández, J. F., 2012. “Quasi-Static Testing of Cantilever Masonry Shear Wall Segments” Master’s thesis, University of Texas, Austin, Texas.

Hetenyi, M.I. 1958 “Beams on elastic foundation: theory with applications in the fields of civil and mechanical engineering”. Ann Arbor: The University of Michigan Press.

Kent, D., C., and R., Park. 1971. “Flexural members with confined concrete”. ASCE Journal of the Structural Division Vol.97, No 7, pp. 1969–1990.

Kikuchi, K., Yoshimura, K., Yoshida, K., Tanaka, A., Urasaki, H., Kijima, Y., & Mizumasa, N. 2004. “Experimental Study On Seismic Capacity Of Reinforced Fully Grounted Concrete Masonry Walls” Proceedings of the 13th World Conference on Earthquake Engineering, Vancouver, Canada, Paper (No. 1880).

Masonry Institute of British Columbia (MIBC), 2009. “Masonry Standards Commentary” Vancouver, B.C., http://www.masonrybc.org/document/manual/3.1.pdf [Accessed: 15 October 2014]

Mast, R.F. 1968 “Auxiliary Reinforcement in Precast Concrete Connections”. ASCE Journal Struct Div 1968, Vol. 94 No. 6, pp 1485–1504.

Matsumura, A., 1987 “Shear Strength of Reinforced Hollow Unit Masonry Walls” Proceedings of the 4th North American Masonry Conference, Los Angeles, California

Mattock, A.H., Hawkins, N.M., 1972 “Shear transfer in reinforced concrete – recent research”. PCI Journal 1972; Vol. 17, No. 2, pp 55–75.

Mazzoni S, McKenna F, Scott MH, Fenves GL. 2006 “ Open system for earthquake engineering simulation, user command-language manual - PINCHING4 Material” Pacific Earthquake Engineering Research Center. [online] Available at: http://opensees.berkeley.edu/OpenSees/manuals/usermanual/1152.htm, [Accessed: 02 July 2013]

McKenna, F., Fenves, G.L. and Scott, M.H., 2000. "Open System for Earthquake Engineering Simulation, University of California Berkeley, California, http://opensees.berkeley.edu. [Accessed: 02 July 2013]

Menegotto, M., and Pinto, P. E. (1973). "Method of anaysis for cyclically loaded reinforced concrete plane frames including changes in geometry and non-elastic behaviour of elements under combined normal force and bending." Proceedings, IABSE Symposium of Resistance and Ultimate Deformability of Structures Acted on by Well Defined Repeated Loads, Vol. 13 pp. 15-22. Lisbon, Portugal.

MSJC 2008a. "Building Code Requirements for Masonry Structures" (TMS 402-08 / ACI 530-08 / ASCE 5-08), The Masonry Society, Boulder, Colorado, the American Concrete Institute, Farmington Hills, Michigan, and the American Society of Civil Engineers, Reston, Virginia.

MSJC 2008b. "Specification for Masonry Structures" (TMS 602-08 / ACI 530.1-08 / ASCE 6-08), The Masonry Society, Boulder, Colorado, the American Concrete Institute, Farmington Hills, Michigan, and the American Society of Civil Engineers, Reston, Virginia.

National Research Council of Canada. (2010) "National Building Code of Canada, (NBCC), 2010 Part 4 Structural Design". Ottawa, Ontario, Canada

Nees.org., 2011. "NEES Project Warehouse - Seismic Design of Reinforced Masonry Shear-wall Structures" [online] Available at: http://nees.org/warehouse/experiments/1045 [Accessed: 20 Jul 2013].

NZSS 1900:1962. "New Zealand Standard Model Building Bylaw, Chapter 9.4, Design and Construction, Masonry." New Zealand Standards Institute, Wellington.

OpenSeesWiki., 2010. "Concrete02 Material -- Linear Tension Softening" - OpenSeesWiki. [ONLINE] Available at: http://opensees.berkeley.edu/wiki/index.php/Concrete02_Material_--_Linear_Tension_Softening [Accessed: 02 July 2013]

OpenSeesWiki., 2012a. "Flat Slider Bearing Element" - OpenSeesWiki. [ONLINE] Available at: http://opensees.berkeley.edu/wiki/index.php/Flat_Slider_Bearing_Element [Accessed: 02 July 2013]

OpenSeesWiki., 2012b. "Truss Element" - OpenSeesWiki. [ONLINE] Available at: http://opensees.berkeley.edu/wiki/index.php/Truss_Element [Accessed: 02 July 2013]

OpenSeesWiki., 2012c. "Steel02 Material -- Giuffré-Menegotto-Pinto Model with Isotropic Strain Hardening" - OpenSeesWiki. [ONLINE] Available at: http://opensees.berkeley.edu/wiki/index.php/Steel02_Material_--_Giuffr%C3%A9-Menegotto-Pinto_Model_with_Isotropic_Strain_Hardening [Accessed: 02 July 2013]

OpenSeesWiki., 2012d. "Pinching4 Material" - OpenSeesWiki. [ONLINE] Available at: http://opensees.berkeley.edu/wiki/index.php/Pinching4_Material [Accessed: 02 July 2013]

OpenSeesWiki., 2013. "Section Aggregator" - OpenSeesWiki. [ONLINE] Available at: http://opensees.berkeley.edu/wiki/index.php/Section_Aggregator [Accessed: 02 July 2013]

Orakcal, K., Massone, L, and Wallace, J. "Analytical Modeling of Reinforced Concrete Walls for Predicting Flexural and Coupled– Shear-Flexural Responses" PEER Report 2006/07, Pacific Earthquake Engineering Research Center, University of California, Berkeley, October 2006.

Park, R., and Paulay, T., 1975. "Reinforced Concrete Structures", Wiley, New York, United States of America.

Paulay, T., Priestley, MJN. and Synge A. J., 1982. "Ductility in Earthquake Resisting Squat Shearwalls", ACI Journal Vol. 79, No. 4, pp. 257-269.

Priestley, MJN. 1977. "Seismic Resistance of Reinforced Masonry Shear walls with High Steel Percentages", Bulletin of the New Zealand National Society for Earthquake Engineering, Vol 10, No. 1, pp 1-16.

Priestley, MJN. 1978. "Discussion: Seismic Resistance of Reinforced Masonry Shear walls with High Steel Percentages", Bulletin of the New Zealand National Society for Earthquake Engineering, Vol 11, No. 1, pp 70-71.

Priestley, MJN., Bridgeman D.O., 1974. "Seismic Resistance of Brick Masonry Walls", Bulletin of the New Zealand National Society for Earthquake Engineering, Vol 7, No. 4, pp 167-187.

Pruijessers A. F. 1988. "Aggregate Interlock and Dowel Action Under Monotonic and Cyclic Loading", PhD thesis, 165 p., Delft University, Netherland, 1988.

Rasmussen, B. H., 1962. "Strength of transversely loaded bolts and dowels cast into concrete", Laboratoriet for bugningastatik, Denmark Technical University, Meddelelse, Vol. 34, No. 2, (in Danisch)

Robazza, Brook, 2013. "Out-of-plane stability of reinforced masonry shear walls under seismic loading: in-plane reversed cyclic testing". Masters Thesis, University of British Columbia.

San Bartolomé A. 2007. http://blog.pucp.edu.pe/albanileria (in Spanish).

San Bartolomé A., Silva W., Melendez E., Castro G., and Quiun D., 2009 "Experimental Study to Avoid the Sliding Failure in Reinforced Masonry Walls Under Lateral Loads" Proceedings of the 11th Canadian Masonry Symposium, Toronto, Ontario.

Santos, P., Júlio, E. N., 2012. “A state-of-the-art review on shear-friction”. Journal of Engineering Structures, Vol. 45, pp 435-448.

Scott, B. D., Park, R., and Priestley, M. J. N. 1982. “Stress-Strain Behaviour of Concrete Confined by Overlapping Hoops at Low and High Strain Rates.” ACI Journal, Vol. 79 No. 2, pp. 13-27.

Shedid, M. T., Drysdale R. G., and El-Dakhakhni, W.W., 2008. “Behaviour of fully grouted reinforced concrete masonry shear walls failing in flexure: flexure: Experimental Results”, Journal of Structural Engineering, Vol. 134, No. 11, pp. 1754-1767.

Shing, P. B., Noland J. L., Klamerus, E. and Spaeh H., 1989. “Inelastic Behaviour of Concrete Masonry Shear Walls, Journal of Structural Engineering”, ASCE, Vol. 115, No. 9. pp 2204-2225.

Shing, P. B., Schuller M., Hoskere V.S. and Carter E., 1990. “Flexural and shear response of Reinforced Masonry Walls”, ACI Structural Journal, Vol. 87, No. 6. pp 646-656.

Soroushian, P., Obaseki, K., Rojas MC., 1987. “Bearing strength and stiffness of concrete under reinforcing bars”. ACI Structural Journal, Vol. 84, No. 3, pp. 179-84.

Soroushian, P., Obaseki, K., Baiyasi, M. I., Basheer, E. and Choi, K., 1988. “Inelastic cyclic behaviour of dowel bars”. ACI Structural Journal, Vol. 85 No. 1, pp. 23–29.

Tanner, J. E., 2003 “Design Provisions for Autoclaved Aerated Concrete (AAC) Structural Systems,” PhD Dissertation, University of Texas, Austin, Texas..

Vintzeleou E. N. and Tassios T. P., 1987. “Behaviour of dowels under cyclic deformations” ACI Structural Journal, Vol. 84, No. 1, pp 18-30.

Voon, K. and Ingham, J. 2006. ”Experimental In-Plane Shear Strength Investigation of Reinforced Concrete Masonry Walls”, Journal of Structural Engineering, Vol. 132, No. 3, pp. 400-408.

Vulcano, A., Bertero, V. V., Cotolli, V., 1988. “Analytical modeling of RC structural walls”. Proceedings of the 9th World Conference on Earthquake Engineering, Tokyo-Kyoto, Japan Vol. VI, pp. 41-46.

Walraven J, Frénay J, Pruijssers A., 1987. “Influence of concrete strength and load history on the shear friction capacity of concrete members”. PCI J 1987;32(1):66–84.

Walraven J.C., 1999. “Biaxial Behaviour of cracked Reinforced Concrete”. In: Fédération Internationale du Béton Structural Concrete: Textbook on “Behaviour, Design and Performance”, Volume 1. Lausanne, Switzerland: International Federation for Structural Concrete, 1999.

Wight, J. K., and MacGregor, J. G., 2009. "Reinforced concrete: Mechanics and design (5th edition)." Pearson Prentice Hall, Upper Saddle River, NJ.

Williams, Scott, 2013. “Numerical Analysis of Reinforced Masonry Shear Walls Using the Nonlinear Truss Approach”. Master’s thesis, Virginia Tech, Blacksburg.

Yassin, M. H. M., 1994. “Nonlinear analysis of prestressed concrete structures under monotonic and cyclic loads”. PhD Dissertation. University of California. Berkeley, California.

Appendix A: Calibration of the 2D Model for Specimens with Cantilever Support Conditions

Calibration of Test Specimen PBS-03

LWall := 2.4 m	fm := 8.5 MPa	Lambda = 1.00	Frict_Coeff = 0.60	DowelCoeff = 1.27	P / (f'm Ag) = 0%
HWall := 2.4 m	fsy := 460 MPa	h := 0.20·HWall	Frict_Yield = 1mm	Dowel_Yield = 1.7 mm	P = 0 kN
ρ_v := 0.33%					

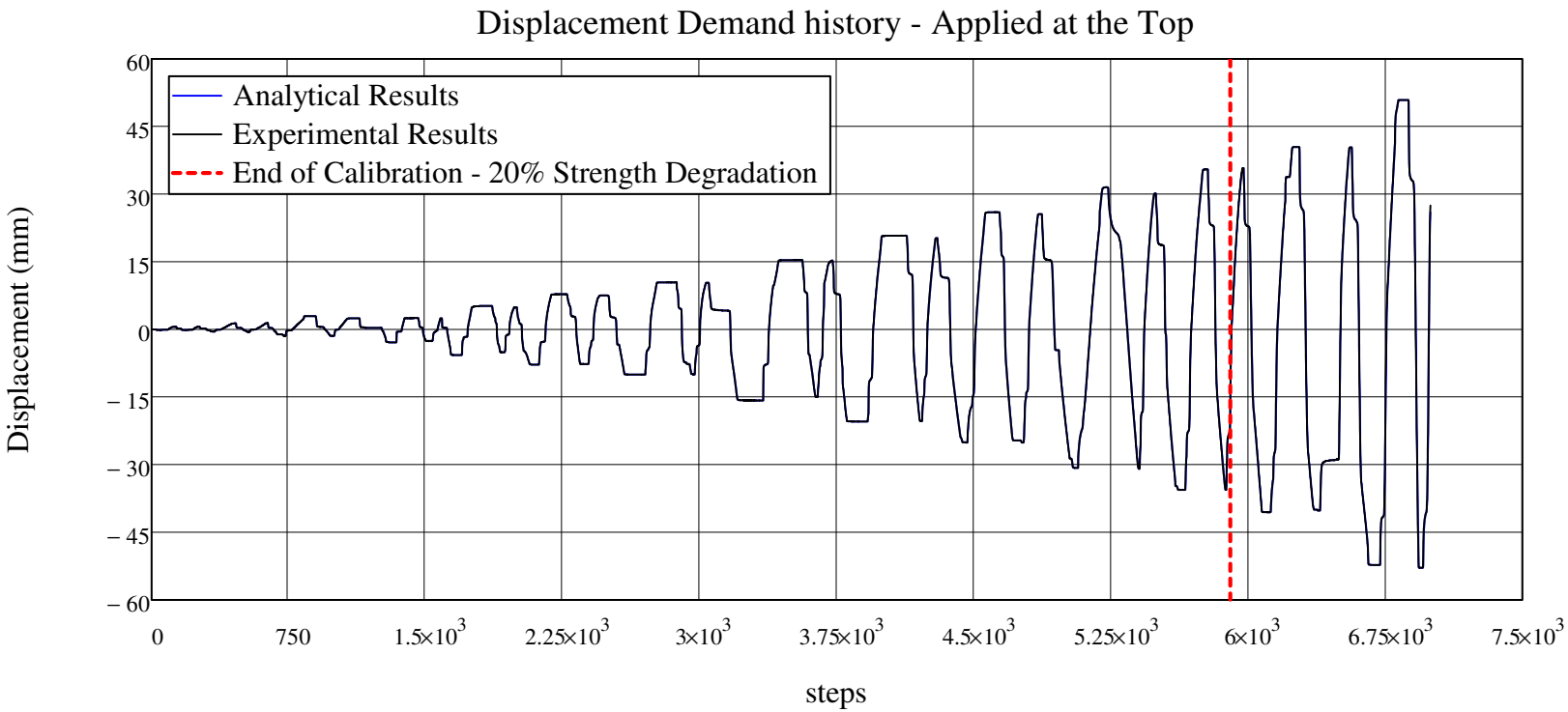

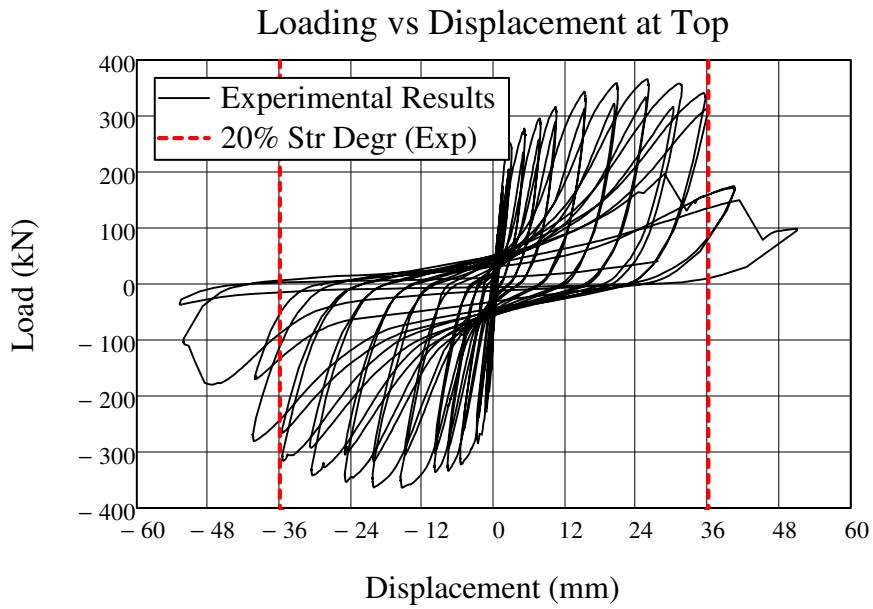
Loading vs Displacement at Top
Experimental Results
20% Str Degr (Exp)
Load (kN)
Displacement (mm)
400
300
200
100
0
– 100
– 200
– 300
– 400
– 60
– 48
– 36
– 24
– 12
0
12
24
36
48
60

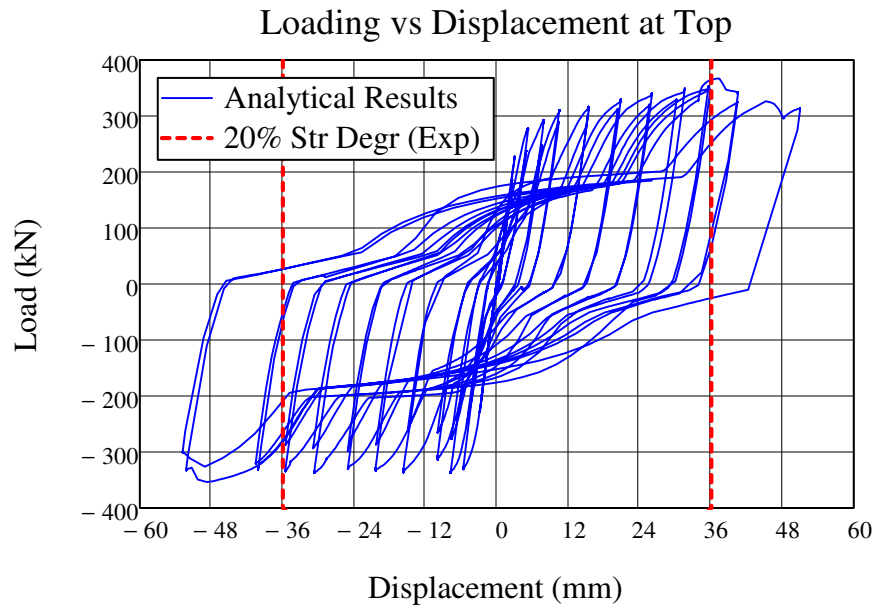
Loading vs Displacement at Top
Analytical Results
20% Str Degr (Exp)
Load (kN)
Displacement (mm)
400
300
200
100
0
– 100
– 200
– 300
– 400
– 60
– 48
– 36
– 24
– 12
0
12
24
36
48
60

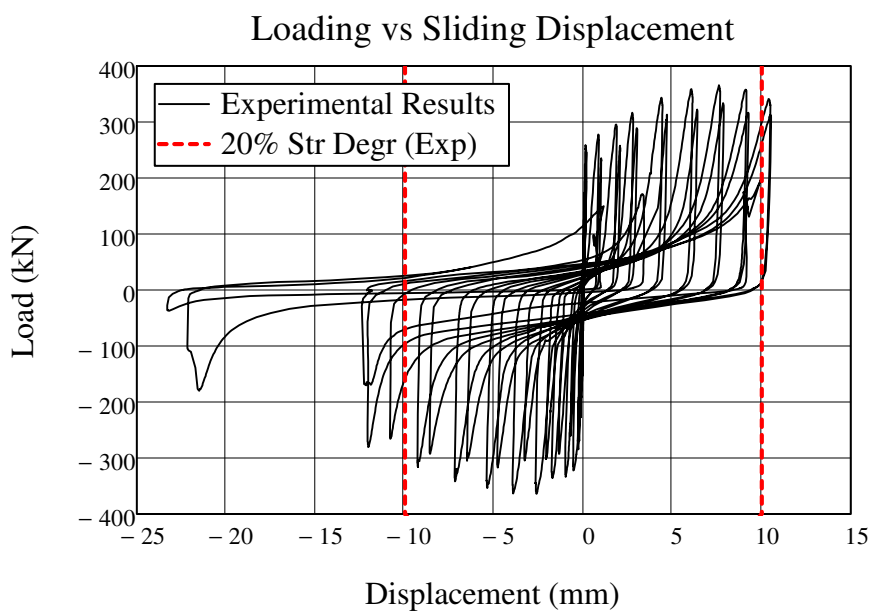
Loading vs Sliding Displacement
Experimental Results
20% Str Degr (Exp)
Load (kN)
Displacement (mm)
400
300
200
100
0
– 100
– 200
– 300
– 400
– 25
– 20
– 15
– 10
– 5
0
5
10
15

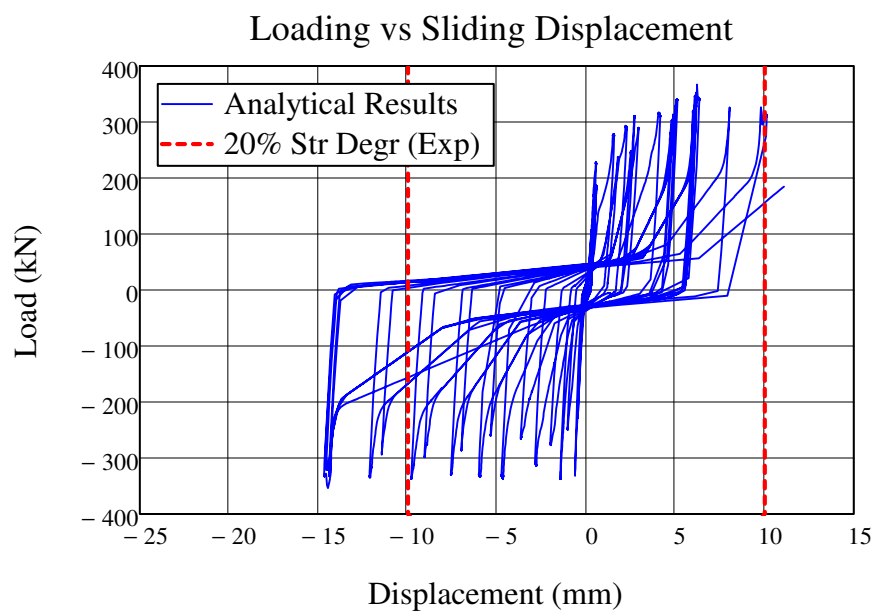
Loading vs Sliding Displacement
Analytical Results
20% Str Degr (Exp)
Load (kN)
Displacement (mm)
400
300
200
100
0
– 100
– 200
– 300
– 400
– 25
– 20
– 15
– 10
– 5
0
5
10
15

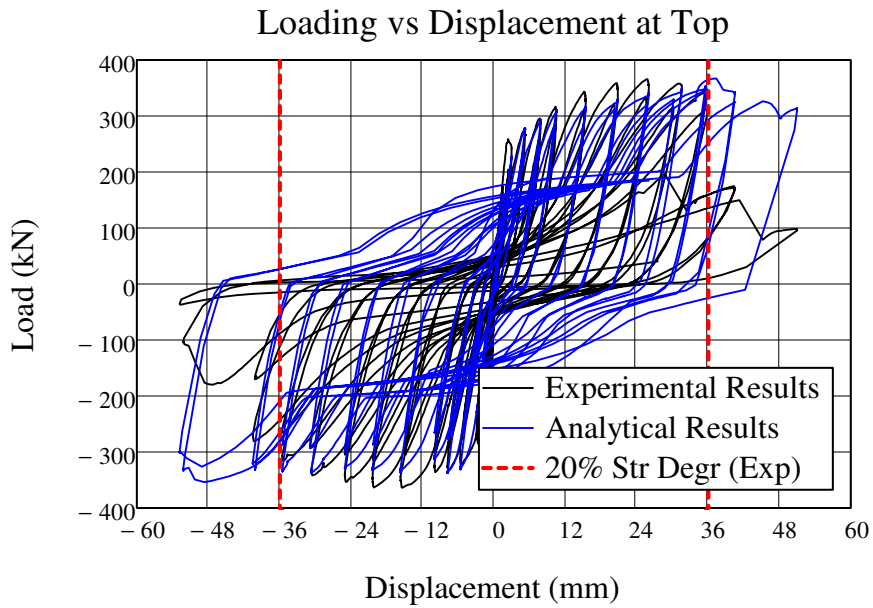
Loading vs Displacement at Top
Load (kN)
400
300
200
100
0
– 100
– 200
– 300
– 400
– 60
– 48
– 36
– 24
– 12
0
12
24
36
48
60
Displacement (mm)
Experimental Results
Analytical Results
20% Str Degr (Exp)

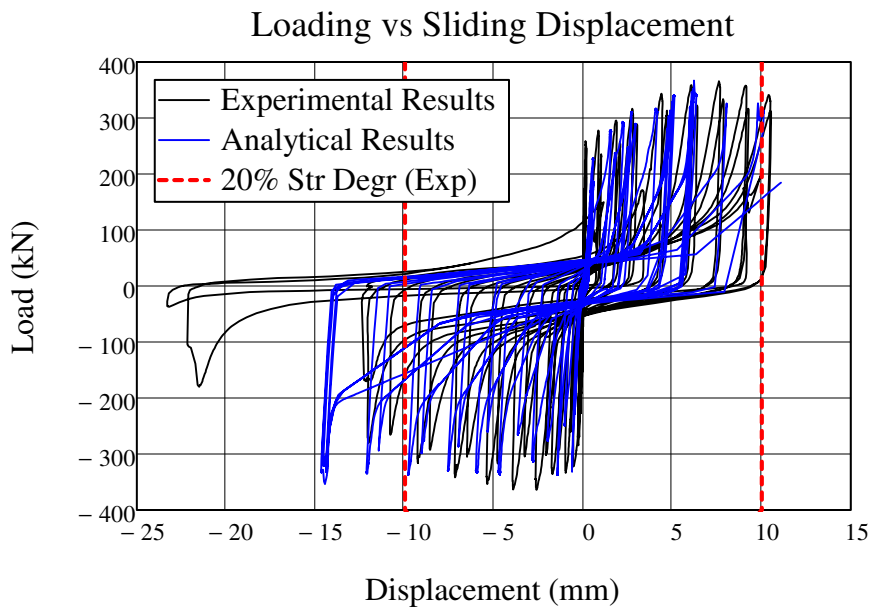
Loading vs Sliding Displacement
Load (kN)
400
300
200
100
0
– 100
– 200
– 300
– 400
– 25
– 20
– 15
– 10
– 5
0
5
10
15
Displacement (mm)
Experimental Results
Analytical Results
20% Str Degr (Exp)

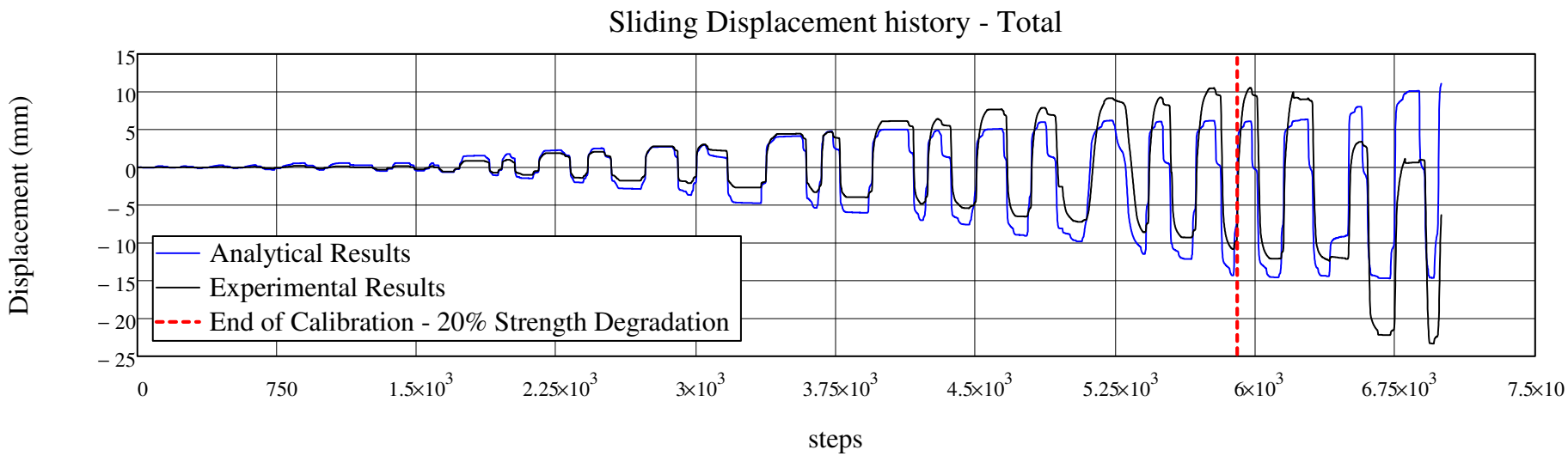

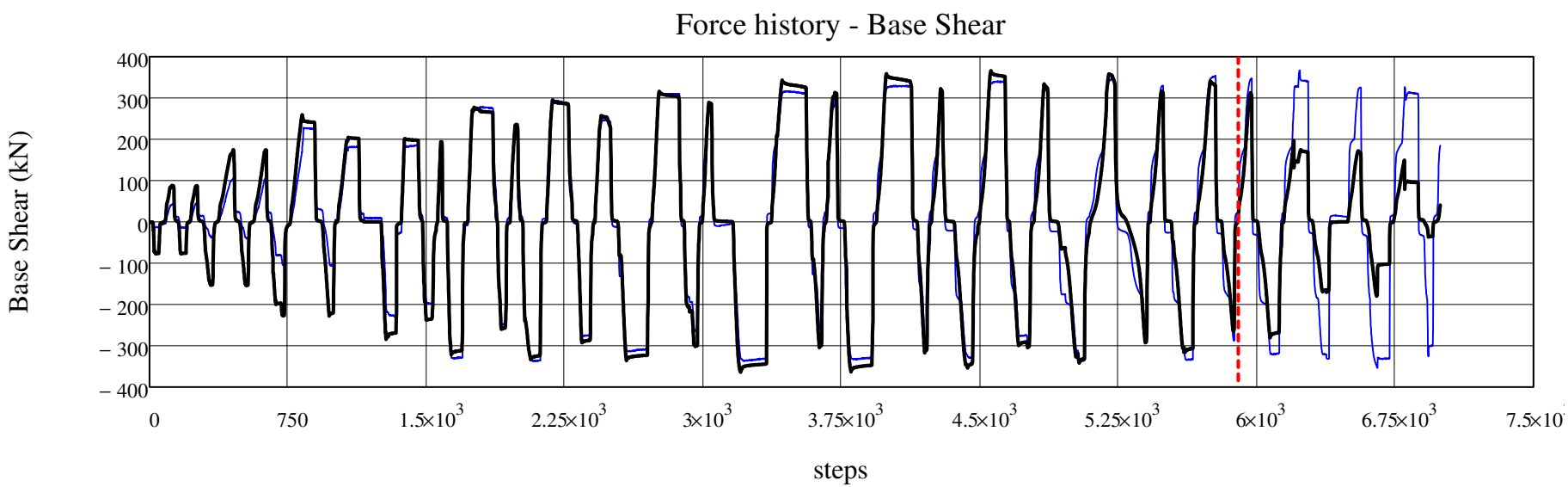

Analytical Results
Experimental Results
20% Strength Degradation

Modeling Predictions prior to Strength Degradation*
Maximum Sliding Disp. = 137% of Experimental Result
Maximum Resistance = 101% of Experimental Result

**Strength Degradation @ step 5900*

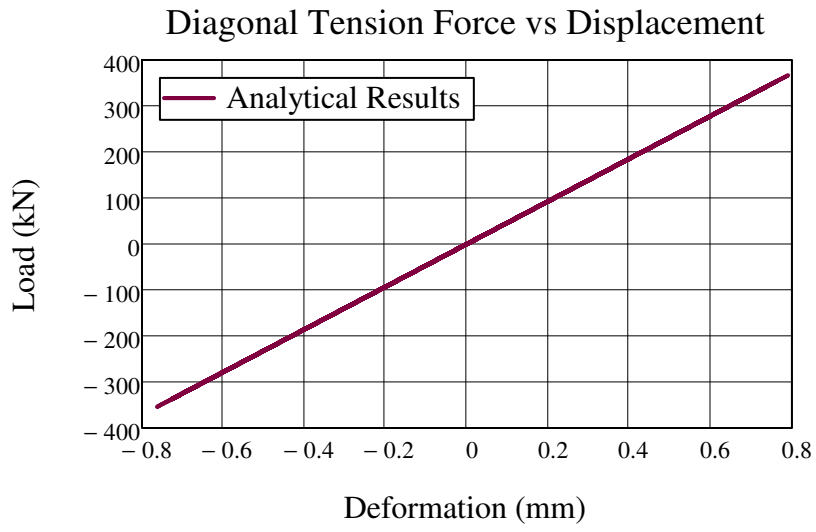
Diagonal Tension Force vs Displacement
Analytical Results
Load (kN)
400
300
200
100
0
− 100
− 200
− 300
− 400
− 0.8
− 0.6
− 0.4
− 0.2
0
0.2
0.4
0.6
0.8
Deformation (mm)

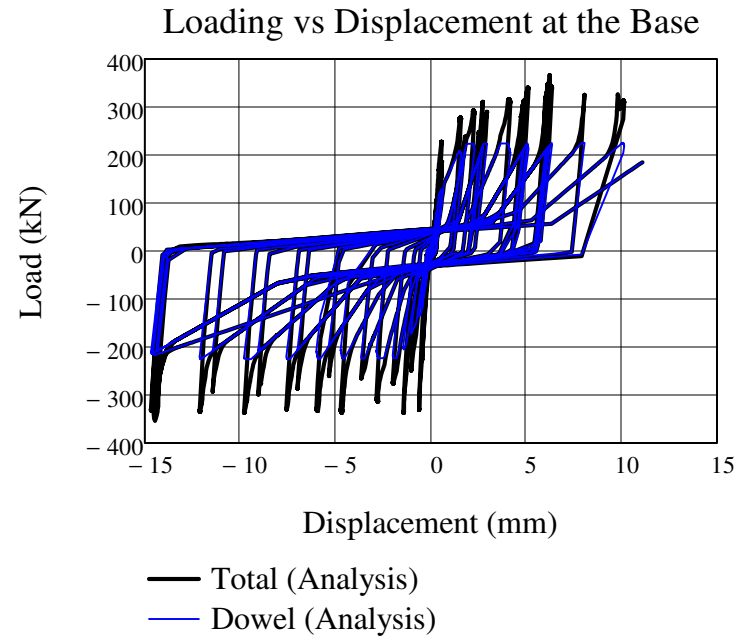
Loading vs Displacement at the Base
Load (kN)
400
300
200
100
0
− 100
− 200
− 300
− 400
− 15
− 10
− 5
0
5
10
15
Displacement (mm)
Total (Analysis)
Dowel (Analysis)

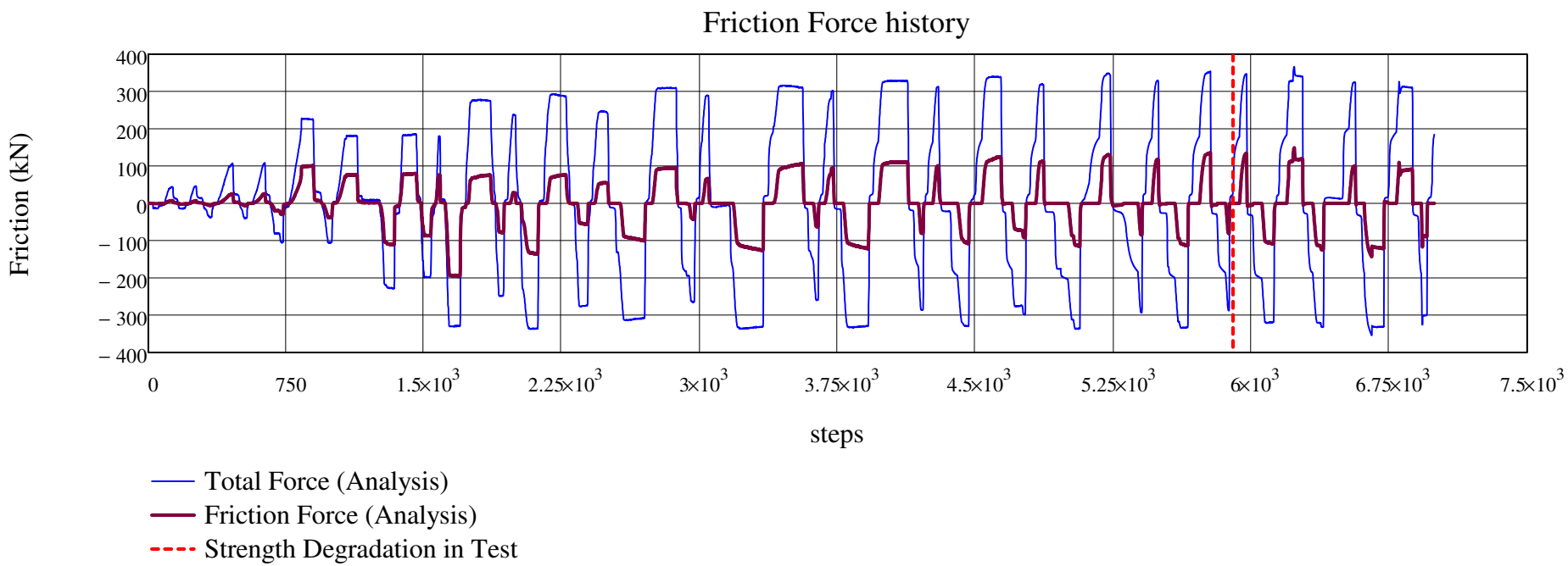
Friction Force history
Friction (kN)
400
300
200
100
0
− 100
− 200
− 300
− 400
0
750
1.5×10^3
2.25×10^3
3×10^3
3.75×10^3
4.5×10^3
5.25×10^3
6×10^3
6.75×10^3
7.5×10^3
steps
Total Force (Analysis)
Friction Force (Analysis)
Strength Degradation in Test

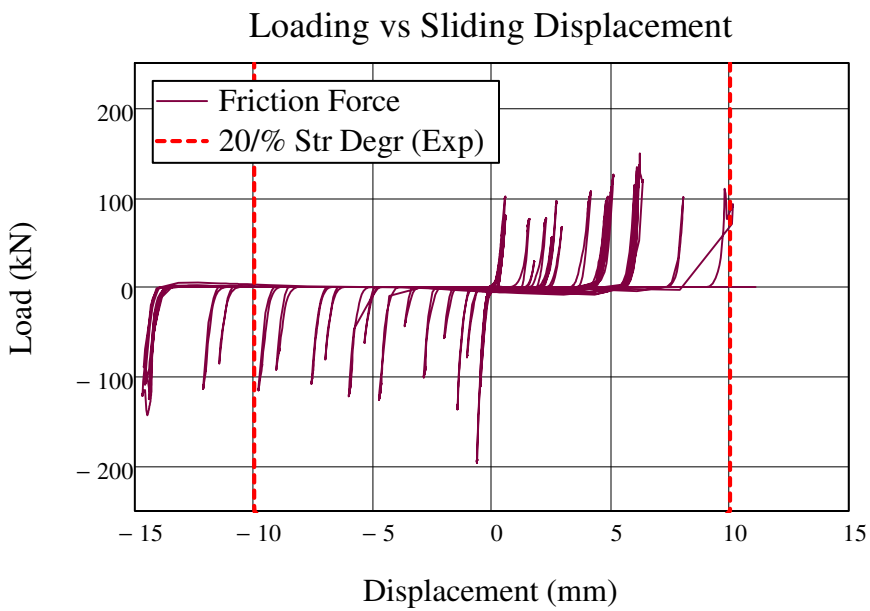
Loading vs Sliding Displacement
Friction Force
20/% Str Degr (Exp)
Load (kN)
200
100
0
− 100
− 200
− 15
− 10
− 5
0
5
10
15
Displacement (mm)

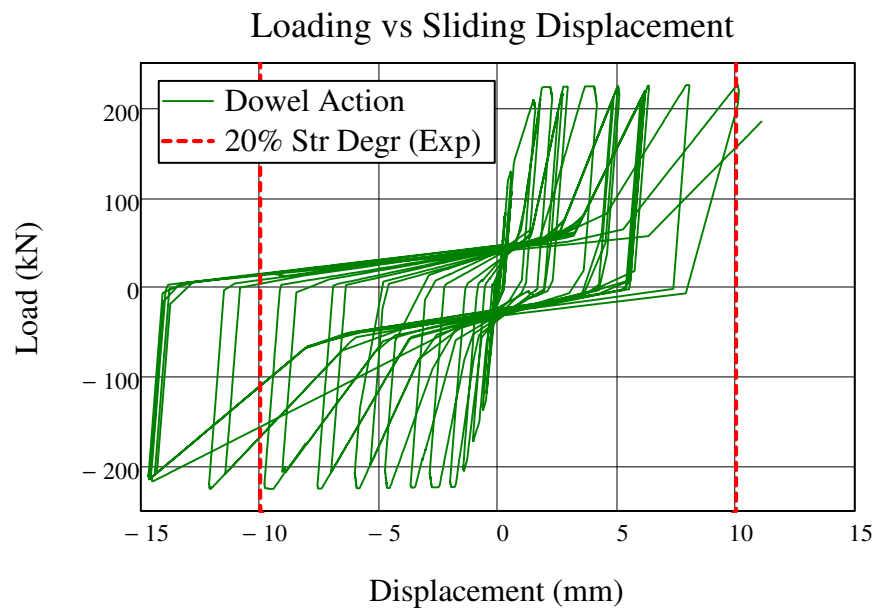
Loading vs Sliding Displacement
Dowel Action
20% Str Degr (Exp)
Load (kN)
200
100
0
− 100
− 200
− 15
− 10
− 5
0
5
10
15
Displacement (mm)

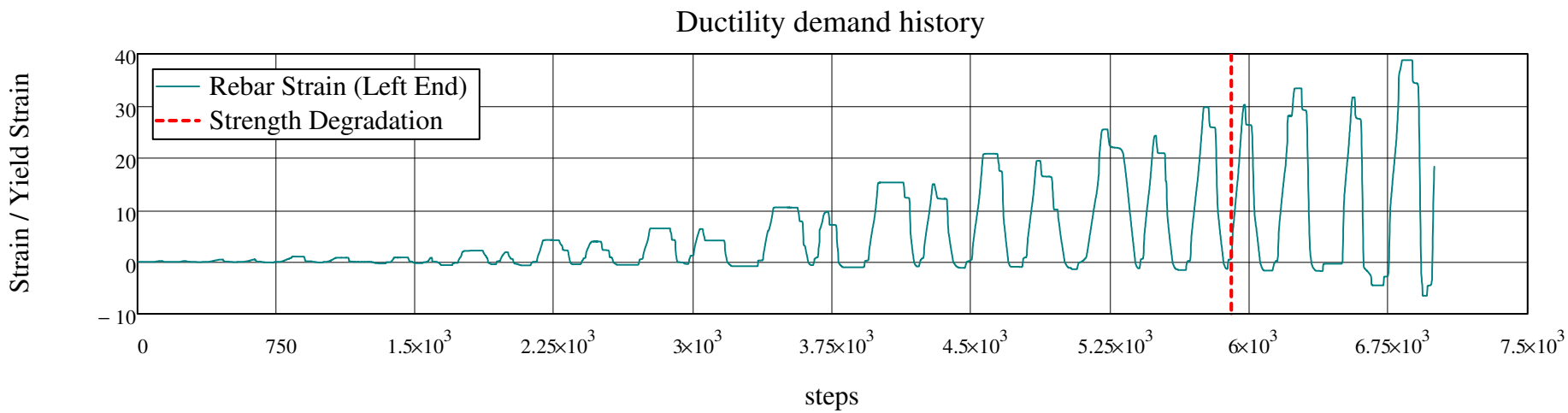
Ductility demand history
Rebar Strain (Left End)
Strength Degradation
Strain / Yield Strain
40
30
20
10
0
− 10
0
750
1.5×10^3
2.25×10^3
3×10^3
3.75×10^3
4.5×10^3
5.25×10^3
6×10^3
6.75×10^3
7.5×10^3
steps

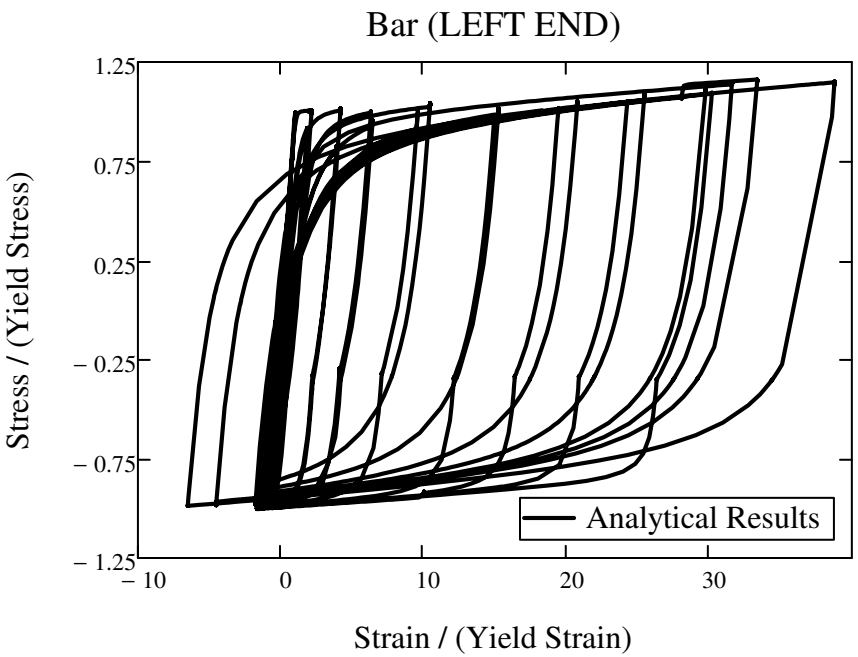
Bar (LEFT END)
Stress / (Yield Stress)
Strain / (Yield Strain)
Analytical Results
1.25
0.75
0.25
– 0.25
– 0.75
– 1.25
– 10
0
10
20
30

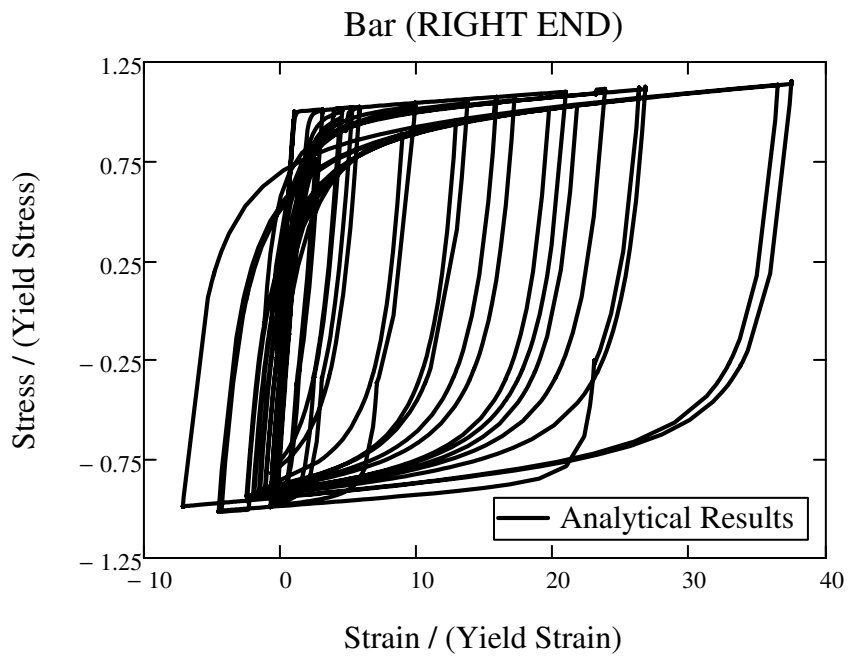
Bar (RIGHT END)
Stress / (Yield Stress)
Strain / (Yield Strain)
Analytical Results
1.25
0.75
0.25
– 0.25
– 0.75
– 1.25
– 10
0
10
20
30
40

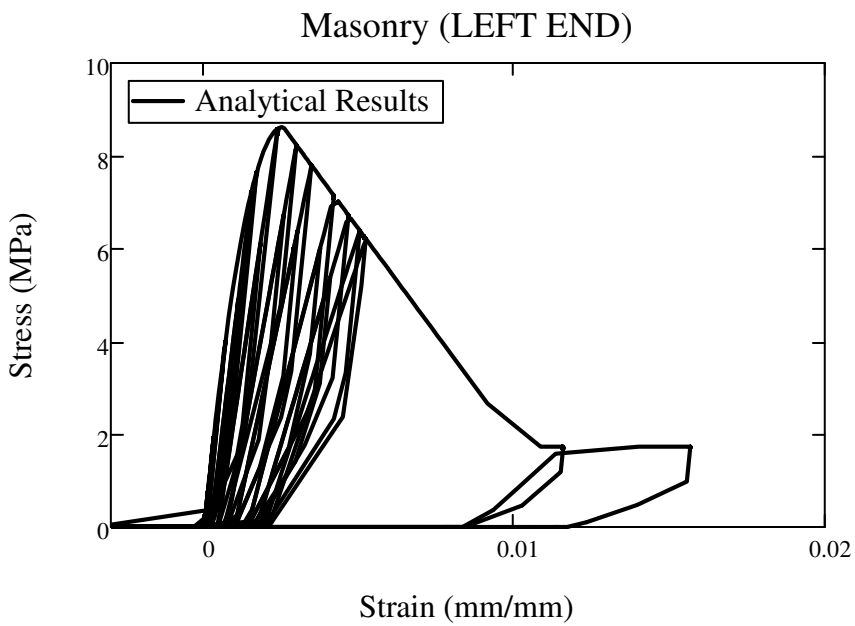
Masonry (LEFT END)
Stress (MPa)
Strain (mm/mm)
Analytical Results
10
8
6
4
2
0
0
0.01
0.02

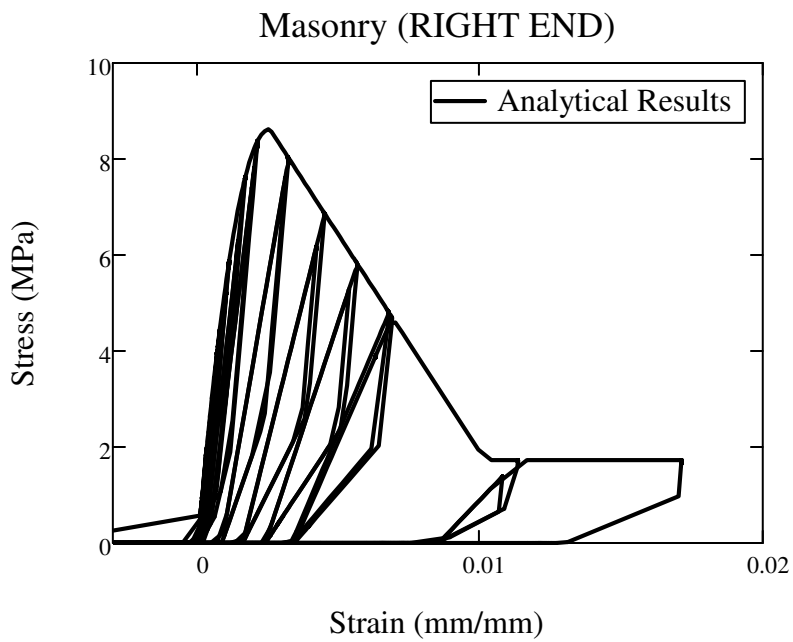
Masonry (RIGHT END)
Stress (MPa)
Strain (mm/mm)
Analytical Results
10
8
6
4
2
0
0
0.01
0.02


Force history - Base Shear
Base Shear (kN)
400
300
200
100
0
– 100
– 200
– 300
– 400
0
1.25×10^3
2.5×10^3
3.75×10^3
5×10^3
6.25×10^3
7.5×10^3
steps
Analytical Results
Instance when Flexural Crack is open across Cross Section
End of Calibration - 20% Strength Degradation

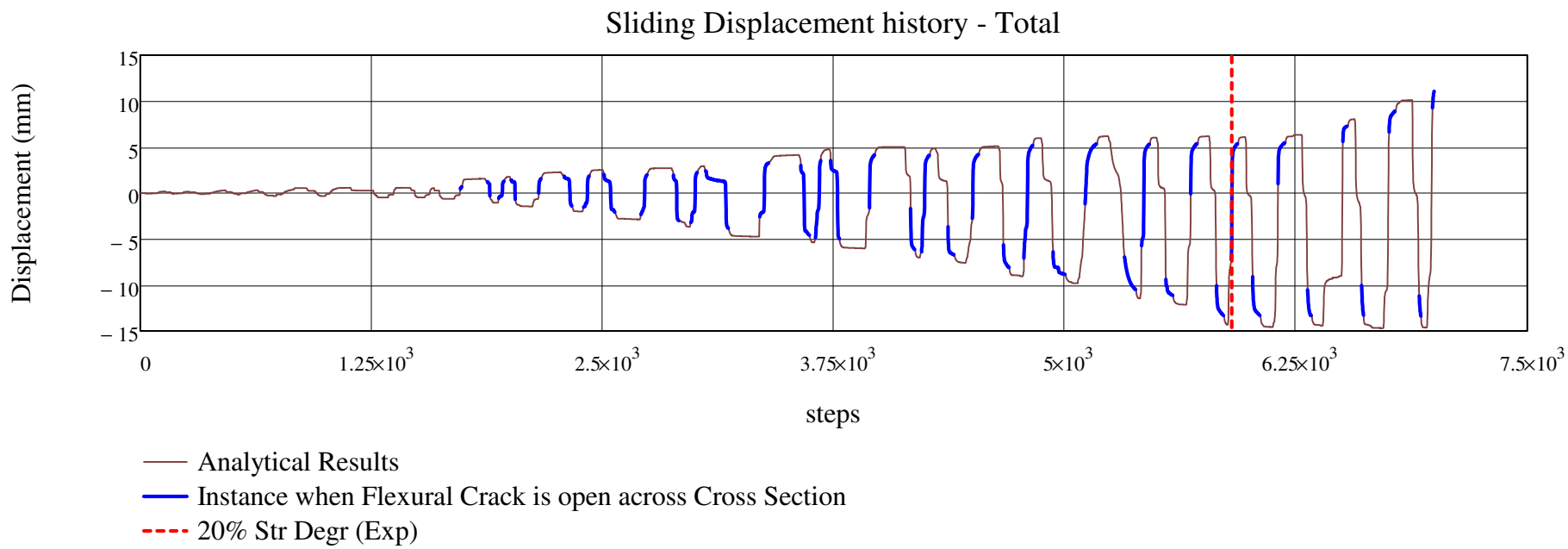
Sliding Displacement history - Total
Displacement (mm)
15
10
5
0
– 5
– 10
– 15
0
1.25×10^3
2.5×10^3
3.75×10^3
5×10^3
6.25×10^3
7.5×10^3
steps
Analytical Results
Instance when Flexural Crack is open across Cross Section
20% Str Degr (Exp)

Calibration of Test Specimen PBS-04

LWall := 2.4 m	fm := 8.5 MPa	Lambda = 1.00	Frict_Coeff = 0.60	DowelCoeff = 1.18	P / (f'm Ag) = 0%
HWall := 2.4 m	fsy := 440 MPa	h := 0.20·HWall	Frict_Yield = 1mm	Dowel_Yield = 1.7mm	P = 0 kN
$\rho_v := 0.18\%$					

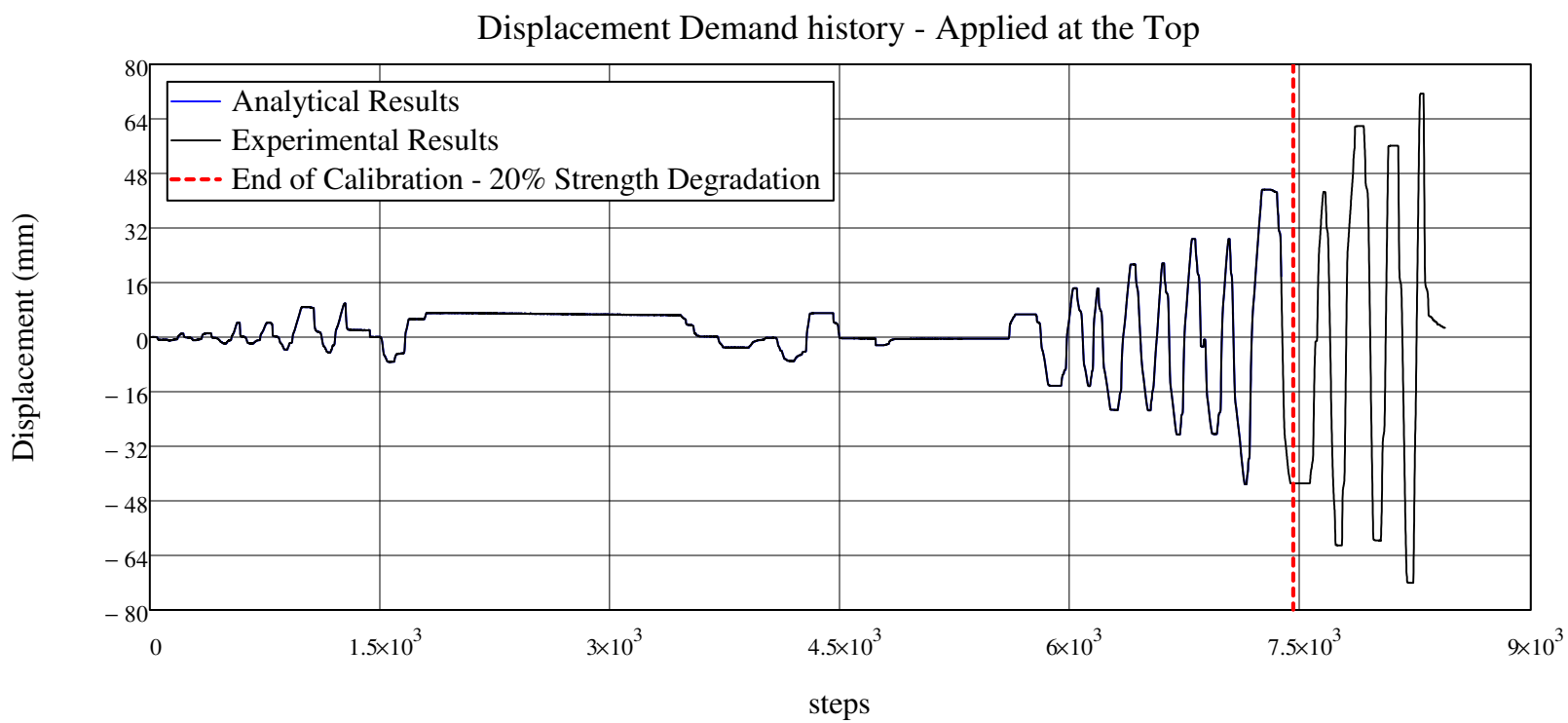

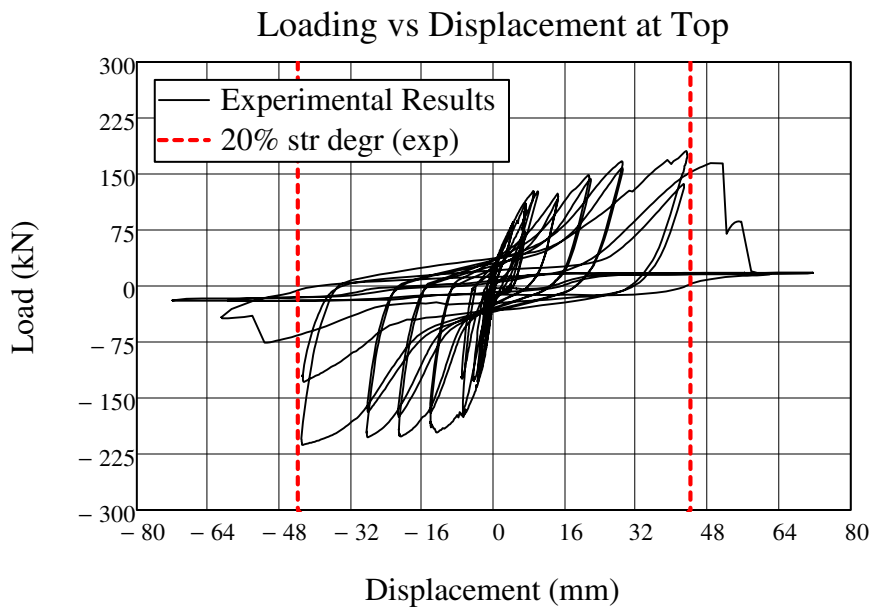
Loading vs Displacement at Top
Experimental Results
20% str degr (exp)
Load (kN)
Displacement (mm)
300
225
150
75
0
– 75
– 150
– 225
– 300
– 80
– 64
– 48
– 32
– 16
0
16
32
48
64
80

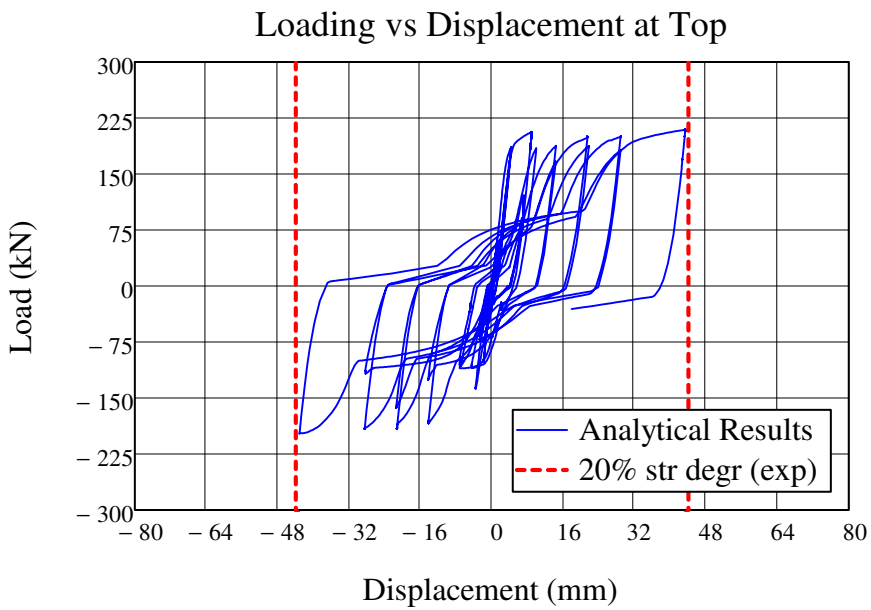
Loading vs Displacement at Top
Analytical Results
20% str degr (exp)
Load (kN)
Displacement (mm)
300
225
150
75
0
– 75
– 150
– 225
– 300
– 80
– 64
– 48
– 32
– 16
0
16
32
48
64
80

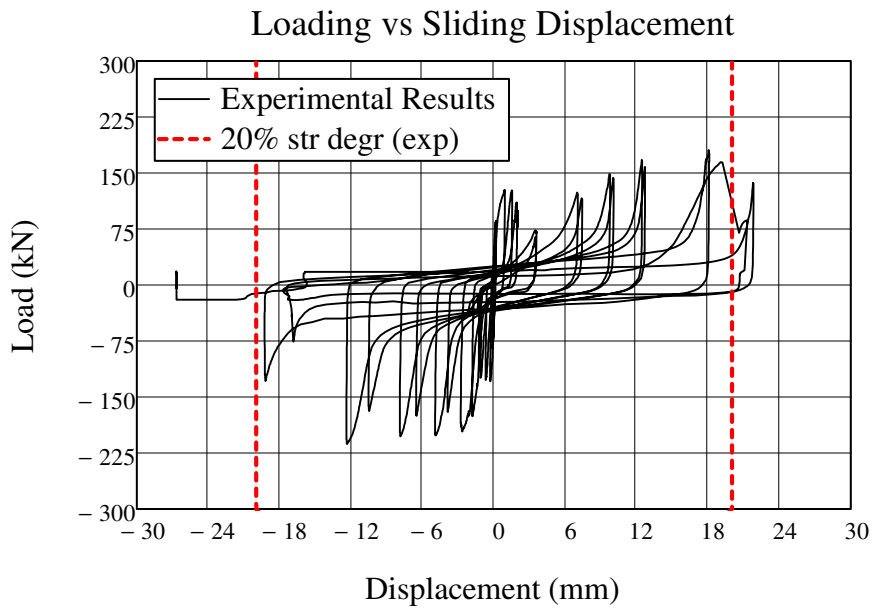
Loading vs Sliding Displacement
Experimental Results
20% str degr (exp)
Load (kN)
Displacement (mm)
300
225
150
75
0
– 75
– 150
– 225
– 300
– 30
– 24
– 18
– 12
– 6
0
6
12
18
24
30

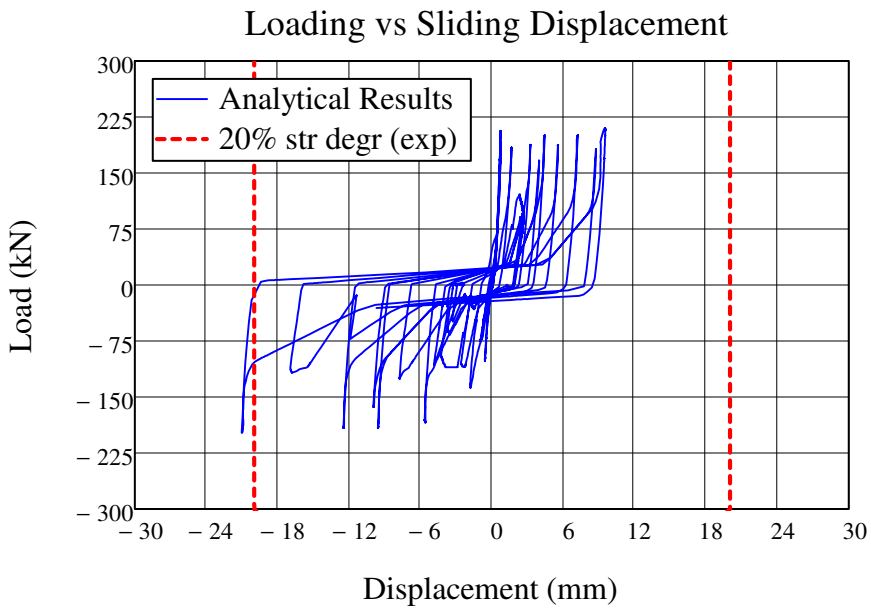
Loading vs Sliding Displacement
Analytical Results
20% str degr (exp)
Load (kN)
Displacement (mm)
300
225
150
75
0
– 75
– 150
– 225
– 300
– 30
– 24
– 18
– 12
– 6
0
6
12
18
24
30

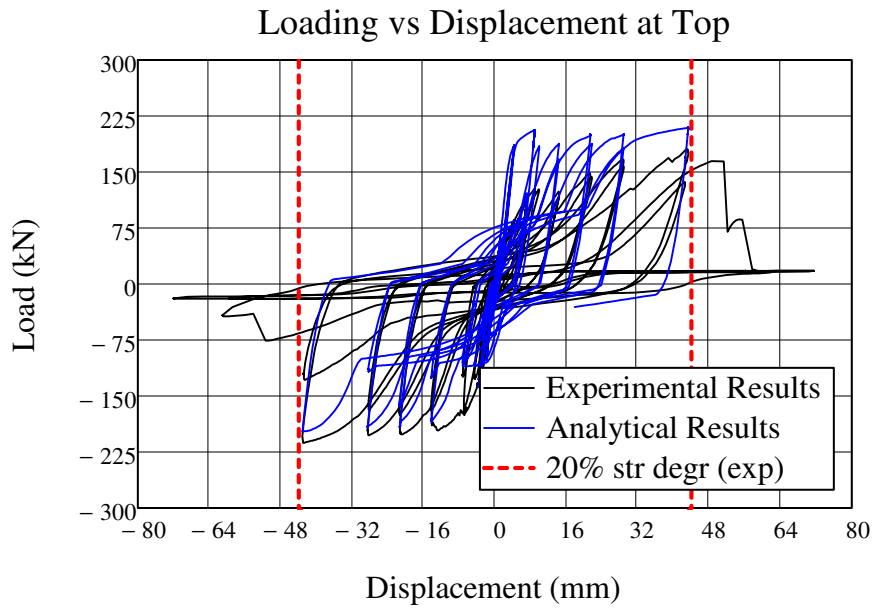
Loading vs Displacement at Top
Load (kN)
300
225
150
75
0
– 75
– 150
– 225
– 300
– 80
– 64
– 48
– 32
– 16
0
16
32
48
64
80
Displacement (mm)
Experimental Results
Analytical Results
20% str degr (exp)

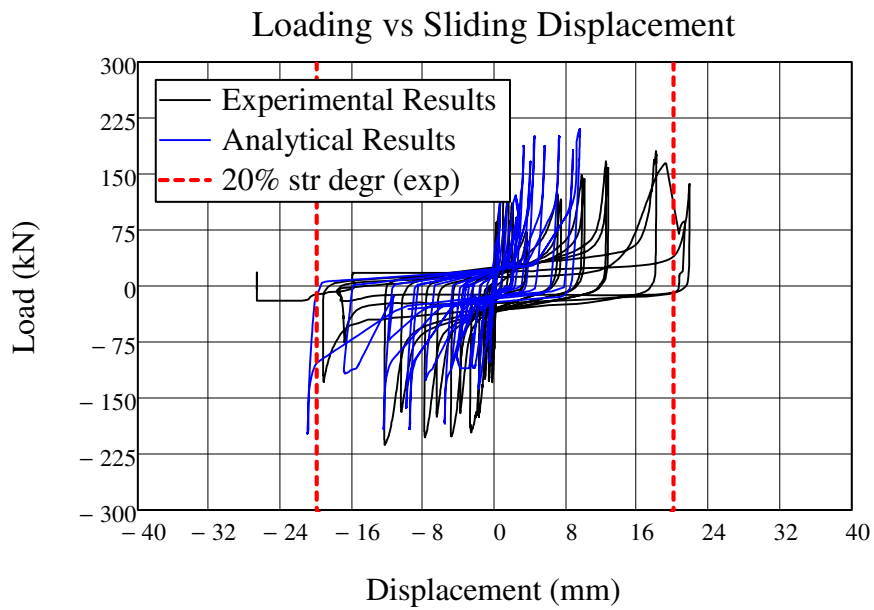
Loading vs Sliding Displacement
Load (kN)
300
225
150
75
0
– 75
– 150
– 225
– 300
– 40
– 32
– 24
– 16
– 8
0
8
16
24
32
40
Displacement (mm)
Experimental Results
Analytical Results
20% str degr (exp)

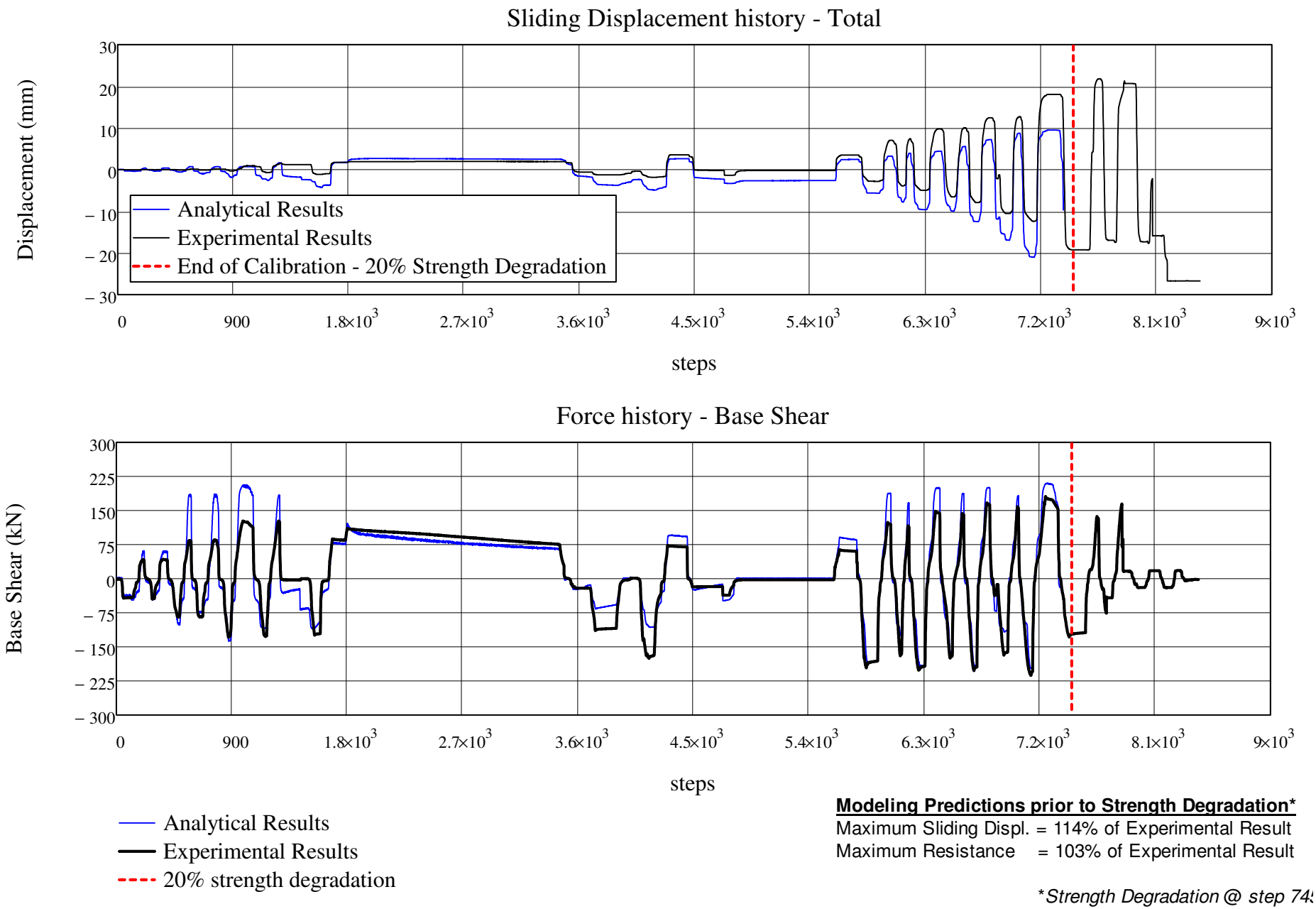

Analytical Results
Experimental Results
20% strength degradation

Modeling Predictions prior to Strength Degradation*
Maximum Sliding Displ. = 114% of Experimental Result
Maximum Resistance = 103% of Experimental Result

**Strength Degradation @ step 74*

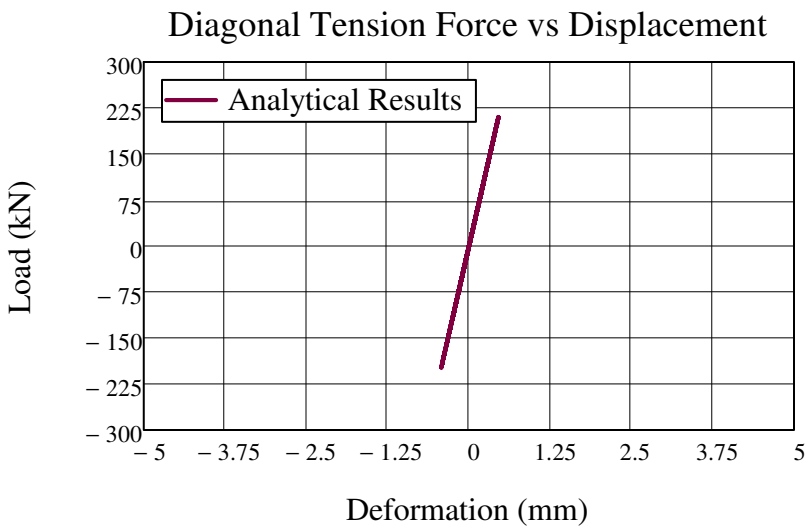
Diagonal Tension Force vs Displacement
Analytical Results
Load (kN)
300
225
150
75
0
− 75
− 150
− 225
− 300
− 5
− 3.75
− 2.5
− 1.25
0
1.25
2.5
3.75
5
Deformation (mm)

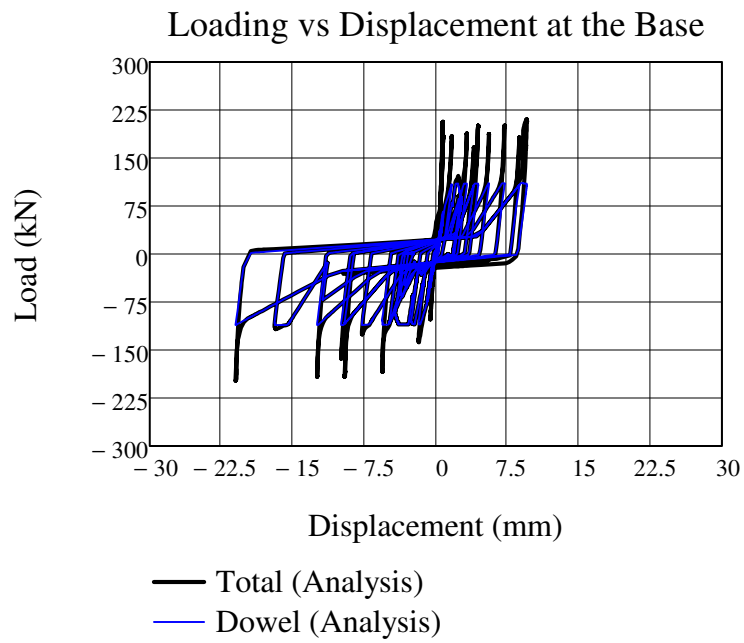
Loading vs Displacement at the Base
Load (kN)
300
225
150
75
0
− 75
− 150
− 225
− 300
− 30
− 22.5
− 15
− 7.5
0
7.5
15
22.5
30
Displacement (mm)
Total (Analysis)
Dowel (Analysis)

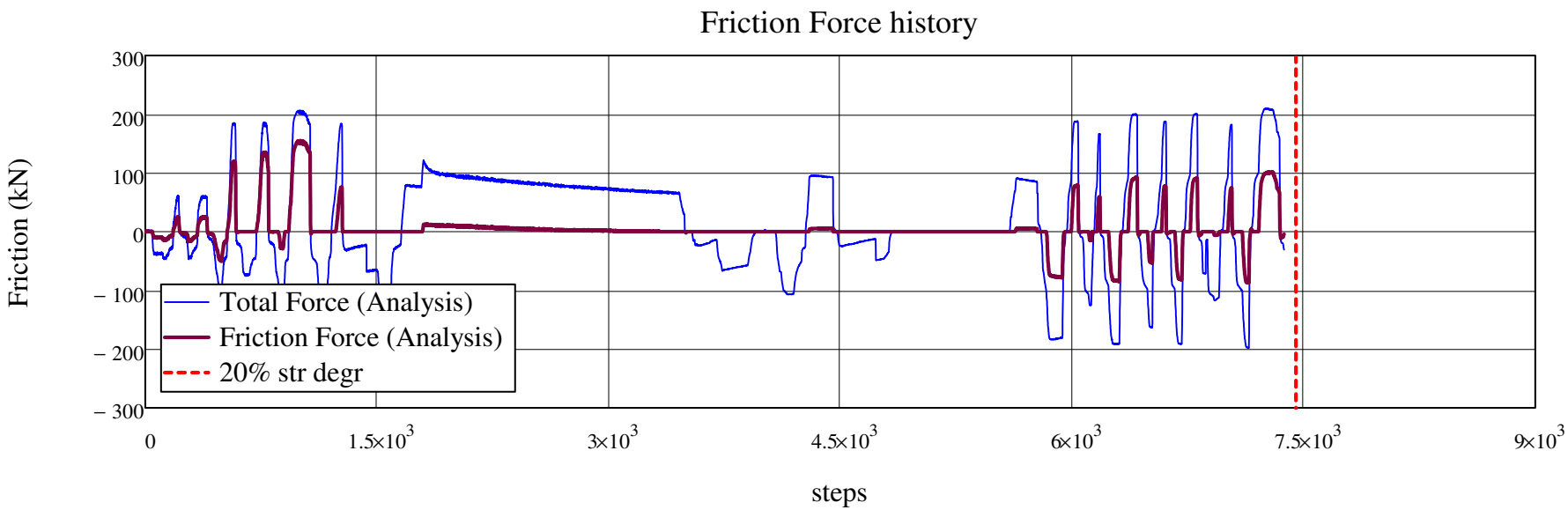
Friction Force history
Friction (kN)
300
200
100
0
− 100
− 200
− 300
Total Force (Analysis)
Friction Force (Analysis)
20% str degr
0
1.5×10^3
3×10^3
4.5×10^3
6×10^3
7.5×10^3
9×10^3
steps

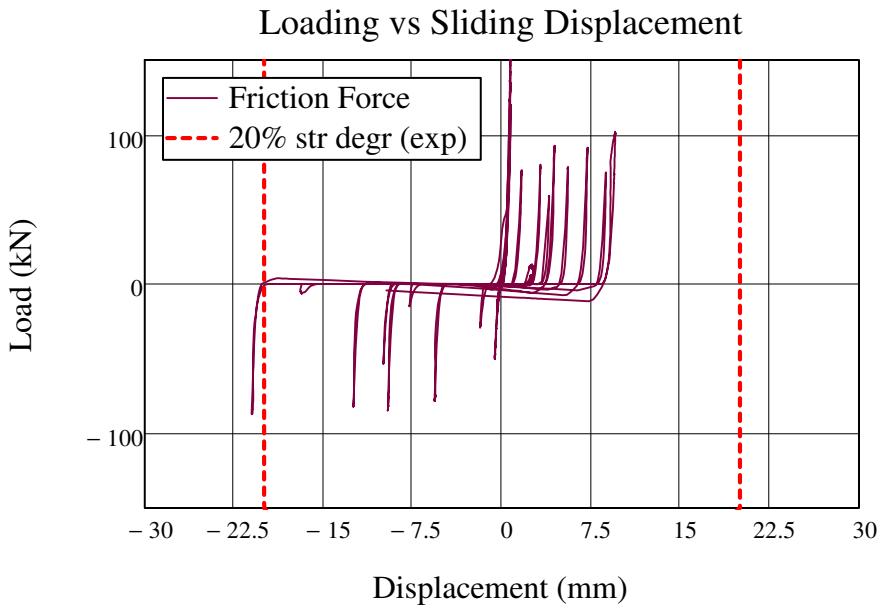
Loading vs Sliding Displacement
Friction Force
20% str degr (exp)
Load (kN)
100
0
– 100
– 30
– 22.5
– 15
– 7.5
0
7.5
15
22.5
30
Displacement (mm)

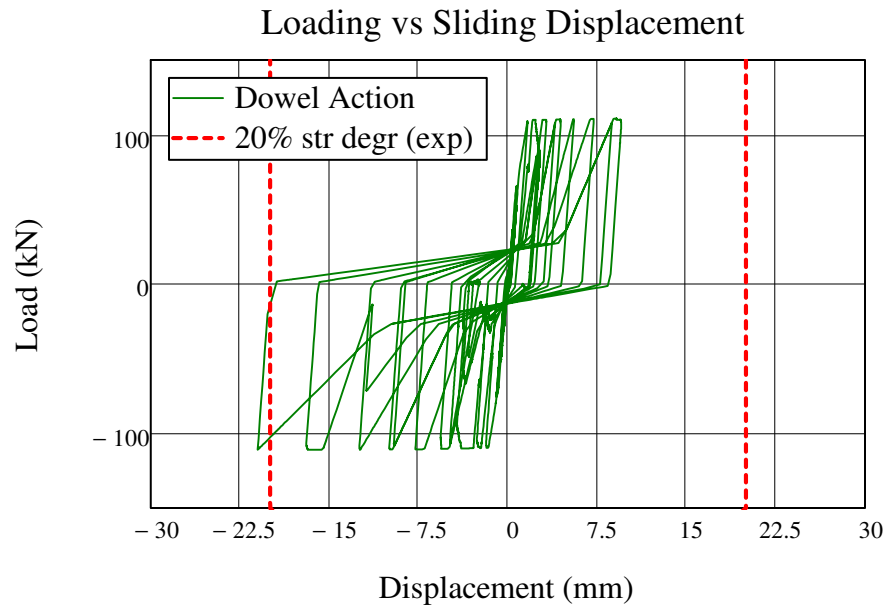
Loading vs Sliding Displacement
Dowel Action
20% str degr (exp)
Load (kN)
100
0
– 100
– 30
– 22.5
– 15
– 7.5
0
7.5
15
22.5
30
Displacement (mm)

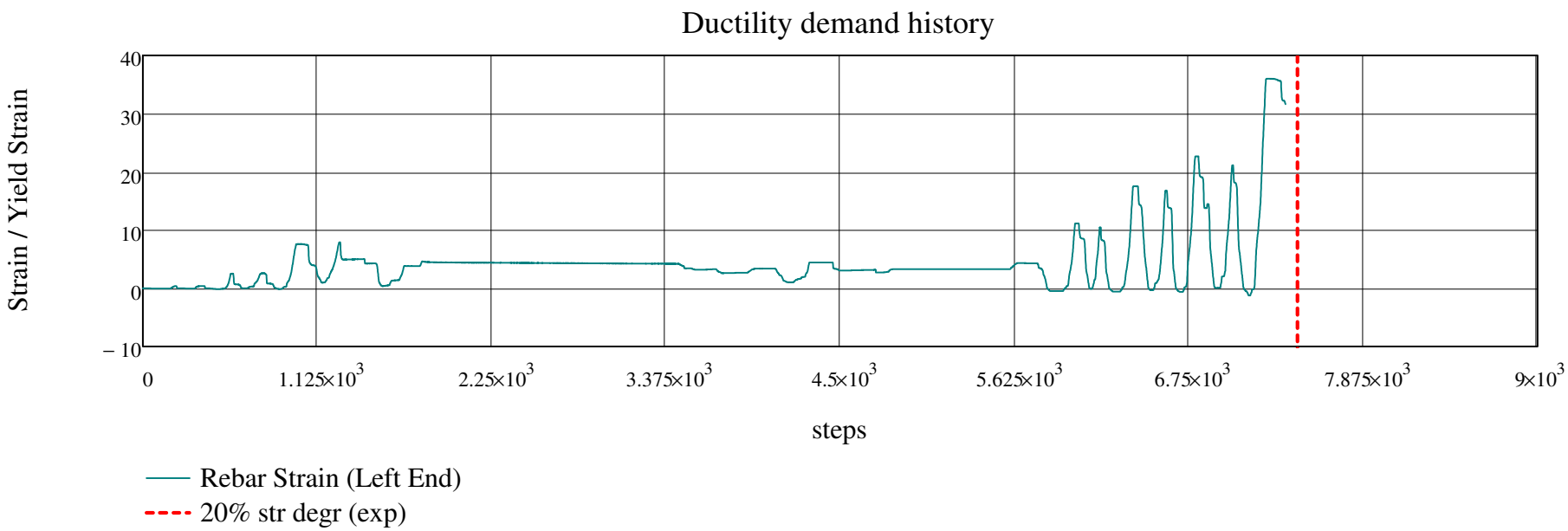
Ductility demand history
Strain / Yield Strain
40
30
20
10
0
– 10
0
1.125×10^3
2.25×10^3
3.375×10^3
4.5×10^3
5.625×10^3
6.75×10^3
7.875×10^3
9×10^3
steps
Rebar Strain (Left End)
20% str degr (exp)

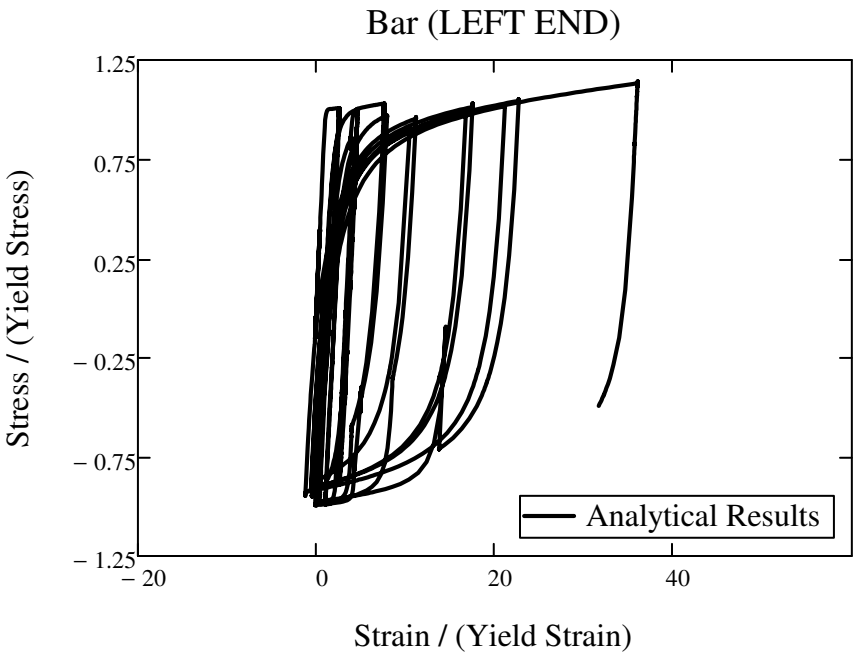
Bar (LEFT END)
Stress / (Yield Stress)
Strain / (Yield Strain)
Analytical Results
1.25
0.75
0.25
– 0.25
– 0.75
– 1.25
– 20
0
20
40

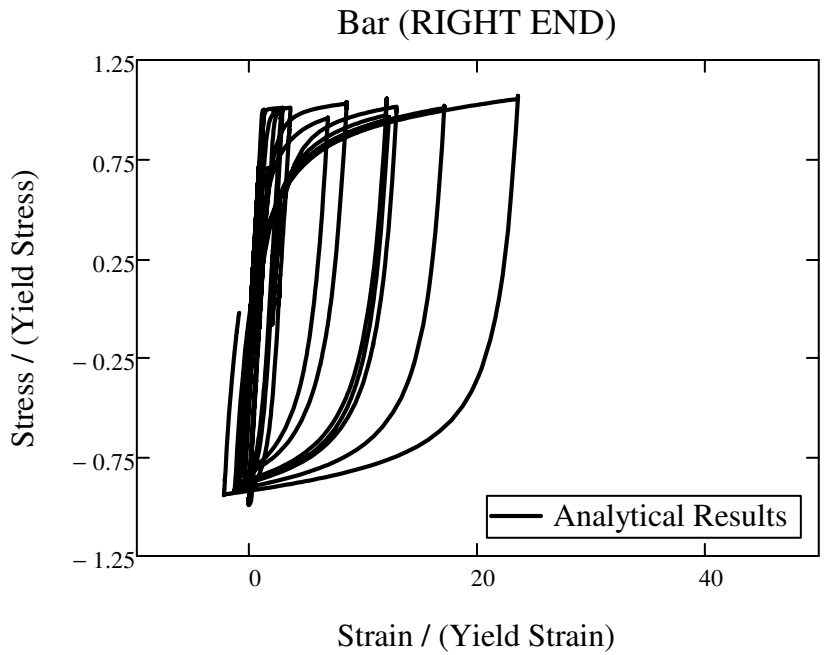
Bar (RIGHT END)
Stress / (Yield Stress)
Strain / (Yield Strain)
Analytical Results
1.25
0.75
0.25
– 0.25
– 0.75
– 1.25
0
20
40

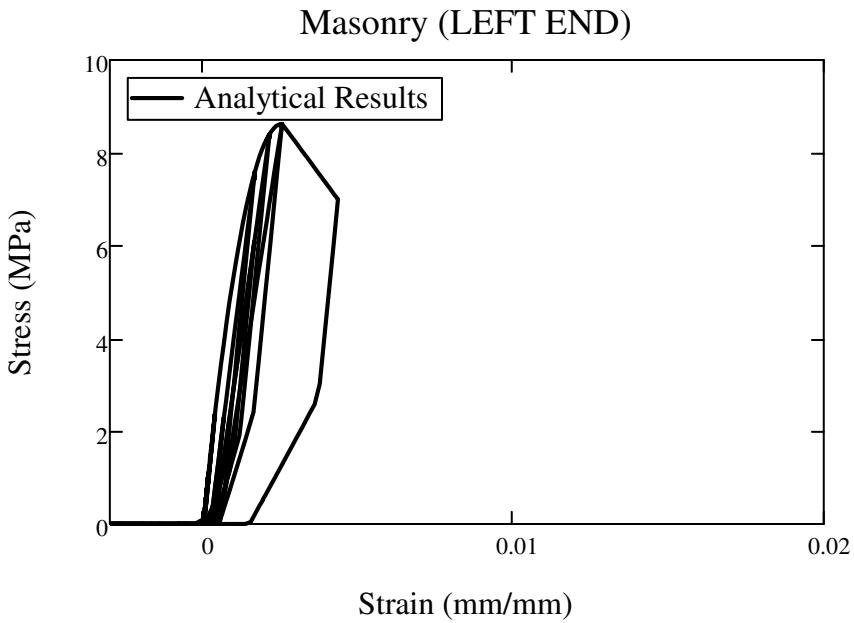
Masonry (LEFT END)
Stress (MPa)
Strain (mm/mm)
Analytical Results
10
8
6
4
2
0
0
0.01
0.02

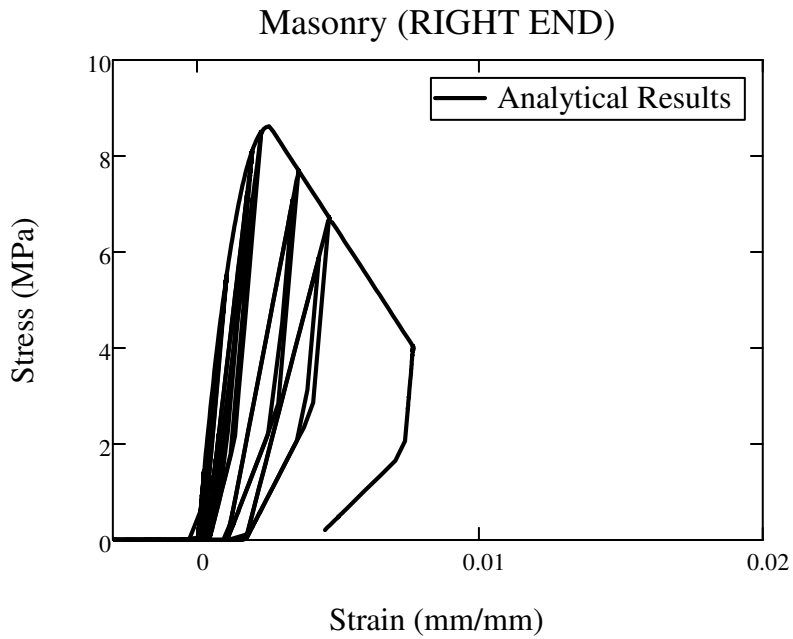
Masonry (RIGHT END)
Stress (MPa)
Strain (mm/mm)
Analytical Results
10
8
6
4
2
0
0
0.01
0.02

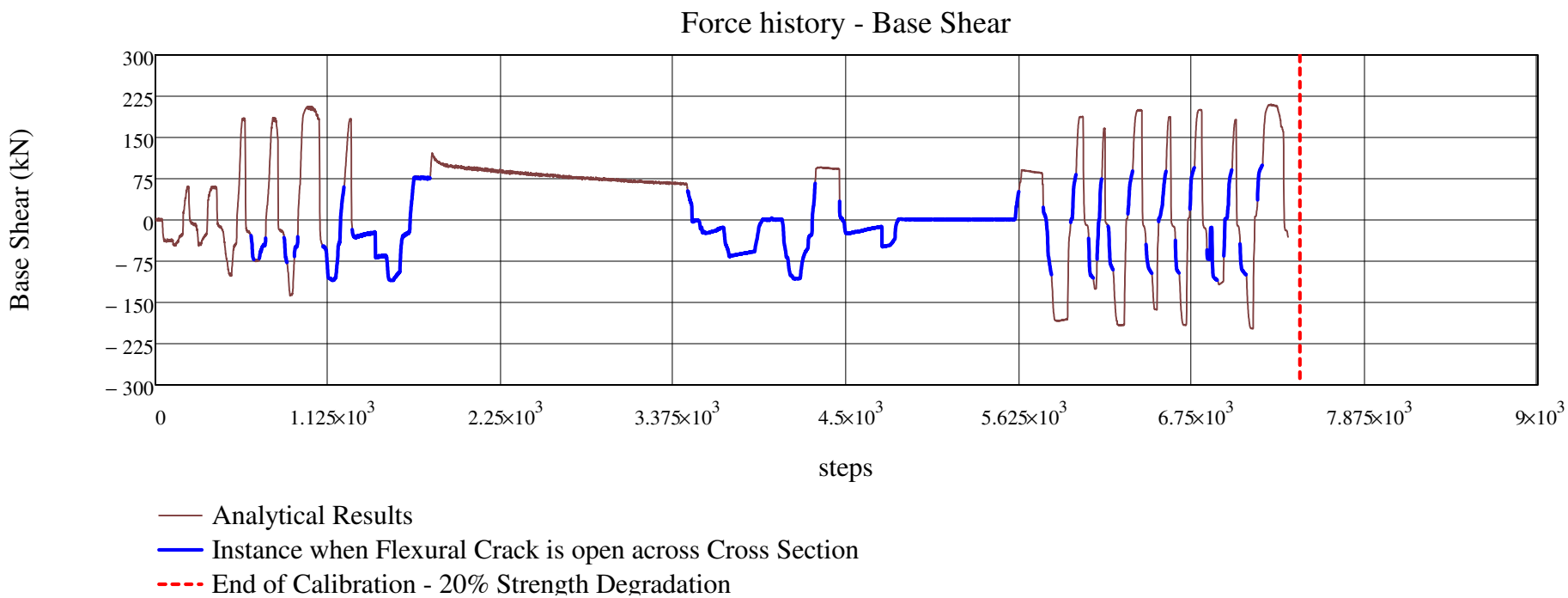
Force history - Base Shear
Base Shear (kN)
300
225
150
75
0
– 75
– 150
– 225
– 300
0
1.125×10^3
2.25×10^3
3.375×10^3
4.5×10^3
5.625×10^3
6.75×10^3
7.875×10^3
9×10^3
steps
Analytical Results
Instance when Flexural Crack is open across Cross Section
End of Calibration - 20% Strength Degradation

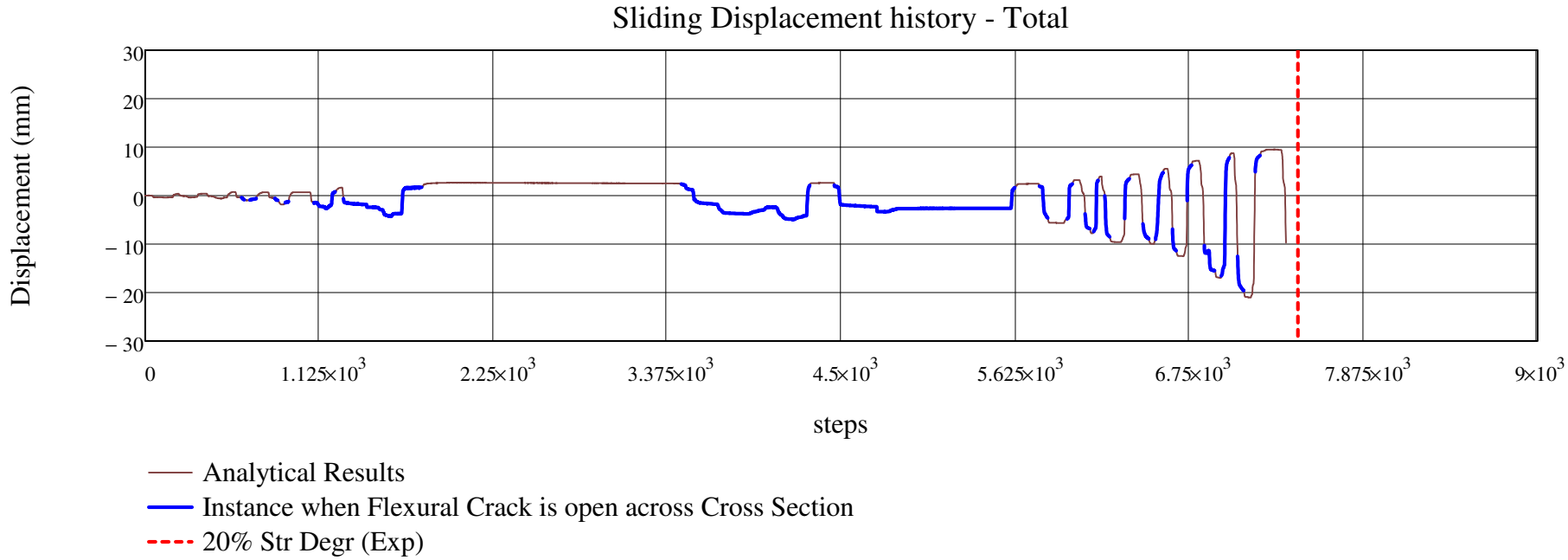
Sliding Displacement history - Total
Displacement (mm)
30
20
10
0
– 10
– 20
– 30
0
1.125×10^3
2.25×10^3
3.375×10^3
4.5×10^3
5.625×10^3
6.75×10^3
7.875×10^3
9×10^3
steps
Analytical Results
Instance when Flexural Crack is open across Cross Section
20% Str Degr (Exp)

Calibration of Test Specimen PBS-04G

LWall := 2.4 m	fm := 8.6 MPa	Lambda = 1.00	Frict_Coeff = 0.60	DowelCoeff = 1.18	P / (f'm Ag) = 0%
HWall := 2.4 m	fsy := 440 MPa	h := 0.15·HWall	Frict_Yield = 1mm	Dowel_Yield = 1mm	P = 0 kN
$\rho_v := 0.18\%$					

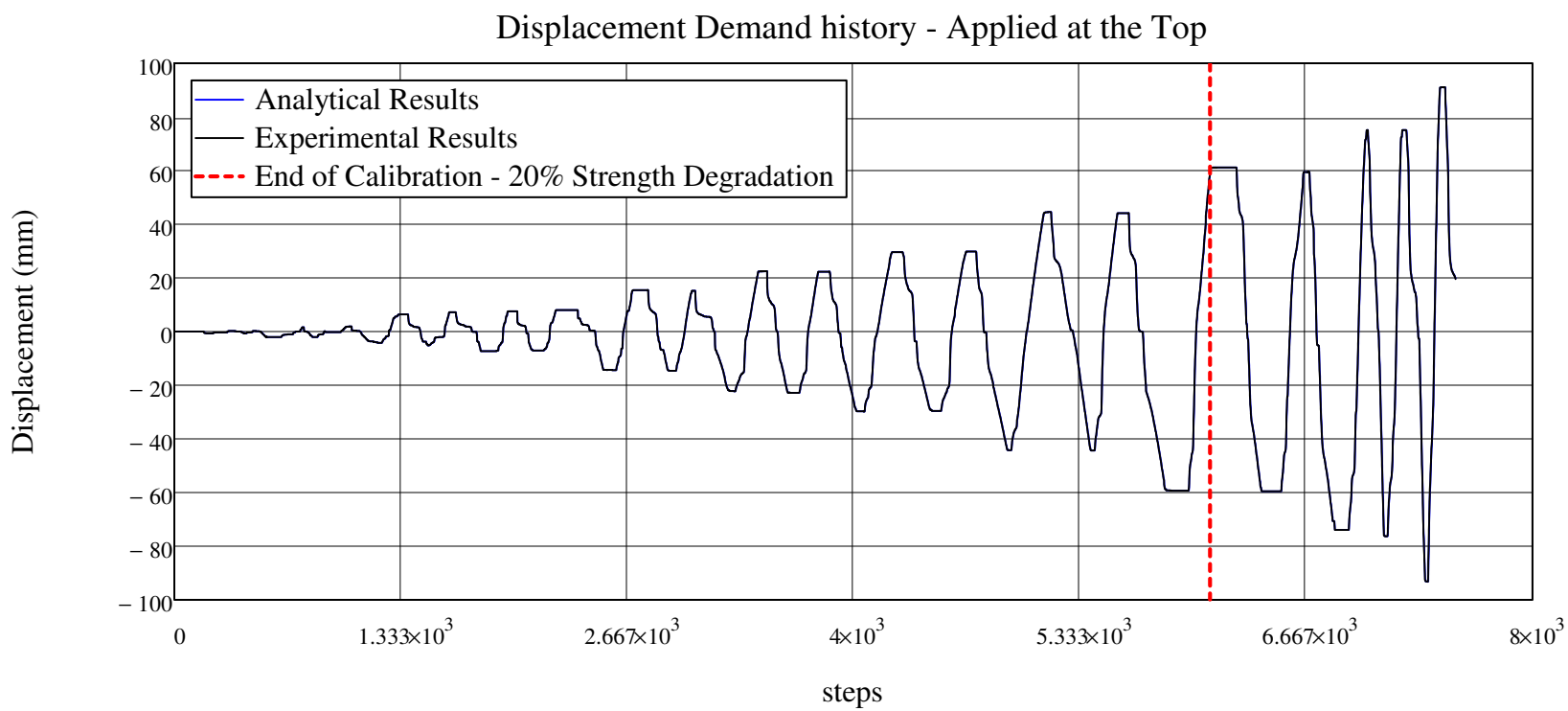

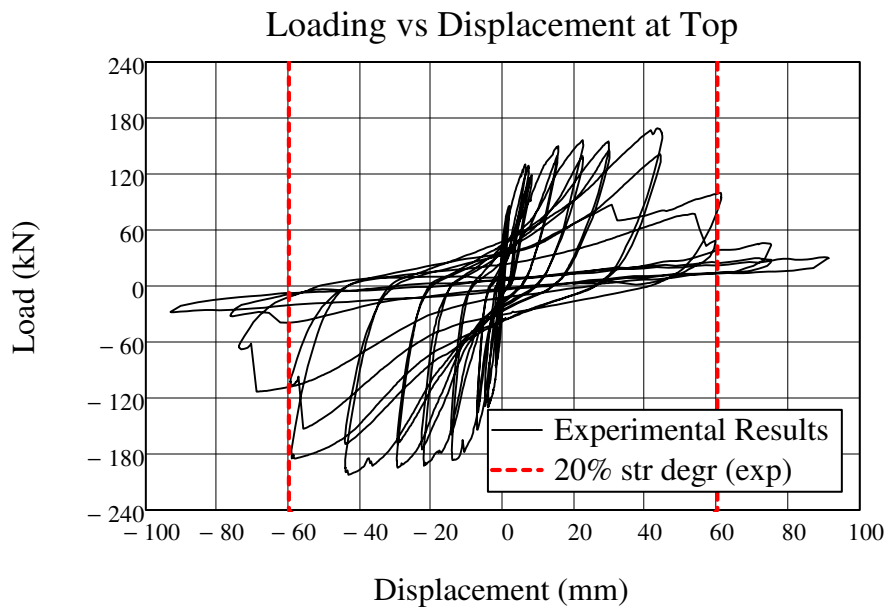
Loading vs Displacement at Top
Load (kN)
Displacement (mm)
Experimental Results
20% str degr (exp)

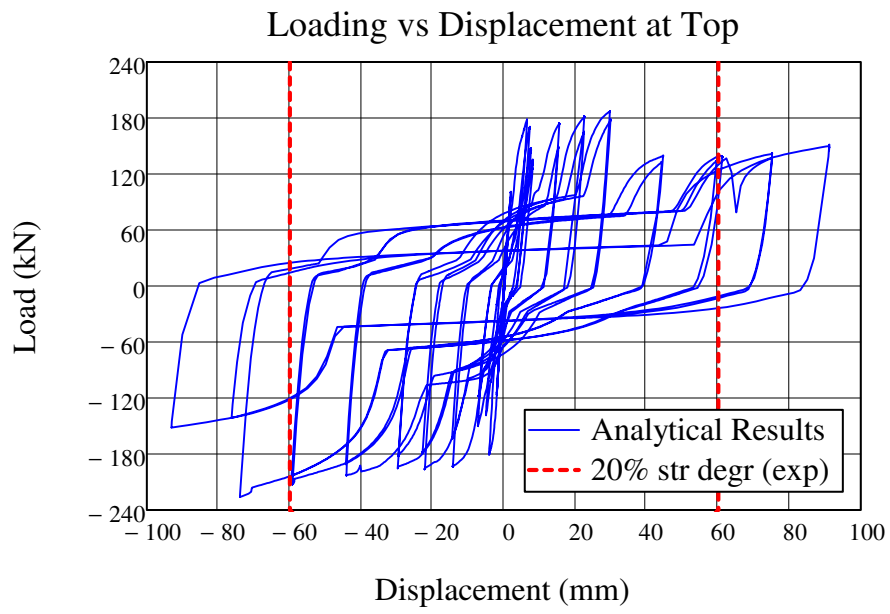
Loading vs Displacement at Top
Load (kN)
Displacement (mm)
Analytical Results
20% str degr (exp)

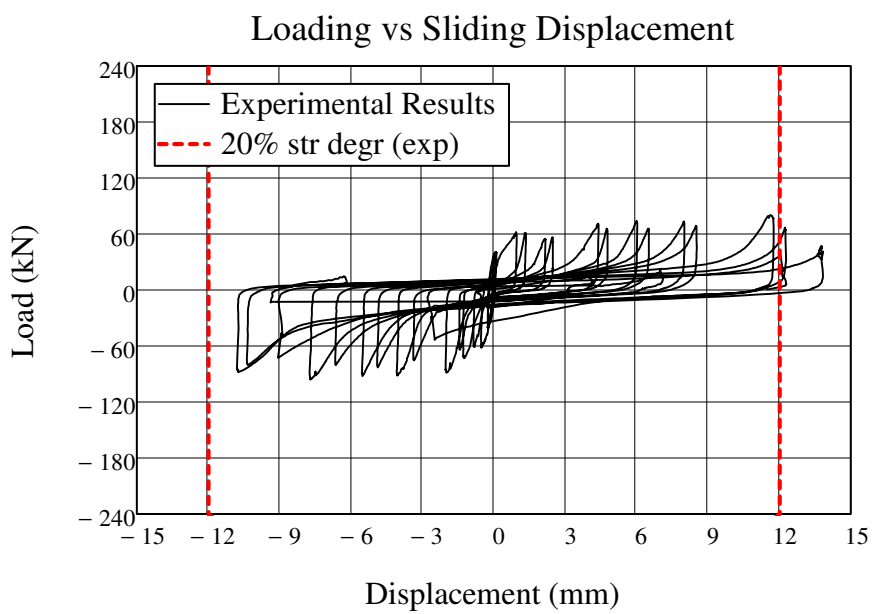
Loading vs Sliding Displacement
Load (kN)
Displacement (mm)
Experimental Results
20% str degr (exp)

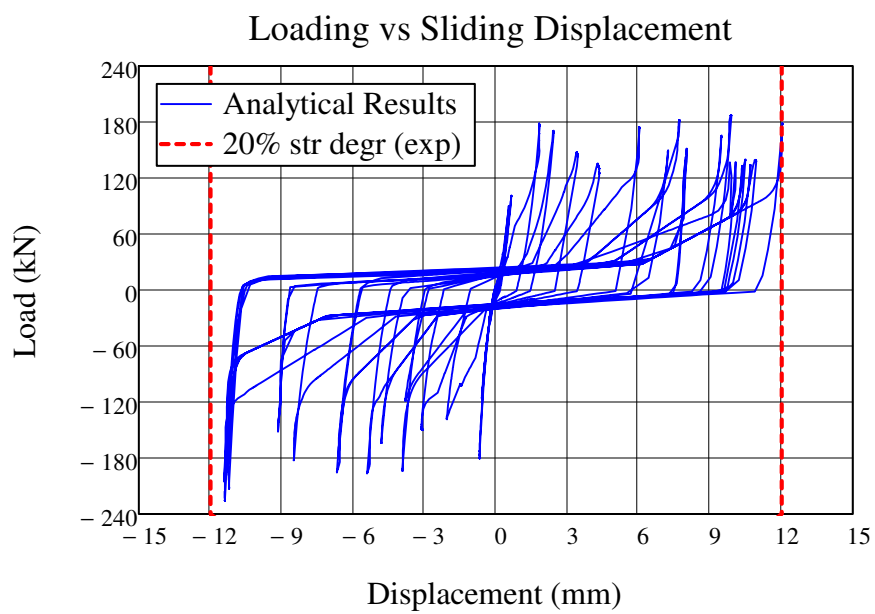
Loading vs Sliding Displacement
Load (kN)
Displacement (mm)
Analytical Results
20% str degr (exp)

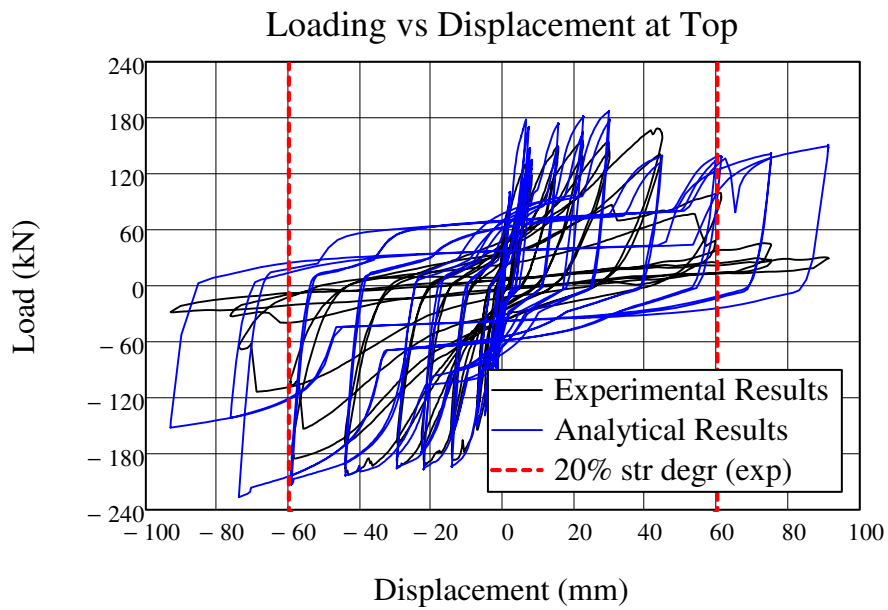
Loading vs Displacement at Top
Load (kN)
240
180
120
60
0
– 60
– 120
– 180
– 240
– 100
– 80
– 60
– 40
– 20
0
20
40
60
80
100
Displacement (mm)
Experimental Results
Analytical Results
20% str degr (exp)

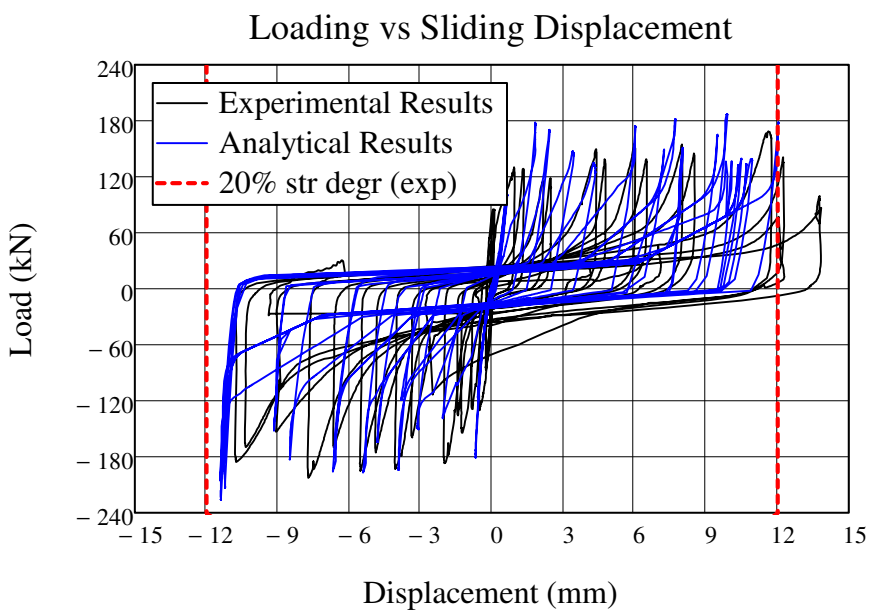
Loading vs Sliding Displacement
Load (kN)
240
180
120
60
0
– 60
– 120
– 180
– 240
– 15
– 12
– 9
– 6
– 3
0
3
6
9
12
15
Displacement (mm)
Experimental Results
Analytical Results
20% str degr (exp)

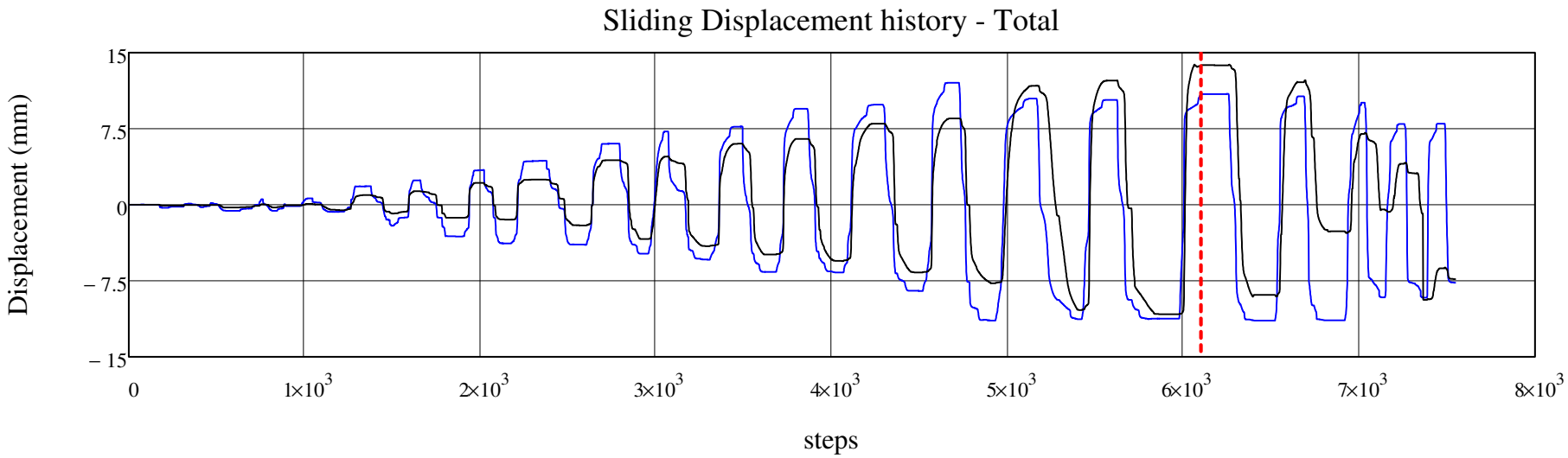

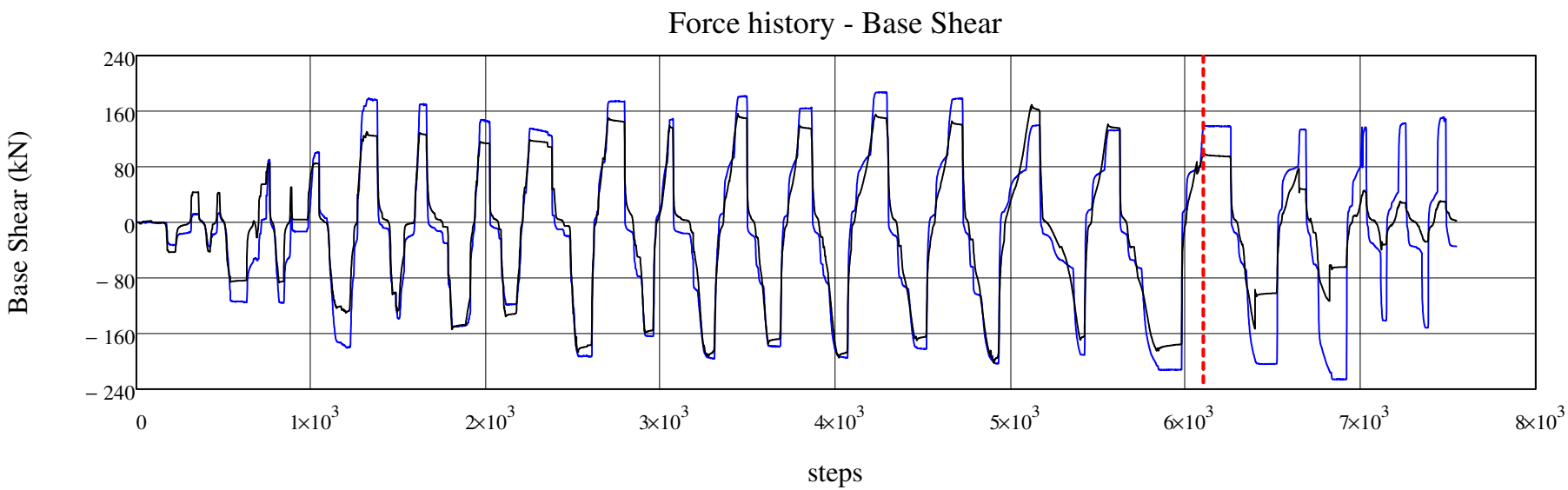

Analytical Results
Experimental Results
End of Calibration - 20% Strength Degradation

Modeling Predictions prior to Strength Degradation*
Maximum Sliding Disp. = 87% of Experimental Result
Maximum Resistance =110% of Experimental Result

**Strength Degradation @ step 6100*

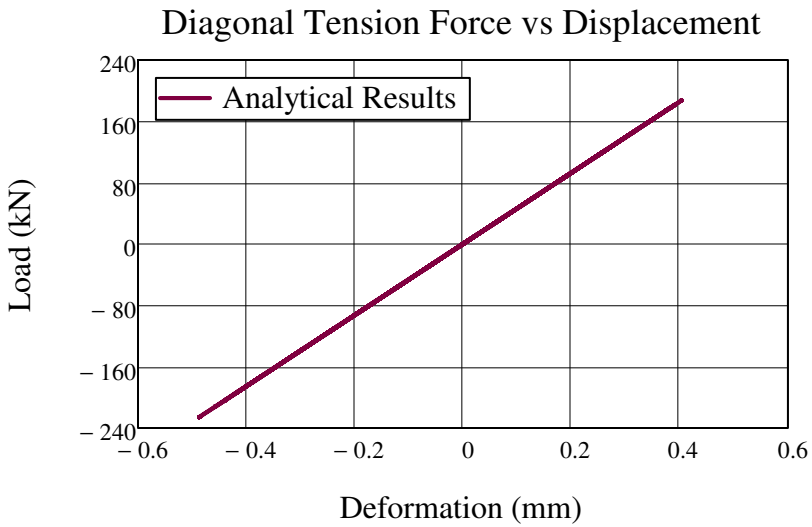
Diagonal Tension Force vs Displacement
Analytical Results
Load (kN)
240
160
80
0
− 80
− 160
− 240
− 0.6
− 0.4
− 0.2
0
0.2
0.4
0.6
Deformation (mm)

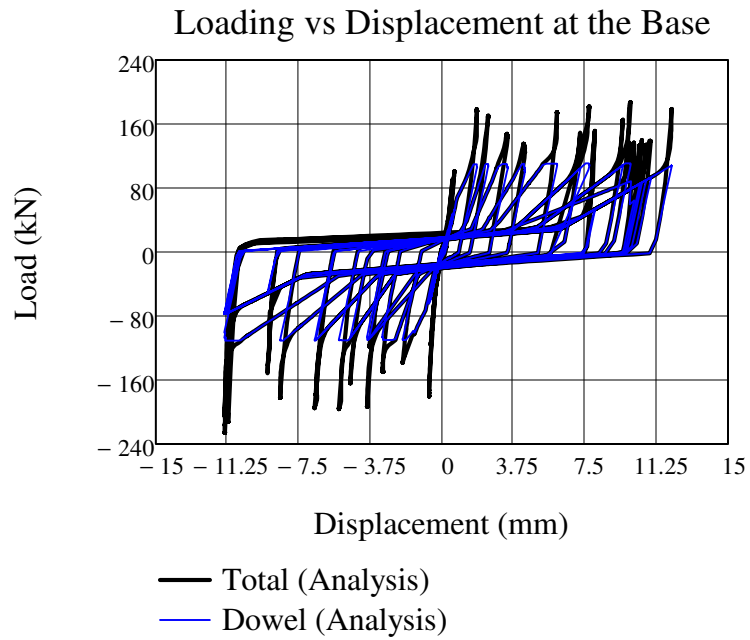
Loading vs Displacement at the Base
Load (kN)
240
160
80
0
− 80
− 160
− 240
− 15
− 11.25
− 7.5
− 3.75
0
3.75
7.5
11.25
15
Displacement (mm)
Total (Analysis)
Dowel (Analysis)

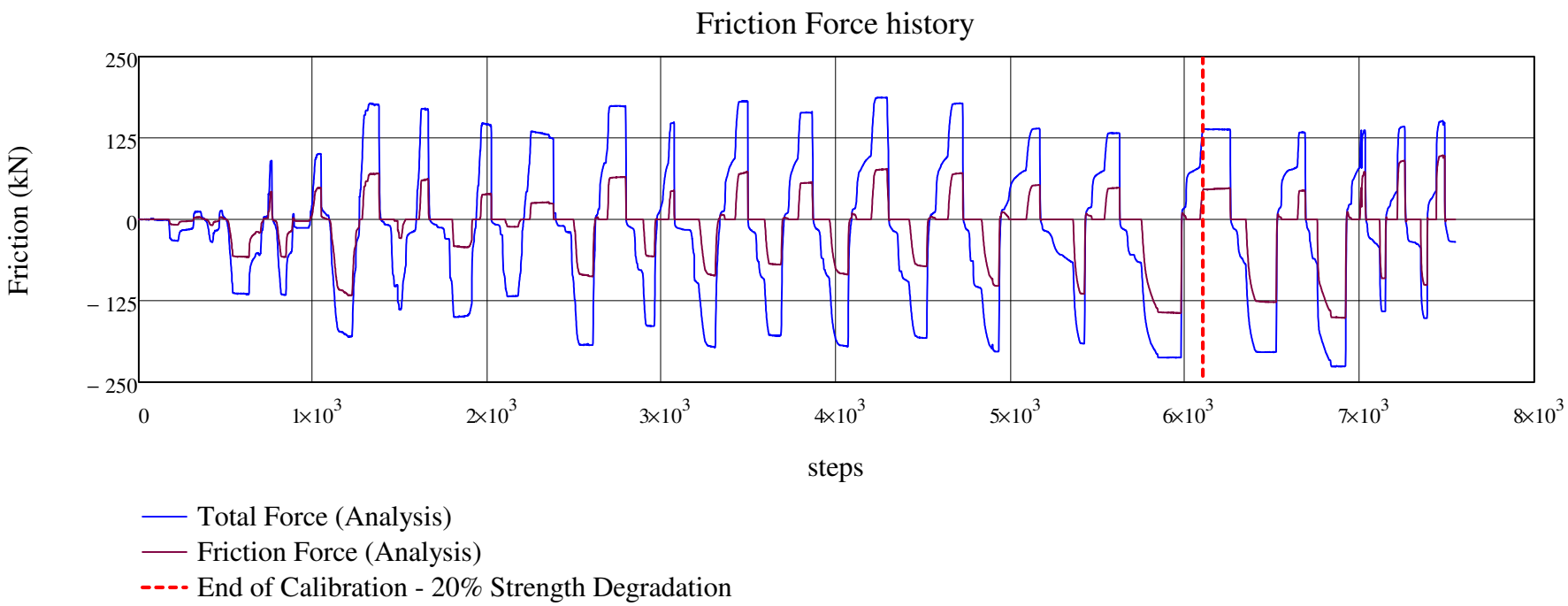
Friction Force history
Friction (kN)
250
125
0
− 125
− 250
0
1×10^3
2×10^3
3×10^3
4×10^3
5×10^3
6×10^3
7×10^3
8×10^3
steps
Total Force (Analysis)
Friction Force (Analysis)
End of Calibration - 20% Strength Degradation

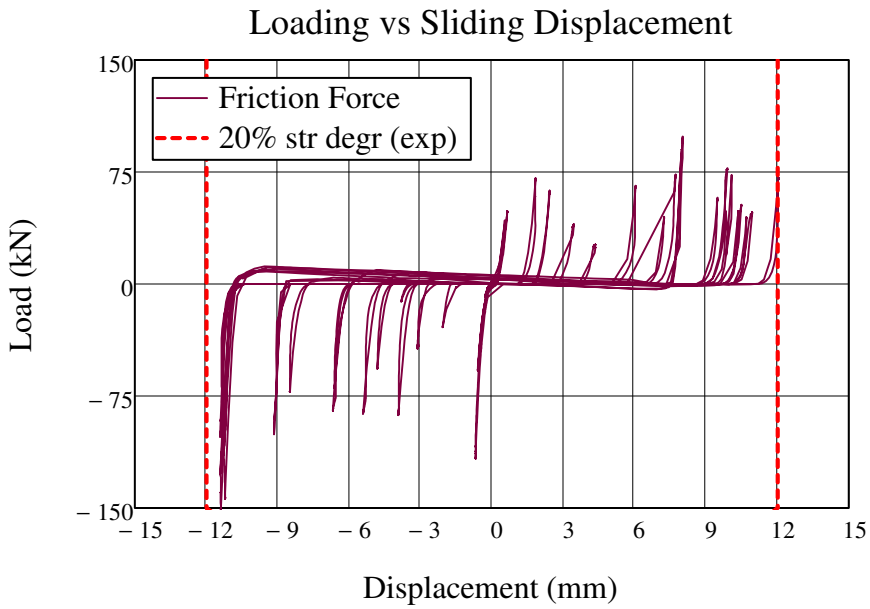
Loading vs Sliding Displacement
Friction Force
20% str degr (exp)
Load (kN)
150
75
0
− 75
− 150
− 15
− 12
− 9
− 6
− 3
0
3
6
9
12
15
Displacement (mm)

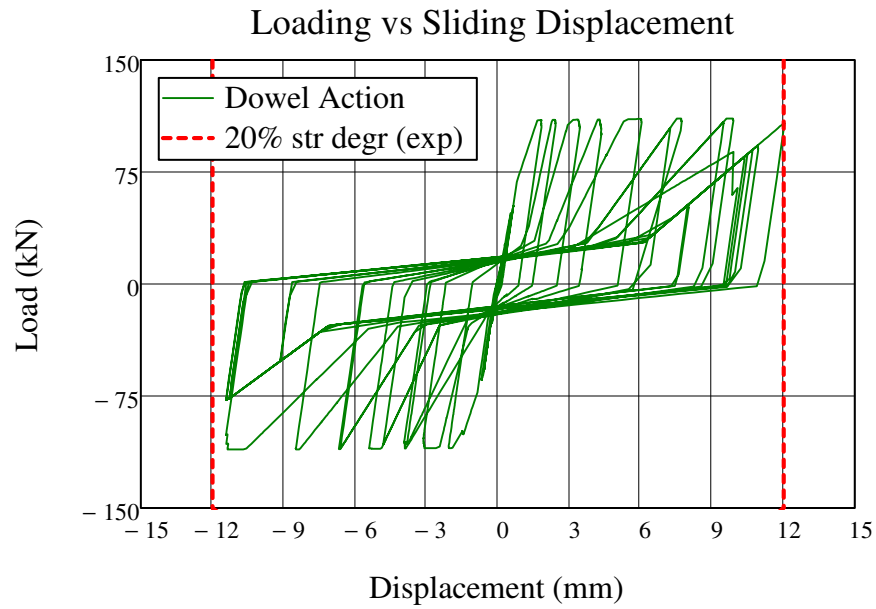
Loading vs Sliding Displacement
Dowel Action
20% str degr (exp)
Load (kN)
150
75
0
− 75
− 150
− 15
− 12
− 9
− 6
− 3
0
3
6
9
12
15
Displacement (mm)

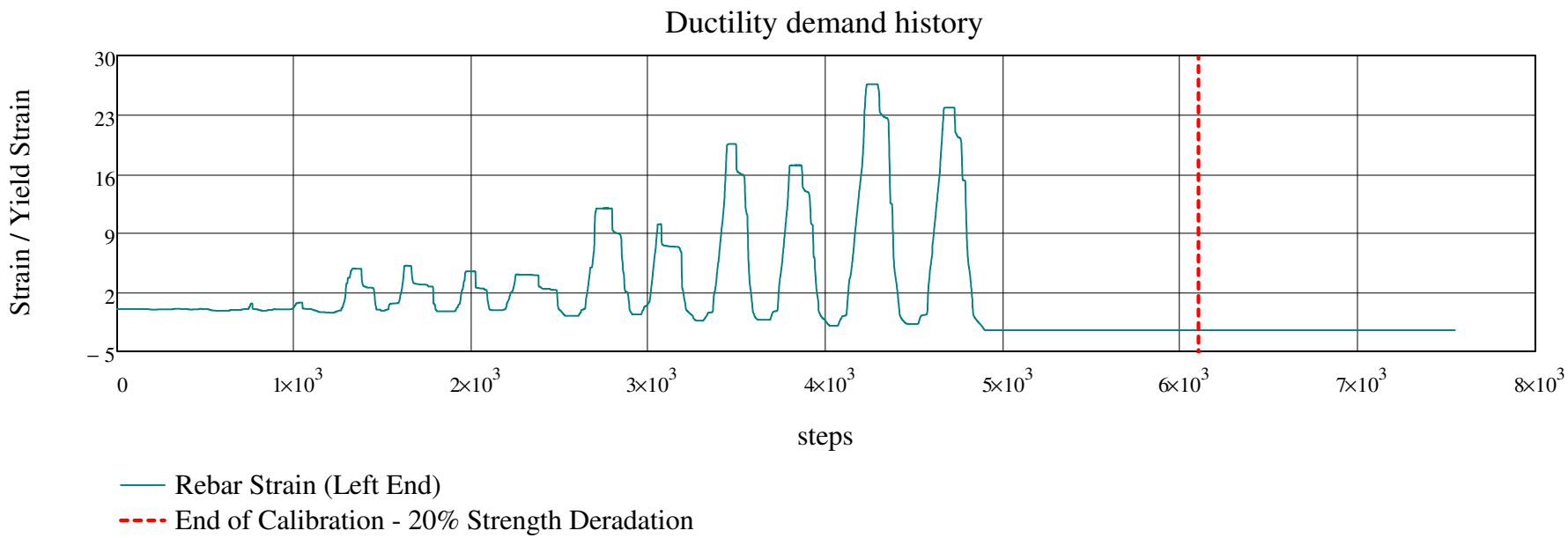
Ductility demand history
Strain / Yield Strain
30
23
16
9
2
− 5
0
1×10^3
2×10^3
3×10^3
4×10^3
5×10^3
6×10^3
7×10^3
8×10^3
steps
Rebar Strain (Left End)
End of Calibration - 20% Strength Deradation

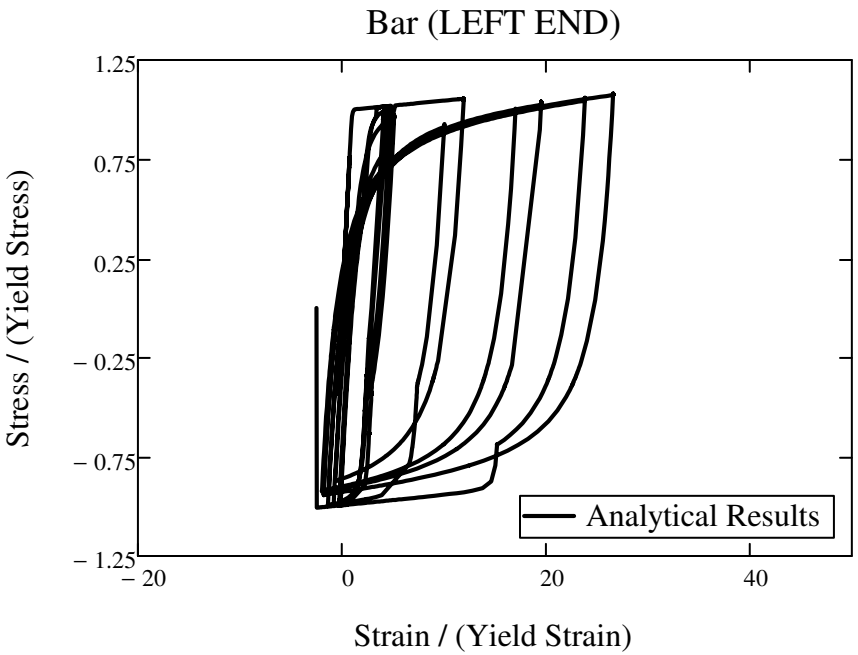
Bar (LEFT END)
Stress / (Yield Stress)
Strain / (Yield Strain)
Analytical Results
1.25
0.75
0.25
− 0.25
− 0.75
− 1.25
− 20
0
20
40

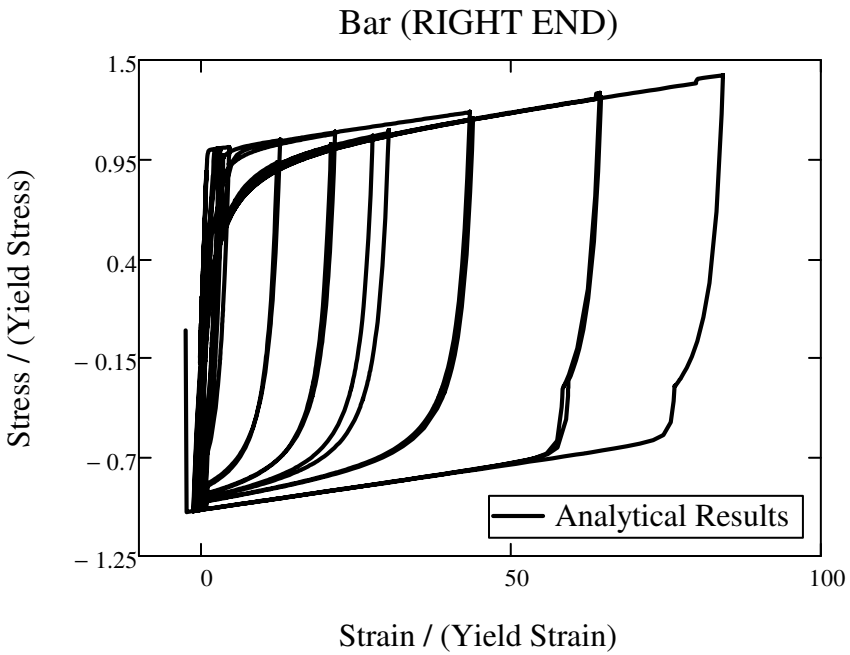
Bar (RIGHT END)
Stress / (Yield Stress)
Strain / (Yield Strain)
Analytical Results
1.5
0.95
0.4
− 0.15
− 0.7
− 1.25
0
50
100

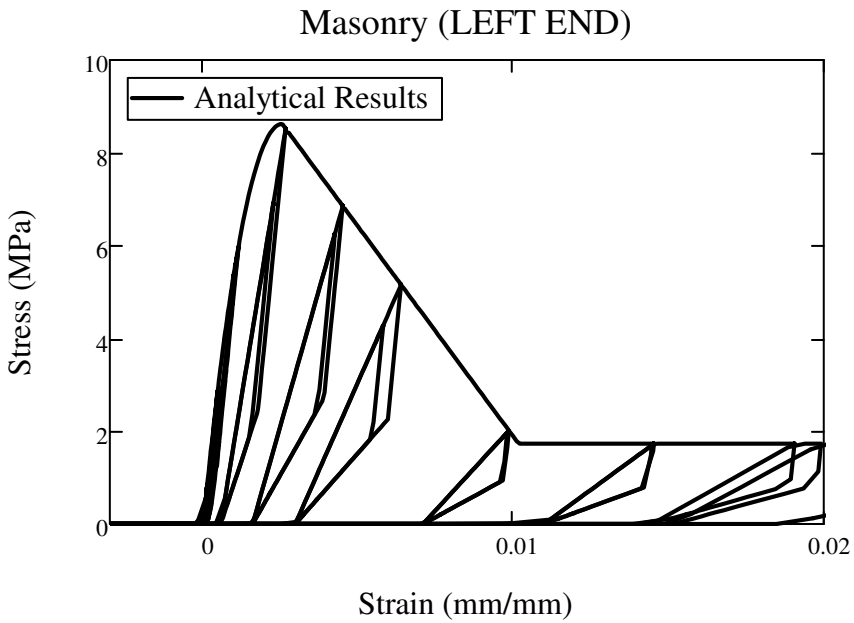
Masonry (LEFT END)
Stress (MPa)
Strain (mm/mm)
Analytical Results
10
8
6
4
2
0
0
0.01
0.02

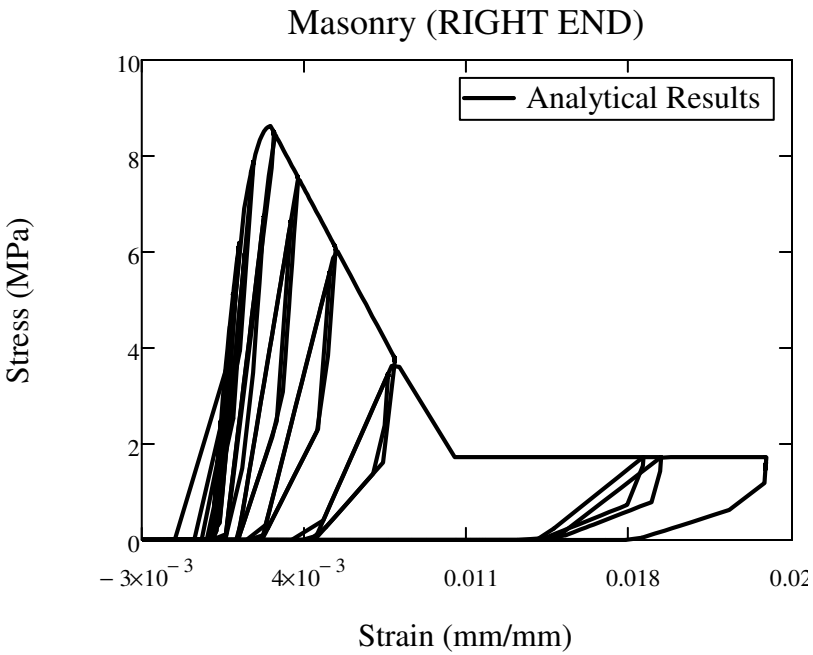
Masonry (RIGHT END)
Stress (MPa)
Strain (mm/mm)
Analytical Results
10
8
6
4
2
0
− 3×10^−3
4×10^−3
0.011
0.018
0.02

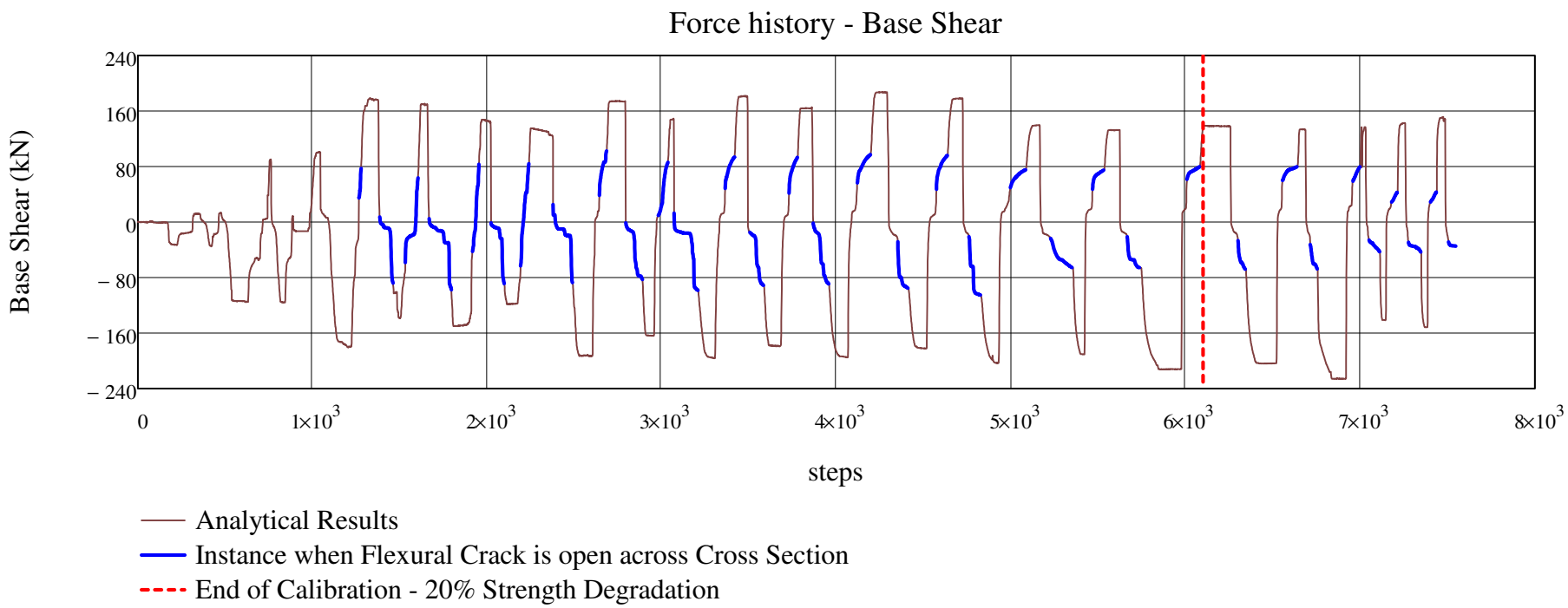
Force history - Base Shear
Base Shear (kN)
240
160
80
0
− 80
− 160
− 240
0
1×10^3
2×10^3
3×10^3
4×10^3
5×10^3
6×10^3
7×10^3
8×10^3
steps
Analytical Results
Instance when Flexural Crack is open across Cross Section
End of Calibration - 20% Strength Degradation

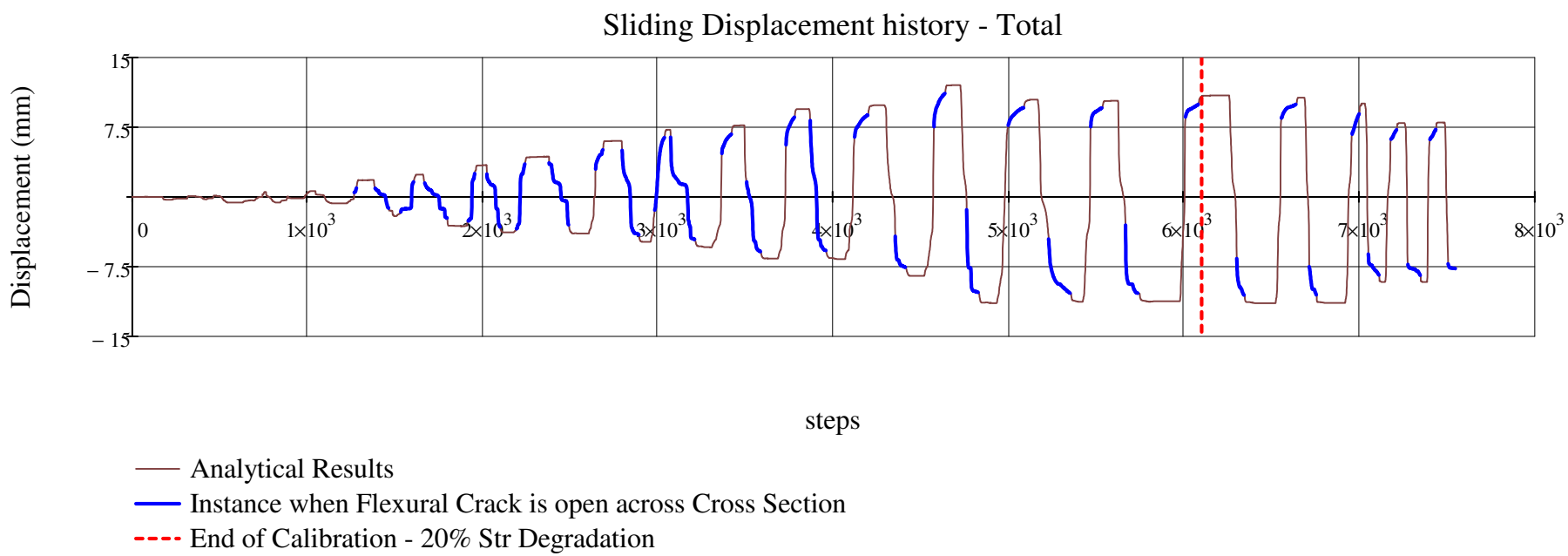
Sliding Displacement history - Total
Displacement (mm)
15
7.5
− 7.5
− 15
0
1×10^3
2×10^3
3×10^3
4×10^3
5×10^3
6×10^3
7×10^3
8×10^3
steps
Analytical Results
Instance when Flexural Crack is open across Cross Section
End of Calibration - 20% Str Degradation

Calibration of Test Specimen PBS-12

LWall := 2.4 m	fm := 8.5 MPa	Lambda = 1.00	Frict_Coeff = 0.55	DowelCoeff = 1.18	P / (f'm Ag) = 10%
HWall := 2.4 m	fsy := 440 MPa	h := 0.20·HWall	Frict_Yield = 1mm	Dowel_Yield = 1mm	P = 814 kN
$\rho_v := 0.18\%$					

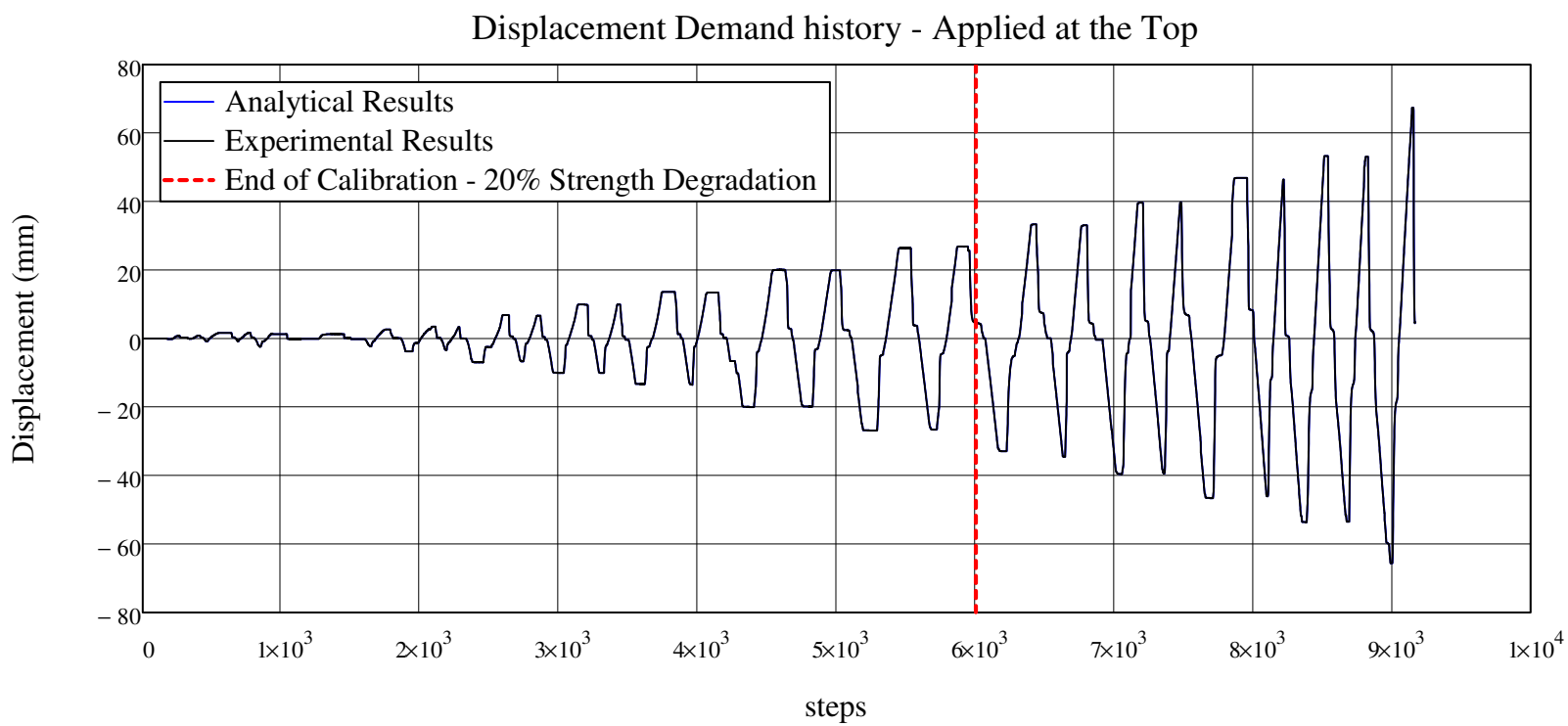

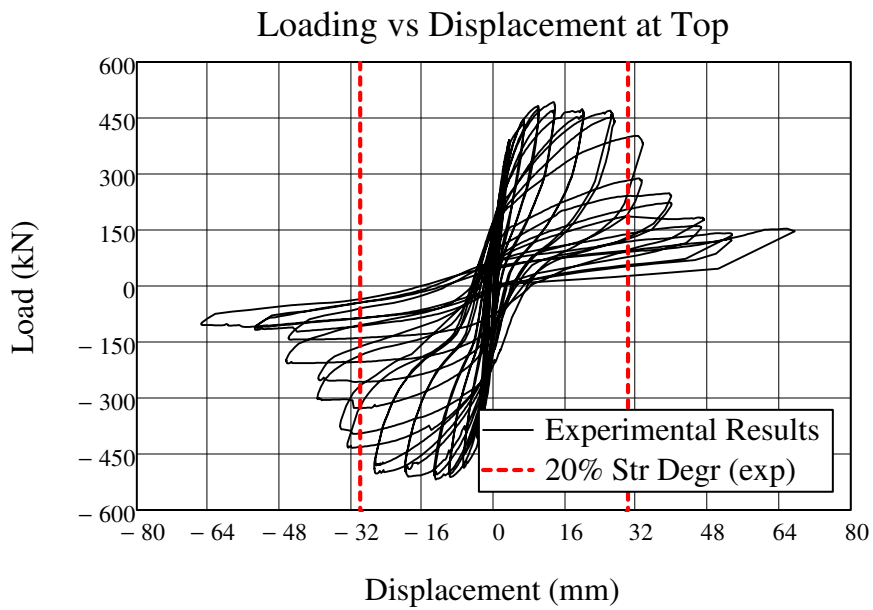
Loading vs Displacement at Top
Load (kN)
600
450
300
150
0
– 150
– 300
– 450
– 600
– 80
– 64
– 48
– 32
– 16
0
16
32
48
64
80
Displacement (mm)
Experimental Results
20% Str Degr (exp)

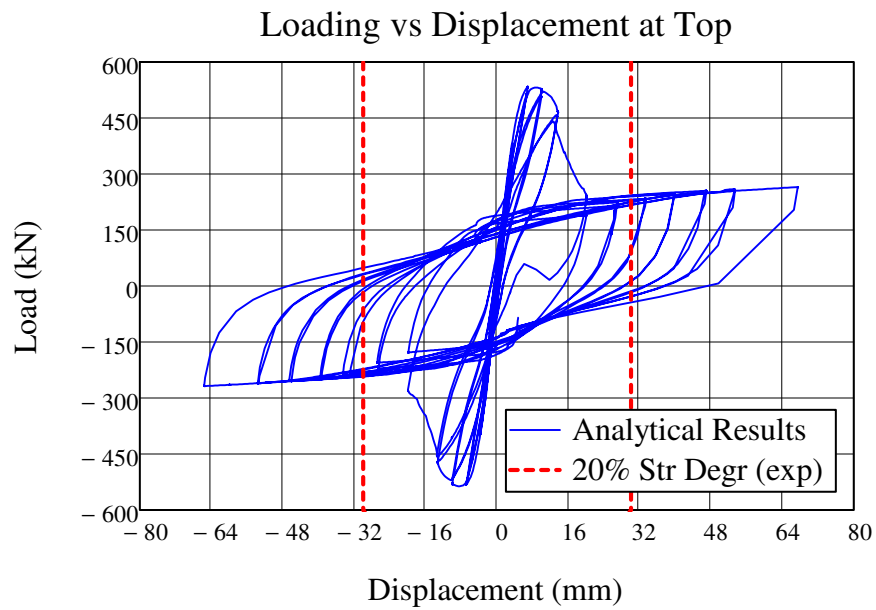
Loading vs Displacement at Top
Load (kN)
600
450
300
150
0
– 150
– 300
– 450
– 600
– 80
– 64
– 48
– 32
– 16
0
16
32
48
64
80
Displacement (mm)
Analytical Results
20% Str Degr (exp)

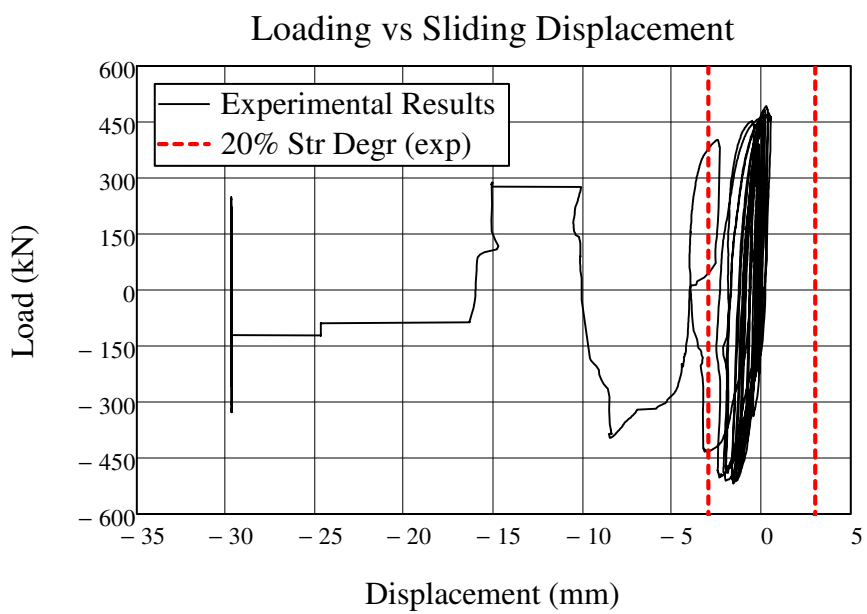
Loading vs Sliding Displacement
Load (kN)
600
450
300
150
0
– 150
– 300
– 450
– 600
– 35
– 30
– 25
– 20
– 15
– 10
– 5
0
5
Displacement (mm)
Experimental Results
20% Str Degr (exp)

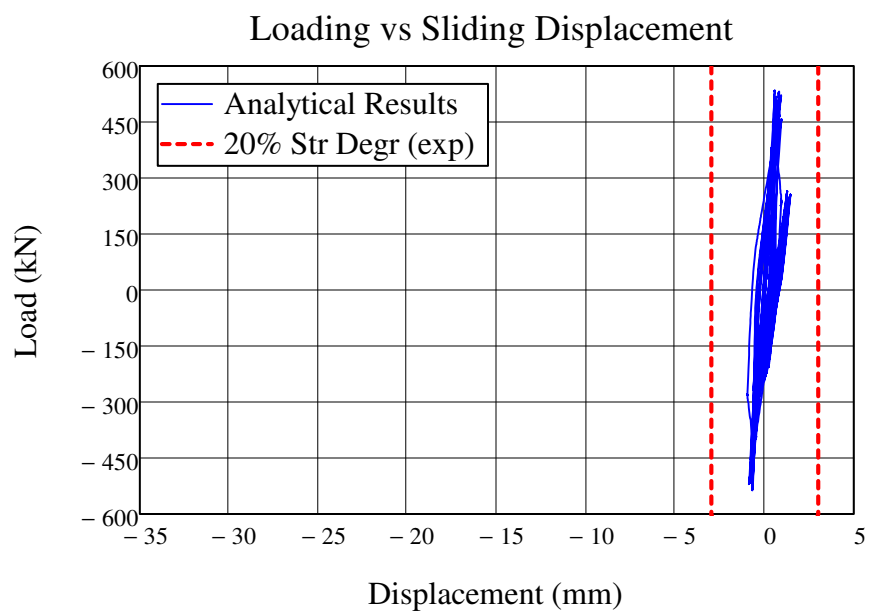
Loading vs Sliding Displacement
Load (kN)
600
450
300
150
0
– 150
– 300
– 450
– 600
– 35
– 30
– 25
– 20
– 15
– 10
– 5
0
5
Displacement (mm)
Analytical Results
20% Str Degr (exp)

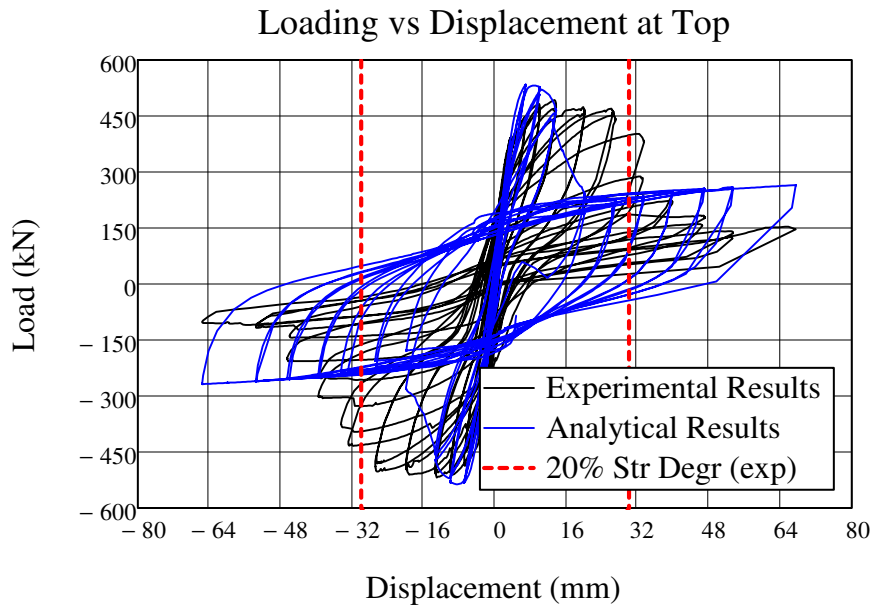
Loading vs Displacement at Top
Load (kN)
600
450
300
150
0
– 150
– 300
– 450
– 600
– 80
– 64
– 48
– 32
– 16
0
16
32
48
64
80
Displacement (mm)
Experimental Results
Analytical Results
20% Str Degr (exp)

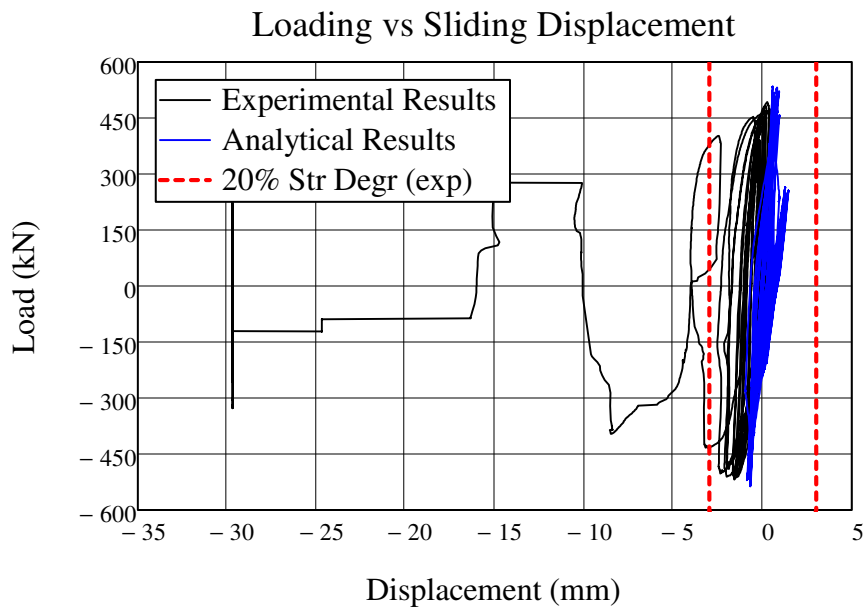
Loading vs Sliding Displacement
Load (kN)
600
450
300
150
0
– 150
– 300
– 450
– 600
– 35
– 30
– 25
– 20
– 15
– 10
– 5
0
5
Displacement (mm)
Experimental Results
Analytical Results
20% Str Degr (exp)

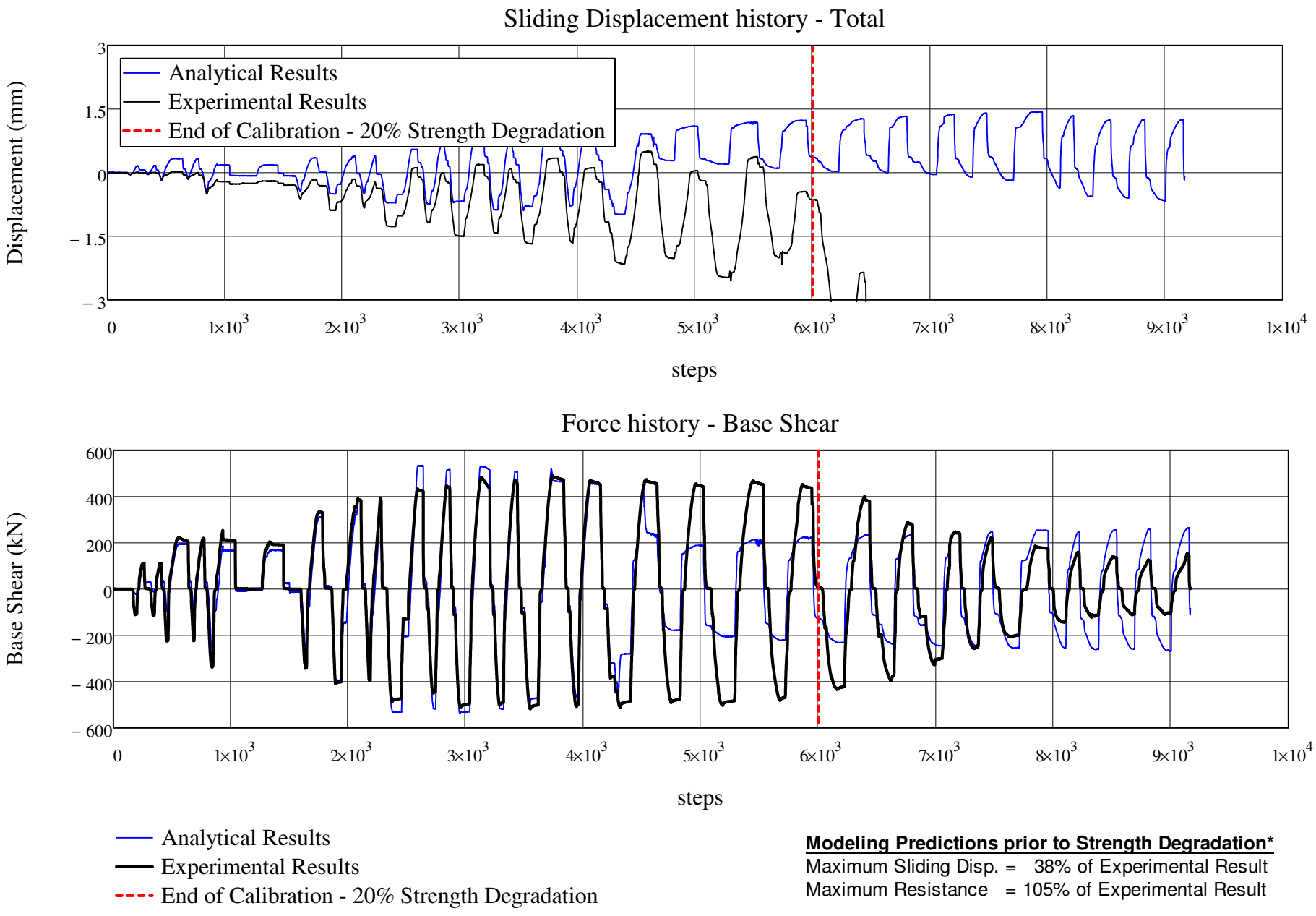

Modeling Predictions prior to Strength Degradation*

Maximum Sliding Disp. = 38% of Experimental Result

Maximum Resistance = 105% of Experimental Result

**Strength Degradation @ step 6000*

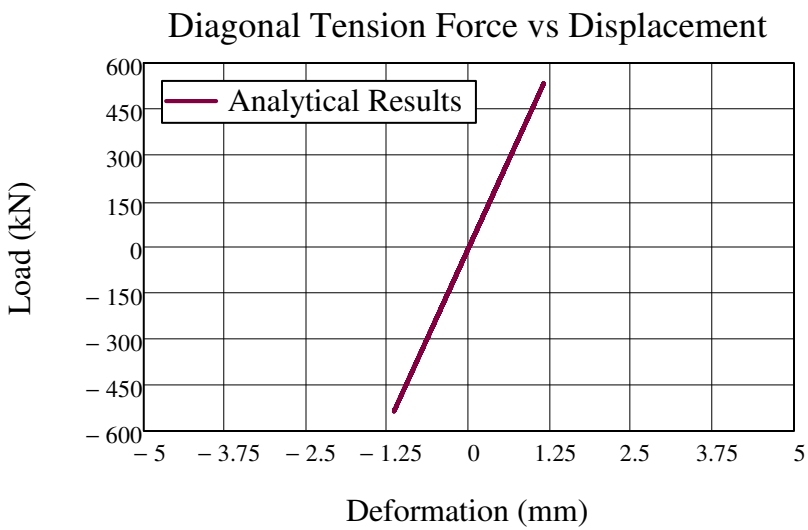
Diagonal Tension Force vs Displacement
Analytical Results
Load (kN)
600
450
300
150
0
– 150
– 300
– 450
– 600
– 5
– 3.75
– 2.5
– 1.25
0
1.25
2.5
3.75
5
Deformation (mm)

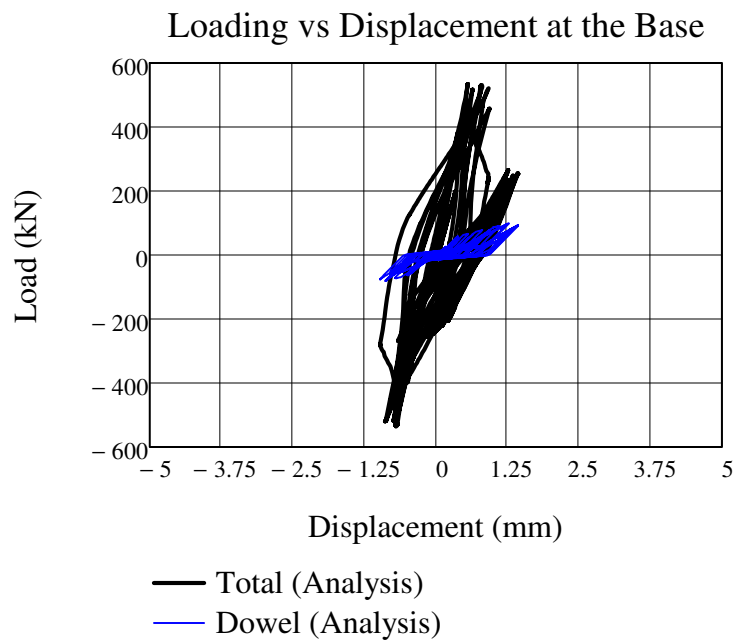
Loading vs Displacement at the Base
Load (kN)
600
400
200
0
– 200
– 400
– 600
– 5
– 3.75
– 2.5
– 1.25
0
1.25
2.5
3.75
5
Displacement (mm)
Total (Analysis)
Dowel (Analysis)

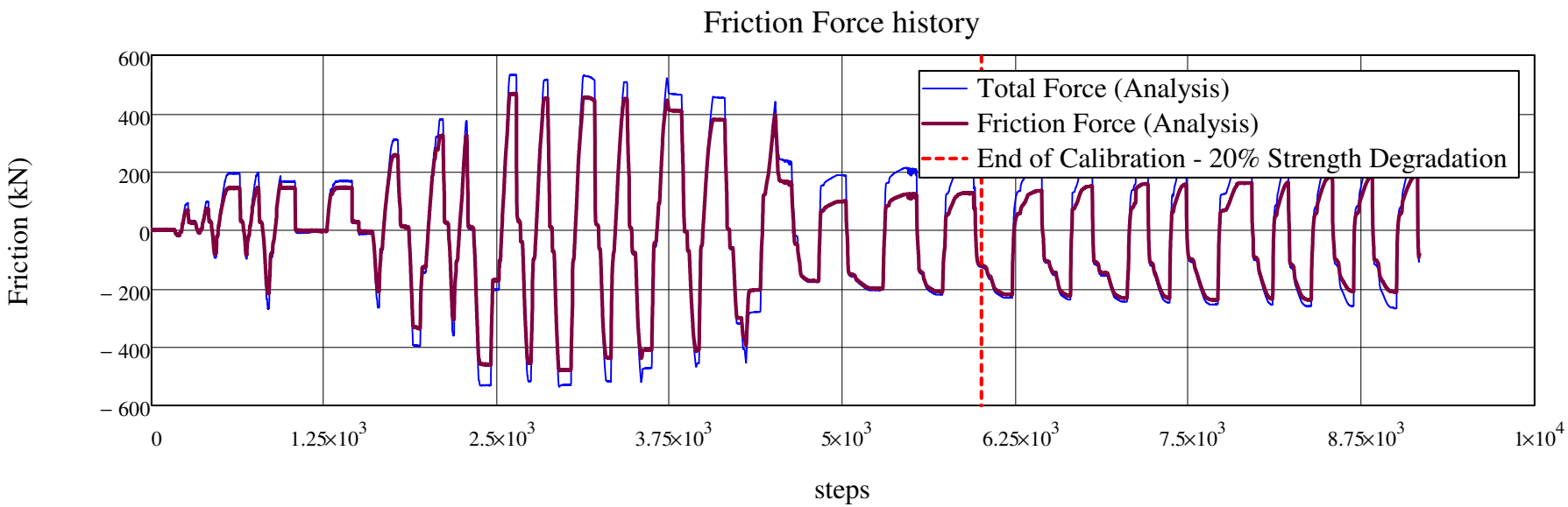
Friction Force history
Total Force (Analysis)
Friction Force (Analysis)
End of Calibration - 20% Strength Degradation
Friction (kN)
600
400
200
0
– 200
– 400
– 600
0
1.25×10^3
2.5×10^3
3.75×10^3
5×10^3
6.25×10^3
7.5×10^3
8.75×10^3
1×10^4
steps

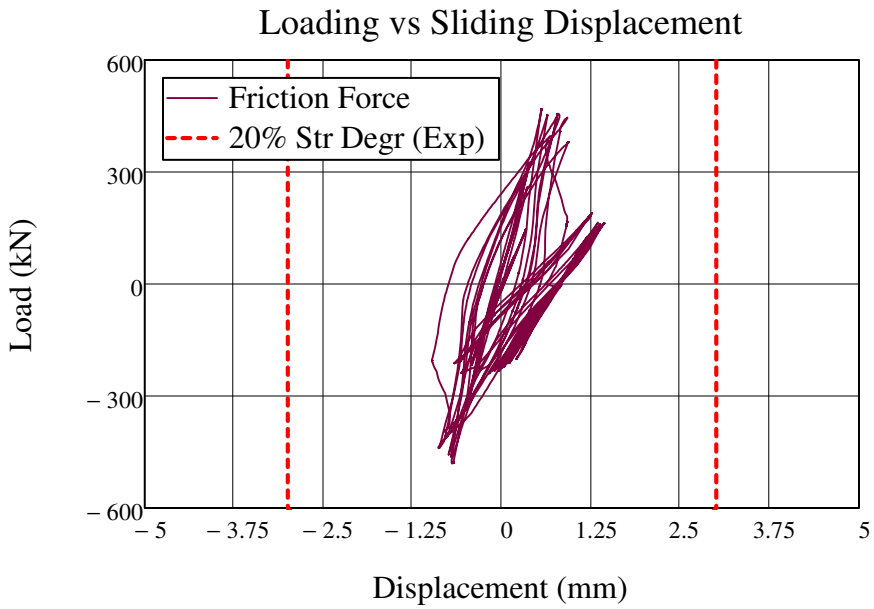
Loading vs Sliding Displacement
Friction Force
20% Str Degr (Exp)
Load (kN)
600
300
0
− 300
− 600
− 5
− 3.75
− 2.5
− 1.25
0
1.25
2.5
3.75
5
Displacement (mm)

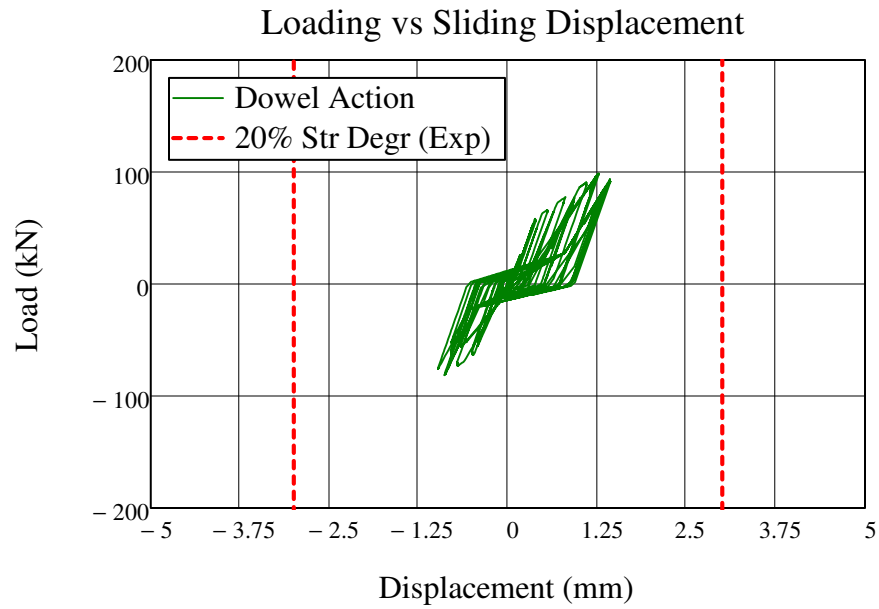
Loading vs Sliding Displacement
Dowel Action
20% Str Degr (Exp)
Load (kN)
200
100
0
− 100
− 200
− 5
− 3.75
− 2.5
− 1.25
0
1.25
2.5
3.75
5
Displacement (mm)

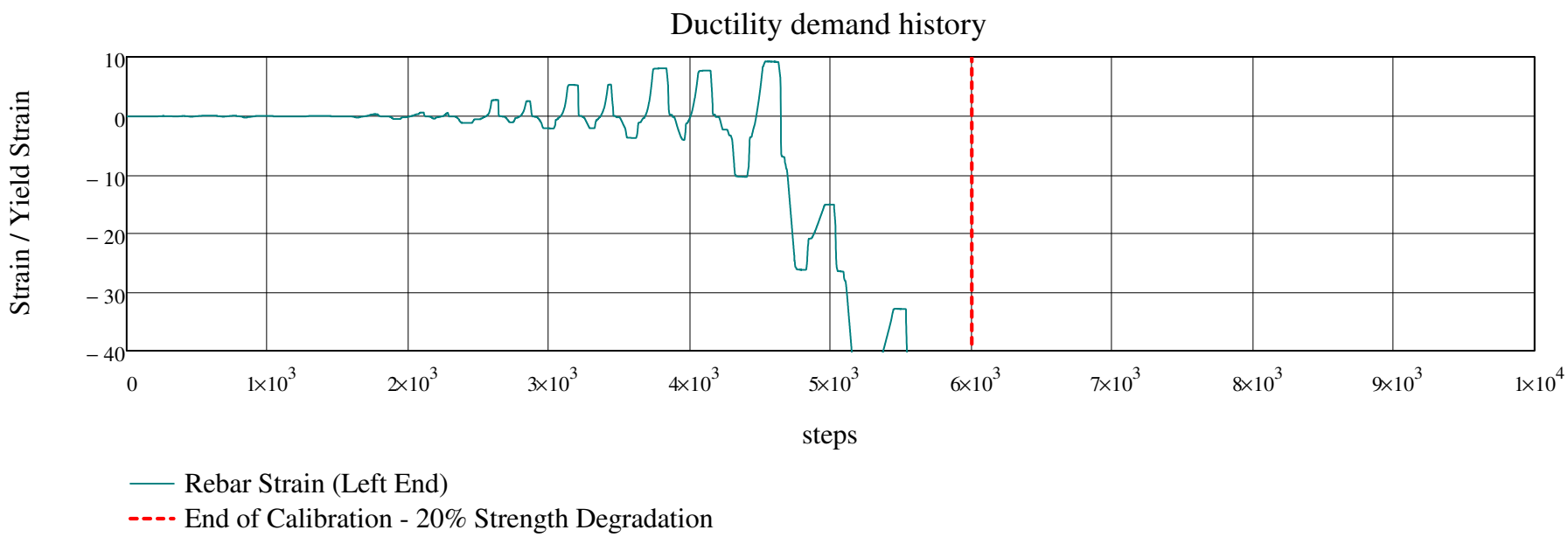
Ductility demand history
Strain / Yield Strain
10
0
− 10
− 20
− 30
− 40
0
1×10^3
2×10^3
3×10^3
4×10^3
5×10^3
6×10^3
7×10^3
8×10^3
9×10^3
1×10^4
steps
Rebar Strain (Left End)
End of Calibration - 20% Strength Degradation

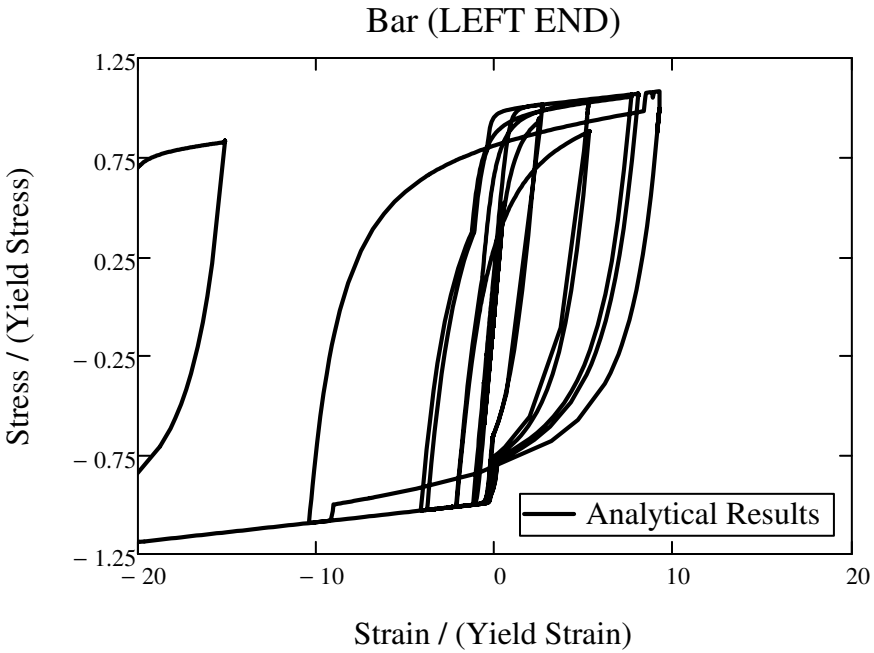
Bar (LEFT END)
Stress / (Yield Stress)
Strain / (Yield Strain)
Analytical Results
1.25
0.75
0.25
– 0.25
– 0.75
– 1.25
– 20
– 10
0
10
20

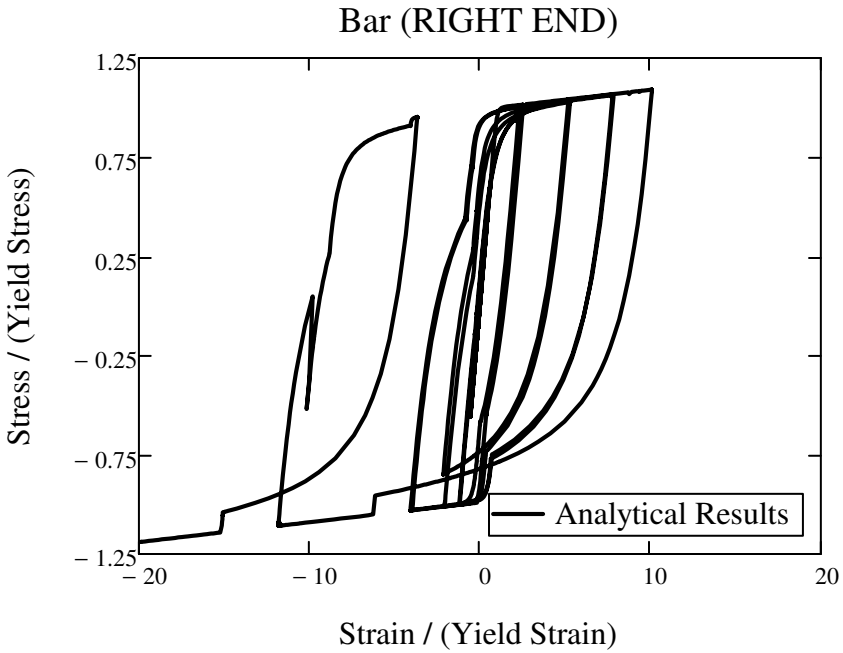
Bar (RIGHT END)
Stress / (Yield Stress)
Strain / (Yield Strain)
Analytical Results
1.25
0.75
0.25
– 0.25
– 0.75
– 1.25
– 20
– 10
0
10
20

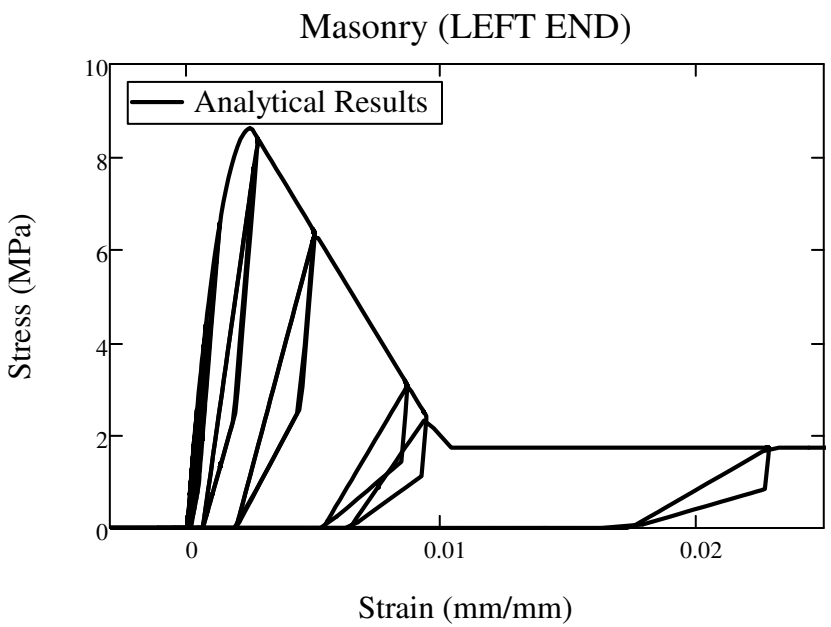
Masonry (LEFT END)
Stress (MPa)
Strain (mm/mm)
Analytical Results
10
8
6
4
2
0
0
0.01
0.02

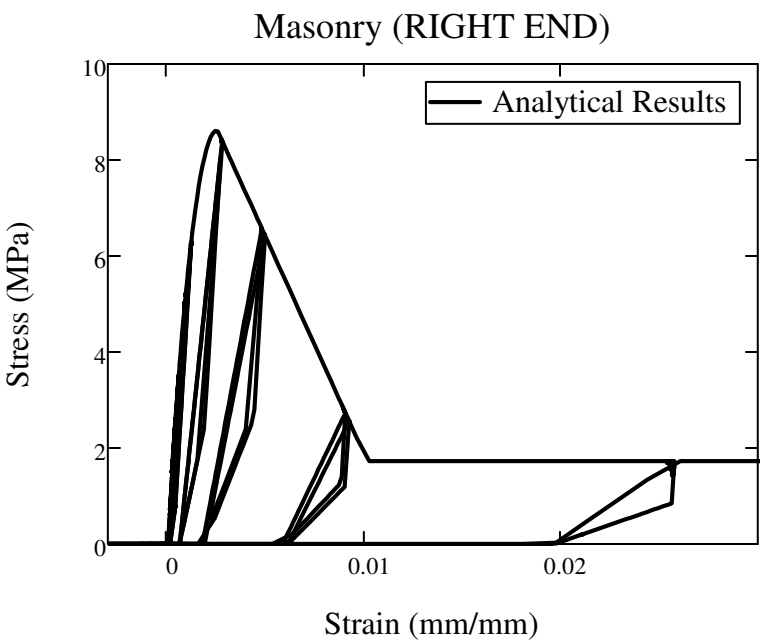
Masonry (RIGHT END)
Stress (MPa)
Strain (mm/mm)
Analytical Results
10
8
6
4
2
0
0
0.01
0.02

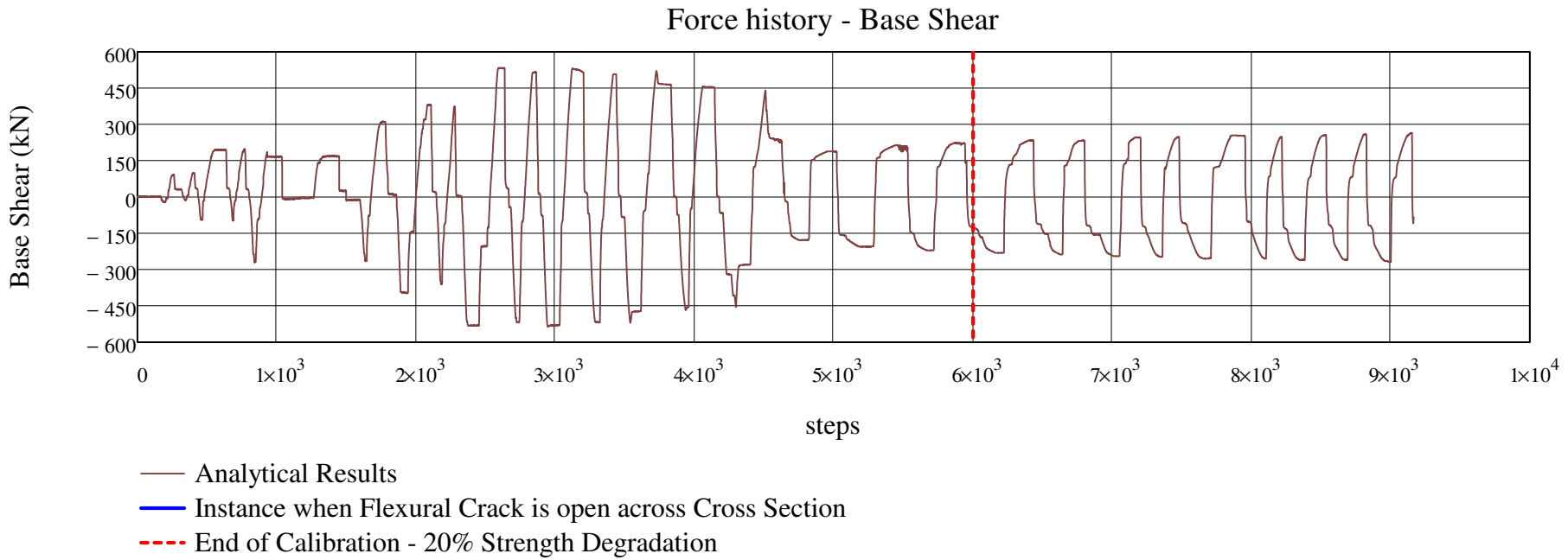
Force history - Base Shear
Base Shear (kN)
600
450
300
150
0
− 150
− 300
− 450
− 600
0
1×10^3
2×10^3
3×10^3
4×10^3
5×10^3
6×10^3
7×10^3
8×10^3
9×10^3
1×10^4
steps
Analytical Results
Instance when Flexural Crack is open across Cross Section
End of Calibration - 20% Strength Degradation

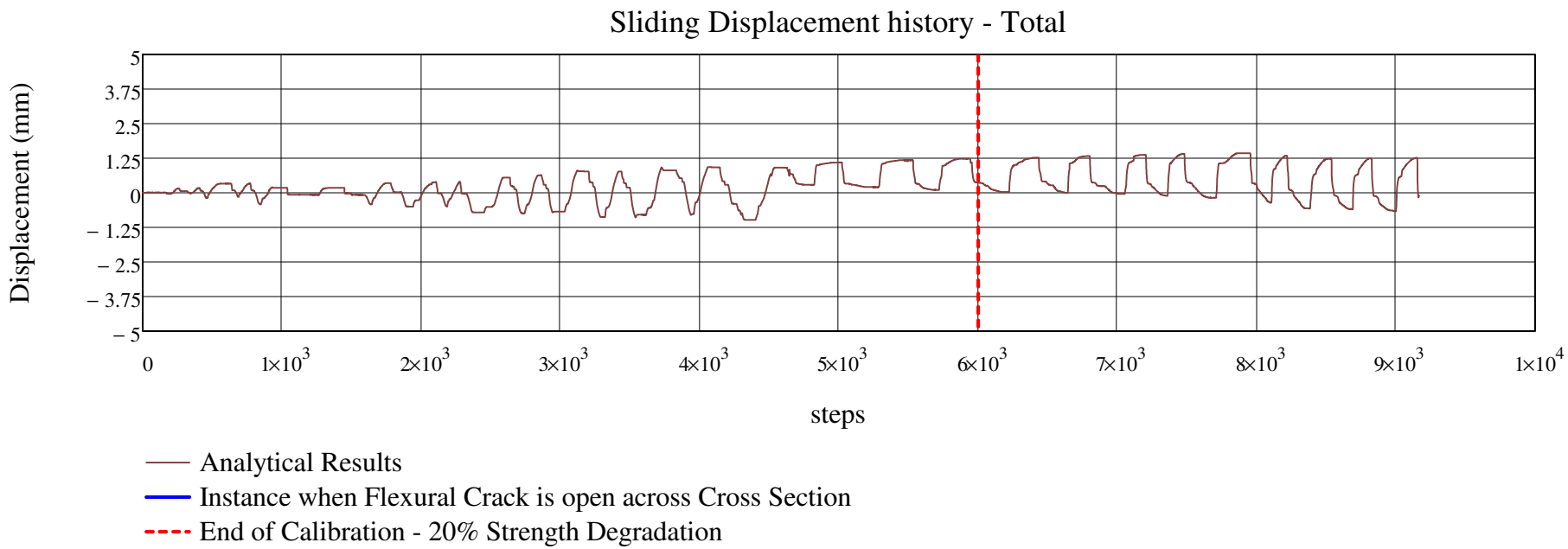
Sliding Displacement history - Total
Displacement (mm)
5
3.75
2.5
1.25
0
− 1.25
− 2.5
− 3.75
− 5
0
1×10^3
2×10^3
3×10^3
4×10^3
5×10^3
6×10^3
7×10^3
8×10^3
9×10^3
1×10^4
steps
Analytical Results
Instance when Flexural Crack is open across Cross Section
End of Calibration - 20% Strength Degradation

Calibration of Test Specimen PBS-12G

LWall := 2.4 m	fm := 8.6 MPa	Lambda = 1.00	Frict_Coeff = 0.55	DowelCoeff = 1.27	P / (f'm Ag) = 10%
HWall := 2.4 m	fsy := 460 MPa	h := 0.22·HWall	Frict_Yield = 1 mm	Dowel_Yield = 1.7 mm	P = 814 kN

$\rho_v := 0.18\%$

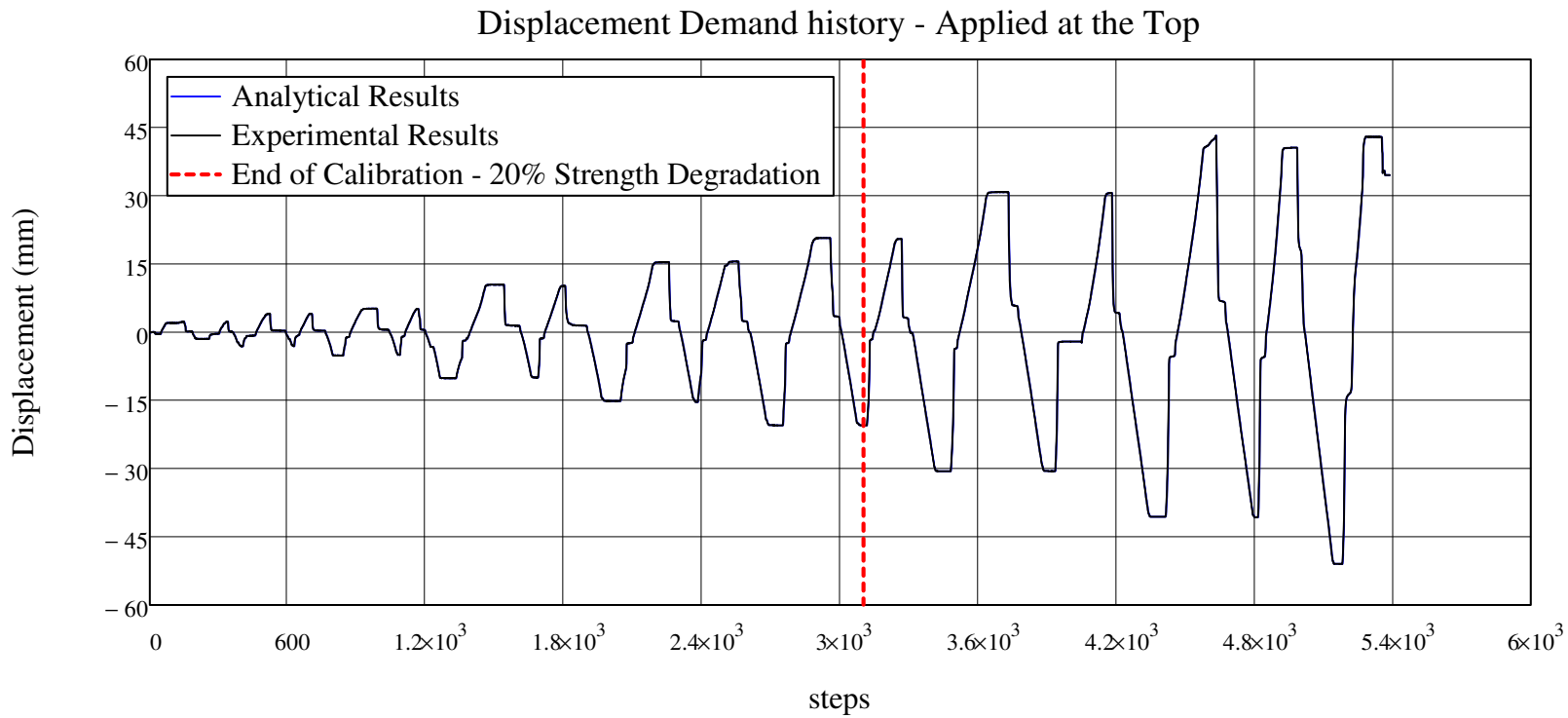

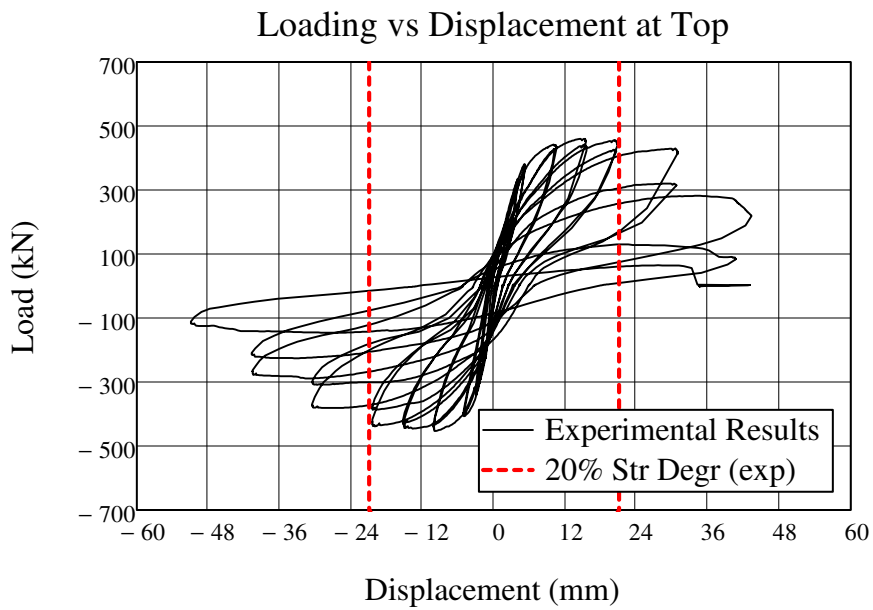
Loading vs Displacement at Top
Load (kN)
700
500
300
100
– 100
– 300
– 500
– 700
– 60
– 48
– 36
– 24
– 12
0
12
24
36
48
60
Displacement (mm)
Experimental Results
20% Str Degr (exp)

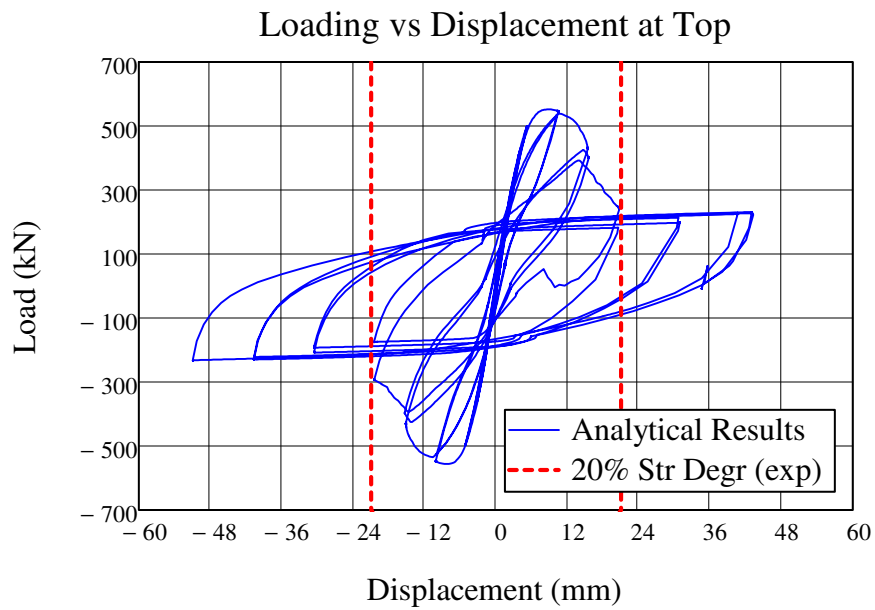
Loading vs Displacement at Top
Load (kN)
700
500
300
100
– 100
– 300
– 500
– 700
– 60
– 48
– 36
– 24
– 12
0
12
24
36
48
60
Displacement (mm)
Analytical Results
20% Str Degr (exp)

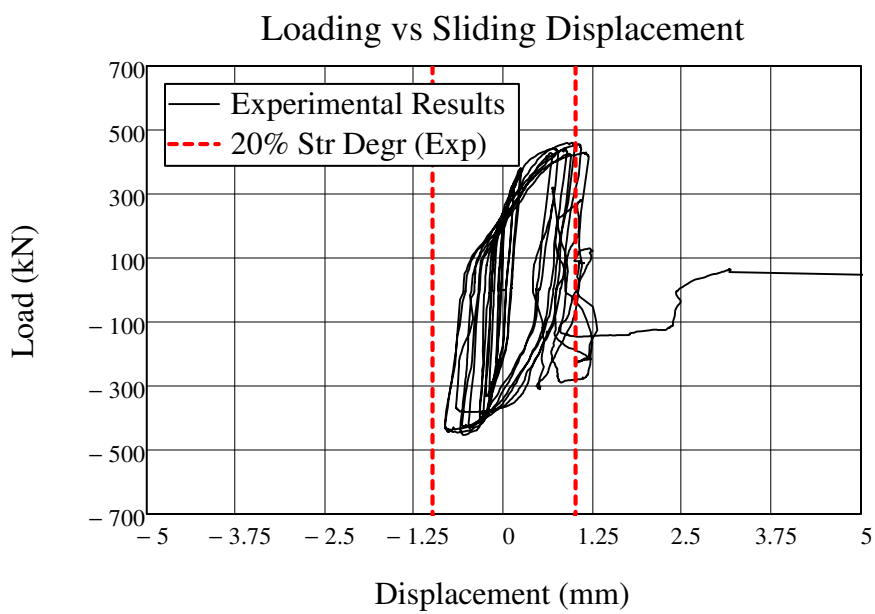
Loading vs Sliding Displacement
Load (kN)
700
500
300
100
– 100
– 300
– 500
– 700
– 5
– 3.75
– 2.5
– 1.25
0
1.25
2.5
3.75
5
Displacement (mm)
Experimental Results
20% Str Degr (Exp)

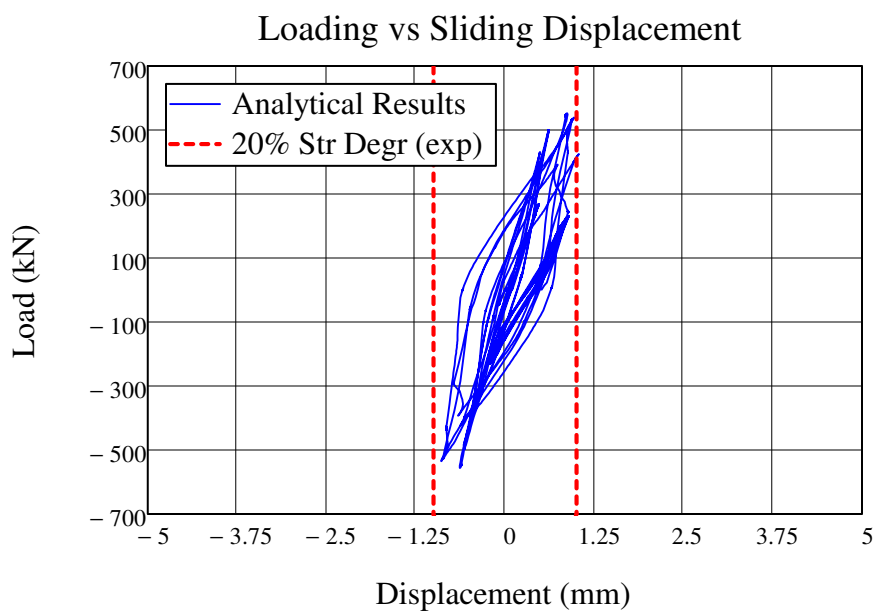
Loading vs Sliding Displacement
Load (kN)
700
500
300
100
– 100
– 300
– 500
– 700
– 5
– 3.75
– 2.5
– 1.25
0
1.25
2.5
3.75
5
Displacement (mm)
Analytical Results
20% Str Degr (exp)

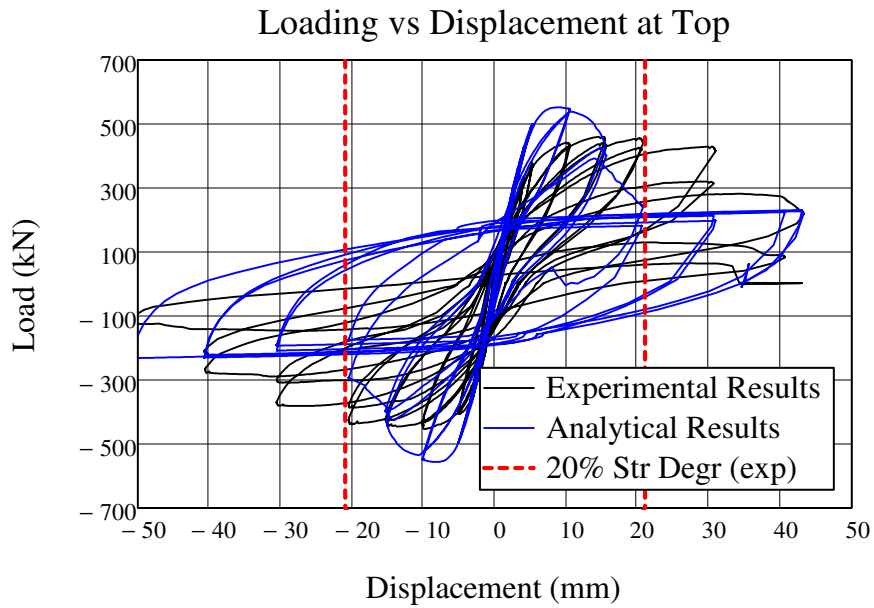
Loading vs Displacement at Top
Load (kN)
700
500
300
100
– 100
– 300
– 500
– 700
– 50
– 40
– 30
– 20
– 10
0
10
20
30
40
50
Displacement (mm)
Experimental Results
Analytical Results
20% Str Degr (exp)

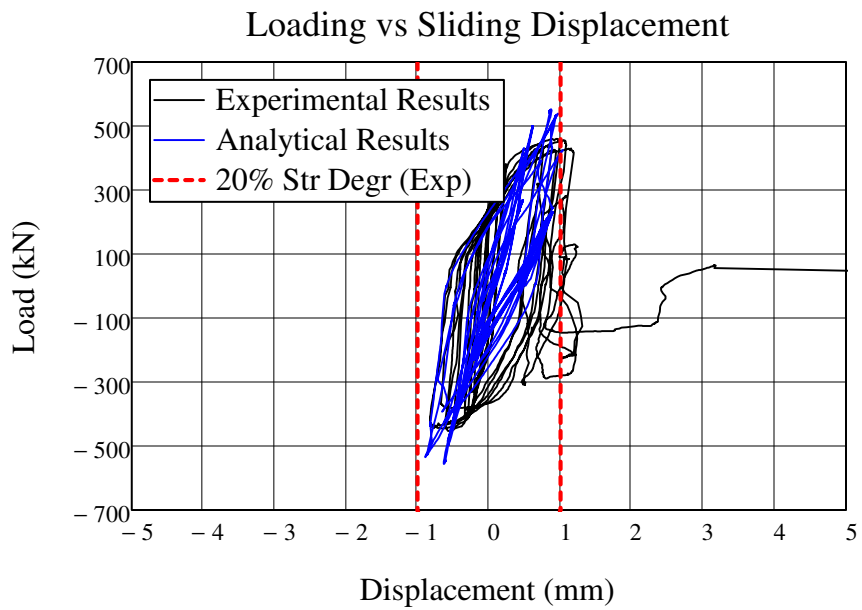
Loading vs Sliding Displacement
Load (kN)
700
500
300
100
– 100
– 300
– 500
– 700
– 5
– 4
– 3
– 2
– 1
0
1
2
3
4
5
Displacement (mm)
Experimental Results
Analytical Results
20% Str Degr (Exp)

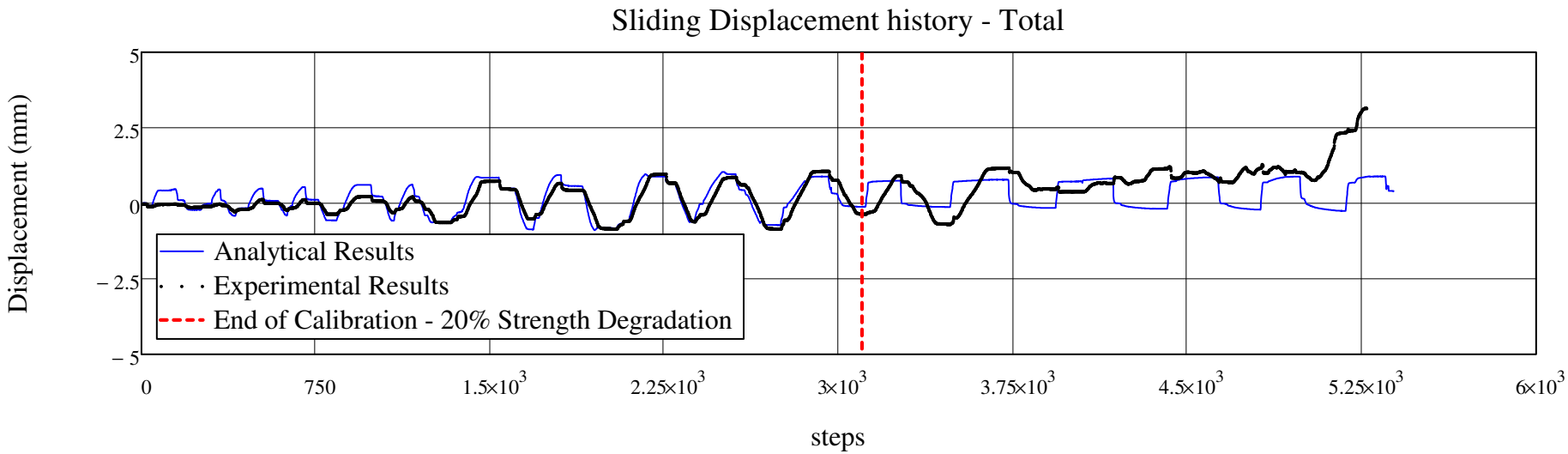

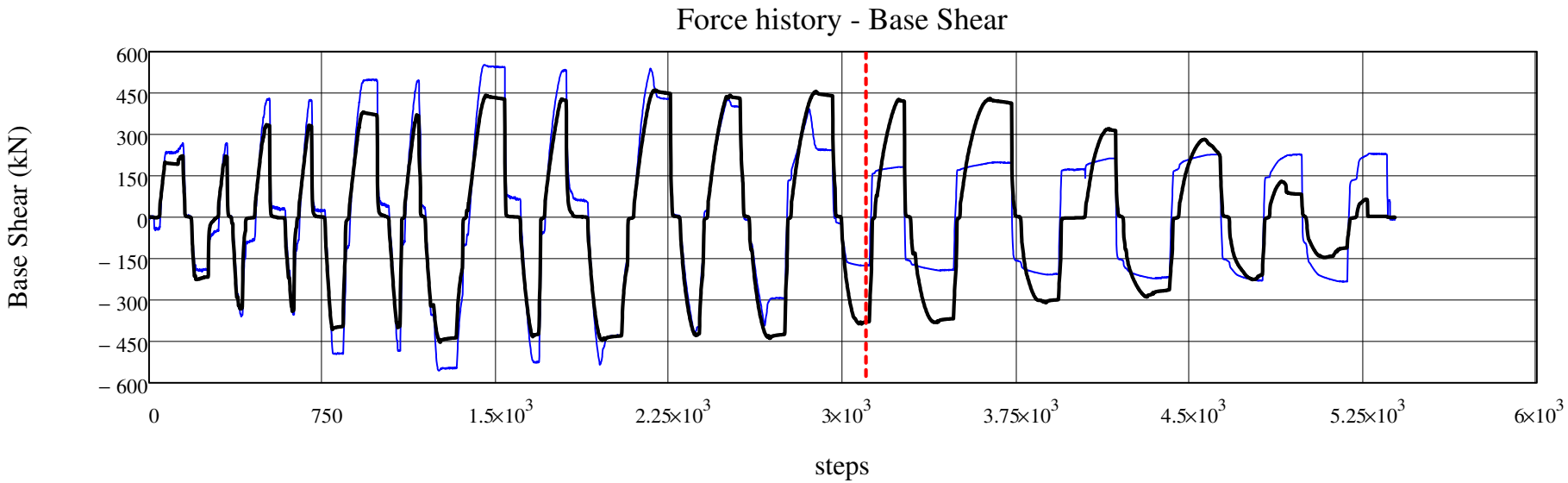

Analytical Results
Experimental Results
End of Calibration - 20% Strength Degradation

Modeling Predictions prior to Strength Degradation*
Maximum Sliding Disp. = 100% of Experimental Result
Maximum Resistance = 122% of Experimental Result

**Strength Degradation @ step 3100*

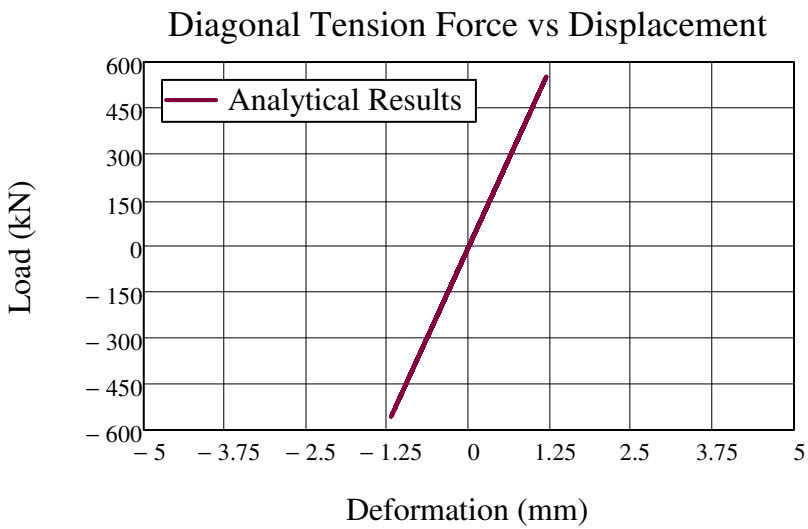
Diagonal Tension Force vs Displacement
Analytical Results
Load (kN)
600
450
300
150
0
– 150
– 300
– 450
– 600
– 5
– 3.75
– 2.5
– 1.25
0
1.25
2.5
3.75
5
Deformation (mm)

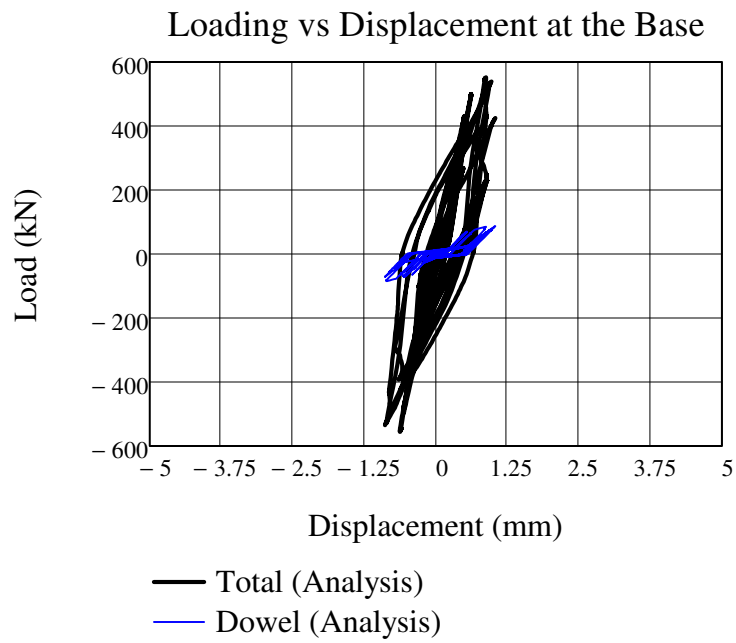
Loading vs Displacement at the Base
Load (kN)
600
400
200
0
– 200
– 400
– 600
– 5
– 3.75
– 2.5
– 1.25
0
1.25
2.5
3.75
5
Displacement (mm)
Total (Analysis)
Dowel (Analysis)

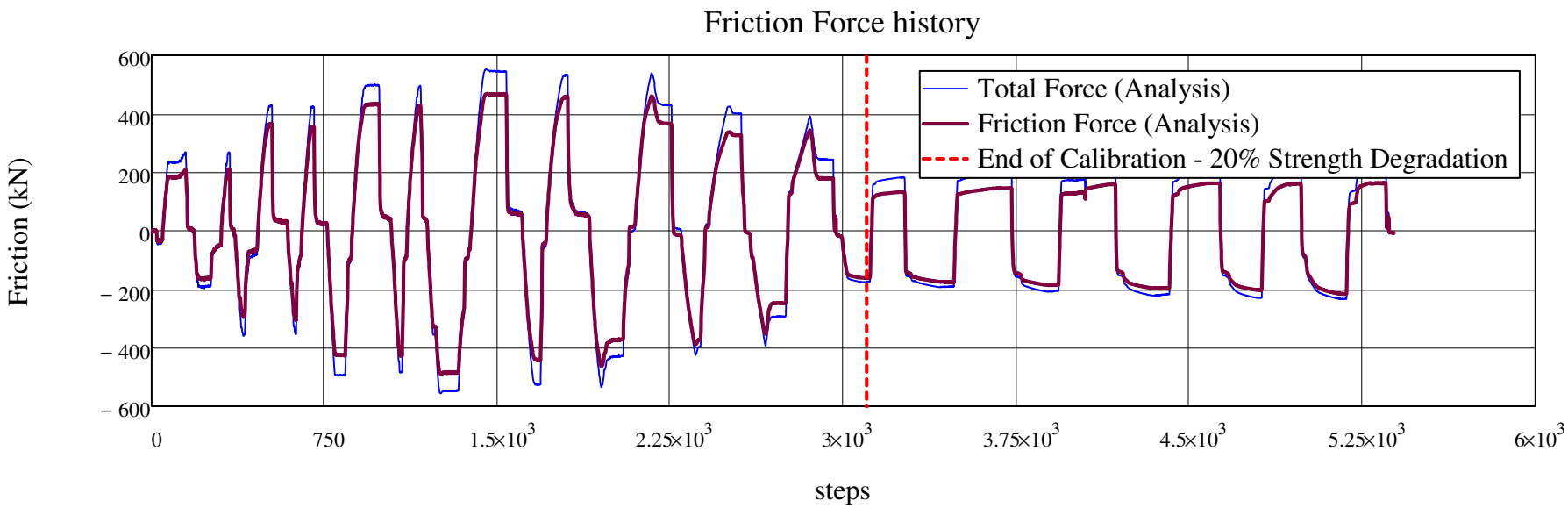
Friction Force history
Total Force (Analysis)
Friction Force (Analysis)
End of Calibration - 20% Strength Degradation
Friction (kN)
600
400
200
0
– 200
– 400
– 600
0
750
1.5×10^3
2.25×10^3
3×10^3
3.75×10^3
4.5×10^3
5.25×10^3
6×10^3
steps

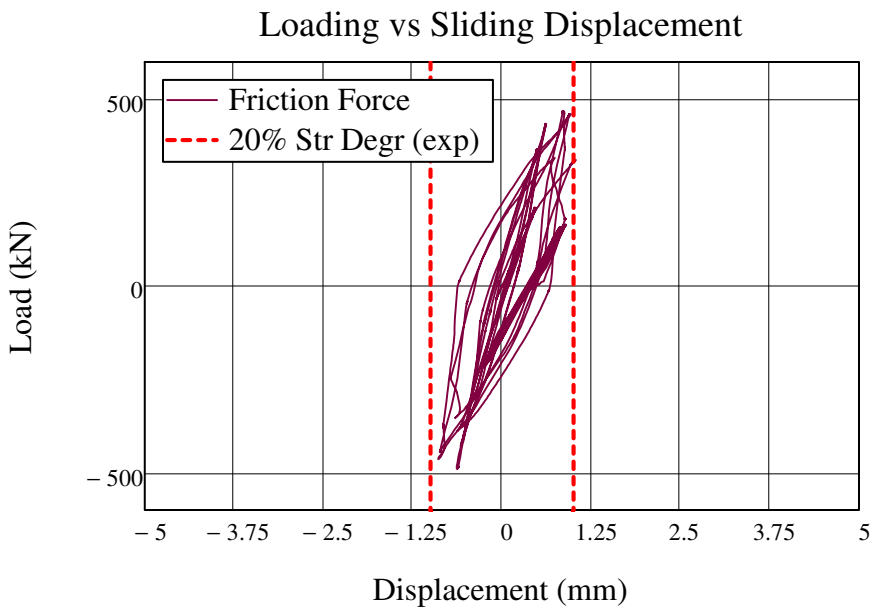
Loading vs Sliding Displacement
Friction Force
20% Str Degr (exp)
Load (kN)
500
0
− 500
− 5
− 3.75
− 2.5
− 1.25
0
1.25
2.5
3.75
5
Displacement (mm)

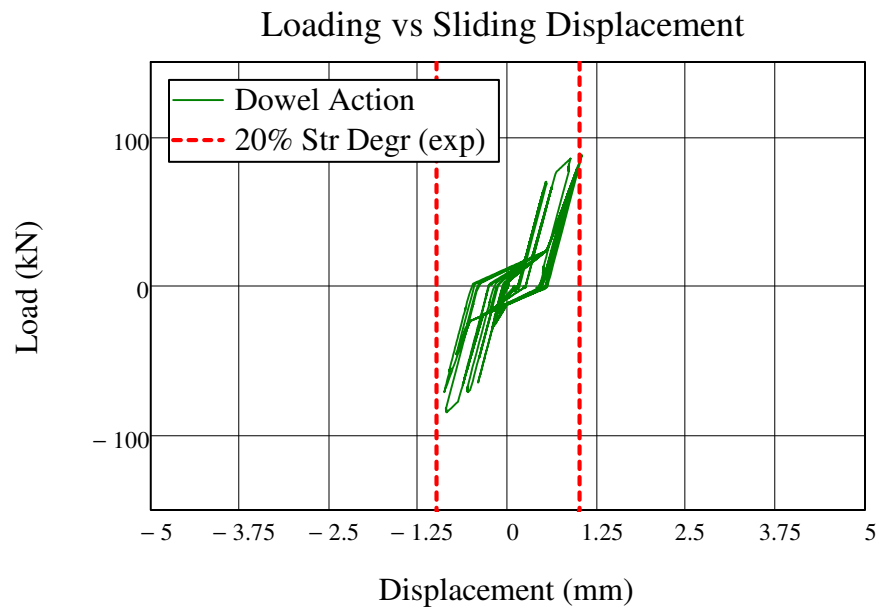
Loading vs Sliding Displacement
Dowel Action
20% Str Degr (exp)
Load (kN)
100
0
− 100
− 5
− 3.75
− 2.5
− 1.25
0
1.25
2.5
3.75
5
Displacement (mm)

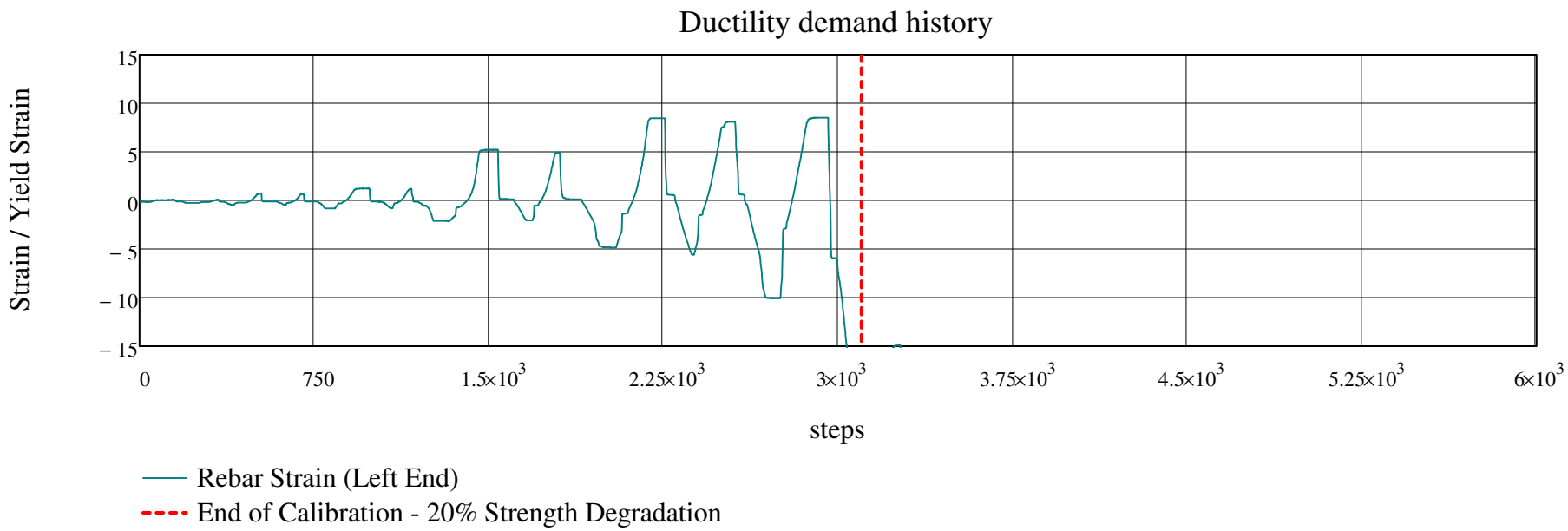
Ductility demand history
Strain / Yield Strain
15
10
5
0
− 5
− 10
− 15
0
750
1.5×10^3
2.25×10^3
3×10^3
3.75×10^3
4.5×10^3
5.25×10^3
6×10^3
steps
Rebar Strain (Left End)
End of Calibration - 20% Strength Degradation

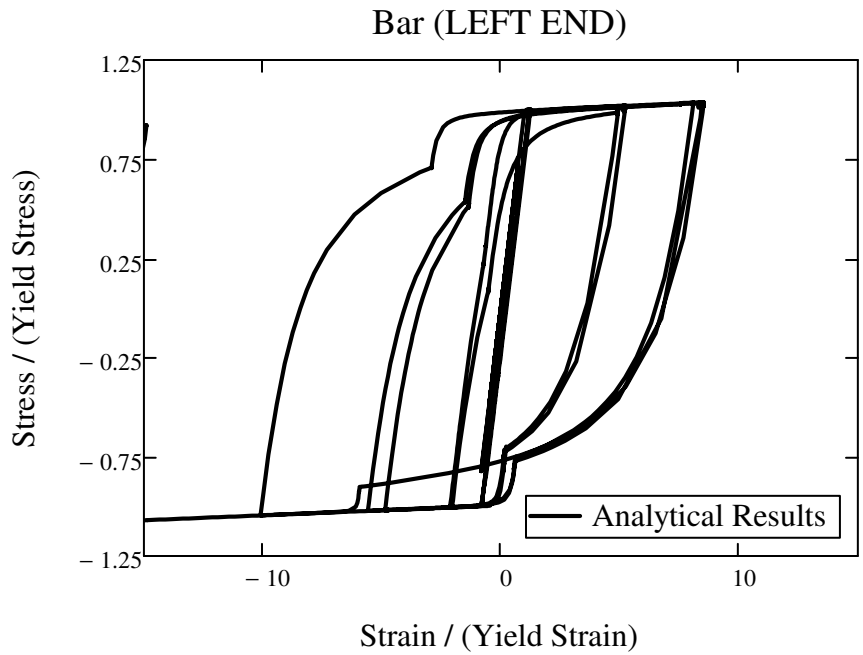
Bar (LEFT END)
Stress / (Yield Stress)
Strain / (Yield Strain)
Analytical Results
1.25
0.75
0.25
− 0.25
− 0.75
− 1.25
− 10
0
10

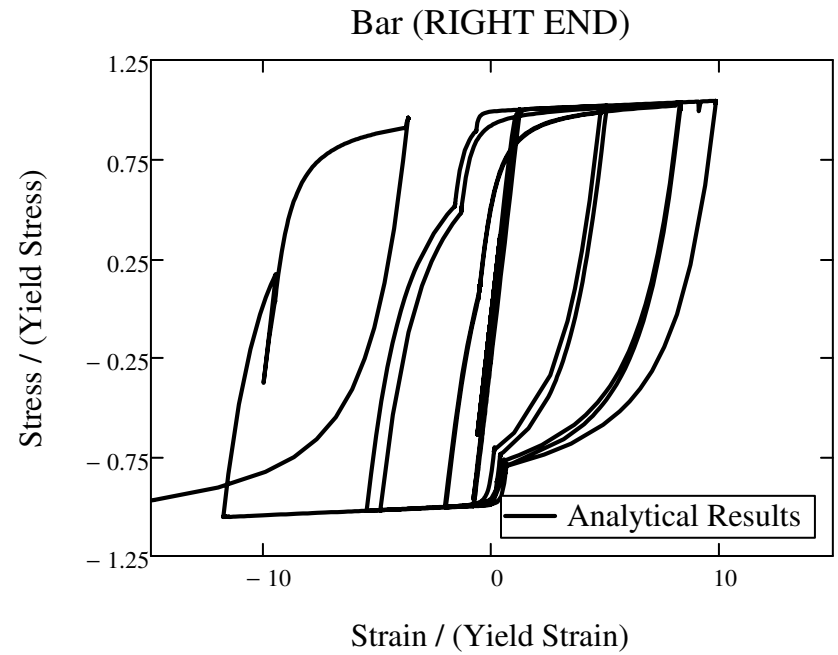
Bar (RIGHT END)
Stress / (Yield Stress)
Strain / (Yield Strain)
Analytical Results
1.25
0.75
0.25
− 0.25
− 0.75
− 1.25
− 10
0
10

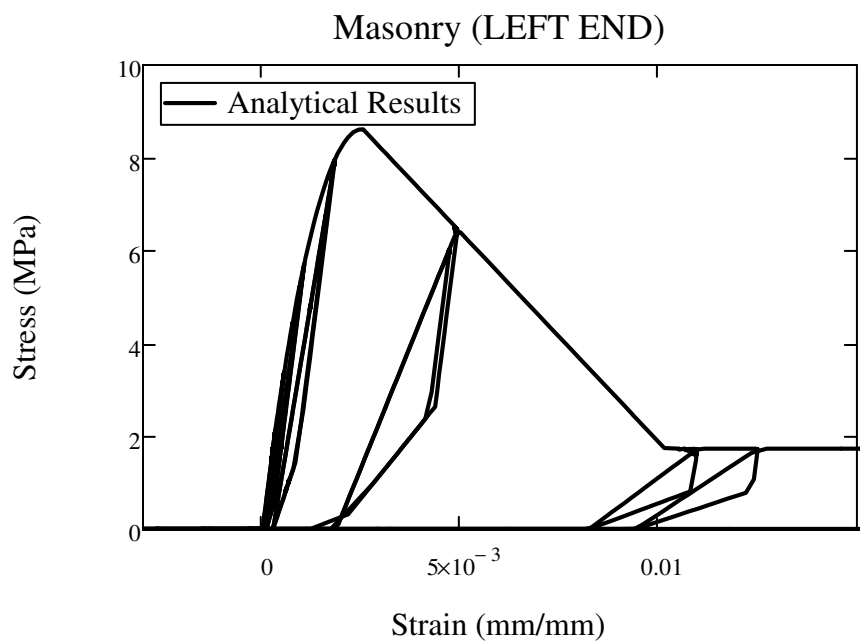
Masonry (LEFT END)
Stress (MPa)
Strain (mm/mm)
Analytical Results
10
8
6
4
2
0
0
5×10− 3
0.01

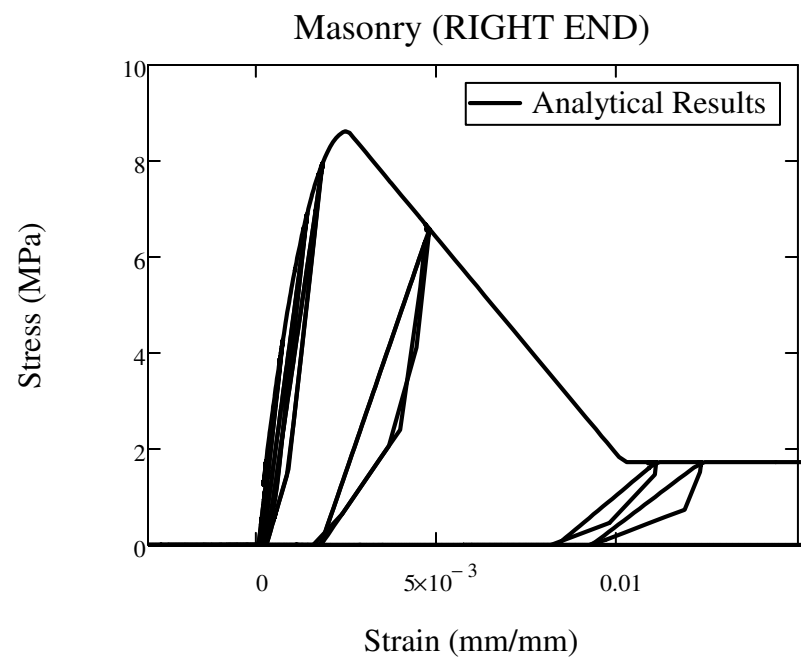
Masonry (RIGHT END)
Stress (MPa)
Strain (mm/mm)
Analytical Results
10
8
6
4
2
0
0
5×10− 3
0.01

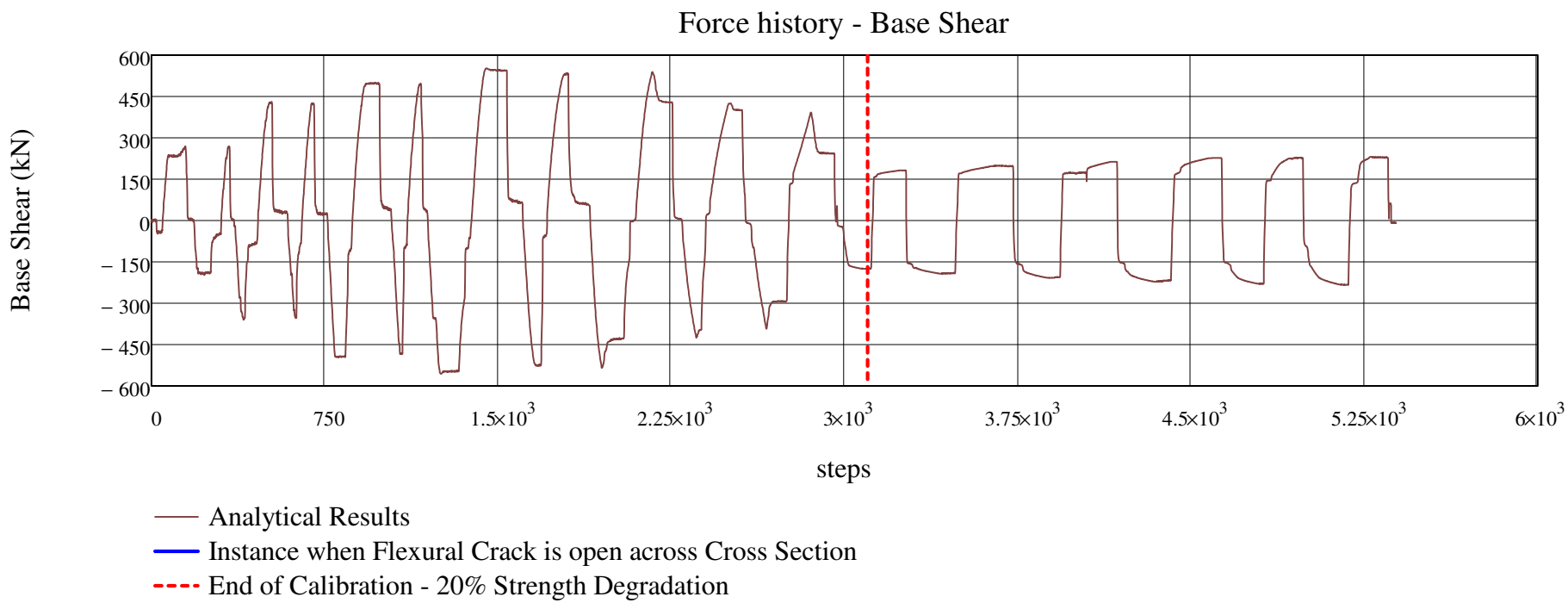
Force history - Base Shear
Base Shear (kN)
600
450
300
150
0
– 150
– 300
– 450
– 600
0
750
1.5×10^3
2.25×10^3
3×10^3
3.75×10^3
4.5×10^3
5.25×10^3
6×10^3
steps
Analytical Results
Instance when Flexural Crack is open across Cross Section
End of Calibration - 20% Strength Degradation

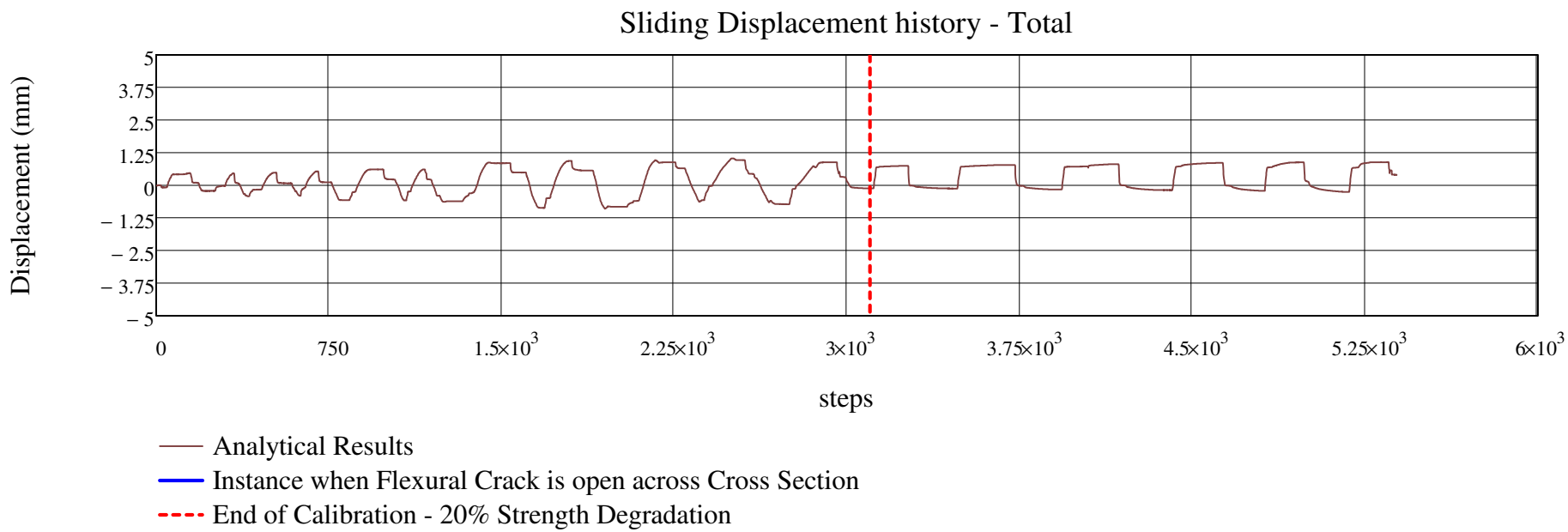
Sliding Displacement history - Total
Displacement (mm)
5
3.75
2.5
1.25
0
– 1.25
– 2.5
– 3.75
– 5
0
750
1.5×10^3
2.25×10^3
3×10^3
3.75×10^3
4.5×10^3
5.25×10^3
6×10^3
steps
Analytical Results
Instance when Flexural Crack is open across Cross Section
End of Calibration - 20% Strength Degradation

Appendix B: Calibration of the 2D Model for Specimens with Fixed-Fixed Support Conditions

Calibration of Test Specimen PBS-01

LWall := 1.8 m	fm := 8.5 MPa	Lambda = 1.00	Frict_Coeff = 0.60	DowelCoeff = 2.51	P / (f'm Ag) =1.4%
HWall := 1.8 m	fsy := 460 MPa	h := 0.15·LWall	Frict_Yield = 1mm	Dowel_Yield = 3.9mm	P = 89 kN
$\rho_v := 0.75\%$					

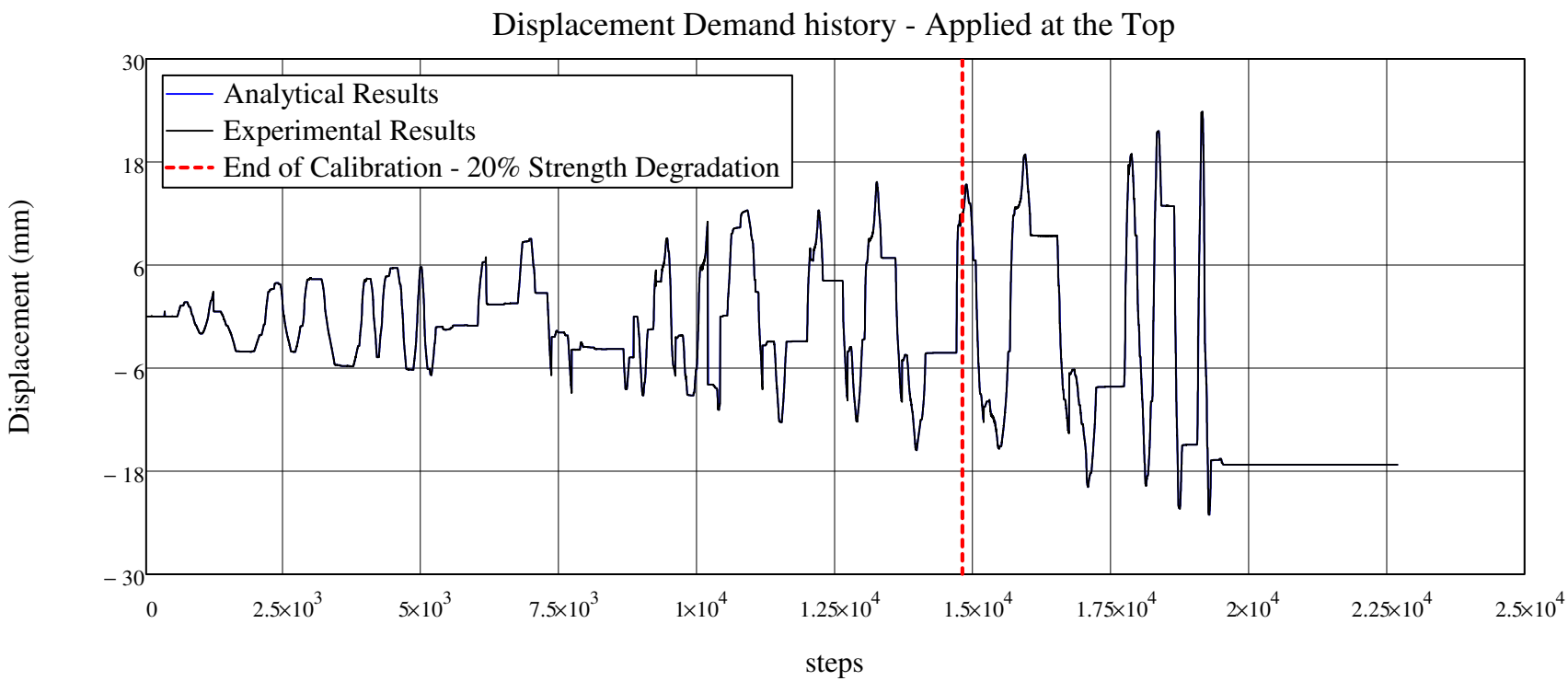

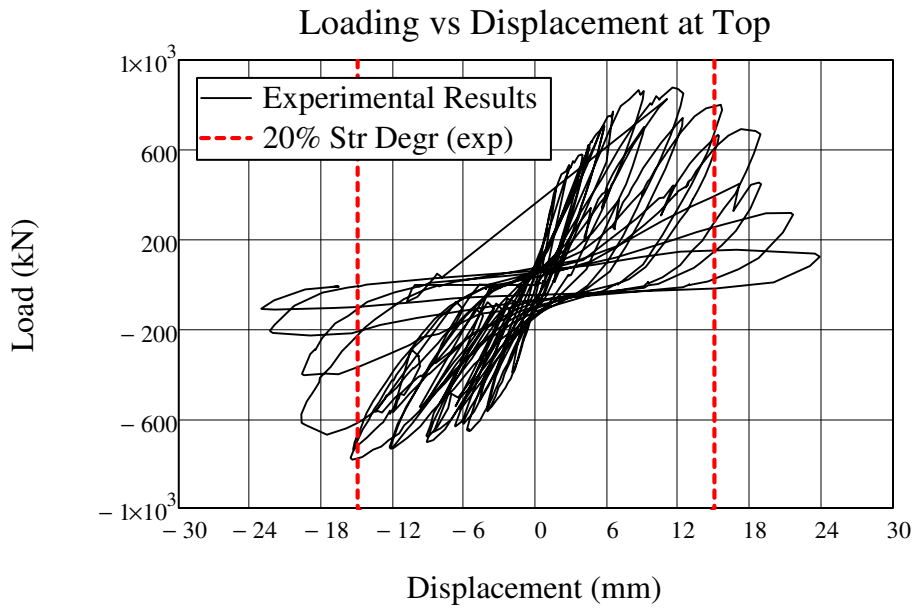
Loading vs Displacement at Top
Experimental Results
20% Str Degr (exp)
Load (kN)
Displacement (mm)
1×10^3
600
200
− 200
− 600
− 1×10^3
− 30
− 24
− 18
− 12
− 6
0
6
12
18
24
30

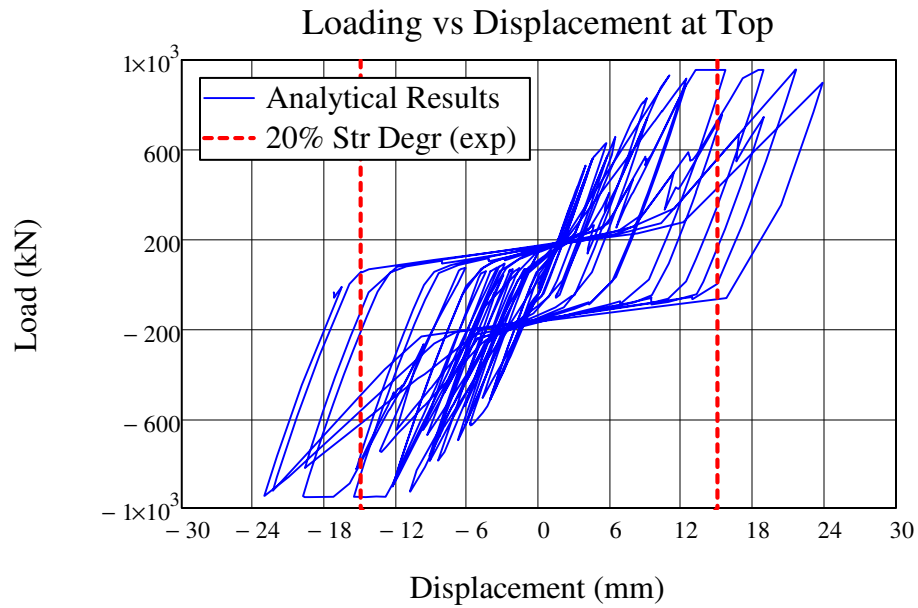
Loading vs Displacement at Top
Analytical Results
20% Str Degr (exp)
Load (kN)
Displacement (mm)
1×10^3
600
200
− 200
− 600
− 1×10^3
− 30
− 24
− 18
− 12
− 6
0
6
12
18
24
30

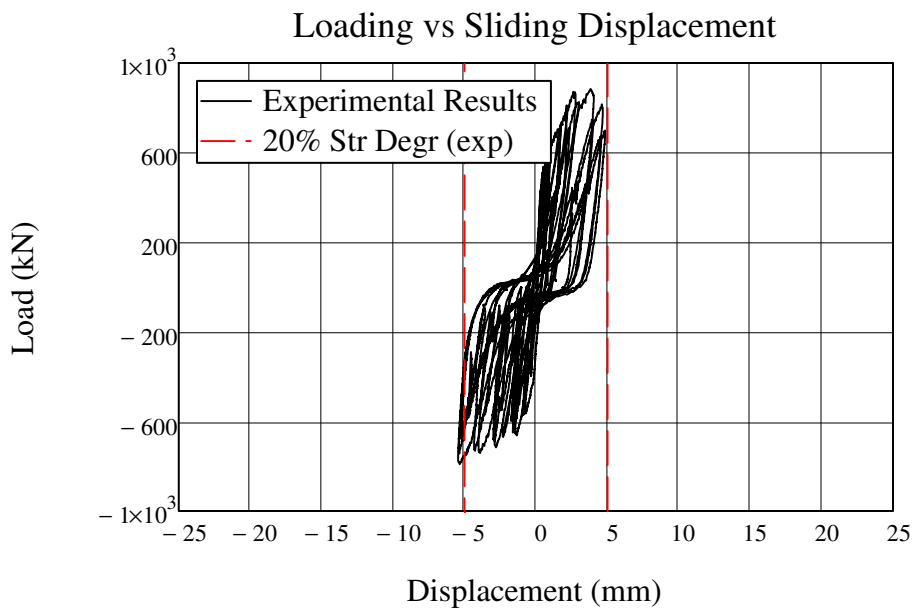
Loading vs Sliding Displacement
Experimental Results
20% Str Degr (exp)
Load (kN)
Displacement (mm)
1×10^3
600
200
− 200
− 600
− 1×10^3
− 25
− 20
− 15
− 10
− 5
0
5
10
15
20
25

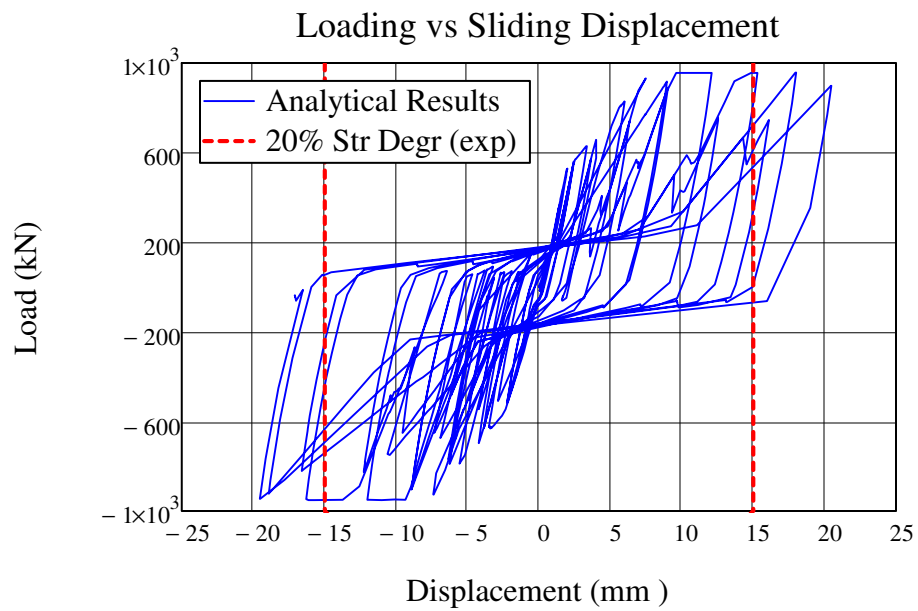
Loading vs Sliding Displacement
Analytical Results
20% Str Degr (exp)
Load (kN)
Displacement (mm)
1×10^3
600
200
− 200
− 600
− 1×10^3
− 25
− 20
− 15
− 10
− 5
0
5
10
15
20
25

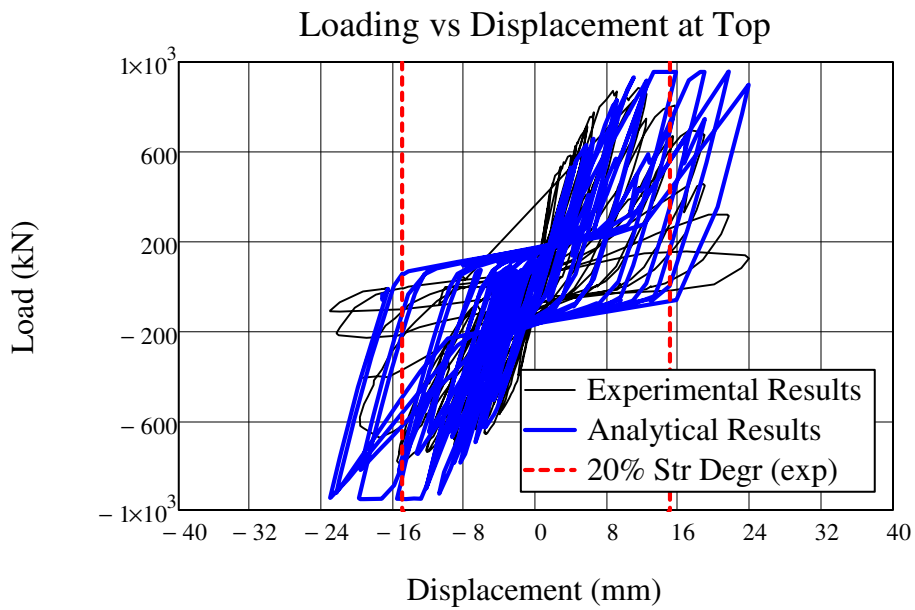
Loading vs Displacement at Top
Load (kN)
1×10^3
600
200
− 200
− 600
− 1×10^3
− 40
− 32
− 24
− 16
− 8
0
8
16
24
32
40
Displacement (mm)
Experimental Results
Analytical Results
20% Str Degr (exp)

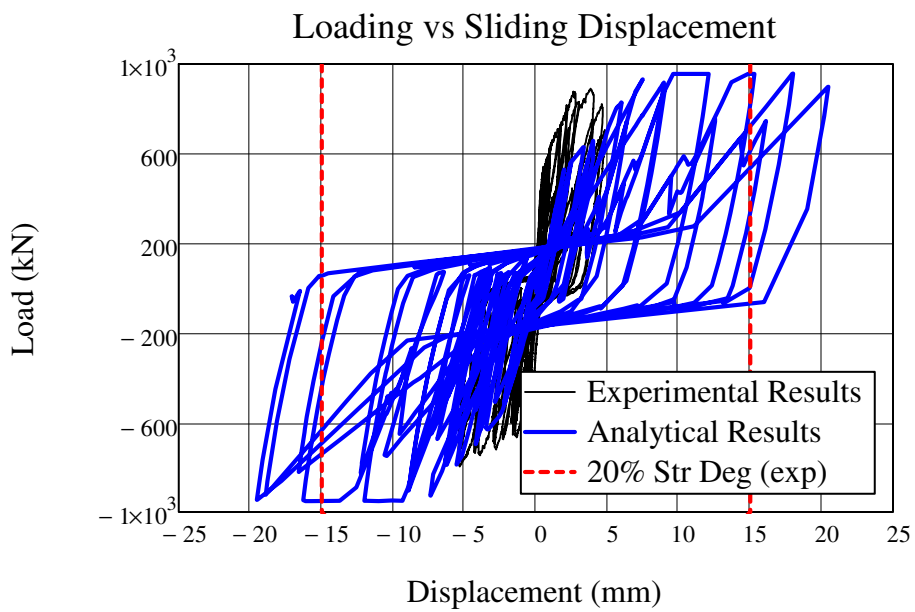
Loading vs Sliding Displacement
Load (kN)
1×10^3
600
200
− 200
− 600
− 1×10^3
− 25
− 20
− 15
− 10
− 5
0
5
10
15
20
25
Displacement (mm)
Experimental Results
Analytical Results
20% Str Deg (exp)

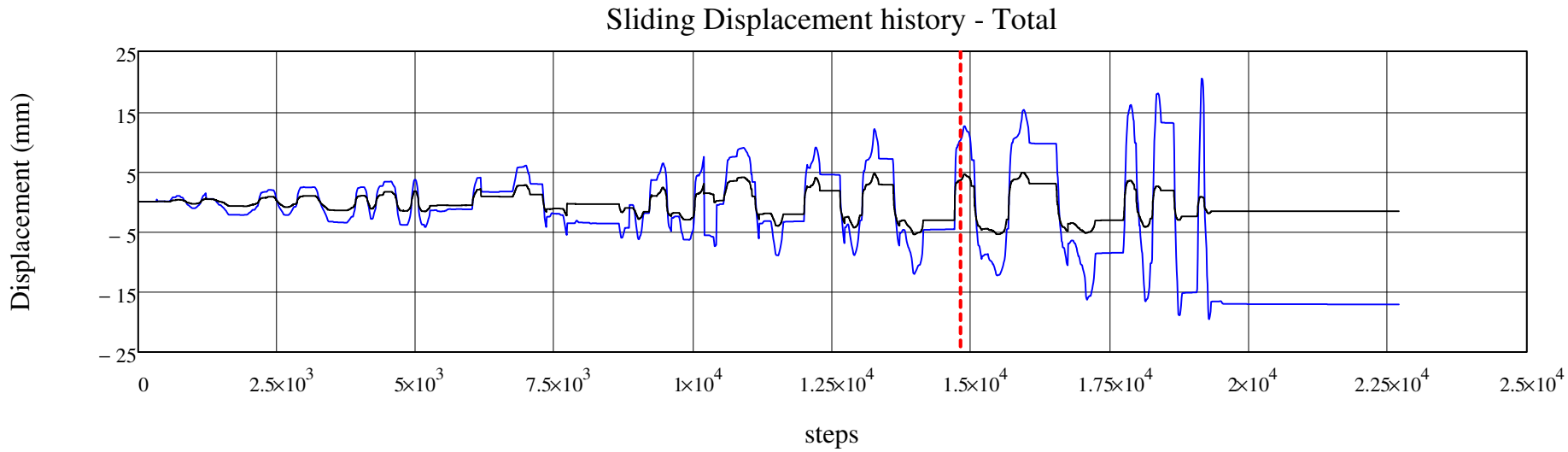

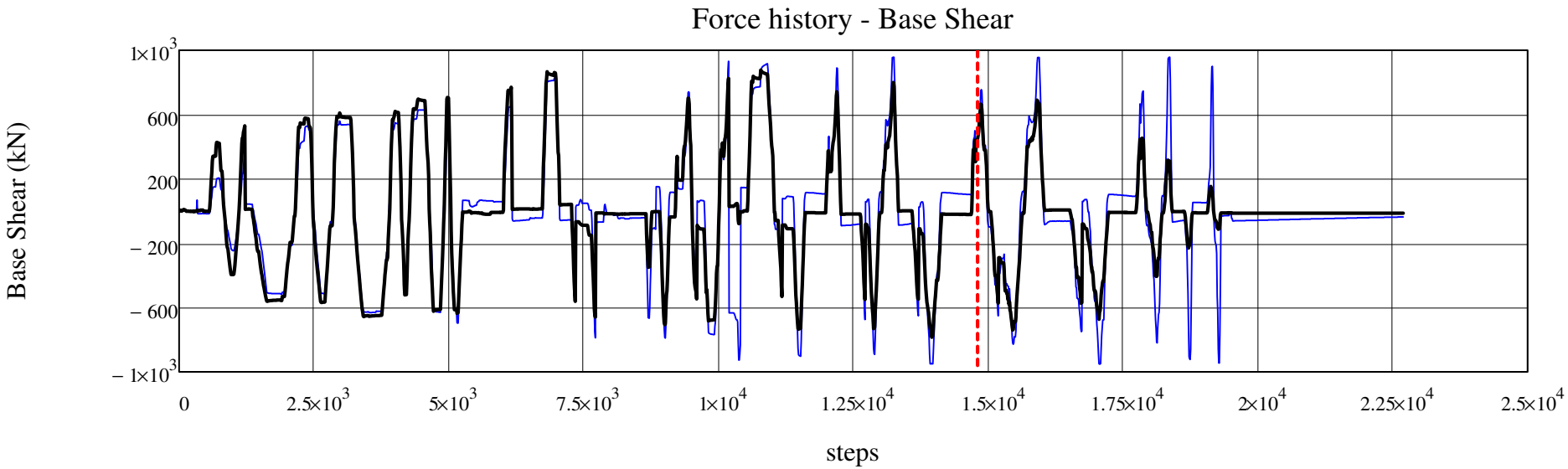

Analytical Results
Experimental Results
End of Calibration - 20% Strength Degradation

Modeling Predictions prior to Strength Degradation*

Sliding Displacement = 267% of Experimental Results
Maximum Resistance = 100% of Experimental Results

**Strength Degradation @ step 14800*

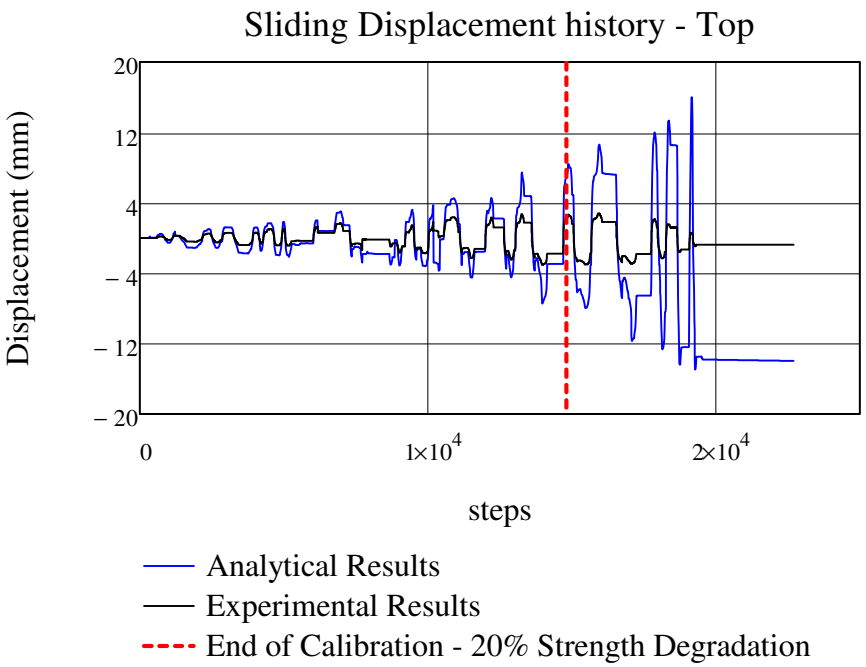
Sliding Displacement history - Top
Displacement (mm)
20
12
4
– 4
– 12
– 20
0
1×10^4
2×10^4
steps
Analytical Results
Experimental Results
End of Calibration - 20% Strength Degradation

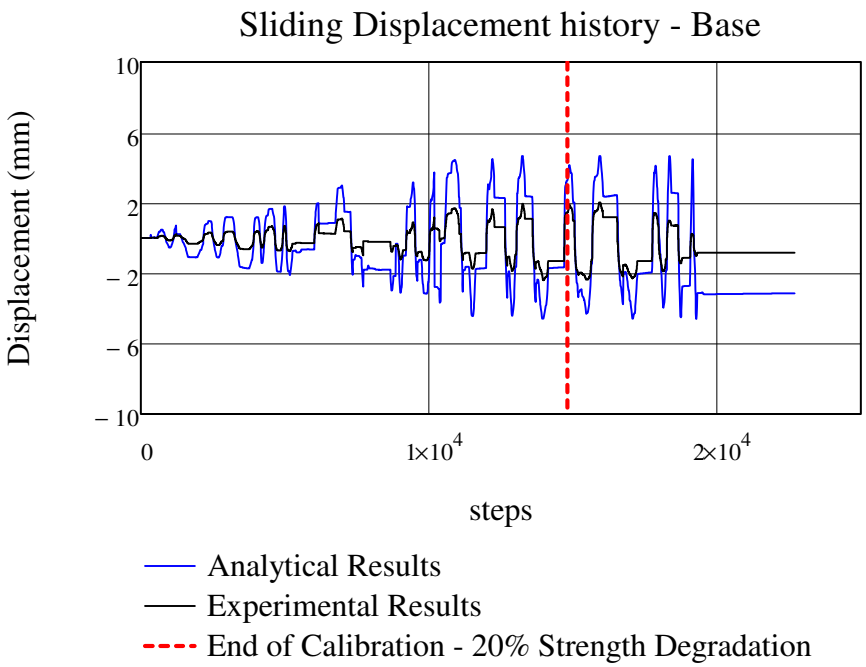
Sliding Displacement history - Base
Displacement (mm)
10
6
2
– 2
– 6
– 10
0
1×10^4
2×10^4
steps
Analytical Results
Experimental Results
End of Calibration - 20% Strength Degradation

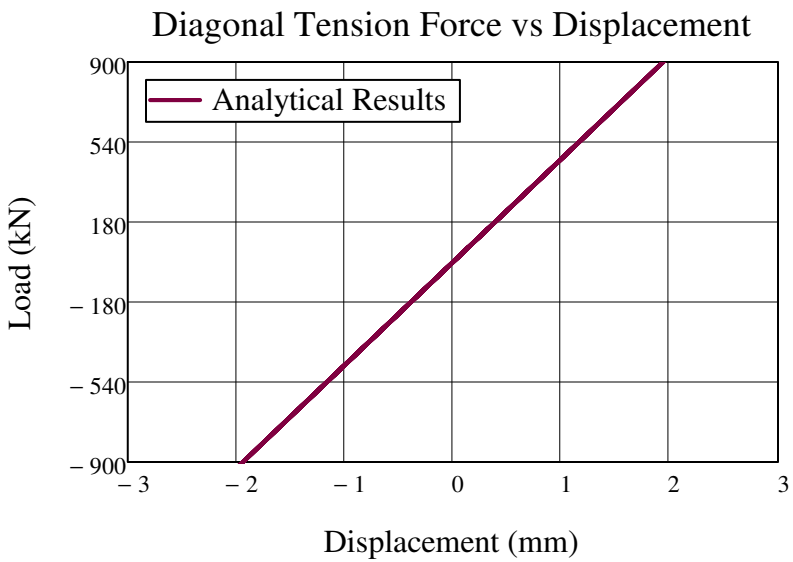
Diagonal Tension Force vs Displacement
Analytical Results
Load (kN)
900
540
180
– 180
– 540
– 900
– 3
– 2
– 1
0
1
2
3
Displacement (mm)

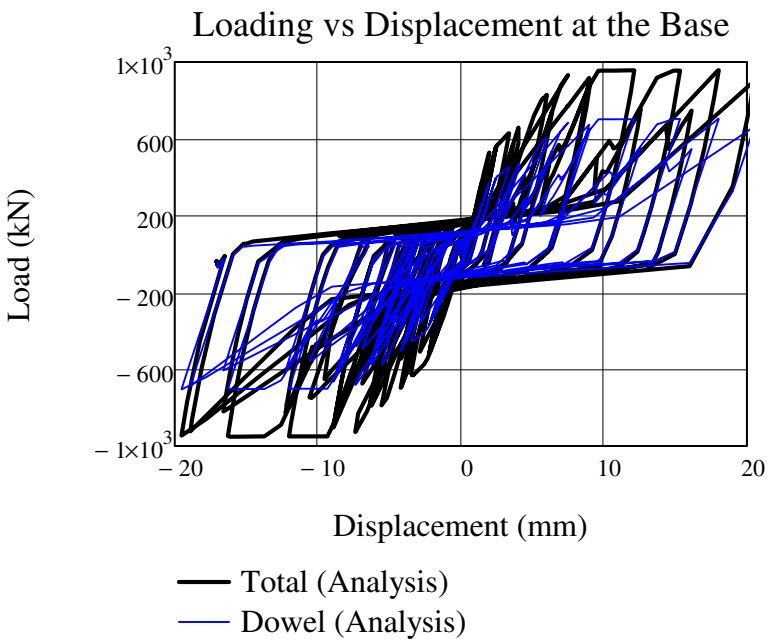
Loading vs Displacement at the Base
Load (kN)
1×10^3
600
200
– 200
– 600
– 1×10^3
– 20
– 10
0
10
20
Displacement (mm)
Total (Analysis)
Dowel (Analysis)

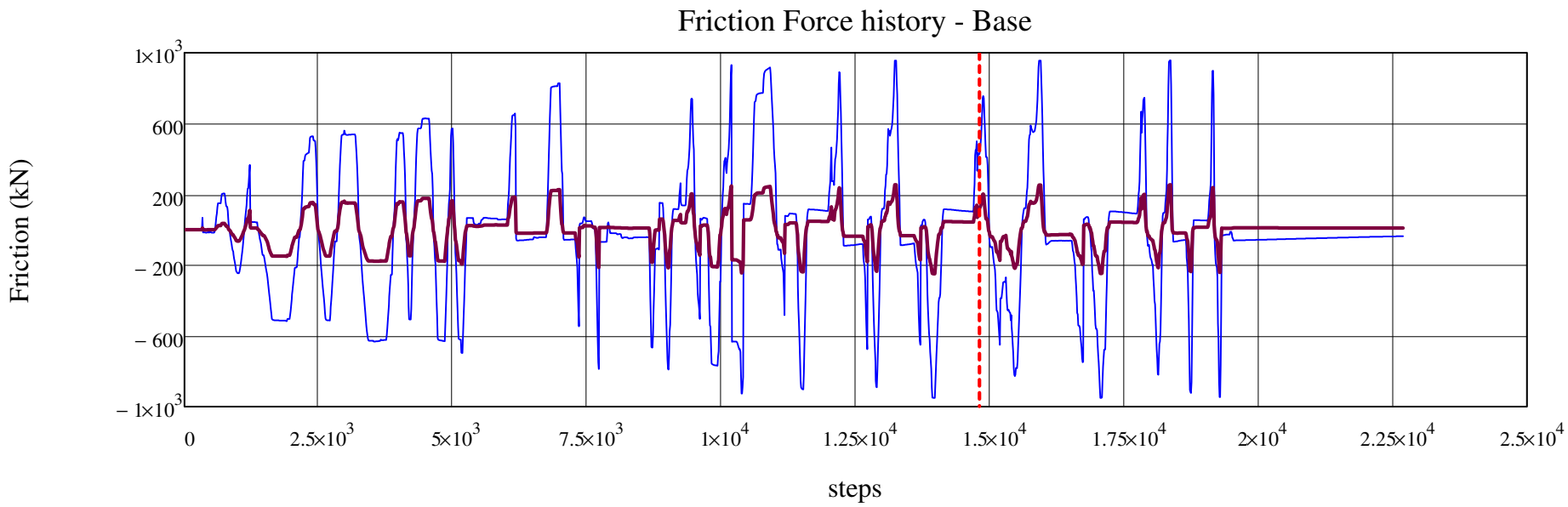

Total Force (Analysis)
Friction Force (Analysis)
End of Calibration - 20% Strength Degradation

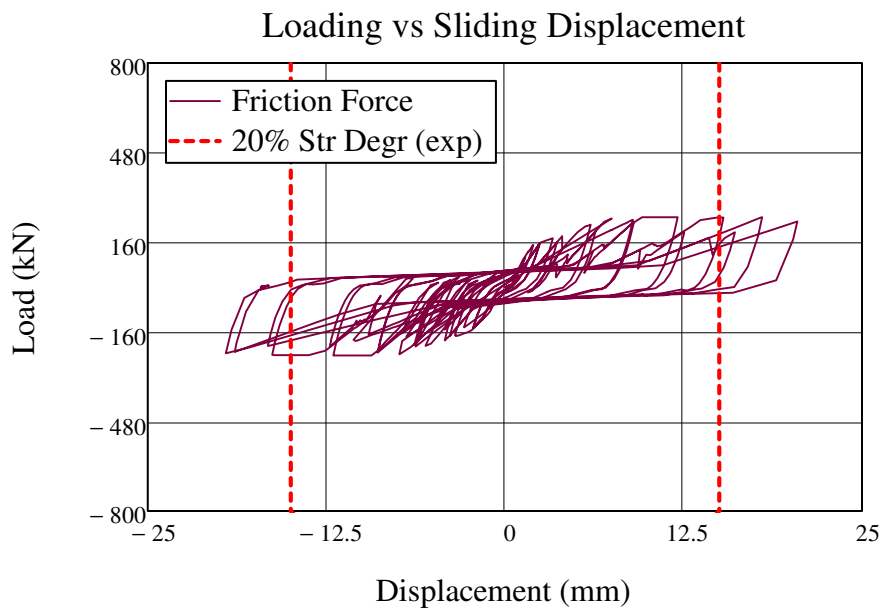
Loading vs Sliding Displacement
Friction Force
20% Str Degr (exp)
Load (kN)
800
480
160
− 160
− 480
− 800
− 25
− 12.5
0
12.5
25
Displacement (mm)

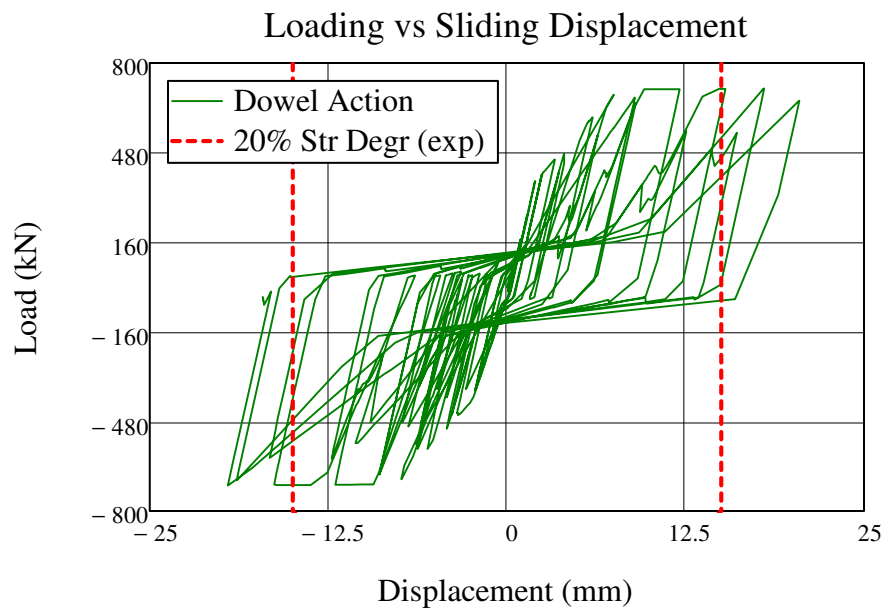
Loading vs Sliding Displacement
Dowel Action
20% Str Degr (exp)
Load (kN)
800
480
160
− 160
− 480
− 800
− 25
− 12.5
0
12.5
25
Displacement (mm)


Ductility demand history
Strain / Yield Strain
1.5
0.875
0.25
− 0.375
− 1
0
2.5×10^3
5×10^3
7.5×10^3
1×10^4
1.25×10^4
1.5×10^4
1.75×10^4
2×10^4
2.25×10^4
2.5×10^4
steps
Rebar Strain (Left End)

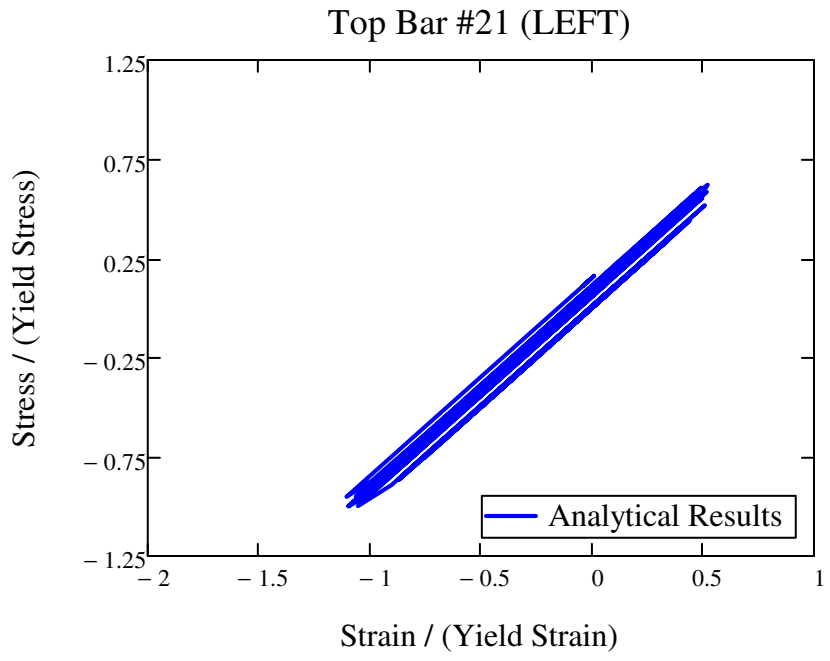
Top Bar #21 (LEFT)
Stress / (Yield Stress)
Strain / (Yield Strain)
Analytical Results
1.25
0.75
0.25
− 0.25
− 0.75
− 1.25
− 2
− 1.5
− 1
− 0.5
0
0.5
1

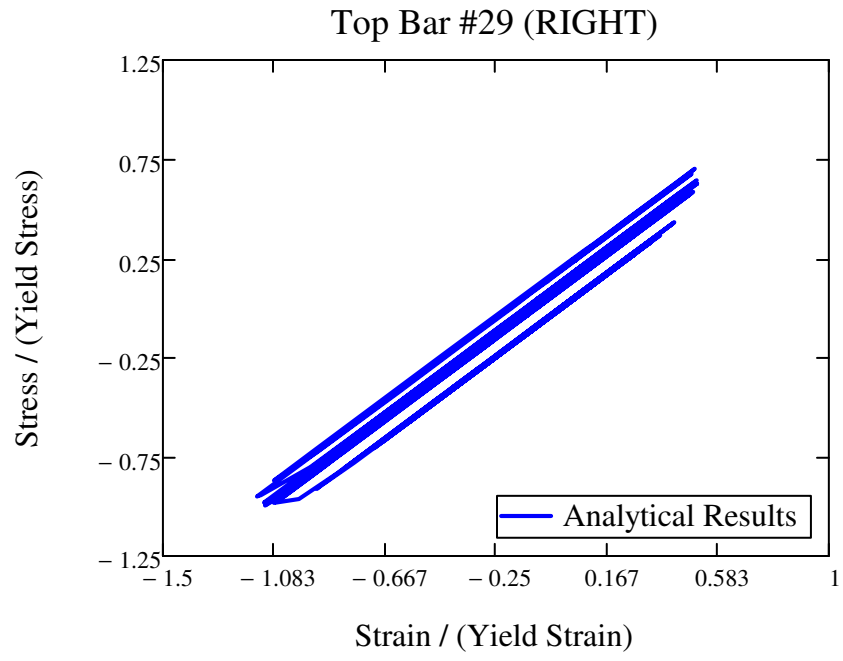
Top Bar #29 (RIGHT)
Stress / (Yield Stress)
Strain / (Yield Strain)
Analytical Results
1.25
0.75
0.25
− 0.25
− 0.75
− 1.25
− 1.5
− 1.083
− 0.667
− 0.25
0.167
0.583
1

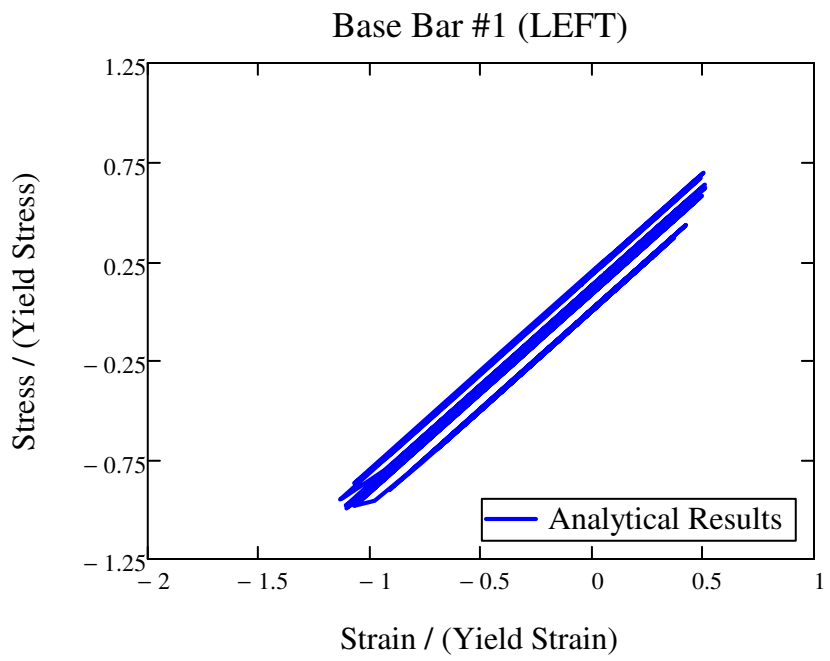
Base Bar #1 (LEFT)
Stress / (Yield Stress)
Strain / (Yield Strain)
Analytical Results
1.25
0.75
0.25
− 0.25
− 0.75
− 1.25
− 2
− 1.5
− 1
− 0.5
0
0.5
1

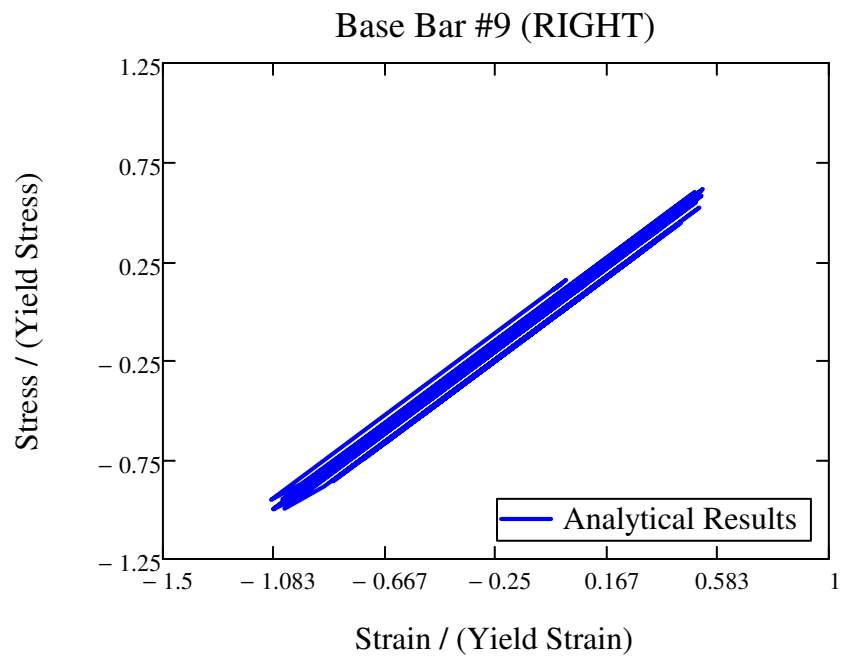
Base Bar #9 (RIGHT)
Stress / (Yield Stress)
Strain / (Yield Strain)
Analytical Results
1.25
0.75
0.25
− 0.25
− 0.75
− 1.25
− 1.5
− 1.083
− 0.667
− 0.25
0.167
0.583
1

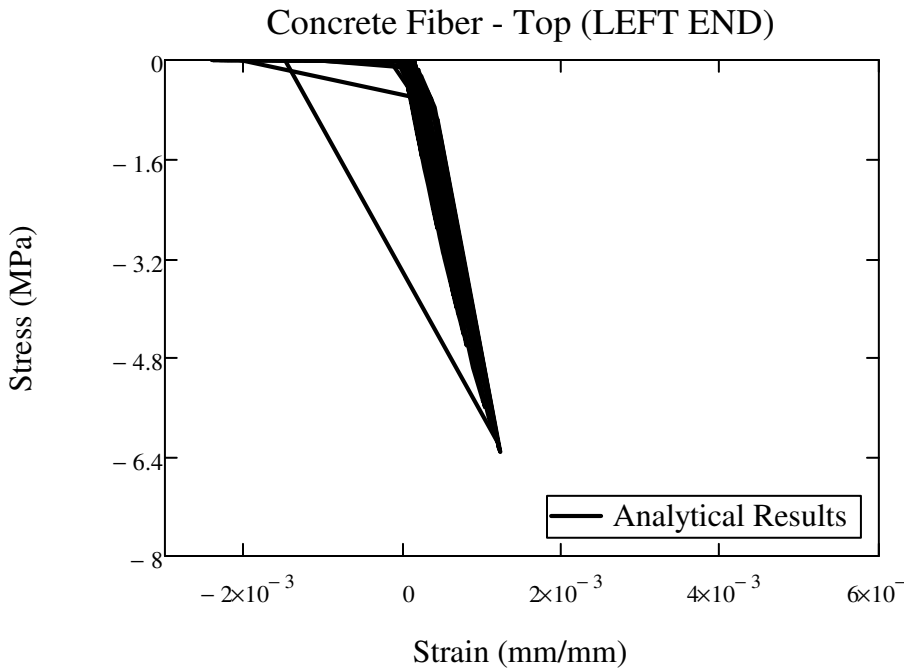
Concrete Fiber - Top (LEFT END)
Stress (MPa)
0
− 1.6
− 3.2
− 4.8
− 6.4
− 8
− 2×10⁻³
0
2×10⁻³
4×10⁻³
6×10⁻
Strain (mm/mm)
Analytical Results

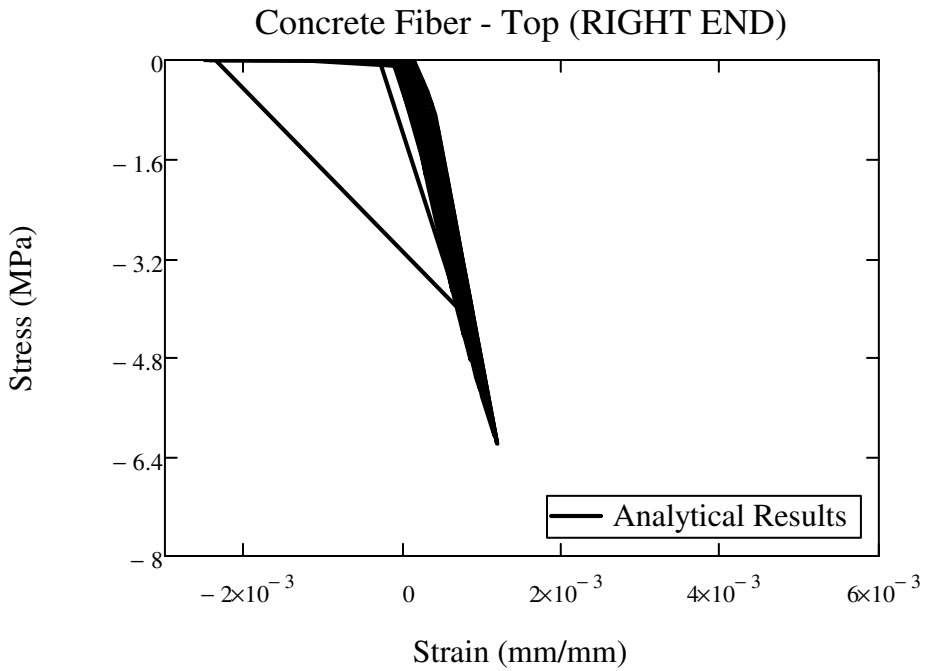
Concrete Fiber - Top (RIGHT END)
Stress (MPa)
0
− 1.6
− 3.2
− 4.8
− 6.4
− 8
− 2×10⁻³
0
2×10⁻³
4×10⁻³
6×10⁻³
Strain (mm/mm)
Analytical Results

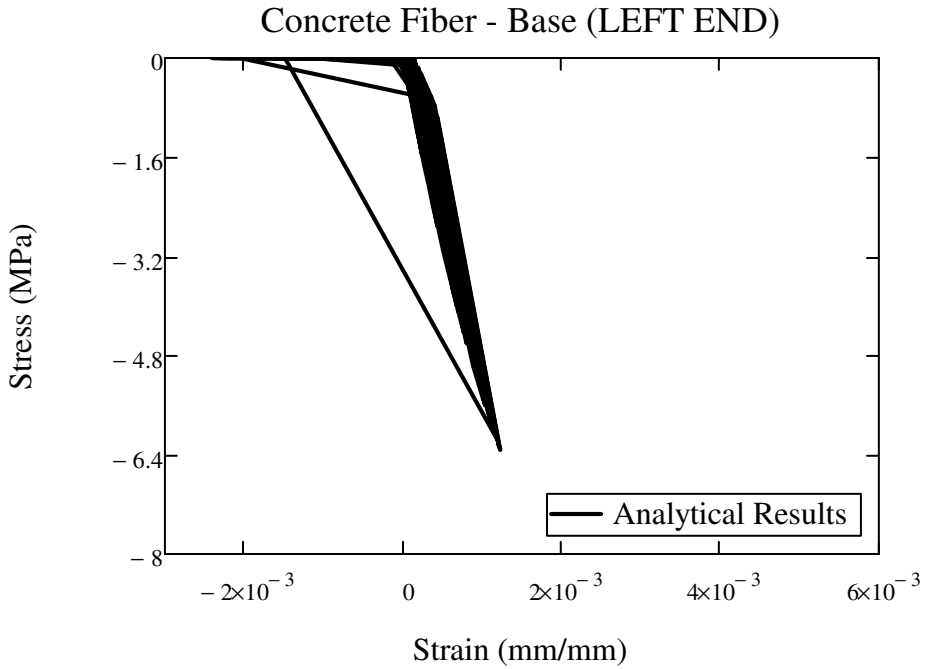
Concrete Fiber - Base (LEFT END)
Stress (MPa)
0
− 1.6
− 3.2
− 4.8
− 6.4
− 8
− 2×10⁻³
0
2×10⁻³
4×10⁻³
6×10⁻³
Strain (mm/mm)
Analytical Results

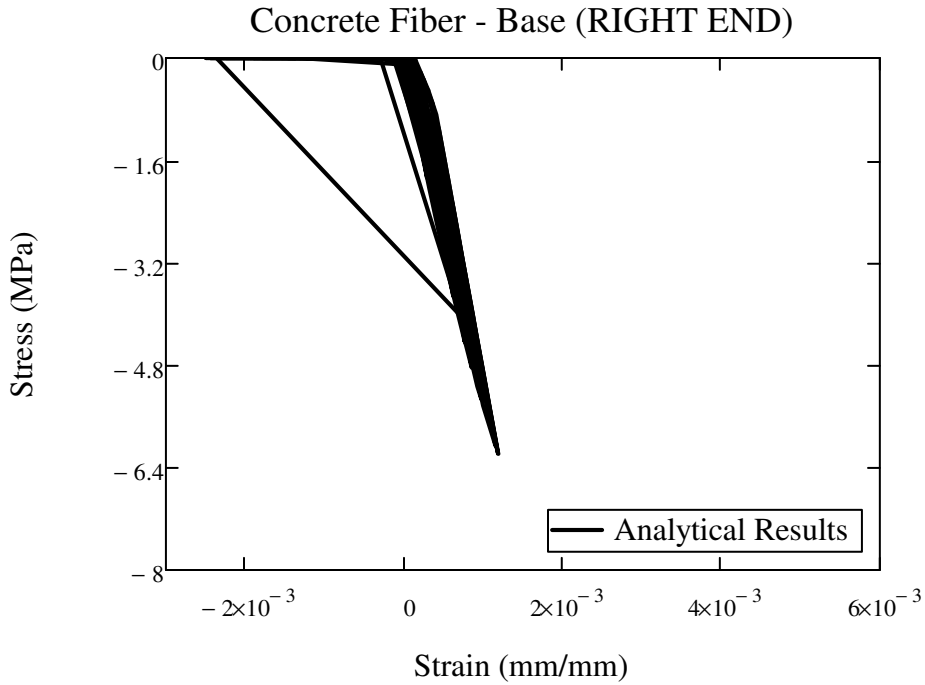
Concrete Fiber - Base (RIGHT END)
Stress (MPa)
0
− 1.6
− 3.2
− 4.8
− 6.4
− 8
− 2×10⁻³
0
2×10⁻³
4×10⁻³
6×10⁻³
Strain (mm/mm)
Analytical Results

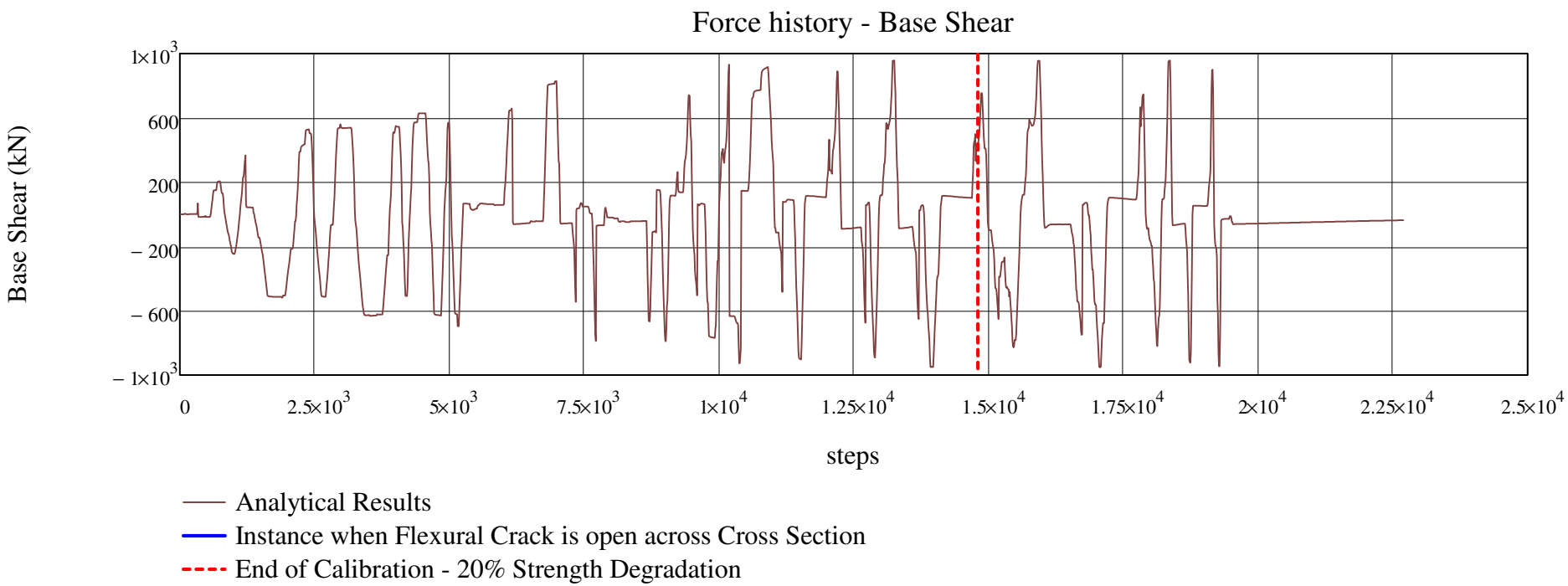
Force history - Base Shear
Base Shear (kN)
1×10^3
600
200
− 200
− 600
− 1×10^3
0
2.5×10^3
5×10^3
7.5×10^3
1×10^4
1.25×10^4
1.5×10^4
1.75×10^4
2×10^4
2.25×10^4
2.5×10^4
steps
Analytical Results
Instance when Flexural Crack is open across Cross Section
End of Calibration - 20% Strength Degradation

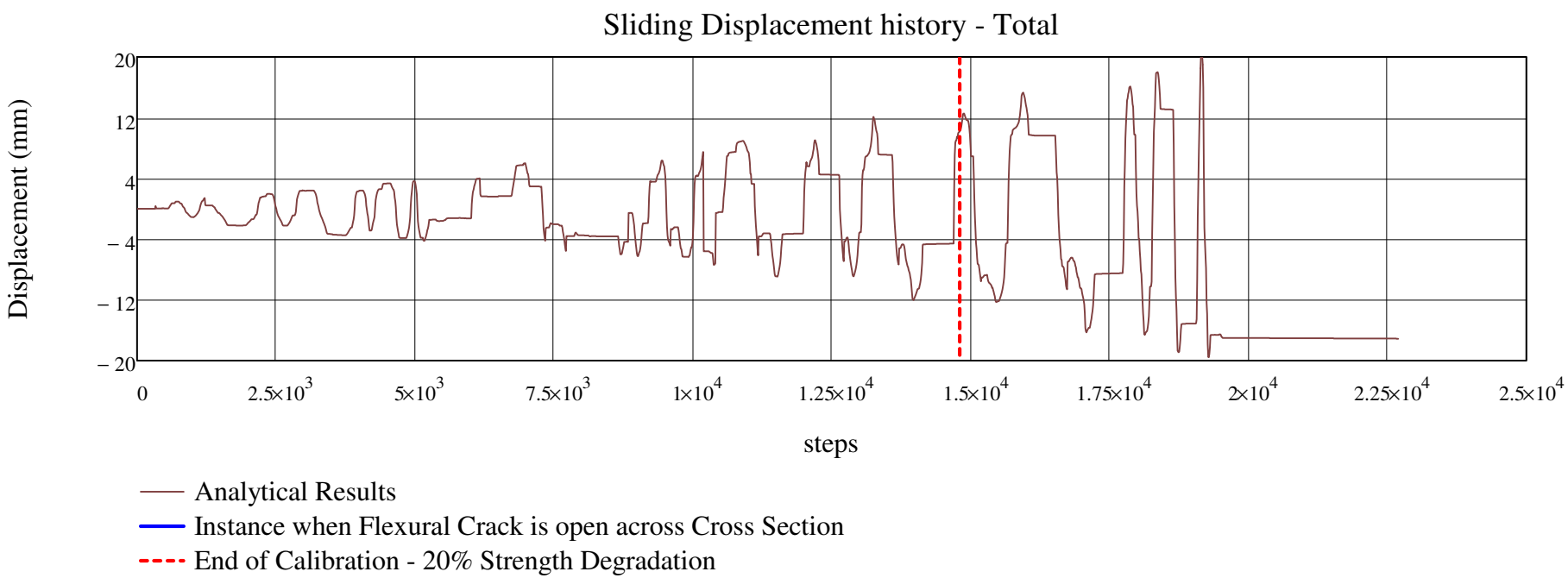
Sliding Displacement history - Total
Displacement (mm)
20
12
4
− 4
− 12
− 20
0
2.5×10^3
5×10^3
7.5×10^3
1×10^4
1.25×10^4
1.5×10^4
1.75×10^4
2×10^4
2.25×10^4
2.5×10^4
steps
Analytical Results
Instance when Flexural Crack is open across Cross Section
End of Calibration - 20% Strength Degradation

Calibration of Test Specimen PBS-05

LWall := 1.8 m	fm := 8.5 MPa	Lambda = 1.00	Frict_Coeff = 0.60	DowelCoeff = 2.51	P / (f'm Ag) = 5%
HWall := 1.8 m	fsy := 460 MPa	h := 0.15·LWall	Frict_Yield = 1mm	Dowel_Yield = 2.7mm	P = 361.6 kN
$\rho_v := 0.33\%$					

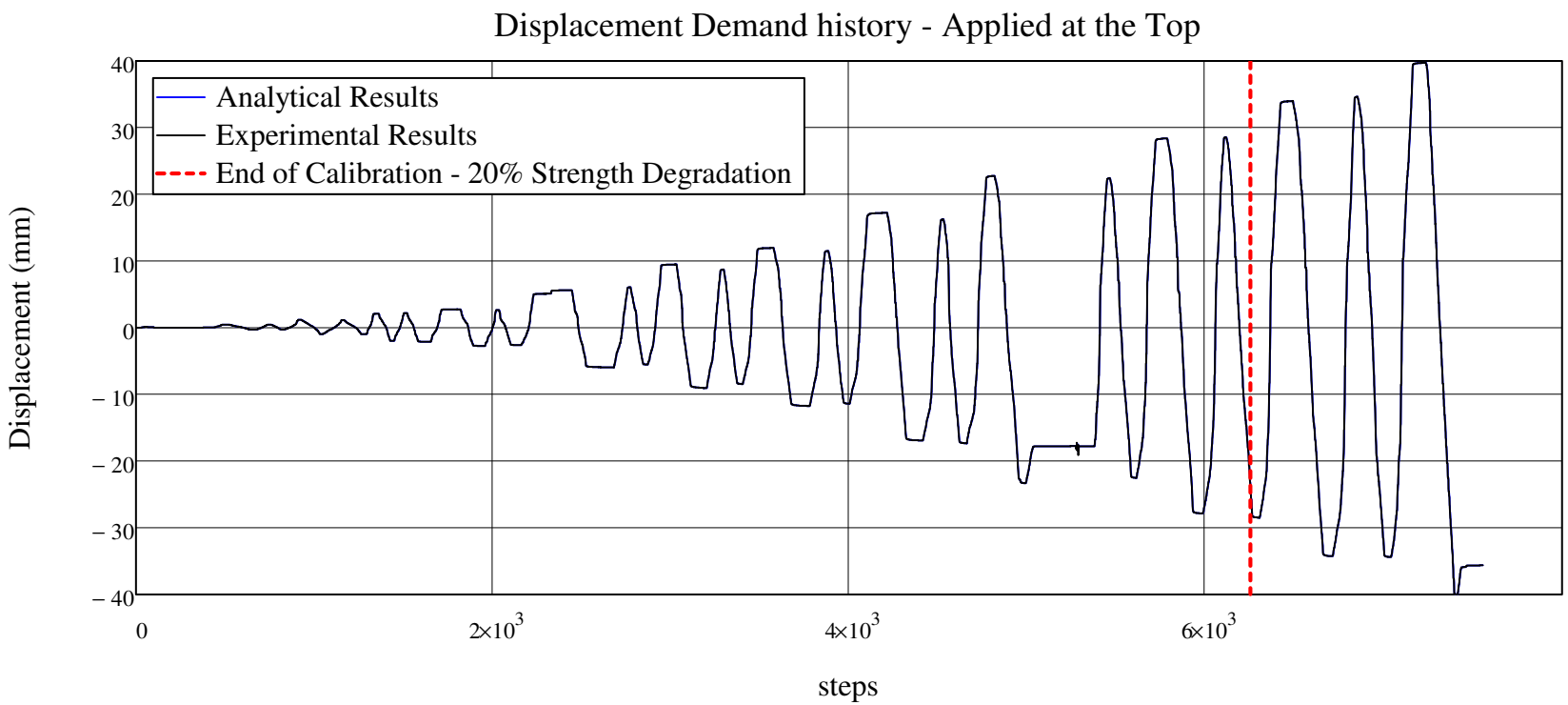

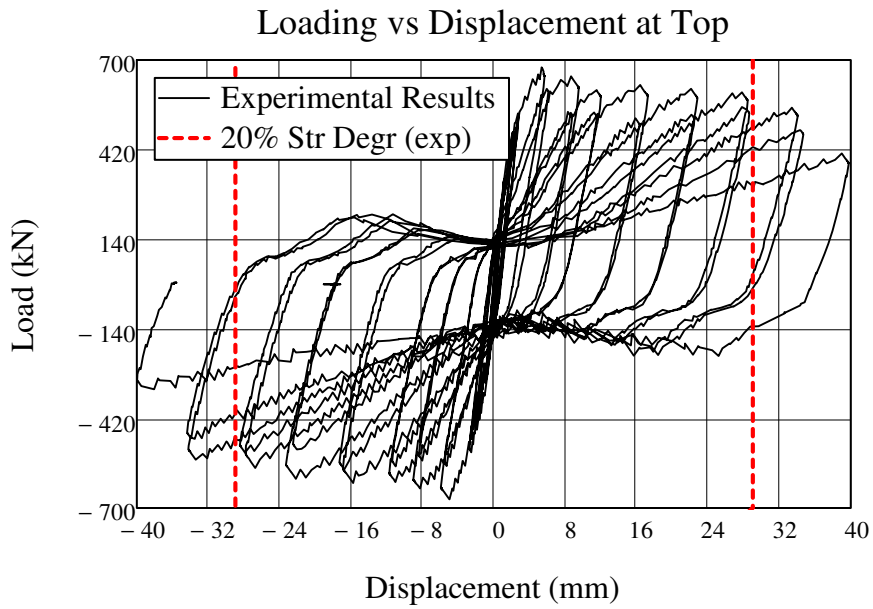
Loading vs Displacement at Top
Experimental Results
20% Str Degr (exp)
Load (kN)
700
420
140
– 140
– 420
– 700
– 40
– 32
– 24
– 16
– 8
0
8
16
24
32
40
Displacement (mm)

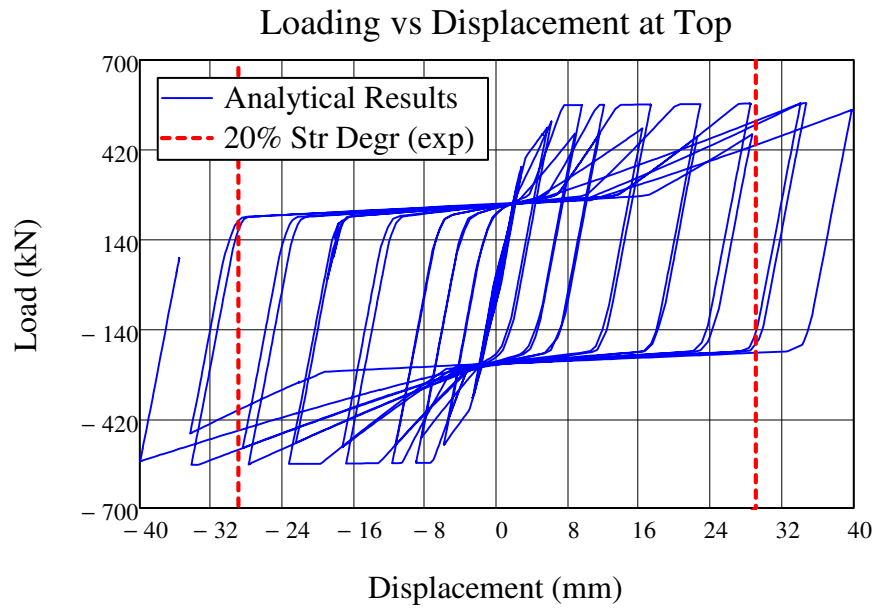
Loading vs Displacement at Top
Analytical Results
20% Str Degr (exp)
Load (kN)
700
420
140
– 140
– 420
– 700
– 40
– 32
– 24
– 16
– 8
0
8
16
24
32
40
Displacement (mm)

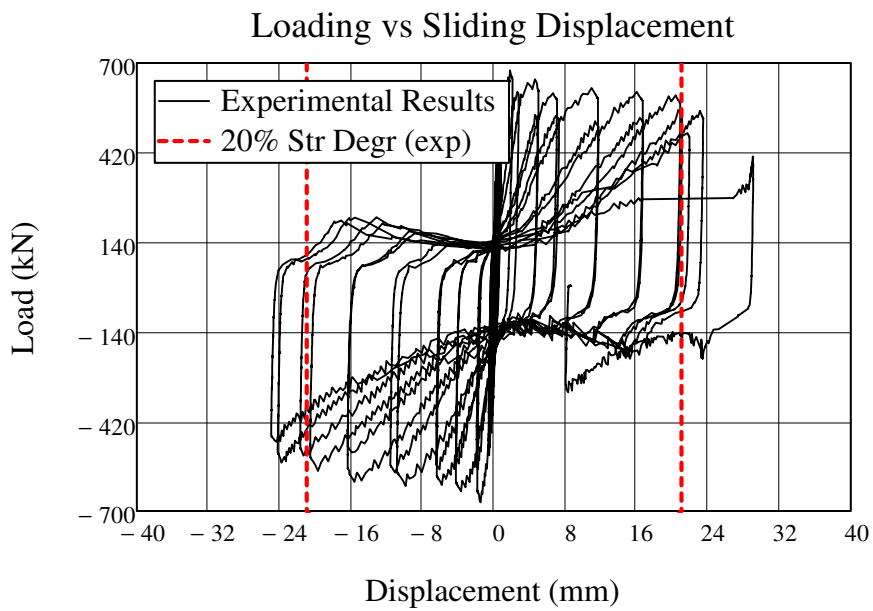
Loading vs Sliding Displacement
Experimental Results
20% Str Degr (exp)
Load (kN)
700
420
140
– 140
– 420
– 700
– 40
– 32
– 24
– 16
– 8
0
8
16
24
32
40
Displacement (mm)

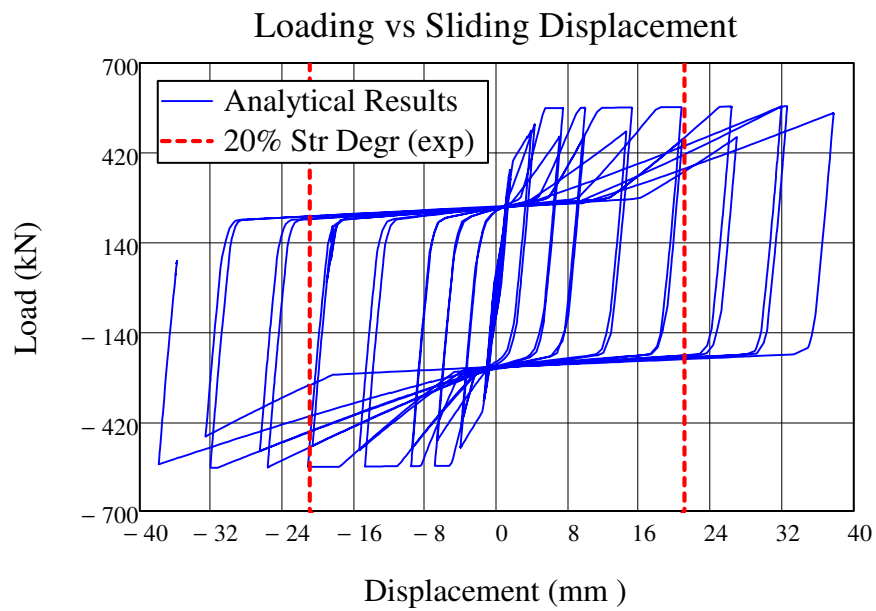
Loading vs Sliding Displacement
Analytical Results
20% Str Degr (exp)
Load (kN)
700
420
140
– 140
– 420
– 700
– 40
– 32
– 24
– 16
– 8
0
8
16
24
32
40
Displacement (mm)

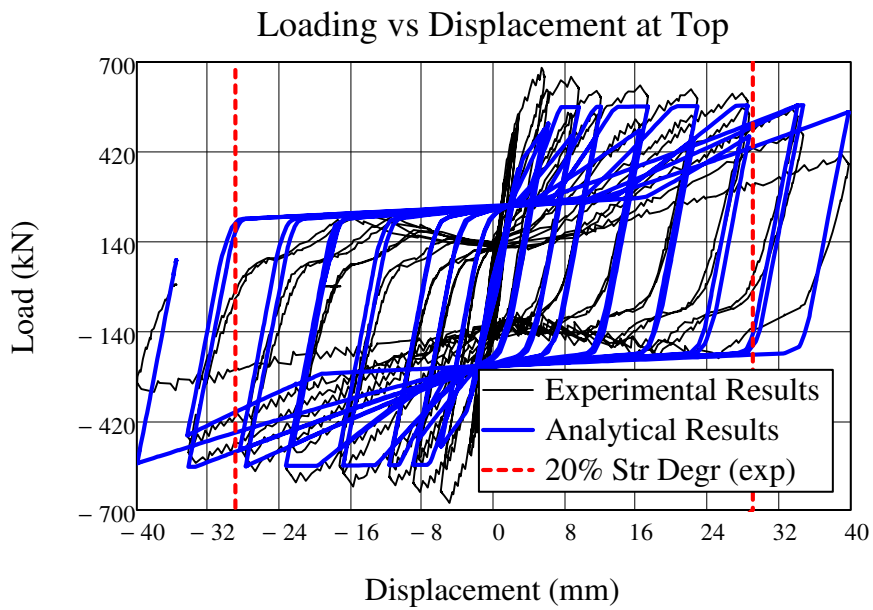
Loading vs Displacement at Top
700
420
140
– 140
– 420
– 700
Load (kN)
– 40
– 32
– 24
– 16
– 8
0
8
16
24
32
40
Displacement (mm)
Experimental Results
Analytical Results
20% Str Degr (exp)

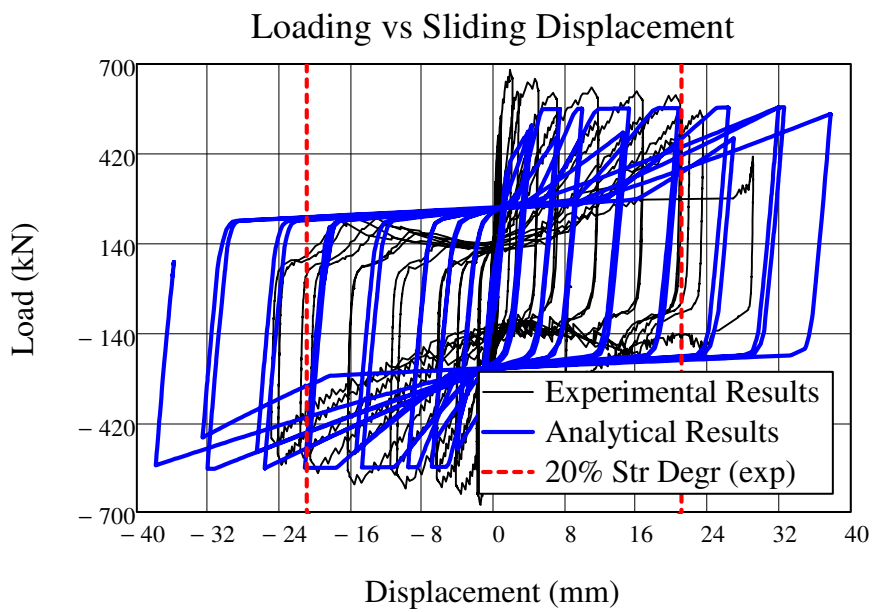
Loading vs Sliding Displacement
700
420
140
– 140
– 420
– 700
Load (kN)
– 40
– 32
– 24
– 16
– 8
0
8
16
24
32
40
Displacement (mm)
Experimental Results
Analytical Results
20% Str Degr (exp)

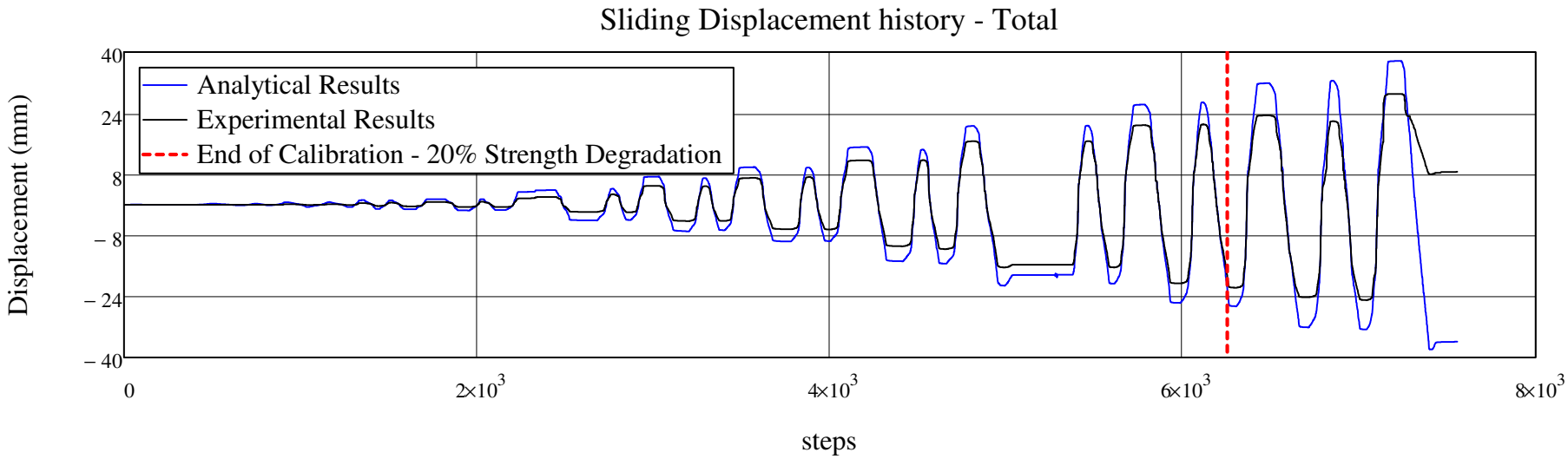

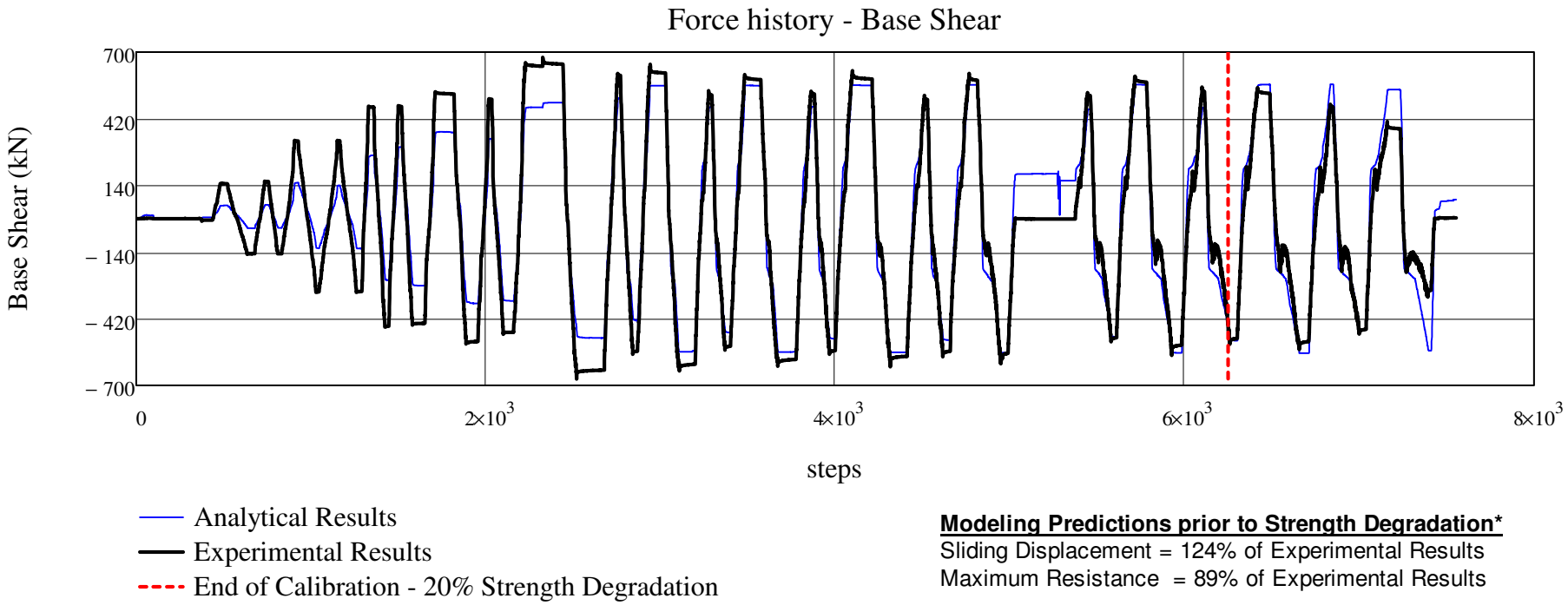

Modeling Predictions prior to Strength Degradation*

Sliding Displacement = 124% of Experimental Results

Maximum Resistance = 89% of Experimental Results

**Strength Degradation @ step 6250*

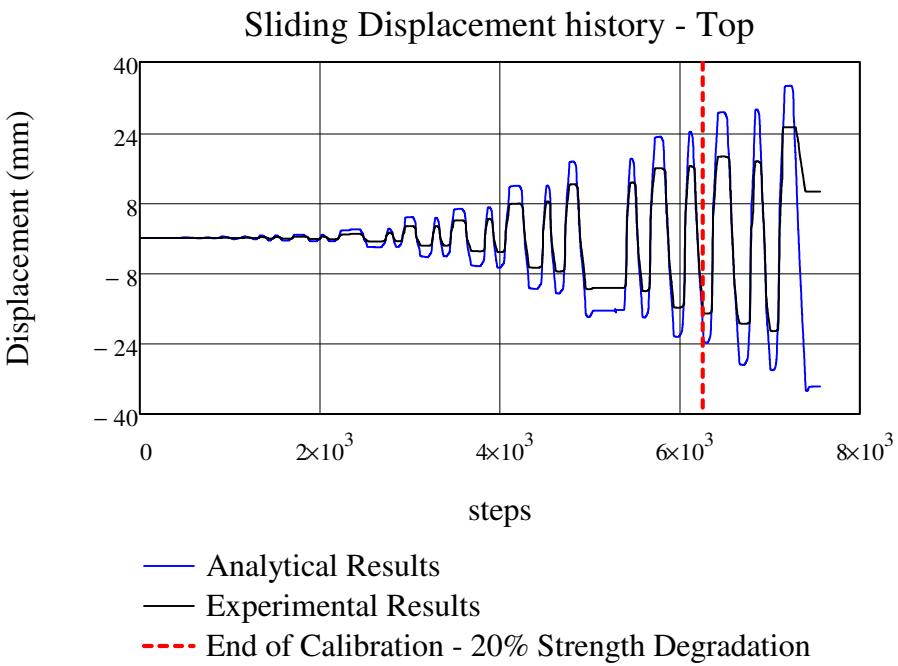
Sliding Displacement history - Top
Displacement (mm)
40
24
8
– 8
– 24
– 40
0
2×10^3
4×10^3
6×10^3
8×10^3
steps
Analytical Results
Experimental Results
End of Calibration - 20% Strength Degradation

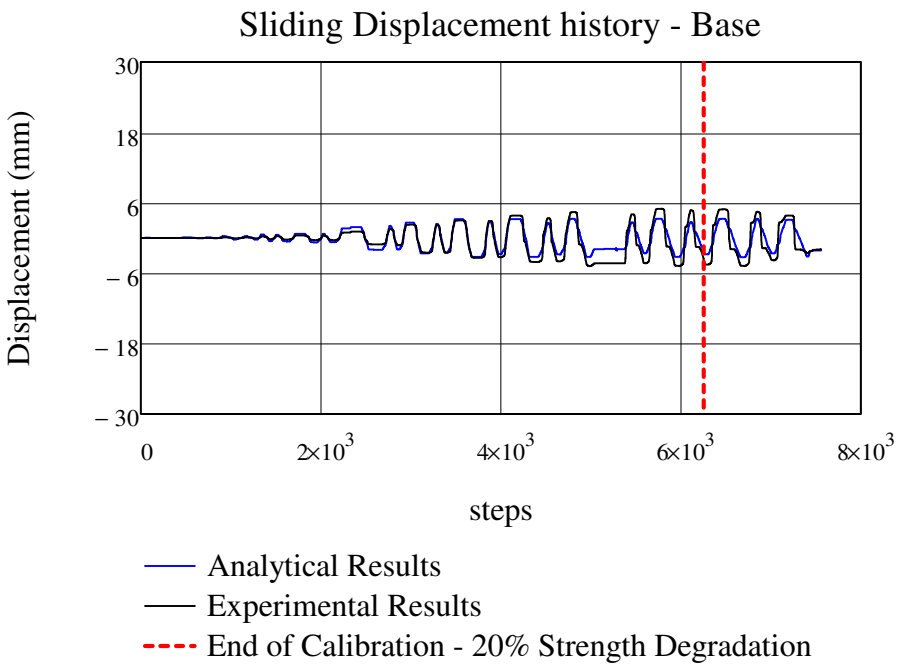
Sliding Displacement history - Base
Displacement (mm)
30
18
6
– 6
– 18
– 30
0
2×10^3
4×10^3
6×10^3
8×10^3
steps
Analytical Results
Experimental Results
End of Calibration - 20% Strength Degradation

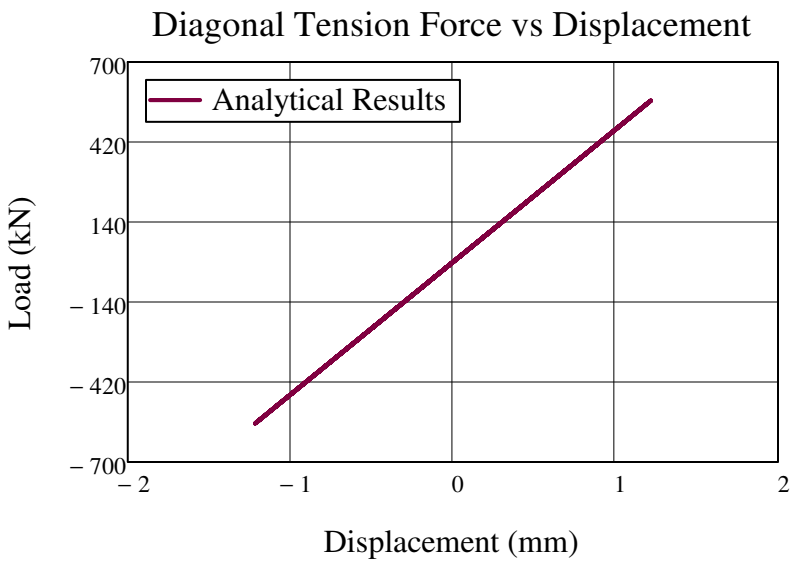
Diagonal Tension Force vs Displacement
Analytical Results
Load (kN)
700
420
140
– 140
– 420
– 700
– 2
– 1
0
1
2
Displacement (mm)

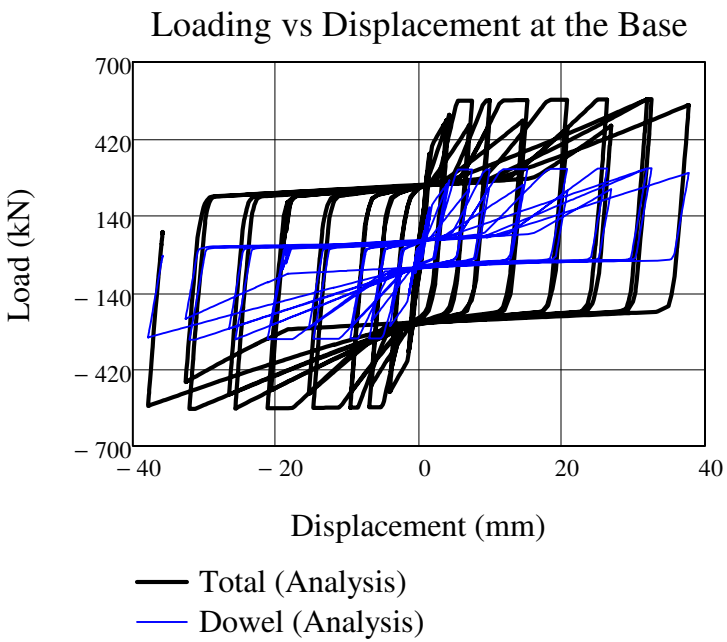
Loading vs Displacement at the Base
Load (kN)
700
420
140
– 140
– 420
– 700
– 40
– 20
0
20
40
Displacement (mm)
Total (Analysis)
Dowel (Analysis)

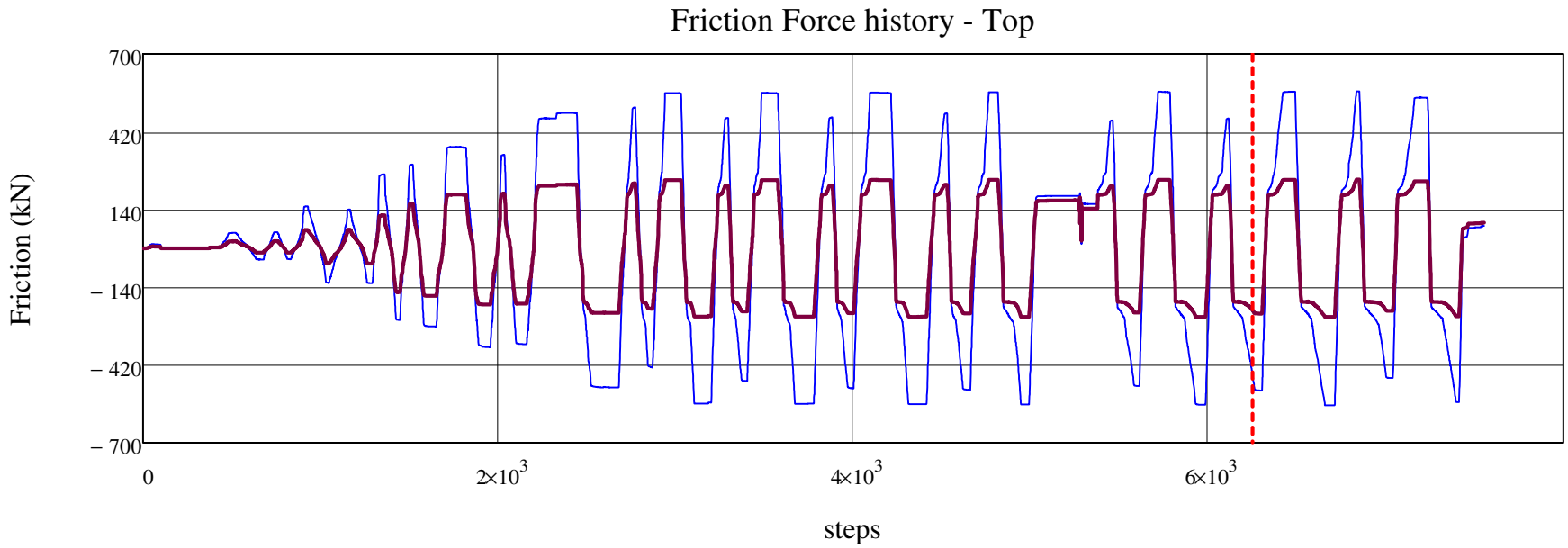

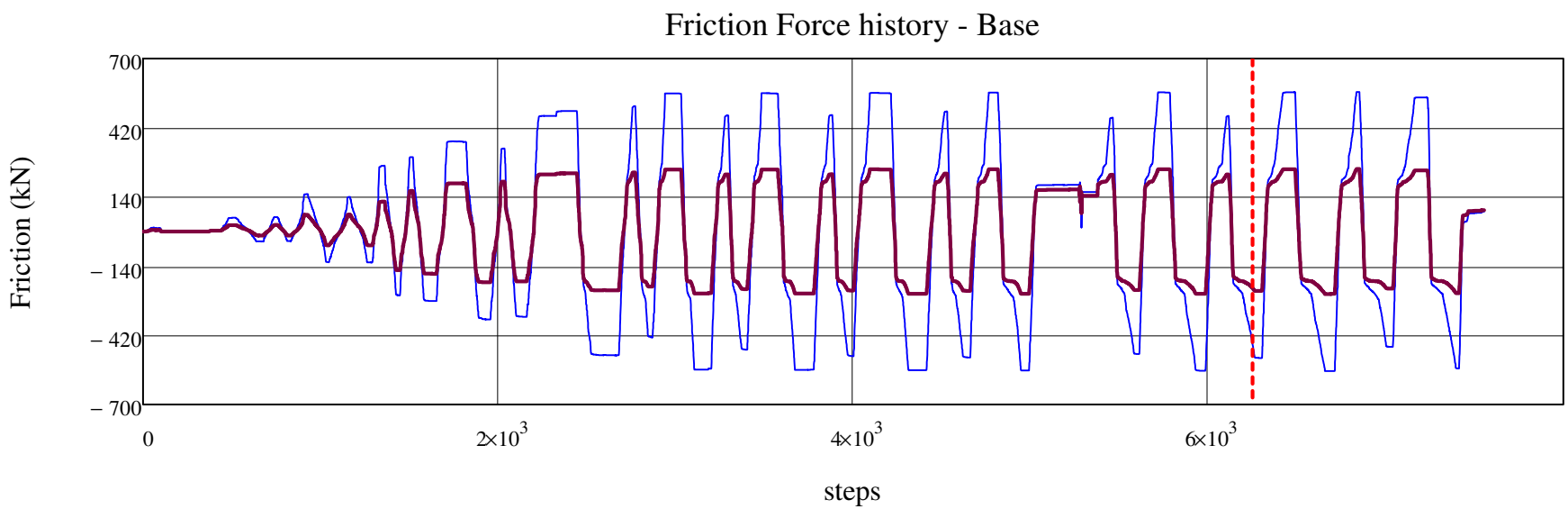

Total Force (Analysis)
Friction Force (Analysis)
End of Calibration - 20% Strength Degradation

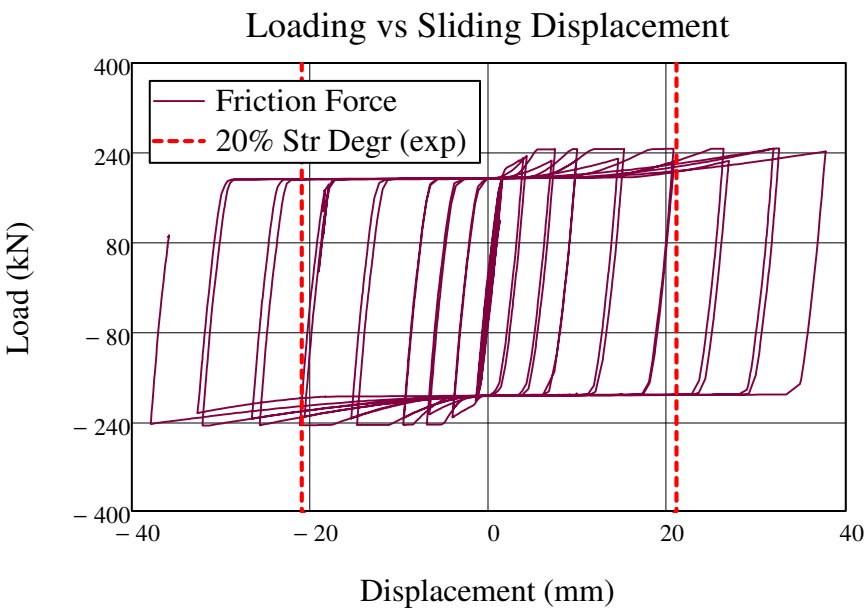
Loading vs Sliding Displacement
Friction Force
20% Str Degr (exp)
Load (kN)
Displacement (mm)
400
240
80
− 80
− 240
− 400
− 40
− 20
0
20
40

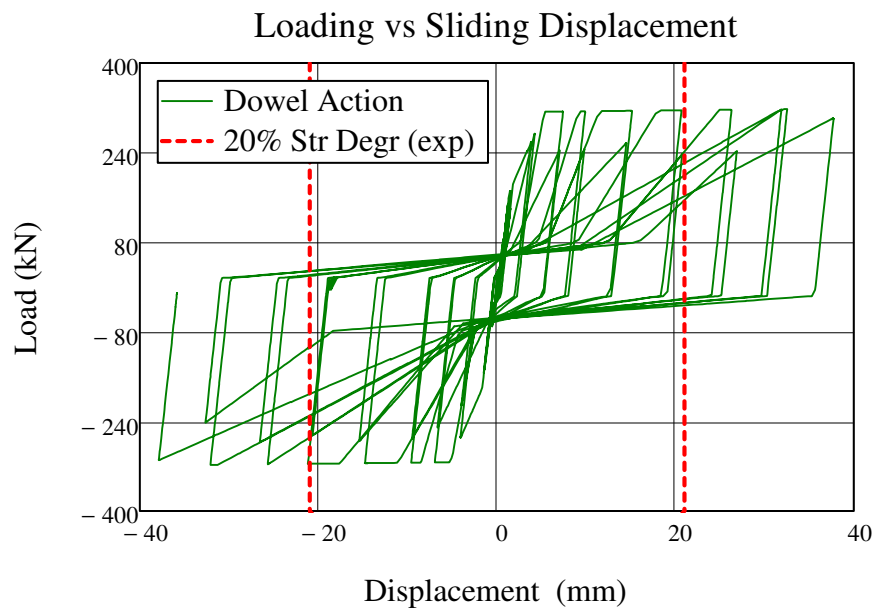
Loading vs Sliding Displacement
Dowel Action
20% Str Degr (exp)
Load (kN)
Displacement (mm)
400
240
80
− 80
− 240
− 400
− 40
− 20
0
20
40

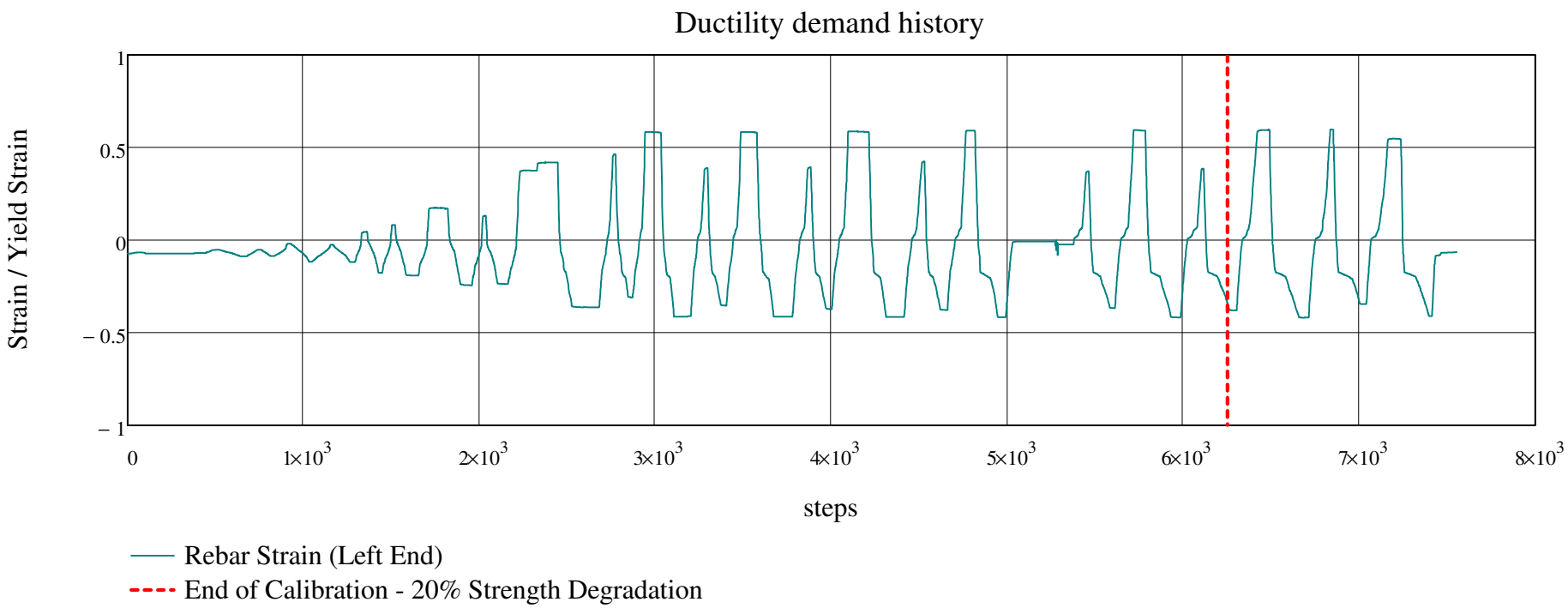
Ductility demand history
Strain / Yield Strain
steps
1
0.5
0
− 0.5
− 1
0
1×10^3
2×10^3
3×10^3
4×10^3
5×10^3
6×10^3
7×10^3
8×10^3
Rebar Strain (Left End)
End of Calibration - 20% Strength Degradation

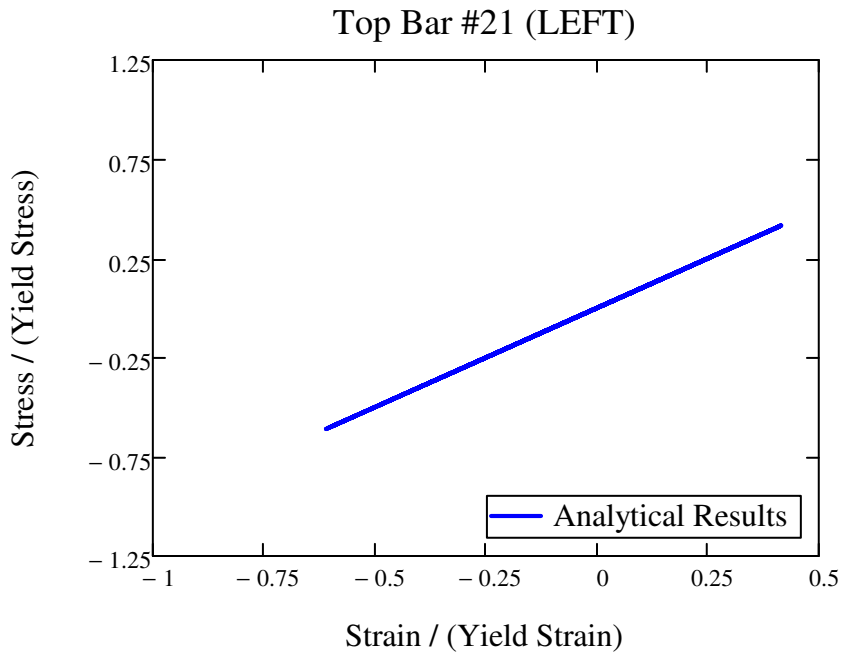
Top Bar #21 (LEFT)
Stress / (Yield Stress)
Strain / (Yield Strain)
Analytical Results
1.25
0.75
0.25
− 0.25
− 0.75
− 1.25
− 1
− 0.75
− 0.5
− 0.25
0
0.25
0.5

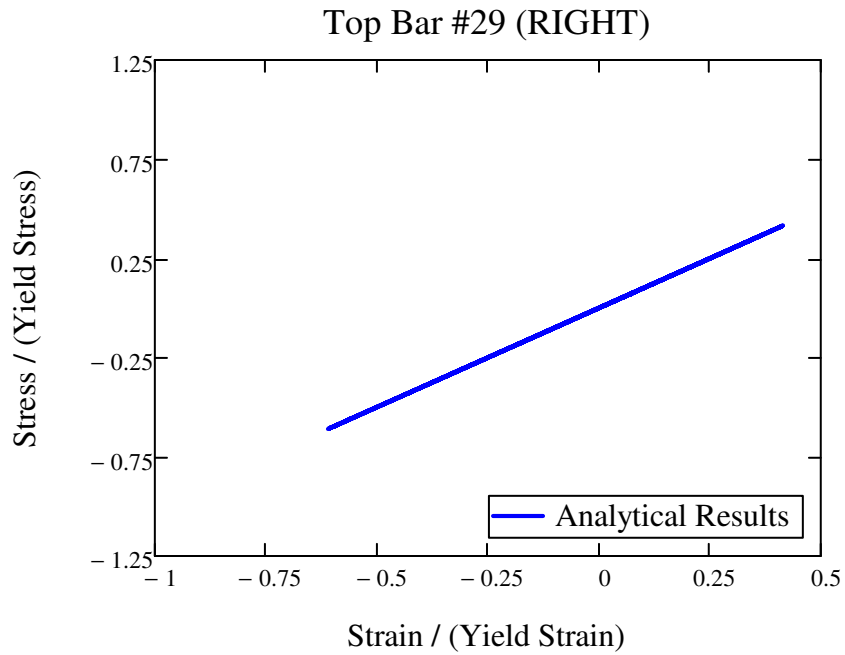
Top Bar #29 (RIGHT)
Stress / (Yield Stress)
Strain / (Yield Strain)
Analytical Results
1.25
0.75
0.25
− 0.25
− 0.75
− 1.25
− 1
− 0.75
− 0.5
− 0.25
0
0.25
0.5

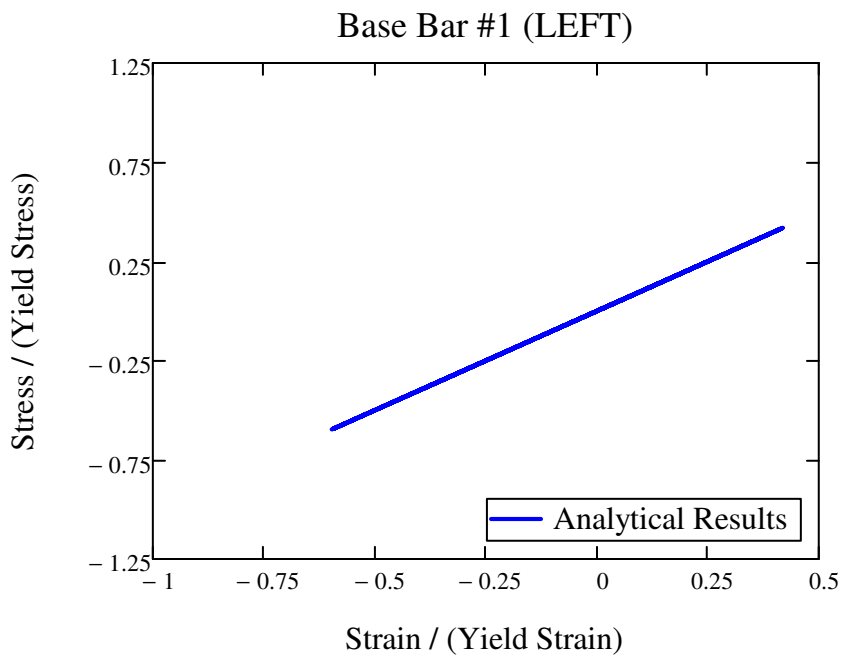
Base Bar #1 (LEFT)
Stress / (Yield Stress)
Strain / (Yield Strain)
Analytical Results
1.25
0.75
0.25
− 0.25
− 0.75
− 1.25
− 1
− 0.75
− 0.5
− 0.25
0
0.25
0.5

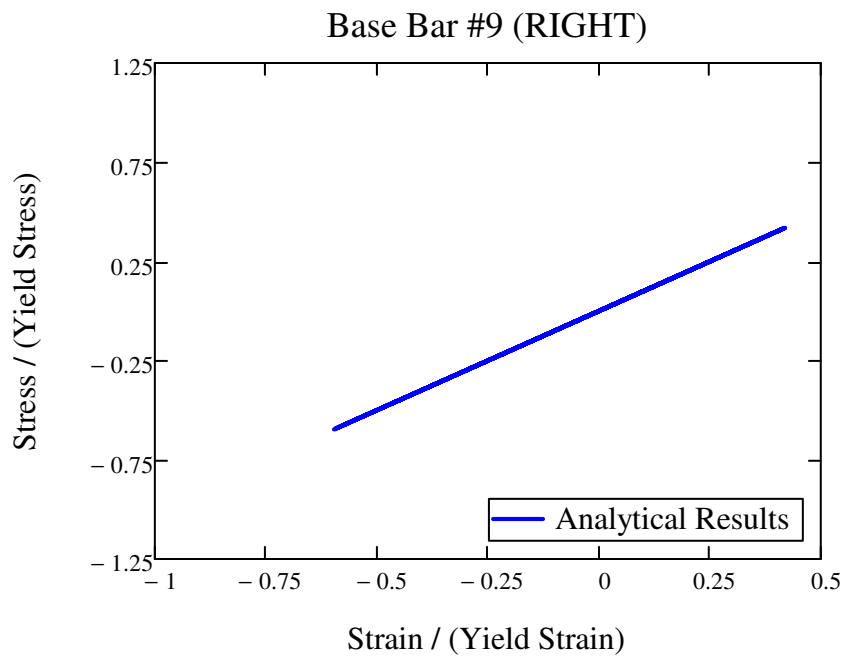
Base Bar #9 (RIGHT)
Stress / (Yield Stress)
Strain / (Yield Strain)
Analytical Results
1.25
0.75
0.25
− 0.25
− 0.75
− 1.25
− 1
− 0.75
− 0.5
− 0.25
0
0.25
0.5

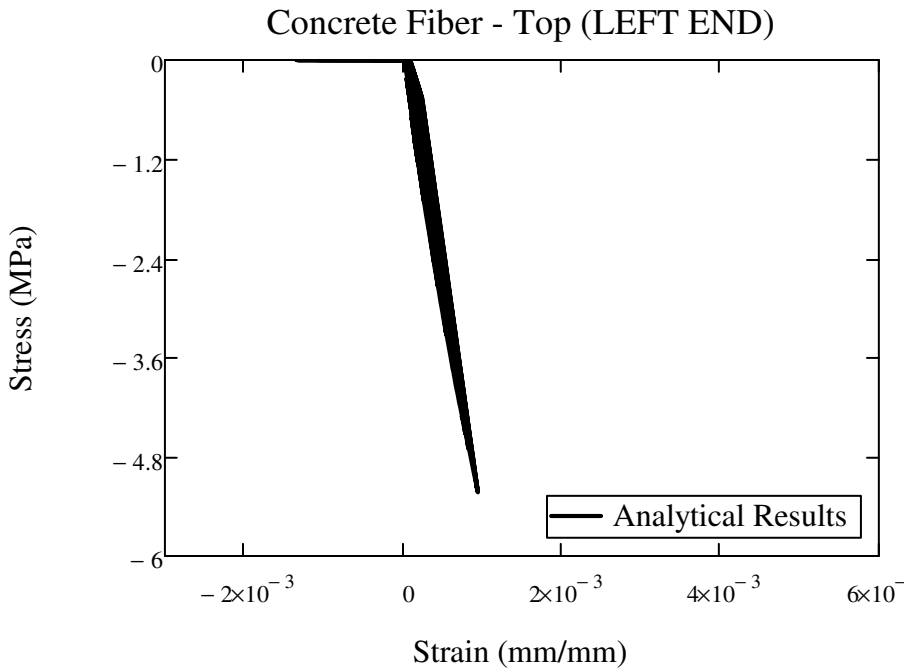
Concrete Fiber - Top (LEFT END)
Stress (MPa)
0
− 1.2
− 2.4
− 3.6
− 4.8
− 6
− 2×10− 3
0
2×10− 3
4×10− 3
6×10−
Strain (mm/mm)
Analytical Results

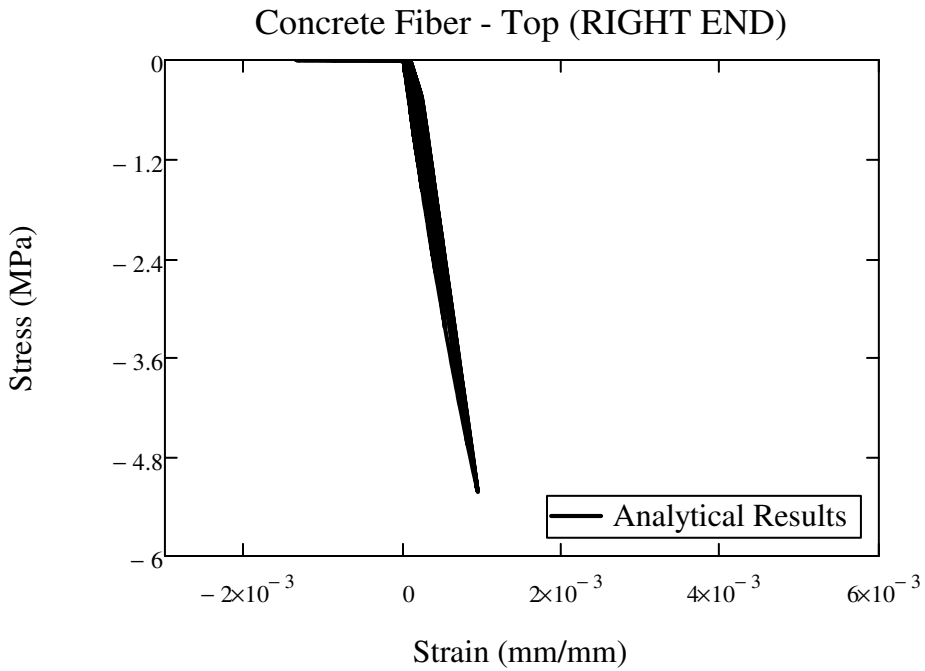
Concrete Fiber - Top (RIGHT END)
Stress (MPa)
0
− 1.2
− 2.4
− 3.6
− 4.8
− 6
− 2×10− 3
0
2×10− 3
4×10− 3
6×10− 3
Strain (mm/mm)
Analytical Results

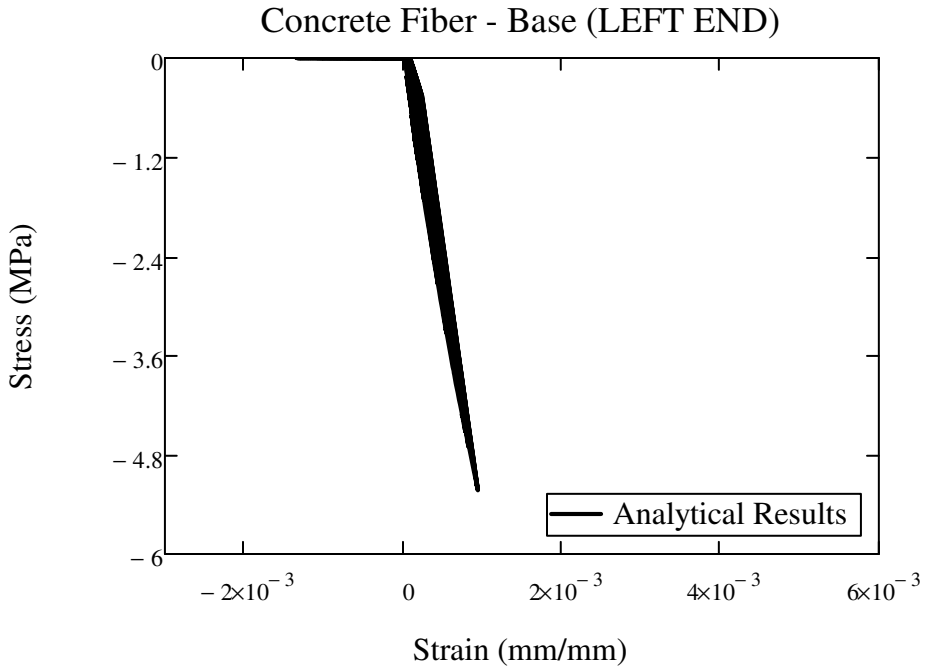
Concrete Fiber - Base (LEFT END)
Stress (MPa)
0
− 1.2
− 2.4
− 3.6
− 4.8
− 6
− 2×10− 3
0
2×10− 3
4×10− 3
6×10− 3
Strain (mm/mm)
Analytical Results

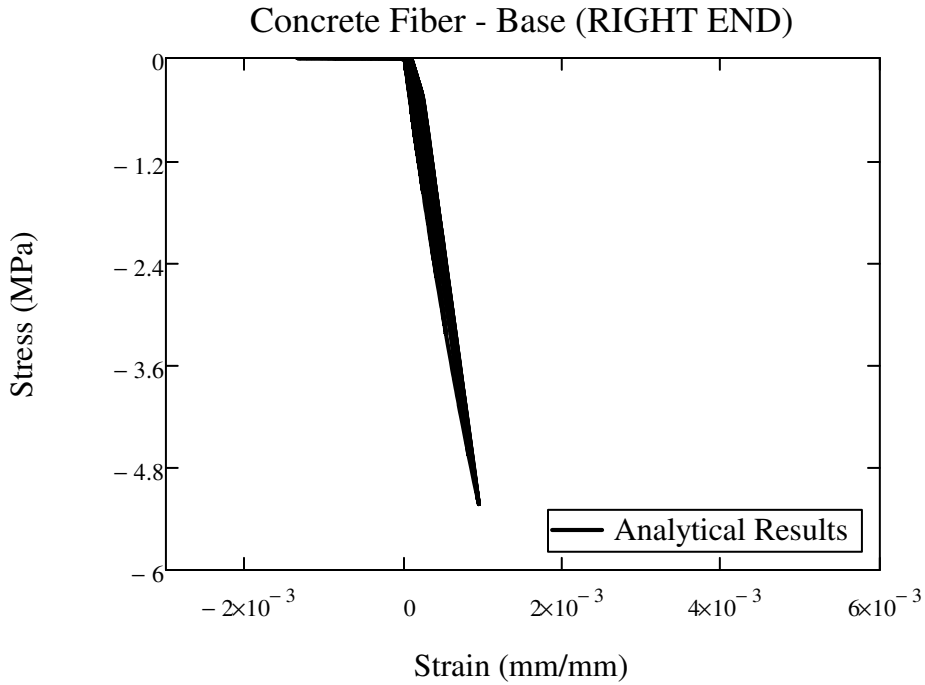
Concrete Fiber - Base (RIGHT END)
Stress (MPa)
0
− 1.2
− 2.4
− 3.6
− 4.8
− 6
− 2×10− 3
0
2×10− 3
4×10− 3
6×10− 3
Strain (mm/mm)
Analytical Results

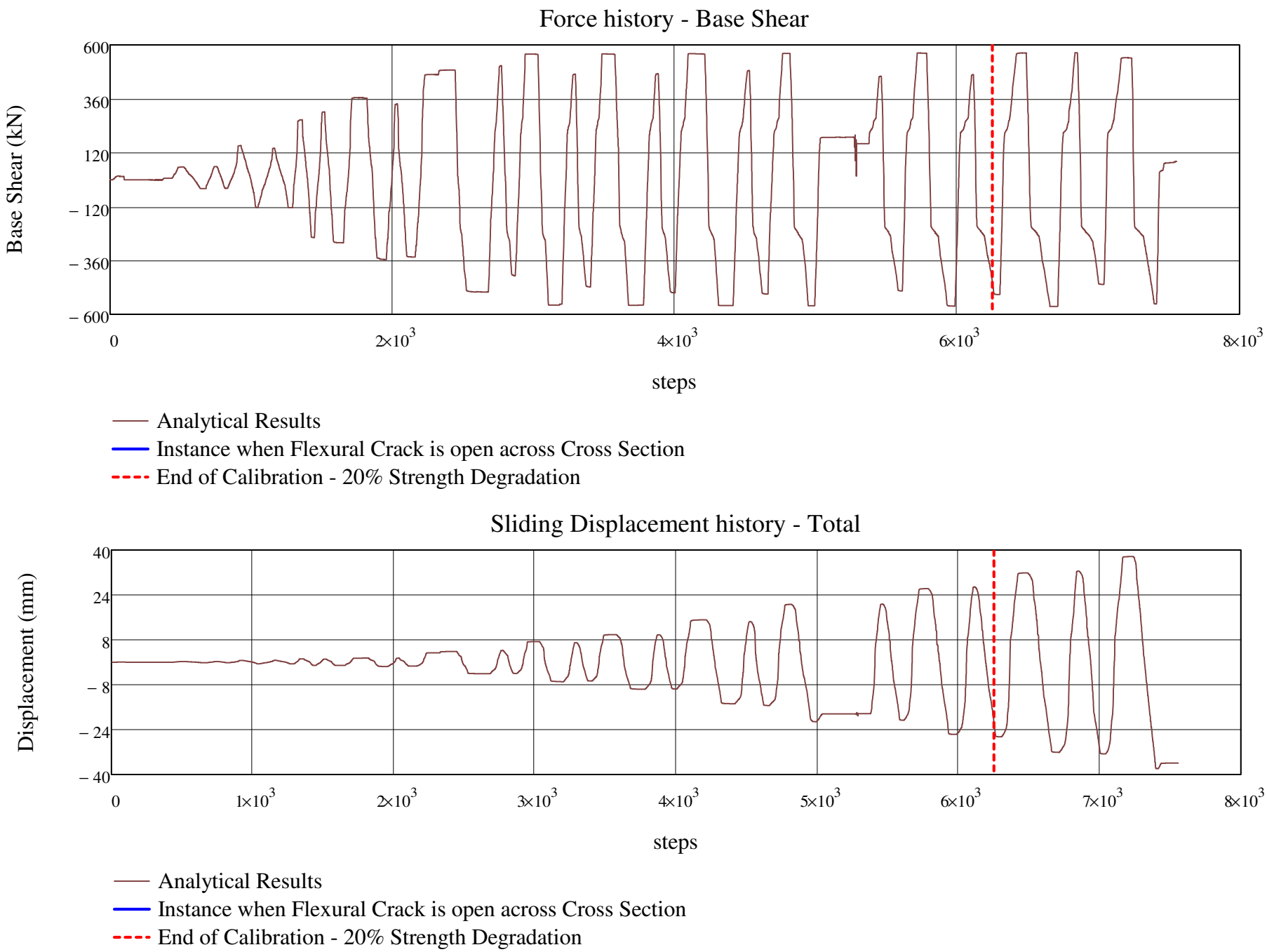
Force history - Base Shear
Base Shear (kN)
600
360
120
− 120
− 360
− 600
0
2×10^3
4×10^3
6×10^3
8×10^3
steps
Analytical Results
Instance when Flexural Crack is open across Cross Section
End of Calibration - 20% Strength Degradation
Sliding Displacement history - Total
Displacement (mm)
40
24
8
− 8
− 24
− 40
0
1×10^3
2×10^3
3×10^3
4×10^3
5×10^3
6×10^3
7×10^3
8×10^3
steps
Analytical Results
Instance when Flexural Crack is open across Cross Section
End of Calibration - 20% Strength Degradation

Calibration of Test Specimen PBS-06

LWall := 1.8 m	fm := 8.5 MPa	Lambda = 1.00	Frict_Coeff = 0.60	DowelCoeff = 2.51	P / (f'm Ag) = 5%
HWall := 1.8 m	fsy := 460 MPa	h := 0.15·LWall	Frict_Yield = 1mm	Dowel_Yield = 2.7mm	P = 303.8 kN
$\rho_v := 0.18\%$					

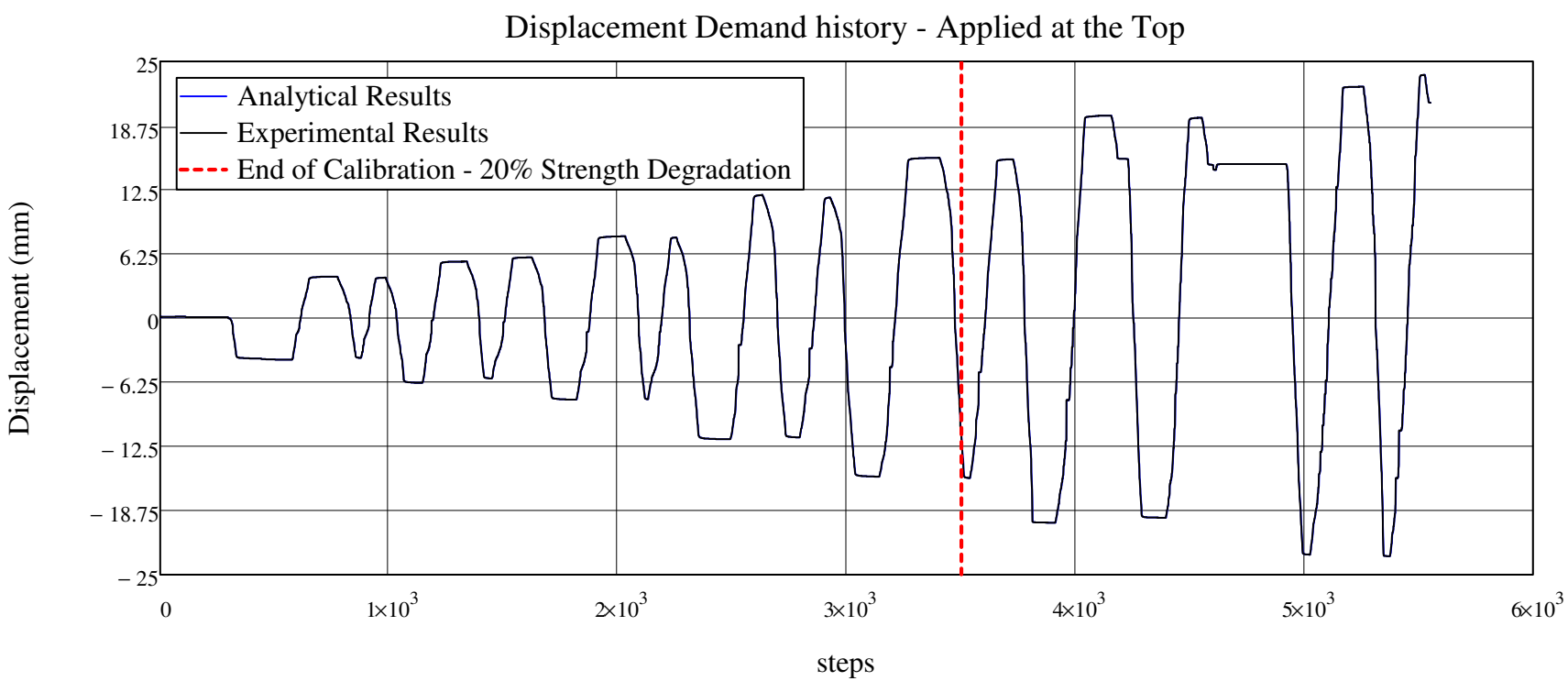

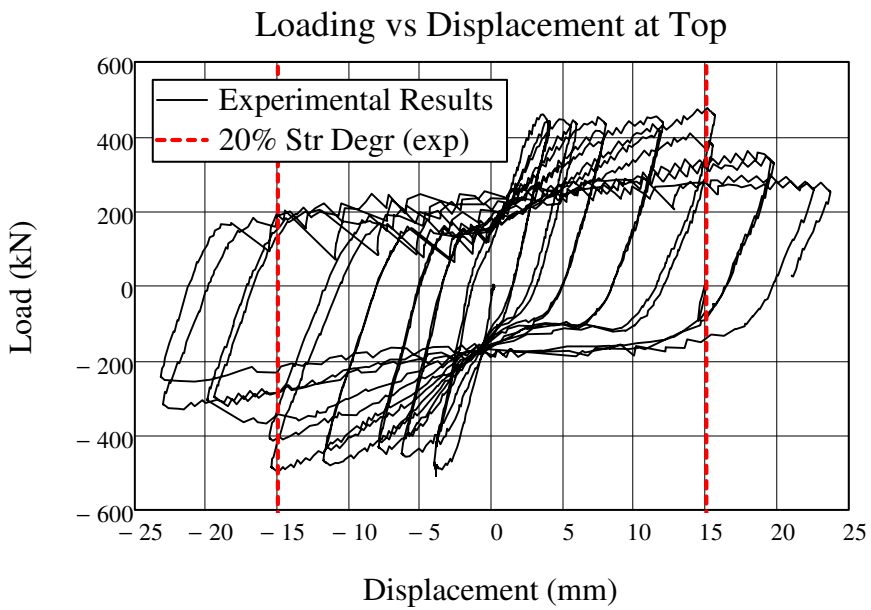
Loading vs Displacement at Top
Experimental Results
20% Str Degr (exp)
Load (kN)
Displacement (mm)
600
400
200
0
– 200
– 400
– 600
– 25
– 20
– 15
– 10
– 5
0
5
10
15
20
25

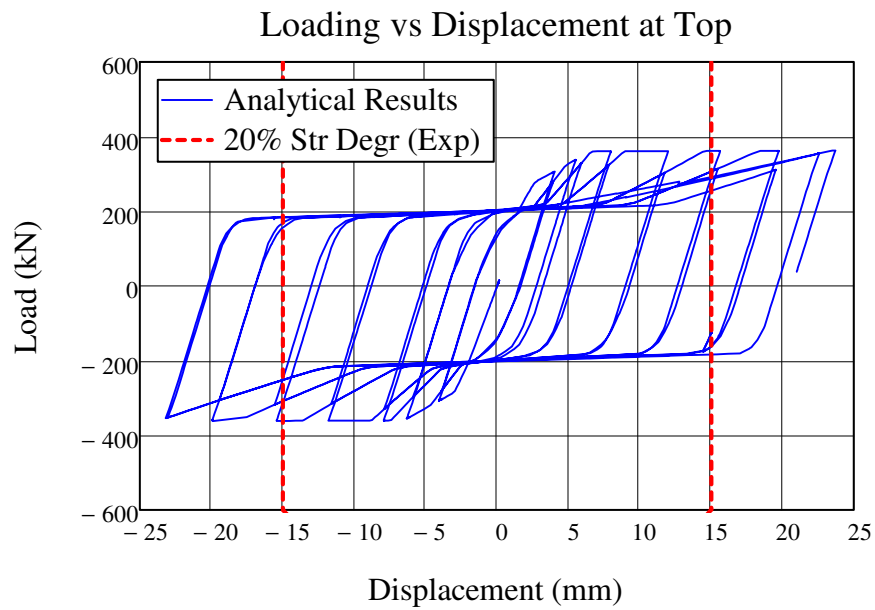
Loading vs Displacement at Top
Analytical Results
20% Str Degr (Exp)
Load (kN)
Displacement (mm)
600
400
200
0
– 200
– 400
– 600
– 25
– 20
– 15
– 10
– 5
0
5
10
15
20
25

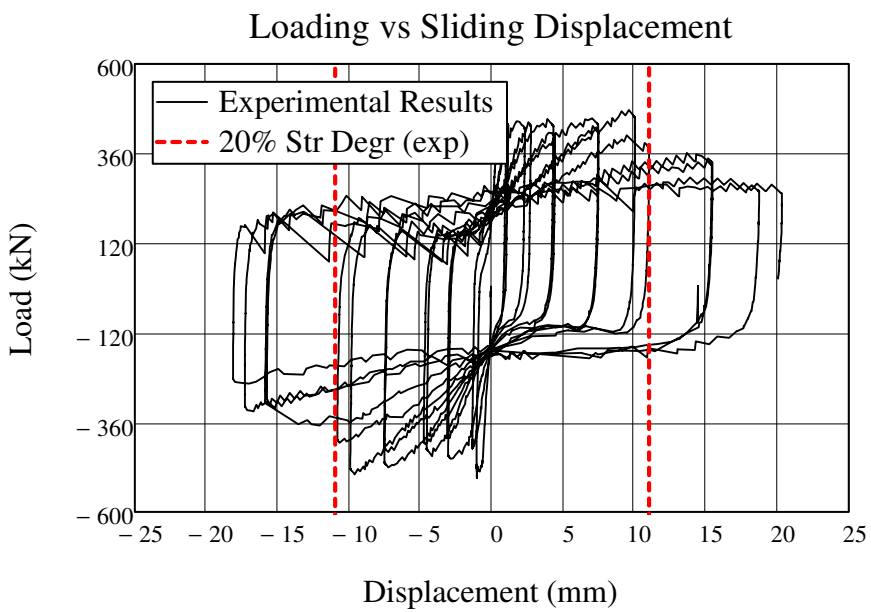
Loading vs Sliding Displacement
Experimental Results
20% Str Degr (exp)
Load (kN)
Displacement (mm)
600
360
120
– 120
– 360
– 600
– 25
– 20
– 15
– 10
– 5
0
5
10
15
20
25

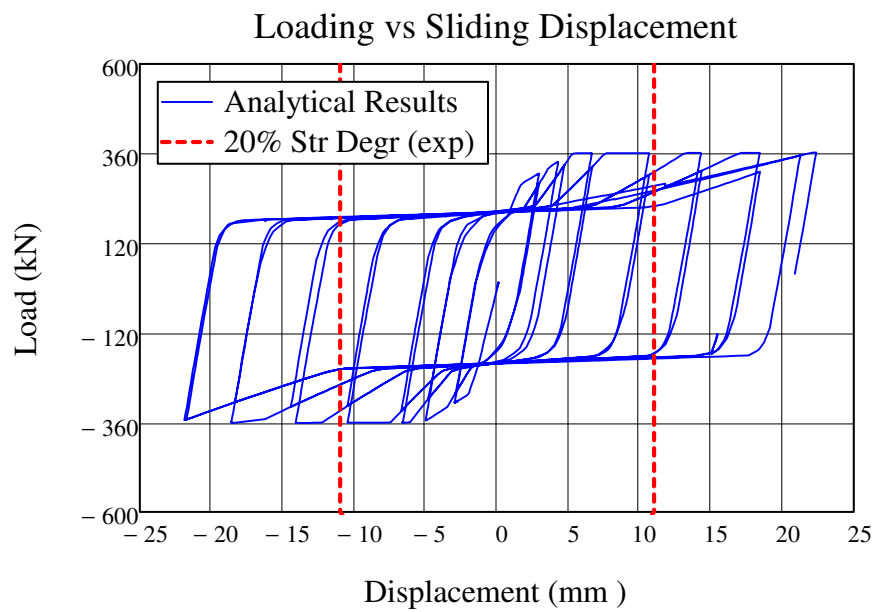
Loading vs Sliding Displacement
Analytical Results
20% Str Degr (exp)
Load (kN)
Displacement (mm)
600
360
120
– 120
– 360
– 600
– 25
– 20
– 15
– 10
– 5
0
5
10
15
20
25

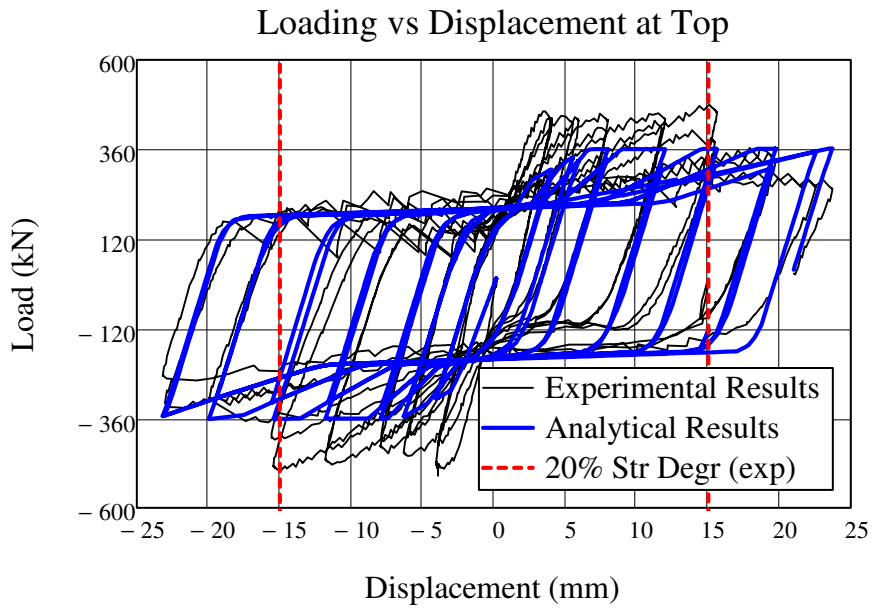
Loading vs Displacement at Top
600
360
120
– 120
– 360
– 600
Load (kN)
– 25
– 20
– 15
– 10
– 5
0
5
10
15
20
25
Displacement (mm)
Experimental Results
Analytical Results
20% Str Degr (exp)

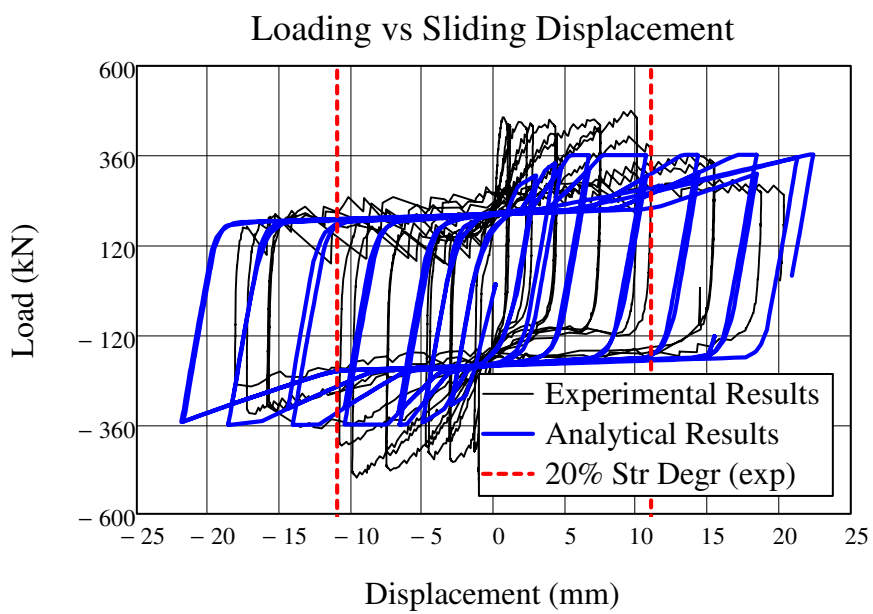
Loading vs Sliding Displacement
600
360
120
– 120
– 360
– 600
Load (kN)
– 25
– 20
– 15
– 10
– 5
0
5
10
15
20
25
Displacement (mm)
Experimental Results
Analytical Results
20% Str Degr (exp)

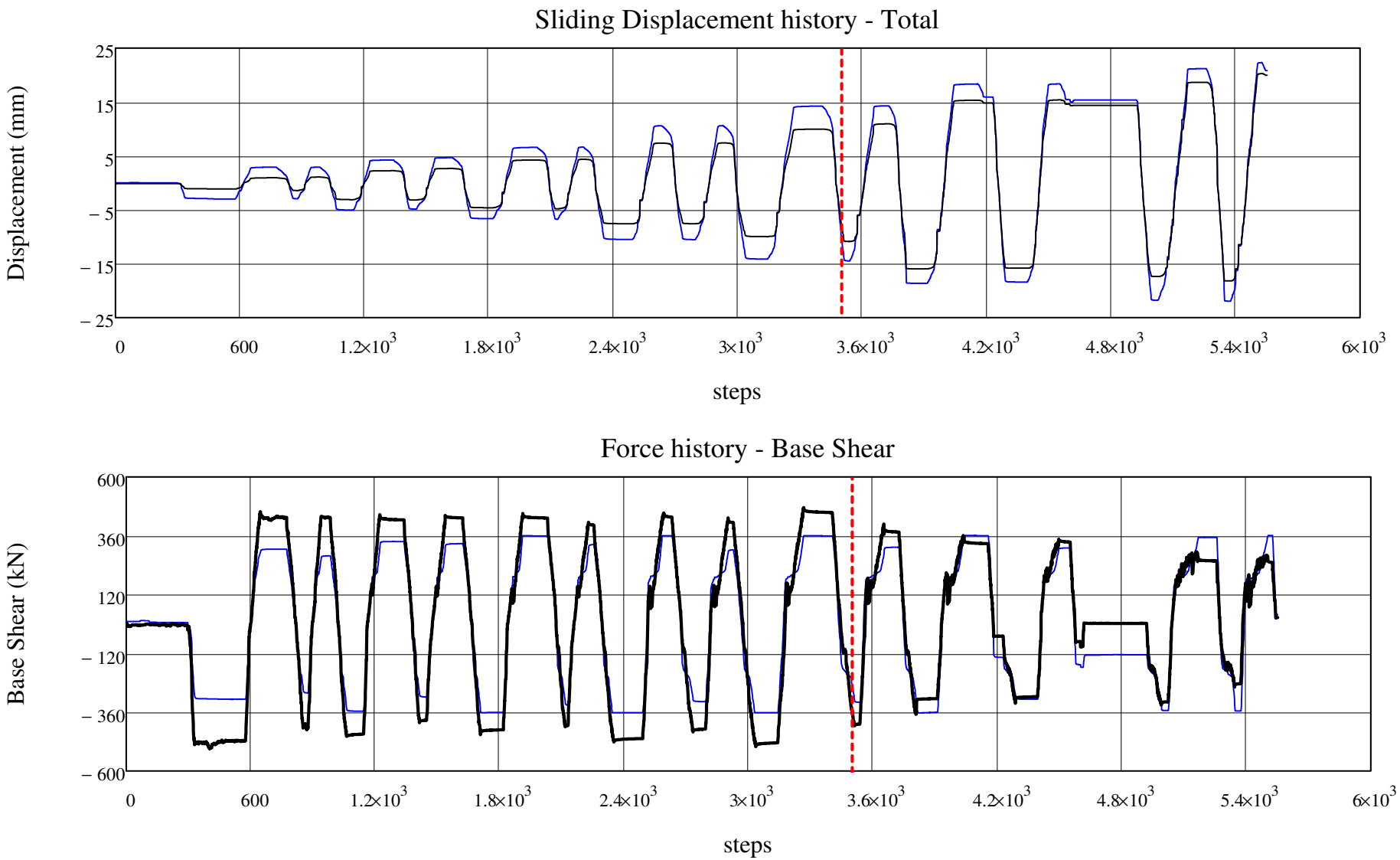

Modeling Predictions prior to Strength Degradation*

Sliding Displacement = 140% of Experimental Results

Maximum Resistance = 78% of Experimental Results

**Strength Degradation @ step 3500*

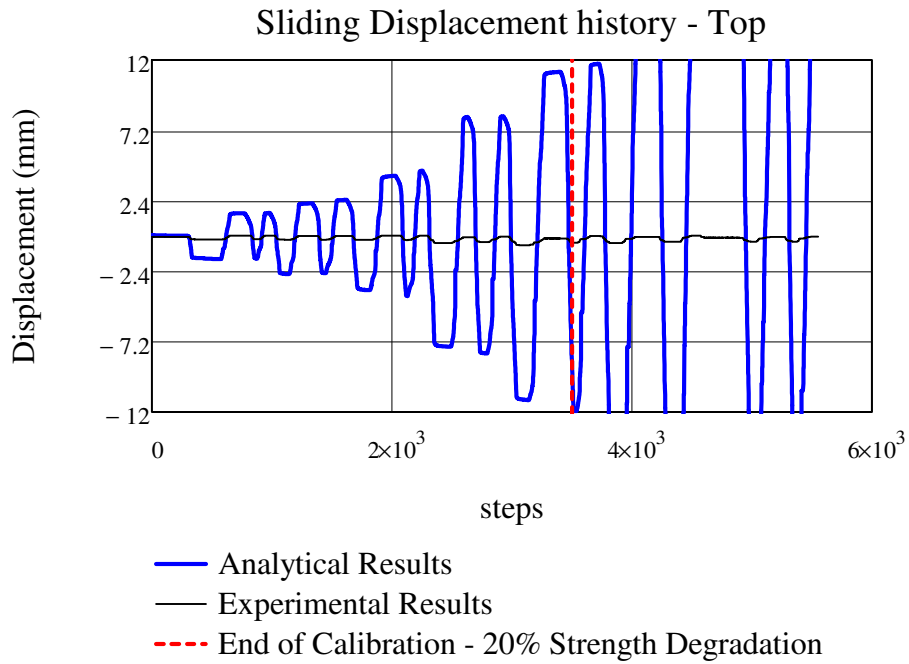
Sliding Displacement history - Top
Displacement (mm)
12
7.2
2.4
– 2.4
– 7.2
– 12
0
2×10^3
4×10^3
6×10^3
steps
Analytical Results
Experimental Results
End of Calibration - 20% Strength Degradation

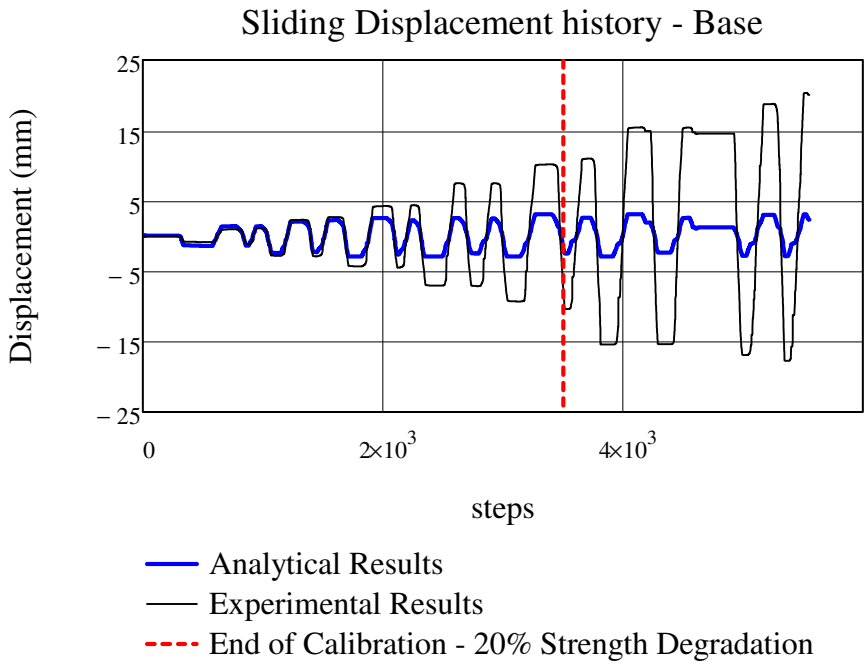
Sliding Displacement history - Base
Displacement (mm)
25
15
5
– 5
– 15
– 25
0
2×10^3
4×10^3
steps
Analytical Results
Experimental Results
End of Calibration - 20% Strength Degradation

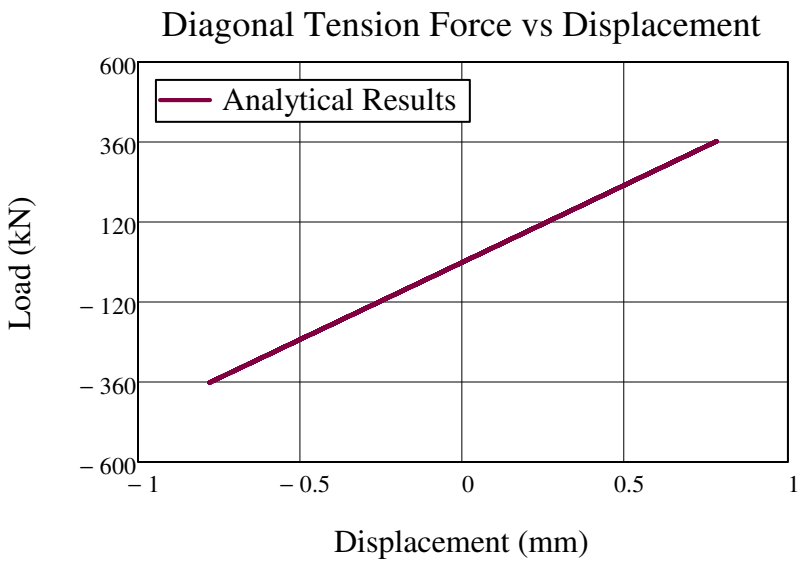
Diagonal Tension Force vs Displacement
Analytical Results
Load (kN)
600
360
120
– 120
– 360
– 600
– 1
– 0.5
0
0.5
1
Displacement (mm)

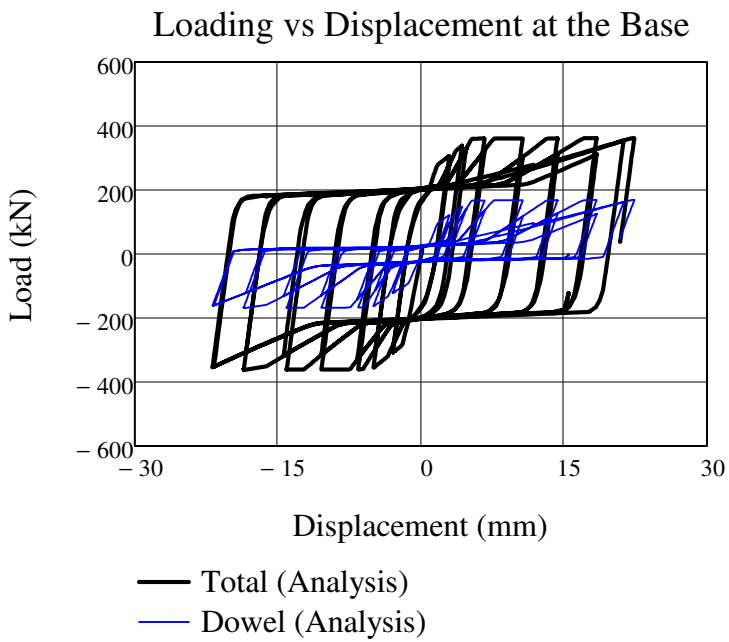
Loading vs Displacement at the Base
Load (kN)
600
400
200
0
– 200
– 400
– 600
– 30
– 15
0
15
30
Displacement (mm)
Total (Analysis)
Dowel (Analysis)

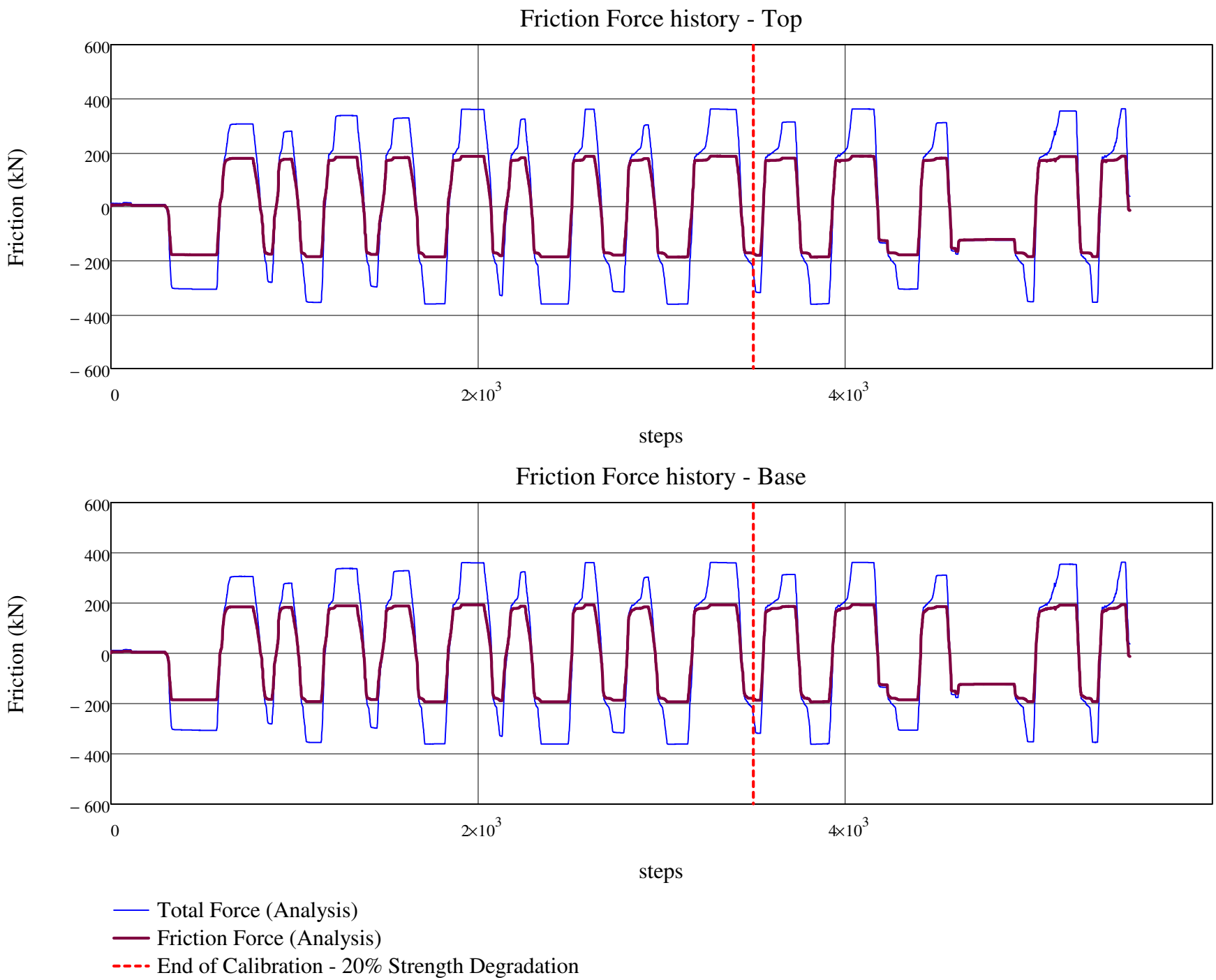
Friction Force history - Top
Friction (kN)
600
400
200
0
– 200
– 400
– 600
0
2×10^3
4×10^3
steps
Friction Force history - Base
Friction (kN)
600
400
200
0
– 200
– 400
– 600
0
2×10^3
4×10^3
steps
Total Force (Analysis)
Friction Force (Analysis)
End of Calibration - 20% Strength Degradation

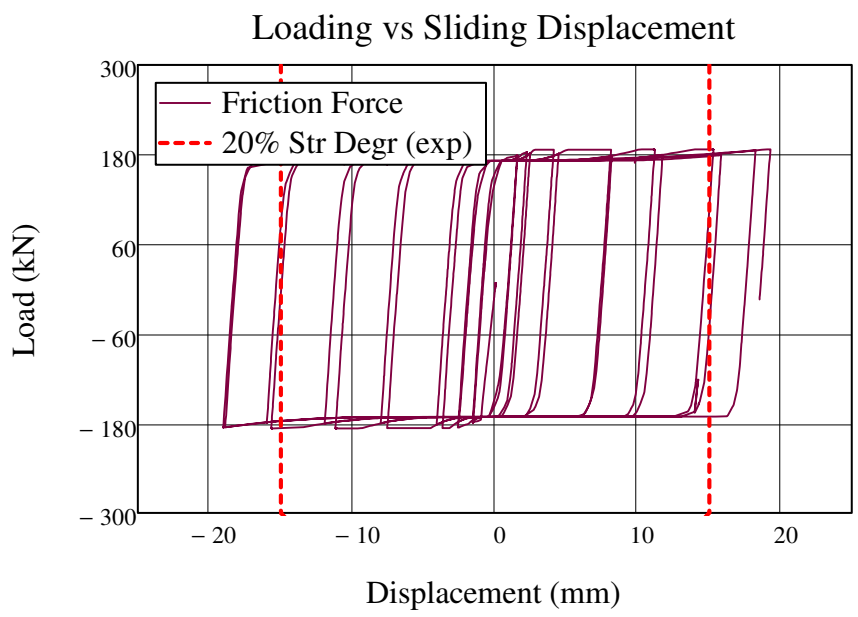
Loading vs Sliding Displacement
Friction Force
20% Str Degr (exp)
Load (kN)
300
180
60
− 60
− 180
− 300
− 20
− 10
0
10
20
Displacement (mm)

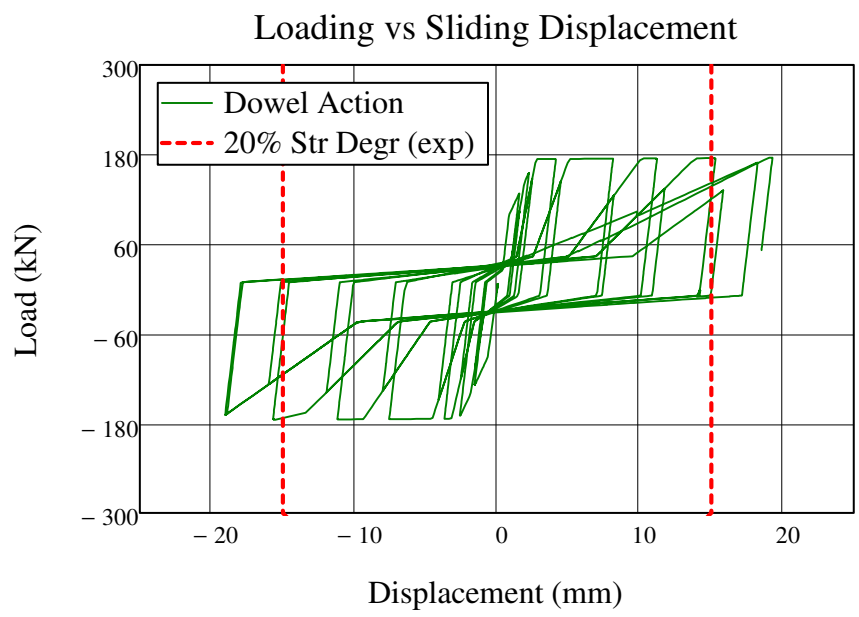
Loading vs Sliding Displacement
Dowel Action
20% Str Degr (exp)
Load (kN)
300
180
60
− 60
− 180
− 300
− 20
− 10
0
10
20
Displacement (mm)

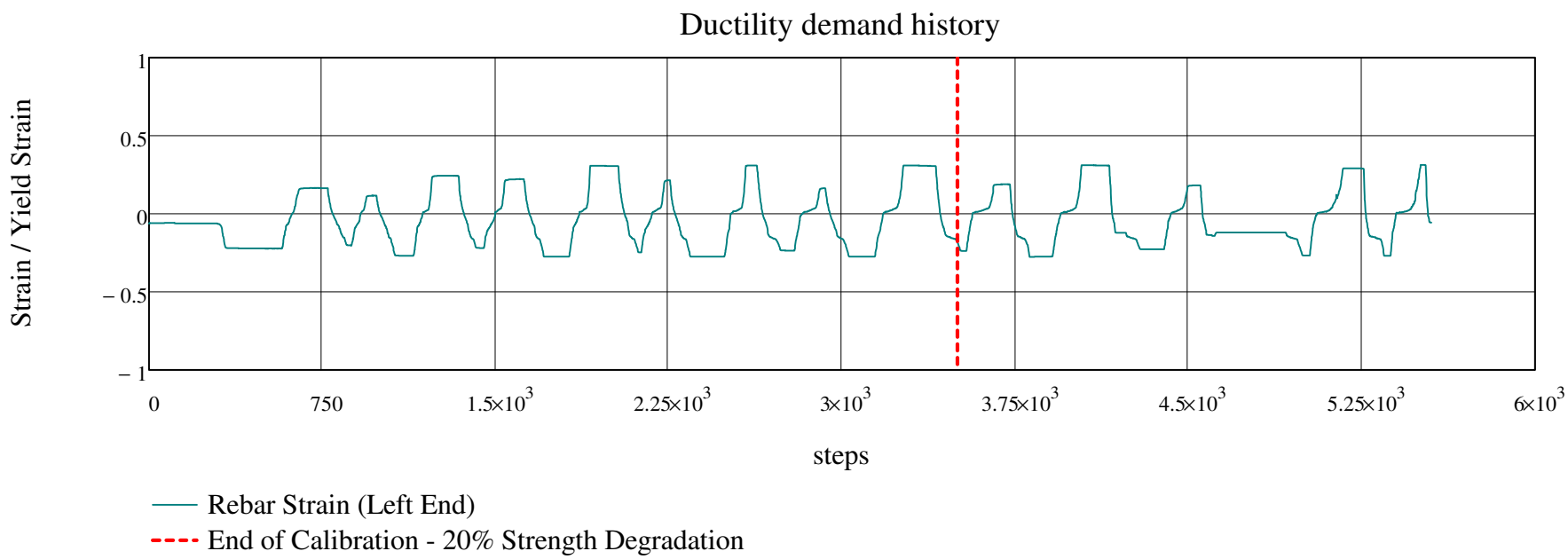
Ductility demand history
Strain / Yield Strain
1
0.5
0
− 0.5
− 1
0
750
1.5×10^3
2.25×10^3
3×10^3
3.75×10^3
4.5×10^3
5.25×10^3
6×10^3
steps
Rebar Strain (Left End)
End of Calibration - 20% Strength Degradation

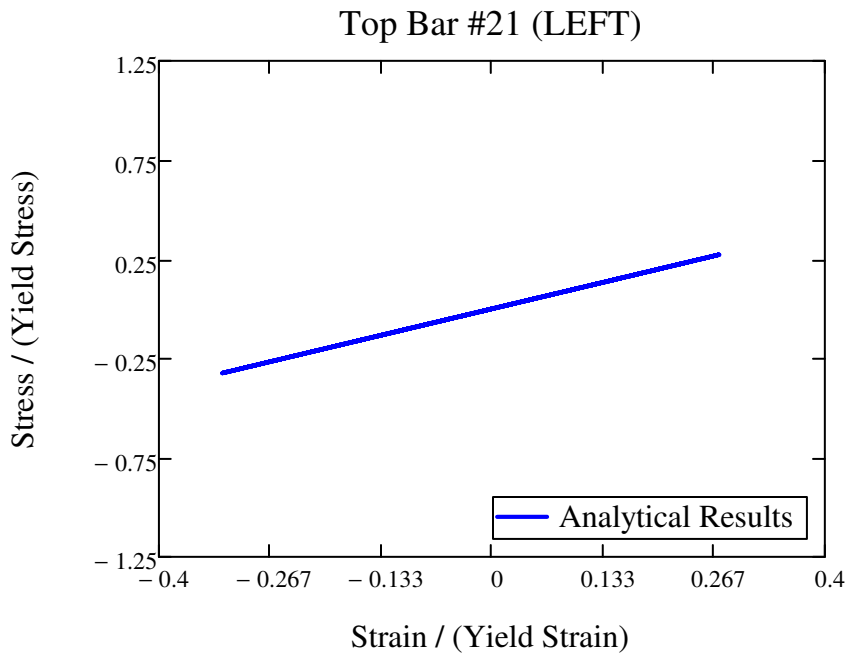
Top Bar #21 (LEFT)
Stress / (Yield Stress)
1.25
0.75
0.25
− 0.25
− 0.75
− 1.25
− 0.4
− 0.267
− 0.133
0
0.133
0.267
0.4
Strain / (Yield Strain)
Analytical Results

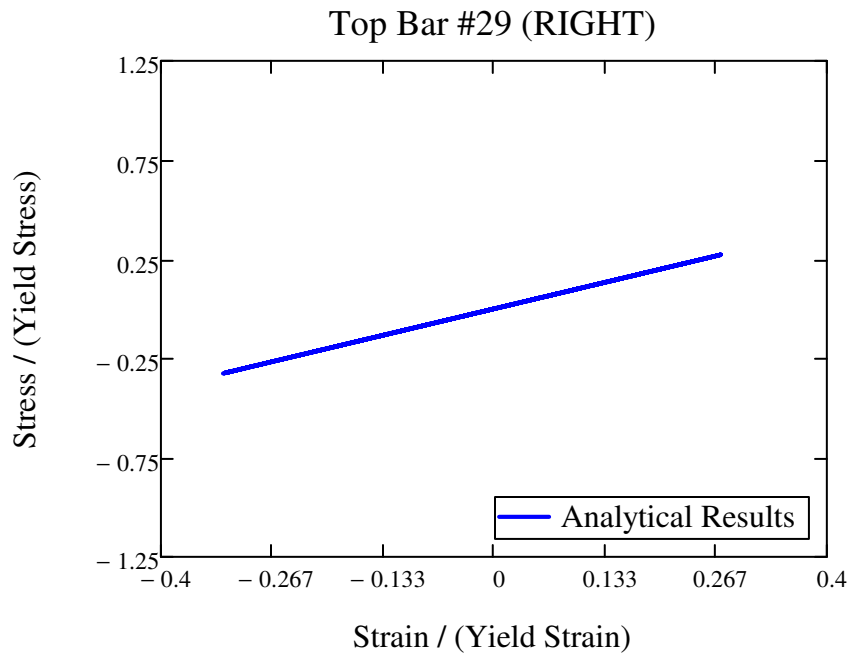
Top Bar #29 (RIGHT)
Stress / (Yield Stress)
1.25
0.75
0.25
− 0.25
− 0.75
− 1.25
− 0.4
− 0.267
− 0.133
0
0.133
0.267
0.4
Strain / (Yield Strain)
Analytical Results

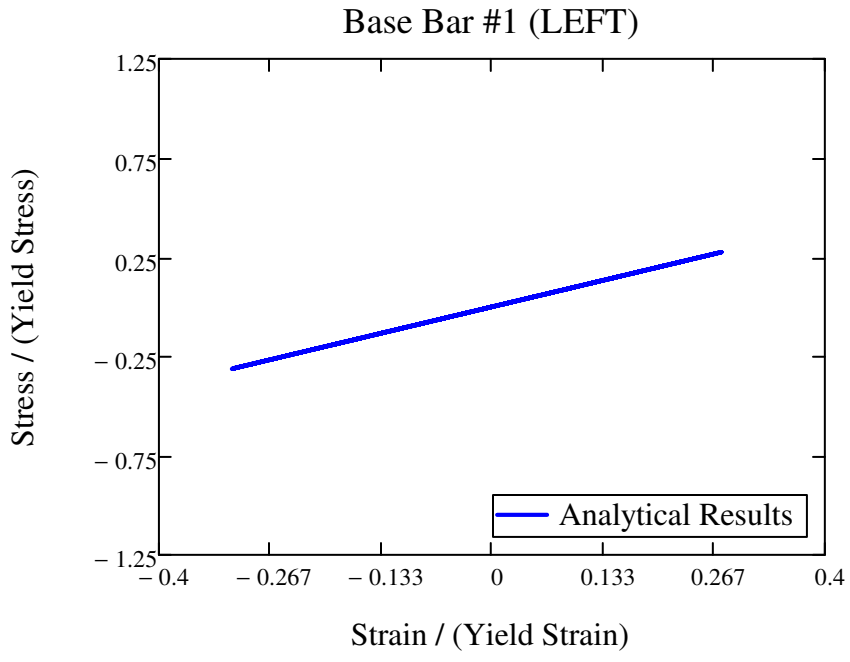
Base Bar #1 (LEFT)
Stress / (Yield Stress)
1.25
0.75
0.25
− 0.25
− 0.75
− 1.25
− 0.4
− 0.267
− 0.133
0
0.133
0.267
0.4
Strain / (Yield Strain)
Analytical Results

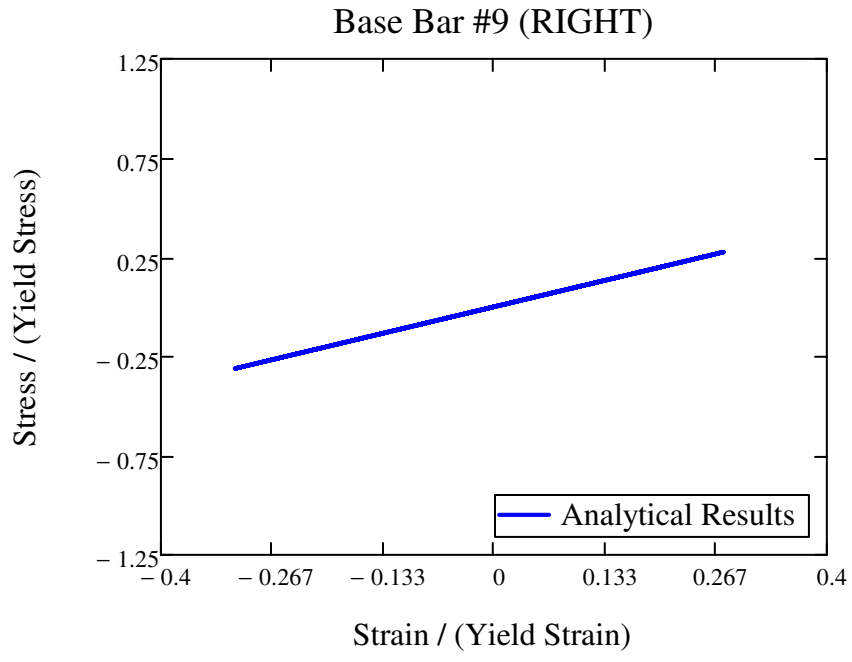
Base Bar #9 (RIGHT)
Stress / (Yield Stress)
1.25
0.75
0.25
− 0.25
− 0.75
− 1.25
− 0.4
− 0.267
− 0.133
0
0.133
0.267
0.4
Strain / (Yield Strain)
Analytical Results

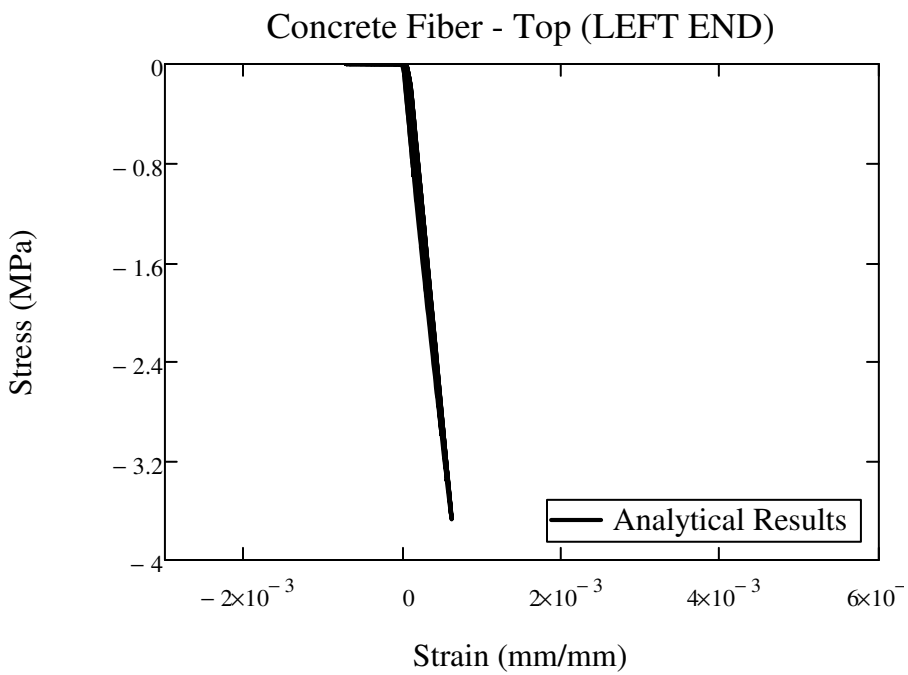
Concrete Fiber - Top (LEFT END)
Stress (MPa)
0
− 0.8
− 1.6
− 2.4
− 3.2
− 4
− 2×10⁻³
0
2×10⁻³
4×10⁻³
6×10⁻
Strain (mm/mm)
Analytical Results

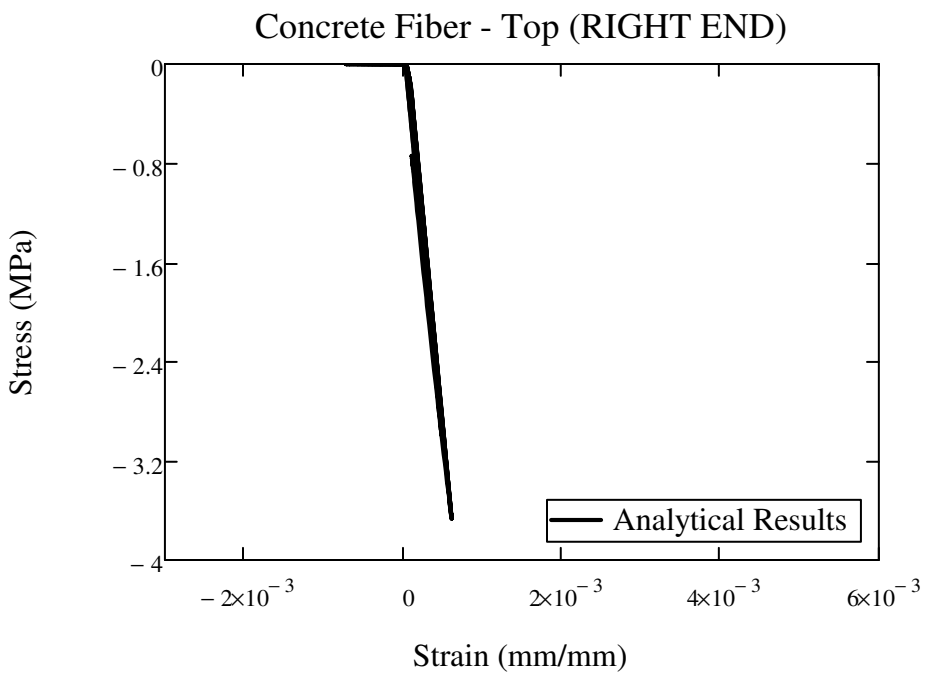
Concrete Fiber - Top (RIGHT END)
Stress (MPa)
0
− 0.8
− 1.6
− 2.4
− 3.2
− 4
− 2×10⁻³
0
2×10⁻³
4×10⁻³
6×10⁻³
Strain (mm/mm)
Analytical Results

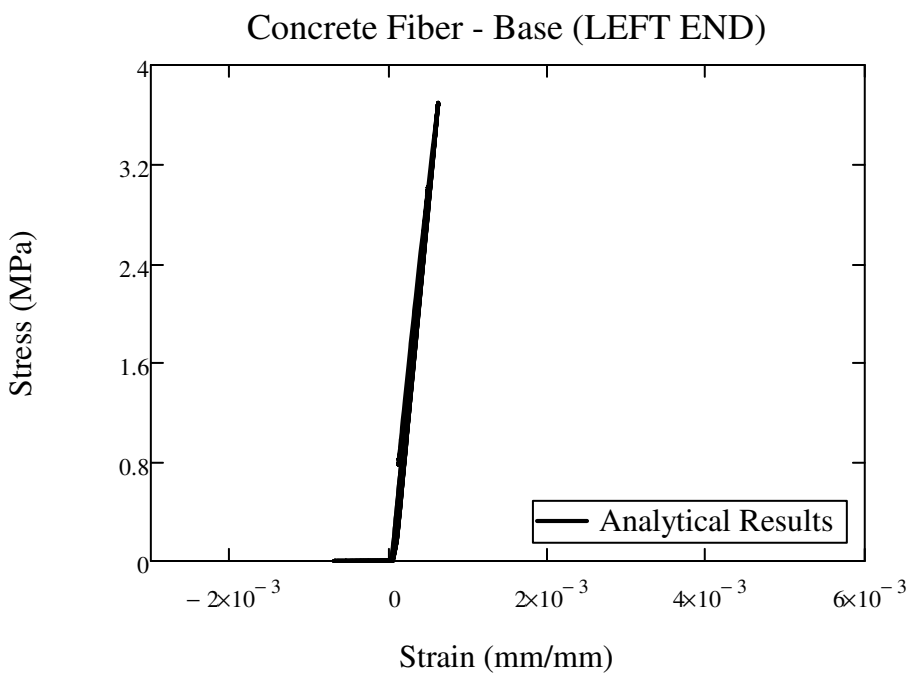
Concrete Fiber - Base (LEFT END)
Stress (MPa)
4
3.2
2.4
1.6
0.8
0
− 2×10⁻³
0
2×10⁻³
4×10⁻³
6×10⁻³
Strain (mm/mm)
Analytical Results

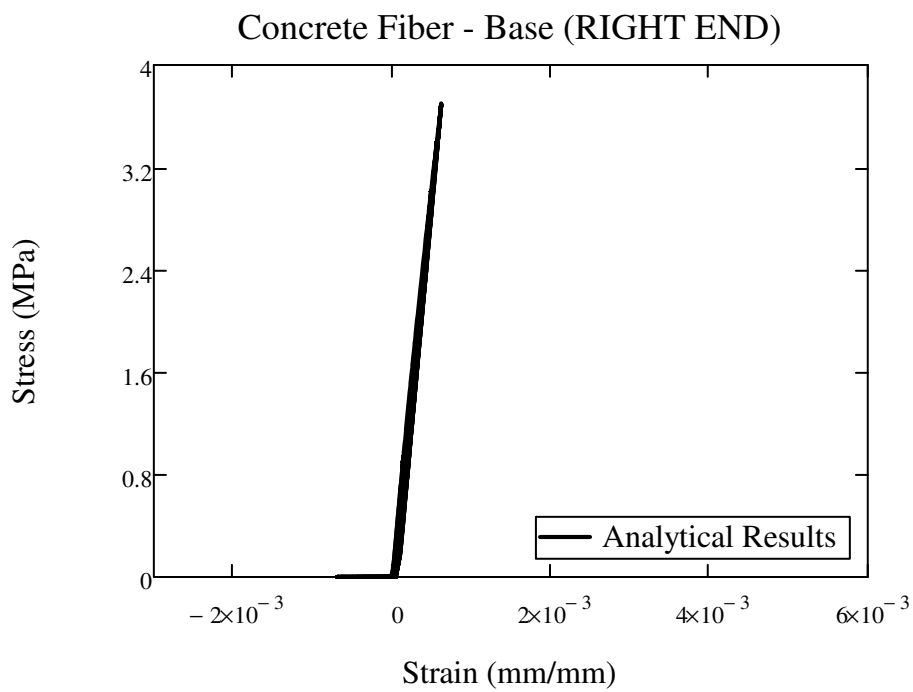
Concrete Fiber - Base (RIGHT END)
Stress (MPa)
4
3.2
2.4
1.6
0.8
0
− 2×10⁻³
0
2×10⁻³
4×10⁻³
6×10⁻³
Strain (mm/mm)
Analytical Results

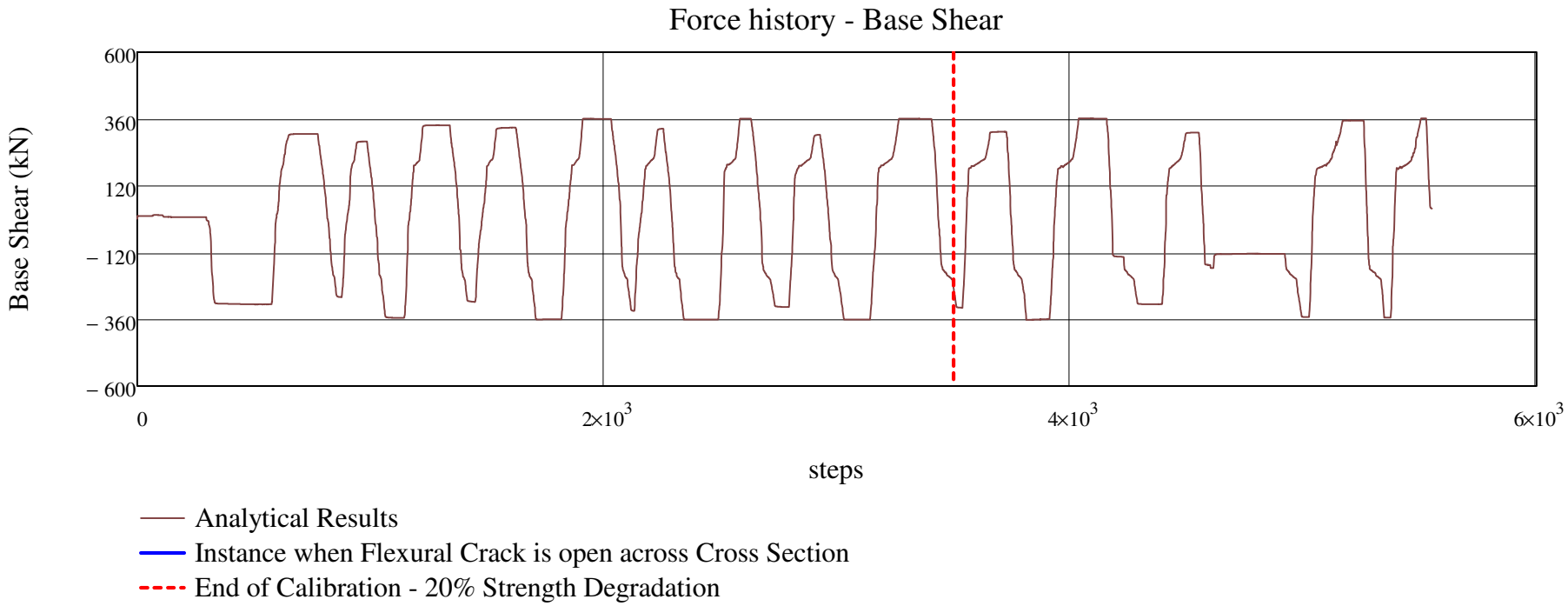
Force history - Base Shear
Base Shear (kN)
600
360
120
– 120
– 360
– 600
0
2×10^3
4×10^3
6×10^3
steps
Analytical Results
Instance when Flexural Crack is open across Cross Section
End of Calibration - 20% Strength Degradation

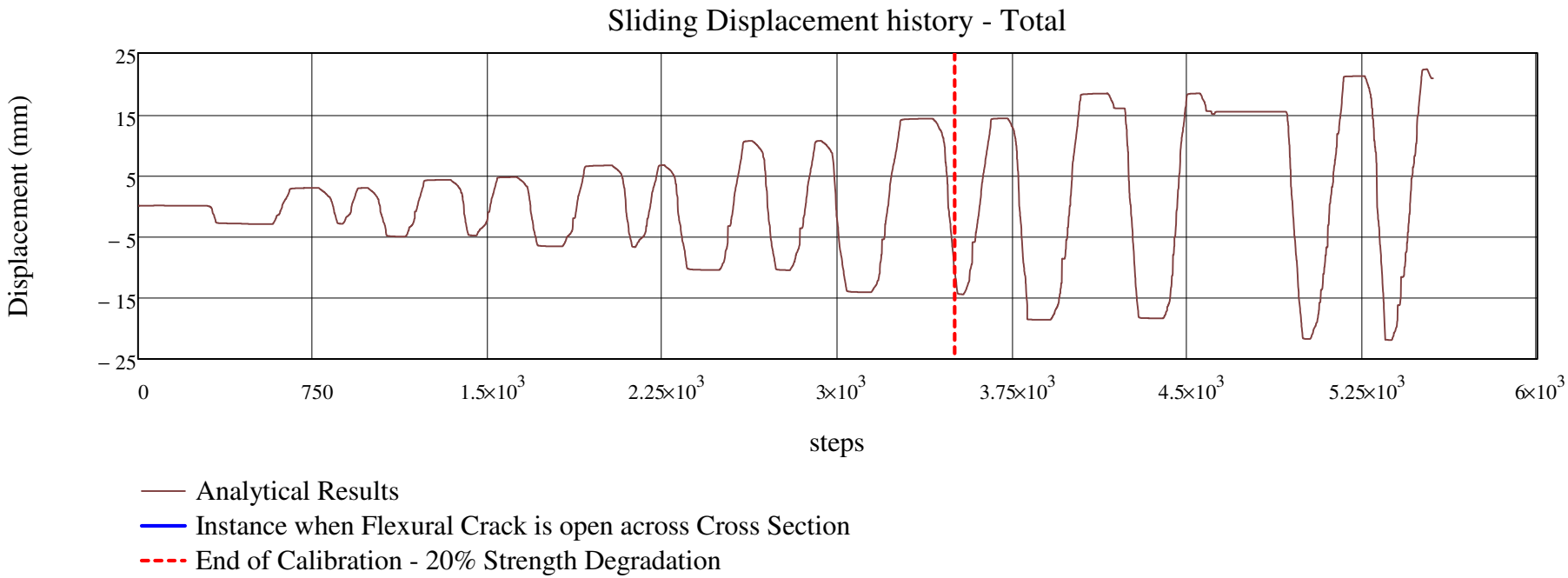
Sliding Displacement history - Total
Displacement (mm)
25
15
5
– 5
– 15
– 25
0
750
1.5×10^3
2.25×10^3
3×10^3
3.75×10^3
4.5×10^3
5.25×10^3
6×10^3
steps
Analytical Results
Instance when Flexural Crack is open across Cross Section
End of Calibration - 20% Strength Degradation

Calibration of Test Specimen PBS-09

LWall := 1.8 m	fm := 8.5 MPa	Lambda = 1.00	Frict_Coeff = 0.60	DowelCoeff = 2.51	P / (f'm Ag) = 10%
HWall := 1.8 m	fsy := 460 MPa	h := 0.15·LWall	Frict_Yield = 1mm	Dowel_Yield = 2.7mm	P = 608 kN

$\rho_v := 0.33\%$

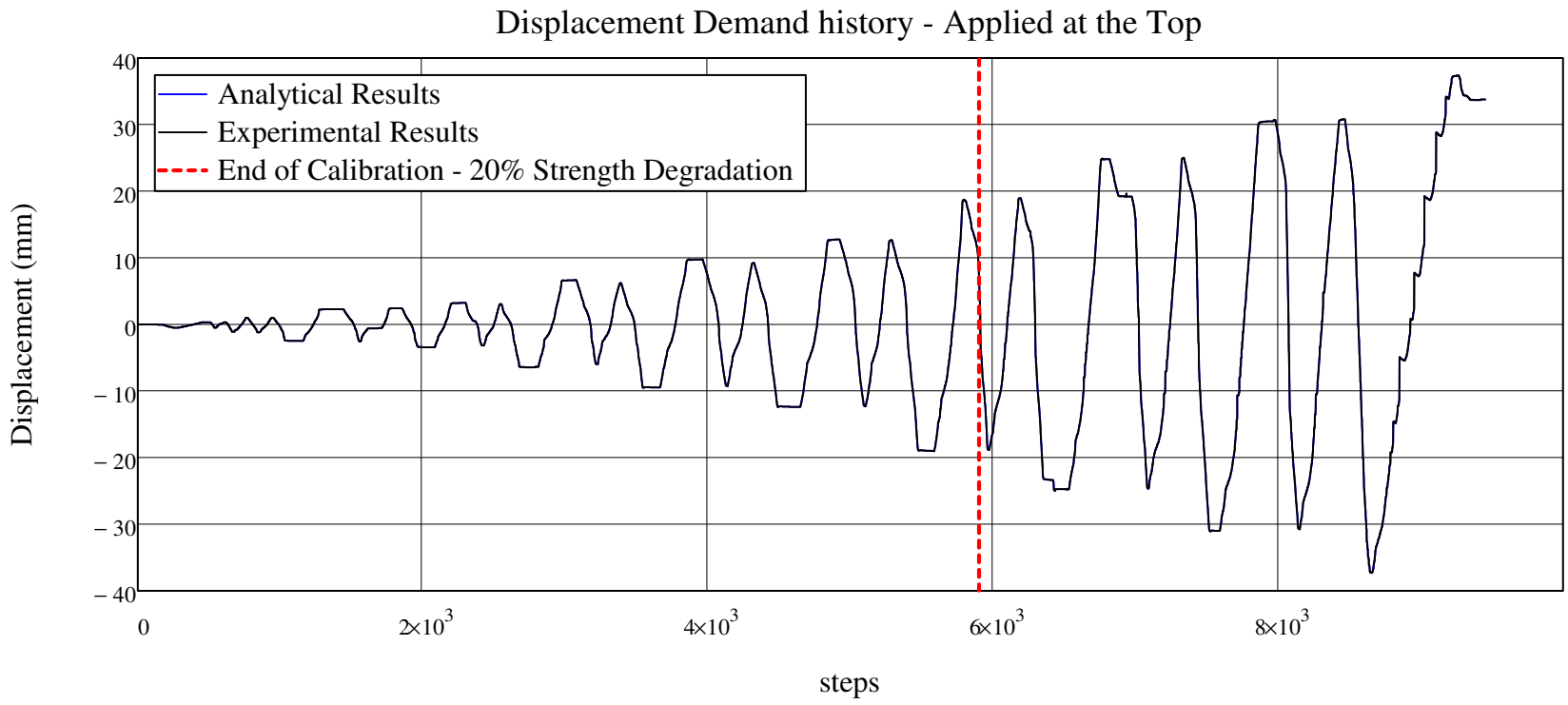

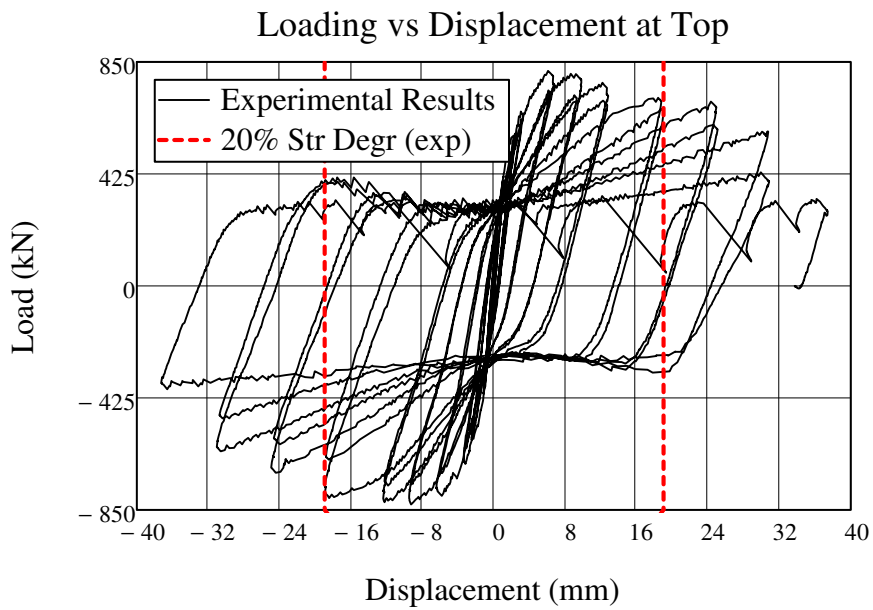
Loading vs Displacement at Top
Experimental Results
20% Str Degr (exp)
Load (kN)
850
425
0
– 425
– 850
– 40
– 32
– 24
– 16
– 8
0
8
16
24
32
40
Displacement (mm)

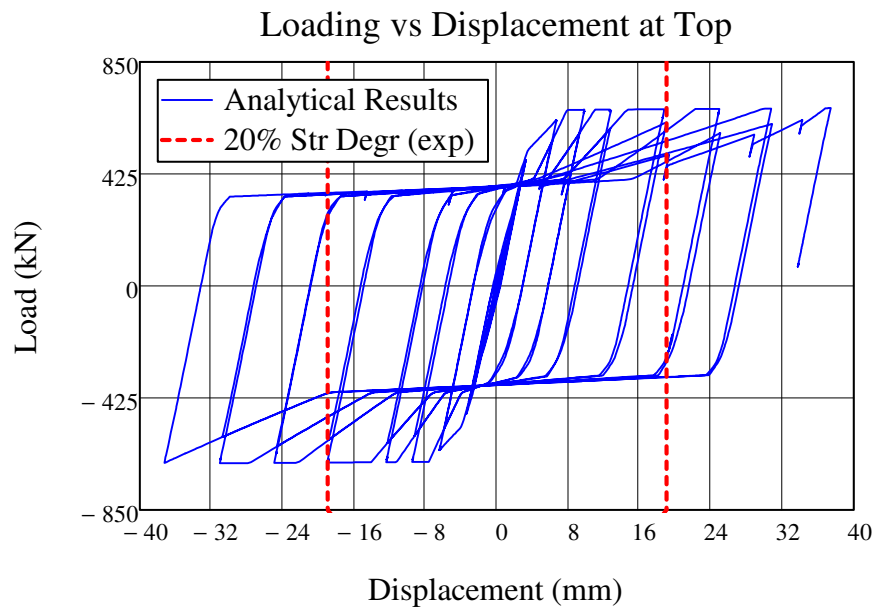
Loading vs Displacement at Top
Analytical Results
20% Str Degr (exp)
Load (kN)
850
425
0
– 425
– 850
– 40
– 32
– 24
– 16
– 8
0
8
16
24
32
40
Displacement (mm)

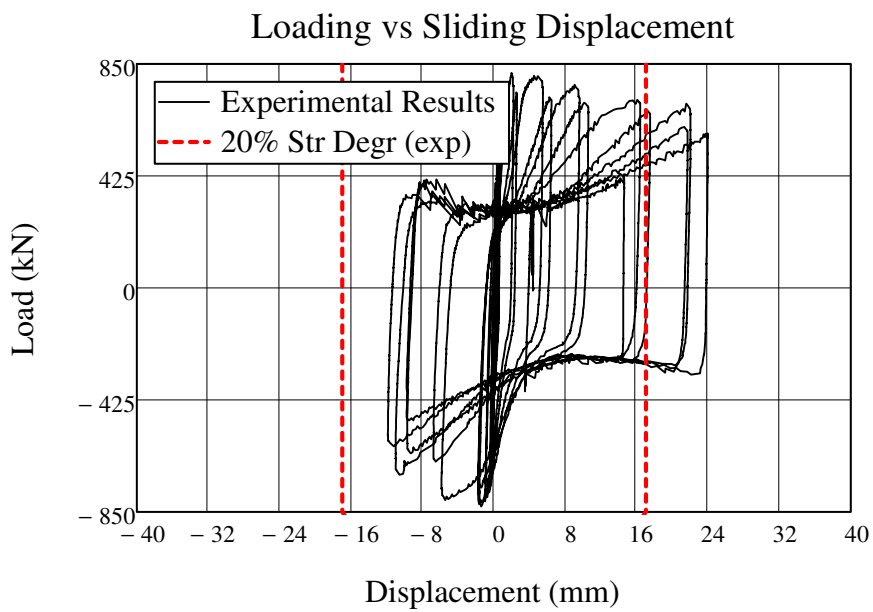
Loading vs Sliding Displacement
Experimental Results
20% Str Degr (exp)
Load (kN)
850
425
0
– 425
– 850
– 40
– 32
– 24
– 16
– 8
0
8
16
24
32
40
Displacement (mm)

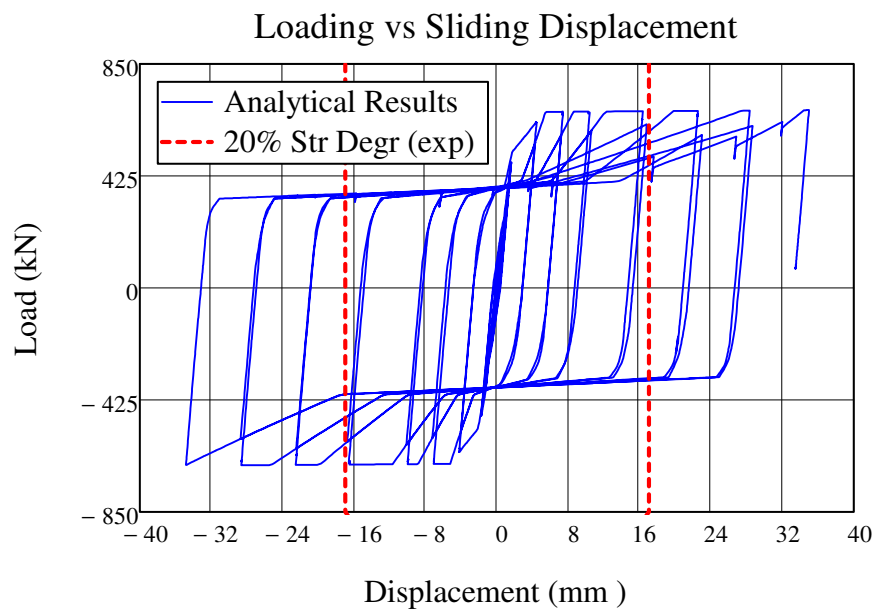
Loading vs Sliding Displacement
Analytical Results
20% Str Degr (exp)
Load (kN)
850
425
0
– 425
– 850
– 40
– 32
– 24
– 16
– 8
0
8
16
24
32
40
Displacement (mm)

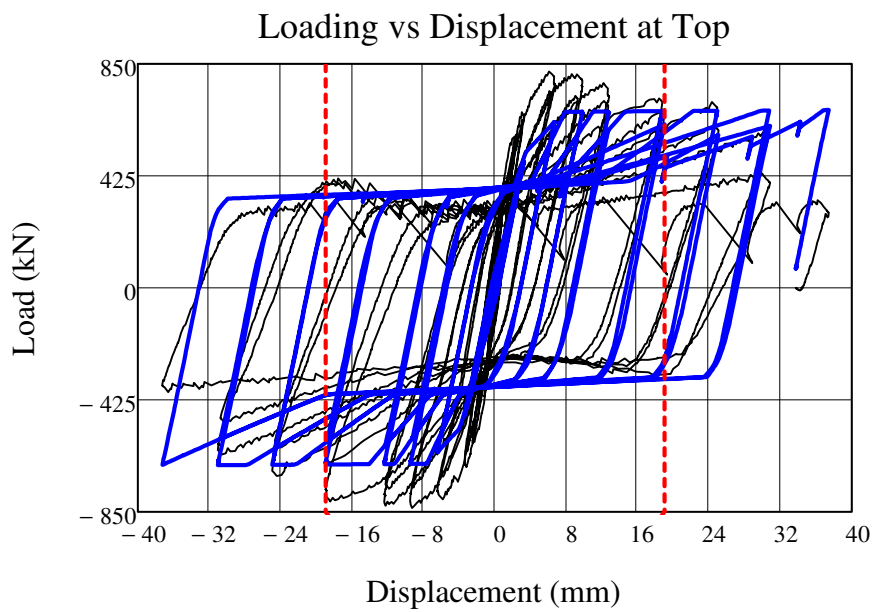

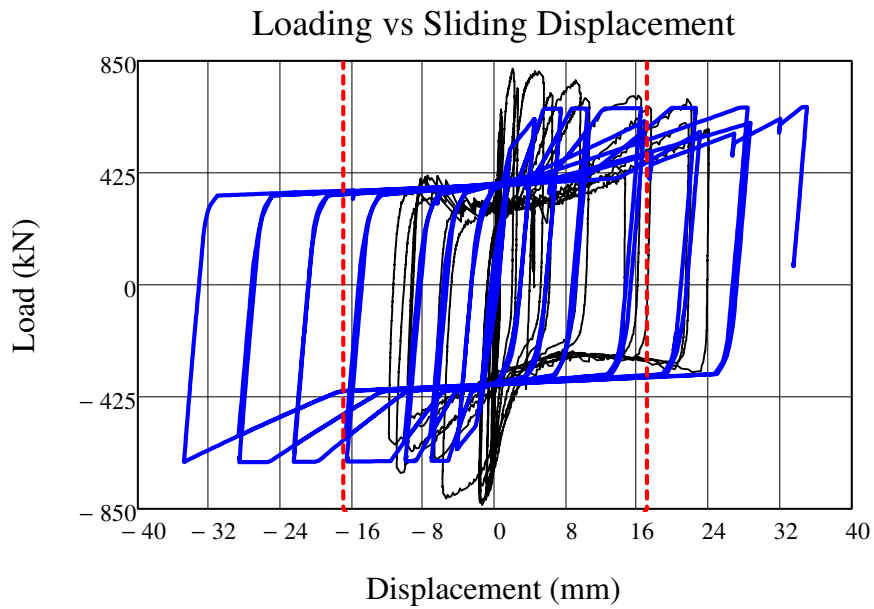

Experimental Results
Analytical Results
20% Str Degr (exp)

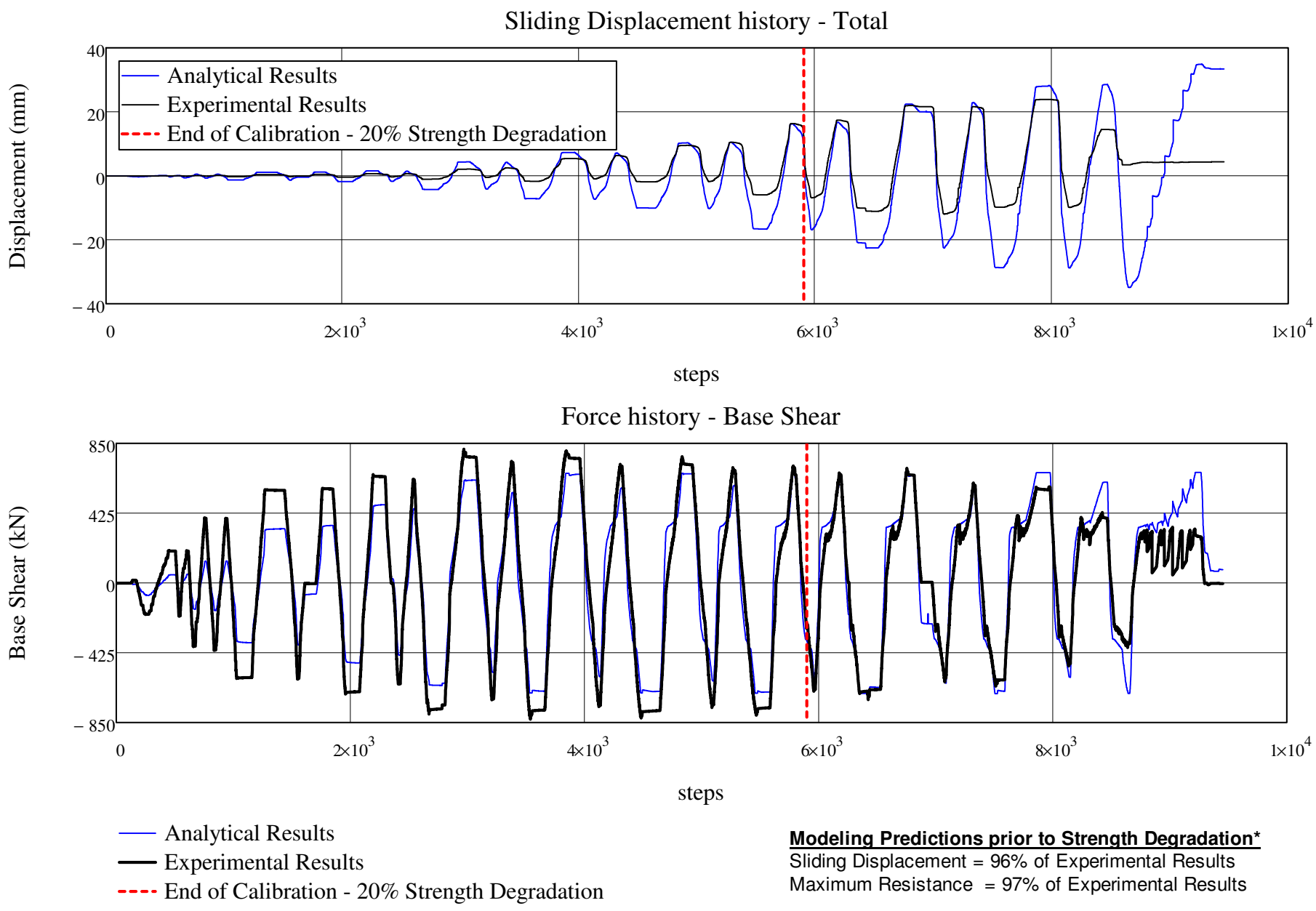

Modeling Predictions prior to Strength Degradation*

Sliding Displacement = 96% of Experimental Results

Maximum Resistance = 97% of Experimental Results

**Strength Degradation @ step 5900*

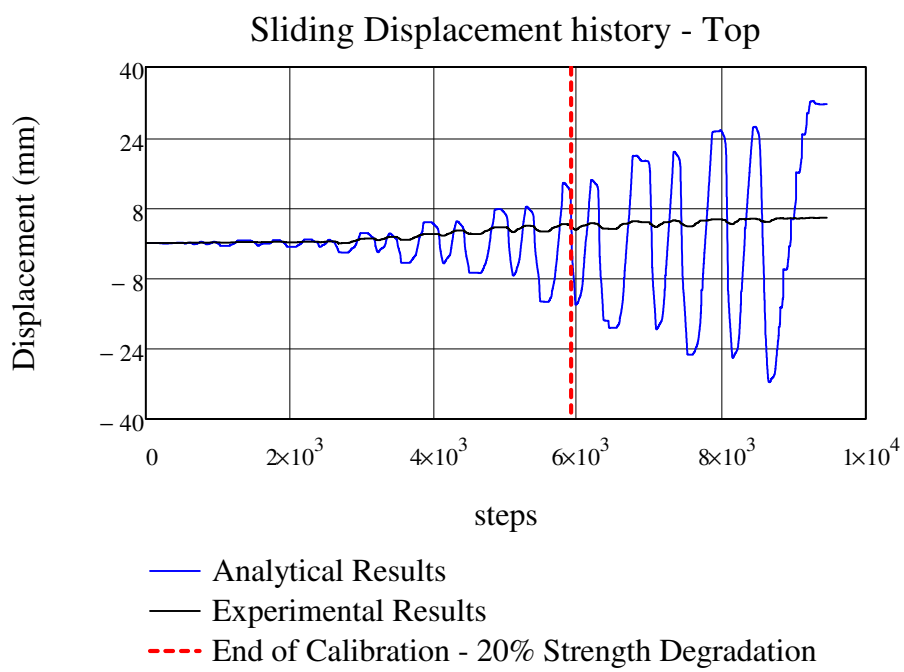
Sliding Displacement history - Top
Displacement (mm)
40
24
8
− 8
− 24
− 40
0
2×10^3
4×10^3
6×10^3
8×10^3
1×10^4
steps
Analytical Results
Experimental Results
End of Calibration - 20% Strength Degradation

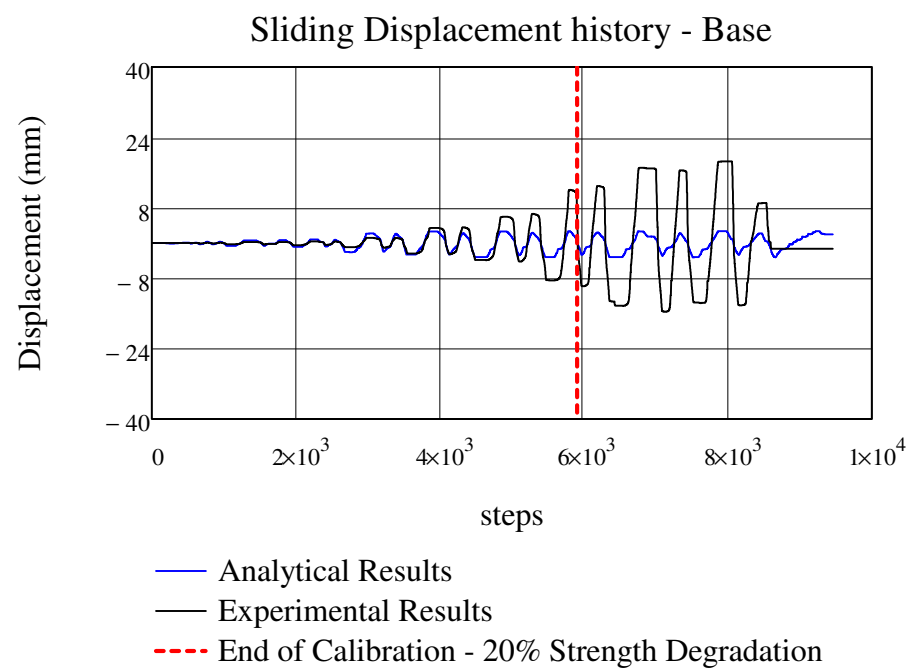
Sliding Displacement history - Base
Displacement (mm)
40
24
8
− 8
− 24
− 40
0
2×10^3
4×10^3
6×10^3
8×10^3
1×10^4
steps
Analytical Results
Experimental Results
End of Calibration - 20% Strength Degradation

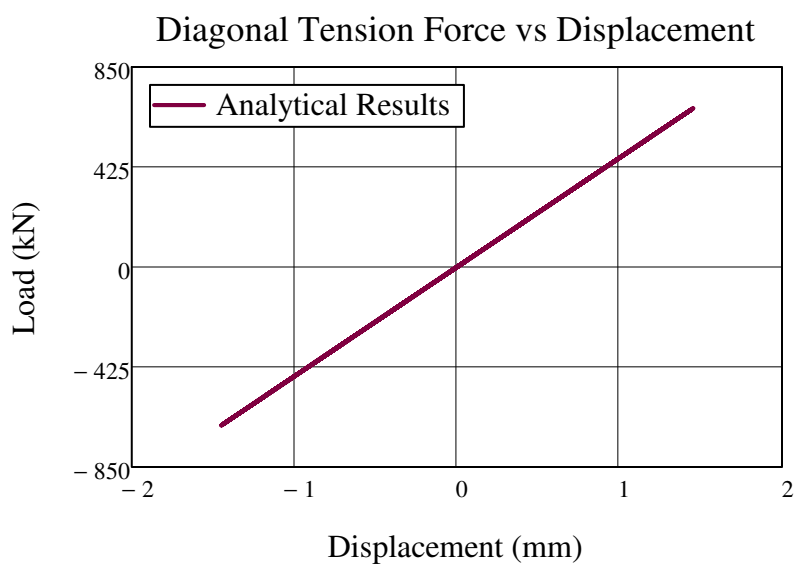
Diagonal Tension Force vs Displacement
Analytical Results
Load (kN)
850
425
0
− 425
− 850
− 2
− 1
0
1
2
Displacement (mm)

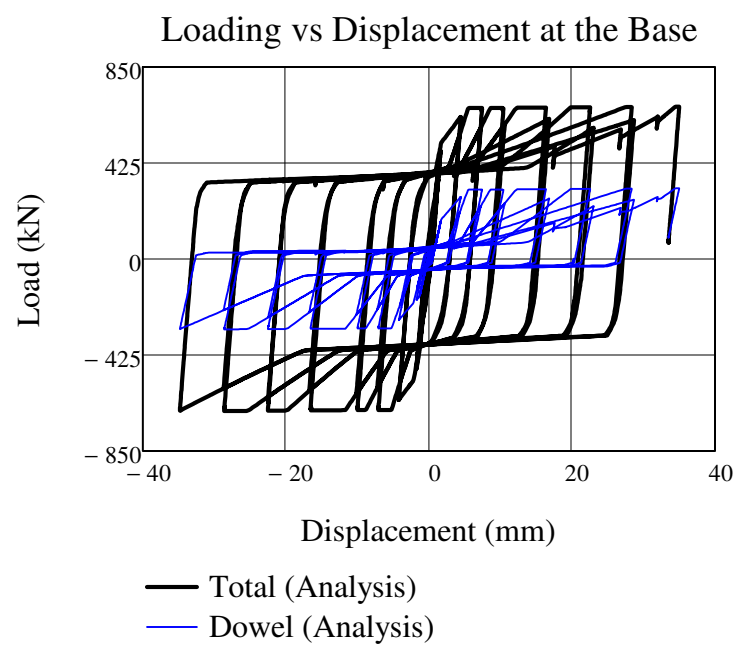
Loading vs Displacement at the Base
Load (kN)
850
425
0
− 425
− 850
− 40
− 20
0
20
40
Displacement (mm)
Total (Analysis)
Dowel (Analysis)

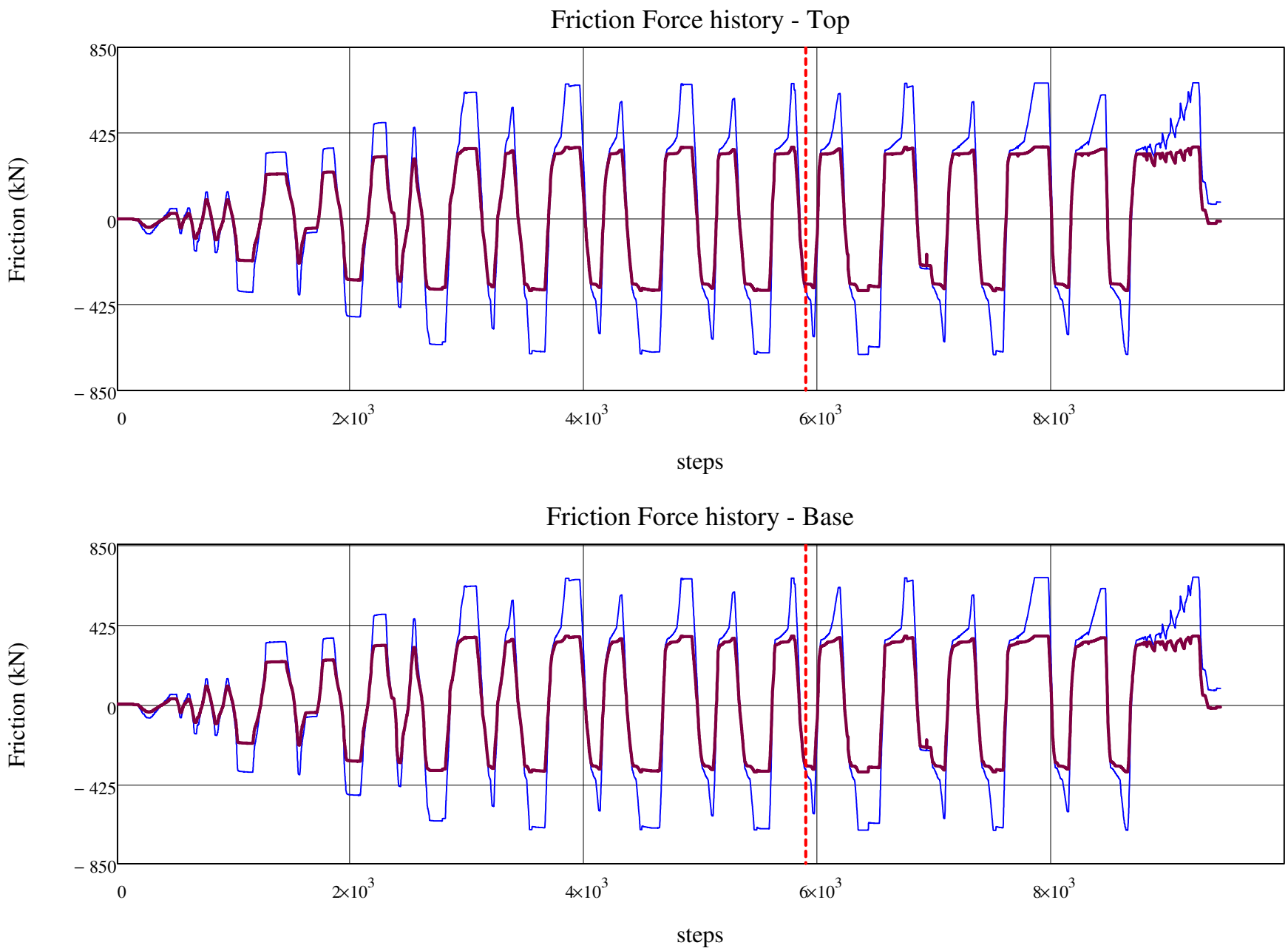
Friction Force history - Top
850
425
0
– 425
– 850
Friction (kN)
0
2×10^3
4×10^3
6×10^3
8×10^3
steps
Friction Force history - Base
850
425
0
– 425
– 850
Friction (kN)
0
2×10^3
4×10^3
6×10^3
8×10^3
steps
Total Force (Analysis)
Friction Force (Analysis)
End of Calibration - 20% Strength Degradation

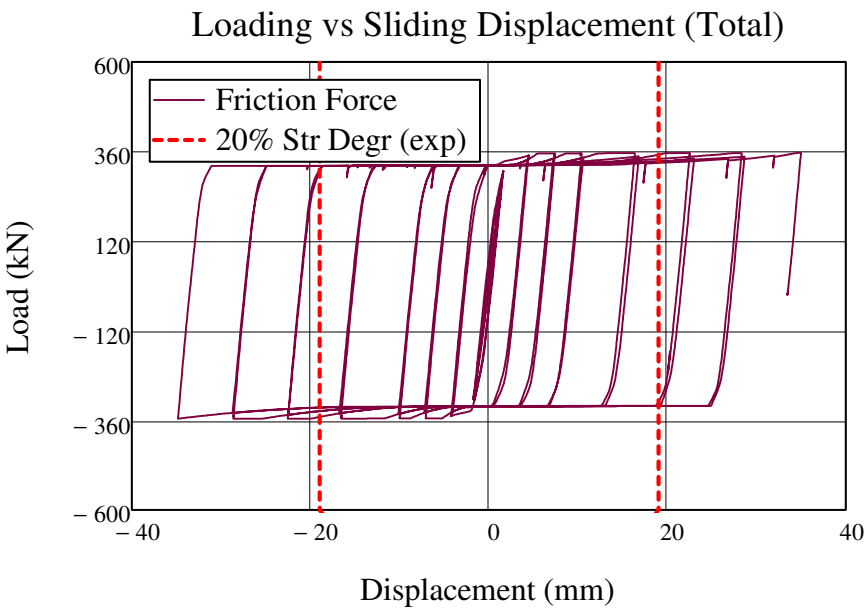
Loading vs Sliding Displacement (Total)
Friction Force
20% Str Degr (exp)
Load (kN)
600
360
120
− 120
− 360
− 600
− 40
− 20
0
20
40
Displacement (mm)

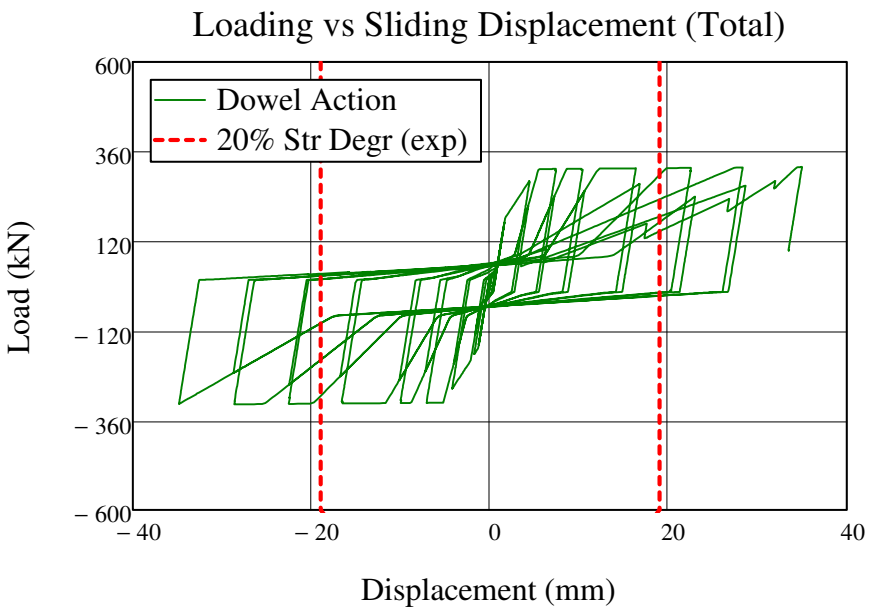
Loading vs Sliding Displacement (Total)
Dowel Action
20% Str Degr (exp)
Load (kN)
600
360
120
− 120
− 360
− 600
− 40
− 20
0
20
40
Displacement (mm)

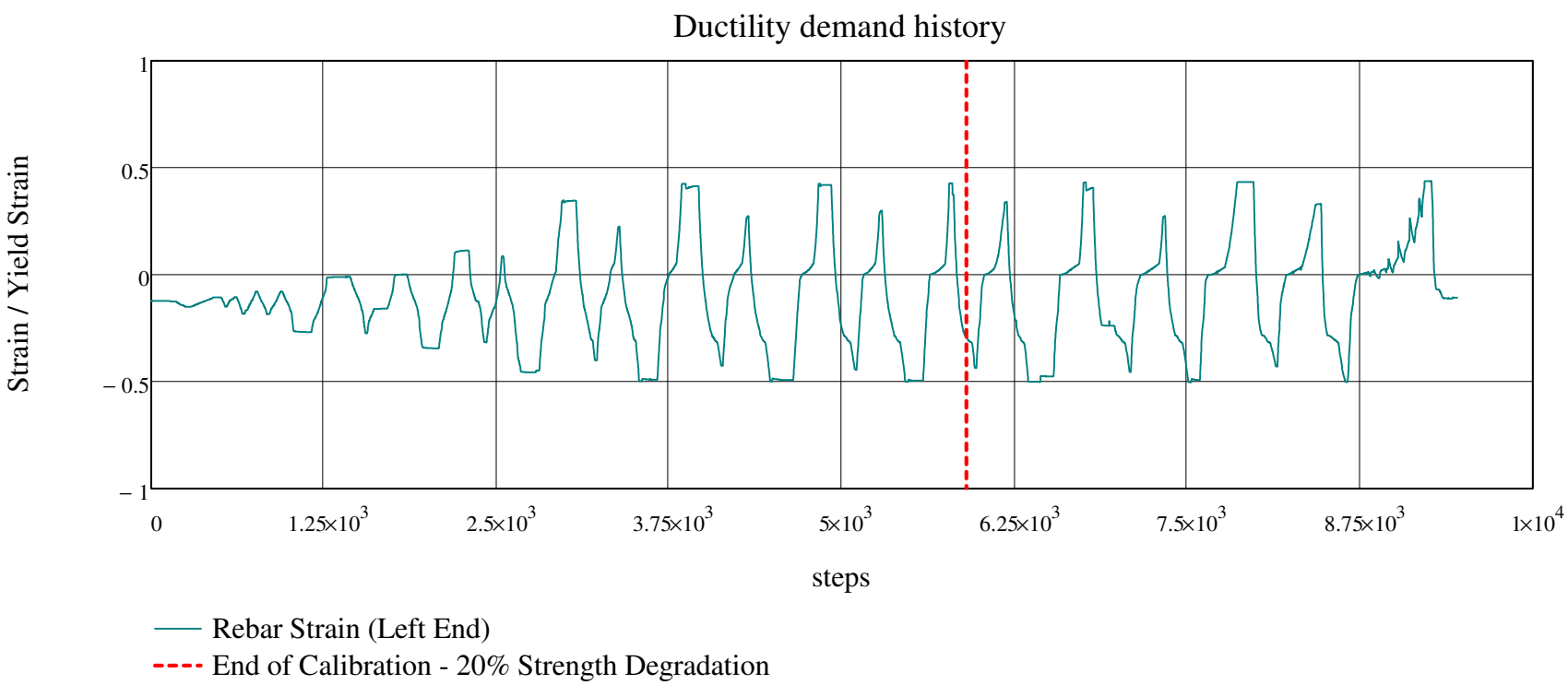
Ductility demand history
Strain / Yield Strain
1
0.5
0
− 0.5
− 1
0
1.25×10^3
2.5×10^3
3.75×10^3
5×10^3
6.25×10^3
7.5×10^3
8.75×10^3
1×10^4
steps
Rebar Strain (Left End)
End of Calibration - 20% Strength Degradation

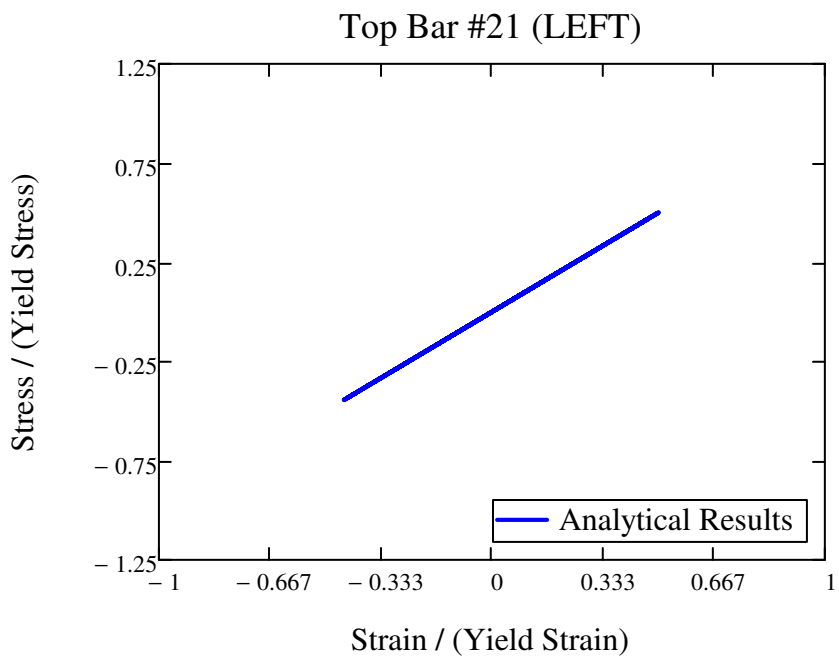
Top Bar #21 (LEFT)
Stress / (Yield Stress)
1.25
0.75
0.25
− 0.25
− 0.75
− 1.25
− 1
− 0.667
− 0.333
0
0.333
0.667
1
Strain / (Yield Strain)
Analytical Results

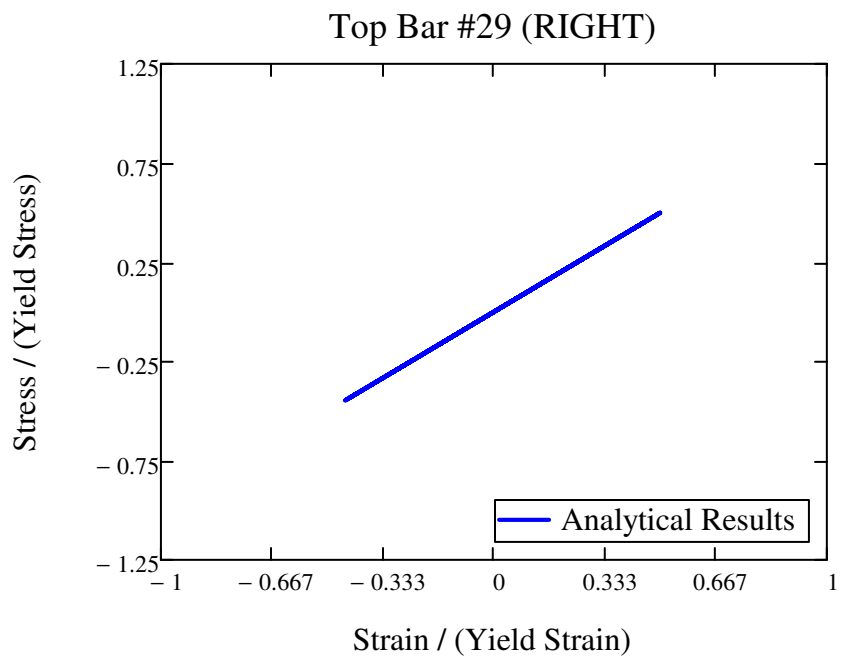
Top Bar #29 (RIGHT)
Stress / (Yield Stress)
1.25
0.75
0.25
− 0.25
− 0.75
− 1.25
− 1
− 0.667
− 0.333
0
0.333
0.667
1
Strain / (Yield Strain)
Analytical Results

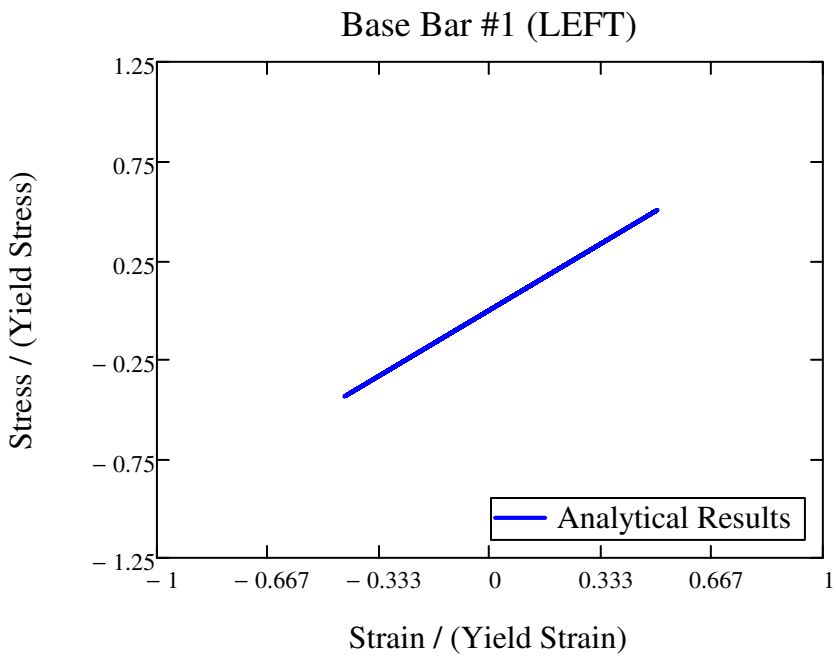
Base Bar #1 (LEFT)
Stress / (Yield Stress)
1.25
0.75
0.25
− 0.25
− 0.75
− 1.25
− 1
− 0.667
− 0.333
0
0.333
0.667
1
Strain / (Yield Strain)
Analytical Results

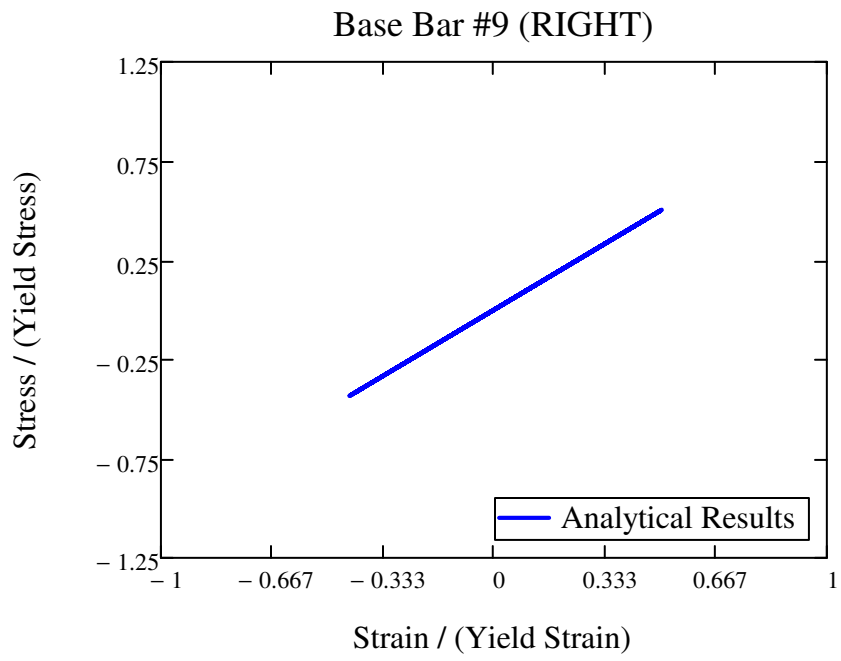
Base Bar #9 (RIGHT)
Stress / (Yield Stress)
1.25
0.75
0.25
− 0.25
− 0.75
− 1.25
− 1
− 0.667
− 0.333
0
0.333
0.667
1
Strain / (Yield Strain)
Analytical Results

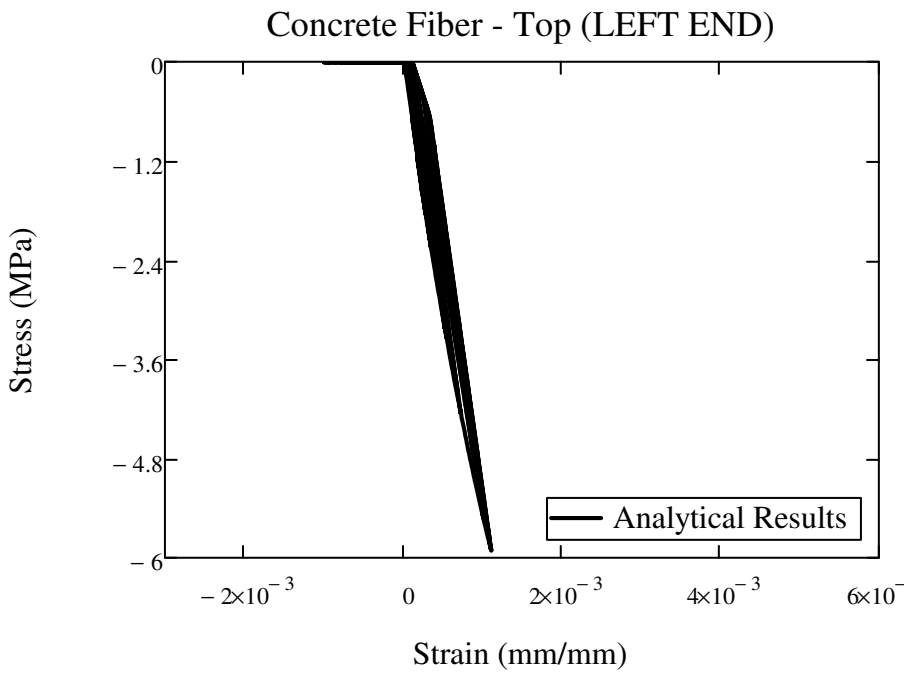
Concrete Fiber - Top (LEFT END)
Stress (MPa)
0
− 1.2
− 2.4
− 3.6
− 4.8
− 6
− 2×10⁻³
0
2×10⁻³
4×10⁻³
6×10⁻
Strain (mm/mm)
Analytical Results

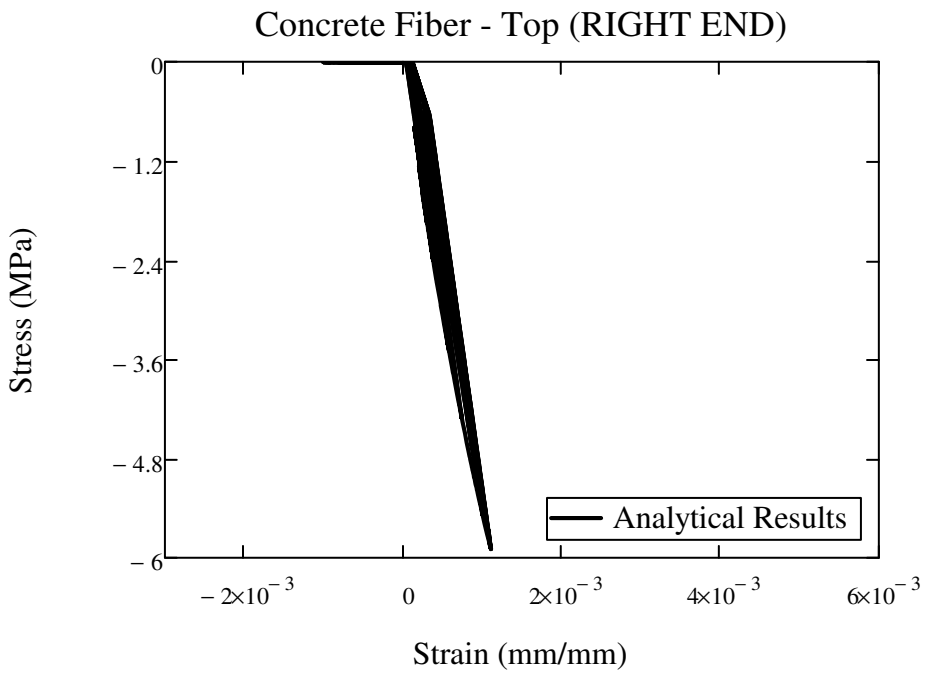
Concrete Fiber - Top (RIGHT END)
Stress (MPa)
0
− 1.2
− 2.4
− 3.6
− 4.8
− 6
− 2×10⁻³
0
2×10⁻³
4×10⁻³
6×10⁻³
Strain (mm/mm)
Analytical Results

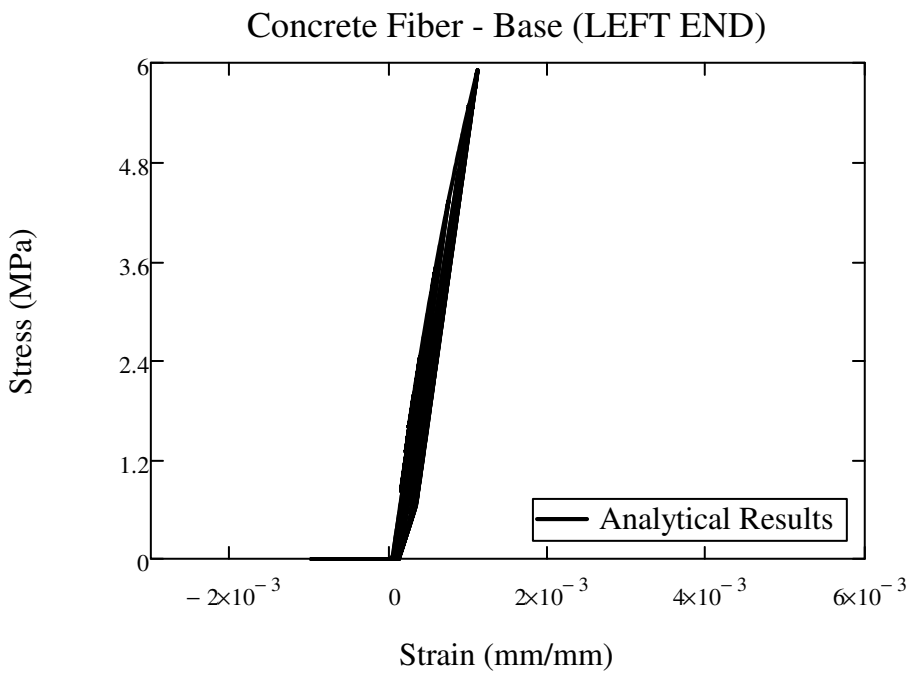
Concrete Fiber - Base (LEFT END)
Stress (MPa)
6
4.8
3.6
2.4
1.2
0
− 2×10⁻³
0
2×10⁻³
4×10⁻³
6×10⁻³
Strain (mm/mm)
Analytical Results

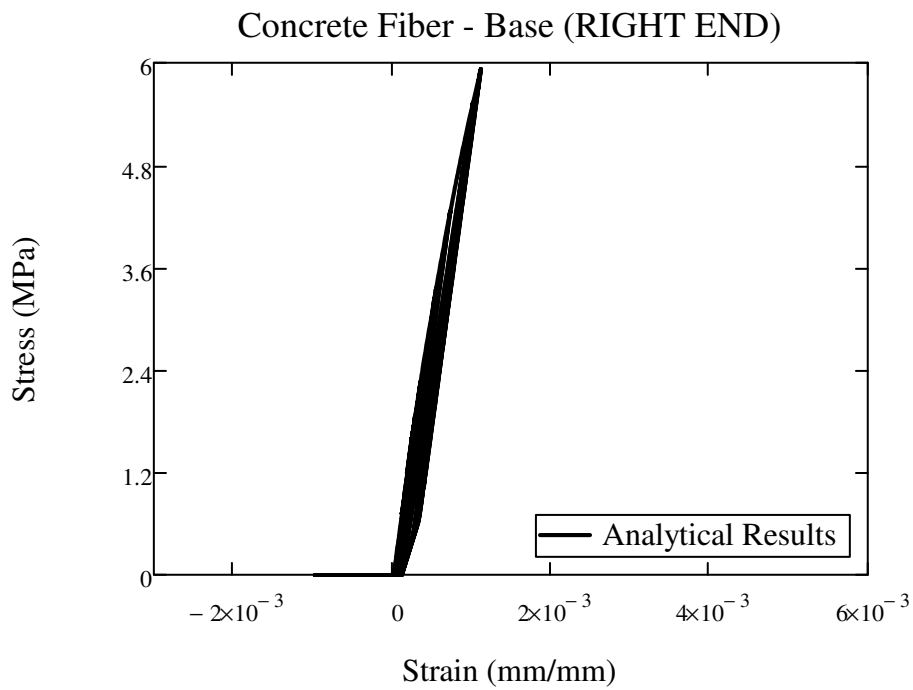
Concrete Fiber - Base (RIGHT END)
Stress (MPa)
6
4.8
3.6
2.4
1.2
0
− 2×10⁻³
0
2×10⁻³
4×10⁻³
6×10⁻³
Strain (mm/mm)
Analytical Results

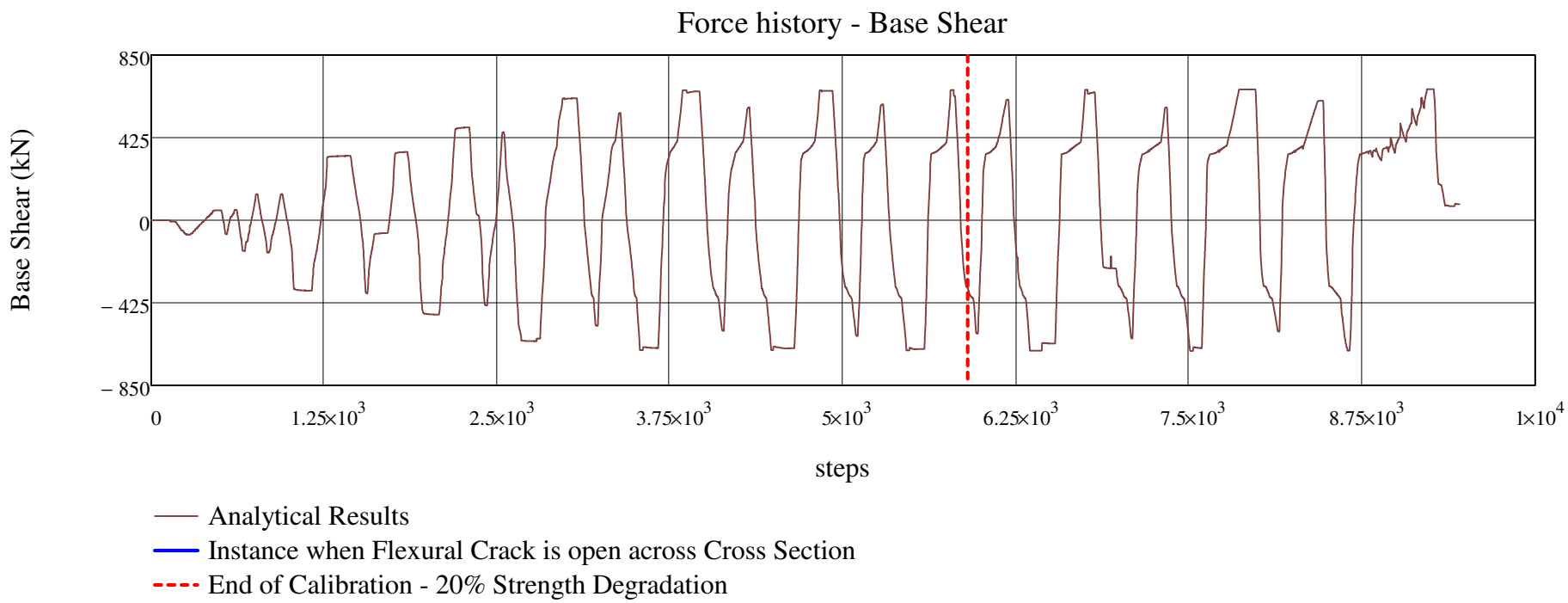
Force history - Base Shear
Base Shear (kN)
850
425
0
– 425
– 850
0
1.25×10^3
2.5×10^3
3.75×10^3
5×10^3
6.25×10^3
7.5×10^3
8.75×10^3
1×10^4
steps
Analytical Results
Instance when Flexural Crack is open across Cross Section
End of Calibration - 20% Strength Degradation

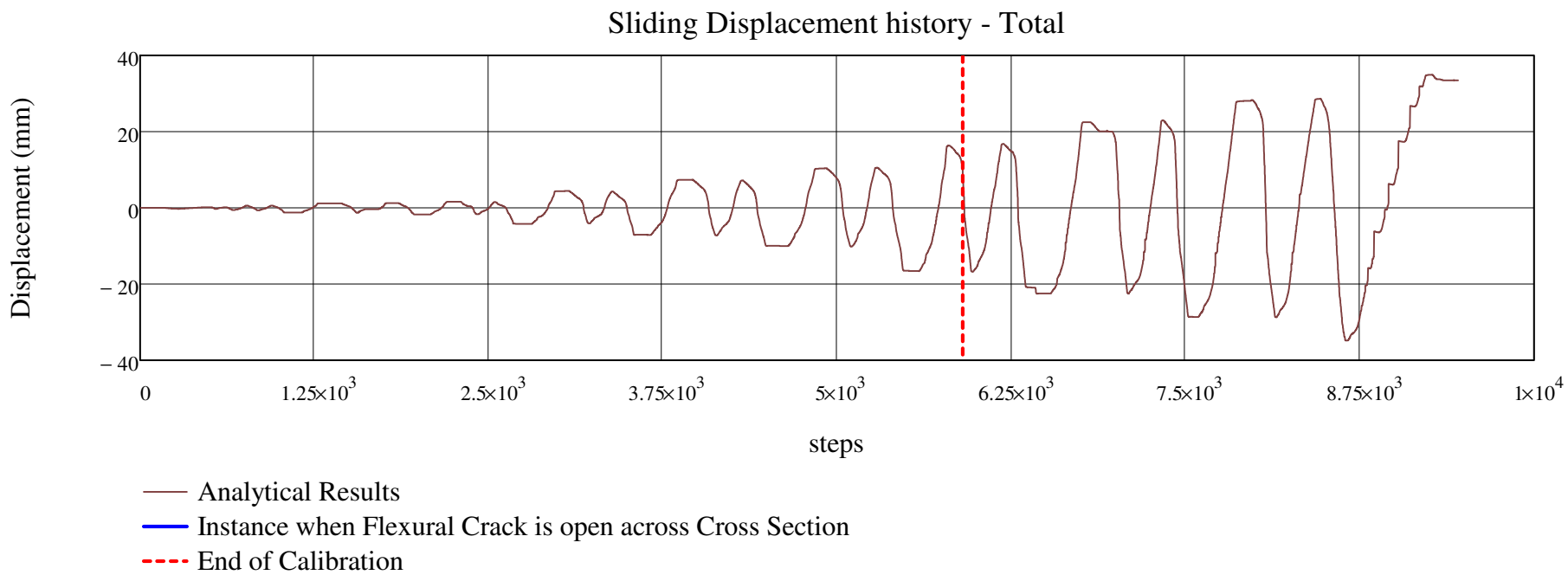
Sliding Displacement history - Total
Displacement (mm)
40
20
0
– 20
– 40
0
1.25×10^3
2.5×10^3
3.75×10^3
5×10^3
6.25×10^3
7.5×10^3
8.75×10^3
1×10^4
steps
Analytical Results
Instance when Flexural Crack is open across Cross Section
End of Calibration

Calibration of Test Specimen PBS-10

LWall := 1.8 m	fm := 8.5 MPa	Lambda = 1.00	Frict_Coeff = 0.60	DowelCoeff = 2.51	P / (f'm Ag) = 10%
HWall := 1.8 m	fsy := 460 MPa	h := 0.15·LWall	Frict_Yield = 1mm	Dowel_Yield = 2.7mm	P = 608 kN

$\rho_v := 0.18\%$

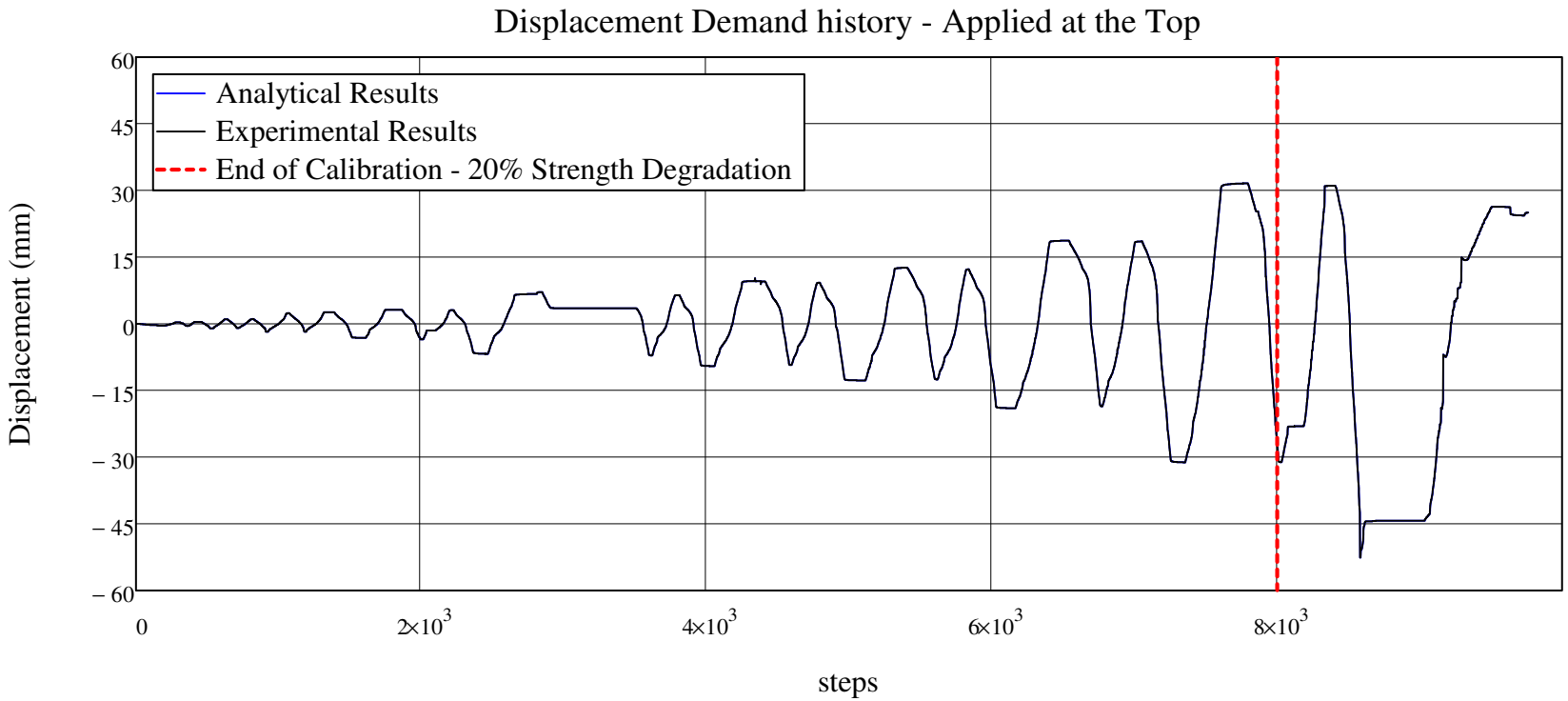

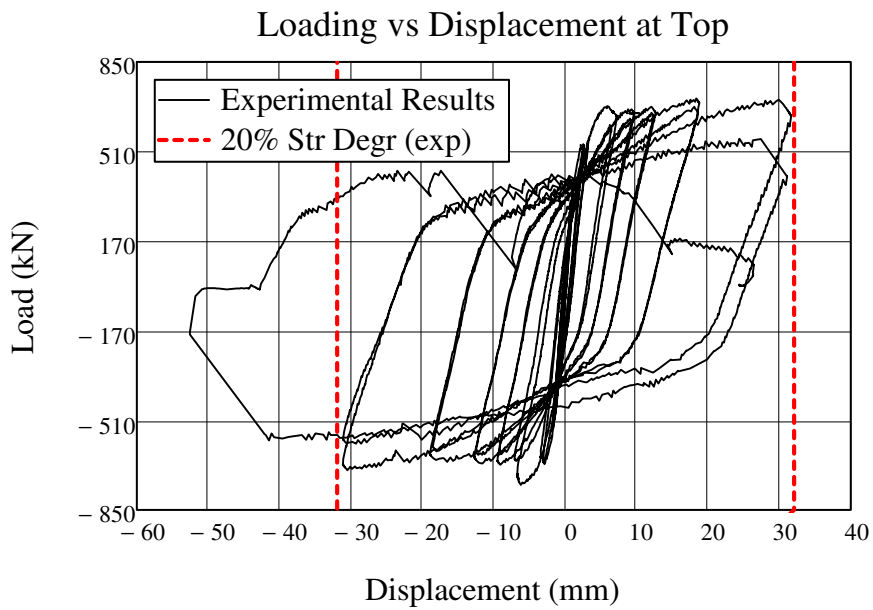
Loading vs Displacement at Top
Experimental Results
20% Str Degr (exp)
Load (kN)
850
510
170
– 170
– 510
– 850
– 60
– 50
– 40
– 30
– 20
– 10
0
10
20
30
40
Displacement (mm)

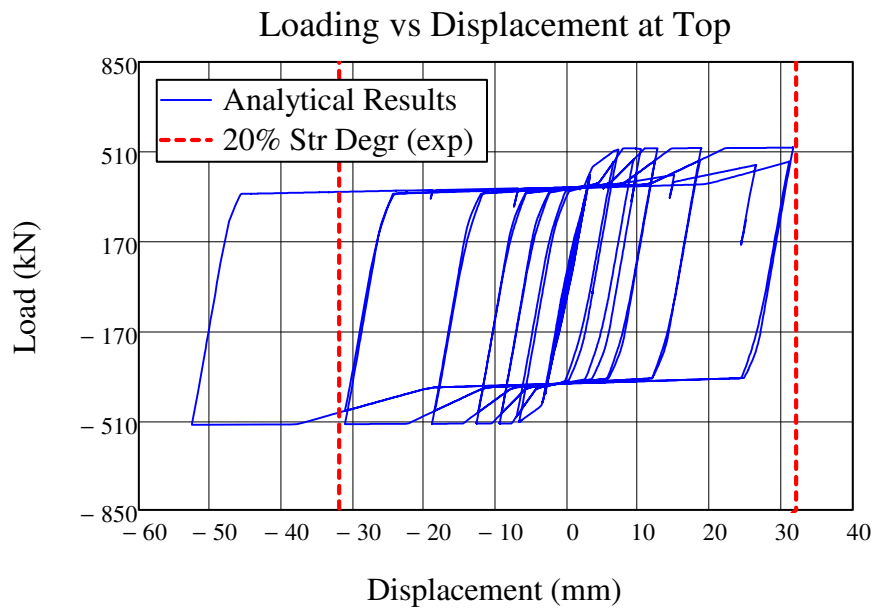
Loading vs Displacement at Top
Analytical Results
20% Str Degr (exp)
Load (kN)
850
510
170
– 170
– 510
– 850
– 60
– 50
– 40
– 30
– 20
– 10
0
10
20
30
40
Displacement (mm)

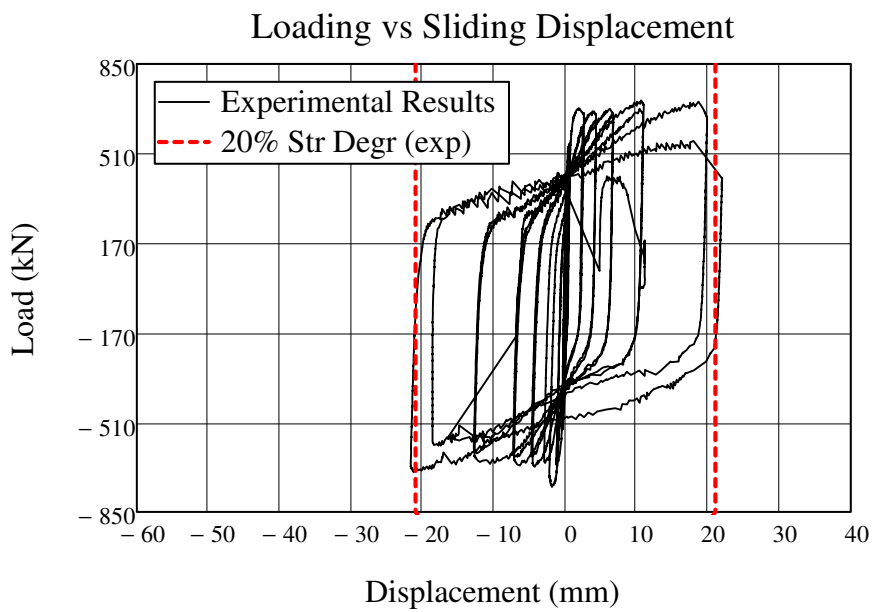
Loading vs Sliding Displacement
Experimental Results
20% Str Degr (exp)
Load (kN)
850
510
170
– 170
– 510
– 850
– 60
– 50
– 40
– 30
– 20
– 10
0
10
20
30
40
Displacement (mm)

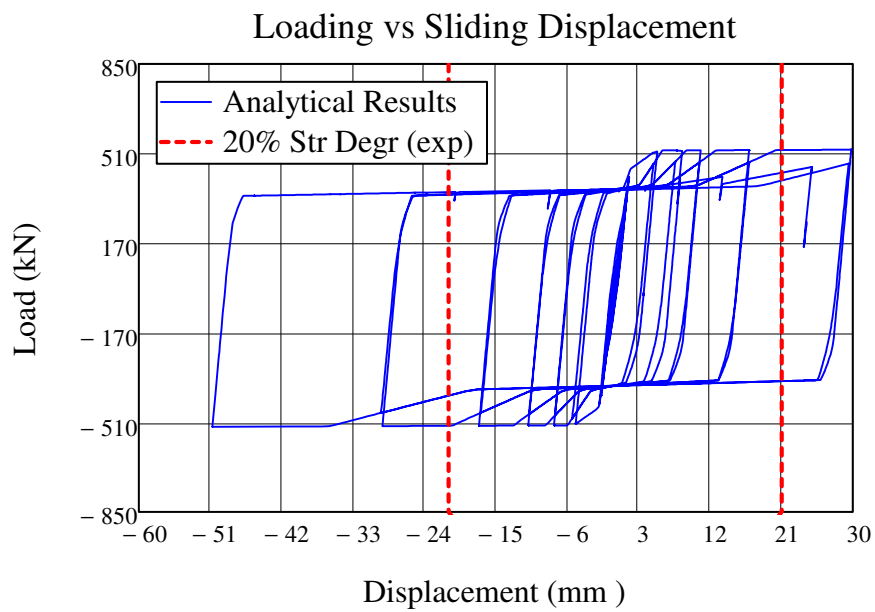
Loading vs Sliding Displacement
Analytical Results
20% Str Degr (exp)
Load (kN)
850
510
170
– 170
– 510
– 850
– 60
– 51
– 42
– 33
– 24
– 15
– 6
3
12
21
30
Displacement (mm)

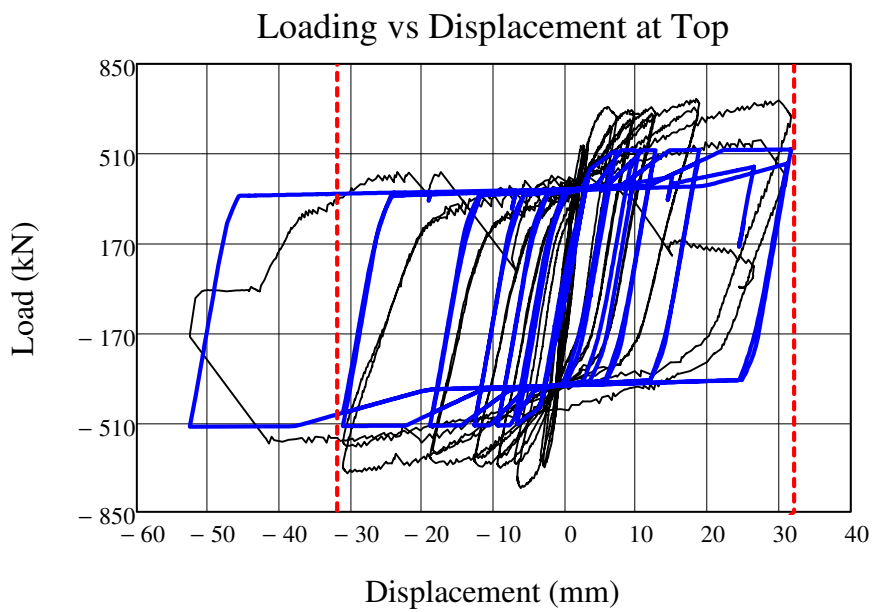

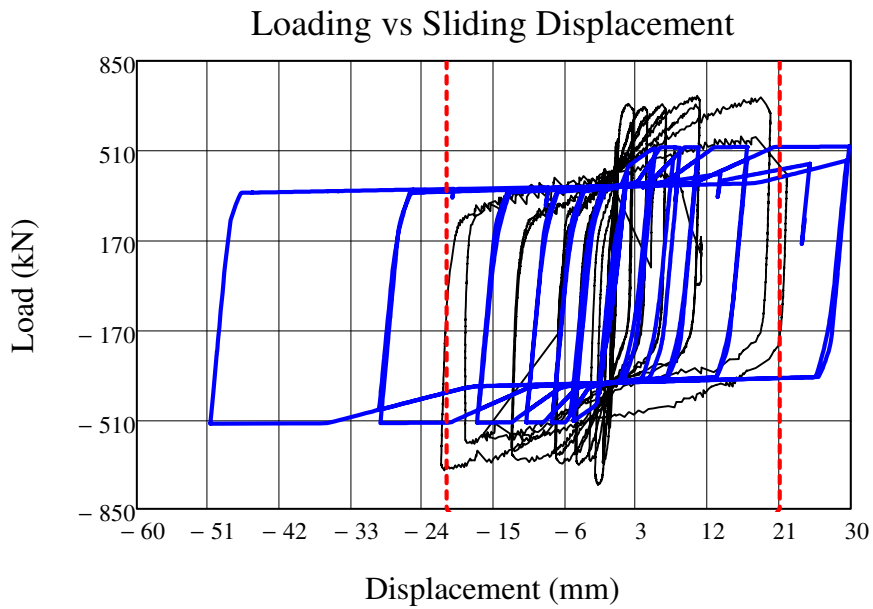

Experimental Results
Analytical Results
20% Str Degr (exp)

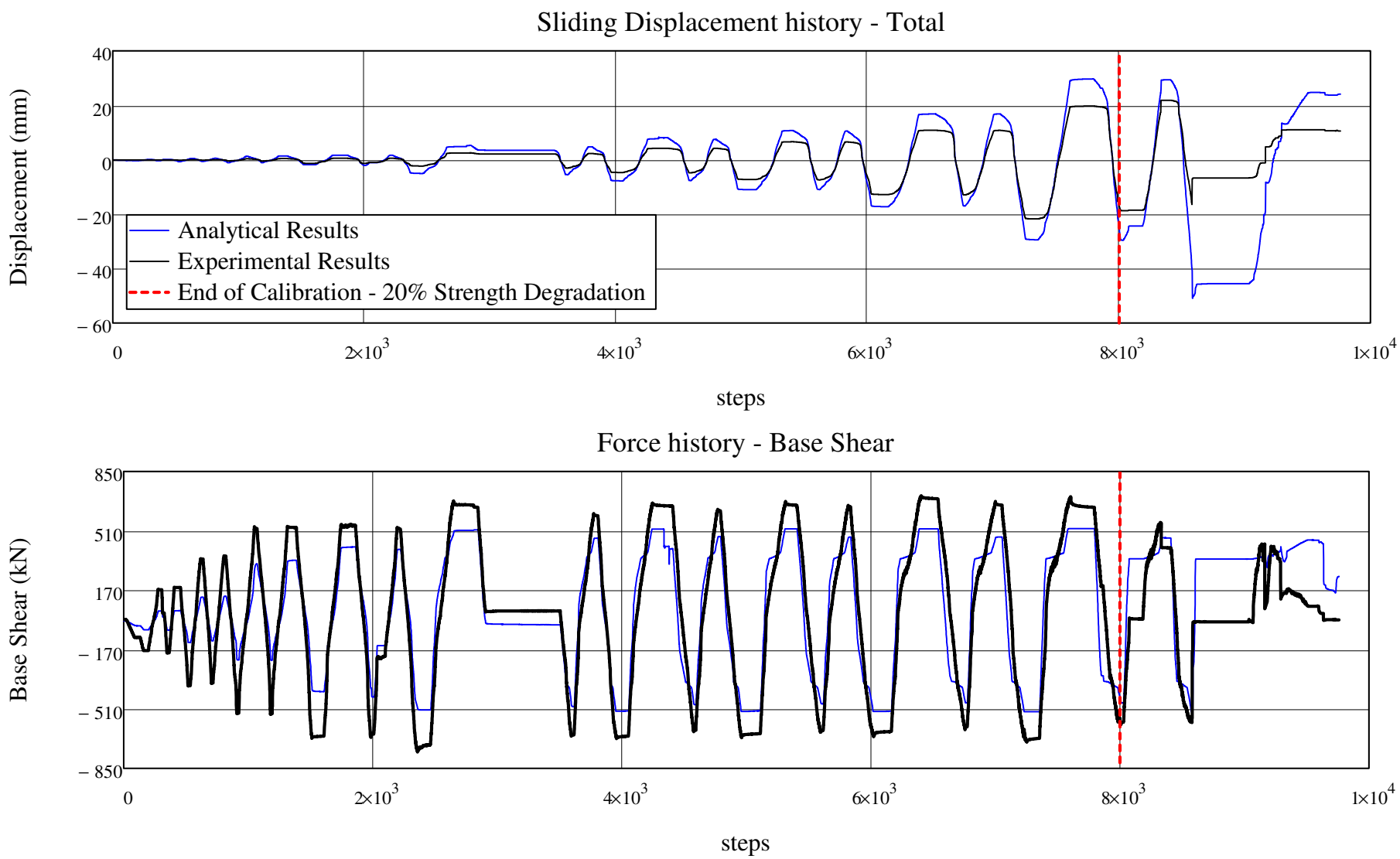

Modeling Predictions prior to Strength Degradation*

Sliding Displacement = 138% of Experimental Results

Maximum Resistance = 72% of Experimental Results

**Strength Degradation @ step 8000*

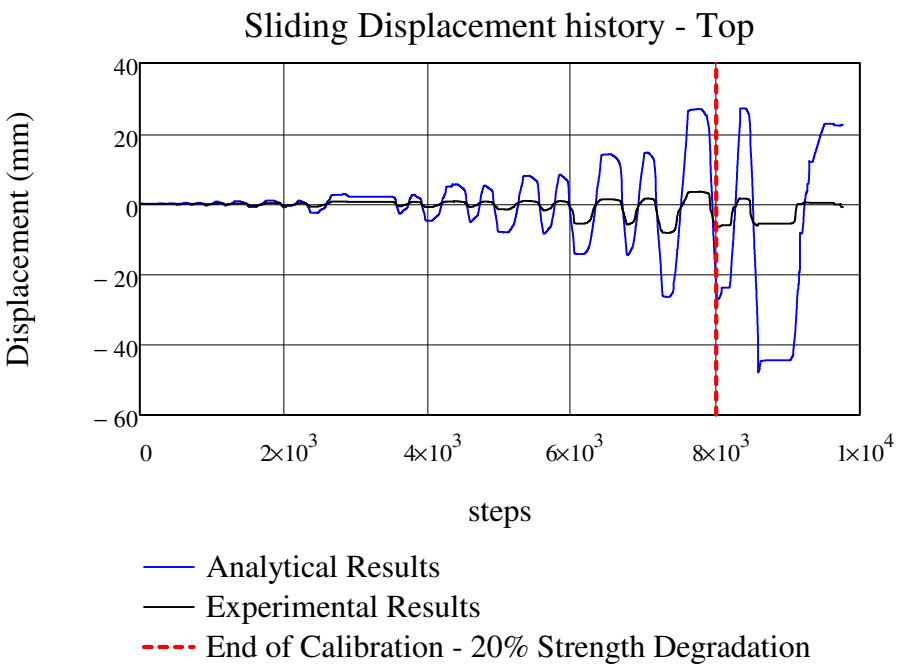
Sliding Displacement history - Top
Displacement (mm)
40
20
0
− 20
− 40
− 60
0
2×10^3
4×10^3
6×10^3
8×10^3
1×10^4
steps
Analytical Results
Experimental Results
End of Calibration - 20% Strength Degradation

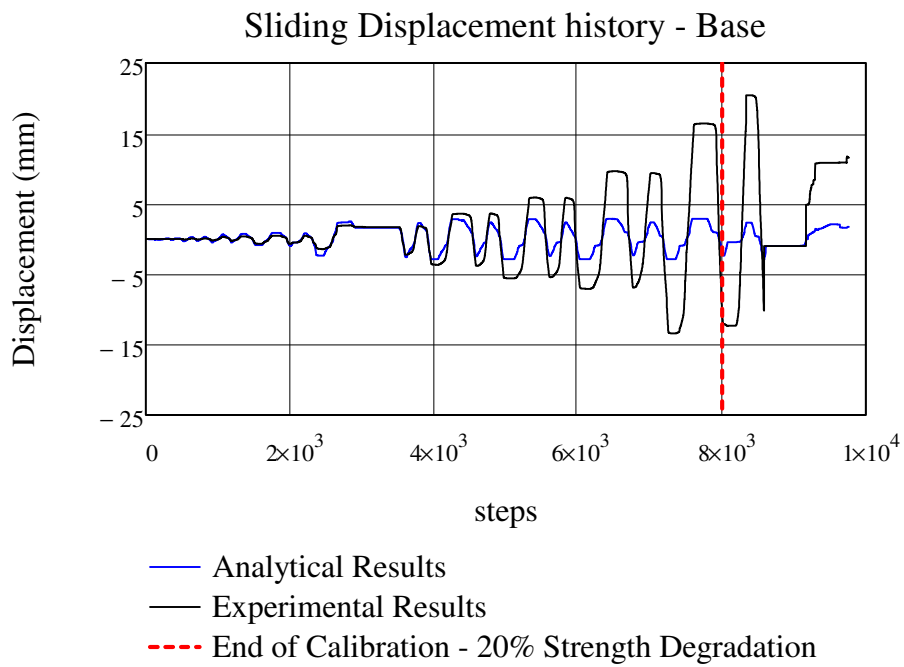
Sliding Displacement history - Base
Displacement (mm)
25
15
5
− 5
− 15
− 25
0
2×10^3
4×10^3
6×10^3
8×10^3
1×10^4
steps
Analytical Results
Experimental Results
End of Calibration - 20% Strength Degradation

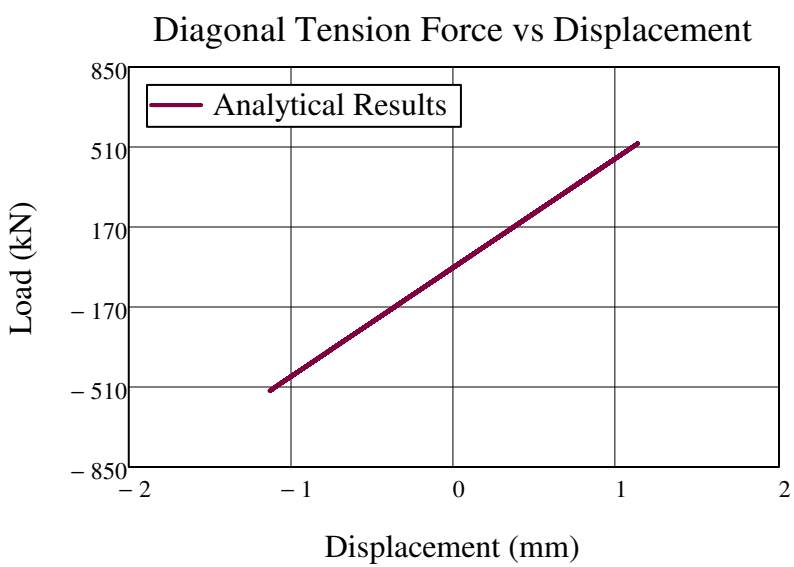
Diagonal Tension Force vs Displacement
Analytical Results
Load (kN)
850
510
170
− 170
− 510
− 850
− 2
− 1
0
1
2
Displacement (mm)

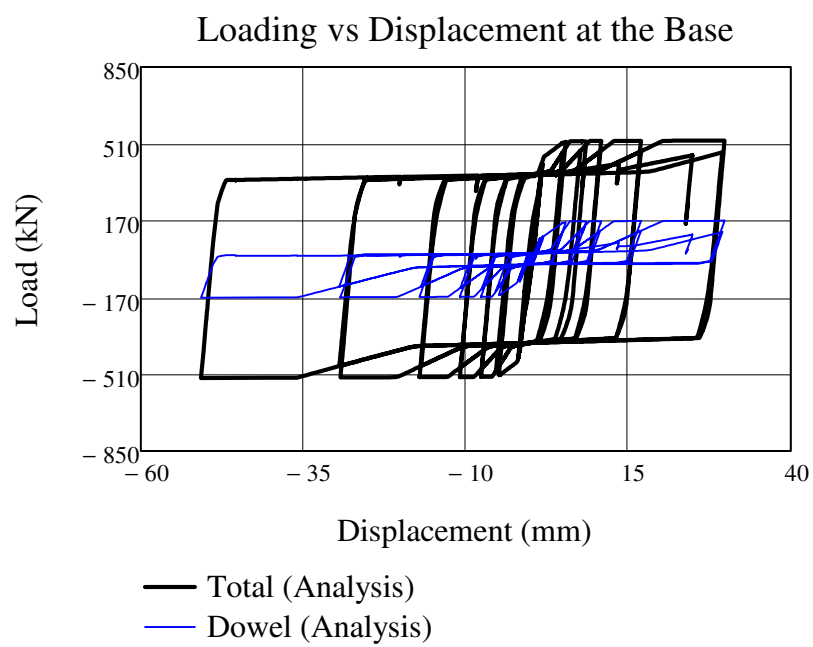
Loading vs Displacement at the Base
Load (kN)
850
510
170
− 170
− 510
− 850
− 60
− 35
− 10
15
40
Displacement (mm)
Total (Analysis)
Dowel (Analysis)

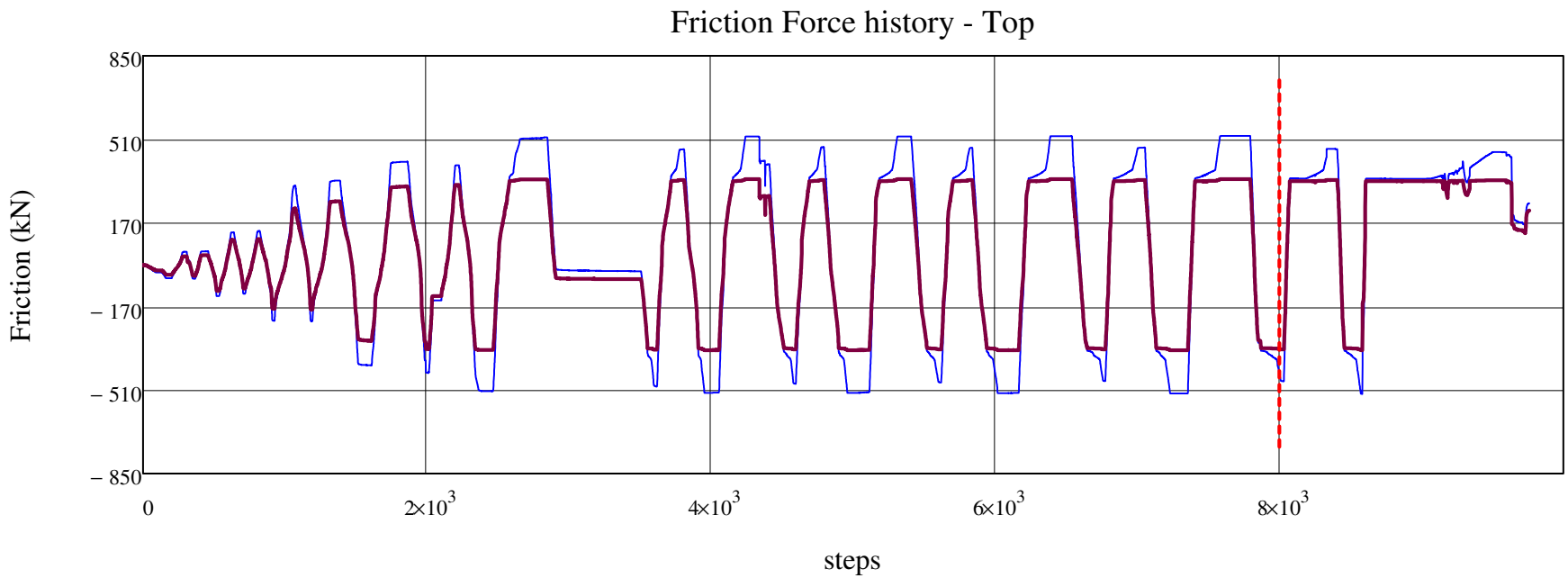

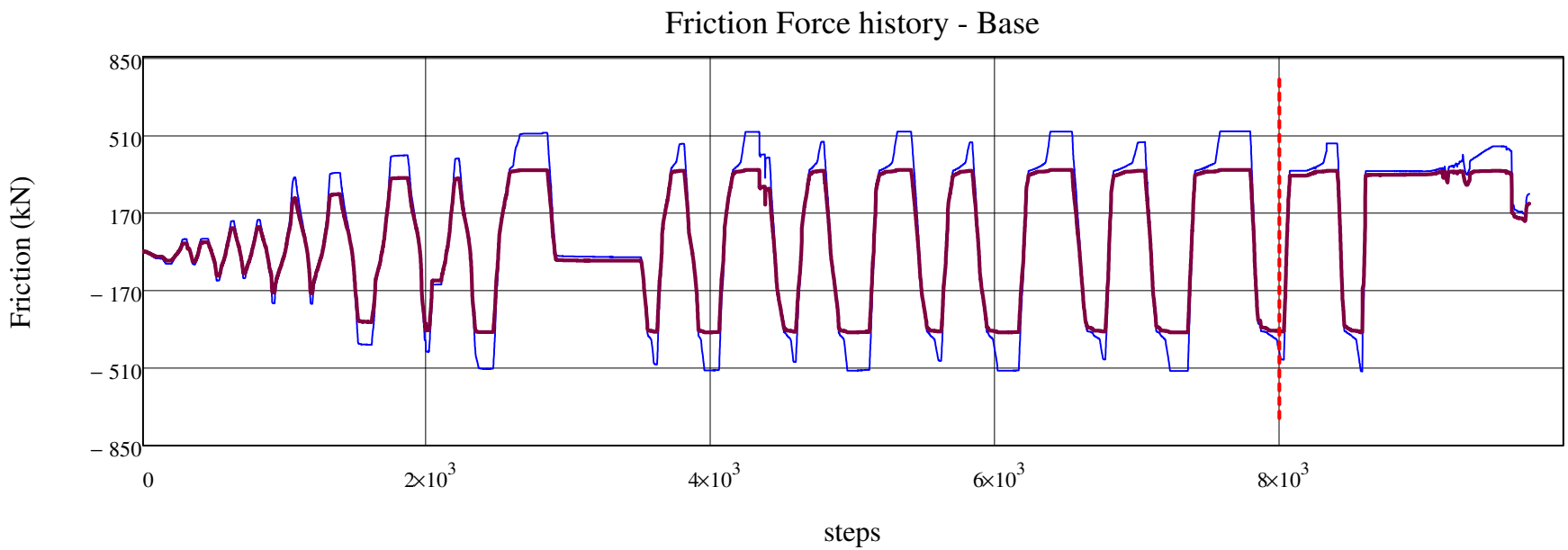

Total Force (Analysis)
Friction Force (Analysis)
End of Calibration – 20% Strength Degradation

End of Calibration - 20% Strength Degradation

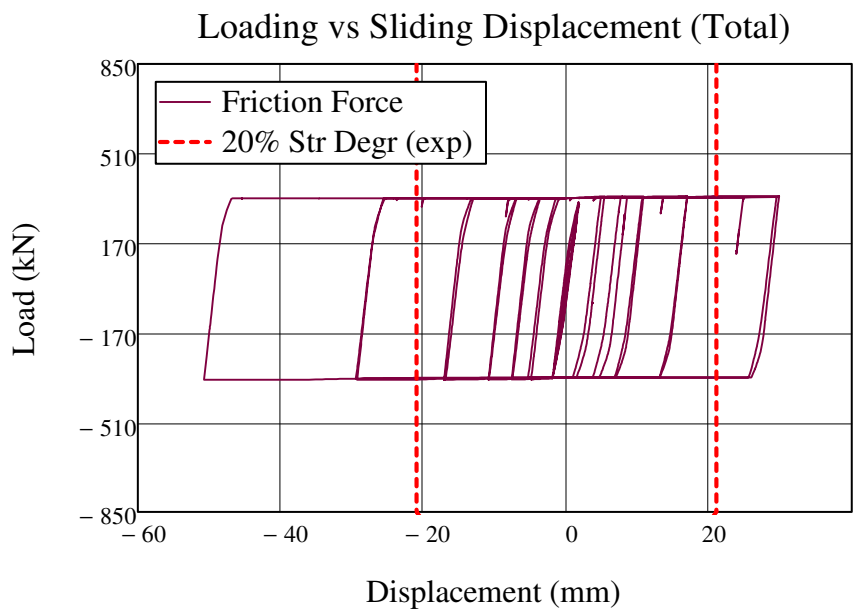

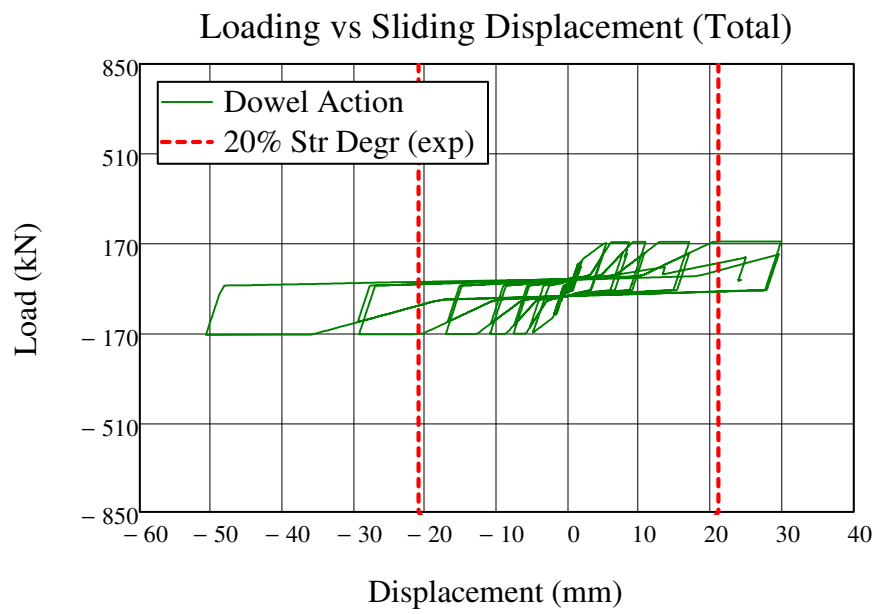

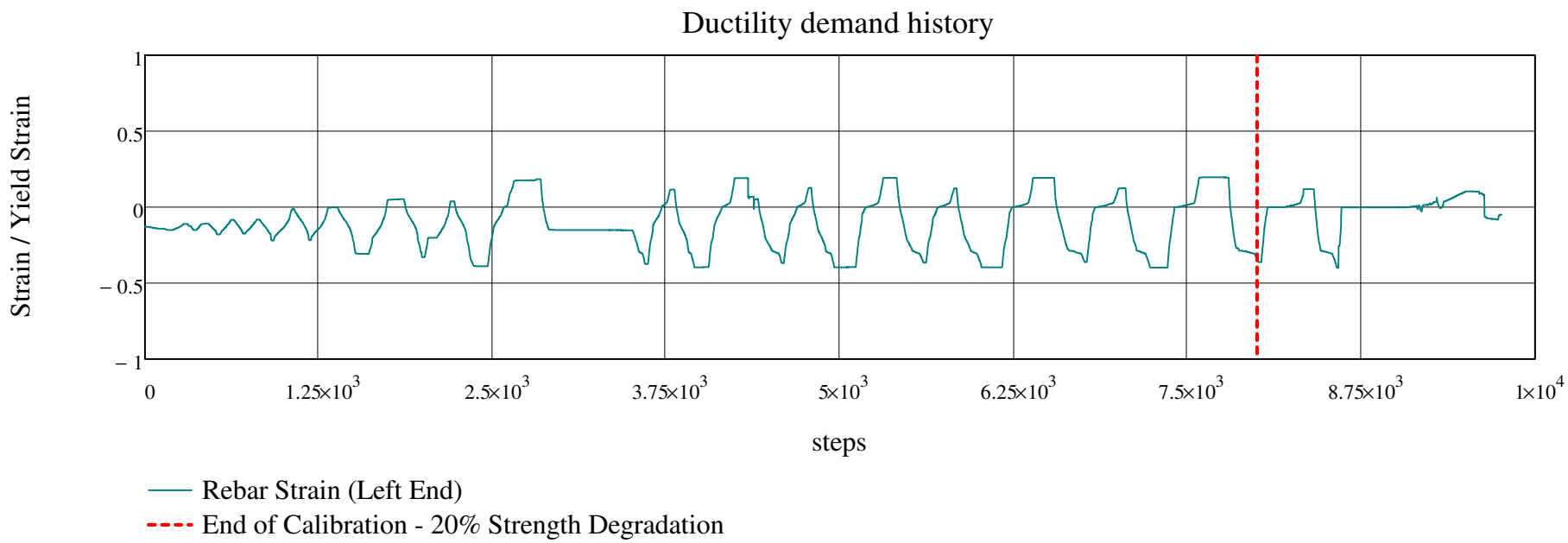

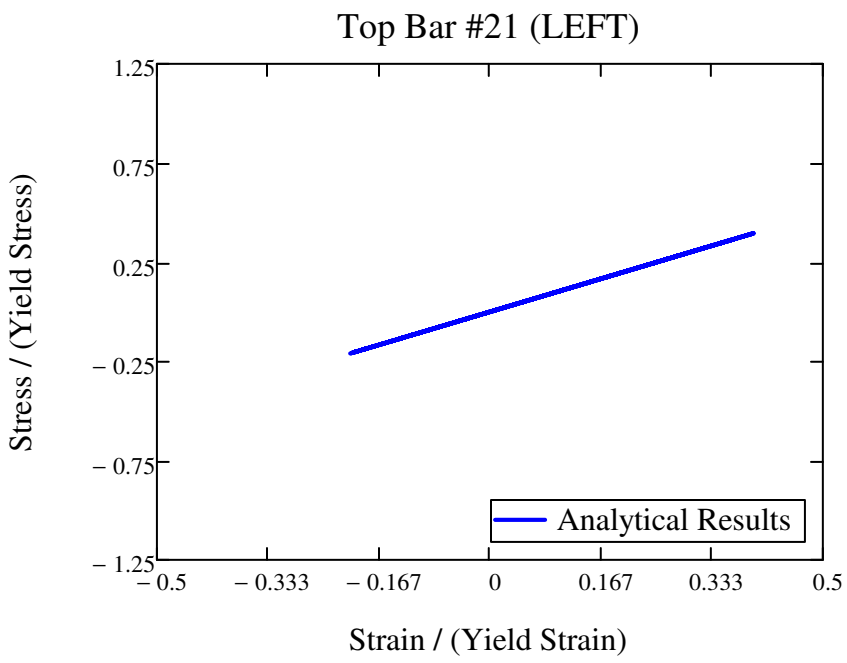
Top Bar #21 (LEFT)
Stress / (Yield Stress)
1.25
0.75
0.25
− 0.25
− 0.75
− 1.25
− 0.5
− 0.333
− 0.167
0
0.167
0.333
0.5
Strain / (Yield Strain)
Analytical Results

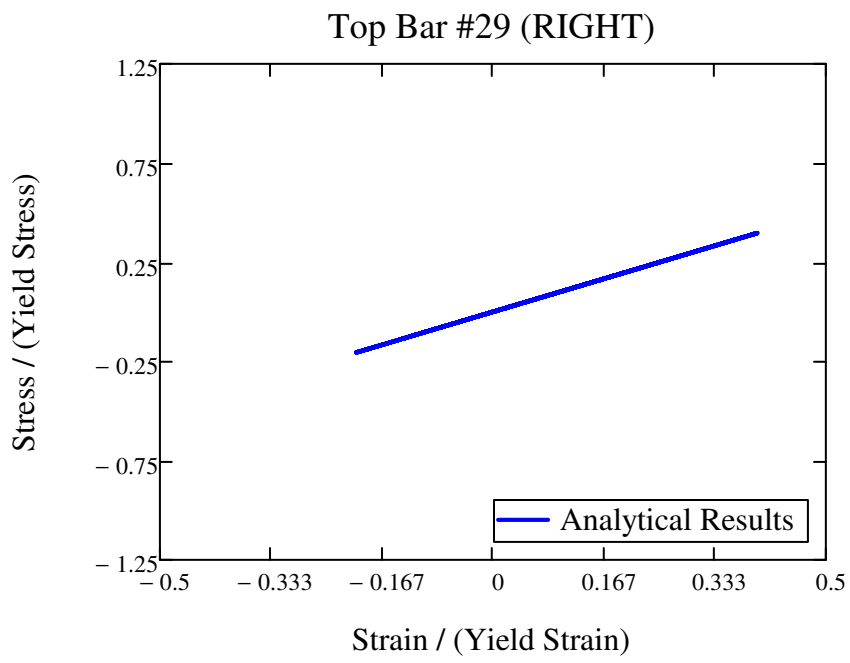
Top Bar #29 (RIGHT)
Stress / (Yield Stress)
1.25
0.75
0.25
− 0.25
− 0.75
− 1.25
− 0.5
− 0.333
− 0.167
0
0.167
0.333
0.5
Strain / (Yield Strain)
Analytical Results

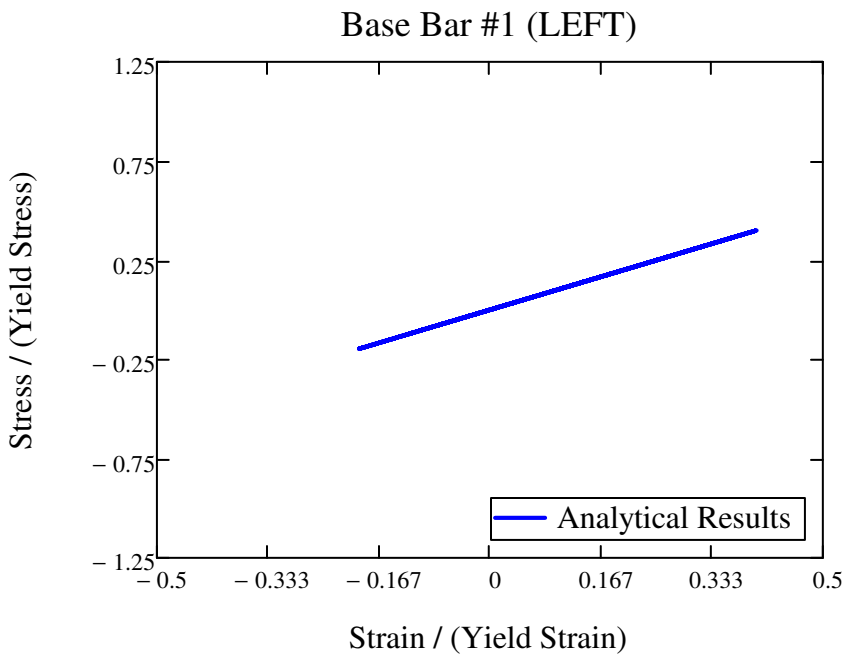
Base Bar #1 (LEFT)
Stress / (Yield Stress)
1.25
0.75
0.25
− 0.25
− 0.75
− 1.25
− 0.5
− 0.333
− 0.167
0
0.167
0.333
0.5
Strain / (Yield Strain)
Analytical Results

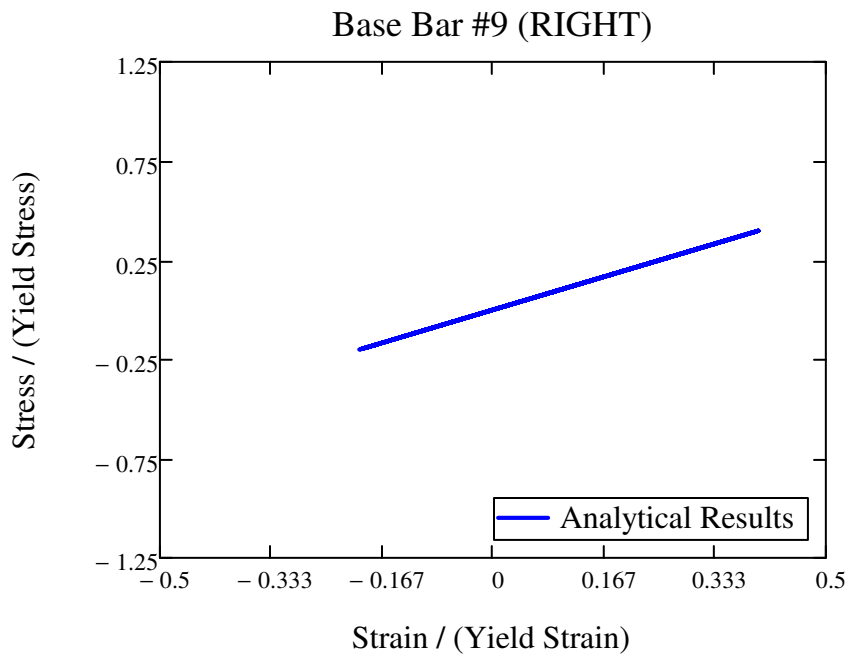
Base Bar #9 (RIGHT)
Stress / (Yield Stress)
1.25
0.75
0.25
− 0.25
− 0.75
− 1.25
− 0.5
− 0.333
− 0.167
0
0.167
0.333
0.5
Strain / (Yield Strain)
Analytical Results

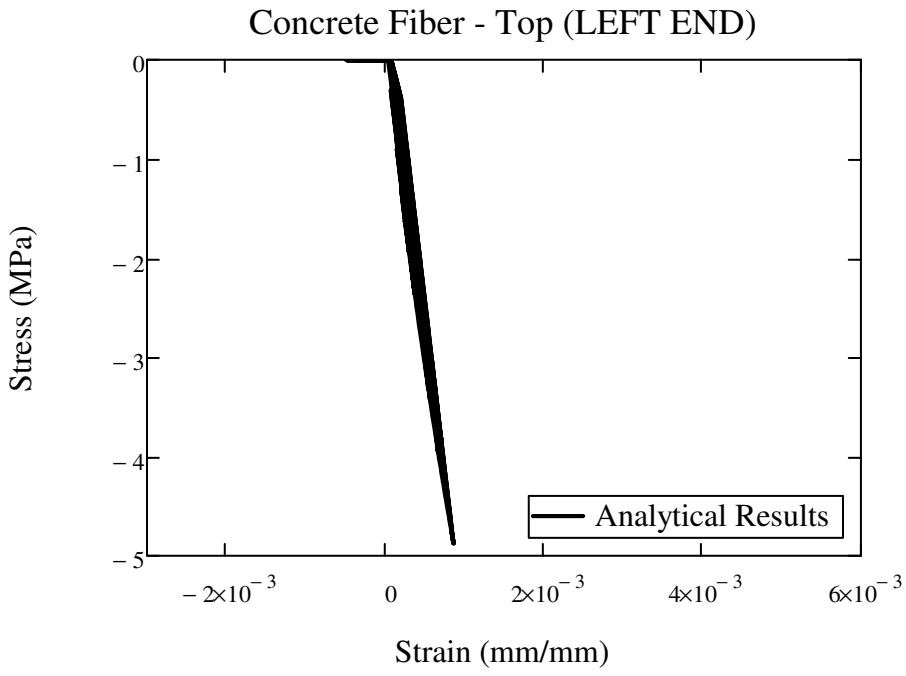
Concrete Fiber - Top (LEFT END)
Stress (MPa)
0
− 1
− 2
− 3
− 4
− 5
− 2×10^−3
0
2×10^−3
4×10^−3
6×10^−3
Strain (mm/mm)
Analytical Results

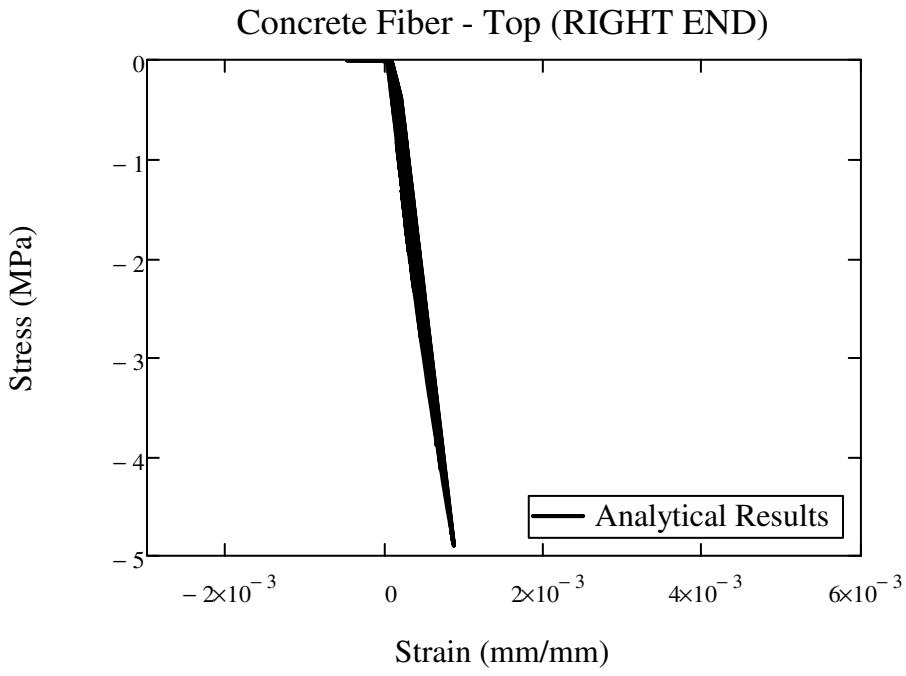
Concrete Fiber - Top (RIGHT END)
Stress (MPa)
0
− 1
− 2
− 3
− 4
− 5
− 2×10^−3
0
2×10^−3
4×10^−3
6×10^−3
Strain (mm/mm)
Analytical Results

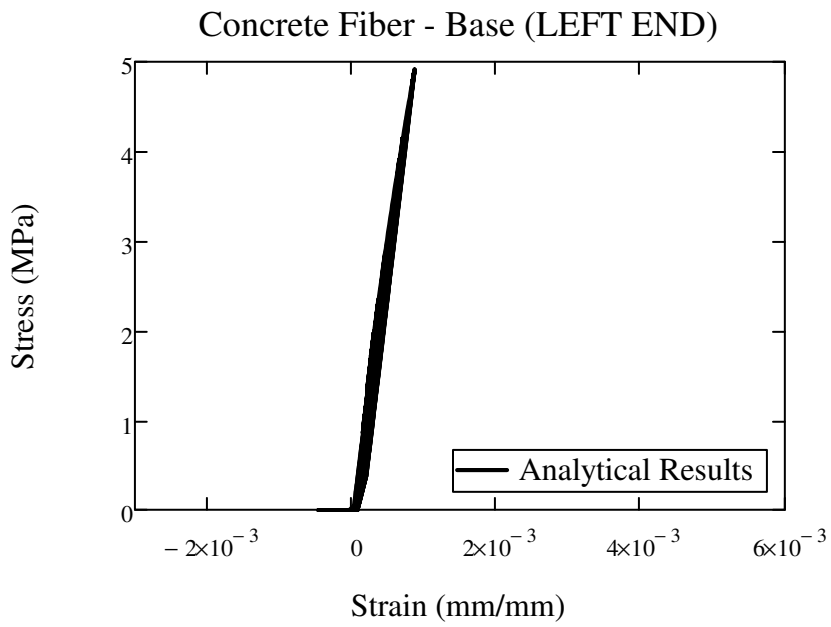
Concrete Fiber - Base (LEFT END)
Stress (MPa)
5
4
3
2
1
0
− 2×10^−3
0
2×10^−3
4×10^−3
6×10^−3
Strain (mm/mm)
Analytical Results

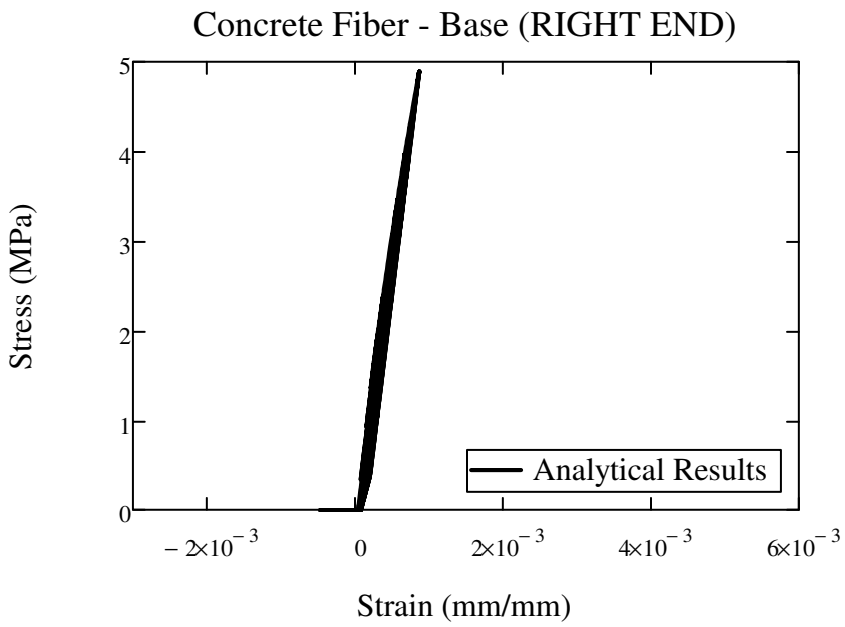
Concrete Fiber - Base (RIGHT END)
Stress (MPa)
5
4
3
2
1
0
− 2×10^−3
0
2×10^−3
4×10^−3
6×10^−3
Strain (mm/mm)
Analytical Results

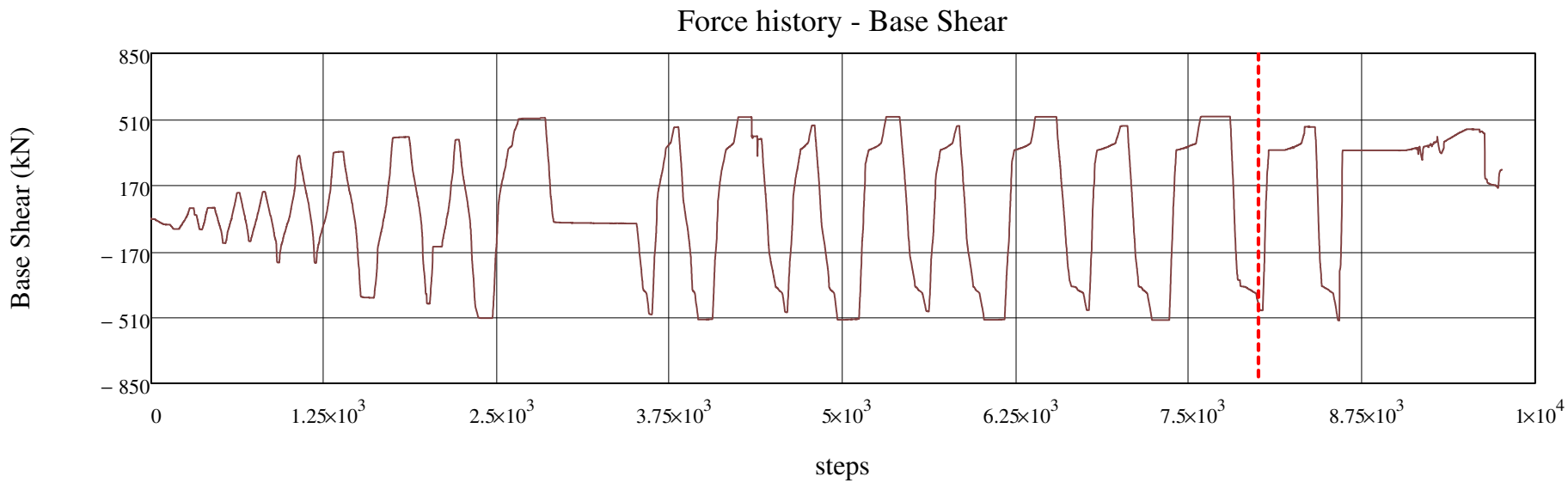

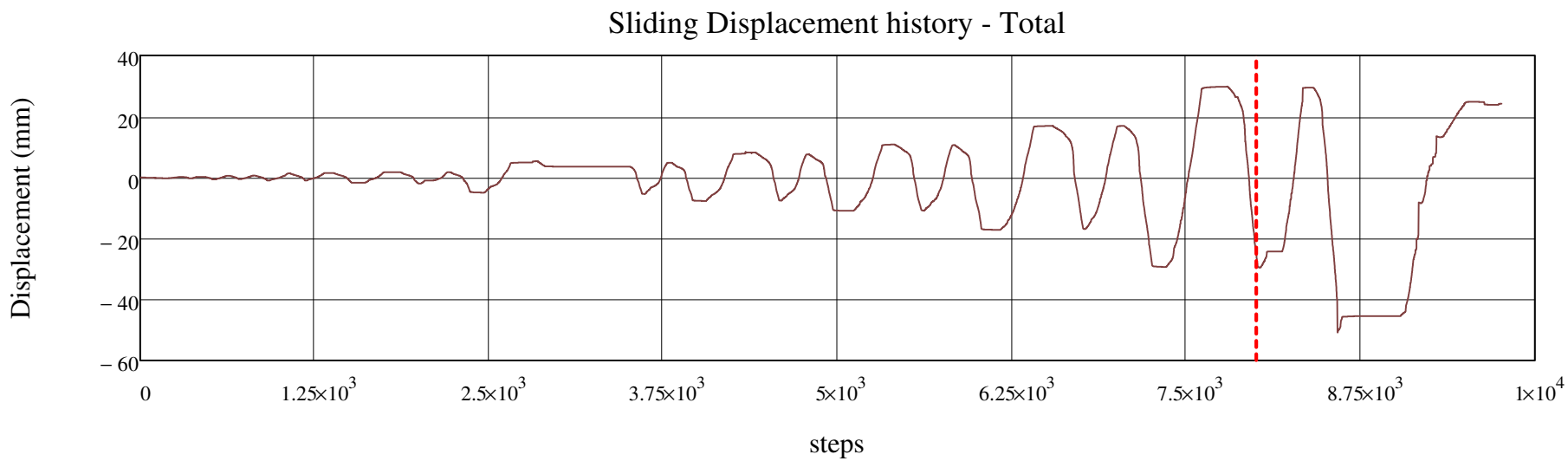

Analytical Results
Instance when Flexural Crack is open across Cross Section
End of Calibration - 20% Strength Degradation